ENVIRONMENTAL BIOENERGETICS

EDITED BY: Anke Marianne Herrmann, Doug LaRowe and Alain F. Plante
PUBLISHED IN: Frontiers in Environmental Science, Frontiers in Microbiology and Frontiers in Earth Science

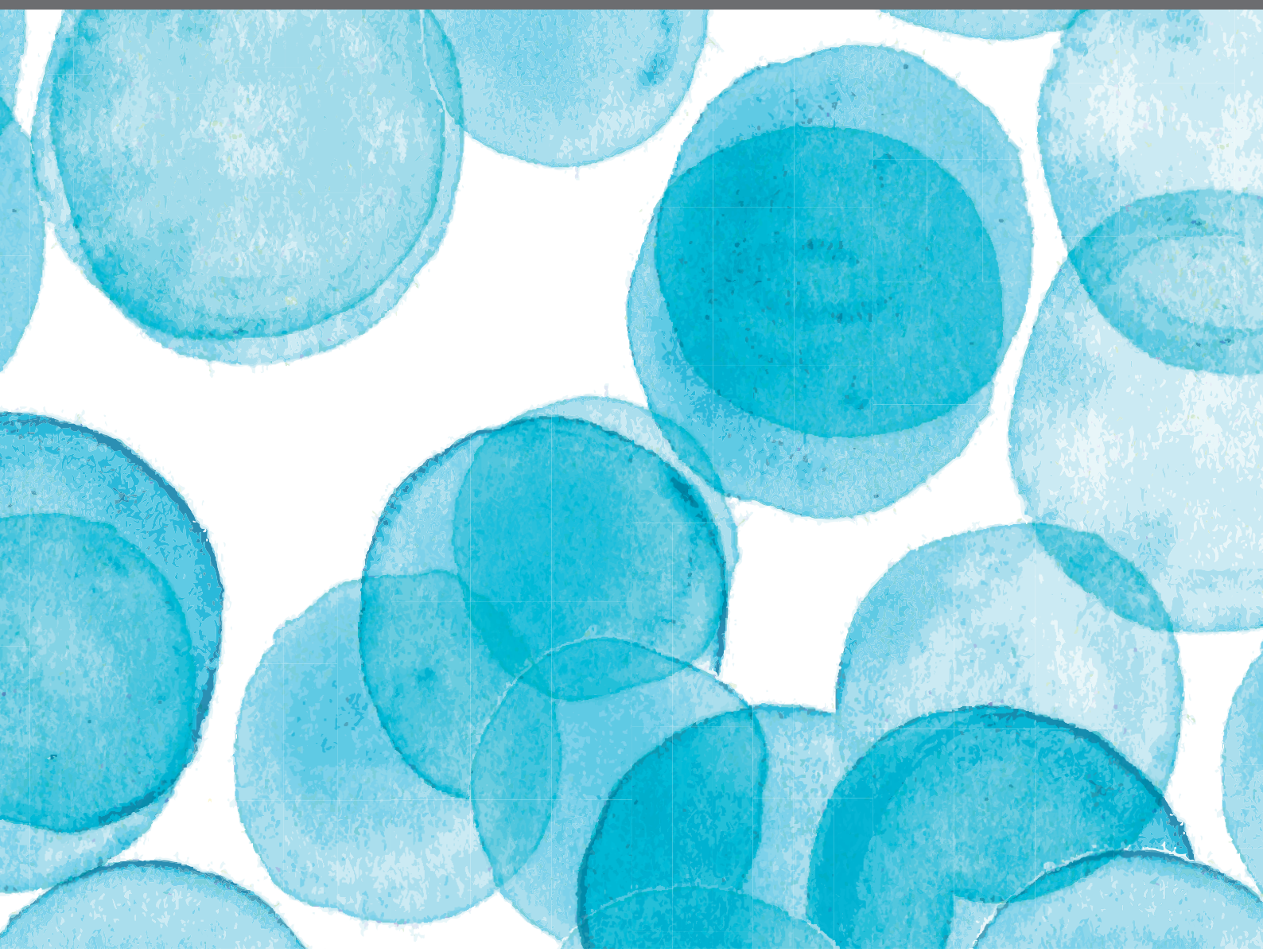

frontiers Research Topics

ISSN 1664-8714
ISBN 978-2-88963-308-1
DOI 10.3389/978-2-88963-308-1

About Frontiers

Frontiers is more than just an open-access publisher of scholarly articles: it is a pioneering approach to the world of academia, radically improving the way scholarly research is managed. The grand vision of Frontiers is a world where all people have an equal opportunity to seek, share and generate knowledge. Frontiers provides immediate and permanent online open access to all its publications, but this alone is not enough to realize our grand goals.

Frontiers Journal Series

The Frontiers Journal Series is a multi-tier and interdisciplinary set of open-access, online journals, promising a paradigm shift from the current review, selection and dissemination processes in academic publishing. All Frontiers journals are driven by researchers for researchers; therefore, they constitute a service to the scholarly community. At the same time, the Frontiers Journal Series operates on a revolutionary invention, the tiered publishing system, initially addressing specific communities of scholars, and gradually climbing up to broader public understanding, thus serving the interests of the lay society, too.

Dedication to Quality

Each Frontiers article is a landmark of the highest quality, thanks to genuinely collaborative interactions between authors and review editors, who include some of the world's best academicians. Research must be certified by peers before entering a stream of knowledge that may eventually reach the public - and shape society; therefore, Frontiers only applies the most rigorous and unbiased reviews.
Frontiers revolutionizes research publishing by freely delivering the most outstanding research, evaluated with no bias from both the academic and social point of view. By applying the most advanced information technologies, Frontiers is catapulting scholarly publishing into a new generation.

What are Frontiers Research Topics?

Frontiers Research Topics are very popular trademarks of the Frontiers Journals Series: they are collections of at least ten articles, all centered on a particular subject. With their unique mix of varied contributions from Original Research to Review Articles, Frontiers Research Topics unify the most influential researchers, the latest key findings and historical advances in a hot research area! Find out more on how to host your own Frontiers Research Topic or contribute to one as an author by contacting the Frontiers Editorial Office: researchtopics@frontiersin.org

ENVIRONMENTAL BIOENERGETICS

Topic Editors:
Anke Marianne Herrmann, Swedish University of Agricultural Sciences, Sweden
Doug LaRowe, University of Southern California, United States
Alain F. Plante, University of Pennsylvania, United States

Citation: Herrmann, A. M., LaRowe, D., Plante, A. F., eds. (2019). Environmental Bioenergetics. Lausanne: Frontiers Media SA. doi: 10.3389/978-2-88963-308-1

Table of Contents

04 ***Editorial: Environmental Bioenergetics***
Anke M. Herrmann, Douglas E. LaRowe and Alain F. Plante

07 ***Resource Legacies of Organic and Conventional Management Differentiate Soil Microbial Carbon Use***
Melissa M. Arcand, David J. Levy-Booth and Bobbi L. Helgason

24 ***Redox Sensing Within the Genus* Shewanella**
Howard W. Harris, Irene Sánchez-Andrea, Jeffrey S. McLean, Everett C. Salas, William Tran, Mohamed Y. El-Naggar and Kenneth H. Nealson

35 ***Adsorption and Desorption Characteristics of Cd^{2+} and Pb^{2+} by Micro and Nano-sized Biogenic $CaCO_3$***
Renlu Liu, Yong Guan, Liang Chen and Bin Lian

44 ***Microbial Diversity and Mineralogical-Mechanical Properties of Calcitic Cave Speleothems* in Natural *and* in Vitro *Biomineralization Conditions***
Navdeep K. Dhami, Abhijit Mukherjee and Elizabeth L. J. Watkin

66 ***Bioenergetic Controls on Microbial Ecophysiology in Marine Sediments***
James A. Bradley, Jan P. Amend and Douglas E. LaRowe

74 ***Low-Light Anoxygenic Photosynthesis and Fe-S-Biogeochemistry in a Microbial Mat***
Sebastian Haas, Dirk de Beer, Judith M. Klatt, Artur Fink, Rebecca McCauley Rench, Trinity L. Hamilton, Volker Meyer, Brian Kakuk and Jennifer L. Macalady

89 ***pH as a Primary Control in Environmental Microbiology: 1. Thermodynamic Perspective***
Qusheng Jin and Matthew F. Kirk

104 ***Discerning Microbially Mediated Processes During Redox Transitions in Flooded Soils Using Carbon and Energy Balances***
Kristin Boye, Anke M. Herrmann, Michael V. Schaefer, Malak M. Tfaily and Scott Fendorf

118 ***Low Energy Subsurface Environments as Extraterrestrial Analogs***
Rose M. Jones, Jacqueline M. Goordial and Beth N. Orcutt

136 ***Corrigendum: Low Energy Subsurface Environments as Extraterrestrial Analogs***
Rose M. Jones, Jacqueline M. Goordial and Beth N. Orcutt

139 ***pH as a Primary Control in Environmental Microbiology: 2. Kinetic Perspective***
Qusheng Jin and Matthew F. Kirk

155 ***A Bioenergetic Framework for Assessing Soil Organic Matter Persistence***
Elizabeth K. Williams and Alain F. Plante

167 ***Using Maximum Entropy Production to Describe Microbial Biogeochemistry Over Time and Space in a Meromictic Pond***
Joseph J. Vallino and Julie A. Huber

frontiers in Environmental Science

EDITORIAL
published: 10 September 2019
doi: 10.3389/fenvs.2019.00132

Editorial: Environmental Bioenergetics

Anke M. Herrmann[1]*, *Douglas E. LaRowe*[2] *and Alain F. Plante*[3]

[1] Department of Soil and Environment, Swedish University of Agricultural Sciences, Uppsala, Sweden, [2] Department of Earth Sciences, University of Southern California, Los Angeles, CA, United States, [3] Department of Earth and Environmental Science, University of Pennsylvania, Philadelphia, PA, United States

Keywords: energy, thermodynamics, calorimetry, energy-limited environments, soil, sediment

Editorial on the Research Topic

Environmental Bioenergetics

Energy is continuously transformed in the environment through the metabolic activities of organisms. Catabolic reactions generate energy (energy-yielding) which are used to fuel anabolic reactions for maintenance and growth (energy-requiring). These transformations of energy (i.e., bioenergetics) underpin most biogeochemical cycles on Earth and allow the delivery of a wide range of life-supporting ecosystem services. It has long been understood that the amount and types of energy available in an environment influence the rates of biological activity and the complexity of interactions in that system. Traditionally, energy fluxes and stocks have not been described in a quantitative manner, and it is not well-understood how physicochemical theorems such as thermodynamic principles are manifested in environmental systems. Theoretical ecological frameworks (Odum, 1969; Addiscott, 1995) have suggested that the more complex ecosystems become in terms of their food webs, the more efficient they are, i.e., relatively less energy is wasted when utilizing resources. However, this has not been rigorously tested experimentally, but in recent years, scientists in a number of fields have increasingly shown interest in quantifying how bioenergetics constrain and define ecosystem functioning. For example, organic matter in soils has distinct energetic signatures, e.g., energy densities and activation energies (Barré et al., 2016; Williams et al., 2018), and microbial bioenergetics provides empirical data for mechanistic models of carbon turnover in soils, work that is relevant to climate change (Sparling, 1983; Herrmann et al., 2014; Barros et al., 2016; Bölscher et al., 2017). Furthermore, geochemists have quantified the amount of chemolithotrophic energy available for microorganisms in a number of extreme environments to infer the dominant metabolic activities (e.g., McCollom and Shock, 1997; Shock et al., 2010; Osburn et al., 2014). These activities are challenging to monitor due to their inaccessibility and incredibly slow rates of energy processing. Although all of these efforts represent significant progress in the field of biogeochemistry, bioenergetics analysis of natural systems is still in its infancy. Nonetheless, there is increasing interest in using bioenergetics tools to better characterize biogeochemical cycling in water, soils, and sediments in terrestrial, freshwater, and marine ecosystems.

In this general context, this Research Topic aims to gather contributions from scientists working in diverse disciplines who have a common interest in evaluating bioenergetics at various spatio-temporal scales in a variety of different environments. The scientific disciplines involved include microbial chemistry, geomicrobiology, extreme microbiology, and soil biogeochemistry, and these articles show the diversity of topics demonstrating the environmental breadth of bioenergetics.

OPEN ACCESS

Edited and reviewed by:
Bradley M. Tebo,
Oregon Health & Science University, United States

***Correspondence:**
Anke M. Herrmann
anke.herrmann@slu.se

Specialty section:
This article was submitted to Microbiological Chemistry and Geomicrobiology, a section of the journal Frontiers in Environmental Science

Received: *25 July 2019*
Accepted: *27 August 2019*
Published: *10 September 2019*

Citation:
Herrmann AM, LaRowe DE and Plante AF (2019) Editorial: Environmental Bioenergetics. Front. Environ. Sci. 7:132. doi: 10.3389/fenvs.2019.00132

MICROBIAL CHEMISTRY

In two companion papers, Jin and Kirk and Jin and Kirk explore how pH affects the thermodynamics and kinetics of microbial respiration using geochemical reaction modeling. Their approach is an expansion of the work proposed by Bethke et al. (2011), and by using such a reductionist approach, they show that pH is an important factor in shaping the composition and functioning of microbial communities. In another reductionist approach, Harris et al. examine the capability of nine *Shewanella* strains to transport extracellular electrons to insoluble electron acceptors such as metal oxides. Five strains are capable of this behavior with some strains showing a preference for a particular metal oxide. Such fundamental studies provide information on underlying basic processes occurring in complex interactions in the environment.

GEOMICROBIOLOGY

Interactions between microorganisms and minerals play an important role in the transformation of rocks in natural systems (Banfield and Nealson, 1997; Shock, 2009). In this Research Topic, Dhami et al. explore the intersection of microbial ecology, geochemistry and the mechanical properties of minerals, and conclude that physicochemical conditions are important in selecting microbial communities under different environmental conditions. Liu et al. address how biologically produced minerals exert influence over the transport of metal ions and thus how microbial behavior modifies ecosystems. Finally, in a modeling article, Vallino and Huber put forward a complementary holistic approach based on thermodynamics. They evaluate the principle of maximum entropy production by combining a metabolic network, a transport model and an entropy production and optimization procedure. In this approach, field observations and modeling are combined and the results support their hypothesis that biological systems evolve and organize to maximize entropy production over a wide range of spatio-temporal scales.

EXTREME MICROBIOLOGY

Marine (sediment, oceanic basement, seep habitats) and continental (crust, ores, and aquifers) environments are energy-limited habitats. Haas et al. explore the biogeochemistry of anoxygenic photosynthesis in a thick microbial mat in Magical Blue Hole in The Bahamas. When iron is present, sulfur cycling slows down considerably. Yet, despite extreme light limitations, green sulfur bacteria were able to carry out anoxygenic photosynthesis, producing a potential biomarker for extreme low-light environments. In a review paper, Bradley et al. summarize diagenetic models (Arndt et al., 2013) commonly used to evaluate microbial energetics in marine sediments (e.g., growth rate, yield maintenance, and the physiological state of microorganisms), and provide a new model where all factors including dormancy are encompassed. Such a modeling tool will advance our understanding of why microbial communities can persist under unfavorable conditions on geological timescales. Marine sediments therefore can serve as a model system for how life could persist on extra-terrestrial settings. In a review paper, Jones et al. present an overview of how energetic limitation in subsurface environments can serve as potential analogs for life on other planetary bodies. The value of these contributions go beyond our understanding of processes on planet Earth.

SOIL BIOGEOCHEMISTRY

Soil organic matter serves as carbon and energy source for microorganisms, and the use of the average nominal oxidation state of carbon has been suggested as a universal metric of the bioenergetics potential of microbial metabolism decomposing organic matter in soils (LaRowe and Van Cappellen, 2011; Nunan et al., 2015; Gunina et al., 2017). In the current Research Topic, Boye et al. extend this approach to make progress on sustainable land-use management issues such as the degradation of organic matter in oxygen-limited rice paddy systems. Using energy balances of redox-processes, their results indicate that water-soluble carbon is key driver of microbial processes with major impacts on ecosystem functioning. Arcand et al. explore the functional importance of soil biota, including their composition, in organic and conventional management systems. Combining isothermal calorimetry with ^{13}C-DNA stable isotope probing, they demonstrate that long-term agricultural management can alter microbially driven carbon processes in soils. Furthermore, Williams and Plante propose a bioenergetics framework for assessing the persistence of organic matter in soil systems. The framework is based on a return-on-investment ratio, the ratio between energy invested in relation to energy density (Harvey et al., 2016). Their framework contradicts traditional humus theory that organic matter is composed of inherently stable macromolecules; instead it supports the idea that organic matter is a continuum of progressively decomposing organic compounds (Lehmann and Kleber, 2015).

CONCLUSIONS

The 12 articles comprising this Research Topic only begin to scratch the surface of the very broad emerging research area of environmental bioenergetics. By taking an energetic view of microbial metabolism in various environments, we may (i) further our understanding of the link between microbial communities and their activities in relation to geochemical processes, and (ii) improve our prediction of microbial feedback mechanisms and ecosystem responses to climate change. The publication of this volume comes at a key moment in which the delivery of ecosystem services is of high importance (IPBES, 2019) and the need to achieve the UN Sustainable Development Goals for 2030 (UN-DSDG, 2019) becomes an increasingly urgent issue. We aspire that this collective work will inform and stimulate more studies on this Research Topic in the coming years, and we advocate that environmental bioenergetics research (including development of new concepts and frameworks) needs to be integrated with targeted scientific research to address the pressing challenges humankind is currently faced with.

AUTHOR CONTRIBUTIONS

All authors listed have made a substantial, direct and intellectual contribution to the work, and approved it for publication.

ACKNOWLEDGMENTS

The editors want to express their profound gratitude to all authors and reviewers for their valuable contributions, which helped to achieve high standards for the contributed papers.

REFERENCES

Addiscott, T. M. (1995). Entropy and sustainability. *Eur. J. Soil Sci.* 46, 161–168. doi: 10.1111/j.1365-2389.1995.tb01823.x

Arndt, S., Jørgensen, B. B., LaRowe, D. E., Middelburg, J., Pancost, R., and Regnier, P. (2013). Quantifying the degradation of organic matter in marine sediments: a review and synthesis. *Earth Sci. Rev.* 123, 53–86. doi: 10.1016/j.earscirev.2013.02.008

Banfield, J. F., and Nealson, K. H. (1997). *Geomicrobiology: Interactions Between Microbes and Minerals*. Washington, DC: Mineralogical Society of America. doi: 10.1515/9781501509247

Barré, P., Plante, A. F., Cecillon, L., Lutfalla, S., Baudin, F., Bernard, S., et al. (2016). The energetic and chemical signatures of persistent soil organic matter. *Biogeochemistry* 130, 1–12. doi: 10.1007/s10533-016-0246-0

Barros, N., Hansen, L. D., Piñeiro, V., Pérez-Cruzado, C., Villanueva, M., Proupín, J., et al. (2016). Factors influencing the calorespirometric ratios of soil microbial metabolism. *Soil Biol. Biochem.* 92, 221–229. doi: 10.1016/j.soilbio.2015.10.007

Bethke, C. M., Sanford, R. A., Kirk, M. F., Jin, Q., and Flynn, T. M. (2011). The thermodynamic ladder in geomicrobiology. *Am. J. Sci.* 311, 183–210. doi: 10.2475/03.2011.01

Bölscher, T., Paterson, E., Freitag, T., Thornton, B., and Herrmann, A. M. (2017). Temperature sensitivity of substrate-use efficiency can result from altered microbial physiology without change to community composition. *Biol. Biochem.* 109, 59–69. doi: 10.1016/j.soilbio.2017.02.005

Gunina, A., Smith, A. R., Kuzyakov, Y., and Jones, D. L. (2017). Microbial uptake and utilization of low molecular weight organic substrates in soil depend on carbon oxidation state. *Biogeochemistry* 133, 89–100. doi: 10.1007/s10533-017-0313-1

Harvey, O. R., Myers-Pigg, A. N., Kuo, L. J., Singh, B. P., Kuehn, K. A., and Louchouarn, P. (2016). Discrimination in degradability of soil pyrogenic organic matter follows a return-on-energy-investment principle. *Environ. Sci. Technol.* 50, 8578–8585. doi: 10.1021/acs.est.6b01010

Herrmann, A. M., Coucheney, E., and Nunan, N. (2014). Isothermal Microcalorimetry provides new insight into terrestrial carbon cycling. *Environ. Sci. Technol.* 48, 4344–4352. doi: 10.1021/es403941h

IPBES (2019). *Global Assessment Report on Biodiversity and Ecosystem Services*. Available online at: https://www.ipbes.net/global-assessment-report-biodiversity-ecosystem-services

LaRowe, D. E., and Van Cappellen, P. (2011). Degradation of natural organic matter: a thermodynamic analysis. *Geochim. Cosmochim. Acta* 75, 2030–2042. doi: 10.1016/j.gca.2011.01.020

Lehmann, J., and Kleber, M. (2015). The contentious nature of soil organic matter. *Nature* 528, 60–68. doi: 10.1038/nature16069

McCollom, T. M., and Shock, E. L. (1997). Geochemical constraints on chemolithoautotrophic metabolism by microorganisms in seafloor hydrothermal systems. *Geochim. Cosmochim. Acta* 61, 4375–4391. doi: 10.1016/S0016-7037(97)00241-X

Nunan, N., Lerch, T. Z., Pouteau, V., Mora, P., Changey, F., Kätterer, T., et al. (2015). Metabolising old soil carbon: Simply a matter of simple organic matter? *Soil Biol. Biochem.* 88, 128–136. doi: 10.1016/j.soilbio.2015.05.018

Odum, E. P. (1969). The strategy of ecosystem development. *Science* 164, 262–270. doi: 10.1126/science.164.3877.262

Osburn, M. R., LaRowe, D. E., Momper, L., and Amend, J. P. (2014). Chemolithotrophy in the continental deep subsurface: Sanford Underground Research Facility (SURF), USA. *Front. Microbiol.* 5:610. doi: 10.3389/fmicb.2014.00610

Shock, E. L. (2009). Minerals as energy sources for microorganisms. *Econ. Geol.* 104, 1235–1248. doi: 10.2113/gsecongeo.104.8.1235

Shock, E. L., Holland, M., Meyer-Dombard, D., Amend, J. P., Osburn, G. R., and Fischer, T. P. (2010). Quantifying inorganic sources of geochemical energy in hydrothermal ecosystems, Yellowstone National Park, USA. *Geochim. Cosmochim. Acta* 74, 4005–4043. doi: 10.1016/j.gca.2009.08.036

Sparling, G. P. (1983). Estimation of microbial biomass and activity in soil using micro-calorimetry. *J. Soil Sci.* 34, 381–390. doi: 10.1111/j.1365-2389.1983.tb01043.x

UN-DSDG (2019). *United Nations Sustainable Development Goals*. Available online at: https://sustainabledevelopment.un.org/

Williams, E. K., Fogel, M. L., Berhe, A. A., and Plante, A. F. (2018). Distinct bioenergetic signatures in particulate versus mineral-associated soil organic matter. *Geoderma* 330, 107–116. doi: 10.1016/j.geoderma.2018.05.024

Conflict of Interest Statement: The authors declare that the research was conducted in the absence of any commercial or financial relationships that could be construed as a potential conflict of interest.

frontiers in Microbiology

ORIGINAL RESEARCH
published: 27 November 2017
doi: 10.3389/fmicb.2017.02293

Resource Legacies of Organic and Conventional Management Differentiate Soil Microbial Carbon Use

*Melissa M. Arcand[1], David J. Levy-Booth[2] and Bobbi L. Helgason[3]**

[1] Department of Soil Science, University of Saskatchewan, Saskatoon, SK, Canada, [2] Department of Microbiology and Immunology, University of British Columbia, Vancouver, BC, Canada, [3] Saskatoon Research Centre, Agriculture and Agri-Food Canada, Saskatoon, SK, Canada

Long-term contrasts in agricultural management can shift soil resource availability with potential consequences to microbial carbon (C) use efficiency (CUE) and the fate of C in soils. Isothermal calorimetry was combined with ^{13}C-labeled glucose stable isotope probing (SIP) of 16S rRNA genes to test the hypothesis that organically managed soils would support microbial communities with greater thermodynamic efficiency compared to conventional soils due to a legacy of lower resource availability and a resultant shift toward communities supportive of more oligotrophic taxa. Resource availability was greater in conventionally managed soils, with 3.5 times higher available phosphorus, 5% more nitrate, and 36% more dissolved organic C. The two management systems harbored distinct glucose-utilizing populations of *Proteobacteria* and *Actinobacteria*, with a higher *Proteobacteria*:*Actinobacteria* ratio (2.4 vs. 0.7) in conventional soils. Organically managed soils also harbored notable activity of *Firmicutes*. Thermodynamic efficiency indices were similar between soils, indicating that glucose was metabolized at similar energetic cost. However, differentially abundant glucose utilizers in organically managed soils were positively correlated with soil organic matter (SOM) priming and negatively correlated to soil nutrient and carbon availability, respiration, and heat production. These correlation patterns were strongly reversed in the conventionally managed soils indicating clear differentiation of microbial functioning related to soil resource availability. Fresh C addition caused proportionally more priming of SOM decomposition (57 vs. 51%) in organically managed soils likely due to mineralization of organic nutrients to satisfy microbial demands during glucose utilization in these more resource deprived soils. The additional heat released from SOM oxidation may explain the similar community level thermodynamic efficiencies between management systems. Restoring fertility to soils with a legacy of nutrient limitation requires a balanced supply of both nutrients and energy to protect stable SOM from microbial degradation. These results highlight the need to consider managing C for the energy it provides to critical biological processes that underpin soil health.

Keywords: thermodynamics, carbon use efficiency, microbial community composition, ^{13}C-DNA-SIP, priming effect, organic agriculture, calorimetry

OPEN ACCESS

Edited by:
Alain F. Plante, University of Pennsylvania, United States

Reviewed by:
Kevin Michael Geyer, University of New Hampshire, United States
Chao Liang, University of Wisconsin–Madison, United States
Mallory Choudoir, University of Colorado Boulder, United States

****Correspondence:***
Bobbi L. Helgason
bobbi.helgason@agr.gc.ca

Specialty section:
This article was submitted to Terrestrial Microbiology, a section of the journal Frontiers in Microbiology

Received: *11 September 2017*
Accepted: *06 November 2017*
Published: *27 November 2017*

Citation:
Arcand MM, Levy-Booth DJ and Helgason BL (2017) Resource Legacies of Organic and Conventional Management Differentiate Soil Microbial Carbon Use. Front. Microbiol. 8:2293. doi: 10.3389/fmicb.2017.02293

INTRODUCTION

Microorganisms are central drivers of soil organic matter (SOM) dynamics and are critical to controlling the flow of carbon (C) through terrestrial ecosystems. Further, microbial residues directly contribute to SOM formation (Ludwig et al., 2015; Kallenbach et al., 2016; Liang et al., 2017). Microbial carbon use efficiency (CUE) is receiving increased attention as an important factor governing the fate of metabolized C and therefore SOM formation, nutrient dynamics, and release of C to the atmosphere (Manzoni et al., 2012; Schimel and Schaeffer, 2012; Cotrufo et al., 2013; Blagodatskaya et al., 2014). Inefficient C use exacerbates CO_2 emissions with concomitant energy losses from terrestrial ecosystems (Janzen, 2015).

Soil microbial community structure (i.e., abundance and composition), resource availability, and substrate quality (nutrient and energy content) are important factors that govern CUE (Manzoni et al., 2012; Sinsabaugh et al., 2013; Herrmann et al., 2014; Lee and Schmidt, 2014; Bölscher et al., 2016). Physiological differences between active microbial populations can occur during shifts in microbial community structure, potentially altering community metabolic capacity and community-level CUE (Geyer et al., 2016). For example, copiotrophic microorganisms flourish under high resource availability while oligotrophs are adapted to resource-deprived environments through efficient use of minimal resources (Fierer et al., 2007; Roller and Schmidt, 2015). As a result, structurally different communities can process the same substrate with varied efficiency. Energy and stoichiometric nutrient balance of substrates can also affect microbial CUE (Manzoni et al., 2012), resulting in identical microbial communities that can manifest different CUE when substrates varying in free energy content are metabolized (Frey et al., 2013; Roller and Schmidt, 2015; Bölscher et al., 2016). Moreover, limitations in nutrient availability can cause microorganisms to mine SOM for nutrients via inefficient mechanisms (Geyer et al., 2016). Microbial CUE at the community level reflects the complex interplay of both microbial community structure and the chemical and energetic properties of the utilized substrates.

Agricultural management practices that alter microbial community structure can affect soil metabolic capacity and C stabilization (Lee and Schmidt, 2014; Kallenbach et al., 2015), particularly if the predominant life-strategy of the community shifts as a result of changing resource availability (Roller and Schmidt, 2015; Finn et al., 2017). Microbial community composition in agricultural and forest soils have been associated with microbial CUE (Harris et al., 2012; Herrmann et al., 2014; Creamer et al., 2015; Bölscher et al., 2016). However, large shifts in microbial community structure due to agricultural management may have little effect on CUE (van Groenigen et al., 2013) and agricultural systems with differing CUE can maintain similar metabolically active communities (Kallenbach et al., 2015). Therefore, there is no clear consensus on how or whether agricultural practices that alter microbial community composition affect microbial CUE.

Organically managed soils can harbor microbial communities that are distinct in structure and function compared to conventionally managed soils due to differences in edaphic factors stemming from legacies of pest management, nutrient inputs, and other agronomic practices such as tillage (García-Ruiz et al., 2008; Joergensen et al., 2010; Kong et al., 2011; Chaudhry et al., 2012; Li et al., 2012; Dai et al., 2014; Hartmann et al., 2014; Arcand et al., 2016). Soil C stocks have been shown to decline with conversion to organic management (Bell et al., 2012), but have also remained on par with conventional soils (Malhi et al., 2009) and even increased due to higher microbial CUE relative to conventionally managed soils (Syswerda et al., 2011; Kallenbach et al., 2015). Organic farming practices can vary markedly among regions and systems (e.g., grain vs. integrated livestock farming), thus the potential to sequester soil C in organically managed soils will not be uniform. For instance, organic grain farming systems in the Canadian prairies use tillage to control for weeds, have limited access to manure, tend to be deficient in plant-available phosphorus (P), produce lower yields, and lower crop residue returns compared to their conventional counterparts (Knight et al., 2010; Dai et al., 2014; Benaragama et al., 2016). Recently, we demonstrated that soil microbial C dynamics during crop residue decomposition differed between organic and conventional prairie grain systems. In organically managed soils, fungi and actinobacteria were more dominant utilizers of crop residue derived-C during early and late stages of decomposition, respectively, and microbial activity and abundance was more responsive to residue additions (Arcand et al., 2016). Investigation of microbial CUE could improve understanding of the fate of C in these contrasting agricultural management systems.

Isothermal calorimetry is capable of detecting minute changes in heat production and can therefore provide valuable insight into microbially driven soil C dynamics (Harris et al., 2012; Herrmann et al., 2014; Barros et al., 2010). Compared to measures of respiration, calorimetric approaches can provide a complementary and more comprehensive picture of microbial metabolism as heat captures the net outcome of anabolic and catabolic processes (Herrmann et al., 2014). Harris et al. (2012) proposed a thermodynamic efficiency index for soils based on Battley's (1960, 1987) enthalpy equations used to describe microbial cell growth on single C substrates. The index is a unit-less measure determined from the ratio of the amount of energy released following substrate addition to the energy input into the system as substrate (Harris et al., 2012). Thermodynamic efficiency indices have been shown to correlate to functional diversity and community structure, suggesting that community composition is an important factor influencing substrate utilization (Harris et al., 2012; Herrmann et al., 2014).

Thermodynamic indices integrate whole community energetics, circumventing the need to open the "microbial black box" to quantify specific metabolic processes within this complex soil ecosystem. Combined with the use of isotopic tracers that can elucidate the membership of active populations within the community, calorimetry and stable isotope probing (SIP) establish the links between energy flows during microbial metabolism and microbial community structure. SIP using enriched substrates (e.g., containing ^{13}C, ^{15}N, or ^{18}O) and subsequent characterization of labeled biomarkers allows

targeting of active microbial populations (Jameson et al., 2017). Targeted amplicon sequencing of ^{13}C-enriched DNA provides phylogenetic information about populations of interest (Neufeld et al., 2007). When combined with functional information, DNA-SIP informs the understanding of resource availability and allocation in complex environments (Li et al., 2011; Coyotzi et al., 2017). Isothermal calorimetry combined with ^{13}C-SIP has the potential to provide valuable insight into the simultaneous identity of active members and physiology of the microbial communities, enabling greater understanding of the role community composition plays in soil C dynamics.

This study combined isothermal calorimetry with ^{13}C-DNA-SIP for the first time to examine microbial metabolism and thermodynamics during glucose metabolism in soils from a long-term agricultural cropping systems field trial known to vary in community composition (Arcand et al., 2016), nutrient availability, and organic matter quality (Malhi et al., 2009). This experimental system represents typical conventional and organic grain production on the Canadian prairies. Our specific objectives were to: (i) examine the thermodynamic efficiency indices and thermal yields in soils subject to long-term history of organic and conventional management and use ^{13}C-glucose to (ii) quantify the degree of SOM priming during the assay and (iii) characterize the glucose-utilizing bacterial and archaeal communities using ^{13}C-DNA-SIP. We hypothesized that soils from conventional management systems and with cropping histories that included perennial crops in rotation have higher resource availability and therefore higher biological activity with lower thermodynamic efficiency than organically managed soils and those under annual crop rotations. We further hypothesized that the bacterial community in conventional soils would contain relatively more copiotrophs with the ability to metabolize simple compounds with low thermodynamic efficiency, while oligotrophs would be more dominant in organically managed soils.

MATERIALS AND METHODS

Field Site Description and Soil Sampling

The soils used in the incubation experiment were collected from a subset of treatments in the Alternative Cropping Systems field study established in 1994 at Scott, SK, Canada (52° 22′, 108° 50′). The field study is arranged as a split-plot design with levels of inputs as main plots and cropping sequence as sub-plots replicated four times, each on a 6-year rotation cycle. Detailed descriptions of the experimental design and management history are outlined in Brandt et al. (2010). The present study focused on two input treatments, herein defined as management systems, each representative of typical conventional and organic grain production systems in this region. The conventional (CON) system uses no-till practices and the judicious use of synthetic inputs to manage pests and nutrients based on crop scouting and soil testing, respectively. The organic (ORG) system does not use any chemical fertilizer or pesticides and weeds are controlled using tillage. The cropping sequence sub-plots sampled for use in the current study included either a diversified annual grains (ANN) or a diversified annual-perennial (PER) rotation. The soils are classified as Dark Brown Chernozems (Typic Boroll) and are loam in texture. Surface soils (0–7.5 cm) from the four field replicates of each treatment were collected following crop harvest on October 31, 2014, which represented the 21st year of the study and the last time these long-term plots were managed according to historical agricultural treatments. All plots had been cropped to wheat (*Triticum aestivum* L.); details of the cropping sequences within each management system are in Supplementary Table S1. Soils were sieved (<2 mm) and stored at 4°C until initiation of the laboratory incubations; field replicates were maintained through the experiment.

Soil Chemical and Biochemical Properties

Soils, prior to pre-incubation, were extracted for inorganic N using 2 M KCl (Maynard et al., 2008) and available P was determined using a modified Kelowna extraction (Ashworth and Mrazek, 1995); 2 M KCl extracts were analyzed for NO_3^--N and NH_4^+-N and Kelowna extracts for PO_4^--P on a Technicon Autoanalyzer (Technicon Industrial Systems, Tarrytown, NY, United States). After HCl treatment to remove carbonates, soil organic C (SOC) was determined by combustion on a LECO Carbonator (LECO Corporation, St. Joseph, MI, United States). Soil pH of air-dried soil was determined in 0.01 M $CaCl_2$ (Hendershot et al., 2008). Subsamples of soil from each field treatment were pre-incubated for 14 days at 45% water holding capacity (WHC) and 25°C. Microbial biomass was determined on these pre-incubated soils using fumigation-extraction (Vance et al., 1987). Extracts were analyzed for total organic C concentrations using a TOC-V (Shimadzu Scientific Instruments, Columbia, MD, United States). Microbial biomass C (MBC) was calculated using a k_{ec} factor of 0.45 (Wu et al., 1990). Dissolved organic C (DOC) was determined in unfumigated extracts. Potential activity of β-glucosidase (BG) which hydrolyzes degradation products of cellulose was assayed based on the colorimetric determination of *p*-nitrophenol released from synthetic substrate (Parham and Deng, 2000). BG activities were determined on 1 g of pre-incubated soil that was amended with 50 mM *p*-nitrophenyl-β-D-glucopyanoside, buffered at pH 5.5, and incubated for 1 h at 37°C. Absorbance of filtered *p*-nitrophenol extracts was determined at 405 nm (Evolution 60S spectrophotometer, Thermo Fisher Scientific, Madison, WI, United States). Phenol oxidase was assayed in 50 mM acetate buffer at pH 5.0 using 10 mM L-3,4-dihydroxy phenylalanine as substrate. Absorbance of filtered extracts was measured at 475 nm.

Soil Incubation for Calorimetry and DNA-SIP

Isothermal Calorimetry

After the 14 days pre-incubation period, 5 g soil was weighed into two sets of glass ampoules. The first set of samples received 350 μL of 0.1 M ^{13}C-glucose (99 atom%) at a rate equivalent

to 500 μg C g^{-1} soil. The glucose solution was made from U-^{13}C-labeled glucose (Cambridge Isotope Laboratories, Inc., Andover, MA, United States) dissolved in autoclaved Milli-Q water. Highly enriched ^{13}C-labeled glucose was added to enable the identification of the bacterial taxa actively assimilating glucose using DNA-SIP. The second set of soil samples served as controls and received 350 μL autoclaved Milli-Q water. The glucose and water additions brought the soil moisture levels up to 65% WHC. The ampoules containing the glucose-amended and corresponding control soils were immediately introduced into an eight channel TAM Air calorimeter (TA Instruments, Sollentuna, Sweden) and real-time heat data was continuously recorded for 48 h at 25°C. Each calorimetric channel is comprised of two heat flow sensors, one for the sample and one for a reference sample, which should be an inert material with approximately the same heat capacity as the sample (TA Instruments, 2012). Autoclaved Milli-Q water without soil was used as the reference; based on the heat capacity of water, the volume equivalent to the estimated heat capacity of the unamended soil could be determined and was added to the reference ampoule. The instrument could accommodate one complete field replicate including the water-control soils in a single assay. Therefore, the heat measurements were staggered by field replicate and the pre-incubation periods for each replicate were adjusted accordingly. After completion of the 48 h calorimetry incubation period, soils were emptied into Whirl-pak bags and immediately stored frozen (−80°C) for DNA extraction.

The total thermodynamic efficiency of soil microbial communities during glucose assimilation was calculated according to Harris et al. (2012) originally adapted from Battley's thermodynamic efficiency enthalpy equations:

$$\eta\text{eff} = 1 - [(Q_{\text{glucose}} - Q_{\text{control}})/\Delta H_{\text{glucose}}]$$

where Q_{glucose} and Q_{control} are the total heat production (J g^{-1} soil) in glucose-amended and water control soils, respectively and $\Delta H_{\text{glucose}}$ is amount of heat energy stored in the glucose (18.05 J g^{-1} soil) added to these soils.

The thermal yield, which is the fraction of heat dissipated from glucose oxidation, was calculated according to Harris et al. (2012), but was modified to account for the number of CO_2-C moles derived from primed SOM:

$$\eta CO_2 - C = \frac{\Delta\, H_C{}^O[n(CO_2)_{\text{glucose}} - (n(CO_2)_{\text{primed}} + n(CO_2)_{\text{control}})]}{\Delta H_{\text{glucose}}}$$

where $n(CO_2)_{\text{glucose}}$ and $n(CO_2)_{\text{control}}$ are the number of CO_2-C moles respired in glucose- and water-amended soils over the 48 h incubation period, respectively, and $n(CO_2)_{\text{primed}}$ is the number of SOM-derived CO_2-C moles that were primed in glucose-amended soils. The sum of $n(CO_2)_{\text{primed}}$ and $n(CO_2)_{\text{control}}$ comprises the total moles of CO_2-C mineralized from SOM in glucose-amended soils. The fraction of glucose-heat retained in the soil, ηsoil, is 1-ηCO_2-C. Details on the methods and calculations used to determine respiration and priming are outlined below.

^{13}C-DNA Stable Isotope Probing

Total genomic DNA was extracted from each of the ^{12}C glucose and ^{13}C glucose-amended soils using the Mo Bio PowerSoil DNA kit according to the manufacturer's instructions (Qiagen Canada). DNA concentration was determined using the Qubit fluorometer (Life Technologies, Thermo Fisher Canada) and 2 μg DNA from of each sample was used for density centrifugation. The separation of different density fractions was performed according to Dunford and Neufeld (2010). Briefly, 500 mL of sterile 7.163 M CsCl gradient stock solution was freshly prepared. The appropriate volume gradient buffer was added to the volume of DNA extract required to contain 2 μg of DNA and 4.8 mL of CsCl stock solution in a 15 mL Falcon tube to achieve a final density of 1.725 g mL^{-1} and inverted to mix. The solutions were then loaded into 5.1 mL Quickseal Polyallomer centrifuge tubes, weighed and balanced, and loaded into a Vti 65.2 rotor and centrifuged using a Beckman optima TLX under vacuum for 40 h at 23°C and 44,100 rpm. Samples were immediately fractionated into 12 μL × 425 μL fractions in sterile 1.5 mL Eppendorf tubes using a calibrated infusion pump (Braintree Scientific Inc.). The DNA was then precipitated by first adding 20 μg polyacrylamide followed by 2 volumes of 30% Polyethylene glycol in NaCl, mixing by inversion after each addition and incubating at room temperature overnight. Pelleted DNA was washed with 70% ethanol, dried at room temperature for 15 min and then suspended in 30 μL of TE buffer. The amount of DNA in each of the fractions was further quantified by using the Qubit assay.

An initial characterization of the fractions was performed by combining aliquots of fractionated DNA from each of the experimental replicates ($n = 4$) and comparing 16S rRNA gene DGGE banding patterns of labeled (^{13}C) and native substrate (^{12}C) samples. Specifically, unique banding patterns in ^{13}C "heavy" fractions that corresponded with high concentration of DNA signaled ^{13}C incorporation into bacterial DNA (Dunford and Neufeld, 2010). We sequenced fraction 6 (heavy, ∼1.722 g ml^{-1}) and 10 (light, ∼1.747 g ml^{-1}) for ^{13}C-glucose amended soils, herein referred to as "glucose utilizers" and fraction 9 (light, ∼1.741 g ml^{-1}) for ^{12}C-glucose amended soil. Concentration of DNA in fractions 5 and 6 (heavy) of the ^{12}C-glucose amended soil was below the threshold of detection in all treatments except for one replicate of the ORG-ANN soils.

DNA sequencing of the bacterial 16S rRNA v4 region was performed using primers 518F and 806R (Caporaso et al., 2011) at the McGill University and Genome Quebec Innovation Centre (Montreal, QC, Canada). Following PCR amplification, amplicons were purified using Ampure XP beads (Beckman Coulter, Canada), ligated to index adapters, quantified with the Quant-iT PicoGreen dsDNA Assay Kit (Thermo Fisher Scientific, Waltham, MA, United States) and pooled at equimolar concentration. DNA was then sequenced according to manufacturer's instructions on the MiSeq DNA Sequencer (Illumina, San Diego, CA, United States). Raw sequencing

reads were deposited in the European Nucleotide Archive at study accession PRJEB22936 and sample accessions ERS1963781-ERS1963826.

Soil Incubation for Respiration and Determination of Priming

An additional subsample of soil from each field treatment was pre-incubated for 14 days at 45% WHC and 25°C as above for determining respiration rates, including priming of SOM. Three separate sets of the pre-incubated soil were weighed (20 g) into 16 dram vials and placed into 1 L Mason jars. The first set received 0.1 M of 19.5 atom% ^{13}C glucose solution. The second set received 0.1 M of glucose containing ^{13}C at natural abundance levels. These soils were used as ^{12}C-glucose-amended controls for DNA-SIP. The third set received autoclaved Milli-Q water. Solutions were added at equal volumes (1.40 mL) across the three sets of soils to bring soil moisture levels up to 65% WHC and at glucose rates equivalent to the 500 μg C g^{-1} soil used in the calorimetry assay. A lower enrichment of ^{13}C-labeled glucose compared to that added to the set of DNA-SIP/calorimetry soils was used to reduce potential analytical difficulty associated with analyzing high enrichment material using IRMS (Watzinger, 2015). Jars were immediately sealed following solution addition, flushed with CO_2-free air and incubated at 25°C.

Gas Sampling and Analysis

Headspace gas samples (20 mL) were taken 4, 12, 24, 36, and 48 h after glucose or water addition and injected into evacuated 12 mL Exetainer® tubes (Labco Limited, United Kingdom) to determine CO_2 concentration using gas chromatography (Bruker 450 GC, Bruker Biosciences, Billerica, MA, United States). A second gas sample (12 mL) was taken and injected into another set of Exetainer® tubes for ^{13}C analysis on a GasBench interfaced to a Thermo Scientific Delta V Plus isotope ratio mass spectrometer (Thermo Scientific, Bremen, DE) at the UC Davis Stable Isotope Facility. Jars were immediately flushed with CO_2-free air after sampling and resealed. Two blank jars without soil were carried throughout the incubation.

The amount of CO_2-C respiration (μg CO_2-C g^{-1} soil) derived from glucose ($R_{glucose}$) was determined using the following mass balance equation:

$$R_{glucose} = \frac{R_t^*[x(^{13}C)_{sample} - x(^{13}C)_{soil}]}{[x(^{13}C)_{glucose} - x(^{13}C)_{soil}]}$$

Where R_t is the total amount of CO_2-C released from glucose-amended soil samples, $x(^{13}C)_{sample}$ is its isotopic abundance, $x(^{13}C)_{glucose}$ is the isotopic abundance of the ^{13}C-labeled glucose, and $x(^{13}C)_{soil}$ is the isotopic abundance of CO_2 from soil receiving water only. Thus, the amount of SOM-derived CO_2 was calculated as:

$$R_{SOM} = R_t - R_{glucose}$$

The amount of CO_2 respired through priming of SOM (R_{primed}) was calculated as:

$$R_{primed} = R_{SOM} - R_{basal}$$

Where R_{Basal} is the amount of CO_2 released during basal respiration (water-only control soils).

In addition to the thermodynamic efficiency indices and thermal yields, we calculated metabolic quotients and calorespirometric ratios, which are often used as proxies for microbial CUE (Hansen et al., 2004; Creamer et al., 2015; Herrmann and Bölscher, 2015; Barros et al., 2016; Bölscher et al., 2016; Bailey et al., 2017). The metabolic quotient (qCO2) was calculated as the ratio of basal respiration and soil MBC (Anderson and Domsch, 1985). Calorespirometric ratios (mJ μg^{-1} CO_2-C) were calculated for both control and glucose-amended soils as the ratio of heat production to CO_2-C respired (Hansen et al., 2004). Calorespirometric ratios are suggested to provide information on both the nature of the substrate being metabolized and its utilization efficiency (Barros et al., 2016). Given metabolism of similar organic material, low ratios indicate high efficiency (Hansen et al., 2004). However, unlike single substrates, the constituents of SOM are variable and complex, making the interpretation of these ratios difficult.

Bioinformatics and Statistical Approaches

The bioinformatics approach of this work was modeled after Caporaso et al. (2010). Paired end joining of Illumina fastq files used FLASH 1.2.11 (Magoc and Salzberg, 2011). Quality filtering at a per-base cutoff of Q13 used USEARCH 9.0.2132 (Edgar and Flyvbjerg, 2015). OTU selection used the QIIME pipeline, with sequencing filtering and alignment using Chimera Slayer and PyNast. Open-reference operational taxonomic unit (OTU) binning was performed using Greengenes at 97% sequence similarity followed by *de novo* clustering of unbinned sequences. Singletons were removed prior to analysis.

Soil chemical and biological variables, relative abundance of phyla, and α-diversity measures were analyzed with a mixed effects model using the *lme* function in the *nlme* package in R. Management system and cropping history were fixed factors, while field replicate and the interaction of field replicate by management system were random effects. Where significant interactions between management system and cropping history were detected ($P < 0.05$), Tukey *post hoc* procedure was used to determine how soil variables under the four treatment combinations (ORG-ANN, ORG-PER, CON-ANN, CON-PER) differed. Respiration, heat production, and calorespirometric ratios were also analyzed with amendment (glucose/water) as an additional fixed factor to management system and cropping history.

To test for differences in β-diversity of OTUs under all treatments and fractions permutational multivariate analysis of variance (PERMANOVA) was used on Bray–Curtis dissimilarity indices calculated using relative abundance on counts rarified to an equal depth (23932) with the same multi-factor ANOVA structure as previously described. PERMANOVA was performed using the *adonis* function in the *vegan* 2.4-3 package (Oksanen et al., 2017) in R 3.2.4 (R Developement Core Team, 2016), as were all analyses reported in this manuscript. β-diversity was

visualized with Principal Coordinate Analysis (PCoA) using the *capscale* in *vegan*.

DESeq2 was used to select positively differentially abundant OTUs that differentiated treatment effects (Love et al., 2014). We used this technique to identify taxa that drove differences between the CON and ORG management systems within each C fraction as well as between ^{13}C-heavy and ^{13}C-light fractions to distinguish between glucose and non-glucose utilizers within each management system. Clustered correlation heatmaps of differentially abundant OTUs [false discovery rate (FDR)-adjusted *P*-values < 0.01] and soil properties were made using the *CIM* function in the *mixOmics* package.

RESULTS

Soil Properties, Basal Heat Production, and Respiration

Available P was 3.5 times greater, NO_3^--N was 5% greater, and DOC was 36% greater in soils under CON compared to ORG management regardless of cropping history (**Table 1**), reflecting different nutrient input regimes and crop residue returns between the two systems over the course of the 20 year field study. Soil pH was significantly lower in the ORG-ANN soils compared to the CON-ANN and ORG-PER soils (**Table 1**).

The effect of management system on MBC depended on cropping history. MBC was greater in CON-ANN compared to CON-PER soils, but there were no significant differences in MBC between the ORG and CON soils (**Table 1**). Without glucose amendment, CON soils supported 48% higher rates of potential PHOX activity (**Table 1**), 26% higher production of CO_2 and 38% more heat (**Table 2**). CON soils produced 32% more CO_2 per unit initial MBC (qCO_2) than ORG soils at basal rates (**Table 2**).

Heat Production, Respiration, and SOM Priming Following Glucose Amendment

Glucose increased cumulative heat production and respiration compared to controls soils after 48 h by 4.6 and 7.1 times, respectively, in CON soils and by 5.8 and 8.7 times, respectively, in ORG soils. These heat measurements represent the energy not conserved in the system during glucose metabolism and are used in the calculation of ηeff. Differences in heat and respiration observed in controls between management systems were maintained, albeit to a lesser extent, following glucose amendment (**Table 2**). Heat production was 7% higher and CO_2 production was 6% higher in CON compared to ORG soils. Calorespirometric ratios (mJ μg^{-1} CO_2-C) declined with glucose addition ($P < 0.0001$).

Isotopic analysis of the ^{13}C-CO_2 released from ^{13}C-glucose-amended soils enabled the partitioning of glucose- vs. SOM-derived CO_2 production (**Table 3**). Cumulative glucose-derived CO_2 did not differ among treatments, but glucose oxidation contributed significantly less to total cumulative CO_2 in CON-ANN soils than ORG and CON-PER soils (71 vs. 73%), corresponding to greater SOM-derived CO_2 in CON-ANN

TABLE 1 | Soil chemical and biological properties from long-term organically (ORG) and conventionally (CON) managed agricultural systems with either annual (ANN) or annual-perennial (PER) cropping histories.

MS	Crop	SOC (%)	DOC (μg g soil^{-1})	NO_3^--N (μg g soil^{-1})	PO_4^--P (μg g soil^{-1})	pH	MBC (μg g soil^{-1})	BG (μmol g^{-1} soil)	PHOX (μmol g^{-1} soil)
Management system means pooled across cropping histories ($n = 8$)									
CON		2.91 ± 0.15[1]	61.5 ± 5.1A	52.2 ± 3.4A	59.6 ± 4.1A	5.15 ± 0.08	308.5 ± 26.8	1.31 ± 0.24	0.54 ± 0.03A
ORG		2.72 ± 0.17	45.3 ± 2.2B	42.3 ± 1.4B	15.5 ± 0.8B	5.13 ± 0.13	302.3 ± 13.0	1.04 ± 0.07	0.37 ± 0.07B
Individual treatment means ($n = 4$)									
CON	ANN	3.09 ± 0.30	61.7 ± 10.1	51.2 ± 7.1	53.7 ± 7.2	5.26 ± 0.14a	362.8 ± 32.9a	1.66 ± 0.37	0.56 ± 0.05
	PER	2.73 ± 0.04	61.3 ± 4.6	53.3 ± 1.1	65.5 ± 2.0	5.03 ± 0.04ab	254.2 ± 17.5b	0.97 ± 0.22	0.52 ± 0.05
ORG	ANN	2.89 ± 0.29	46.3 ± 3.4	41.7 ± 1.1	14.8 ± 1.3	4.91 ± 0.15b	298.4 ± 17.6ab	1.10 ± 0.11	0.36 ± 0.11
	PER	2.55 ± 0.20	44.2 ± 3.3	42.9 ± 2.8	16.2 ± 1.1	5.35 ± 0.16a	306.2 ± 21.6ab	0.98 ± 0.11	0.37 ± 0.11
Analysis of variance[2]									
MS		NS	**	*	***	NS	NS	NS	*
Crop		NS	NS	NS	NS	NS	NS	NS	NS
MS × Crop		NS	NS	NS	NS	**	*	NS	NS

[1]*Values are means ± standard error; data displayed are pooled across management systems ($n = 8$) and for each individual treatment ($n = 4$). Same letters indicate no significant difference between treatment means after Tukey's HSD post hoc test.* [2]*Asterisks indicate P-values (*$P < 0.05$, **$P < 0.01$, ***$P < 0.001$; NS, not significant) from the analysis of variance of management system (MS) and cropping history (Crop) and their interactions on soil properties.*

soils. The greater SOM-derived CO_2 in CON-ANN soils can be attributed to both higher basal respiration and priming of SOM. We found that priming of SOM comprised 15% of total cumulative respiration across all treatments and glucose primed the decomposition of 11% more organic matter in CON-ANN compared to the other soils. In spite of lower quantities of primed SOM in ORG soils, a higher proportion of the total SOM-derived CO_2 produced was primed under ORG compared to CON soils (57 vs. 51%), regardless of cropping history.

There were no significant differences in any of the thermodynamic efficiency indices among the long-term field treatments using glucose as an available substrate (**Table 4**). The thermal yield in soil (ηsoil) was 0.56 across all treatments and the thermodynamic efficiency index (ηeff) was 0.68.

TABLE 2 | Long-term differences in organic (ORG) and conventional (CON) management systems (MS) affect respiration, heat, and metabolic properties without labile substrate amendment, but differences were attenuated with glucose addition.

MS	Crop[1]	Control soils				Glucose-amended soils		
		Respiration μg CO_2-C g^{-1} soil	Heat J g^{-1} soil	Caloresp. ratio mJ μg^{-1} CO_2-C	Metabolic quotient μg CO_2-C μg^{-1} MBC	Respiration μg CO_2-C g^{-1} soil	Heat J g^{-1} soil	Caloresp. ratio mJ μg^{-1} CO_2-C
Management system means pooled across cropping histories ($n = 8$)[2]								
CON		34.3 ± 2.3A[3]	1.65 ± 0.12A	48.4 ± 2.8	0.12 ± 0.009A	243.4 ± 4.9A	7.44 ± 0.07A	30.6 ± 0.5
ORG		26.5 ± 0.8B	1.20 ± 0.04B	45.3 ± 1.4	0.09 ± 0.003B	229.8 ± 2.6B	6.93 ± 0.04B	30.2 ± 0.3
Individual treatment means ($n = 4$)								
CON	ANN	37.4 ± 4.0	1.76 ± 0.21	47.7 ± 5.3	0.11 ± 0.014	248.1 ± 9.7	7.47 ± 0.12	30.2 ± 1.1
	PER	31.2 ± 1.1	1.54 ± 0.11	49.2 ± 2.7	0.13 ± 0.013	238.6 ± 2.2	7.41 ± 0.1	31.0 ± 0.3
ORG	ANN	26.1 ± 0.6	1.18 ± 0.04	45.4 ± 2.1	0.09 ± 0.006	229.6 ± 5.2	7.01 ± 0.06	30.6 ± 0.5
	PER	26.9 ± 1.6	1.22 ± 0.07	45.3 ± 2.0	0.09 ± 0.004	230.1 ± 2.2	6.86 ± 0.04	29.8 ± 0.4
		Analysis of variance[4]						
MS		**	**	NS	*	*	***	NS
Crop		NS	NS	NS	NS	NS	NS	NS
MS × Crop		NS	NS	NS	NS	NS	NS	NS

[1]*Crop refers to the annual (ANN) or annual-perennial (PER) cropping history subplots used in the incubation experiment.* [2]*Values are means ± standard error; data displayed are pooled across management systems (n = 8) and for each individual treatment (n = 4).* [3]*Different letters indicate significant differences between management systems based on analysis of variance.* [4]*Asterisks indicate P-values (*P < 0.05, **P < 0.01, ***P < 0.001; NS, not significant) from the analysis of variance of management system (MS) and cropping history and their interactions on soil properties.*

TABLE 3 | Source partitioning of CO_2 and priming effects following glucose amendment to soils from contrasting long-term organic (ORG) and conventional (CON) management systems (MS).

MS	Crop[1]	Glucose-derived	SOM-derived	Primed	Glucose-derived	Primed	Primed
		μg CO_2-C g^{-1} soil			% total CO_2-C		% SOM-derived CO_2-C
Management system means pooled across cropping histories ($n = 8$)[2]							
CON		173.0 ± 3.1	70.6 ± 3.4	36.2 ± 1.2	71.3 ± 0.9B	14.9 ± 0.5	51.4 ± 1.5B
ORG		168.4 ± 2.5	61.5 ± 0.8	34.9 ± 0.5	73.3 ± 0.4A	15.4 ± 0.2	56.9 ± 0.9A
Individual treatment means ($n = 4$)							
CON	ANN	172.5 ± 5.7	75.6 ± 4.3a	38.2 ± 1.0a	69.8 ± 0.8b	15.5 ± 0.6	51.0 ± 2.7
	PER	173.6 ± 0.8	63.9 ± 2.6b	33.4 ± 1.3b	73.3 ± 0.7a	14.0 ± 0.6	52.0 ± 0.6
ORG	ANN	168.8 ± 4.9	60.8 ± 0.3b	34.7 ± 0.7b	73.5 ± 0.5a	15.3 ± 0.3	57.0 ± 1.1
	PER	168.0 ± 2.1	62.1 ± 1.5b	35.2 ± 0.7b	73.0 ± 0.7a	15.5 ± 0.3	56.8 ± 1.6
		Analysis of variance[3]					
MS		NS	NS	NS	*	NS	*
Crop		NS	NS	NS	NS	NS	NS
MS × Crop		NS	*	*	*	NS	NS

[1]*Crop refers to the annual (ANN) or annual-perennial (PER) cropping history subplots used in the incubation experiment.* [2]*Values are means ± standard error; data displayed are pooled across management systems (n = 8) and for each individual treatment (n = 4). Same letters indicate no significant difference between treatment means after Tukey's HSD post hoc test.* [3]*Asterisk * indicates P < 0.05 and NS, not significant from the analysis of variance of management system (MS) and cropping history (Crop) and their interactions on soil properties.*

TABLE 4 | Thermodynamic efficiency indices did not differ between soils under contrasting long-term organic (ORG) and conventional (CON) management system when supplied with glucose.

Management system	Cropping history	ηeff*	ηCO_2*	ηsoil*
CON	ANN	0.684 ± 0.012	0.448 ± 0.013	0.553 ± 0.013
	PER	0.675 ± 0.001	0.443 ± 0.003	0.558 ± 0.003
ORG	ANN	0.677 ± 0.005	0.435 ± 0.012	0.565 ± 0.012
	PER	0.687 ± 0.002	0.433 ± 0.005	0.568 ± 0.005

*Microbial thermodynamic efficiency (ηeff) and thermal yields of heat dissipated as CO_2 (ηCO_2) or retained in the soil (ηsoil) during glucose oxidation. Heat production and respiration rates were measured using isothermal calorimetry and sampling of headspace CO_2, respectively, of glucose-amended surface soils (0–7.5 cm) from CON and ORG management system treatments planted to annual (ANN) or annual-perennial (PER) cropping history subplots that were incubated for 48 h. No significant effect of long-term management system or cropping history was detected based on analysis of variance ($P > 0.05$).

Structure and Diversity of Glucose-Utilizing Communities

Community Structure

The ^{12}C-light fraction represents the total community following amendment of unlabeled glucose for 48 h. The ^{13}C-light fraction represents community members that did not utilize glucose and the ^{13}C-heavy fraction represents community members that have incorporated ^{13}C from labeled glucose.

Principal coordinate analysis of Bray–Curtis dissimilarity of 16S rRNA gene OTU relative abundance profiles showed that the glucose-utilizing bacterial and archaeal communities (^{13}C-heavy) were distinct from the non-glucose utilizing communities (^{13}C-light) and (^{12}C-light) (**Figure 1A**). When community analyses of the fractions were separated, total (**Figure 1B**) and non-glucose utilizing (**Figure 1C**) communities were significantly different under CON and ORG management, as were communities under different cropping histories (ANN vs. PER). In the fraction representing glucose-utilizers (**Figure 1D**), only communities under different management systems were significantly different, accounting for 22% of variation following PERMANOVA.

Regression of Bray–Curtis dissimilarity with soil variables showed the influence of soil C on glucose utilization. Soil pH was the only significant variable ($R^2 = 0.13$, $P = 0.017$) to affect total community structure. DOC ($R^2 = 0.13$, $P = 0.013$) and SOC concentration ($R^2 = 0.14$, $P = 0.019$) were significantly correlated with non-glucose utilizing community structure, and DOC concentration was the only variable that significantly correlated with glucose-utilizing community structure ($R^2 = 0.14$, $P = 0.031$).

Bacterial and archaeal relative abundance in each fraction was investigated at the phylum level. The number of total sequencing counts was similar between fractions, although the ^{13}C-heavy community contained 4,323 and 10,834 fewer OTUs than the ^{13}C-light and ^{12}C-light fractions, respectively. Within the ^{12}C-light fraction, *Proteobacteria* had a relative abundance of 29.3% and were significantly more abundant in soil under CON management and in ANN compared to PER cropping histories (**Figure 2** and Supplementary Table S2). In the ORG-ANN soils, relative abundance of *Actinobacteria* was significantly lower, while *Verrucomicrobia, Firmicutes,* and *Acidobacteria* were relatively more abundant. Compared to the total community, the *Bacteroidetes*, *Crenarchaeota*, and *Firmicutes* were relatively more abundant in the ^{13}C-light fraction, representing members that did not likely directly assimilate labeled glucose. *Bacteroidetes* and *Crenarchaeota* were significantly more abundant under CON management, while *Chloroflexi* was greater under ORG. Within the ^{13}C-heavy fraction, *Actinobacteria* had a relative abundance of 49.4%, and were significantly more abundant under ORG, as were *Firmicutes* while *Proteobacteria* were more abundant under CON management. In comparison, *Actinobacteria* represented 31.3 and 19.2% of ^{12}C-light and ^{13}C-light communities, respectively.

Differential Abundance between Management Systems

As only management system was a significant factor in structuring the ^{13}C-heavy community (**Figure 1D**), DeSeq2 differential abundance testing was used to determine the most important microbial community members driving differences between these management systems and their relationships with soil attributes. Overall, 331 different OTUs, or 1.0% of ^{13}C-enriched OTUs, were differentially abundant between ORG and CON management systems at a FDR-corrected *p*-value cut-off of 0.01 (**Figure 3A**). This accounted for 29% of ^{13}C-enriched OTUs based on counts. There were 114 glucose-utilizing OTUs that were significantly more abundant in CON systems, 55% of which were *Proteobacteria* (**Figure 3C**). The 26 glucose-utilizing *Actinobacteria* OTUs enriched in CON systems resolved to the genera *Thermomonospora* sp., *Actinoallomurus* sp., *Cellulomonas* sp. and *Gaiella* sp. Of the 217 glucose-utilizing OTUs with significant abundance in ORG systems 32% were *Proteobacteria*, with taxonomic difference to CON system-selected *Proteobacteria*. The majority of ORG-*Proteobacteria* were *Burkholderia* sp., *Janthinobacterium* sp., *Variovorax paradoxus,* and *Rhizobium leguminosarum*. Glucose-utilizing *Actinobacteria* appeared enriched in ORG systems, and were almost entirely made up of *Arthrobacter* sp. Additionally, ORG systems appeared to select for *Firmicutes* including *Paenibacillus chondroitinus* and *Bacillus flexus*.

Of the 112 differentially abundant OTUs between management systems in the ^{13}C-light fraction (0.3% of total ^{13}C-light OTUs), 97 were significantly more abundant in CON systems (**Figure 3D**). These primarily included *Bacteroidetes* (46 OTUs), *Proteobacteria* (30 OTUs) and

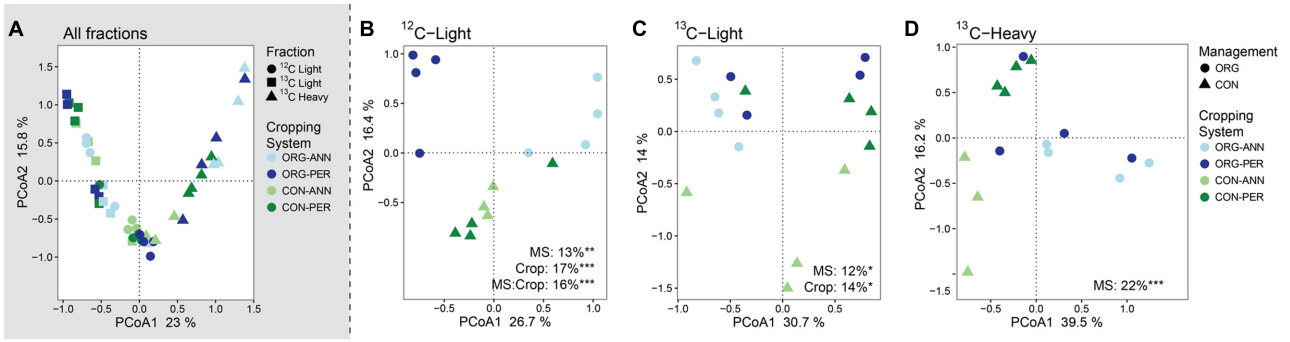

FIGURE 1 | Bacterial and archaeal community structure differed according to long-term organic (ORG) and conventionally (CON) managed agricultural treatments. Unconstrained multivariate ordination of Bray–Curtis dissimilarity indicating β-diversity of ANN and PER cropping systems under ORG and CON management systems with **(A)** all C isotopic fractions (^{12}C-light, ^{13}C-light, ^{13}C-heavy), **(B)** ^{12}C-light fraction, **(C)** ^{13}C-light fraction, **(D)** ^{13}C-heavy fraction using Principal Component Analysis (PCoA). PERMANOVA for cropping system (Crop) and management system (MS) is shown for fraction-specific PCoA in each panel. Asterisks denote *p*-value range following PERMANOVA: $*p < 0.05$, $**p < 0.01$, $***p < 0.001$.

Actinobacteria (14 OTUs), although one *Crenarchaeota* OTU mapping to *Nitrososphaera* clone SCA1145 was significantly more abundant in ^{13}C-Light CON vs. ORG (**Figure 3D**). The remaining OTUs selected for by ORG systems, primarily *Proteobacteria* (4 OTUs), *Actinobacteria* (4 OTUs) and *Acidobacteria* (3 OTUs) showed poor taxonomic resolution. These 111 differentially abundant OTUs comprised only 2.8% of the counts, compared to the much higher proportion of the community (29.2%) differentiated in the ^{13}C-heavy fraction.

Differentially abundant OTUs between glucose-utilizers in ORG and CON management systems gave rise to substantially different correlation patterns with soil attributes. Correlation heatmaps indicate that both glucose-utilizing (**Figure 3A**) and non-utilizing (**Figure 3B**) organisms were differentiated between CON and ORG management systems according to soil resource availability and function. The CON OTU cluster correlated negatively with the proportion of SOM-derived CO_2 that was primed (pSOMprimed) and positively with PO_4-P, NO_3-N, and DOC concentrations, phenol oxidase activity (PHOX), metabolic quotients, ηCO_2, respiration, and heat production. ORG-enriched OTUs demonstrated opposing correlative trends. Correlation patterns between differentially abundant OTUs in the ^{12}C-light (i.e., total community) and soil attributes were similar (Supplementary Figure S1).

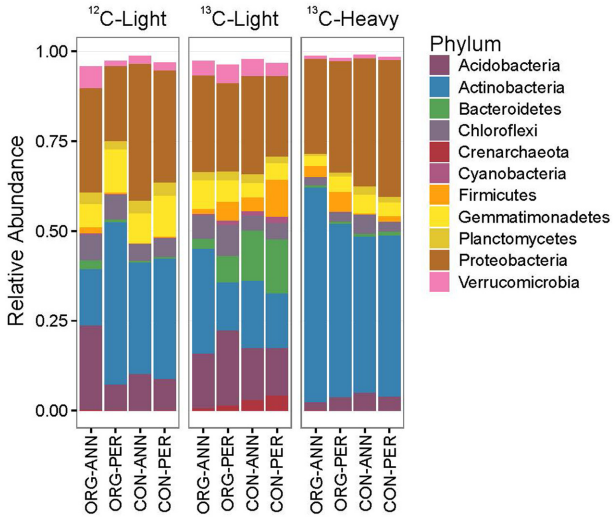

FIGURE 2 | Phyla relative abundance of 16S OTUs in carbon fractions differed according to long-term agricultural management treatments. The panels show relative abundance of 16S OTUs in the total bacterial (^{12}C-light), the non-glucose utilizing bacteria (^{13}C-light) and the glucose-utilizing bacterial (^{13}C-heavy) communities from management system (ORG, CON) and cropping history (ANN, PER) treatments following glucose amendment. Only phyla with a relative abundance greater than 0.005 shown. Each bar represents the mean of four replicates.

Differential Abundance between ^{13}C-Fractions

To verify that ^{13}C-glucose incubation selected for unique microbial populations, and that ^{13}C-glucose utilization differed between CON and ORG management systems, DESeq2 was again applied to identify OTUs that were differentially abundant between ^{13}C-heavy (glucose utilizers) and ^{13}C-light (non-glucose utilizers) fractions for each management system (**Figure 4A**). Of the 978 differentially abundant OTUs in CON soil (1.1% of CON OTUs), 312 were significantly more abundant in ^{13}C-heavy treatments, indicating glucose utilization (**Figure 4C**). These OTUs were predominately from the phyla *Actinobacteria* (57%), including *Streptomyces* sp., *Modestobacter* sp. and *Nocardioides* sp. The most-abundant *Proteobacteria* (38% of CON OTUs differentially abundant in the ^{13}C-heavy fraction) were largely *Burkholderia* sp. and *Devosia* sp. In contrast, 666 non-glucose utilizing OTUs in CON ^{13}C-light fractions were primarily from the phyla *Bacteroidetes* (31%), *Acidobacteria* (21%) and *Proteobacteria* (13.4%), with minor populations of *Verrucomicrobia* (9.0%) and *Firmicutes* (8 %). The *Acidobacteria* were *Koribacter versatilis* and *Solibacter* sp. non-glucose-utilizing *Proteobacteria* included several

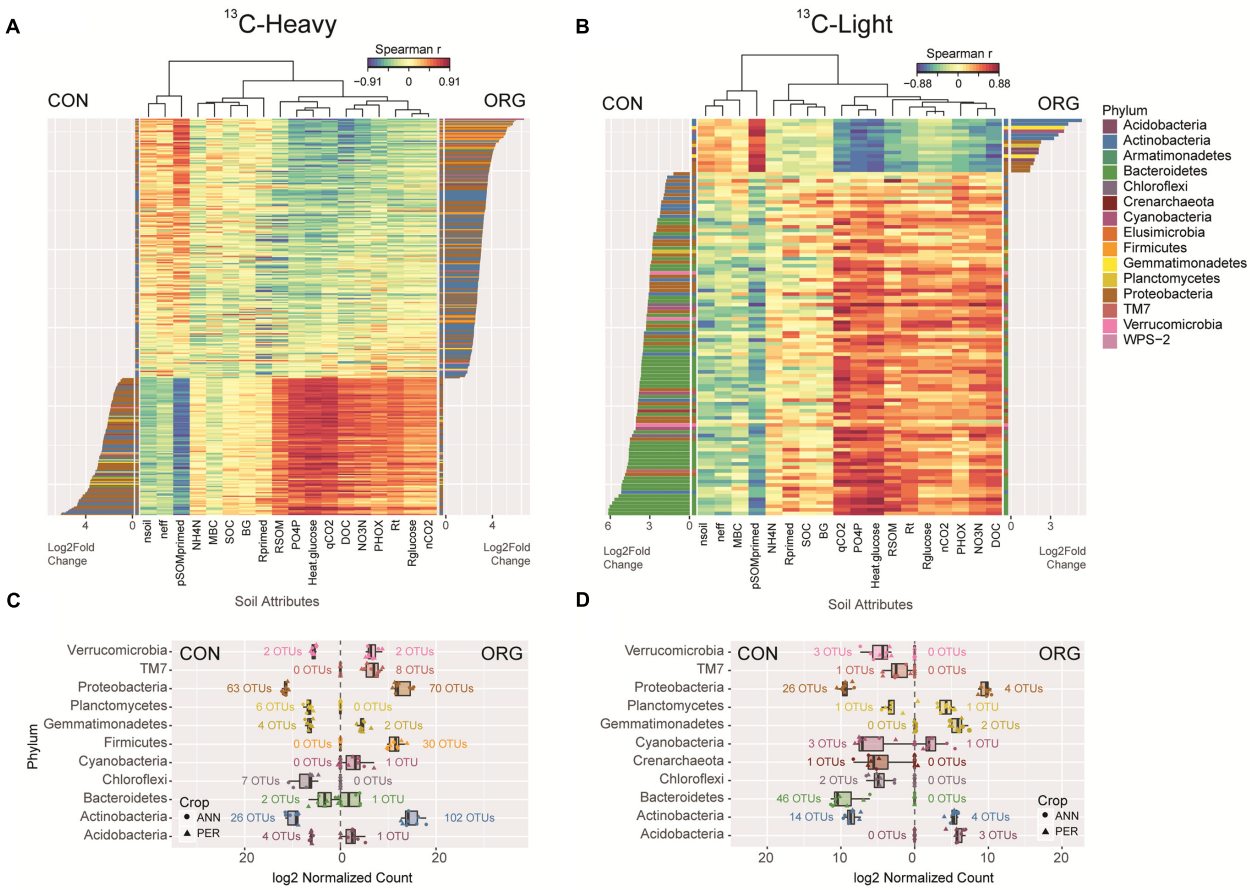

FIGURE 3 | Glucose-utilizing and non-utilizing bacteria in conventional and organically managed soils were differentiated by soil attributes. DeSeq2 differential abundance analysis of OTUs in CON and ORG managed soils in ^{13}C-heavy **(A)** and ^{13}C-light **(B)** fractions (FDR-adjusted $p < 0.01$). Heat map of Spearman correlations between OTU differential abundance and soil variables ordered by $\log_2$-fold-change. Abundance of each phylum in CON and ORG managed soil in ^{13}C-heavy **(C)** and ^{13}C-light **(D)** fractions corresponding to the differentially abundant OTUs, annotated with the number of OTUs per phyla. MBC, microbial biomass carbon; SOC, soil organic carbon; DOC, dissolved organic carbon; R_t, total CO_2-C production; R_{primed}, total primed CO_2-C; $R_{glucose}$, total glucose-derived CO_2-C; RSOM, total soil organic matter-derived CO_2-C; pSOMprimed, proportion of soil organic matter derived CO_2-C that was primed; qCO_2, metabolic quotient; PHOX, phenol oxidase; BG, β-glucosidase; ηeff, thermodynamic efficiency index; ηCO_2, thermal yield of glucose heat in CO_2-C; ηsoil, thermal yield of glucose heat in soil.

methanotrophic and N-fixing taxa, as well as *Nitrosovibrio tenus*.

In ORG management systems, a direct comparison of ^{13}C-heavy and ^{13}C-light fractions using DeSeq2 differential abundance analysis was also used to investigate glucose-utilizing and non-utilizing populations, respectively (**Figure 4B**). About half of the 952 differentially abundant OTUs (1.2% of all ORG OTUs) were enriched by glucose addition over 48 h (**Figure 4D**). As with previous comparisons, *Actinobacteria*, including *Arthrobacter psychrolactophilus, Streptomyces mirabilis,* and *Cellulomonas xylanilytica* represented 53% of ORG glucose-utilizing OTUs. Likewise, *Proteobacteria* such as *Burkholderia tuberum*, *Sphingomonas wittichii,* and *Variovorax paradoxus* represent 34% of glucose-utilizing OTUs in ORG systems. OTUs differentially abundant in ^{13}C-light fractions from ORG systems had similar OTU identities and distribution as from CON systems, albeit with substantially fewer *Bacteroidetes*. This comparison of ^{13}C-heavy and ^{13}C-light fractions in each cropping system provided additional information regarding taxonomic identity and ecology of glucose-utilizing and non-utilizing populations, respectively.

DISCUSSION

Microbial Thermodynamic Indices under Organic and Conventional Management

Soil microbial CUE plays a critical role in C sequestration, nutrient availability, and SOM formation. Microbial communities produced similar amounts of heat per unit glucose-derived energy applied (ηeff) between management systems and cropping histories (**Table 4**). The thermodynamic efficiencies were slightly lower than those reported in an arable soil (Bölscher et al., 2016), but closely coincided to those found in soils under contrasting agricultural management

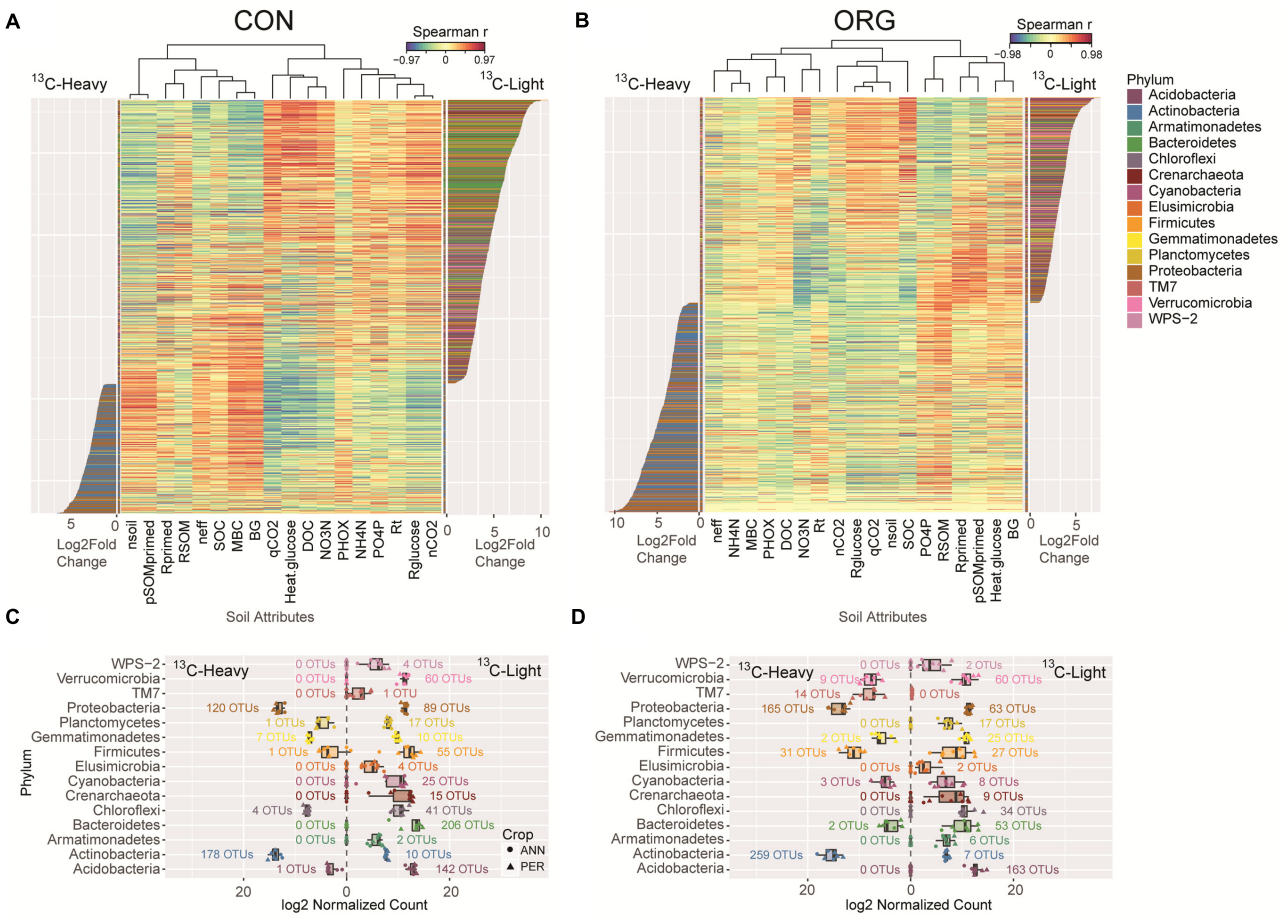

FIGURE 4 | Differentially abundant glucose-utilizing (^{13}C-heavy) and non-utilizing bacteria (^{13}C-light) in CON compared to ORG managed soils and correlation to soil attributes. DeSeq2 differential abundance analysis of OTUs between glucose utilizers (^{13}C-heavy) and non-utilizers (^{13}C-light) between CON **(A)** and ORG **(B)** management systems. Heat map of Spearman correlations between OTU differential abundance and soil variables ordered by $\log_2$-fold-change. Abundance of each phylum in CON **(C)** and ORG **(D)** managed soil in ^{13}C-heavy and ^{13}C-light fractions corresponding to the differentially abundant OTUs, annotated with the number of OTUs per phyla. MBC, microbial biomass carbon; SOC, soil organic carbon; DOC, dissolved organic carbon; R_t, total CO_2-C production; R_{primed}, total primed CO_2-C; $R_{glucose}$, total glucose-derived CO_2-C; RSOM, total soil organic matter-derived CO_2-C; pSOMprimed, proportion of soil organic matter derived CO_2-C that was primed; qCO_2, metabolic quotient; PHOX, phenol oxidase; BG, β-glucosidase; ηeff, thermodynamic efficiency index; ηCO_2, thermal yield of glucose heat in CO_2-C; ηsoil, thermal yield of glucose heat in soil.

reported by Harris et al. (2012). However, Harris et al. (2012) differentiated the effects of long-term agricultural inputs on ηeff whereas we could not. Heavy metal toxicity and low soil pH can result from repeated applications of sewage sludge and $(NH_4)_2SO_4$, respectively, which potentially disturbed microbial communities, resulting in low ηeff (Harris et al., 2012). In contrast, the agricultural inputs in our study likely did not induce toxicity-related stress or soil acidification.

We hypothesized that (i) ORG soils would support microbial communities with higher thermodynamic efficiency than CON soils and (ii) that cropping history would modify the efficiencies. However, thermodynamic efficiency indices (ηeff) and thermal yields (ηCO_2 and ηsoil) did not differ between management systems or cropping history (**Table 4**). Incubating soils with ^{13}C-labeled glucose enabled us quantify glucose-derived ^{13}C released during glucose oxidation based on isotopic mass balance. Any CO_2-C released due to priming of SOM decomposition following glucose addition would not confound calculations of ηCO_2 and ηsoil (Harris et al., 2012). Therefore, similar ηCO_2 between the two communities suggests that ^{13}C-glucose was oxidized with equal efficiency. The simplicity of glucose enables it to be consumed rapidly (minutes to hours), without enzymatic breakdown (Frey et al., 2013; Gunina and Kuzyakov, 2015), and calorespirometric ratios suggest that this labile C substrate was processed efficiently compared to SOC (**Table 2**). Glucose has been used as a model substrate in calorimetric studies of soil microbial energetics (Nuñez et al., 1994; Barja and Nuñez, 1999; Barros et al., 2010; Harris et al., 2012), and is frequently used to assess microbial activity and in isotopic tracer experiments (Hill et al., 2008; Strickland et al., 2012). However, studies using

multiple substrates have shown that assessments of metabolic efficiency is substrate dependent (Frey et al., 2013; Bölscher et al., 2016). Microbial thermodynamic efficiency under these contrasting soils might be better resolved with multiple substrates ranging in energy content and chemical complexity, reflecting the heterogeneous nature of organic materials comprising SOM.

In contrast to thermal yields, ηeff calculations include heat released due to oxidation of primed SOM in addition to glucose. Thus, similarities in ηeff in glucose-amended soils may be due to varying degrees of SOM priming between soils. Glucose amendment rates (500 μg C g^{-1} soil, 165% of MBC) were likely high enough to induce microbial growth, which can increase microbial nutrient demand as well as affect priming (Blagodatskaya and Kuzyakov, 2008). The proportionally higher priming of SOM decomposition in ORG compared to CON soils (**Table 3**) following glucose amendment may be due overflow respiration (Manzoni et al., 2012; Geyer et al., 2016), which occurs when excess C is mineralized due to nutrient limitations to growth (Sinsabaugh et al., 2013) and microorganisms seek out nutrients in SOM (Geyer et al., 2016). The microbial community in the ORG soil likely mineralized organic nutrients to satisfy stoichiometric demand (Chen et al., 2013). The observed positive correlations between the differentially abundant OTUs in ORG soil and SOM-derived CO_2, as well as negative correlations between nutrient and C availability with heat production (**Figure 3**), likely reflect differences in SOM chemistry, inorganic nutrient supply, and prevailing life strategies of the dominant heterotrophs (van der Wal and de Boer, 2017).

Metabolic quotients and calorespirometric ratios were also determined as they have been used as proxies for microbial CUE (Barros et al., 2010; Bölscher et al., 2016; Bailey et al., 2017). The metabolic quotient during basal metabolism was 32% higher in CON soils (**Table 2**), indicating that proportionally more C was respired by the microbial biomass and could suggest that the ORG communities utilized indigenous resources more efficiently. Metabolic quotients have been questioned for their utility in discerning the effects of stress and disturbance on microbial metabolism (Wardle and Ghani, 1995; Bölscher et al., 2016), but they have been useful ecophysiological indicators especially when combined with other measures of microbial growth and activity (Blagodatskaya et al., 2014). Management history had no significant effect on calorespirometric ratios (**Table 2**). However, calorespirometric ratios and metabolic quotients are not necessarily related (Barros et al., 2011; Bölscher et al., 2016) as metabolism of more reduced (i.e., higher energy content) substrate can increase calorespirometric ratios without affecting qCO_2 (Barros et al., 2011). As such, the calorespirometric ratio may not be a good approximation for CUE when different substrates are being consumed (Bölscher et al., 2016). Despite similar SOC between systems, less light fraction OM and DOC in the ORG soils indicate differences in organic matter quality between management systems (Malhi et al., 2009). Therefore, though differences in metabolic quotients were detected, the lack of differences in calorespirometric ratios may reflect variation in the amounts and the specific oxidation states of C substrates present in the soils from the two contrasting management systems.

Organic and Conventional Systems Select for Microbial Populations with Distinct Carbon Utilization Profiles

Soil organisms, including bacteria and fungi, contribute to processing and stabilization of carbon inputs from plant biomass litter, root exudates, and microbial turnover (Liang et al., 2017). We focused our ^{13}C-DNA-SIP analyses on 16S rRNA genes rather than fungal targets based on phospholipid fatty acid profiling that showed that fungi played a minimal role in short-term glucose utilization (<5% of ^{13}C-glucose C incorporated into fungal biomarkers and fungi to bacteria ratios declined with glucose addition; data not shown), which is supported by other work (Gunina et al., 2017). Despite importance to long-term C cycling in these agricultural soils (Arcand et al., 2016), fungi may play a relatively minor role in priming effects following glucose addition (Di Lonardo et al., 2017).

Amendment of labile substrates such as glucose to soil can select for copiotrophic members of the microbial community. Copiotrophic organisms in niches of high resource availability tend to exhibit r-selection, characterized by high growth rates with relatively inefficient resource use, while oligotrophs in low-resource niches tend toward K-selection with efficient, slow growth (Grayston et al., 1998; Blagodatskaya et al., 2007; Fierer et al., 2007; Berg and Smalla, 2009). This categorization can explain the low CUE exhibited by communities in high-nutrient niches (i.e., rhizospheres) relative to those for which nutrients are limited (i.e., bulk soil) (Blagodatskaya et al., 2014). Our results partially support these broad categorizations as we found relationships between phylum-level (and class-level within the *Proteobacteria*) differential abundance (log fold change) and soil resource availability and metabolic properties (**Figures 3**, **4**). Results also indicate that (i) C metabolism emerges as a property of the total soil community under a particular management system rather than being linked to relative abundance of specific phyla and (ii) OTUs in the same phylum had markedly different taxonomic identity and relationships to soil resource availability in CON and ORG soil.

The two management systems supported taxonomically distinct *Actinobacteria* and *Proteobacteria* populations below the phylum level that had drastically different relationships with soil attributes, indicating major differences in glucose-utilization and adaptation to resource availability. In the CON soils, potentially oligotrophic *Alphaproteobacteria,* which are found in environments where complex C dominates (e.g., in decomposing wood; Kielak et al., 2016), were the primary glucose-utilizers within the *Proteobacteria*. These *Alphaproteobacteria* included the photoheterotrophic *Rhodoplanes* sp. (Oren and Xu, 2014), contaminant-degrading *Sphingomonas* sp. (Leys et al., 2004), and putatively polysaccharide-degrading Ellin 329 (Harbison et al., 2016). In contrast, *Betaproteobacteria*, primarily from the genus *Burkholderia,* were indicative of

glucose-utilizers in ORG soils and were shown to positively relate to C-mineralization and sucrose-amendment rates (Fierer et al., 2007). *Burkholderia*, including strains in the *Burkholderia cepacia* complex, are fast-growing heterotrophs common in crop rhizospheres (Fiore et al., 2001) and capable of plant growth promotion, antifungal activities, and degradation of chlorinated aromatic pollutants (Chiarini et al., 2006). The majority of ORG-associated *Actinobacteria* can degrade macromolecules from plant-litter, SOM, and other complex substrates, including *Streptomyces* sp. and *Arthrobacter* sp. (de Boer et al., 2005; Manteca and Sanchez, 2009; Bai et al., 2016). *Actinobacteria* can also rapidly assimilate ^{13}C-glucose (Dungait et al., 2013) and ^{13}C-xylose (Pepe-Ranney et al., 2016), and respond to increased C supply after soil rewetting (Placella et al., 2012). Thus, they encompass a variety of life strategies and ability to degrade complex and labile substrates (Fierer et al., 2007, 2012; Morrissey et al., 2016; Pepe-Ranney et al., 2016). Indeed, *Actinobacteria*, which showed no relationships with soil C-mineralization or sucrose amendment rates (Fierer et al., 2007), were highly enriched by glucose addition in both CON and ORG soil and were important crop residue decomposers in these soils, particularly in the ORG system (Arcand et al., 2016).

Glucose amendment selected for a high-proportion of active *Firmicutes* in ORG, but not in CON soils (**Figures 2**, **3C**). These bacteria included plant-growth promoting *Paenibacillus* sp. and *Bacillus* sp., that have the capacity to metabolize labile substrates such as glucose and xylose (Verastegui et al., 2014; Pepe-Ranney et al., 2016), and whose diversity and abundance is positively influenced by resource availability (Ling et al., 2014). *Bacillus* sp. can be considered SOC-degraders (Mau et al., 2015) and are well adapted to organic systems due to their synthesis of extracellular enzymes that degrade complex substrates under low nutrient availability (Priest, 1977; Panikov, 1995). Their high fold change in ORG soil ^{13}C-heavy fraction relative to CON soil (**Figure 3A**) suggests that in contrast to the findings of Mau et al. (2015), *Bacillus* sp. are also able to take up ^{13}C from glucose. It is likely that glucose uptake in *Bacillus* sp. and other *Firmicutes* resulted in the liberation of organic nutrients from SOM, indicative of their importance in priming. This is supported by their high degree of positive correlation with pSOMprimed (**Figure 3A**).

The ^{13}C-light populations have been categorized as "non-glucose-utilizing"; however, it is possible that they incorporated some labeled substrate due to differences in genome GC content between ^{13}C-heavy and ^{13}C-light OTUs. The mol% GC of the ^{13}C-heavy fraction OTUs from *Actinobacteria* and *Proteobacteria* are within 59–75% (Rosenberg et al., 2014), making their genomes denser than the *Bacteroidetes* (40–48%) and *Nitrososphaera* (48–52.7%; Stieglmeier et al., 2014) that are found in the CON ^{13}C-light fraction. *Actinobacteria* and *Proteobacteria* show the strongest density shifts compared to other phyla when incubated with ^{13}C-glucose (Hungate et al., 2015). With binary fractionation, glucose-utilizing organisms with low-GC genomes may not shift sufficiently to the "heavy" fraction for accurate categorization (Hungate et al., 2015). However, the high abundance of *Firmicutes* (37.7–44 mol% GC) in the ^{13}C-heavy fraction of ORG soil indicates that the enrichment of low-GC taxa can be detected using binary DNA-SIP. Meanwhile, glucose-amended CON soil may select for distinct populations that do not directly utilize glucose for growth, including *Bacteroidetes* (**Figures 3B,D**), through bacterial micro-predation (Lueders et al., 2006) or rapid turnover (Malik et al., 2015).

Glucose-utilizing bacteria were strongly differentiated between CON and ORG systems based on resource availability and metabolic properties (**Figure 3**). Compared to CON soils, ORG soils harbored twice as many differentially abundant OTUs of glucose-utilizing bacteria, which were associated with priming of SOM decomposition, thermodynamic efficiency, and low nutrient availability. This suggests that this subset of glucose-utilizing bacteria in the ORG soils co-metabolized SOM, likely to gain access to inorganic nutrients in these more nutrient deficient soils (Chen et al., 2013). These bacteria were also associated with high retention of glucose-derived energy in soil and thermodynamic efficiency (**Figure 3A**), possibly due to energy investment in enzymes required to mineralize nutrients. Previous work has demonstrated that under N limiting conditions, K strategists are dominant contributors to SOM priming, while r strategists are dominant in nutrient rich soils (Chen et al., 2013). Therefore, glucose addition in ORG soils likely provided sufficient energy to K strategists to overcome previous limitations on nutrient acquisition from SOM. However, these energy and nutrient limitations were not present to the same extent in the CON soils, where differentially abundant glucose-utilizing OTUs were associated with high nutrient availability (e.g., NO_3-N, PO_4-P, DOC), respiration and heat production, metabolic quotients, and negatively with thermodynamic efficiency indices and the proportion of primed SOM-derived CO_2-C.

Stable SOM formation rates develop from the balance of SOM degradation via the priming effect and anabolism by soil microorganisms (Liang et al., 2017). A priming effect was measured in both CON and ORG soils with greater primed CO_2 released in the CON soils (**Table 3**). However, a higher magnitude of priming can be balanced by equally greater accumulation of microbial-derived C into stable SOM (Liang et al., 2017), protecting the net SOC balance and rates of accrual. In contrast, the ORG soils emitted proportionally more CO_2 due to priming than to basal respiration suggesting that this balance was tipped toward CO_2-C loss. The effect of organic management on C sequestration is contentious (Leifeld and Fuhrer, 2010) and is site and system dependent with reports of losses, accruals, and no net changes (Malhi et al., 2009; Syswerda et al., 2011; Bell et al., 2012; Kallenbach et al., 2015). Here, the metabolism of SOM-derived C, in particular the priming of SOM degradation in ORG soil, indicates that the SOM and DOC patterns observed in ORG and CON soils is partially explained by the liberation of SOM-derived organic nutrients to resolve stoichiometric imbalance following glucose amendment in ORG soil. While sources of microbial N and P between ORG and CON soil have yet to be fully identified, it is likely that lower soil C in ORG soils results

from a microbial community adapted to SOM degradation, thus hindering rates of soil C sequestration in this organically managed system.

CONCLUSION

By combining isothermal calorimetry with ^{13}C-DNA-SIP and high-throughput sequencing of 16S rRNA genes, we were able to elucidate differences in soil microbial carbon use in organic and conventionally managed grain systems. Thermodynamic efficiency indices were not different between CON and ORG soils during glucose utilization. Yet priming of SOM degradation in ORG soils indicated soil communities under low-nutrient availability satisfy stoichiometric demand by mineralizing organic nutrients, indicating that calorespirometric ratios can be uncoupled from metabolic quotients and microbial strategies of C-utilization. Further, differential abundance analysis showed that glucose-utilizing and non-utilizing microbial populations were indicative of long-term differences in agricultural management histories. Metabolic activity of the microbial community following glucose amendment under ORG conditions favored thermodynamically efficient SOM degrading oligotrophic bacteria vs. inefficient metabolism of available C in high-nutrient CON systems. While more work is required to determine if C accumulation in soil under organic management is limited by microbial catabolism of SOM resulting from stoichiometric imbalance in soil nutrients, this work demonstrates that long-term agricultural management can alter microbially driven soil C processes.

AUTHOR CONTRIBUTIONS

MA conceived, designed, and performed the experiments, analyzed and interpreted data, and wrote the manuscript. DL-B performed bioinformatics, data analysis and generated figures, and contributed to the writing. BH was the principle investigator of this work, conceived and designed the experiments, interpreted results, and contributed to the writing of the manuscript.

FUNDING

This work was funded through Agriculture and Agri-Food Canada Growing Forward II.

ACKNOWLEDGMENTS

We are grateful to S. Kumicz for performing DNA extractions and density fractionations for the DNA-SIP analyses and to J. Dechka for laboratory assistance. We also acknowledge the Agriculture and Agri-Food Canada scientists and staff who conceived and managed this long-term experimental field trial.

SUPPLEMENTARY MATERIAL

The Supplementary Material for this article can be found online at: https://www.frontiersin.org/articles/10.3389/fmicb.2017.02293/full#supplementary-material

REFERENCES

Anderson, T.-H., and Domsch, K. H. (1985). Determination of ecophysiological maintenance carbon requirements of soil microorganisms in a dormant state. *Biol. Fertil. Soils* 1, 81–89. doi: 10.1007/BF00255134

Arcand, M. M., Helgason, B. L., and Lemke, R. L. (2016). Microbial crop residue decomposition dynamics in organic and conventionally managed soils. *Appl. Soil Ecol.* 107, 347–359. doi: 10.1016/j.apsoil.2016.07.001

Ashworth, J., and Mrazek, K. (1995). "Modified Kelowna" test for available phosphorus and potassium in soil. *Commun. Soil Sci. Plant Anal.* 26, 731–739. doi: 10.1080/00103629509369331

Bai, Z., Liang, C., Bodé, S., Huygens, D., and Boeckx, P. (2016). Phospholipid ^{13}C stable isotopic probing during decomposition of wheat residues. *Appl. Soil Ecol.* 98, 65–74. doi: 10.1016/j.apsoil.2015.09.009

Bailey, V. L., Bond-Lamberty, B., DeAngelis, K., Grandy, A. S., Hawkes, C. V., Heckman, K., et al. (2017). Soil carbon cycling proxies: understanding their critical role in predicting climate change feedbacks. *Glob. Chang. Biol.* doi: 10.1111/gcb.13926 [Epub ahead of print].

Barja, I., and Nuñez, L. (1999). Microcalorimetric measurements of the influence of glucose concentration on microbial activity in soils. *Soil Biol. Biochem.* 31, 441–447. doi: 10.1016/S0038-0717(98)00149-7

Barros, N., Feijóo, S., and Hansen, L. D. (2011). Calorimetric determination of metabolic heat, CO_2 rates and the calorespirometric ratio of soil basal metabolism. *Geoderma* 160, 542–547. doi: 10.1016/j.geoderma.2010.11.002

Barros, N., Hansen, L. D., Piñeiro, V., Pérez-Cruzado, C., Villanueva, M., Proupín, J., et al. (2016). Factors influencing the calorespirometric ratios of soil microbial metabolism. *Soil Biol. Biochem.* 92, 221–229. doi: 10.1016/j.soilbio.2015.10.007

Barros, N., Salgado, J., Rodríguez-Añón, J., Proupín, J., Villanueva, M., and Hansen, L. (2010). Calorimetric approach to metabolic carbon conversion efficiency in soils. *J. Therm. Anal. Calorim.* 99, 771–777. doi: 10.1007/s10973-010-0673-4

Battley, E. H. (1960). Enthalpy changes accompanying the growth of *Saccharomyces cerevisiae* (Hansen). *Physiol. Plant.* 13, 628–640. doi: 10.1111/j.1399-3054.1960.tb08085.x

Battley, E. H. (1987). *Energetics of Microbial Growth*. New York: Wiley-Interscience.

Bell, L. W., Sparling, B., Tenuta, M., and Entz, M. H. (2012). Soil profile carbon and nutrient stocks under long-term conventional and organic crop and alfalfa-crop rotations and re-established grassland. *Agric. Ecosyst. Environ.* 158, 156–163. doi: 10.1016/j.agee.2012.06.006

Benaragama, D., Shirtliffe, S. J., Gossen, B. D., Brandt, S. A., Lemke, R., Johnson, E. N., et al. (2016). Long-term weed dynamics and crop yields under diverse crop rotations in organic and conventional cropping systems in the Canadian prairies. *Field Crops Res.* 196, 357–367. doi: 10.1016/j.fcr.2016.07.010

Berg, G., and Smalla, K. (2009). Plant species and soil type cooperatively shape the structure and function of microbial communities in the rhizosphere. *FEMS Microbiol. Ecol.* 68, 1–13. doi: 10.1111/j.1574-6941.2009.00654.x

Blagodatskaya, E., Blagodatsky, S., Anderson, T.-H., Kuzyakov, Y., and Mohn, W. (2014). Microbial growth and carbon use efficiency in the rhizosphere and root-free soil. *PLOS ONE* 9:e93282. doi: 10.1371/journal.pone.0093282

Blagodatskaya, E., and Kuzyakov, Y. (2008). Mechanisms of real and apparent priming effects and their dependence on soil microbial biomass and community structure: critical review. *Biol. Fertil. Soils* 45, 115–131. doi: 10.1007/s00374-008-0334-y

Blagodatskaya, E. V., Blagodatsky, S. A., Anderson, T.-H., and Kuzyakov, Y. (2007). Priming effects in Chernozem induced by glucose and N in relation to microbial growth strategies. *Appl. Soil Ecol.* 37, 95–105. doi: 10.1016/j.apsoil.2007.05.002

Bölscher, T., Wadsö, L., Börjesson, G., and Herrmann, A. M. (2016). Differences in substrate use efficiency: impacts of microbial community composition, land use management, and substrate complexity. *Biol. Fertil. Soils* 52, 547–559. doi: 10.1007/s00374-016-1097-5

Brandt, S. A., Thomas, A. G., Olfert, O. O., Leeson, J. Y., Ulrich, D., and Weiss, R. (2010). Design, rationale and methodological considerations for a long term alternative cropping experiment in the Canadian plain region. *Eur. J. Agron.* 32, 73–79.

Caporaso, J. G., Kuczynski, J., Stombaugh, J., Bittinger, K., Bushman, F. D., Costello, E. K., et al. (2010). QIIME allows analysis of high-throughput community sequencing data. *Nat. Methods* 7, 335–336. doi: 10.1038/nmeth.f.303

Caporaso, J. G., Lauber, C. L., Walters, W. A., Berg-Lyons, D., Lozupone, C. A., Turnbaugh, P. J., et al. (2011). Global patterns of 16S rRNA diversity at a depth of millions of sequences per sample. *Proc. Natl. Acad. Sci. U.S.A.* 108(Suppl. 1), 4516–4522. doi: 10.1073/pnas.1000080107

Chaudhry, V., Rehman, A., Mishra, A., Chauhan, P. S., and Nautiyal, C. S. (2012). Changes in bacterial community structure of agricultural land due to long-term organic and chemical amendments. *Microb. Ecol.* 64, 450–460. doi: 10.1007/s00248-012-0025-y

Chen, R., Senbayram, M., Blagodatsky, S., Myachina, O., Dittert, K., Lin, X., et al. (2013). Soil C and N availability determine the priming effect: microbial N mining and stoichiometric decomposition theories. *Glob. Chang. Biol.* 20, 2356–2367. doi: 10.1111/gcb.12475

Chiarini, L., Bevivino, A., Dalmastri, C., Tabacchioni, S., and Visca, P. (2006). *Burkholderia cepacia* complex species: health hazards and biotechnological potential. *Trends Microbiol.* 14, 277–286. doi: 10.1016/j.tim.2006.04.006

Cotrufo, M. F., Wallenstein, M. D., Boot, C. M., Denef, K., and Paul, E. (2013). The microbial efficiency-matrix stabilization (MEMS) framework integrates plant litter decomposition with soil organic matter stabilization: do labile plant inputs form stable soil organic matter? *Glob. Chang. Biol.* 19, 988–995. doi: 10.1111/gcb.12113

Coyotzi, S., Doxey, A. C., Clark, I. D., Lapen, D. R., Van Cappellen, P., and Neufeld, J. D. (2017). Agricultural soil denitrifiers possess extensive nitrite reductase gene diversity. *Environ. Microbiol.* 19, 1189–1208. doi: 10.1111/1462-2920.13643

Creamer, C. A., de Menezes, A. B., Krull, E. S., Sanderman, J., Newton-Walters, R., and Farrell, M. (2015). Microbial community structure mediates response of soil C decomposition to litter addition and warming. *Soil Biol. Biochem.* 80, 175–188. doi: 10.1016/j.soilbio.2014.10.008

Dai, M., Hamel, C., Bainard, L. D., Arnaud, M. S., Grant, C. A., Lupwayi, N. Z., et al. (2014). Negative and positive contributions of arbuscular mycorrhizal fungal taxa to wheat production and nutrient uptake efficiency in organic and conventional systems in the Canadian prairie. *Soil Biol. Biochem.* 74, 156–166. doi: 10.1016/j.soilbio.2014.03.016

de Boer, W., Folman, L. B., Summerbell, R. C., and Boddy, L. (2005). Living in a fungal world: impact of fungi on soil bacterial niche development. *FEMS Microbiol. Rev.* 29, 795–811. doi: 10.1016/j.femsre.2004.11.005

Di Lonardo, D. P., De Boer, W., Klein Gunnewiek, P. J. A., Hannula, S. E., and Van der Wal, A. (2017). Priming of soil organic matter: chemical structure of added compounds is more important than the energy content. *Soil Biol. Biochem.* 108, 41–54. doi: 10.1016/j.soilbio.2017.01.017

Dunford, E. A., and Neufeld, J. D. (2010). DNA stable-isotope probing (DNA-SIP). *J. Vis. Exp.* 42:e2027. doi: 10.3791/2027

Dungait, J. A. J., Kemmitt, S. J., Michallon, L., Guo, S., Wen, Q., Brookes, P. C., et al. (2013). The variable response of soil microorganisms to trace concentrations of low molecular weight organic substrates of increasing complexity. *Soil Biol. Biochem.* 64, 57–64. doi: 10.1016/j.soilbio.2013.03.036

Edgar, R. C., and Flyvbjerg, H. (2015). Error filtering, pair assembly and error correction for next-generation sequencing reads. *Bioinformatics* 31, 3476–3482. doi: 10.1093/bioinformatics/btv401

Fierer, N., Bradford, M. A., and Jackson, R. B. (2007). Toward an ecological classification of soil bacteria. *Ecology* 88, 1354–1364.

Fierer, N., Lauber, C. L., Ramirez, K. S., Zaneveld, J., Bradford, M. A., and Knight, R. (2012). Comparative metagenomic, phylogenetic and physiological analyses of soil microbial communities across nitrogen gradients. *ISME J.* 6, 1007–1017. doi: 10.1038/ismej.2011.159

Finn, D., Kopittke, P. M., Dennis, P. G., and Dalal, R. C. (2017). Microbial energy and matter transformation in agricultural soils. *Soil Biol. Biochem.* 111, 176–192. doi: 10.1016/j.soilbio.2017.04.010

Fiore, A., Laevens, S., Bevivino, A., Dalmastri, C., Tabacchioni, S., Vandamme, P., et al. (2001). Burkholderia cepacia complex: distribution of genomovars among isolates from the maize rhizosphere in Italy. *Environ. Microbiol.* 3, 137–143. doi: 10.1046/j.1462-2920.2001.00175.x

Frey, S. D., Lee, J., Melillo, J. M., and Six, J. (2013). The temperature response of soil microbial efficiency and its feedback to climate. *Nat. Clim. Chang.* 3, 395–398. doi: 10.1038/nclimate1796

García-Ruiz, R., Ochoa, V., Hinojosa, M. B., and Carreira, J. A. (2008). Suitability of enzyme activities for the monitoring of soil quality improvement in organic agricultural systems. *Soil Biol. Biochem.* 40, 2137–2145. doi: 10.1016/j.soilbio.2008.03.023

Geyer, K. M., Kyker-Snowman, E., Grandy, A. S., and Frey, S. D. (2016). Microbial carbon use efficiency: accounting for population, community, and ecosystem-scale controls over the fate of metabolized organic matter. *Biogeochemistry* 127, 173–188. doi: 10.1007/s10533-016-0191-y

Grayston, S. J., Wang, S., Campbell, C. D., and Edwards, A. C. (1998). Selective influence of plant species on microbial diversity in the rhizosphere. *Soil Biol. Biochem.* 30, 369–378. doi: 10.1016/S0038-0717(97)00124-7

Gunina, A., Dippold, M., Glaser, B., and Kuzyakov, Y. (2017). Turnover of microbial groups and cell components in soil: ¹³C analysis of cellular biomarkers. *Biogeosciences* 14, 271–283. doi: 10.5194/bg-14-271-2017

Gunina, A., and Kuzyakov, Y. (2015). Sugars in soil and sweets for microorganisms: review of origin, content, composition and fate. *Soil Biol. Biochem.* 90, 87–100. doi: 10.1016/j.soilbio.2015.07.021

Hansen, L. D., Macfarlane, C., McKinnon, N., Smith, B. N., and Criddle, R. S. (2004). Use of calorespirometric ratios, heat per CO_2 and heat per O_2, to quantify metabolic paths and energetics of growing cells. *Thermochim. Acta* 422, 55–61. doi: 10.1016/j.tca.2004.05.033

Harbison, A. B., Carson, M. A., Lamit, L. J., Basiliko, N., and Auer, S. L. B. (2016). A novel isolate and widespread abundance of the candidate alphaproteobacterial order (Ellin 329), in southern Appalachian peatlands. *FEMS Microbiol. Lett.* 363:fnw151. doi: 10.1093/femsle/fnw151

Harris, J. A., Ritz, K., Coucheney, E., Grice, S. M., Lerch, T. Z., Pawlett, M., et al. (2012). The thermodynamic efficiency of soil microbial communities subject to long-term stress is lower than those under conventional input regimes. *Soil Biol. Biochem.* 47, 149–157. doi: 10.1016/j.soilbio.2011.12.017

Hartmann, M., Frey, B., Mayer, J., Mäder, P., and Widmer, F. (2014). Distinct soil microbial diversity under long-term organic and conventional farming. *ISME J.* 9, 1177–1194. doi: 10.1038/ismej.2014.210

Hendershot, W. H., Lalande, H., and Duquette, M. (2008). "Soil reaction and exchangeable acidity," in *Soil Sampling and Methods of Analysis Second Edition*, eds M. R. Carter and E. G. Gregorich (Boca Raton, FL: Taylor & Francis Group), 173–178.

Herrmann, A. M., and Bölscher, T. (2015). Simultaneous screening of microbial energetics and CO_2 respiration in soil samples from different ecosystems. *Soil Biol. Biochem.* 83, 88–92. doi: 10.1016/j.soilbio.2015.01.020

Herrmann, A. M., Coucheney, E., and Nunan, N. (2014). Isothermal microcalorimetry provides new insight into terrestrial carbon cycling. *Environ. Sci. Technol.* 48, 4344–4352. doi: 10.1021/es403941h

Hill, P. W., Farrar, J. F., and Jones, D. L. (2008). Decoupling of microbial glucose uptake and mineralization in soil. *Soil Biol. Biochem.* 40, 616–624. doi: 10.1016/j.soilbio.2007.09.008

Hungate, B. A., Mau, R. L., Schwartz, E., Caporaso, J. G., Dijkstra, P., van Gestel, N., et al. (2015). Quantitative microbial ecology through stable isotope probing. *Appl. Environ. Microbiol.* 81, 7570–7581. doi: 10.1128/AEM.02280-15

Jameson, E., Taubert, M., Coyotzi, S., Chen, Y., Eyice, Ö, Schäfer, H., et al. (2017). DNA-, RNA-, and protein-based stable-isotope probing for high-throughput biomarker analysis of active microorganisms. *Methods Mol. Biol.* 1539, 57–74. doi: 10.1007/978-1-4939-6691-2_5

Janzen, H. H. (2015). Beyond carbon sequestration: soil as conduit of solar energy. *Eur. J. Soil Sci.* 66, 19–32. doi: 10.1111/ejss.12194

Joergensen, R. G., Mäder, P., and Fließbach, A. (2010). Long-term effects of organic farming on fungal and bacterial residues in relation to microbial energy metabolism. *Biol. Fertil. Soils* 46, 303–307. doi: 10.1007/s00374-009-0433-4

Kallenbach, C. M., Frey, S. D., and Grandy, A. S. (2016). Direct evidence for microbial-derived soil organic matter formation and its ecophysiological controls. *Nat. Commun.* 7:13630. doi: 10.1038/ncomms13630

Kallenbach, C. M., Grandy, A. S., Frey, S. D., and Diefendorf, A. F. (2015). Microbial physiology and necromass regulate agricultural soil carbon accumulation. *Soil Biol. Biochem.* 91, 279–290.

Kielak, A. M., Scheublin, T. R., Mendes, L. W., van Veen, J. A., and Kuramae, E. E. (2016). Bacterial community succession in pine-wood decomposition. *Front. Microbiol.* 7:231. doi: 10.3389/fmicb.2016.00231

Knight, J. D., Buhler, R., Leeson, J. Y., and Shirtliffe, S. (2010). Classification and fertility status of organically managed fields across Saskatchewan. *Canada. Can. J. Soil Sci.* 90, 667–678. doi: 10.4141/cjss09082

Kong, A. Y. Y., Scow, K. M., Córdova-Kreylos, A. L., Holmes, W. E., and Six, J. (2011). Microbial community composition and carbon cycling within soil microenvironments of conventional, low-input, and organic cropping systems. *Soil Biol. Biochem.* 43, 20–30. doi: 10.1016/j.soilbio.2010.09.005

Lee, Z. M., and Schmidt, T. M. (2014). Bacterial growth efficiency varies in soils under different land management practices. *Soil Biol. Biochem.* 69, 282–290. doi: 10.1016/j.soilbio.2013.11.012

Leifeld, J., and Fuhrer, J. (2010). Organic farming and soil carbon sequestration: what do we really know about the benefits? *Ambio* 39, 585–599. doi: 10.1007/s13280-010-0082-8

Leys, N. M. E. J., Ryngaert, A., Bastiaens, L., Verstraete, W., Top, E. M., and Springael, D. (2004). Occurrence and phylogenetic diversity of *Sphingomonas* strains in soils contaminated with polycyclic aromatic hydrocarbons. *Appl. Environ. Microbiol.* 70, 1944–1955. doi: 10.1128/AEM.70.4.1944-1955.2004

Li, R., Khafipour, E., Krause, D. O., Entz, M. H., de Kievit, T. R., and Fernando, W. G. D. (2012). Pyrosequencing reveals the influence of organic and conventional farming systems on bacterial communities. *PLOS ONE* 7:e51897. doi: 10.1371/journal.pone.0051897

Li, Y., Lee, C. G., Watanabe, T., Murase, J., Asakawa, S., and Kimura, M. (2011). Identification of microbial communities that assimilate substrate from root cap cells in an aerobic soil using a DNA-SIP approach. *Soil Biol. Biochem.* 43, 1928–1935. doi: 10.1016/j.soilbio.2011.05.016

Liang, C., Schimel, J. P., and Jastrow, J. D. (2017). The importance of anabolism in microbial control over soil carbon storage. *Nat. Microbiol.* 2, 17105. doi: 10.1038/nmicrobiol.2017.105

Ling, N., Wang, D., Zhu, C., Song, Y., Yu, G., Ran, W., et al. (2014). Response of the population size and community structure of *Paenibacillus* spp. to different fertilization regimes in a long-term experiment of red soil. *Plant Soil* 383, 87–98. doi: 10.1007/s11104-014-2146-1

Love, M. I., Huber, W., and Anders, S. (2014). Moderated estimation of fold change and dispersion for RNA-seq data with DESeq2. *Genome Biol.* 15, 550. doi: 10.1186/s13059-014-0550-8

Ludwig, M., Achtenhagen, J., Miltner, A., Eckhardt, K.-U., Leinweber, P., Emmerling, C., et al. (2015). Microbial contribution to SOM quantity and quality in density fractions of temperate arable soils. *Soil Biol. Biochem.* 81, 311–322. doi: 10.1016/j.soilbio.2014.12.002

Lueders, T., Kindler, R., Miltner, A., Friedrich, M. W., and Kaestner, M. (2006). Identification of bacterial micropredators distinctively active in a soil microbial food web. *Appl. Environ. Microbiol.* 72, 5342–5348. doi: 10.1128/AEM.00400-06

Magoc, T., and Salzberg, S. L. (2011). FLASH: fast length adjustment of short reads to improve genome assemblies. *Bioinformatics* 27, 2957–2963. doi: 10.1093/bioinformatics/btr507

Malhi, S., Brandt, S., Lemke, R., Moulin, A., and Zentner, R. (2009). Effects of input level and crop diversity on soil nitrate-N, extractable P, aggregation, organic C and N, and nutrient balance in the Canadian Prairie. *Nutr. Cycl. Agroecosystems* 84, 1–22. doi: 10.1007/s10705-008-9220-0

Malik, A. A., Dannert, H., Griffiths, R. I., Thomson, B. C., and Gleixner, G. (2015). Rhizosphere bacterial carbon turnover is higher in nucleic acids than membrane lipids: implications for understanding soil carbon cycling. *Front. Microbiol.* 6:268. doi: 10.3389/fmicb.2015.00268

Manteca, A., and Sanchez, J. (2009). Streptomyces development in colonies and soils. *Appl. Environ. Microbiol.* 75, 2920–2924. doi: 10.1128/AEM.02288-08

Manzoni, S., Taylor, P., Richter, A., Porporato, A., and Agren, G. I. (2012). Environmental and stoichiometric controls on microbial carbon-use efficiency in soils. *New Phytol.* 196, 79–91. doi: 10.1111/j.1469-8137.2012.04225.x

Mau, R. L., Liu, C. M., Aziz, M., Schwartz, E., Dijkstra, P., Marks, J. C., et al. (2015). Linking soil bacterial biodiversity and soil carbon stability. *ISME J.* 9, 1477–1480. doi: 10.1038/ismej.2014.205

Maynard, D. G., Kalra, Y. P., and Crumbaugh, J. A. (2008). "Nitrate and exchangeable ammonium nitrogen," in *Soil Sampling and Methods of Analysis Second Edition*, eds M. R. Carter and E. G. Gregorich (Boca Raton, FL: Taylor & Francis Group), 71–80.

Morrissey, E. M., Mau, R. L., Schwartz, E., Caporaso, J. G., Dijkstra, P., van Gestel, N., et al. (2016). Phylogenetic organization of bacterial activity. *ISME J.* 10, 2336–2340. doi: 10.1038/ismej.2016.28

Neufeld, J. D., Wagner, M., and Murrell, J. C. (2007). Who eats what, where and when? Isotope-labelling experiments are coming of age. *ISME J.* 1, 103–110. doi: 10.1038/ismej.2007.30

Nuñez, L., Barros, N., and Barja, I. (1994). A kinetic analysis of the degradation of glucose by soil microorganisms studied by microcalorimetry. *Thermochim. Acta* 237, 73–81. doi: 10.1016/0040-6031(94)85185-9

Oksanen, J., Guillaume, B., Friendly, M., Kindt, R., Legendre, P., and McGlinn, D. (2017). *Vegan: Community Ecology Package. R Package Version 2.4-3.* Available at: https://cran.r-project.org/package=vegan

Oren, A., and Xu, X.-W. (2014). *The Family Hyphomicrobiaceae in the Prokaryotes*. Berlin: Springer, 247–281.

Panikov, N. S. (1995). *Microbial Growth Kinetics*. London: Chapman and Hall.

Parham, J. A., and Deng, S. P. (2000). Detection, quantification and characterization of β-glucosaminidase activity in soil. *Soil Biol. Biochem.* 32, 1183–1190. doi: 10.1016/S0038-0717(00)00034-1

Pepe-Ranney, C., Campbell, A. N., Koechli, C. N., Berthrong, S., and Buckley, D. H. (2016). Unearthing the ecology of soil microorganisms using a high resolution DNA-SIP approach to explore cellulose and xylose metabolism in soil. *Front. Microbiol.* 7:703. doi: 10.3389/fmicb.2016.00703

Placella, S. A., Brodie, E. L., and Firestone, M. K. (2012). Rainfall-induced carbon dioxide pulses result from sequential resuscitation of phylogenetically clustered microbial groups. *Proc. Natl. Acad. Sci. U.S.A.* 109, 10931–10936. doi: 10.1073/pnas.1204306109

Priest, F. G. (1977). Extracellular enzyme synthesis in the genus Bacillus. *Bacteriol. Rev.* 41, 711–753.

R Developement Core Team (2016). *R: A Language and Environment for Statistical Computing*. Vienna: R Foundation for Statistical Computing.

Roller, B. R., and Schmidt, T. M. (2015). The physiology and ecological implications of efficient growth. *ISME J.* 9, 1481–1487. doi: 10.1038/ismej.2014.235

Rosenberg, E., DeLong, E. F., Lory, S., Stackebrandt, E., and Thompson, F. (2014). *The Prokaryotes*. New York, NY: Springer.

Schimel, J. P., and Schaeffer, S. M. (2012). Microbial control over carbon cycling in soil. *Front. Microbiol.* 3:348. doi: 10.3389/fmicb.2012.00348

Sinsabaugh, R. L., Manzoni, S., Moorhead, D. L., and Richter, A. (2013). Carbon use efficiency of microbial communities: stoichiometry, methodology and modelling. *Ecol. Lett.* 16, 930–939. doi: 10.1111/ele.12113

Stieglmeier, M., Klingl, A., Alves, R. J. E., Rittmann, S. K.-M. R., Melcher, M., Leisch, N., et al. (2014). *Nitrososphaera viennensis* gen. nov., sp. nov., an aerobic and mesophilic, ammonia-oxidizing archaeon from soil and a member of the archaeal phylum *Thaumarchaeota*. *Int. J. Syst. Evol. Microbiol.* 64, 2738–2752. doi: 10.1099/ijs.0.063172-0

Strickland, M. S., Wickings, K., and Bradford, M. A. (2012). The fate of glucose, a low molecular weight compound of root exudates, in the belowground foodweb of forests and pastures. *Soil Biol. Biochem.* 49, 23–29. doi: 10.1016/j.soilbio.2012.02.001

Syswerda, S. P., Corbin, A. T., Mokma, D. L., Kravchenko, A. N., and Robertson, G. P. (2011). Agricultural management and soil carbon storage in surface vs. deep layers. *Soil Sci. Soc. Am. J.* 75, 92–101. doi: 10.2136/sssaj2009.0414

TA Instruments (2012). *TAM Air Getting Started Guide*. New Castle, DE: TA Instruments.

van der Wal, A., and de Boer, W. (2017). Dinner in the dark: illuminating drivers of soil organic matter decomposition. *Soil Biol. Biochem.* 105, 45–48. doi: 10.1016/j.soilbio.2016.11.006

van Groenigen, K. J., Forristal, D., Jones, M., Smyth, N., Schwartz, E., Hungate, B., et al. (2013). Using metabolic tracer techniques to assess the impact of tillage and straw management on microbial carbon use efficiency in soil. *Soil Biol. Biochem.* 66, 139–145. doi: 10.1016/j.soilbio.2013.07.002

Vance, E. D., Brookes, P. C., and Jenkinson, D. S. (1987). An extraction method for measuring soil microbial biomass C. *Soil Biol. Biochem.* 19, 703–707. doi: 10.1016/0038-0717(87)90052-6

Verastegui, Y., Cheng, J., Engel, K., Kolczynski, D., Mortimer, S., Lavigne, J., et al. (2014). Multisubstrate isotope labeling and metagenomic analysis of active soil bacterial communities. *mBio* 5:e1157-14. doi: 10.1128/mBio.01157-14

Wardle, D. A., and Ghani, A. (1995). A critique of the microbial metabolic quotient (qCO_2) as a bioindicator of disturbance and ecosystem development. *Soil Biol. Biochem.* 27, 1601–1610. doi: 10.1016/0038-0717(95)00093-T

Watzinger, A. (2015). Microbial phospholipid biomarkers and stable isotope methods help reveal soil functions. *Soil Biol. Biochem.* 86, 98–107. doi: 10.1016/j.soilbio.2015.03.019

Wu, J., Joergensen, R. G., Pommerening, B., Chaussod, R., and Brookes, P. C. (1990). Measurement of soil microbial biomass C by fumigation-extraction—an automated procedure. *Soil Biol. Biochem.* 22, 1167–1169. doi: 10.1016/0038-0717(90)90046-3

Conflict of Interest Statement: The authors declare that the research was conducted in the absence of any commercial or financial relationships that could be construed as a potential conflict of interest.

frontiers in Microbiology

ORIGINAL RESEARCH
published: 25 January 2018
doi: 10.3389/fmicb.2017.02568

Redox Sensing within the Genus *Shewanella*

Howard W. Harris[1], Irene Sánchez-Andrea[2], Jeffrey S. McLean[3,4], Everett C. Salas[5], William Tran[1], Mohamed Y. El-Naggar[1] and Kenneth H. Nealson[1]*

[1] Department of Earth Sciences, Biological Sciences and Physics, University of Southern California, Los Angeles, CA, United States, [2] Laboratory of Microbiology, Wageningen University, Wageningen, Netherlands, [3] Department of Periodontics, University of Washington, Seattle, WA, United States, [4] Microbial and Environmental Genomics, J. Craig Venter Institute, San Diego, CA, United States, [5] Chevron, San Ramon, CA, United States

A novel bacterial behavior called congregation was recently described in *Shewanella oneidensis* MR-1 as the accumulation of cells around insoluble electron acceptors (IEA). It is the result of a series of "run-and-reversal" events enabled by modulation of swimming speed and direction. The model proposed that the swimming cells constantly sense their surroundings with specialized outer membrane cytochromes capable of extracellular electron transport (EET). Up to this point, neither the congregation nor attachment behavior have been studied in any other strains. In this study, the wild type of *S. oneidensis* MR-1 and several deletion mutants as well as eight other *Shewanella* strains (*Shewanella putrefaciens* CN32, *S.* sp. ANA-3, *S.* sp. W3-18-1, *Shewanella amazonensis* SB2B, *Shewanella loihica* PV-4, *Shewanella denitrificans* OS217, *Shewanella baltica* OS155, and *Shewanella frigidimarina* NCIMB400) were screened for the ability to congregate. To monitor congregation and attachment, specialized cell-tracking techniques, as well as a novel cell accumulation after photo-bleaching (CAAP) confocal microscopy technique were utilized in this study. We found a strong correlation between the ability of strain MR-1 to accumulate on mineral surface and the presence of key EET genes such as *mtrBC/omcA* (SO_1778, SO_1776, and SO_1779) and gene coding for methyl-accepting protein (MCPs) with Ca^{+} channel *che*motaxis receptor (Cache) domain (SO_2240). These EET and taxis genes were previously identified as essential for characteristic run and reversal swimming around IEA surfaces. CN32, ANA-3, and PV-4 congregated around both $Fe(OH)_3$ and MnO_2. Two other *Shewanella* spp. showed preferences for one oxide over the other: preferences that correlated with the metal content of the environments from which the strains were isolated: e.g., W3-18-1, which was isolated from an iron-rich habitat congregated and attached preferentially to $Fe(OH)_3$, while SB2B, which was isolated from a MnO_2-rich environment, preferred MnO_2.

Keywords: redox sensing, MR-1, *Shewanella oneidensis,* energy taxis, extracellular electron transport, congregation, insoluble electron acceptors, dissimilatory

OPEN ACCESS

Edited by:
Alain F. Plante, University of Pennsylvania, United States

Reviewed by:
Johannes Gescher, Karlsruhe Institute of Technology, Germany
Michaela TerAvest, Michigan State University, United States

****Correspondence:***
Howard W. Harris
wayneharris1@me.com

Specialty section:
This article was submitted to Extreme Microbiology, a section of the journal Frontiers in Microbiology

Received: *26 June 2017*
Accepted: *11 December 2017*
Published: *25 January 2018*

Citation:
Harris HW, Sánchez-Andrea I, McLean JS, Salas EC, Tran W, El-Naggar MY and Nealson KH (2018) Redox Sensing within the Genus Shewanella. Front. Microbiol. 8:2568. doi: 10.3389/fmicb.2017.02568

INTRODUCTION

In the late 1980's, *Shewanella oneidensis* MR-1 (Myers and Nealson, 1988a) and later several species of *Geobacter* (Lovley et al., 1993; Champine et al., 2000) were shown to be capable of electron transfer to insoluble electron acceptors (IEAs), such as insoluble metal oxides and/or charged electrodes: a process called extracellular electron transport (EET) (Myers and Nealson, 1988b; Venkateswaran et al., 1999; Bond and Lovley, 2003). This ability attracted considerable interest with regard to biogeochemical cycling, bioremediation, corrosion, nanomaterials processing, and energy production (Bretschger et al., 2007; Kan et al., 2011; Hsu et al., 2012). While several groups of microbes are known to be capable of EET, major mechanistic studies have been done with only two model systems, *Shewanella* (Fredrickson et al., 2008; Shi et al., 2009), and *Geobacter* (Lovley et al., 2004).

Thus far, more than 100 other strains of *Shewanella* have been isolated from a wide variety of habitats including open water column, sandstone shale, marine and fresh water sediments, oil-pipelines, oil brine, and even algal communities atop Antarctic Ice (Hau and Gralnick, 2007). The genomes of more than 20 of these species have been fully sequenced (Fredrickson et al., 2008). Several of these species have been shown to be capable of EET to IEA, including *S. oneidensis* MR-1, *Shewanella putrefaciens* CN32, *S.* sp. ANA-3, *S.* sp. W3-18-1, *Shewanella amazonensis* SB2B, *Shewanella frigidimarina* NCIMB 400, and *Shewanella loihica* PV-4 (Fredrickson et al., 1998; Venkateswaran et al., 1998; Gao et al., 2006; Bretschger, 2008). Other members of the *Shewanella* genus such as *Shewanella baltica* OS217 and *Shewanella denitrificans* OS155 (**Table 1**) are not capable of EET (Brettar et al., 2002). Of all these strains, the congregation in response to IEA has only been studied for MR-1.

Within the genus *Shewanella*, the EET mechanism of MR-1 has been the most extensively characterized. MR-1 employs several approaches for insoluble IEAs reduction: (1) direct EET via extracellular multiheme cytochromes (Beliaev and Saffarini, 1998; Myers and Myers, 2001, 2002; Meyer et al., 2004; Mitchell et al., 2012; Kracke et al., 2015) (**Figure 1A**); (2) mediated EET using soluble electron shuttles bound to membrane cytochromes (Lovley et al., 1996; Marsili et al., 2008; Li et al., 2012; Kotloski and Gralnick, 2013; Okamoto et al., 2014); (3) mediated EET utilizing conductive outer membrane extensions that contain cytochromes (Gorby et al., 2006; El-Naggar et al., 2010); and (4) conductive extracellular matrices containing conductive and semiconductive minerals (Kato et al., 2010). Several genes have been identified in strain MR-1 and shown to be essential for EET (**Figure 1A** and **Table 2**), including the tetraheme cytochrome *c cymA* (SO_4591) and the combination of *mtrBC/omcA* (SO_1776, SO_1778, and SO_1779) that code for the decaheme cytochrome *c* component and tetraheme cytochrome *c* necessary for reduction of several anaerobic electron acceptors, including metal oxides (Myers and Myers, 2001, 2002; Schwalb et al., 2003). Because all these mechanisms rely on the cell proximity to IEA for EET, it is important to understand the cell sensing and net swimming migration toward the IEA. With regard to congregation, redox taxis or energy taxis, many studies have been conducted on MR-1 due to its versatile electron acceptor utilization (Bencharit and Ward, 2005; Baraquet et al., 2009; Harris et al., 2010). Energy taxis is a term that broadly encompasses aerotaxis, phototaxis, redox taxis, taxis to alternative electron acceptors, and chemotaxis to oxidizable substrates (Alexandre et al., 2004).

It is well-documented that the accumulation of MR-1 cells in response to soluble electron acceptors is a form of energy taxis, which depends on H^+ flux and the establishment of a proton motive force (Baraquet et al., 2009) (**Figure 1**). A part of this response includes more rapid swimming, as also seen with electron shuttles such as riboflavin or anthraquinone 2.6-disulfonate (AQDS) (Bencharit and Ward, 2005; Harris et al., 2010; Li et al., 2012). In contrast, the accumulation of cells around IEA, which has been called congregation (Nealson et al., 1995), involves both increased swimming speed upon contact with the IEA (called electrokinesis), and increased swimming reversals upon a decrease in PMF. Swimming reversals allow multiple transient cell-IEA encounters (lasting for 1–100 ms), and the rate at which swimming cells transition to irreversible attachment to IEA during congregation has not yet been quantified.

The mechanism(s) that cells utilize to locate IEAs remain unclear (Nealson et al., 1995; Bencharit and Ward, 2005; Harris et al., 2010). Early reports proposed that the other studied model organism *Geobacter,* accumulates around IEAs by sensing a gradient of reduced metal ions (Childers et al., 2002), however, reduced metal ions are not involved with the sensing mechanism used by MR-1 (Bencharit and Ward, 2005). Bacterial congregation in response to poised electrodes was recently described, pointing to the redox sensing, rather than metal ion sensing, as the trigger for response (Harris et al., 2010). The positive applied potentials to electrode (200–600 mV vs. Ag/AgCl) caused MR-1 to congregate similar to that seen with metal oxides (Harris et al., 2012). Redox potentials of MnO_2 containing minerals range between 400 and 600 mV vs. Ag/AgCl and accept electrons more readily than $Fe(OH)_3$ minerals, which carry the equivalent poised potential of 100 to 300 mV vs. Ag/AgCl (Burdige, 1993). In a previous study, the characteristic swimming of MR-1 around IEA was hypothesized to be regulated by two self-sensing chemotaxis receptors, methyl-accepting proteins (MCPs) with, Ca^+ channel *che*motaxis receptor (Cache) domain (SO_2240) and Per/Arnt/Sim (PAS) domains (SO_1385), and by the chemotaxis signal transduction protein kinase CheA-3 (SO_3207) to allow the cell to sample the redox potential, or electron accepting ability of a surface (**Table 2** and **Figure 1B**) (Harris et al., 2012). Before this study, the genes responsible for the motility driven attachment of cells on and around IEA were unknown.

In this report, we study the congregation mechanism of different *Shewanella* strains by monitoring swimming patterns and cell attachments to MnO_2 and $Fe(OH)_3$. In addition to screening the WT and several deletion mutants of MR-1, other *Shewanella* species (see **Table 1**) were screened. Many strains were shown to be capable of congregation around

TABLE 1 | Genetic comparison of *Shewanella* spp. and their original habitat.

Strain	MCP PAS like gene	MCP Cache like gene	mtrF like genes (SO_1780)	octaheme cytochrome-c like gene (SO_4142)	Habitat	References
S. oneidensis MR-1	+	+	+	+	Sediment of lake Oneida, NY	Venkateswaran et al., 1999
S. amazonensis SB2B	+	+	+		Intertidal sediments of Amazon River delta, Brazil	Venkateswaran et al., 1998
S. baltica OS155		+			Oil brine water column of Baltic sea	Ziemke et al., 1998
S. denitrificans OS217					Oxic–anoxic interface of water column of Baltic Sea	Brettar et al., 2002
S. frigidimarina NCIMB 400		+			Water column of North Sea	Bowman et al., 1997
S. putrefaciens CN32	+	+		+	Shale sandstone in Albuquerque, New Mexico, USA	Fredrickson et al., 1998
S. sp. ANA-3	+	+	+	+	Arsenic-treated wooden poll in brackish water, Woods Hole, Massachusetts, USA	Saltikov et al., 2003
S. sp. W3-18-1	+	+		+	Iron-rich marine sediment, Washington coast, Pacific Ocean	Murray et al., 2001
S. loihica PV-4		+	+	+	Iron-rich microbial mat near a hydrothermal vent, Loihi Seamount, Pacific Ocean	Gao et al., 2006

both MnO_2 and $FeOH_3$, while others responded selectively to MnO_2 (SB2B) or $Fe(OH)_3$ (W3-18-1). When cell attachment to the mineral surfaces was monitored we observed a strong correlation between the ability of the cell to congregate, and the attachment of the cells to the IEA surface. We then compared the genomes of these species to find candidate genes involved in the congregation swimming, accumulation, and cell attachment phenotypes in response to specific IEA surface.

RESULTS

Cell Accumulation and Attachment to Mineral Requires Chemotaxis and Extracellular Electron Transport Genes in *S. oneidensis* MR-1

Most of the early studies of energy taxis in MR-1 utilized a method of swarm plate assays (Nealson et al., 1995; Baraquet et al., 2009; Li et al., 2012). Here, we offer a more in-depth characterization of these yet unknown energy taxis mechanisms by using a quantitative method of tracking the swimming of individual cells through liquid media in response to IEA and cell accumulation after photo-bleaching (CAAP) to measure cell attachment rate (Li et al., 2010). CAAP utilizes irradiation from a confocal microscope UV laser to irreversibly darken (quench the fluorescence of) GFP-labeled cells on and around a given IEA. By quantifying fluorescent cells as they move into the darkened zone, the rates of accumulation and attachment can be quantified, and different strains compared. To be considered attached, the position of the motile cell is verified by analyzing a 3D image of the field of view. If the cell comes to rest on the mineral surface then the cell is then considered "attached." The strength of bonds between stationary MR-1 cells and surfaces was measured with optical tweezers in a separate study (Gross and El-Naggar, 2015). This method allows distinction between directed cell-attachment, and random electrostatic attachment.

As shown in **Figure 2**, the WT MR-1 cells attached to mineral surface after 30 min with some large deviation in number, 2,655 $\pm$ 1,352 cells/mm^2. During this time, the cells exhibit "touch and go" swimming, making transient contact with the MnO_2 mineral surface. After 2 h, the number of new cells attached to the mineral surface increased to 4,300 $\pm$ 584 cells/mm^2 of mineral surface while additional motile cells continued to congregate (Videos S1, S2, and S17). Mutants with triple deletions in key EET genes *mtrBC/omcA* (SO_1776, SO_1778, SO_1779), single deletion of *cymA* (SO_4591) and the major energy taxis chemoreceptor MCP Cache (SO_2240) have been previously linked to swimming congregation phenotype (Harris et al., 2012). Deletion mutants (Δ*cymA*, Δ*mcp_cache,* and Δ*mtrBC/omcA*) were all motile and capable of reversing swimming direction, but were incapable of congregation and showed little or no attachment to MnO_2 during the experiment (**Figure 2C** and Figures S1A,B). WT accumulation in bleached zone at $t = 2$ h averages 4,300 $\pm$ 584 cells/mm^2 while Δ*mcp_cache*, and Δ*mtrBC/omcA* mutants accumulate in negligible numbers (**Figure 2C** and S1CD).

Characterizing Congregation around IEA in Other *Shewanella* Strains

Nine strains of *Shewanella* were tested for their ability to congregate around mineral surfaces of MnO_2 and $Fe(OH)_3$ with time series assay of cell attachment to mineral (**Table 3** and Videos S3–S14). As with MR-1, all nine strains examined had a single polar flagellum and reversal of swimming direction was accomplished by reversal of flagellar rotation (data not shown). The swimming tracks within the same experiment were sorted into two separate groups based on swimming

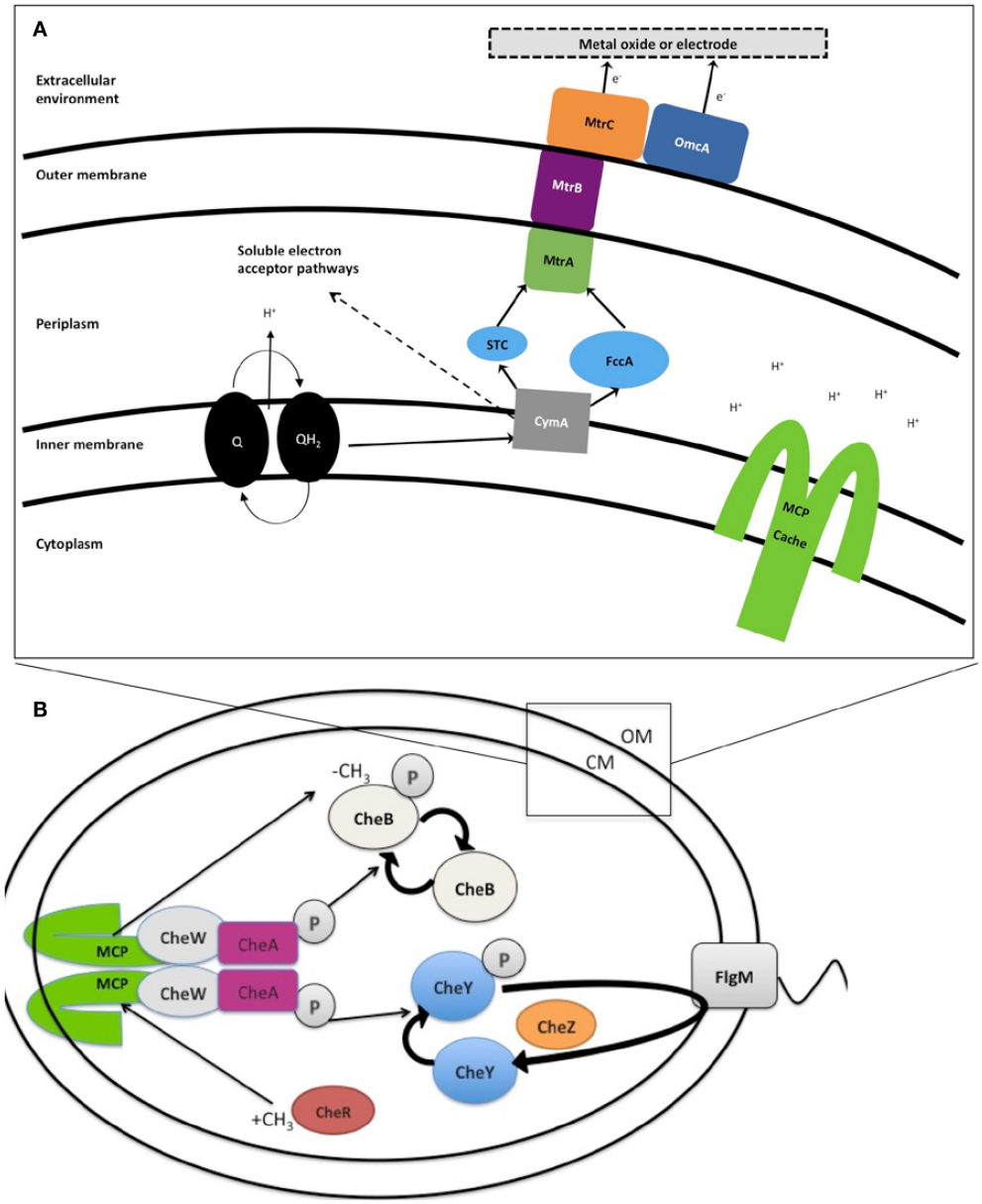

FIGURE 1 | (A) Extracellular electron transport (EET) in *Shewanella oneidensis* MR-1 builds proton motive force (pmf). Under anaerobic conditions members of the genus *Shewanella* can transport electrons from the inner membrane, periplasm, outer membrane, and an electrode via a chain of cytochromes and menaquinones (MQ) known collectively as extracellular electron transport (EET). Expression of EET cytochromes can fluctuate based on the electron acceptor available in the environment. The number of iron containing *c*-type heme groups are indicated inside (parenthesis). Electron flows from electron donors, such as lactate, to reduce quinones (Q), which simultaneously transfer H^+ into periplasm, building pmf, while also passing electrons to CymA. In the absence of soluble electron acceptors the electrons are transferred to MtrCAB outer membrane complex. This MtrCAB complex can donate electrons directly to terminal electron acceptor, either mineral or anode electrode, or via flavin molecules. The pmf drives the production of ATP and rotation of the polar flagella. "Self-sensing" methyl-accepting chemotaxis proteins (MCPs) control flagella rotation via the chemotaxis signal transduction system **(B)** and may detect changes in H^+ concentration during metal reduction. **(B)** Likely chemotaxis signal transduction pathway in *Shewanella*. In response to stimulation, the structure of MCP shifts like a piston, causing the auto phosphorylation of CheA to slow or stop. CheY and CheB are, therefore, not phosphorylated, and this lack of CheY-P allows smooth swimming. This stimulation also has another effect—the CheB is inactive without phosphorylation (it cannot perform as a methylesterase) and this allows for the CheR protein (a continually active methyltransferase) to outcompete and freely methylate the dimer methyl-accepting region of MCP (HAMP domain). This methylation of the MCP acts to increase the auto-phosphorylation rate of CheA Histidine residue. Therefore, the signal transduction system has control over the flagellar reversal frequency in the presence of increased or decreased stimuli, leading to a series of "run-and-reversal" swimming.

TABLE 2 | Genes of MR-1 described in the text.

Gene name	Locus tag	Description	Role	References
cymA	SO_4591	Tetraheme cytochrome *c*	Necessary for reduction of several anaerobic electron acceptors, including metal oxides	Myers and Myers, 1997; Schwalb et al., 2003
NA	SO_4142	Periplasmic monoheme cytochrome c	Unknown	
mtrC	SO_1778	Surface decaheme cytochrome c component	Extracellular metal oxide respiration	Coursolle and Gralnick, 2010
mtrF	SO_1780	Decaheme cytochrome c component	Unknown	
mtrB	SO_1776	Periplasmic EET component	Extracellular metal oxide respiration	Beliaev and Saffarini, 1998
omcA	SO_1779	Surface decaheme cytochrome c component	Extracellular metal oxide respiration	Beliaev and Saffarini, 1998; Myers and Myers, 2001
mtrBC/omcA	SO_1778, SO_1776, SO_1779	Outer-membrane decaheme *c*-type cytochromes and periplasmic EET component	Extracellular metal oxide respiration	Myers and Myers, 2001; Coursolle and Gralnick, 2010
cheA-3	SO_3207	Histidine protein kinase	Chemotactic signal transduction	Li et al., 2007; Coursolle and Gralnick, 2010
mcp cache	SO_2240	MCP with a Cache domain	Energy taxis in response to soluble electron acceptors and congregation	Baraquet et al., 2009
mcp pas	SO_1385	MCP with PAS domain	Energy taxis and congregation around $Fe(OH)_3$	Baraquet et al., 2009; Harris et al., 2012

path (**Table 3**): those that contacted insoluble metal oxide surface (swam within 2 μm) compared with those that did not contact (swam >2 μm). Contacting swimmers that demonstrated significant increase in reversal frequency and swimming velocity than non-contacting group ($P < 0.05$) are classified as positive for congregation behavior as designated with superscript letters (**Table 3**).

Strains ANA3, CN32, and PV-4, in addition to MR-1, were positive for congregation around both MnO_2 and $Fe(OH)_3$ (**Table 3**, **Figure 3**; Videos S1–S8). They showed maximum reversal rates when they were located between 5 and 40 μm from the MnO_2 or $FeOH_3$ particle surface (**Figure 3**). Three strains: OS217, NCIMB400, and OS155 were not motile at time $t = 30$ min—in response to $Fe(OH)_3$ or MnO_2 minerals (**Table 3**). For example, the reversal frequency of the swimming MR-1 cells contacting MnO_2 was 0.94 ± 0.53 reversals/s, while the reversal frequency of the non-contacting cells was 0.62 ± 0.73 reversals/s. The speed also increased in the contacting group of MR-1 from 19.26 ± 11.2 μm/s in the non-contacting group to 24.37 ± 6 μm/s in the contacting group. Because there was both a statistically significant increase in swimming speed and reversals so as to allow the cells to remain near the metal oxide particle this strain was said to be congregation positive.

Shewanella spp. swimming tracks (30 s) that demonstrated a preference for metal oxide minerals are highlighted in **Figures 4A–F**. Figure SB2B cells displayed no swimming response to $Fe(OH)_3$ (**Figure 4D**) while exhibiting active congregation around MnO_2 particles (**Figure 4A**). In contrast, W3-18-1 cells congregated around $Fe(OH)_3$ particles (**Figure 4C**) but showed significantly diminished swimming and reversal activity around MnO_2 (**Figure 4F**; Videos S9, S14).

DISCUSSION

Members of the genus *Shewanella* are comprised of heterotrophic, facultative aerobes capable of utilizing a wide range of organics and inorganics as energy sources. Many *Shewanella* strains have been isolated from water column and sediment habitats in locations all across the globe. In addition to soluble electron acceptors, many of these organisms can respire a wide assortment of naturally occurring insoluble metal oxides under anoxic conditions.

In our study of congregation behavior in eight *Shewanella* species, we used cell tracking with computer analysis and time series assay of cell attachment to MnO_2 or $Fe(OH)_3$ to demonstrate that five out of eight shewanellae were capable of this behavior CN32, ANA-3, W3-18-1, SB2B, and PV-4) and that some strains (W3-18-1, SB2B) show a preference for one metal oxide over the other under these conditions (**Figure 4**). Such findings are consistent with the notion that these bacteria have adapted to the prevalent insoluble electron acceptor found in the habitat from which they were isolated. Furthermore, three *Shewanella* strains that were isolated from the water column did not congregate in response to IEA. Whether these differences derive from the absence of genes involved in EET (as in the OS217) or other reasons will be a point for future studies.

In other studies, overnight growth of the *Shewanella* strains comparing reduction rates of various metal oxides in head to head comparison, have been shown to reduce metal oxide preferentially from their environmental niche (Bretschger et al., 2007). The results presented here are consistent with the hypothesis that *Shewanella* species have evolved a congregation and attachment behavior consistent with the environments from which they were isolated (**Table 3**). For example, W3-18-1 seems to reveal significant inclination for congregation in the presence of and attachment to $Fe(OH)_3$ minerals native to Pacific continental shelf (Harris et al., 2012) while SB2B prefers MnO_2 (Venkateswaran et al., 1998) similar to that of the Amazon river sediment.

The genomic comparison in **Table 1** suggests that the presence of octaheme cytochrome (SO_4142) may be important for

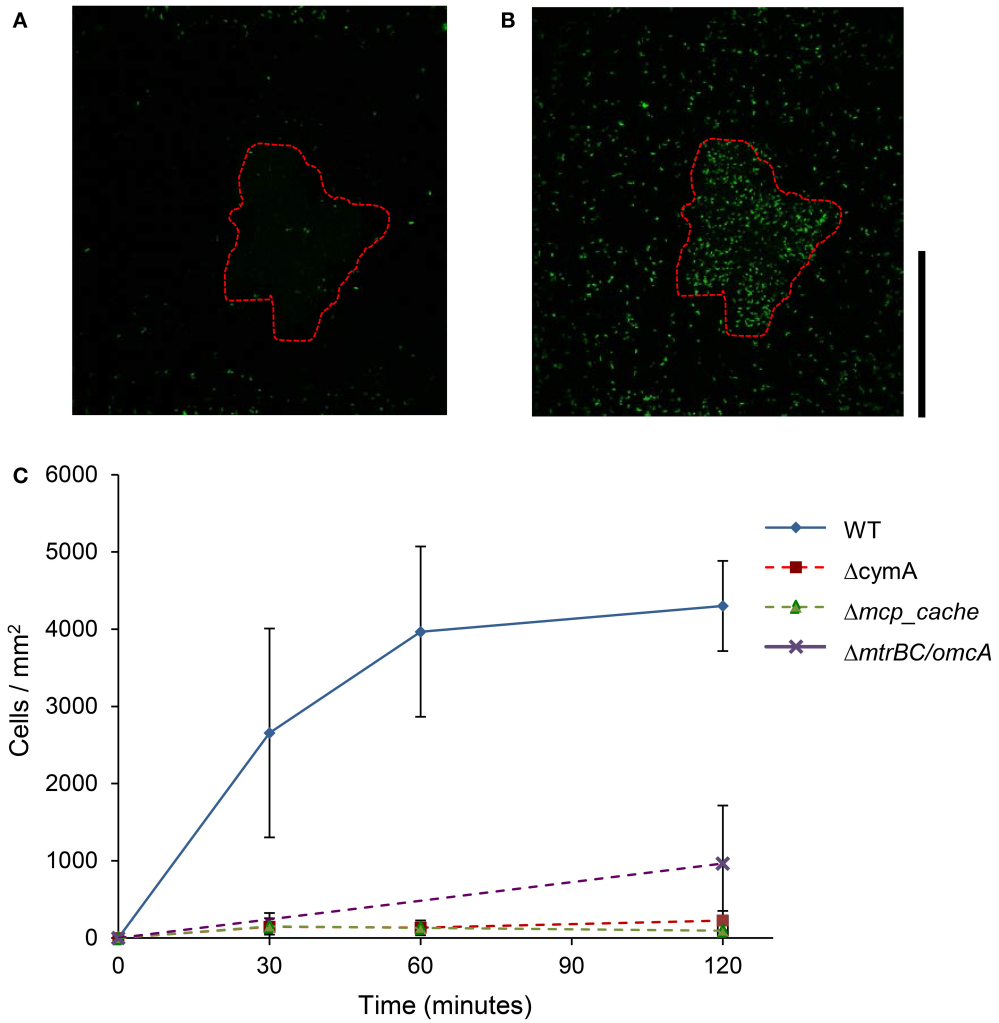

FIGURE 2 | Swimming MR-1 can migrate toward insoluble electron acceptor minerals and attach**.** Representative confocal fluorescence microscopy image of WT MR-1 cells at $t = 0$ and $t = 120$ min **(A,B)**. Swimming WT MR-1 GFP cells were introduced to MnO_2 particle (red dotted outline) in anaerobic sealed capillary. At $t = 0$ all the cells were irreversibly *photo-bleached* in a 250 by 250 μm area around particle **(A)**. Fluorescent cells from outside bleached zone that swim into frame and attach to mineral surface were then counted. The black vertical scale bar on the right represents 100 μm. Graph **(C)** compares WT MR-1 attachment on MnO_2 particle over 120 min with chemotaxis and extracellular electron transfer deletion mutants (MR-1 Δ*mcp_cache,* Δ*cymA,* and Δ*mtrBC/omcA*). The error bars include 2 std deviations.

swimming in response to relatively "low" redox potentials (100–300 mV vs. Ag/AgCl) of $Fe(OH)_3$. While *mtrF* (SO_1780) may be needed for response to relatively "higher" redox potentials of MnO_2 (between 400 and 600 mV vs. Ag/AgCl). This hypothesis could then be tested with deletion mutants in MR-1. This work complements previous work of Harris et al. (2012), by revealing that genes involved with the net effect of the motility behavior toward IEA minerals or electrodes is cumulative through relevant time scales of 1–30 min (**Figure 2**) (Harris et al., 2012). Our findings with CAAP confocal microscopy technique, demonstrated that congregation leads to a slow migration of cells toward IEA minerals with eventual attachment. Thus, this behavior is appropriately termed congregation, as it describes the gathering or accumulation of motile bacteria around IEA. We showed here that genes *mcp cache* and *mtrBC/omcA* are essential for accumulation and attachment phenotype in MR-1, in addition to being responsible for the characteristic swimming patterns of increased speed and run-and-reversal type behavior that was identified previously (Harris et al., 2012).

The results of the experiments with Δ*cymA*, Δ*mtrBC/omcA,* and Δ*mcp_cache* mutants in MR-1 show an inhibition of accumulation, attachment and congregation behavior in response to all IEAs. Therefore, it can be hypothesized that the presence of homologous EET genes (*cymA, mtrB, mtrC, omcA*), and methyl accepting chemotaxis gene (*mcp_cache*) determines the phenotypic responses we see in other *Shewanella* spp. (**Table 3**). Genetic comparison of strains, which could respond

TABLE 3 | Bacteria swimming speed and reversal frequency around metal oxide minerals.

Strain	Mineral	Reversal frequency (reversals/s)		Speed (μm/s)	
		≤2 μm	>2 μm	≤2 μm	>2 μm
MR-1	MnO_2	0.97 ± 0.58^{a}	0.32 ± 0.48^{a}	24.37 ± 6^{k}	19.26 ± 11.2^{k}
	$Fe(OH)_3$	0.74 ± 0.5^{b}	0.21 ± 0.39^{b}	18.12 ± 5.4^{l}	12.6 ± 5.4^{l}
SB2B	MnO_2	1.657 ± 0.925^{c}	0.320 ± 0.462^{c}	37.7 ± 14.7^{m}	23.5 ± 8.79^{m}
	$Fe(OH)_3$	nr	nr	nr	nr
PV-4	MnO_2	0.930 ± 0.3^{d}	0.519 ± 0.7^{d}	56.05 ± 35.8^{n}	48.49 ± 59.8^{n}
	$Fe(OH)_3$	0.177 ± 0.34^{e}	0.586 ± 0.59^{e}	12.73 ± 6.1	13.57 ± 4.4
W3-18-1	MnO_2	nr	nr	nr	nr
	$Fe(OH)_3$	0.228 ± 0.39	0.298 ± 0.27	15.54 ± 9.7^{p}	9.48 ± 1.5^{p}
CN32	MnO_2	1.371 ± 0.98^{g}	0.622 ± 0.49^{g}	34.98 ± 10.18^{q}	22.6 ± 8.4^{q}
	$Fe(OH)_3$	0.573 ± 0.47^{h}	0.342 ± 0.39^{h}	17.86 ± 6.5^{r}	13.62 ± 5.1^{r}
ANA3	MnO_2	1.240 ± 0.91^{i}	0.416 ± 0.47^{i}	20.38 ± 3.7^{s}	14.71 ± 6.7^{s}
	$Fe(OH)_3$	0.786 ± 0.45^{j}	0.426 ± 0.49^{j}	21.79 ± 7.7^{t}	13.87 ± 5.7^{t}

Results $^{a-t}$ *indicates significant difference of ± 2 S.D. nr = no response. OS155, NCIMB400, and OS217 did not show response to minerals.*

to "lower" redox potential IEA, indicates that peripheral outer membrane octaheme cytochromes (such as SO_4142) may play some role in responding to "lower" redox potential IEA. Hence these observations on sustained swimming around specific minerals corresponded with specific genotypes of the different species.

During many MFC (Kotloski and Gralnick, 2013) and metal reducing batch culture experiments, extracellular electron transfer-mediated energy taxis, or congregation ability, was not measured (Kotloski and Gralnick, 2013). In metal oxide reduction assays the 3D distribution of cells and cell motility could greatly influence metal reduction due to incubator shaker speed, culture flask dimensions, or mixing. Congregation behavior directly influences cell attachment to IEAs. The relationship between congregation and nanowire-like appendage formation is still unknown (Pirbadian et al., 2015), although the motility and congregation parameters are rarely monitored in these studies (Gorby et al., 2005; Reguera et al., 2005). Transforming these core congregation genes (*cymA*, *mtrB*, *mtrA*, *omcA*, *mcp_pas*, and *mcp_cache*) into other bacteria species, with single polar flagellum, may someday improve bioremediation capabilities by being able to induce bacterial attachment and colonization of surfaces that would otherwise be difficult or impossible.

MATERIALS AND METHODS

Cultivation and Strains

MR-1 and several deletion mutants originated from MR-1 were examined in this study (**Table 2**) (Beliaev and Saffarini, 1998; Myers and Myers, 2002). Strains were inoculated from glycerol stocks stored at −80°C onto Luria-Bertani (LB) plates and grown overnight at 30°C. Individual colonies were then selected and inoculated into 5 mL of defined minimal media (M1) (Bretschger et al., 2007) supplemented with 18 mM lactate as an energy source (Bretschger et al., 2007) in 15 mL tubes (VWR International LLC, Randor, Pennsylvania, USA) and incubated horizontally in a shaker (180 rpm) for 48 h at 30 °C. Optical Density was measured using a spectrophotometer (Unico 1100RS spectrophotometer, Dayton, New Jersey, USA). Cells were sampled at an OD_{600} of 0.5 ± 0.2 (after ∼48 h). In swimming experiments, five milliliter cultures were sampled when the cells reached an OD of 0.4, mixed with manganese or iron oxides, and introduced to a glass capillary (0.02 × 0.20 mm) (Vitrocom, Mountain Lakes, New Jersey, USA) that was then sealed using vacuum grease as described previously (Harris et al., 2010).

Mineral Synthesis

The $Fe(OH)_3$ stock solution was prepared according to the protocol by Cornell and Schwertmann and then verified by X-ray defraction (Schwertmann and Cornell, 2008). This preparation of colloidal MnO_2 began with 8 g $KMnO_4$ dissolved in 200 mL, while utilizing all possible safety precautions. The solution was continuously mixed using a magnetic stir bar on high and heated below boiling temperature. Then, 5 mL of 10 M sodium hydroxide was added to neutralize the acid produced by the reaction. In a separate flask, 15 g of manganese chloride was dissolved into 75 mL of distilled water. Finally, the solution was then slowly mixed with the permanganate solution (in a chemical fume hood) for 75 min. After cooling the solution, it was then washed by centrifugation and rinsed with deionized water (DI) (18 Meg-Ohm cm) water over five times. The final precipitate was allowed to dry by vacuum filter in a clean bench and desiccated for 36 h. The resulting minerals were analyzed via X-ray diffraction to confirm the production of $Fe(OH)_3$ and MnO_2 (Bretschger et al., 2007; Salas et al., 2010).

Suspended mineral particles were mixed with culture at a final concentration of 300 mg/mL of MnO_2 or $Fe(OH)_3$. Cells

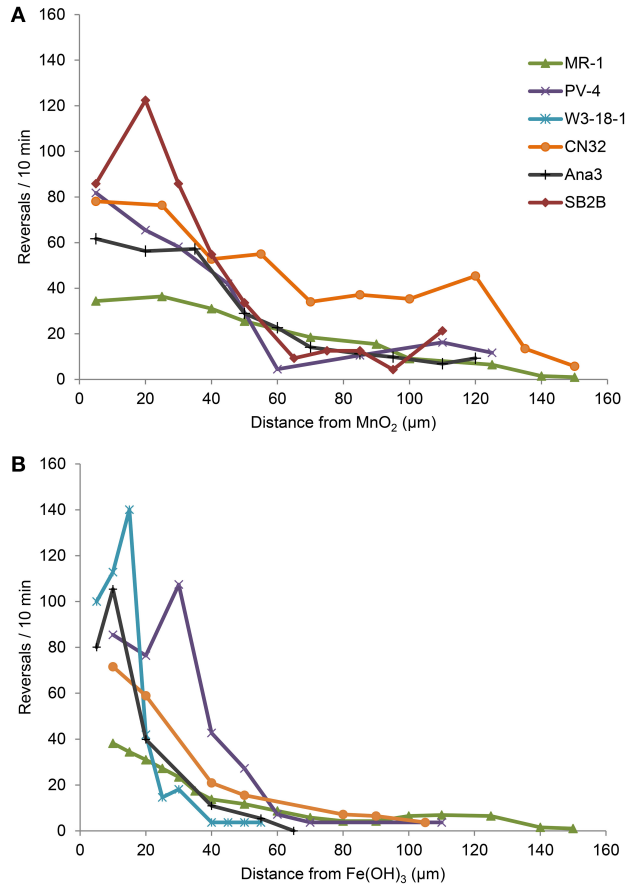

FIGURE 3 | (A,B) Reversal frequency (y-axis) of swimming *Shewanella* cells vs. distance (x-axis) from IEA particle. The average reversal frequencies of individual tracked swimming cells are divided into bins of 5 μm along the x-axis for experiments with MnO_2 **(A)** or $Fe(OH)_3$ particle **(B)**.

were then immersed by capillary into rectangular capillary tubes (0.02 × 0.20 mm) (Vitrocom, Mountain Lakes, New Jersey, USA). Tubes were sealed with Silicon vacuum grease (Dow Corning, Midland, Milwaukie, USA) and observed with light microscopy, fluorescence microscopy, and confocal microscopy.

Cell Accumulation after Photo-Bleaching (CAAP) Time-Lapse Experiments

All fluorescently labeled strains (GFP) were transformed as previously described (McLean et al., 2008) and then grown aerobically on a defined minimal medium with 25 μg/ml kanamycin and 18 mM lactate for 48 h at 30°C. Five milliliter cultures were sampled when the cells reached an OD of 0.4, mixed with manganese or iron oxides, and introduced to a glass capillary (0.02 × 0.20 mm) (Vitrocom, Mountain Lakes, New Jersey, USA) that was then sealed using vacuum grease as described previously (Harris et al., 2010). GFP labeled WT MR-1, Δ*cymA*, Δ*mcp_cache*, and Δ*mtrBC/omcA* cells were bleached using maximum light intensity settings with 60X lenses, of an inverted Leica TCS SPE confocal microscope (Wetzlar, Germany) for 15 min. To ensure that bleaching occurred, time-lapse captured a screen area (250 × 250 μm selected area) every minute until the original cells appeared dark and the surrounding cells remained brightly fluorescent. Images were then captured using 588 nm excitation and 530 nm emission. A time-lapse video of the entire section of the tube was captured using Leica Imaging software and the "auto focus" feature for the next 3 h. Cells were also observed under transmitted light mode to verify that bleached cells were motile and intact. A separate negative control, with GFP labeled Δ*mcp_cache*, was captured for 3 h. No cells were seen accumulating in the dark zone in this negative control, nor did bleached cells recover GFP fluorescence. The response of the entire capillary (height of 30 μm) was captured using time-lapse photography and the sum of cells in all 20 z-axis stacks was determined (using computer analysis method below) for each time point.

Microscopy Capture of Cell Movements

The methods for bacterial tracking and analysis were identical to previous studies utilized for **Figure 3** and recorded in **Table 3** (Harris et al., 2012). Both computer and manual bacterial swimming tracks were standardized using a scale ruler (100 μm). From each experiment, the overall swimming activity within the video frame—equivalent to a 107 × 193 μm field of view—was recorded and the video was time-normalized to give swimming speeds in μm/s. Several parameters were measured for each bacterial swimming track such as the total distance moved, the time of track since the bacteria first appear and disappear, the number of reversals, the distance between each reversal and the metal oxide, and the distance between the metal oxide and the start of the bacteria track.

Swimming Analysis

Cells were tracked by hand from video data (30 frames/s), frame-by-frame, and measured by ImageJ image analysis software. Data inputs include the swimming speed, the starting position of the bacteria with respect to the nearest IEA surface and position of each bacterial reversal event was identified and logged with respect to the distance from the nearest IEA surface (**Figure 3** and **Table 3**). For determining the swimming activity after contact with IEA, the swimming cells were divided into two groups for analysis: cells that swam within 2 μm of a particle were considered "contacting" and those that did not swim within 2 μm from the particle surface were considered "non-contacting." In addition to the hand tracking methods described above, experimental data was then computer sorted and analyzed by an algorithm previously described to yield the calculated swimming data (Crocker and Grier, 1996; Harris et al., 2012; Harris, 2013). To produce **Figures 3**, **4**, all experimental data from four separate biological replicates were combined, pooled and averaged into bins according to distance from the IEA particle. Because this data was pooled into distances, error bars are overlapping; no comparison of reversal frequency, at a given distance can be made between

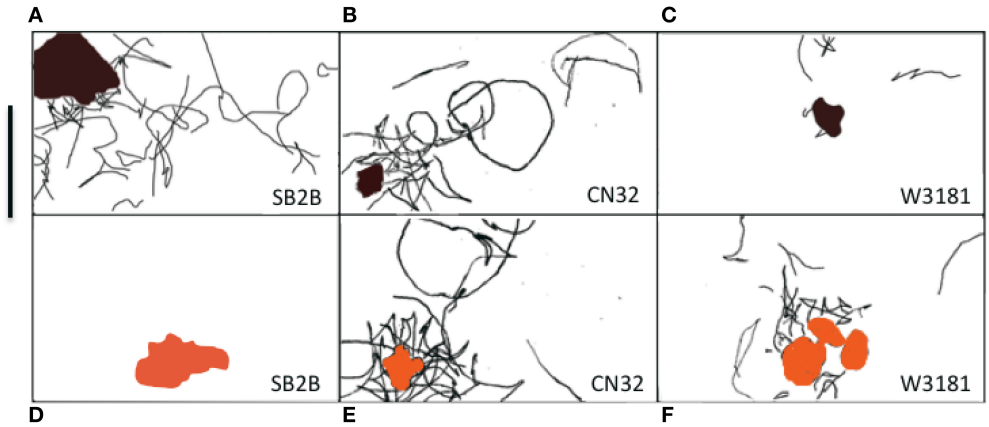

FIGURE 4 | (A–F) Panel of three *Shewanella* spp. swimming tracks (30 s) demonstrated a preference for metal oxide minerals. The swimming behavior of three motile *Shewanella* spp. in response to MnO_2 (top row—black colored particle) and $Fe(OH)_3$ (bottom row—orange colored particle) was studied. Congregation occurs in anaerobic conditions, swimming tracks are shown in black. SB2B (left), CN32 (center), and W3181 (right). The cell swimming was tracked by hand. The scale bar on the upper left = 50 μm. The brown color shape represents MnO_2 and the orange represents $Fe(OH)_3$. When there are no motile cells detected this is indicated by the absence of black lines.

strains, as this method of visualization precludes experiment identifiers.

AUTHOR CONTRIBUTIONS

HH: designed and performed the experiments; HH and IS-A: wrote and revised paper; ES, ME-N, and JM: helped design experiments; WT: helped to perform the data analysis; JM and KN: revised the manuscript.

ACKNOWLEDGMENTS

Special thanks to Mandy J. Ward and Gijs Kuenen for advice on research and experiment design. We thank Meaghan Sullivan for her manual tracking analyses. We thank Cecile Jourlin-Castelli, Samantha Reed, Jun Li, and David Culley for supplying the Δ*mcp_cache*, Δ*mtrBC/omcA*, and Δ*cymA* mutants. Funding for this work was provided by an Air Force Office of Scientific Research Award [grant number FA9550-06-1-0292]. IS-A research was supported by the NASA Planetary Biology Internship fellowship.

SUPPLEMENTARY MATERIAL

The Supplementary Material for this article can be found online at: https://www.frontiersin.org/articles/10.3389/fmicb.2017.02568/full#supplementary-material

REFERENCES

Alexandre, G., Greer-Phillips, S., and Zhulin, I. B. (2004). Ecological role of energy taxis in microorganisms. *FEMS Microbiol. Rev.* 28, 113–126. doi: 10.1016/j.femsre.2003.10.003

Baraquet, C., Théraulaz, L., Iobbi-Nivol, C., Méjean, V., and Jourlin-Castelli, C. (2009). Unexpected chemoreceptors mediate energy taxis towards electron acceptors in *Shewanella oneidensis*. *Mol. Microbiol.* 73, 278–290. doi: 10.1111/j.1365-2958.2009.06770.x

Beliaev, A. S., and Saffarini, D. A. (1998). *Shewanella putrefaciens* mtrB encodes an outer membrane protein required for Fe(III) and Mn(IV) Reduction. *J. Bacteriol.* 180, 6292–6297.

Bencharit, S., and Ward, M. J. (2005). Chemotactic responses to metals and anaerobic electron acceptors in *Shewanella oneidensis* MR-1. *J. Bacteriol.* 187, 5049–5053. doi: 10.1128/JB.187.14.5049-5053.2005

Bond, D. R., and Lovley, D. R. (2003). Electricity production by *Geobacter sulfurreducens* attached to electrodes. *Appl. Environ. Microbiol.* 69, 1548–1555. doi: 10.1128/AEM.69.3.1548-1555.2003

Bowman, J. P., McCammon, S. A., Nichols, D. S., Skerratt, J. H., Rea, S. M., Nichols, P. D., et al. (1997). *Shewanella gelidimarina* sp. nov. and *Shewanella frigidimarina* sp. nov., novel antarctic species with the ability to produce eicosapentaenoic acid (20:5ω3) and grow anaerobically by dissimilatory Fe(III) reduction. *Int. J. Syst. Bacteriol.* 47, 1040–1047. doi: 10.1099/00207713-47-4-1040

Bretschger, O. (2008). *Electron Transfer Capability and Metabolic Processes of the Genus Shewanella with Applications to the Optimization of Microbial Fuel Cells*. University of Southern California, ProQuest Dissertations Publishing, 3325185.

Bretschger, O., Obraztsova, A., Sturm, C. A., Chang, I. S., Gorby, Y. A., Reed, S. B., et al. (2007). Current production and metal oxide reduction by *Shewanella oneidensis* MR-1 wild type and mutants. *Appl. Environ. Microbiol.* 73:7003. doi: 10.1128/AEM.01087-07

Brettar, I., Christen, R., and Höfle, M. G. (2002). *Shewanella denitrificans* sp nov., a vigorously denitrifying bacterium isolated from the oxic-anoxic interface of the Gotland Deep in the central Baltic Sea. *Int. J. Syst. Evol. Microbiol.* 52, 2211–2217. doi: 10.1099/00207713-52-6-2211

Burdige, D. J. (1993). The biogeochemistry of manganese and iron reduction in marine sediments. *Earth Sci. Rev.* 35, 249–284. doi: 10.1016/0012-8252(93)90040-E

Champine, J. E., Underhill, B., Johnston, J. M., Lilly, W. W., and Goodwin, S. (2000). Electron transfer in the dissimilatory iron-reducing bacterium *Geobacter metallireducens*. *Anaerobe* 6, 187–196. doi: 10.1006/anae.2000.0333

Childers, S. E., Ciufo, S., and Lovley, D. R. (2002). *Geobacter metallireducens* accesses insoluble Fe(III) oxide by chemotaxis. *Nature* 416, 767–769. doi: 10.1038/416767a

Coursolle, D., and Gralnick, J. A. (2010). Modularity of the Mtr respiratory pathway of *Shewanella oneidensis* strain MR-1. *Mol. Microbiol.* 77, 995–1008. doi: 10.1111/j.1365-2958.2010.07266.x

Crocker, J. C., and Grier, D. G. (1996). Methods of digital video microscopy for colloidal studies. *J. Colloid Interface Sci.* 179, 298–310. doi: 10.1006/jcis.1996.0217

El-Naggar, M. Y., Wanger, G., Leung, K. M., Yuzvinsky, T. D., Southam, G., Yang, J., et al. (2010). Electrical transport along bacterial nanowires from *Shewanella oneidensis* MR-1. *Proc. Natl Acad. Sci. U.S.A.* 107, 18127–18131. doi: 10.1073/pnas.1004880107

Fredrickson, J. K., Romine, M. F., Beliaev, A. S., Auchtung, J. M., Driscoll, M. E., Gardner, T. S., et al. (2008). Towards environmental systems biology of Shewanella. *Nat. Rev. Microbiol.* 6, 592–603. doi: 10.1038/nrmicro1947

Fredrickson, J. K., Zachara, J. M., Kennedy, D. W., Dong, H., Onstott, T. C., Hinman, N. W., et al. (1998). Biogenic iron mineralization accompanying the dissimilatory reduction of hydrous ferric oxide by a groundwater bacterium. *Geochim. Cosmochim. Acta* 62, 3239–3257. doi: 10.1016/S0016-7037(98)00243-9

Gao, H., Obraztova, A., Stewart, N., Popa, R., Fredrickson, J. K., Tiedje, J. M., et al. (2006). *Shewanella loihica* sp. nov., isolated from iron-rich microbial mats in the Pacific Ocean. *Int. J. Syst. Evol. Microbiol.* 56, 1911–1916. doi: 10.1099/ijs.0.64354-0

Gorby, Y. A., Beveridge, T. J., and Wiley, W. R. (2005). "Composition, reactivity, and regulation of extracellular metal-reducing structures (nanowires) produced by dissimilatory metal reducing bacteria," in *Annual NABIR PI Meeting* (Warrenton, VA).

Gorby, Y. A., Yanina, S., McLean, J. S., Rosso, K. M., Moyles, D., Dohnalkova, A., et al. (2006). Electrically conductive bacterial nanowires produced by *Shewanella oneidensis* strain MR-1 and other microorganisms. *Proc. Natl. Acad. Sci. U.S.A.* 103, 11358–11363. doi: 10.1073/pnas.0604517103

Gross, B. J., and El-Naggar, M. Y. (2015). A combined electrochemical and optical trapping platform for measuring single cell respiration rates at electrode interfaces. *Rev. Sci. Instrum.* 86:064301. doi: 10.1063/1.4922853

Harris, H. W. (2013). *Identification of a New Bacterial Sensing Mechanism: Characterization of Bacterial Insoluble Electron Acceptor Sensing*. University of Southern California.

Harris, H. W., El-Naggar, M. Y., Bretschger, O., Ward, M. J., Romine, M. F., Obraztsova, A. Y., et al. (2010). Electrokinesis is a microbial behavior that requires extracellular electron transport. *Proc. Natl. Acad. Sci. U.S.A.* 107, 326–331. doi: 10.1073/pnas.0907468107

Harris, H. W., Naggar, M. Y., and Nealson, K. H. (2012). *Shewanella oneidensis* MR-1 chemotaxis proteins and electron-transport chain components essential for congregation near insoluble electron acceptors. *Biochem. Soc. Trans.* 40, 1167–1177. doi: 10.1042/BST20120232

Hau, H. H., and Gralnick, J. A. (2007). Ecology and biotechnology of the genus Shewanella. *Annu. Rev. Microbiol.* 61, 237–258. doi: 10.1146/annurev.micro.61.080706.093257

Hsu, L., Masuda, S. A., Nealson, K. H., and Pirbazari, M. (2012). Evaluation of microbial fuel cell *Shewanella biocathodes* for treatment of chromate contamination. *R. Soc. Chem. Adv.* 2, 5844–5855. doi: 10.1039/c2ra20478a

Kan, J., Hsu, L., Cheung, A. C. M., Pirbazari, M., and Nealson, K. H. (2011). Current production by bacterial communities in microbial fuel cells enriched from wastewater sludge with different electron donors. *Environ. Sci. Technol.* 45, 1139–1146. doi: 10.1021/es102645v

Kato, S., Nakamura, R., Kai, F., Watanabe, K., and Hashimoto, K. (2010). Respiratory interactions of soil bacteria with (semi)conductive iron-oxide minerals. *Environ. Microbiol.* 12, 3114–3123. doi: 10.1111/j.1462-2920.2010.02284.x

Kotloski, N. J., and Gralnick, J. A. (2013). Flavin electron shuttles dominate extracellular electron transfer by *Shewanella oneidensis*. *MBio* 4:e00553. doi: 10.1128/mBio.00553-12

Kracke, F., Vassilev, I., and Krömer, J. O. (2015). Microbial electron transport and energy conservation – the foundation for optimizing bioelectrochemical systems. *Front. Microbiol.* 6:575. doi: 10.3389/fmicb.2015.00575

Li, J., Go, A. C., Ward, M. J., and Ottemann, K. M. (2010). The chemical-in-plug bacterial chemotaxis assay is prone to false positive responses. *BMC Res. Notes* 3:77. doi: 10.1186/1756-0500-3-77

Li, J., Romine, M. F., and Ward, M. J. (2007). Identification and analysis of a highly conserved chemotaxis gene cluster in Shewanella species. *FEMS Microbiol. Lett.* 273, 180–186. doi: 10.1111/j.1574-6968.2007.00810.x

Li, R., Tiedje, J. M., Chiu, C., and Worden, R. M. (2012). Soluble electron shuttles can mediate energy taxis toward insoluble electron acceptors. *Environ. Sci. Technol.* 46, 2813–2820. doi: 10.1021/es204302w

Lovley, D. R., Coates, J. D., Blunt-Harris, E. L., Phillips, E. J. P., and Woodward, J. C. (1996). Humic substances as electron acceptors for microbial respiration. *Nature* 382, 445–448. doi: 10.1038/382445a0

Lovley, D. R., Giovannoni, S. J., White, D. C., Champine, J. E., Phillips, E. J., Gorby, Y. A., et al. (1993). *Geobacter metallireducens* gen. nov. sp. nov., a microorganism capable of coupling the complete oxhidation of organic compounds to the reduction of iron and other metals. *Arch. Microbiol.* 159, 336–344. doi: 10.1007/BF00290916

Lovley, D. R., Holmes, D. E., and Nevin, K. P. (2004). Dissimilatory Fe(III) and Mn(IV) reduction. *Adv. Microb. Physiol.* 49, 219–286. doi: 10.1111/j.1462-2920.2004.00593.x

Marsili, E., Baron, D. B., Shikhare, I. D., Coursolle, D., Gralnick, J. A., Bond, D. R., et al. (2008). Shewanella secretes flavins that mediate extracellular electron transfer. *Proc. Natl. Acad. Sci. U.S.A.* 105, 3968–3973. doi: 10.1073/pnas.0710525105

McLean, J. S., Majors, P. D., Reardon, C. L., Bilskis, C. L., Reed, S. B., Romine, M. F., et al. (2008). Investigations of structure and metabolism within *Shewanella oneidensis* MR-1 biofilms. *J. Microbiol. Methods* 74, 47–56. doi: 10.1016/j.mimet.2008.02.015

Meyer, T. E., Tsapin, A. I., Vandenberghe, I., de Smet, L., Frishman, D., Nealson, K. H., et al. (2004). Identification of 42 possible cytochrome C genes in the *Shewanella oneidensis* genome and characterization of six soluble cytochromes. *Omics* 8, 57–77. doi: 10.1089/153623104773547499

Mitchell, A. C., Peterson, L., Reardon, C. L., Reed, S. B., Culley, D. E., Romine, M. R., et al. (2012). Role of outer membrane c-type cytochromes MtrC and OmcA in *Shewanella oneidensis* MR-1 cell production, accumulation, and detachment during respiration on hematite. *Geobiology* 10, 355–370. doi: 10.1111/j.1472-4669.2012.00321.x

Murray, A. E., Lies, D., Li, G., Nealson, K., Zhou, J., and Tiedje, J. M. (2001). DNA/DNA hybridization to microarrays reveals gene-specific differences between closely related microbial genomes. *Proc. Natl. Acad. Sci. U.S.A.* 98, 9853–9858. doi: 10.1073/pnas.171178898

Myers, C. R., and Myers, J. M. (1997). Cloning and sequence of cymA, a gene encoding a tetraheme cytochrome c required for reduction of iron(III), fumarate, and nitrate by *Shewanella putrefaciens* MR-1. *J. Bacteriol.* 179, 1143–1152. doi: 10.1128/jb.179.4.1143-1152.1997

Myers, C. R., and Myers, J. M. (2002). MtrB Is required for proper incorporation of the cytochromes OmcA and OmcB into the outer membrane of *Shewanella putrefaciens* MR-1. *Appl. Environ. Microbiol.* 68, 5585–5594. doi: 10.1128/AEM.68.11.5585-5594.2002

Myers, C. R., and Nealson, K. H. (1988a). Bacterial manganese reduction and growth with manganese oxide as the sole electron acceptor. *Science* 240, 1319–1321. doi: 10.1126/science.240.4857.1319

Myers, C. R., and Nealson, K. H. (1988b). Microbial reduction of manganese oxides: Interactions with iron and sulfur. *Geochim. Cosmochim. Acta* 52, 2727–2732. doi: 10.1016/0016-7037(88)90041-5

Myers, J. M., and Myers, C. R. (2001). Role for outer membrane cytochromes OmcA and OmcB of *Shewanella putrefaciens* MR-1 in reduction of manganese dioxide. *Appl. Environ. Microbiol.* 67, 260–269. doi: 10.1128/AEM.67.1.260-269.2001

Nealson, K. H., Moser, D. P., and Saffarini, D. A. (1995). Anaerobic electron acceptor chemotaxis in *Shewanella putrefaciens*. *Appl. Environ. Microbiol.* 61, 1551–1554.

Okamoto, A., Kalathil, S., Deng, X., Hashimoto, K., Nakamura, R., and Nealson, K. H. (2014). Cell-secreted flavins bound to membrane cytochromes dictate electron transfer reactions to surfaces with diverse charge and pH. *Sci. Rep.* 4:5628. doi: 10.1038/srep05628

Pirbadian, S., Barchinger, S. E., Leung, K. M., Byun, H. S., Jangir, Y., Bouhenni, R. A., et al. (2015). Bacterial nanowires of *Shewanella oneidensis* MR-1 are outer membrane and periplasmic extensions of the extracellular electron transport components. *Biophys. J.* 108:368a. doi: 10.1016/j.bpj.2014.11.2016

Reguera, G., McCarthy, K. D., Mehta, T., Nicoll, J. S., Tuominen, M. T., Lovely, D. R., et al. (2005). Extracellular electron transfer via microbial nanowires. *Nature* 435, 1098–1101. doi: 10.1038/nature03661

Salas, E. C., Berelson, W. M., Hammond, D. E., Kampf, A. R., and Nealson, K. H. (2010). The impact of bacterial strain on the products of dissimilatory iron reduction. *Geochim. Cosmochim. Acta* 74, 574–583. doi: 10.1016/j.gca.2009.10.039

Saltikov, C. W., Cifuentes, A., Venkateswaran, K., and Newman, D. K. (2003). The ars detoxification system is advantageous but not required for As(V) respiration by the genetically tractable Shewanella species strain ANA-3. *Appl. Environ. Microbiol.* 69, 2800–2809. doi: 10.1128/AEM.69.5.2800-2809.2003

Schwalb, C., Chapman, S. K., and Reid, G. A. (2003). The tetraheme cytochrome CymA is required for anaerobic respiration with dimethyl sulfoxide and nitrite in *Shewanella oneidensis*. *Biochemistry* 42, 9491–9497. doi: 10.1021/bi034456f

Schwertmann, U., and Cornell, R. M. (2008). *Iron Oxides in the Laboratory*. Weinheim: John Wiley & Sons.

Shi, L., Richardson, D. J., Wang, Z., Kerisit, S. N., Rosso, K. M., Zachara, J. M., et al. (2009). The roles of outer membrane cytochromes of Shewanella and Geobacter in extracellular electron transfer. *Environ. Microbiol. Rep.* 1, 220–227. doi: 10.1111/j.1758-2229.2009.00035.x

Venkateswaran, K., Dollhopf, M. E., Aller, R., Stackebrandt, E., and Nealson, K. H. (1998). *Shewanella amazonensis* sp. nov., a novel metal-reducing facultative anaerobe from Amazonian shelf muds. *Int. J. Syst. Bacteriol.* 48, 965–972.

Venkateswaran, K., Moser, D. P., Dollhopf, M. E., Lies, D. P., Saffarini, D. A., MacGregor, B. J., et al. (1999). Polyphasic taxonomy of the genus Shewanella and description of *Shewanella oneidensis* sp. nov. *Int. J. Syst. Bacteriol.* 49, 705–724. doi: 10.1099/00207713-49-2-705

Ziemke, F., Höfle, M. G., Lalucat, J., and Rossellö-Mora, R. (1998). Reclassification of *Shewanella putrefaciens* Owen's genomic group II as *Shewanella baltica* sp. nov. *Int. J. Syst. Bacteriol.* 48, 179–186. doi: 10.1099/00207713-48-1-179

Conflict of Interest Statement: The authors declare that the research was conducted in the absence of any commercial or financial relationships that could be construed as a potential conflict of interest.

frontiers in Microbiology

ORIGINAL RESEARCH
published: 26 January 2018
doi: 10.3389/fmicb.2018.00041

Adsorption and Desorption Characteristics of Cd^{2+} and Pb^{2+} by Micro and Nano-sized Biogenic $CaCO_3$

Renlu Liu[1], *Yong Guan*[2], *Liang Chen*[2] *and Bin Lian*[1]*

[1] *Jiangsu Key Laboratory for Microbes and Functional Genomics, Jiangsu Engineering and Technology Research Center for Microbiology, College of Life Sciences, Nanjing Normal University, Nanjing, China,* [2] *National Synchrotron Radiation Laboratory, University of Science and Technology of China, Hefei, China*

The purpose of this study was to elucidate the characteristics and mechanisms of adsorption and desorption for heavy metals by micro and nano-sized biogenic $CaCO_3$ induced by *Bacillus subtilis*, and the pH effect on adsorption was investigated. The results showed that the adsorption characteristics of Cd^{2+} and Pb^{2+} are well described by the Langmuir adsorption isothermal equation, and the maximum adsorption amounts for Cd^{2+} and Pb^{2+} were 94.340 and 416.667 mg/g, respectively. The maximum removal efficiencies were 97% for Cd^{2+}, 100% for Pb^{2+}, and the desorption rate was smaller than 3%. Further experiments revealed that the biogenic $CaCO_3$ could maintain its high adsorption capability for heavy metals within wide pH ranges (3–8). The FTIR and XRD results showed that, after the biogenic $CaCO_3$ adsorbed Cd^{2+} or Pb^{2+}, it did not produce a new phase, which indicated that biogenic $CaCO_3$ and heavy metal ions were governed by a physical adsorption process, and the high adsorptive capacity of biogenic $CaCO_3$ for Cd^{2+} and Pb^{2+} were mainly attributed to its large total specific surface area. The findings could improve the state of knowledge about biogenic $CaCO_3$ formation in the environment and its potential roles in the biogeochemical cycles of heavy metals.

Keywords: biogenic $CaCO_3$, heavy metals, adsorption, desorption, mechanism

OPEN ACCESS

Edited by:
Alain F. Plante, University of Pennsylvania, United States

Reviewed by:
Mustafa Yucel, Middle East Technical University, Turkey
Rachel Narehood Austin, Columbia University, United States

***Correspondence:**
Bin Lian
bin2368@vip.163.com

Specialty section:
This article was submitted to Microbiological Chemistry and Geomicrobiology, a section of the journal Frontiers in Microbiology

Received: *10 July 2017*
Accepted: *09 January 2018*
Published: *26 January 2018*

Citation:
Liu R, Guan Y, Chen L and Lian B (2018) Adsorption and Desorption Characteristics of Cd^{2+} and Pb^{2+} by Micro and Nano-sized Biogenic $CaCO_3$. Front. Microbiol. 9:41. doi: 10.3389/fmicb.2018.00041

INTRODUCTION

The main current environmental problems are the increasing atmospheric greenhouse effect and environmental pollution of large areas. Moreover, the increase of population and industrial or agricultural production makes such environmental issues more prominent. Heavy metal pollution in water and soil is already a global problem, and it is especially serious in soils (Zhao et al., 2014a). For example, the proportion of heavy metal pollution has exceeded 2.5% by land area, covering 2.32 million hectares in China, and the exceedances of permissible threshold values for Cd, Hg, As, Cu, Pb, Cr, Zn, and Ni are 7, 1.6, 2.7, 2.1, 1.5, 1.1, 0.9, and 4.8%, respectively (The Ministry of Environmental Protection, 2014; Zhao et al., 2014a; The Ministry of Land and Resources, 2015).

Microbial methods are become favored due to their low cost and environmentally—friendly nature (Lian et al., 2008; Kavamura and Esposito, 2010; Moreau et al., 2013; Santos et al., 2017), but the adsorbed heavy metals may re-enter the environment and cause re-pollution with the change in environmental conditions (Pavasant et al., 2006; Pan et al., 2007; Apiratikul and Pavasant, 2008; Tsekova et al., 2010). A sequestration method seems to be the most convenient and most commonly

chosen method (Lagadic et al., 2001; Babel and Kurniawan, 2003; Kobya et al., 2005; Ren et al., 2013); however, currently available heavy metals adsorbents remain limited, and most traditional adsorbents come with high utilization costs. Therefore, it is necessary to develop a new high-efficiency, low-cost, environmentally-friendly heavy metal adsorbent.

$CaCO_3$ is one of the most abundant bio-minerals found in nature, and it has aroused great interest in many branches of science. The biosynthesis of $CaCO_3$ is of great significance. It can promote carbon deposition, thus contributing to mitigate global warming (Dupraz et al., 2009; Mitchell et al., 2010; Phillips et al., 2013). $CaCO_3$ is reported to adsorb heavy metal ions in water or soil with good effect, and increasing the amount of $CaCO_3$ in the soil or water can significantly reduce the migration of heavy metals (Al-Degs et al., 2006; Yavuz et al., 2007; Aziz et al., 2008; Cai et al., 2010; Zhao et al., 2014a). However, the use of biogenic $CaCO_3$ combined with microbial technology to remediate heavy metal pollution, including the related process and the microscopic mechanism, has not yet been reported.

Natural $CaCO_3$ from limestone has limited further development prospects as a result of its low purity and efficiency. The traditional CO_2-bubble method for synthesizing $CaCO_3$ cannot sufficiently regulate the product size, morphology, or crystal type, and the cost is higher. But it is feasible to produce biogenic $CaCO_3$ particles with morphological diversity (such as: spherical, rhabditiform, flower, dumbbell-shape, reticular structure aggregates, etc.) and low cost by microbial mineralisation technology (Lian et al., 2006; Han et al., 2013; Cao et al., 2016). On this basis, developing the application of biogenic $CaCO_3$ in the treatment of heavy metals can not only deepen our understanding of the environmental significance of bio-mineralisation, but also develop a potential means with which to control heavy metal pollution.

The adsorption of heavy metal ions is subject to many factors, such as contact time, temperature, pH, and so on. Since the surface charge of an adsorbent in a solution could be altered by changing its pH value, the pH is one of the most important factors affecting the adsorption process of metal ions (Farrah and Pickering, 1979; Chen et al., 1997; Abollino et al., 2003; Üçer et al., 2006; Wolthers et al., 2008; Meng et al., 2009; Ma et al., 2012). Here, the adsorption-desorption properties of Cd^{2+} and Pb^{2+} by $CaCO_3$ induced by *Bacillus subtilis* and the pH effect on adsorption were investigated. This study will improve our knowledge of biogenic $CaCO_3$ formation in the environment and its potential role in the remediation of heavy metals.

MATERIALS AND METHODS

Preparation of Micro and Nano-sized Biogenic $CaCO_3$ and Its Morphology and Chemical Composition Analysis

Experimental Strain

B. subtilis (GenBank accession number KT343639), derived from the National Research and Extension Centre of Microbial Fertilizer Technology of China, is the legal functional microbial fertilizer strain in China.

We inoculated two or three rings with *B. subtilis* in 200 mL LB liquid culture medium [tryptone 0.1% (W/V), yeast extract 0.5% (W/V), NaCl 1% (W/V), $6.5 \leq pH \leq 7.5$], shaking-cultured for 10 h at 30°C and 180 rpm, to prepare the bacterial liquid [$(7.75 \pm 1.19) \times 10^7$ cfu/mL]. We added 100 mL LB liquid medium (containing $CaCl_2$ 0.2 g) to a clean 250 mL conical flask. Afterwards, we inoculated 2 mL strain from the aforementioned bacterial liquid to form the experimental group, and set up 20 parallel, shaking-cultured samples (30°C, 180 rpm, for 7 days) to induce $CaCO_3$ synthesis. The culture solution was centrifuged at 8000 rpm for 15 min at 4°C, and then the centrifuged sediments were collected and dried at 55°C, then milled to 200 mesh size or finer by agate mortar in readiness for testing. To verify whether the acquisition of micro- and nano-sized biogenic $CaCO_3$ was successful, or not, we smeared the precipitate evenly on clean cover-glasses, drying naturally, then, subjected them to field emission scanning electron microscopy and energy dispersive spectrometry (FESEM-EDS) analysis. In addition, the XRD and TEM-SAED (selected area electron diffraction) methods were used to analyse the crystal structure of the precipitate.

The Adsorption and Desorption of Cd^{2+} and Pb^{2+} by Micro and Nano-sized Biogenic $CaCO_3$

To investigate the environmental remediation benefits of biogenic $CaCO_3$, the adsorption and desorption characteristics of two common heavy metal ions (Cd^{2+} and Pb^{2+}) under the action of biogenic $CaCO_3$ were investigated. The Langmuir and Freundlich equations were used to fit an adsorption model, and this was then employed to obtain the maximum adsorption capacity of such heavy metals (Wang et al., 2007b; Mikutta et al., 2012; Musso et al., 2014).

Adsorption Experiments

Some 0.10 g biogenic $CaCO_3$ was added to a 50 mL polyethylene centrifuge tube containing 20 mL solution with different Cd^{2+} ($CdCl_2$), and Pb^{2+} ($Pb(NO_3)_2$) concentrations (0, 5, 10, 30, 60, 100, 150, 180, 220, and 260 mg/L: concentration based on actual measurements). The mixture was shaken at 25°C, and 100 rpm in a shaker for 24 h, and each group was tested as a set of three replicates. After shaking, the supernatant was separated by centrifuging at 8000 rpm for 15 min. The concentration of metal ions was determined by atomic absorption spectrometer (AAS, AA-6300C, Shimadzu). The adsorption amount of Cd^{2+} and Pb^{2+} by biogenic $CaCO_3$ (Q_e) was calculated based on Equation (1), the adsorption isotherms were obtained by use of C_e with Q_e, and the heavy metal adsorption rates were calculated by using of Equation (2), the formulae are as follows (Argun et al., 2007; Wang et al., 2007b; Lian et al., 2008; Ma et al., 2012; Yao et al., 2013; Zhao et al., 2014b; Liu et al., 2016):

$$Q_e(\text{mg/g}) = \frac{C_0 - C_e}{W1} \times V \quad (1)$$

$$\text{The rate of absorption (\%)} = \frac{C_0 - C_e}{C_0} \times 100 \quad (2)$$

Where C_0 and C_e are the initial, and equilibrium concentrations of the metal ions (mg/L), respectively; V represents the volume of

equilibrium liquid in the centrifuge tube (L), and W_1 is the mass of biogenic $CaCO_3$ (g).

Experimental results were analyzed with reference to the Langmuir and Freundlich isotherms (Equations 3, 4), respectively (Grimm et al., 2008; Ma et al., 2012; Mikutta et al., 2012; Wang et al., 2015):

$$\mathrm{L}: \frac{1}{\mathrm{Q_e}} = \frac{1}{Q_m \bullet K_L} \cdot \frac{1}{C_\mathrm{e}} + \frac{1}{Q_m} \quad (3)$$

$$\mathrm{F}: \mathrm{Log}\, Q_\mathrm{e} = n_\mathrm{f} \cdot \mathrm{Log}\, C_\mathrm{e} + \mathrm{Log}\, K_\mathrm{f} \quad (4)$$

Where C_e denotes the equilibrium concentration of metal ions in the supernatant (mg/L), Q_e is the adsorption amount of metal ions by biogenic $CaCO_3$ (mg/g), Q_m denotes the maximum adsorption amount of metal ions (mg/g), K_L is the adsorption coefficient of the Langmuir model (L/mg), K_f is the Freundlich constant, and n_f is the adsorption intensity constant of the Freundlich equation.

Desorption Experiments

We added 20 mL desorption liquid (Dong-Mei et al., 2003; Arias et al., 2006; Gherasim and Bourceanu, 2013; 1 mol/L $NaNO_3$, pH = 7.0) to the centrifugal tube with the precipitates therein after adsorbing any Cd^{2+} or Pb^{2+}, then the samples were shocked at 25°C, and 100 rpm for 12 h. Afterwards, the samples were centrifuged at 8000 rpm for 15 min, and AAS was used to determine the Cd^{2+} or Pb^{2+} concentrations in supernatant (C_1). Each desorption experiment was conducted in triplicate.

The desorption amount of heavy metals (Q_de) (Equation 5) and the rate of desorption (Equation 6) were calculated as follows (Gao et al., 2003; Wang et al., 2007a; Zhao et al., 2014b):

$$Q_\mathrm{de}(\mathrm{mg/g}) = \frac{C_1 \times V}{W_1} \quad (5)$$

$$\text{The rate of desorption (\%)} = \frac{Q_{de}}{Q_e} \times 100 \quad (6)$$

Where Q_de is the desorption amount of heavy metals (mg/g), V is the volume of desorption solution (L), C_1 represents the metal ion concentration of desorption supernatant (mg/L), and W_1 is the mass of biogenic $CaCO_3$ (g).

The Mechanism of Adsorption

To elucidate the adsorption mechanism of biogenic $CaCO_3$, we collected the biogenic $CaCO_3$ before and after adsorbing Cd^{2+} or Pb^{2+}, and dried it at 55°C, Afterwards, using FTIR (NEXUS670, Thermo Nicolet), XRD (Ultima IV Multipurpose, Rigaku), FESEM-EDS, and soft X-ray microscopy techniques were used to analyse the changes in structures, morphologies and elemental compositions. Meanwhile, the adsorption and desorption of Cd^{2+} (74 mg/L) and Pb^{2+} (94 mg/L) by vaterite biogenic $CaCO_3$ (prepared in LB liquid medium containing 0.8 g $CaCl_2$, referenced in Section Preparation of Micro and Nano-sized Biogenic $CaCO_3$ and Its Morphology and Chemical Composition Analysis) were also studied, and the structural changes of

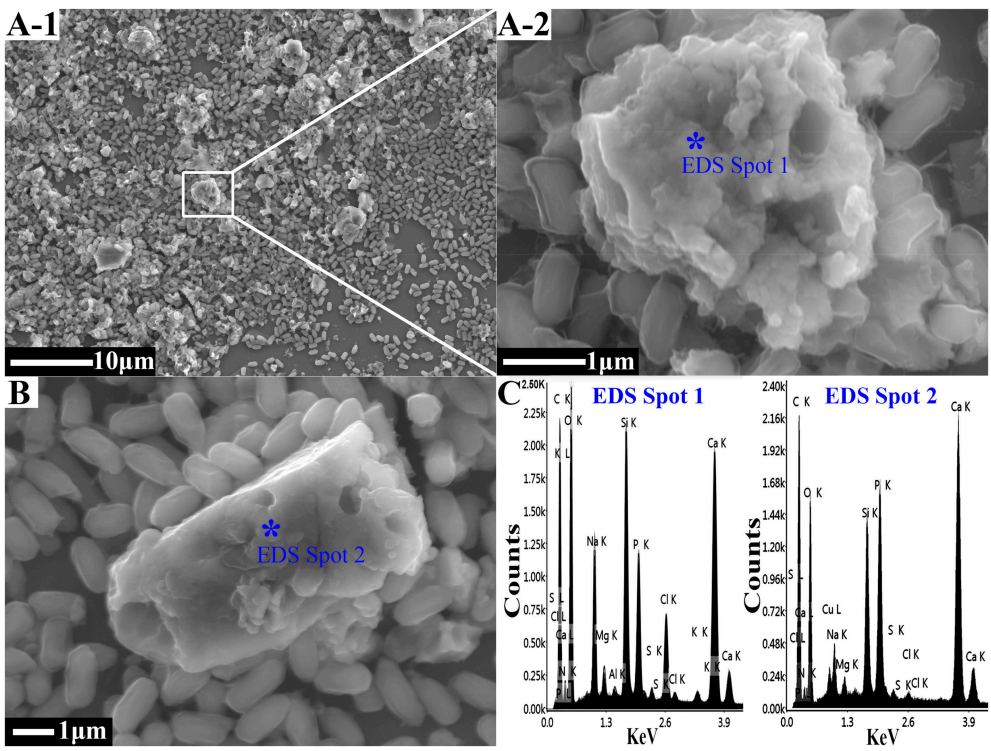

FIGURE 1 | The FESEM-EDS analysis of biogenic $CaCO_3$. **(A,B)** The FESEM images of the biogenic $CaCO_3$; among them, **A–2** is the magnification for the marked area in **A–1**. **(C)** The EDS results for the asterisk site. The "*" showed the site of the EDS analysis.

vaterite before, and after, adsorbing Cd^{2+} or Pb^{2+} were analyzed by XRD.

The Comparison of Adsorption and Desorption for Heavy Metals by Biogenic $CaCO_3$ and Bacterial Cells

We added 100 mL LB liquid medium to a clean 250 mL conical flask, sterilized it at 115°C for 20 min, then inoculated 2 mL strain from the bacterial liquid mentioned above in the experimental group, set up 10 parallel trials, and subjected them to shaking-culturation at 30°C and 180 rpm for 7 days. Then, the culture solution was centrifuged at 8000 rpm for 15 min at 4°C, whereafter, the bacterial cells were collected and dried at 55°C, and then milled to 200 mesh or finer, by agate mortar in readiness for testing.

The biogenic $CaCO_3$ including $CaCO_3$ and bacterial cells was used to clarify the advantages of biogenic $CaCO_3$ for heavy metals the adsorption. The adsorption and desorption experiments of Cd^{2+} (74 mg/L), and Pb^{2+} (94 mg/L) by biogenic $CaCO_3$ and bacterial cells were carried out using the method described in section The Adsorption and Desorption of Cd^{2+} and Pb^{2+} by Micro and Nano-sized Biogenic $CaCO_3$.

The Effect of pH on Adsorption of Biogenic $CaCO_3$ for Heavy Metals

To study the influence of pH on the removal efficiency, 0.05 g biogenic $CaCO_3$ was placed into a 50 mL polyethylene centrifuge tube containing 20 mL solution with different pH values (1, 2, 3, 4, 5, 6, 7, and 8) of 83.13 mg/g Cd^{2+} ($CdCl_2$), or 99.30 mg/g Pb^{2+} ($Pb(NO_3)_2$), respectively. The mixture was shaken at 25°C and 100 rpm for 24 h, and each group was replicated three times. The supernatant was obtained by centrifuging at 8000 rpm for 15 min. The concentrations of Cd^{2+} or Pb^{2+} in the supernatant were determined by AAS, and the heavy metal adsorption rates were calculated by use of Equation (2).

TABLE 1 | Isotherms coefficients according to Langmuir and Freundlich.

Elements	Langmuir			Freundlich		
	K_L (L/g)	Q_m (mg/g)	R^2	LogK_F(L/g)	n_f	R^2
Cd^{2+}	0.033	94.340	0.994	0.531	1.056	0.981
Pb^{2+}	0.004	416.667	0.953	0.255	0.976	0.914

RESULTS AND DISCUSSION

The Morphological and Elemental Composition Analysis of Biogenic $CaCO_3$ Sediments

Different morphologies of crystals in the sediments were observed by using FESEM. These morphologies included cauliflower-like forms, scaly aggregates, and various irregular aggregates of sediment (part of them shown in **Figures 1A,B**). EDS was used to determine the main component as being $CaCO_3$ (**Figure 1C**). The biogenic $CaCO_3$ exhibited its porous surface, corner-incomplete form, and visible irregular fine lines on its surface, thus it had both a larger internal and external specific surface area and pore volume.

The Adsorption and Desorption of Biogenic $CaCO_3$ for Cd^{2+} and Pb^{2+}

Although both Freundlich and Langmuir equations could be used to fit the isothermal adsorption process of Cd^{2+} and Pb^{2+} by biogenic $CaCO_3$, the fitting effect of Langmuir adsorption isotherm equation was more favorable, which suggested that the adsorption process was a single-molecule adsorption process (Mikutta et al., 2012; Wang et al., 2015). The maximum adsorption amounts of Cd^{2+} and Pb^{2+} by biogenic $CaCO_3$ were 94.340 and 416.667 mg/g, respectively (**Table 1**). $CaCO_3$ is an important mineral that is ubiquitous in soils, shallow grand water aquifers and marine sediments which has good adsorption properties for heavy metals (Davis et al., 1987; Garcia-Sánchez and Alvarez-Ayuso, 2002; Al-Degs et al., 2006; Lee et al., 2007; Yavuz et al., 2007). Yavuz et al. (2007) found that the maximum adsorption capacities of Cd^{2+} and Pb^{2+} by natural $CaCO_3$ were

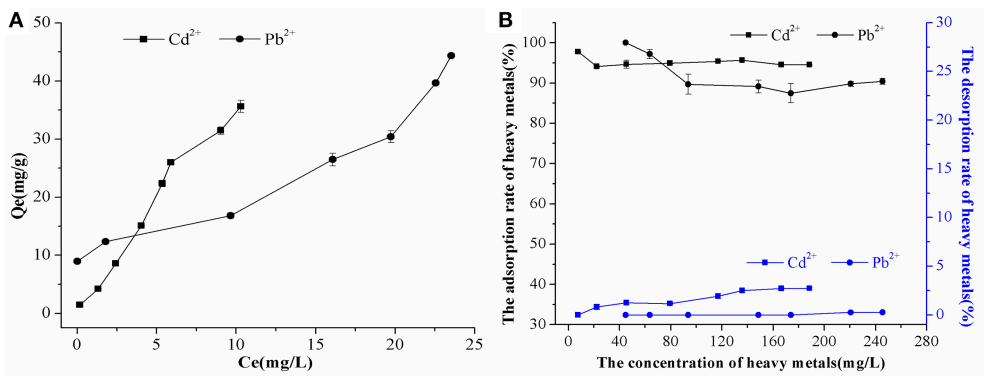

FIGURE 2 | The adsorption and desorption characteristics of Cd^{2+} and Pb^{2+} by biogenic $CaCO_3$. **(A)** The adsorption isotherm curves. **(B)** The adsorption and desorption rates. The black line represents the adsorption rate data, and the blue line represents the desorption rate data. Data represent the mean ± standard deviation (SD) of three independent experiments.

determined as 18.52 and 19.92 mg/g, respectively. This research on the adsorption of heavy metals with biogenic $CaCO_3$ induced by the strain (as a legal strain used in microbial fertilizer) is the first report, and the maximum adsorption capacities of biogenic $CaCO_3$ for heavy metals are apparently higher than that of natural calcite ($p < 0.01$), which suggests a considerable potential to immobilize or passivate heavy metals in contaminated soil.

Figure 2A showed that the adsorption amount (Q_e) of Cd^{2+} or Pb^{2+} on biogenic $CaCO_3$ increased with increasing Cd^{2+} or Pb^{2+} concentration in the equilibrium solution (C_e). When the concentration of Cd^{2+} or Pb^{2+} was between 5 and 260 mg/L, the rate of adsorption of heavy metals on biogenic $CaCO_3$ was as high as 87–100%, while the rate of desorption remained steady at 0.1–3% (**Figure 2B**), which suggest that biogenic $CaCO_3$ has a high adsorption capacity for heavy metals and carries little environmental risk. The results provide evidence that bacterial fertilizer and biogenic $CaCO_3$ may play important roles in various environments, and indeed more than previously acknowledged.

The Adsorption Mechanism

The FTIR results showed that it did not undergo a chemical precipitation reaction to produce new substances after the $CaCO_3$ had adsorbed Cd^{2+} (74 mg/L) or Pb^{2+} (94 mg/L)

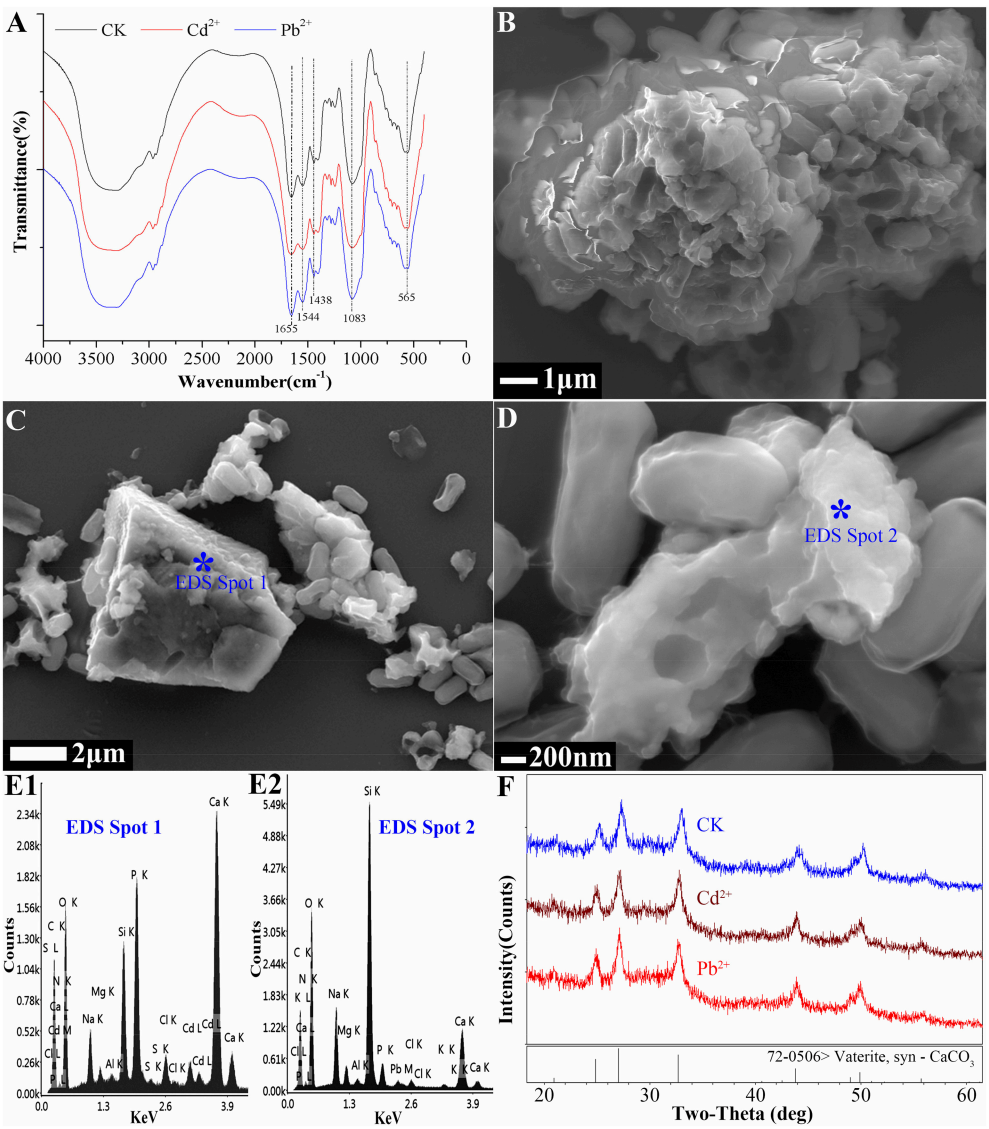

FIGURE 3 | The adsorptive mechanism analysis of Cd^{2+} and Pb^{2+} by biogenic $CaCO_3$. **(A)** The results of FTIR spectra of biogenic $CaCO_3$ before, and after, adsorbing Cd^{2+} or Pb^{2+} (CK: before adsorbing Cd^{2+} or Pb^{2+} by biogenic $CaCO_3$). **(B)** The reticular structure of biogenic $CaCO_3$ by FESEM. **(C,E1)** The result of biogenic $CaCO_3$ after adsorbing Cd^{2+} (74 mg/L) by FESEM-EDS: Cd^{2+} is visible on the surface of the biogenic $CaCO_3$. **(D,E2)** The result of biogenic $CaCO_3$ after adsorbing Pb^{2+} (94 mg/L) by FESEM-EDS: Pb^{2+} is visible on the surface of the biogenic $CaCO_3$. **(F)** The XRD results of biogenic vaterite before, and after, adsorbing Cd^{2+} and Pb^{2+} (CK: before adsorbing Cd^{2+} and Pb^{2+} by biogenic $CaCO_3$). The "*" inside the figure is the site of the EDS spot.

(**Figure 3A**); which indicated that the reaction between the biogenic $CaCO_3$ and Cd^{2+} or Pb^{2+} was mainly based on physical adsorption. The FESEM-EDS analysis showed that the adsorbed Cd^{2+} and Pb^{2+} were visible on the surface of biogenic $CaCO_3$ (**Figures 3C,E1,D,E2**). Chemical $CaCO_3$ morphology is essentially a diamond-shaped cubic structure with smooth surfaces (Lian et al., 2006; Xiao et al., 2015; Cao et al., 2016), but the biogenic $CaCO_3$ surface is porous, micro and nano-sized, the edge is incomplete, and it can stack to form a fragmented structure or form a reticular aggregate with other different forms of $CaCO_3$ according to FESEM and soft X-ray microscopy analysis (**Figures 1A,B,3B**, **Supplementary Video 1**); thus it has a larger internal and external specific surface area and pore volume, which can provide more adsorption sites and accommodation spaces for heavy metals. The XRD and TEM-SAED results indicated that the biogenic $CaCO_3$ used in this test was mainly amorphous $CaCO_3$ (**Figure 4**), and according to the reports that the amorphous $CaCO_3$ surface area is 20 times that of other crystalline forms of $CaCO_3$ (Yan and Lu, 2012), therefore, it exhibits strong adsorption properties for Cd^{2+} and Pb^{2+}.

Since there were no diffraction peaks observed from the amorphous biogenic $CaCO_3$ in the XRD result (**Figure 4A**), to clarify the adsorptive mechanism of biogenic $CaCO_3$ for heavy metals, vaterite-type biogenic $CaCO_3$ was used to adsorb Cd^{2+} (74 mg/L) or Pb^{2+} (94 mg/L), and the adsorption rates were 98.42 and 100%, respectively, moreover, the desorption rates were all zero. The XRD results revealed that, there was no new phase diffraction peak after the biogenic vaterite had adsorbed the Cd^{2+} and Pb^{2+} (**Figure 3F**), which also showed that the reaction between the biogenic $CaCO_3$ and Cd^{2+} or Pb^{2+} was mainly based on physical adsorption. It was also indicated that the Cd^{2+} or Pb^{2+} was stable in the mineral as a result of binding to the $CaCO_3$ surface adsorption sites, or entry to the $CaCO_3$ crystal pores. Consequently, biogenic $CaCO_3$ offered better adsorption properties for heavy metals. Our findings suggested that the biogenic $CaCO_3$ could be expected to be developed into a new type of heavy metals adsorbent, and might achieve the dual environmental benefits of carbon sequestration and heavy metal immobilization.

The Comparison of Adsorption and Desorption of Cd^{2+} and Pb^{2+} by Biogenic $CaCO_3$ and Bacterial Cells

Figure 5 illustrates that the adsorption rate of Cd^{2+} (74 mg/L) and Pb^{2+} (94 mg/L) by biogenic $CaCO_3$, was significantly higher than that of the bacterial cells, and the desorption rate was significantly smaller than that of the desorption rate of bacterial cells ($p < 0.01$), it suggested that the adsorption of $CaCO_3$ crystal for heavy metals was dominant and its environmental risk was

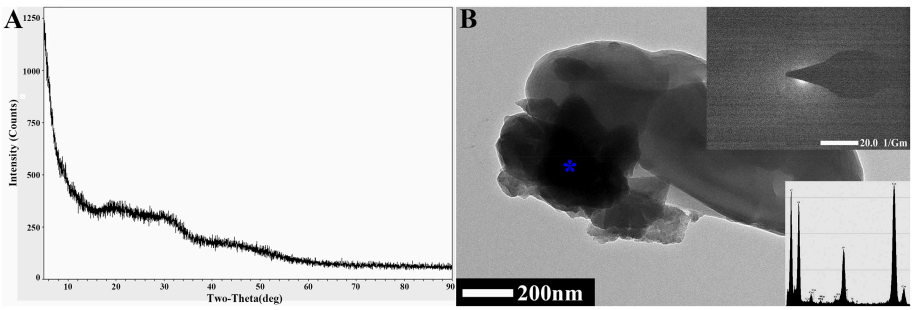

FIGURE 4 | The detection and analysis of biogenic $CaCO_3$ by XRD and TEM-SAED. **(A)** XRD detection. **(B)** TEM-SAED analysis. The "*" in the figure is the site of the EDS analysis.

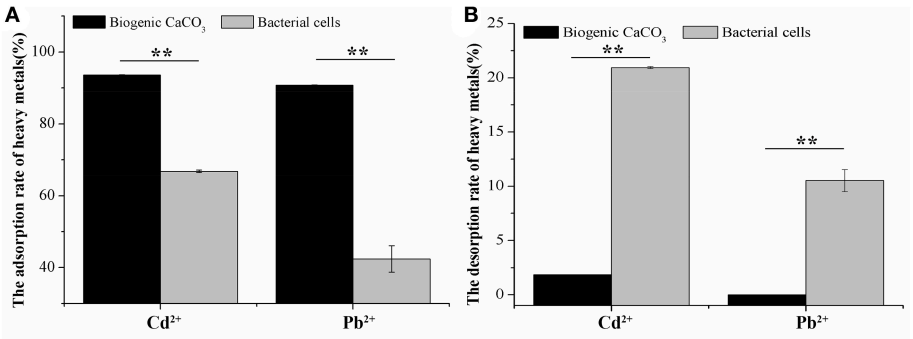

FIGURE 5 | The adsorption and desorption of Cd^{2+} or Pb^{2+} by biogenic $CaCO_3$ and bacterial cells. **(A)** The rate of adsorption (%). **(B)** The rate of desorption (%). The "*" indicates statistically significant differences between the two treatments (*t*-test, $*p < 0.05$, $**p < 0.01$). Data represent the mean ± SD of three independent experiments.

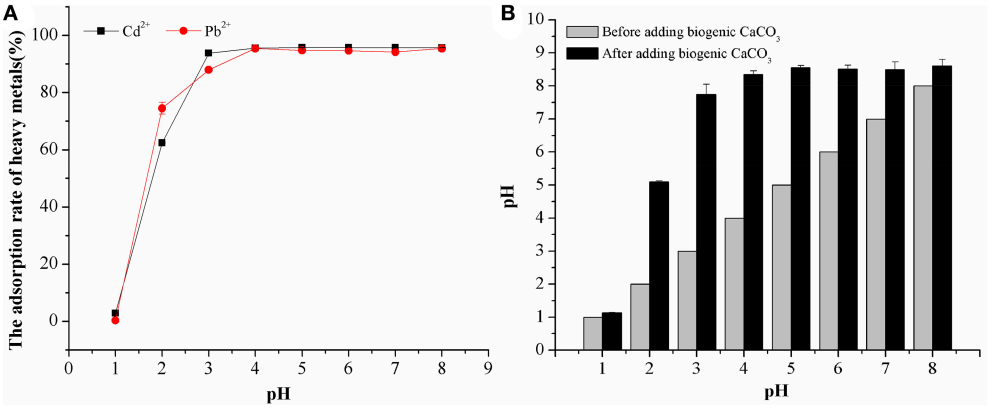

FIGURE 6 | The effect of pH on the adsorption of heavy metals by biogenetic $CaCO_3$. **(A)** The adsorption rate of biogenetic $CaCO_3$ for heavy metals under different pH conditions (%). **(B)** The variation of pH before, and after, adding biogenetic $CaCO_3$. Data represent the mean ±SD of three independent experiments.

very low, but the adsorption rate of bacterial cells for heavy metals was not only low, but also the adsorbed heavy metals would be released to the environment easily, therefore, it posed a higher environmental risk. This also suggested that the biogenic $CaCO_3$ had a larger specific surface area and rich reticular structures which contributed to its high adsorption and low desorption performance. This significant retaining ability of heavy metal ions indicates the remarkable efficiency of biogenic $CaCO_3$ as an adsorbent.

The Effect of pH on Adsorption of Biogenic $CaCO_3$ for Heavy Metals

The results in **Figure 6A** demonstrate the effects of pH on Cd^{2+} and Pb^{2+} adsorption by biogenic $CaCO_3$. The adsorption rate of these heavy metals was quite low at pH $\leq$ 1, as biogenic $CaCO_3$ could not exist at such a low pH value. At pH values from 1.0 to 4.0, the adsorption percentage increased rapidly with increasing pH; thereafter (pH >4) it did not change to any significant extent with further increases in pH and the adsorption percentage was stable at around 95% (**Figure 6A**). Similar experimental results, such as those from Ma et al. (2012) who used use chemogenic $CaCO_3$ for the adsorption of Cd^{2+} and Pb^{2+} and Merrikhpour and Jalali (2012) who used natural $CaCO_3$ for Cd^{2+}, Pb^{2+}, Cu^{2+}, Zn^{2+} adsorption, etc., can also obtain good adsorption effect when starting from an acidic pH value. Furthermore, we found that the pH value of the adsorption system was increased after adding biogenic $CaCO_3$, and the final pH value after adsorption is around 8.61 (**Figure 6B**), which should be attributable by the biogenic $CaCO_3$ and alkaline metabolites produced by *B. subtilis*. In addition, the adsorption percentages of Cd^{2+} and Pb^{2+} at pH 8 were 16.22 and 41.23% when we did not add biogenic $CaCO_3$, which were significantly lower than biogenic $CaCO_3$ adsorption percentages ($p < 0.01$). This indicated that the adsorption rate of heavy metals was mainly influenced by the biogenic $CaCO_3$ rather than the formation of heavy metal hydroxides in alkaline conditions. In summary, the high adsorption capability of the biogenic $CaCO_3$ within a wide pH range (3–8) indicated its potential application in the control of the fate of heavy metals in the natural environment.

CONCLUSIONS

The Langmuir isotherm was preferred to describe the adsorption characteristics of Cd^{2+} and Pb^{2+} by biogenic $CaCO_3$ which suggested that the adsorption process was a single molecule layer adsorption process, and the maximum adsorption amounts (Q_m) of Cd^{2+} and Pb^{2+} were 94.340 and 416.667 mg/g, respectively. Moreover, biogenic $CaCO_3$ could maintain a high adsorption capability for heavy metals within a wide pH range. The biogenic $CaCO_3$ and heavy metal ions formed a physical adsorption process, and the high efficiency and stability of the adsorption of biogenic $CaCO_3$ for Cd^{2+} and Pb^{2+} were mainly attributed to its large total specific surface area and their porous structure. These findings revealed a new perspective on the remediation of heavy metal pollution by using biogenic $CaCO_3$.

AUTHOR CONTRIBUTIONS

BL: designed this study; RL, YG, and LC: performed the laboratory work; RL, YG, LC, and BL: analyzed the data; RL and BL: wrote this manuscript; All authors have read and approved the final manuscript.

ACKNOWLEDGMENTS

This work was jointly supported by the National Natural Science Foundation of China (Grant No. 41373078) and the Priority Academic Program Development of Jiangsu Higher Education Institutions (PAPD).

SUPPLEMENTARY MATERIAL

The Supplementary Material for this article can be found online at: https://www.frontiersin.org/articles/10.3389/fmicb.2018.00041/full#supplementary-material

Supplementary Video 1 | The video of biogenic $CaCO_3$ by soft x-ray microscopy.

REFERENCES

Abollino, O., Aceto, M., Malandrino, M., Sarzanini, C., and Mentasti, E. (2003). Adsorption of heavy metals on Na-montmorillonite. Effect of pH and organic substances. *Water Res.* 37, 1619–1627. doi: 10.1016/S0043-1354(02)00524-9

Al-Degs, Y. S., El-Barghouthi, M. I., Issa, A. A., Khraisheh, M. A., and Walker, G. M. (2006). Sorption of Zn (II), Pb (II), and Co (II) using natural sorbents: equilibrium and kinetic studies. *Water Res.* 40, 2645–2658. doi: 10.1016/j.watres.2006.05.018

Apiratikul, R., and Pavasant, P. (2008). Batch and column studies of biosorption of heavy metals by *Caulerpa lentillifera*. *Bioresour. Technol.* 99, 2766–2777. doi: 10.1016/j.biortech.2007.06.036

Argun, M. E., Dursun, S., Ozdemir, C., and Karatas, M. (2007). Heavy metal adsorption by modified oak sawdust: thermodynamics and kinetics. *J. Hazard. Mater.* 141, 77–85. doi: 10.1016/j.jhazmat.2006.06.095

Arias, M., Pérez-Novo, C., López, E., and Soto, B. (2006). Competitive adsorption and desorption of copper and zinc in acid soils. *Geoderma* 133, 151–159. doi: 10.1016/j.geoderma.2005.07.002

Aziz, H. A., Adlan, M. N., and Ariffin, K. S. (2008). Heavy metals (Cd, Pb, Zn, Ni, Cu and Cr(III)) removal from water in Malaysia: post treatment by high quality limestone. *Bioresour. Technol.* 99, 1578–1583. doi: 10.1016/j.biortech.2007.04.007

Babel, S., and Kurniawan, T. A. (2003). Low-cost adsorbents for heavy metals uptake from contaminated water: a review. *J. Hazard. Mater.* 97, 219–243. doi: 10.1016/S0304-3894(02)00263-7

Cai, G. B., Zhao, G. X., Wang, X. K., and Yu, S. H. (2010). Synthesis of polyacrylic acid stabilized amorphous calcium carbonate nanoparticles and their application for removal of toxic heavy metal ions in water. *J. Phys. Chem C* 114, 12948–12954. doi: 10.1021/jp103464p

Cao, C., Jiang, J., Sun, H., Huang, Y., Tao, F., and Lian, B. (2016). Carbonate mineral formation under the influence of limestone-colonizing actinobacteria: morphology and polymorphism. *Front. Microbiol.* 7:366. doi: 10.3389/fmicb.2016.00366

Chen, X. B., Judith, V. W., Conca J. L., and Peurrung, L. M. (1997). Effects of pH on heavy metal sorption on mineral apatite. *Environ. Sci. Technol.* 31, 624–631. doi: 10.1021/es950882f

Davis, J. A., Fuller, C. C., and Cook, A. D. (1987). A model for trace metal sorption processes at the calcite surface: adsorption of Cd^{2+} and subsequent solid solution formation. *Geochim. Cosmochim. Acta* 51, 1477–1490. doi: 10.1016/0016-7037(87)90330-9

Dong-Mei, Z., Huai-Man, C., Shen-Qiang, W., and Chun-Rong, Z. (2003). Effects of organic acids, o-phenylenediamine and pyrocatechol on cadmium adsorption and desorption in soil. *Water Air Soil Pollut.* 145, 109–121. doi: 10.1023/A:1023636330221

Dupraz, C., Reid, R. P., Braissant, O., Decho, A. W., Norman, R. S., and Visscher, P. T. (2009). Processes of carbonate precipitation in modern microbial mats. *Earth Sci. Rev.* 96, 141–162. doi: 10.1016/j.earscirev.2008.10.005

Farrah, H., and Pickering, W. F. (1979). pH effects in the adsorption of heavy metal ions by clays. *Chem. Geol.* 25, 317–326. doi: 10.1016/0009-2541(79)90063-9

Gao, Y., Kan, A. T., and Tomson, M. B. (2003). Critical evaluation of desorption phenomena of heavy metals from natural sediments. *Environ. Sci. Technol.* 37, 5566–5573. doi: 10.1021/es034392w

Garcia-Sánchez, A., and Alvarez-Ayuso, E. (2002). Sorption of Zn, Cd and Cr on calcite. Application to purification of industrial wastewaters. *Miner. Eng.* 15, 539–547. doi: 10.1016/S0892-6875(02)00072-9

Gherasim, C., and Bourceanu, G. (2013). Removal of chromium (VI) from aqueous solutions using a polyvinyl-chloride inclusion membrane: experimental study and modelling. *Chem. Eng. J.* 220, 24–34. doi: 10.1016/j.cej.2013.01.058

Grimm, A., Zanzi, R., Björnbom, E., and Cukierman, A. L. (2008). Comparison of different types of biomasses for copper biosorption. *Bioresour. Technol.* 99, 2559–2565. doi: 10.1016/j.biortech.2007.04.036

Han, J., Lian, B., and Ling, H. (2013). Induction of calcium carbonate by *Bacillus cereus*. *Geomicrobiol. J.* 30, 682–689. doi: 10.1080/01490451.2012.758194

Kavamura, V. N., and Esposito, E. (2010). Biotechnological strategies applied to the decontamination of soils polluted with heavy metals. *Biotechnol. Adv.* 28, 61–69. doi: 10.1016/j.biotechadv.2009.09.002

Kobya, M., Demirbas, E., Senturk, E., and Ince, M. (2005). Adsorption of heavy metal ions from aqueous solutions by activated carbon prepared from apricot stone. *Bioresour. Technol.* 96, 1518–1521. doi: 10.1016/j.biortech.2004.12.005

Lagadic, I. L., Mitchell, M. K., and Payne, B. D. (2001). Highly effective adsorption of heavy metal ions by a thiol-functionalized magnesium phyllosilicate clay. *Environ. Sci. Technol.* 35, 984–990. doi: 10.1021/es001526m

Lee, M., Paik, I. S., Kim, I., Kang, H., and Lee, S. (2007). Remediation of heavy metal contaminated groundwater originated from abandoned mine using lime and calcium carbonate. *J. Hazard. Mater.* 144, 208–214. doi: 10.1016/j.jhazmat.2006.10.007

Lian, B., Chen, Y., Zhao, J., Teng, H. H., Zhu, L., and Yuan, S. (2008). Microbial flocculation by *Bacillus* mucilaginosus: applications and mechanisms. *Bioresour. Technol.* 99, 4825–4831. doi: 10.1016/j.biortech.2007.09.045

Lian, B., Hu, Q., Chen, J., Ji, J., and Teng, H. H. (2006). Carbonate biomineralization induced by soil bacterium *Bacillus megaterium*. *Geochim. Cosmochim. Acta* 70, 5522–5535. doi: 10.1016/j.gca.2006.08.044

Liu, J., Ge, X., Ye, X., Wang, G., Zhang, H., Zhou, H., et al. (2016). 3D graphene/δ-MnO 2 aerogels for highly efficient and reversible removal of heavy metal ions. *J. Mater. Chem. A* 4, 1970–1979. doi: 10.1039/C5TA08106H

Ma, X., Li, L., Yang, L., Su, C., Wang, K., Yuan, S., et al. (2012). Adsorption of heavy metal ions using hierarchical $CaCO_3$-maltose meso/macroporous hybrid materials: adsorption isotherms and kinetic studies. *J. Hazard. Mater.* 209–210, 467. doi: 10.1016/j.jhazmat.2012.01.054

Meng, Y. T., Zheng, Y. M., Zhang, L. M., and He, J. Z. (2009). Biogenic Mn oxides for effective adsorption of Cd from aquatic environment. *Environ. Pollut.* 157, 2577–2583. doi: 10.1016/j.envpol.2009.02.035

Merrikhpour, H., and Jalali, M. (2012). Waste calcite sludge as an adsorbent for the removal of cadmium, copper, lead, and zinc from aqueous solutions. *Clean Technol. Environ.* 14, 845–855. doi: 10.1007/s10098-012-0450-0

Mikutta, R., Baumgärtner, A., Schippers, A., Haumaier, L., and Guggenberger, G. (2012). Extracellular polymeric substances from *Bacillus subtilis* associated with minerals modify the extent and rate of heavy metal sorption. *Environ. Sci. Technol.* 46, 3866–3873. doi: 10.1021/es204471x

Mitchell, A. C., Dideriksen, K., Spangler, L. H., Cunningham, A. B., and Gerlach, R. (2010). Microbially enhanced carbon capture and storage by mineral-trapping and solubility-trapping. *Environ. Sci. Technol.* 44, 5270–5276. doi: 10.1021/es903270w

Moreau, J. W., Fournelle, J. H., and Banfield, J. F. (2013). Quantifying heavy metals sequestration by sulfate-reducing bacteria in an Acid mine drainage-contaminated natural wetland. *Front. Microbiol.* 4:43. doi: 10.3389/fmicb.2013.00043

Musso, T. B., Parolo, M. E., Pettinari, G., and Francisca, F. M. (2014). Cu (II) and Zn (II) adsorption capacity of three different clay liner materials. *J. Environ. Manage.* 146, 50–58. doi: 10.1016/j.jenvman.2014.07.026

Pan, J., Liu, R., and Tang, H. (2007). Surface reaction of *Bacillus cereus* biomass and its biosorption for lead and copper ions. *J. Environ. Sci. China* 19, 403–408. doi: 10.1016/S1001-0742(07)60067-9

Pavasant, P., Apiratikul, R., Sungkhum, V., Suthiparinyanont, P., Wattanachira, S., and Marhaba, T. F. (2006). Biosorption of Cu^{2+}, Cd^{2+}, Pb^{2+}, and Zn^{2+} using dried marine green macroalga *Caulerpa lentillifera*. *Bioresour. Technol.* 97, 2321–2329. doi: 10.1016/j.biortech.2005.10.032

Phillips, A. J., Lauchnor, E., Eldring, J., Esposito, R., Mitchell, A. C., Gerlach, R., et al. (2013). Potential CO_2 leakage reduction through biofilm-induced calcium carbonate precipitation. *Environ. Sci. Technol.* 47, 142–149. doi: 10.1021/es301294q

Ren, Y., Abbood, H. A., He, F., Peng, H., and Huang, K. (2013). Magnetic EDTA-modified chitosan/SiO_2/Fe_3O_4 adsorbent: preparation, characterization, and application in heavy metal adsorption. *Chem. Eng. J.* 226, 300–311. doi: 10.1016/j.cej.2013.04.059

Santos, D. K., Resende, A. H., and de Almeida, D. G. (2017). Candida lipolytica UCP0988 biosurfactant: potential as a bioremediation agent and in formulating a commercial related product. *Front. Microbiol.* 8:767. doi: 10.3389/fmicb.2017.00767

The Ministry of Environmental Protection (2014). *The Ministry of Land and Resources Report on the National Soil Contamination Survey*. Available online at: http://www.mep.gov.cn/gkml/hbb/qt/201404/t20140417_270670.htm (Accessed April 17, 2014).

The Ministry of Land and Resources (2015). *Geological Survey Bureau of China, The Report on the Geochemical Survey of Cultivated Land in China*. Available online at: http://www.cgs.gov.cn/xwl/ddyw/201603/t20160309_302254.html (Accessed June 25, 2015).

Tsekova, K., Todorova, D., Dencheva, V., and Ganeva, S. (2010). Biosorption of copper(II) and cadmium(II) from aqueous solutions by free and immobilized biomass of *Aspergillus niger*. *Bioresour. Technol.* 101, 1727–1731. doi: 10.1016/j.biortech.2009.10.012

Üçer, A., Uyanik, A., and Aygün, S. F. (2006). Adsorption of Cu (II), Cd (II), Zn (II), Mn (II) and Fe (III) ions by tannic acid immobilised activated carbon. *Sep. Purif. Technol.* 47, 113–118. doi: 10.1016/j.seppur.2005.06.012

Wang, B., Lehmann, J., Hanley, K., Hestrin, R., and Enders, A. (2015). Adsorption and desorption of ammonium by maple wood biochar as a function of oxidation and pH. *Chemosphere* 138, 120–126. doi: 10.1016/j.chemosphere.2015.05.062

Wang, L. K., Hung, Y.-T., and Shammas, N. K. (2007a). *Advanced Physicochemical Treatment Technologies*. Totowa, NJ: Humana Press.

Wang, S., Nan, Z., Zeng, J., and Hu, T. (2007b). Desorption of zinc by the kaolin from Suzhou, China. *Appl. Clay Sci.* 37, 221–225. doi: 10.1016/j.clay.2006.12.003

Wolthers, M., Charlet, L., and Van Cappellen, P. (2008). The surface chemistry of divalent metal carbonate minerals; a critical assessment of surface charge and potential data using the charge distribution multi-site ion complexation model. *Am. J. Sci.* 308, 905–941. doi: 10.2475/08.2008.02

Xiao, L., Lian, B., Hao, J., Liu, C., and Wang, S. (2015). Effect of carbonic anhydrase on silicate weathering and carbonate formation at present day CO_2 concentrations compared to primordial values. *Sci. Rep.* 5:7733. doi: 10.1038/srep07733

Yan, X., and Lu, Y. (2012). *The Key Technologies of Light and Nano Calcium Carbonate*. Beijing: Chemical Industry Press.

Yao, M., Lian, B., Dong, H., Hao, J., and Liu, C. (2013). Iron and lead ion adsorption by microbial flocculants in synthetic wastewater and their related carbonate formation. *J. Environ. Sci. China* 25, 2422–2428. doi: 10.1016/S1001-0742(12)60151-X

Yavuz, Ö., Guzel, R., Aydin, F., Tegin, I., and Ziyadanogullari, R. (2007). Removal of cadmium and lead from aqueous solution by calcite. *Pol. J. Environ. Stud.* 16, 467–471. Available online at: https://www.researchgate.net/publication/279574155

Zhao, F., Ma, Y., Zhu, Y., Tang, Z., and McGrath, S. P. (2014a). Soil contamination in China: current status and mitigation strategies. *Environ. Sci. Technol.* 49, 750–759. doi: 10.1021/es5047099

Zhao, X., Jiang, T., and Du, B. (2014b). Effect of organic matter and calcium carbonate on behaviors of cadmium adsorption–desorption on/from purple paddy soils. *Chemosphere* 99, 41–48. doi: 10.1016/j.chemosphere.2013.09.030

Conflict of Interest Statement: The authors declare that the research was conducted in the absence of any commercial or financial relationships that could be construed as a potential conflict of interest.

frontiers in Microbiology

ORIGINAL RESEARCH
published: 02 February 2018
doi: 10.3389/fmicb.2018.00040

Microbial Diversity and Mineralogical-Mechanical Properties of Calcitic Cave Speleothems *in Natural* and *in Vitro* Biomineralization Conditions

Navdeep K. Dhami[1], Abhijit Mukherjee[1] and Elizabeth L. J. Watkin[2]*

[1] Biologically Activated Materials Laboratory, Department of Civil Engineering, Curtin University, Perth, WA, Australia, [2] School of Biomedical Sciences, Curtin Health Innovation Research Institute-Biosciences, Curtin University, Perth, WA, Australia

OPEN ACCESS

Edited by:
Doug LaRowe, University of Southern California, United States

Reviewed by:
Amy Michele Grunden, North Carolina State University, United States
Juliane Hopf, University of Notre Dame, United States

***Correspondence:**
Navdeep K. Dhami
navdeep.dhami@curtin.edu.au

Specialty section:
This article was submitted to Microbiological Chemistry and Geomicrobiology, a section of the journal Frontiers in Microbiology

Received: *09 April 2017*
Accepted: *09 January 2018*
Published: *02 February 2018*

Citation:
Dhami NK, Mukherjee A and Watkin ELJ (2018) Microbial Diversity and Mineralogical-Mechanical Properties of Calcitic Cave Speleothems in Natural and in Vitro Biomineralization Conditions. Front. Microbiol. 9:40. doi: 10.3389/fmicb.2018.00040

Natural mineral formations are a window into important processes leading to carbon storage and mineralized carbonate structures formed through abiotic and biotic processes. In the current study, we made an attempt to undertake a comprehensive approach to characterize the mineralogical, mechanical, and microbial properties of different kinds of speleothems from karstic caves; with an aim to understand the bio-geo-chemical processes in speleothem structures and their impact on nanomechanical properties. We also investigated the biomineralization abilities of speleothem surface associated microbial communities *in vitro*. Mineralogical profiling using techniques such as X-ray powder Diffraction (XRD) and Tescan Integrated Mineral Analyzer (TIMA) demonstrated that calcite was the dominant mineral in the majority of speleothems with Energy Dispersive X-ray Analysis (EDS) indicating a few variations in the elemental components. Differing proportions of polymorphs of calcium carbonate such as aragonite and vaterite were also recorded. Significant variations in trace metal content were recorded through Inductively Coupled Plasma Mass Spectrometer (ICP-MS). Scanning Electron Microscopy (SEM) analysis revealed differences in morphological features of the crystals which varied from triangular prismatic shapes to etched spiky forms. Microbial imprints and associations were seen in a few sections. Analysis of the associated microbial diversity showed significant differences between various speleothems at Phylum level; although Proteobacteria and Actinobacteria were found to be the predominant groups. Genus level microbial associations showed a relationship with the geochemistry, mineralogical composition, and metal content of the speleothems. The assessment of nanomechanical properties measured by Nanoindentation revealed that the speleothems with a dominance of calcite were stronger than the speleothems with mixed calcium carbonate polymorphs and silica content. The *in vitro* metabolic activity of the microbial communities associated with the surfaces of the speleothems resulted in calcium carbonate crystal precipitation. Firmicutes and Proteobacteria dominated these populations, in contrast to the

populations seen in natural systems. The precipitation of calcium carbonate crystals *in vitro* indicated that microbial metabolic activity may also play an important role in the synthesis and dissociation of biominerals in the natural environment. Our study provides novel evidence of the close relationship between mineralogy, microbial ecology, geochemistry, and nanomechanical properties of natural formations.

Keywords: speleothem, biomineralization, microbial diversity, nanoindentation, calcium carbonate precipitation, mineralogy

INTRODUCTION

Biomineralization is a naturally occurring process where microbial metabolic activity influences the formation of geological structures (Lowenstam, 1981; Hammes and Verstraete, 2002; Hamilton, 2003). A variety of microbial metabolic pathways including photosynthesis, ammonification, denitrification, ureolysis, and methane oxidation have been shown to influence redox conditions and lead to the precipitation of carbonates in different natural environments (Fortin et al., 1997; Douglas and Beveridge, 1998; Zhu and Dittrich, 2016). Bacterial surfaces including cell walls and extracellular polymeric substances (EPS) have also been reported to act as important sites for carbonate mineral nucleation and growth (Douglas and Beveridge, 1998; Bains et al., 2015). The potential for microbes to synthesize carbonates has recently emerged as a prospective technology, called as Microbially Induced Calcium Carbonate Precipitation (MICCP), for civil and environmental engineering applications (Skinner and Jahren, 2004; Phillips et al., 2013; Zhu and Dittrich, 2016). Current usage of the technology includes remediation of heavy metal polluted sites, sequestration of CO_2, and the construction of biocement (Dhami et al., 2012, 2014, 2016, 2017b; Dejong et al., 2013; Zhu and Dittrich, 2016). Several breakthroughs have been made at laboratory and field scale in the creation and utilization of biomineralized carbonates (De Muynck et al., 2010; Phillips et al., 2013; Dhami et al., 2017a; Porter et al., 2017). The application of this technology offers the advantage of high sustainability due to its synthesis at ambient temperatures and has spurred research into exploration of the properties of naturally mineralized structures (Cacchio et al., 2003; Phillips et al., 2013). Although researchers from specializations such as Geology, Microbiology, Environment, and Engineering have contributed to the information on geological formations from separate perspectives; a connection linking mineralogy, microbiology, and mechanical characterization of such biogenically/abiogenically formed natural formations is lacking. A deeper and fundamental understanding of bio-geo-chemical properties of naturally mineralized structures along with the mechanical properties of these materials is imperative (Northup and Lavoie Diana, 2001; Dhami et al., 2012, 2013b; Zepeda Mendoza et al., 2016).

Geological formations such as caves provide a window into one such environment where mineralized carbonate deposits are formed over geological timescales (Buhmann and Dreybrodt, 1984; Short et al., 2005; Rusznyak et al., 2012). The myriad of rock like deposits in caves are commonly known as speleothems; which vary in range of shapes. These structures are known by different names as stalactites, stalagmites, moonmilk, drip stones, and flowstones depending upon their location (from floors, walls to ceilings) and appearance (soft, spongy, fibrous, or stony) (Borsato et al., 2000; Jones, 2001; Melim et al., 2008). The inorganic and physical chemistry that drive these phenomena is well established (Banks et al., 2010; Pacton et al., 2013), however, a growing body of research indicates that microorganisms can play an important role in carbonate precipitation during speleothem growth (Banks et al., 2010; Rusznyak et al., 2012; Ronholm et al., 2014). Several studies on the analysis of the mineralogy and geochemistry of different cave environments have been conducted (White, 1962; Harmon et al., 1983; Hill and Forti, 1986; Leél-Őssy et al., 2011). The majority of speleothems have been found to be calcareous and composed of calcium carbonate polymorphs such as calcite, vaterite, and aragonite (Ronholm et al., 2014; Demény et al., 2016; Garcia et al., 2016). The growth of speleothems through calcite precipitation has long been viewed as an abiogenic process (Kendall and Broughton, 1978; Broughton, 1983a,b,c). However, mineral deposits that are difficult to explain through geologic or inorganic processes raise the possibility of microbial activity in caves (Jones, 2001). For example, in the case of moonmilk, carbonate precipitation is formed either by direct precipitation of calcite via microbial metabolic activity or by the formation of nucleation surface on which minerals precipitate (Northup et al., 2003; Cuezva et al., 2012). A few studies have also reported the biogenic origins of calcified structures such as "pool fingers" and "U-loops" (Tomczyk-Żak and Zielenkiewicz, 2015). Some studies claim that bacteria produce carbonate minerals as a result of passive growth while others report that chemically reactive cell walls of bacteria act as nucleation sites binding mineral forming elements leading to growth of crystals in oversaturated solutions (Fortin et al., 1997; Barabesi et al., 2007; Dhami et al., 2013a). Researchers have demonstrated that by interacting with minerals, microorganisms play an important role in the formation of caves although little cause and effect has been elucidated (Tomczyk-Żak and Zielenkiewicz, 2015). Cave geochemistry, physico-chemical conditions, and mineralogy has also been reported to have a significant impact on the microbiome and the interactions of these microbes with minerals further play a significant role in the formation and characteristics of biomineralized speleothems (Zepeda Mendoza et al., 2016).

A number of studies have investigated microbial biofilms on cave surfaces (Adetutu et al., 2012; Pacton et al., 2013; Barton et al., 2014; Wu et al., 2015) and others have reported the microbial diversity of caves such as the Lechuguilla Cave in New Mexico (Cunningham et al., 1995; Northup et al., 2003), the

sulfidic Frasassi Cave system in Italy, the Movile Cave in Romania (Macalady et al., 2007; Chen et al., 2009), the nitrate/nitrite-dominated Nullarbor Cave in Australia (Holmes et al., 2001), karstic caves of Herrenberg Germany (Rusznyak et al., 2012), and Tjuv-Ante's Cave in Sweden (Zepeda Mendoza et al., 2016). The existence of varying calcium carbonate polymorphs in these materials has also been related to biogenic activity. A few authors have attributed the precipitation of different types of carbonate deposits in moonmilk to the activity of indigenous microbial populations. These deposits vary from nano-fibers to micro-meter sized needle-fiber crystals in a form of monocrystalline rods and polycrystalline chains (Baskar et al., 2008b; Cuezva et al., 2012; Maciejewska et al., 2017). Microbes have also been reported to mediate a wide range of processes that affect the internal crystal fabric (Jones, 2010) with carbonate precipitation and heterotrophic processes through nitrogen metabolism including ureolysis, ammonification, and nitrate reduction have been reported to play more important roles than photosynthesis (low light conditions) and methanogenesis (Castanier et al., 2000; Banks et al., 2010). Although a few studies have been conducted on the microbial diversity and mineralogy of different cave deposits and speleothems, this area remains relatively unexplored.

Mechanical properties of biomineralized geological formations can provide insights for exploring the potential of microbial carbonate based cements for engineering applications. But in many cases, the non-availability of sufficient quantities of such structures for standard material testing (due to their heritage status) makes it difficult to investigate their mechanical properties. For mechanical testing on (sub) micrometer scale, nanoindentation (also referred to as load and depth-sensing indentation (DSI)) has recently gained attention (Presser et al., 2010). This technique offers the advantage of high accuracy and reliability along with the ability to test small amounts of material; making this method particularly suitable for the speleothems. Fortunately, a few such results are available for rock minerals (Zhu et al., 2007), single calcite crystals (Calvaresi et al., 2013; Dhami et al., 2016), hydroxyapatite crystals (Zamiri and De, 2011), carp otoliths (Ren et al., 2013), and sponge spicules (Müller et al., 2014). This encourages the use of this tool to investigate nano-mechanical properties of different cave speleothems.

Whether the formation of cave speleothems is biogenic or abiogenic or a combination of both is a matter of debate. A few studies have demonstrated that bacteria isolated from cave environments are capable of forming similar crystals from organic calcium salts *in vitro* using acetate rich B4 medium (Rusznyak et al., 2012; Garcia et al., 2016). Maciejewska et al. (2017) found amino acid/peptide ammonification to be more widespread compared to ureolysis in moonmilk formation. The investigation of microbial communities associated with cave speleothems for their biomineralization potential under supplementation of similar organic calcium salts will shed light on the biogenic routes of mineralization, as well as exploring the change in microbial community dynamics under enrichment conditions *in vitro* compared to the native profiles.

This paper aims to characterize the mineralogical, elemental and nano-mechanical properties of different cave speleothems as well as the associated microbiomes. We investigated the biomineralization potential of surface associated microbial communities along with microbial community dynamics under *in vitro* conditions. This is the first study on the collective characterization of mineralogical, microbial, and mechanical properties of cave speleothems to elucidate biogenic mineralization processes.

The Leeuwin-Naturaliste ridge in the Margaret River region of Southwest Western Australia is home to a number of karstic caves stretching for approximately 90 km between Cape Leeuwin and Cape Naturaliste with the Indian Ocean to the west, Geographe Bay to the north and the Southern Ocean to the south (Jasinska, 1997; Eberhard, 2004; Eberhard and Davies, 2011). This provided us with the opportunity to investigate distinctly different cave formations. We examined different cave deposits (stalagmites, stalactites, moonmilk) from three unexplored caves where permission was granted for access. An investigation of mineralized cave speleothems in their natural state as well as under enriched conditions *in vitro* is presented with the aim to: (a) evaluate mineralogical, chemical, and nanomechanical properties of different cave speleothems, (b) elucidate the microbial diversity associated with different cave speleothems and, (c) investigate the potential of speleothem associated microbial communities in the formation of carbonate minerals under *in vitro* conditions as well as identification of microbial communities co-responsible for carbonate precipitation in laboratory conditions for analysis of microbial community shifts in comparison to Natural environments.

MATERIALS AND METHODS

Description of Caves

Margaret River is located in Western Australia, 277 km (172 mi) SSW of Perth and 48 km (30 mi) SW of Busselton at 33°57′18″S 115°04′30″E. The climate is humid Mediterranean with an average annual rainfall of around 1,130 mm (44 in) (Eberhard, 2004). Complete details about the cave formations and the environment involved have been reported by Eberhard (2004). Permission for the current study was provided by the Augusta Margaret River Tourism Association for sampling calcitic deposits and speleothem sections in a limited number of locations in three caves (Lake Cave, Moondyne Cave, Mammoth Cave) (**Figures 1i,ii**). The speleothems sampled are highlighted in **Figure 2**. In the case of Mammoth Cave, parts of stalactite and stalagmite that had been already shed were provided.

Sampling of Cave Speleothems

Sampling of calcitic deposits from different formations in each cave (up to 10 g) was conducted using sterile forceps, spatula and chisel. Moonmilk, stalagmite, and stalactite samples were collected from Lake Cave, calcitic deposits were collected from the floor of Moondyne Cave and deposits of stalagmites and stalactites were provided from Mammoth Cave (**Figure 2** and **Table 1**). Sampling locations were selected based on

FIGURE 1 | (i,ii) Geographical location of Margaret River Caves, Western Australia, Australia [source: Google (Googlemaps, 2016)].

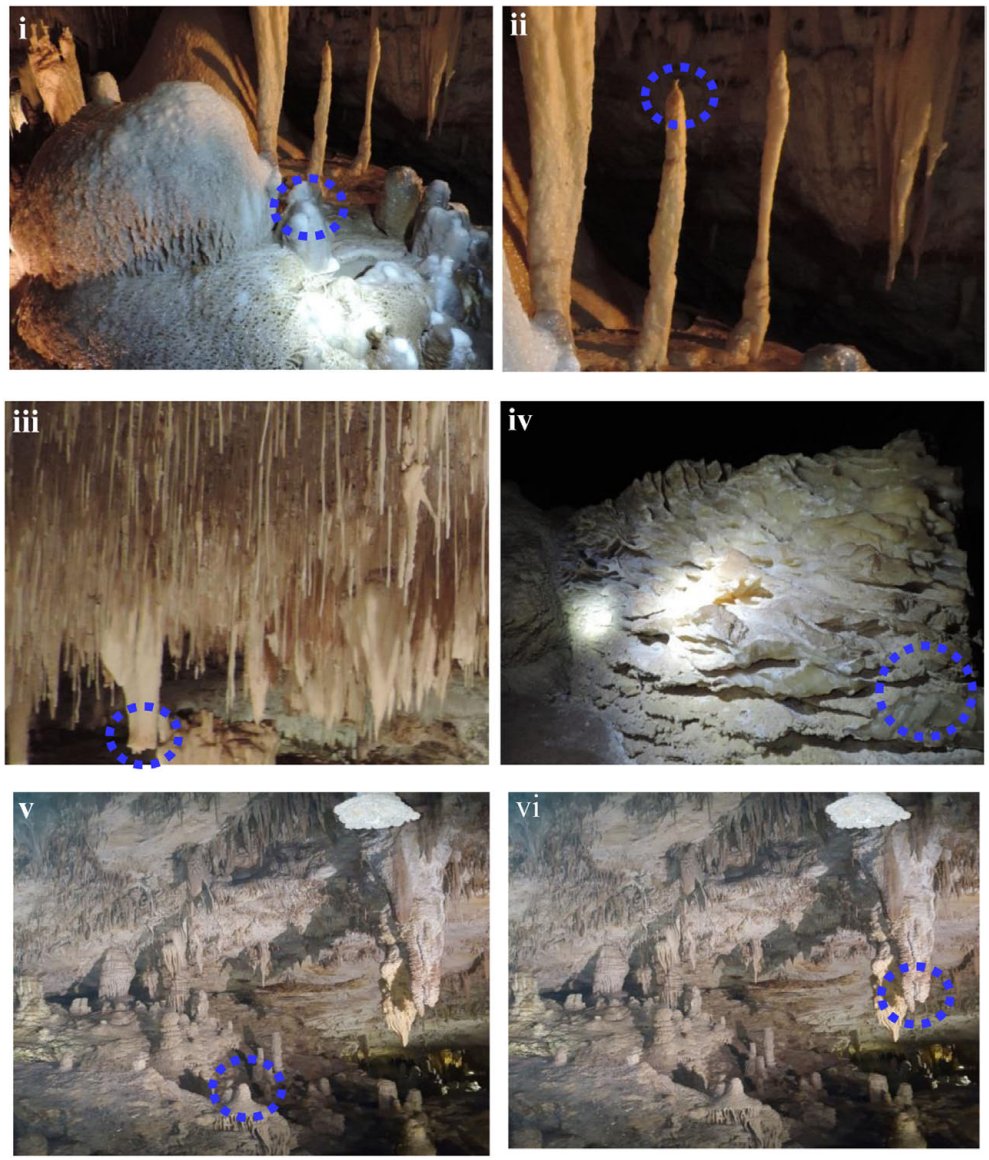

FIGURE 2 | Cave speleothems collected from **(i–iii)** Lake Cave **(iv)** Moondyne Cave **(v,vi)** Mammoth Cave.

TABLE 1 | Cave speleothem type, site and labeling.

Site	Speleothem
Lake Cave	
1	Moonmilk
2	Stalagmite
3	Stalactite
Moondyne Cave	
1	Calcitic floor stalagmite deposit
Mammoth Cave	
1	Stalagmite
2	Stalactite

accessibility, regulatory restrictions and special features observed. All the specimens were collected aseptically, transported under refrigeration to the laboratory, and stored at −20°C until use. The samples were separated into three sections in order to correlate mineralogical, mechanical, and microbial characteristics.

Determination of Carbon, Nitrogen, and Metal Content

One gram of each sample was added to 10 mL deionized water and shaken briefly. Total Al, Mg, Ca, Fe, Mn, and Na analyses were conducted on samples that were dried at 100°C, extracted with aqua regia (Hoffman, 1991) and analyzed with an inductively coupled plasma mass spectrometer (ICP-MS) (PQ3S; Thermo Electron, United Kingdom) following Rusznyak et al. (2012). For the estimation of Carbon and Nitrogen, the samples were freeze dried, finely ground to 200 mesh size (<75 μm), homogenized and analyzed using a CN analyser (Vario Max; Elementary Analysensysteme GmbH, Germany). Inorganic carbon was determined by measuring the total amount of carbon after removal of organic carbon (OC) and ignition of samples for 4 h at 550°C (Grüneberg et al., 2010). OC concentrations were then calculated from the difference between total and inorganic carbon concentrations. For each test triplicate samples were analyzed.

Morphological Characterization of Speleothems by SEM

For scanning electron microscopic analysis (SEM) all samples were fixed in 4% formaldehyde in phosphate-buffered saline (PBS) and kept at 4°C until examination. The samples were rinsed in 0.2 M PBS (pH 7.4) for 1 h and dehydrated in a series of graded ethyl alcohol then sputter coated with platinum (thickness of approximately 8 nm) using a SCD005 sputter coater (BAL-TEC, Liechtenstein) to avoid surface charging. Finally, the specimens were investigated with Zeiss Neon 40 EsB dual beam FESEM/FIB-SEM for imaging at 10 kV and WD = 10–11 mm.

Chemical Characterization of Speleothems by XRD, EDS, and TIMA

X ray diffraction (XRD) spectra were obtained by crushing around 1 g sample of each speleothem and subjecting it to X' Pert PRO diffractometer with a Cu anode (40 kV and 30 mA). The scanning was done from 3° to 60° 2θ with increments of 0.02° 2θ and a counting time of 10 s per step. The components of the sample were identified by comparing them with standards established by the International Centre for Diffraction Data. For elemental analysis of the samples, the same SEM equipped with Oxford energy dispersive spectrometer (EDS), coupled with INCA 250 system was used to generate elemental maps in the samples. EDS qualitative analysis and elemental mapping was performed at an accelerating voltage of 20 kV. Data acquisition and analysis was done using AZtec software (Oxford instruments, United Kingdom). Five frames, each with an area varying between 0.5 mm^2 to 1 mm^2 were mapped. As it can be difficult to identify mineral phases through XRD due to low concentrations or overlapping peaks, poorly crystalline nature of materials with high amorphous content, or high and low temperature variants, the speleothems were also characterized by Tescan Integrated Mineral Analyzer (TIMA). The conditions used for the current analysis were: beam energy 25000 eV, current 6.32 nA, beam intensity 19.56, working distance 15 mm, SEM type TIMA3FE GMU with Pulse Tor 30 detector model at 7.009 μm pixel.

Mechanical Characterization of Speleothems by Nanoindentation

Cubes of approximately 1 cm were cut from each specimen, embedded in epoxy resin (Buehler eco-thin, Buehler, Lake Bluff, Illinois) and allowed to cure for 24 h (in molds 32 mm × 8 mm). Initial grinding and polishing of samples was performed using silicon carbide paper of reducing gradation 52, 35, 22, and 15 μm to expose the surface. Samples were finally ground and polished using diamond suspensions of reducing gradations as 9, 6, 3, 1, and 0.05 μm on a polishing cloth. Nanoindentation was performed using a G200 nanoindenter (Agilent Technologies) fitted with a Berkovich shaped diamond tip at a Poisson ratio of 0.31. The optical microscope fitted with the nanoindenter was used at 40x magnification to select the points of indentation and a matrix of indentation points on the particles of interest was chosen. At least 50 indentation points were selected for each sample with a minimum spacing between the indents of 10 μm and a maximum depth of indentation set to 1000 nm. The surface approach velocity was set to 20 nm/s and the loading time set to 15 s with a peak hold time of 10 s. On completion, indentation sites were re-inspected with an optical microscope and load-indentation diagrams were plotted. From this data the mechanical properties were estimated (Müller et al., 2014). From the initial slope of the unloading curve, the depth of indentation was estimated. The force corresponding to the displacement was utilized to determine the hardness of the material. The elastic modulus was estimated from the unloading segment of the load–indentation curve. Hardness reflects the resistance of the geological samples to deformation, while the elastic modulus represents the elastic deformation of the material following force application (Müller et al., 2014). A power law function was fitted to the initial unloading portion to determine its slope. The calculations were performed with the software NanoTest Platform Four V.40.08 (Micro Materials Ltd.). We determined Young's modulus, E, as the

maximum slope in the corresponding stress–strain curve. Non-linear behavior at low strains is the result of varying alignment inaccuracy.

Microbial Characterization of Cave Speleothems

Bacterial cellular activity or Adenosine triphosphate (ATP) activity of the speleothems was analyzed immediately after returning to the laboratory using the BacTiter-Glo Microbial Cell Viability kit (Promega, United States) as described by Barton et al. (2014).

DNA Extraction from Speleothem Samples

Genomic DNA (gDNA) was extracted in triplicate from all deposits and speleothems. The speleothem sample (1 g) was suspended in sterile phosphate buffer saline and vortexed at high speed followed by sonication in ultrasonic water bath to detach the surface cells. The cell suspension was harvested by microfiltration (0.2 μm pore size filter; Millipore) and the filter washed in PBS. DNA extraction was conducted using the Power Soil DNA kit (MO BIO Laboratories, Carlsbad, CA, United States) following the manufacturer's instructions. The recovered genomic DNA was pooled and the concentration was quantified using a Nanodrop 8000 Spectrophotometer (Thermo Scientific, Wilmington, DE, United States).

Amplicon Diversity Sequencing

PCR amplification and sequencing of the V3/V4 region of the 16S rRNA gene was performed by Australian Genome Research Facility (Brisbane, QLD, Australia) using Illumina MiSeq (San Diego, CA, United States) with 2 × 300 base pairs paired-end chemistry. Briefly, extracted gDNA from each of the sample was PCR amplified using primers 341F (5′-CCTAYGGGRBGCASCAG-3′) and 806R (5′-GGACTAC NNGGGTATCTAAT-3′). Thermocycling was performed in a Bio-Rad C100 (Bio-Rad Laboratories, Richmond, CA, United States) using AmpliTaq Gold 360 mastermix (Life Technologies, Australia).

Sequence Analysis

Paired-ends reads were assembled by aligning the forward and reverse reads using PEAR (version 0.9.5) (Zhang et al., 2014). Primers were trimmed using Seqtk (version 1.0)[1] and the trimmed sequences were processed using Quantitative Insights into Microbial Ecology (QIIME 1.8) (Caporaso et al., 2010) USEARCH (version 7.1.1090) and UPARSE (Edgar et al., 2011) software. Using USEARCH sequences were quality filtered, full length duplicate sequences were removed and sorted by abundance. Singletons or unique reads in the data set were discarded. Sequences were clustered followed by chimera filtering using "rdp_gold" database as the reference. To obtain the number of reads in each Operational Taxonomic Unit (OTU), reads were mapped back to OTUs with a minimum identity of 97%. Using QIIME, taxonomy was assigned using SILVA database (version silva_119) (Quast et al., 2013). The obtained sequences were submitted to National Centre for Biotechnology Information (NCBI) (accession number SAMN07489237 to SAMN07489242 and SAMN07498254 to SAMN07498259). The results are provided as percentage of sequencing reads for the identified OTUs in each sample.

Enrichment of Speleothem Surface Associated Bacterial Communities and Characterization of Precipitated Carbonate Biominerals

In order to investigate the microbial dynamics and biogenic carbonate mineralization potential of the microbial communities associated with speleothem samples under *in vitro* conditions, one gram of speleothem sample collected from each site was inoculated into flasks containing 100 ml autoclaved B4 medium (4 g yeast extract, 2.5 g calcium acetate, 10 g of glucose) (Banks et al., 2010; Rusznyak et al., 2012). For abiogenic controls, one gram of speleothem samples from each site were subjected to autoclaving in order to remove the associated microbes and then inoculated into sterile B4 media flasks as above. Dry autoclaving may have impacted the mineralogy to but as the aim of this experiment was to differentiate biotic vs. abiotic mineralization, we assumed little effect of the mineral change on crystal precipitations. All the flasks were incubated at 50 rpm in an orbital shaker for 10 days at 30°C in the dark (the very low rpm were to ensure the least loss of surface deposits from the speleothems which may interfere with the precipitates). These cultures were subcultured and grown for another 10 days to monitor the microbial growth (OD_{600}) as well as precipitate formation as per Rusznyak et al. (2012). The conditions for *in vitro* carbonate precipitation were significantly different from the actual cave environments with low temperature, high humidity, CO_2, and minimal nutrients, but the aim of this experiment was to investigate the biomineralization potential of heterotrophic communities associated with speleothems in a shorter time frame. After 10 days, five ml of culture broth was taken from each set, centrifuged at 13,000 × *g* (4°C) for 10 min and the pellet was harvested for DNA extraction using the Bacterial DNA Isolation Kit (Qiagen®) following the manufacturer's instructions. The microbial diversity of the enriched cultures was analyzed as previously described. For the analysis of the carbonate mineralization potential of the enriched cultures, 10 ml of the culture was filtered using Whatman No. 1 filter paper and the precipitated crystals were harvested as per Zamarreno et al. (2009). The crystals were washed with sterile distilled water, dried at room temperature for 48 h and analyzed for morphological and chemical constituents with SEM and XRD as described previously. All experiments were conducted in triplicate as biological replicates. The data were analyzed by Analysis of Variance (ANOVA) and the means were compared with Tukey's test. All analyses were performed using Graph Pad Prism software® version 6.0.

[1] https://github.com/lh3/seqtk

RESULTS AND DISCUSSION

Carbon Nitrogen and Trace Metal Compositions

Carbon/Nitrogen content and major metal concentrations of different cave deposits were analyzed as per Rusznyak et al. (2012) and shown in **Table 2**. The proportion of Ca was very high in all the samples although Si, Mg, Al, S and Fe were also consistently present in varying amounts. Other metals such as K, Na, and P were recorded in small quantities. The calcium content was lower in the Mammoth Cave speleothems than those of the other two caves. This was also seen for the calcium proportion as carbonate with Lake Cave and Moondyne Cave speleothems having a higher content compared to Mammoth Cave speleothems. Interestingly, the Mammoth Cave samples were the only ones with detectable levels of Silica. Mineral dissolution was observed in the speleothems of Mammoth Cave (shown in the SEM images in next section). The high amount of silica in this case may be an indicative of sandy sediments being washed into the cave or be due to the dissolution of the speleothem or speleogenesis. Previous studies have reported the role of microbial activity in speleogenesis (Banks et al., 2010). Notably the presence of Mg, S, Al and Fe were also higher in Mammoth Cave speleothems suggesting different formation mechanisms and siliceous mineralogy in these samples. A number of cave speleothems have been reported to have similar calcium contents due to the calcitic nature of these formations but variations in the distribution of other metals and elements in the different samples of the study may influence the microbiomes of the speleothems as well as their mechanical properties (Melim et al., 2001; Baskar et al., 2008a; Cacchio et al., 2012; Rusznyak et al., 2012; Banerjee and Joshi, 2014).

Morphological, Mineralogical and Mechanical Properties

Scanning electron microscopy observations of the speleothems showed a variety of crystalline mineral formations together with a variety of microbial morphotypes and mineralized cells/filaments (**Figure 3**). While there were morphological differences between the different speleothems, most of them displayed associations with hyphae or biofilms. Elemental analysis by EDS, mineralogical analysis by XRD and TIMA demonstrated the presence of multiple mineral polymorphs in the speleothem samples (**Figures 4–6**). The microstructures of the speleothem sections for indentation can be seen in **Figure 7**. The elastic modulus and hardness was determined from the load indentation graphs and the values are presented in **Table 3**.

The moonmilk sample was characterized by a mixture of thickly laminated columnar crystals which were widely distributed (**Figures 3i,ii**). The contacts between different layers were associated with rhombohedral crystals and a few cavities were also noticed. The size of the crystals generally varied from 20 to 200 μm but some larger crystals were recorded. A few regions appeared to be covered by a filamentous network of hyphae and cells. The elemental and mineralogical analysis revealed that the sample consisted entirely of calcite and was composed of Ca, C,

TABLE 2 | Carbon, Nitrogen, $CaCO_3$ and trace metal content of different cave speleothems**.

Sample	C (%)	N (%)	Ca as $CaCO_3$ (%)	Ca (mg/kg)	Si (mg/kg)	K (mg/kg)	Mg (mg/kg)	Na (mg/kg)	S (mg/kg)	Al (mg/kg)	Fe (mg/kg)	P (mg/kg)
Lake Cave												
Moonmilk	4.2 ± 1.3	0.01	99 ± 0.1	408000 ± 1500	<100	<100	924 ± 23	273 ± 5	1360 ± 43	138 ± 27	53 ± 18	115 ± 21
Stalagmite	4.8 ± 1.2	0.01	99 ± 0.2	403000 ± 2100	<100	<100	1160 ± 87	136 ± 18	1290 ± 36	376 ± 29	298 ± 46	62 ± 11
Stalactite	4.9 ± 1.7	0.02	93 ± 3.6	392000 ± 2700	<100	<100	1470 ± 65	437 ± 29	1310 ± 68	1390 ± 76	655 ± 54	859 ± 42
Moondyne Cave												
Stalagmite	4.8 ± 1.8	0.02	94 ± 2.3	391000 ± 1900	<100	<100	1380 ± 84	415 ± 16	1270 ± 37	1310 ± 82	620 ± 42	825 ± 52
Mammoth Cave												
Stalagmite	5.4 ± 1.5	0.01	77 ± 4.9	321000 ± 1600	180 ± 24	<100	3190 ± 76	597 ± 22	1710 ± 122	2640 ± 53	1080 ± 85	145 ± 28
Stalactite	5.3 ± 1.3	0.02	75 ± 3.8	320000 ± 2900	198 ± 32	<100	3380 ± 88	458 ± 31	1660 ± 88	2790 ± 48	1280 ± 94	125 ± 19

***Values are mean ± SD (n = 3).*

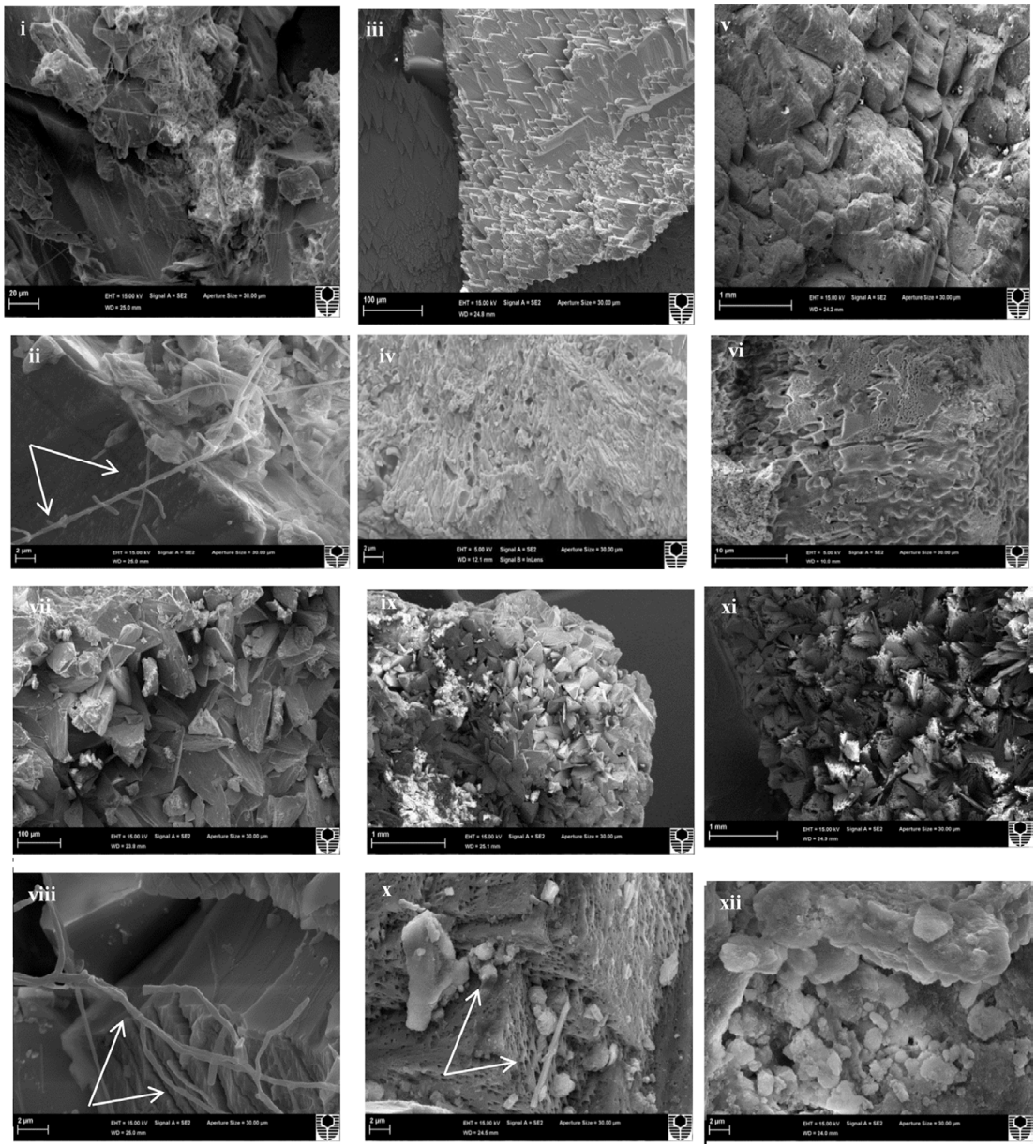

FIGURE 3 | Scanning electron micrographs of: **(i,ii)** Lake Cave moonmilk; **(iii,iv)** Lake Cave stalagmite; **(v,vi)** Lake Cave stalactite; **(vii,viii)** Moondyne Cave stalagmite; **(ix,x)** Mammoth Cave stalagmite and **(xi,xii)** Mammoth Cave stalactite (Arrows indicate hyphal networks and microborings) at lower and higher magnifications.

and O (**Figures 4i**, **5i**, **6i**). The organic composition appeared to be high as analyzed from a high Carbon peak in the elemental analysis. XRD and TIMA both demonstrated the presence of pure calcite as the mineral phase. Similar structures were also reported in moonmilk deposits of the Ballynamintra karstic Cave (Rooney et al., 2010). The precipitation of calcite moonmilk is generally attributed to inorganic processes but a few studies have suggested the formation of it through both biogenic and abiogenic processes (Onac and Ghergari, 1993; Hill and Forti, 1997).

The stalagmite sample from Lake Cave had an abundance of triangular crystals interconnected by smaller cementing binders (**Figures 3iii,iv**). All the components seemed radially arranged. Jones (2001) reported similar structures to be formed in cave deposits due to destructive processes of etching and boring. The formation of spiky calcite crystals was reported to be influenced by microbial activity and mucus leading to irregular shaped depressions (Folk et al., 1985). A closer view revealed encrustations of some bacterial cell like fossilized imprints. EDS analysis revealed the presence of Ca, C, and O along with small peaks of Si and Na (**Figure 4ii**). The carbonates were identified as calcite by XRD while TIMA also confirmed the presence of aragonite (**Figures 5ii**, **6ii**).

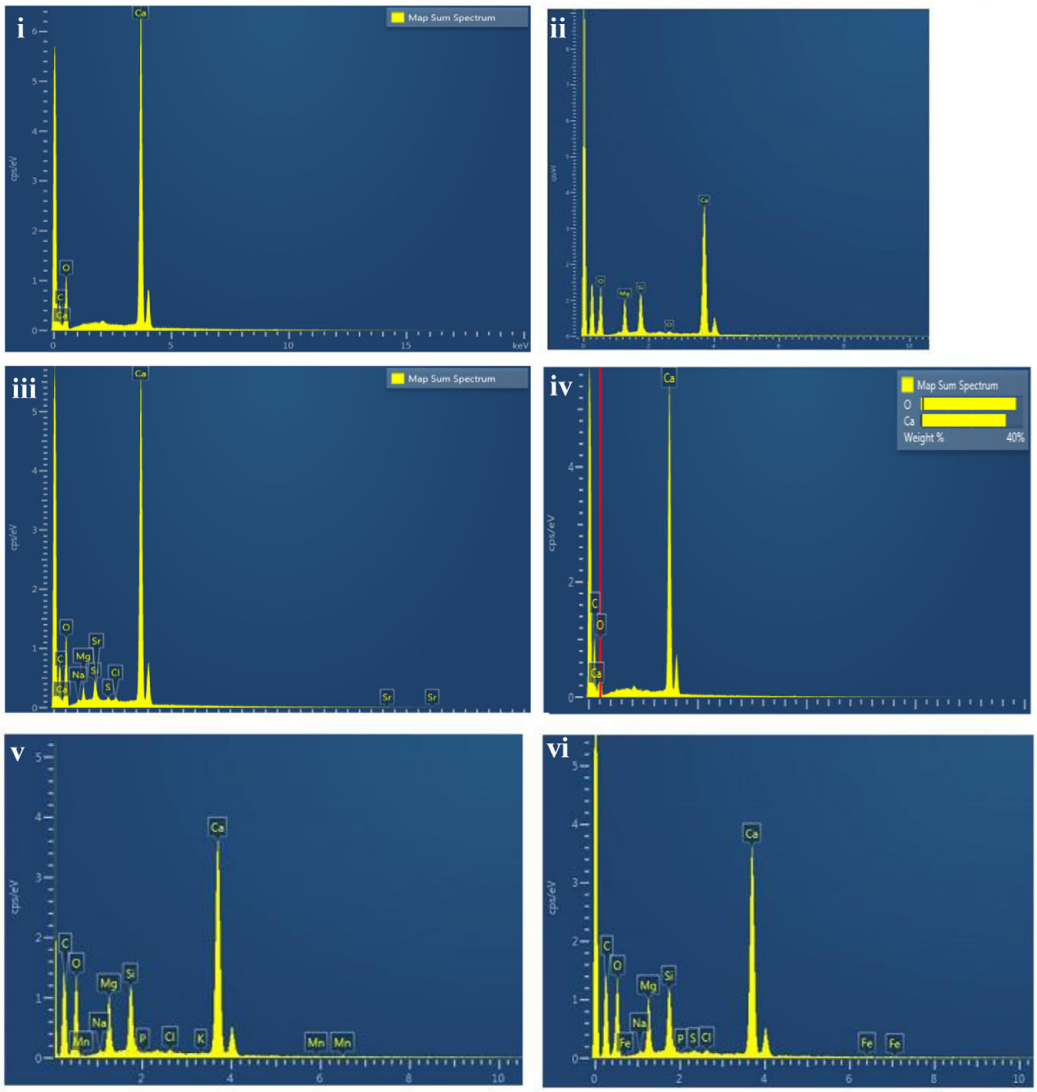

FIGURE 4 | Energy dispersive X ray spectrum of: **(i)** Lake Cave moonmilk; **(ii)** Lake Cave stalagmite; **(iii)** Lake Cave Stalactite; **(iv)** Moondyne Cave stalagmite; **(v)** Mammoth Cave stalagmite and **(vi)** Mammoth Cave stalactite.

The stalactite sample of Lake Cave was characterized by alteration of thickly laminated columnar and accretionary crystals in the size range of 500 μm to 1mm which were widely distributed (**Figures 3v,vi**). In some areas the crystals seemed to be compactly cemented. A cover of matrix like film was also recorded in a few sections with some bacterial like imprints. The current sample displayed microbial like associations on the surface, but whether they are playing an associative or dissociative role is not certain. The hypothesis that the growth of stalagmites and stalactites is mediated by microbial activity is postulated in many studies but there are several challenges to identify these processes in natural systems due to fossilization (Barton et al., 2007; Melim et al., 2008). Elemental analysis again revealed the presence of high C, Ca, O, and Mg along with small peaks of Cl and Na (**Figure 4iii**). Unusual mineral morphologies coupled with high Mg content have also been related to EPS influenced mineralization as biofilms help initiate layer formation on the stalactites via organomineralization processes (Banks et al., 2010; Adetutu et al., 2012). The mineralogical analysis demonstrated the presence of calcite and aragonite though XRD along with dolomite identified through TIMA (**Figures 5ii**, **6iii**).

The stalagmite sample from the Moondyne Cave displayed a slightly different morphology with sharp triangular prismatic crystals with acicular needles in a radial arrangement (**Figures 3vii,viii**). The size of the crystals varied from 20 μm to 100 μm with the bigger crystals cemented by smaller crystals. In this case, the rhomboids had regular outlines with possible microbial hyphae over them. Pacton et al. (2013) reported the presence of cement filled microborings in stalactites of the

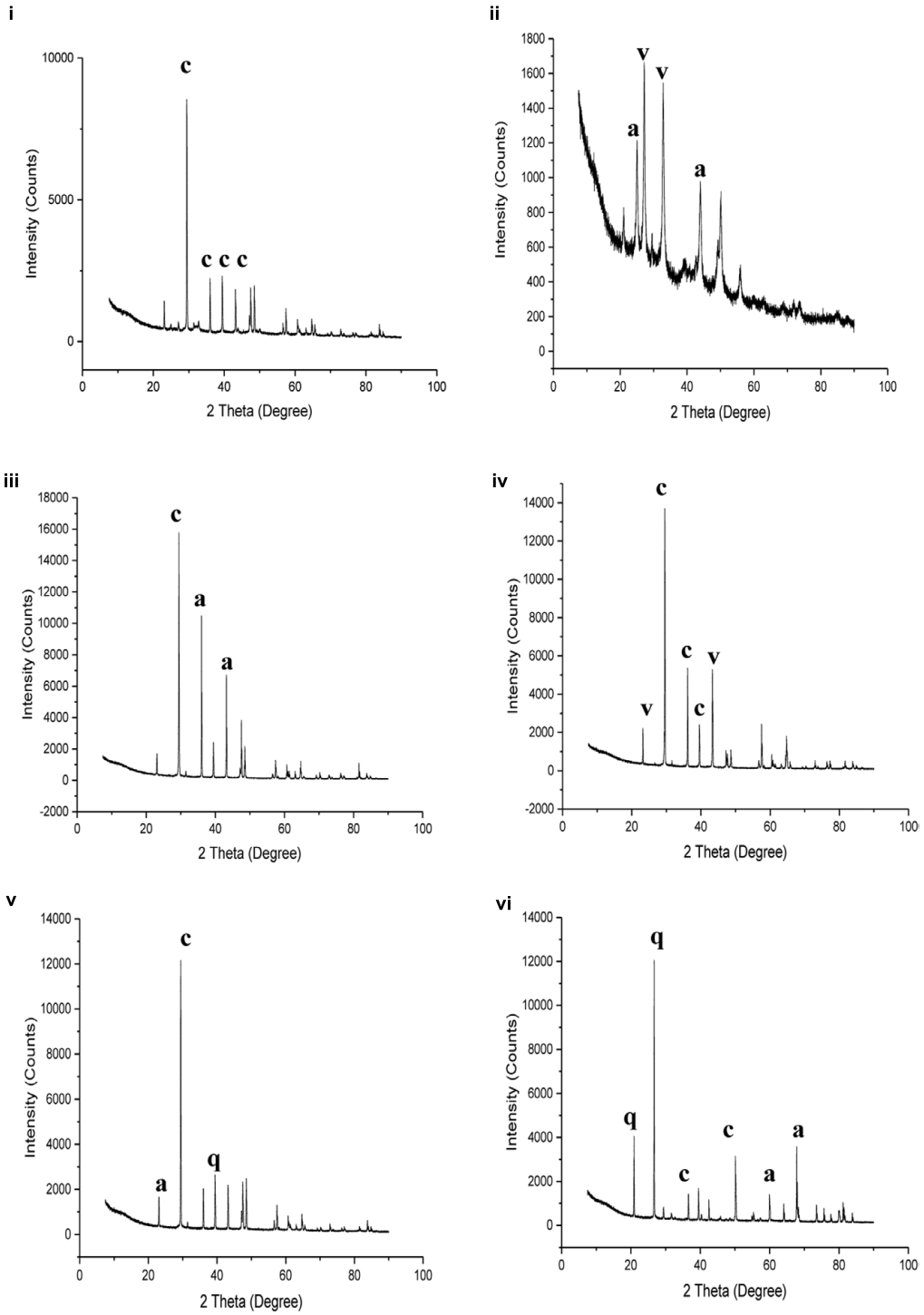

FIGURE 5 | X ray diffraction analysis of: **(i)** Lake Cave moonmilk; **(ii)** Lake Cave stalagmite; **(iii)** Lake Cave Stalactite; **(iv)** Moondyne Cave stalagmite; **(v)** Mammoth Cave stalagmite and **(vi)** Mammoth Cave stalactite (where c denotes calcite; a denotes aragonite; v denotes vaterite; q denotes quartz).

Botovskaya Caves. Mineralogical analysis of the speleothems in Moondyne Cave revealed that they are composed of calcium carbonates in the form of calcite and vaterite along with a feldspar mineral plagioclase (**Figures 4iv**, **5iv**, **6iv**).

The speleothems collected from Mammoth Cave had different morphological features to those from the other caves due to variety of diagenetic processes, climate and associated environments (Demény et al., 2016). The stalactite sample

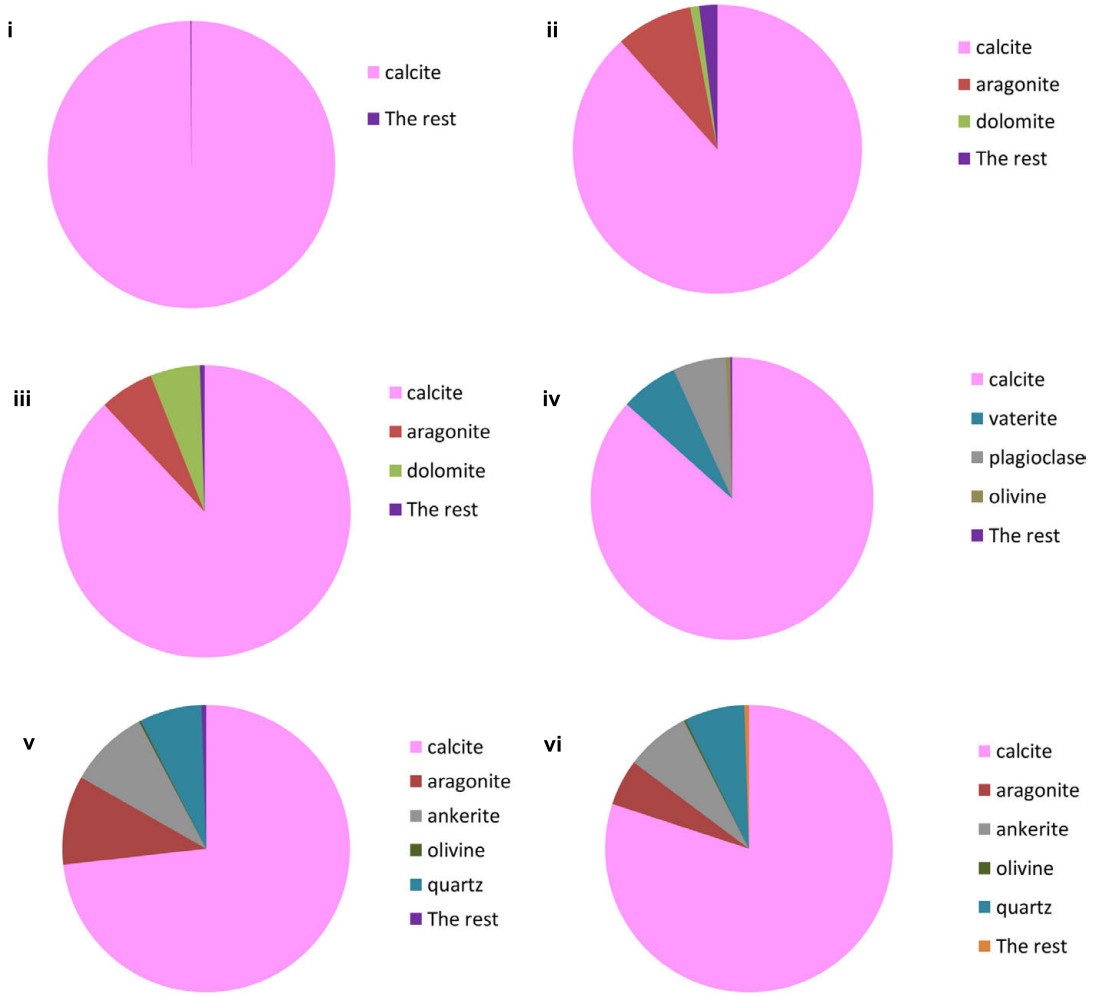

FIGURE 6 | TIMA analysis of: **(i)** Lake Cave moonmilk; **(ii)** Lake Cave stalagmite; **(iii)** Lake Cave Stalactite; **(iv)** Moondyne Cave stalagmite; **(v)** Mammoth Cave stalagmite and **(vi)** Mammoth Cave stalactite.

displayed sharper trigonal prismatic crystals (**Figures 3ix,x**). The empty microborings were clearly seen on the surface of calcite crystals that were open and flaky. Pacton et al. (2013) in their study found that microborings were generally composed of high Fe-Si phases and Mg-calcite precipitates which are corroded by iron oxides. The microborings were seen associated with EPS in their study. In this case also, partial dissolution of the rhombohedral crystals was observed in some sections. The previous elemental analysis of these samples displayed high content of Si and Fe along with Ca, C, and O (**Figure 4v**) paving way to the hypothesis that iron oxides might be responsible for corroding these sections and hinting the role of EPS. XRD and TIMA revealed the crystal phases as a mixture of calcite and aragonite along with quartz and ankerite (**Figures 5v**, **6v**). Ankerite is closely related to dolomite differing in the presence of iron and manganese instead of magnesium. This mineral has also been found in the Jenolan Caves in New South Wales, Australia (Pogson et al., 2014).

Another speleothem from the Mammoth Cave had rosette like crystals surrounded by flaky aggregates (**Figures 3xi,xii**). The contacts between adjacent crystals appeared to be filled by cement like binders with EPS encrusted mineral precipitates. Some areas revealed a breakdown of the substrate which could be related to the etching/boring activity of microbes (Jones, 2001). Some crusts showed corroded features. Similar features were displayed in stalactites of the Botovskaya Cave (Pacton et al., 2013). EDS analysis in this case also showed the presence of high amounts of Si together with Ca, C, O, Mg, and Fe while the mineralogical analysis demonstrated the presence of calcite, aragonite, dolomite, and quartz (**Figures 4vi**, **5vi**, **6vi**). The presence of intermediate forms and higher amounts of Mg in the Mammoth Cave may be an indicator of active mineralization. The mineralogical and micrographical analysis was closely related to the metal composition.

The variety of textures, morphology, and mineralogy of the different speleothems indicates different processes and controls in the formation of these structures. Different mineralogies

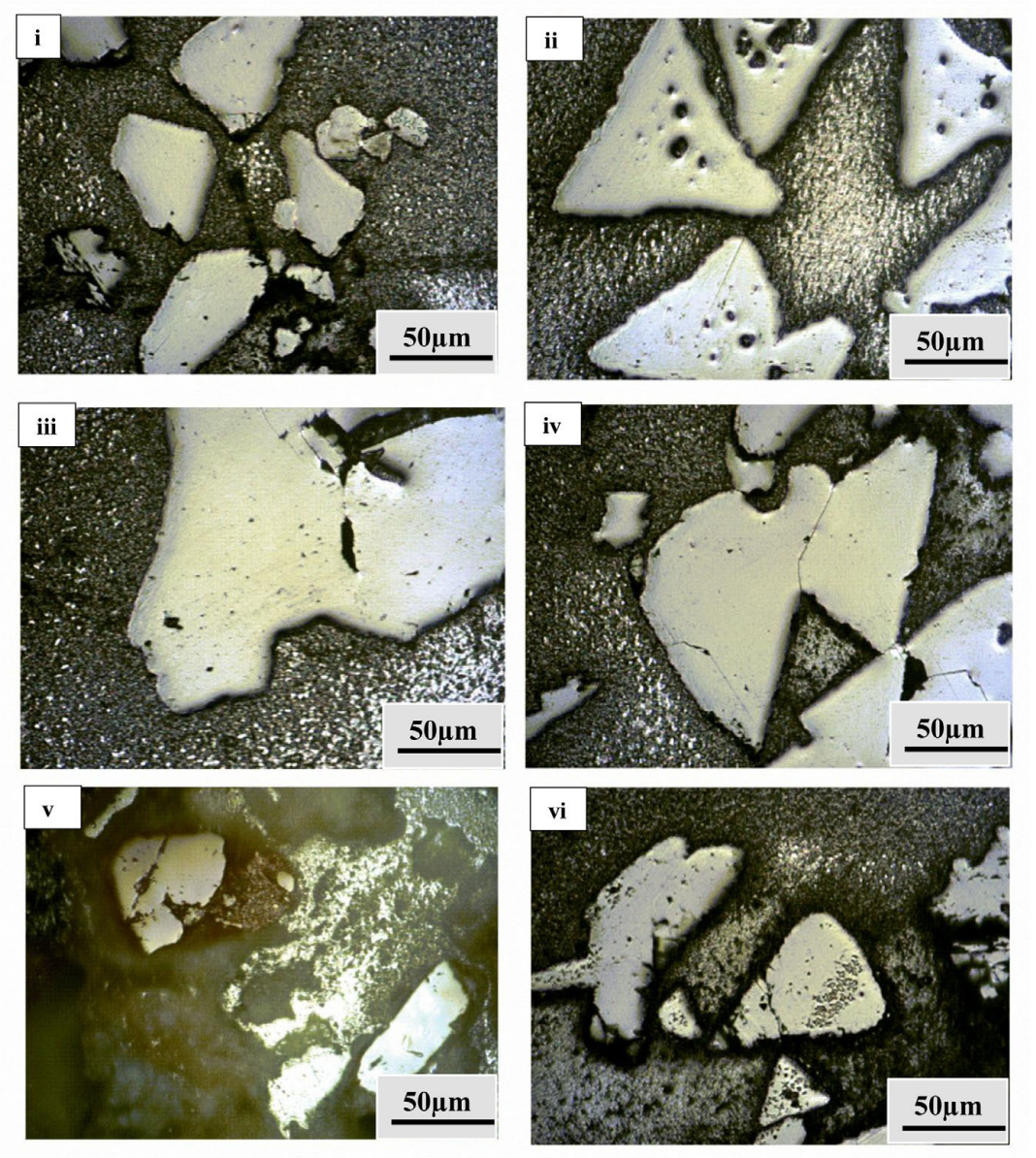

FIGURE 7 | Microstructures for nanoindentation through optical microscope fitted with Nanoindenter for: **(i)** Lake Cave moonmilk; **(ii)** Lake Cave stalagmite; **(iii)** Lake Cave Stalactite; **(iv)** Moondyne Cave stalagmite; **(v)** Mammoth Cave stalagmite and **(vi)** Mammoth Cave stalactite.

and polymorphs such as calcite, vaterite, and aragonite have been analyzed by several studies (Sánchez-Román et al., 2007; Pacton et al., 2013; Demény et al., 2016). Self and Hill (2003) reported that the precipitation of calcite causes enrichment of Mg which favors the formation of aragonite and in a few cases leads to the precipitation of hydro magnesite. In another study, Morse (1983) and Sánchez-Román et al. (2007) explained differences in the mineralogies by kinetic analysis. It was reported that aragonite and calcite nucleate and grow at the same time, but in different settings within the cave. A more continuous water supply in pools and some stalactites promote calcite nucleation, whereas seepage and drip water provided a more favorable environment for aragonite, which forms more delicate speleothems. The variations of mineralogies may also be indicative of different stages of speleothem formation and a varying geochemistry. A recent study of cave speleothems by Demény et al. (2016) reported the transformation of amorphous calcium carbonate into calcite in the presence of cave drip waters where aragonite and vaterite were seen to be intermediate forms, whose formation is dependent upon pH and the concentration of Mg.

Nanoindentation was used to study the microscale mechanical properties of these formations (**Figures 7**, **8** and **Table 3**). This tool also helps in the analysis of the different phases of a

material together with the properties of the interfacial regions. Maintenance of sterile conditions is difficult as the methodology depends upon casting of the materials within resins. Therefore we aimed to determine the overall mechanical properties of the different speleothem samples and investigate the relationship to mineralogy rather than the effect of microbial interactions on the mineral surface. Further tests to determine microbial-mineral interactions and their effect on the nanomechanical properties in the original samples can be conducted using Atomic Force Microscopic techniques.

The mineral constituents of the exposed surface of the speleothem samples after polishing were carefully indented without the interference of the resin matrix (Dhami et al., 2016). The typical microstructures of different speleothem samples recorded through an optical microscope fitted with the Nanoindenter are shown in **Figure 7**. The sites for indentation were selected to cover at least 50% of the image area. Any analysis points on the resin or the interphase between the resin and the sample were discarded from the final analysis. The load indentation curves of the samples are presented in **Figure 8**. Significant variations were recorded between the different speleothems which in some cases were related to their mineralogy. It was observed that the elastic modulus of the speleothems varied within a range of 76–126 GPa while the hardness varied from 2.20 to 20.10 GPa. The Lake Cave Moonmilk had a hardness value of 14–20 GPa and modulus in the range of 120–132 GPa while the stalagmite sample had a hardness value of 10–14.4 GPa with an elastic modulus of 77–84 GPa (**Figures 8i,ii** and **Table 3**). In the case of the Lake Cave stalactite, the hardness and modulus values varied from 5.3–7.5 GPa to 72–83 GPa (**Figure 8iii**). The variation in the mechanical properties was smaller for the stalagmite sample compared to the stalactite sample. It was noticed that the Moonmilk specimen had the highest strength properties which may be in relation to its higher calcite content. In both of the other speleothems, other polymorphs of calcium carbonate were also recorded along with calcite which may play a role in determining the properties of these mineralized formations. However, further investigations of different sections of the same speleothem would be necessary to obtain a more accurate picture. The Moondyne Cave stalagmite had a slightly lower hardness property compared to the Lake Cave samples with a hardness values of 8–10.2 GPa and an elastic modulus value of 75–82 GPa (**Figure 8iv** and **Table 3**). In this case, there was also considerable variation across the cross section of the specimen. The previous mineralogical analysis of this sample had revealed the presence of mixed crystals (small and large) composed of different mineral phases such as calcite, vaterite, and plagioclase and these may be responsible for variations observed. The Mammoth Cave speleothems had the lowest mechanical properties (**Figures 8v,vi**). The stalactite demonstrated hardness in the range of 2.15–4.9 GPa and a modulus value of 64–74 GPa compared to the stalactite sample with hardness and modulus values varying from 2.3-3.9 GPa to 62–66 GPa. Both of these deposits had a much higher content of silicate mineral along with Mg–Fe, and there were also signs of dissolution which may have affected their pore fraction (**Figures 3ix,x**, **4v,vi**). These features may have been responsible for the lower mechanical properties compared to the calcite rich mineralized deposits.

TABLE 3 | Mechanical properties of different cave speleothems**.

Sample	Elastic Modulus at Max Load (GPa)	Hardness at Max Load (GPa)
Resin	6 ± 0.8	0.08 ± 0.02
Quartz (Zhu et al., 2007)	105 ± 5	13 ± 1
Feldspar (Zhu et al., 2007)	85 ± 5	9 ± 1
Calcite (Ren et al., 2013)	72 ± 11	1.98 ± 0.31
Vaterite (Ren et al., 2013)	39.13 ± 8.04	1.38 ± 0.39
Lake Cave moonmilk	126.4 ± 6.2	17.10 ± 3.2
Lake Cave stalagmite	80.5 ± 3.9	12.86 ± 2.1
Lake Cave stalactite	77.5 ± 5.4	6.2 ± 1.5
Moondyne Cave stalagmite	78.7 ± 3.68	9.1 ± 1.15
Mammoth Cave stalagmite	69.13 ± 5.5	3.5 ± 1.41
Mammoth Cave stalactite	64.39 ± 1.95	3.12 ± 0.8

**Values are mean ± SD (n = 10).*

It is believed that different crystal orientations are responsible for differences in mechanical properties (Alonso-Zarza and Wright, 2010). Even within the same sample, there appeared considerable variation in the properties which may be related to the age of the variable accretions inside the geological structures but further studies are required to investigate this hypothesis. There have only been a few reports on the nanomechanical properties of multiphase materials (Constantinides and Ulm, 2007; DeJong and Ulm, 2007; Zhu et al., 2007). Zhu et al. (2007) found that for quartz, the modulus values were 100–110 GPa and the hardness values were 12–14 GPa while orthoclase feldspar recorded modulus values of 80–90 GPa and hardness values of 8–10 GPa. They reported that different crystal orientations of isotropic minerals contribute to the differences in their mechanical properties. The calcium atoms in calcite have a sixfold coordination, nine-fold in aragonite and eightfold coordination in vaterite playing a role in their mechanical properties (Wang and Becker, 2009). It has also been found that the position of CO_3^{2-} ions in different polymorphs such as vaterite are uncertain (disorder displacement); where Ca^{2+} and CO_3^{2-} are not as closely packed as in calcite and aragonite crystals and therefore their mechanical properties are variable (Ren et al., 2013). Müller et al. (2014) found that the elastic modulus of pure calcite prisms is 72.83 ± 11.68 GPa in comparison to vaterite deposits at 39.13 ± 8.04 GPa but as geological formations are mixtures of different minerals and elements, their final properties vary based upon the crystal orientations and growth stages. This study is the first where an attempt to investigate the mechanical properties of mineralized natural formations was made, however, a comparison of nanoindentation with bulk property testing is essential for a full understanding.

Along with the physical, climatic, environmental, geographical, and chemical factors that play a role in speleothem formation, a few studies have found that microbes can also influence the growth (and dissolution) of these structures by microbially mediated mineralization through trapping and

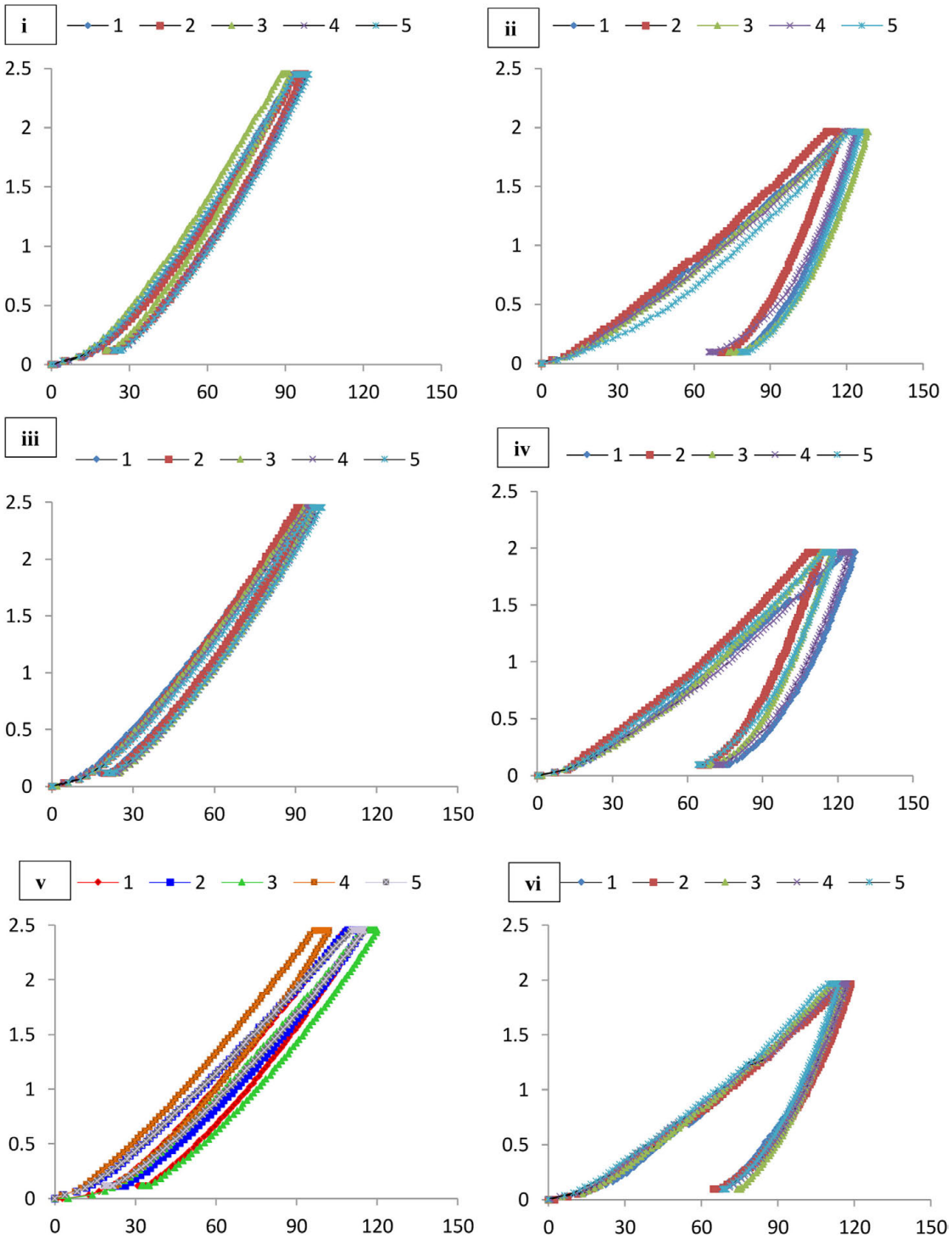

FIGURE 8 | Load indentation graphs of **(i)** Lake Cave moonmilk; **(ii)** Lake Cave stalagmite; **(iii)** Lake Cave Stalactite; **(iv)** Moondyne Cave stalagmite; **(v)** Mammoth Cave stalagmite and **(vi)** Mammoth Cave stalactite.

binding of detrital grains on the substrate, and/or by mediating mineral precipitation (Cañveras and Sanchez-Moral, 2001; Jones, 2001; Baskar et al., 2008a; Banks et al., 2010; Pacton et al., 2013). It is difficult to investigate the role of microbes or demonstrate a cause and effect relationship at this stage, but the study of their associations and diversities may shed more light on biogenic and abiogenic processes in naturally mineralized structures.

Microbial Characterization of Cave Speleothems

In order to test for the presence of active microbes associated with the speleothems, a luminescence based ATP test was conducted. Relative luminescent units (RLU) varied from 240 in the Lake Cave stalagmite to 2320 RLUs in the Moondyne Cave stalagmites which signified high microbial activity. Similar microbial activity was seen In the case of speleothems of Venezuelan Cave (Barton et al., 2014). While the detection of microbial activity is not necessarily an indicator of microbial mineralization/dissolution processes in the speleothems, it does confirm their presence in these oligotrophic environments.

The diversity of microbial communities from the speleothems was analyzed. The sequences were grouped into OTUs and classified using the GreenGene database. Information regarding OTUs and sequencing reads is available in the Supplementary Section. Large variation in microbial community structure associated with the different cave speleothems was observed at phylum level (Family and genus level in Supplementary Data) (**Figure 9**).

The microbial community structure of the Lake Cave speleothems revealed huge richness and variability in OTUs. The Moonmilk sample from Lake Cave was associated mainly with Actinobacteria (59%), Proteobacteria (24%) along with Firmicutes (2%). In contrast, the stalagmite sample was dominated by Actinobacteria (46%) and Proteobacteria (34.2%). In the case of the stalactite sample from this cave, again there was a prevalence of Proteobacteria (47%) and Actinobacteria (40%). The Lake Cave stalactite had a relative abundance of both α and β Proteobacteria (*Sphingomonadaceae* and *Oxalobacteraceae*) at family level (Supplementary Material) while the Lake Cave stalagmite sample had a higher prevalence of *Streptomycetaceae* as was also seen by Maciejewska et al. (2017). The stalagmite from Moondyne Cave was dominated by Actinobacteria (43%) and Proteobacteria (39%) along with Chloroflexi (5%). In the case of the Mammoth Cave speleothems, noticeable variations were observed compared to the other speleothems. At phylum level Actinobacteria (46%) dominated the stalagmite sample followed by Proteobacteria (29%) and Acidobacteria (9.2%). In the stalactite, Proteobacteria were more abundant (39%) followed by Actinobacteria (32.3%) with a higher level of Acidobacteria (13%). The Mammoth Cave speleothems had a much higher proportion of Acidobacteria compared to the other speleothems. At family level, an abundance of Solirubrobacterales and Rhizobiales from the Actinobacteria and α Proteobacteria was observed.

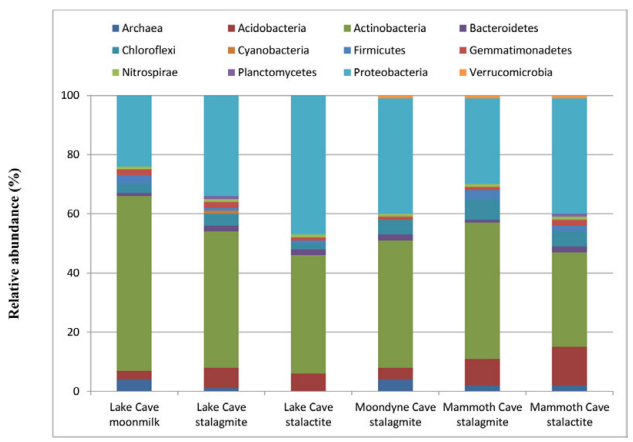

FIGURE 9 | Bacterial population composition at Phylum level associated with different Cave speleothems (based upon 16S rRNA gene sequencing presented as a fraction from total population).

The major phyla in all speleothems were Proteobacteria, Actinobacteria, and Acidobacteria. In general, the dominance of Proteobacteria has been related to their chemoorganotrophic/chemolithotrophic nature. Success of Proteobacteria colonization in several cave environments may be attributed, in part, to their ability to degrade a wide range of organic compounds, their ability to fix atmospheric carbon and transform nitrogen (Tomczyk-Żak and Zielenkiewicz, 2015). An abundance of Proteobacteria (Alpha, Beta, Delta, and Gammaproteobacteria subclass) has also reported in the karstic caves of Lascaux, Tito Bustillo Caves, Altamira Caves, and Herrenberg Cave Germany (Portillo et al., 2008; Bastian et al., 2009; Rusznyak et al., 2012). The dominance of Sphingomonodales and Rhizobiales in speleothems from Lake and Moondyne Caves support high nitrogen fixation abilities in such oligotrophic environments (Larouche et al., 2012). The presence of a large number of heterotrophic, nitrogen fixing species suggests that microorganisms depend on surface derived carbon for growth, while their ability to fix nitrogen plays a critical role in their survival. Actinobacteria have been reported to play an active role in carbonate biomineralization. Their prevalence was highest in the moonmilk sample from Lake Cave that was composed of pure calcite. Although the formation of moonmilk through biogenic or abiogenic process is controversial, and the dominance of biomineralizing Actinobacteria does not indicate whether these communities subsided on these minerals either during or after their formation, there is a close relationship between the mineralogy and the type of microbial structures. The dominance of Streptomyces in high calcium carbonate rich speleothems was also noted which agrees with previous reports of carbonate mineralization potential of such microbes (Maciejewska et al., 2017). In the case of the Altamira Caves, Streptomyces played a major role in capturing CO_2 and precipitating calcium carbonates under low humidity/ CO_2 conditions (Cuezva et al., 2012). Firmicutes (*Bacillus*) have been widely found to be involved in calcite precipitation (Zepeda Mendoza et al., 2016) and were quite noticeable in the Lake and Moondyne Cave calcitic speleothems. At genus level, a large number of previously reported carbonate precipitating bacteria associated with cave speleothems of Lake and Moondyne Cave were observed including species of *Sporosarcina, Bacillus, Lysinibacillus, Exiguobacterium, Myxococcus, Paenibacillus, Geobacillus, Syneccococcus, Arthrobacter, Nitrospira, Pseudomonas* (Rusznyak et al., 2012; Wu et al., 2015; Garcia et al., 2016). The phylum Acidobacteria, which was found to be more dominating in Mammoth Cave speleothems, has previously been reported to

play an active role in sulfur and iron reduction (Baskar et al., 2008a). The Mammoth Cave speleothems had a lower carbonate content, high Fe and S content as well as surface borings which indicate that these microbes may be playing an active role on the surface of such substrates. Wu et al. (2015) emphasized the impact of cave habitat types such as wall deposits, soils, and aquatic sediments on the bacterial community composition. Previous studies have postulated that the growth of stalactites and stalagmites is mediated by microbes (Cunningham et al., 1995; Jones, 2001; Melim et al., 2001; Baskar et al., 2008b). The diversity studies have confirmed the presence of specific classes of bacteria associated with the speleothems in close connection to their mineralogical composition, however, it does not inform us of the role of microbial formative or dissociative during growth and development. Although mineralogy seems to be the driving force behind the microbial community composition in this study, affecting the properties of these structures, further studies of active cave formations using recent OMICS tools should be conducted to gain further knowledge of the influence of microbes in real environments.

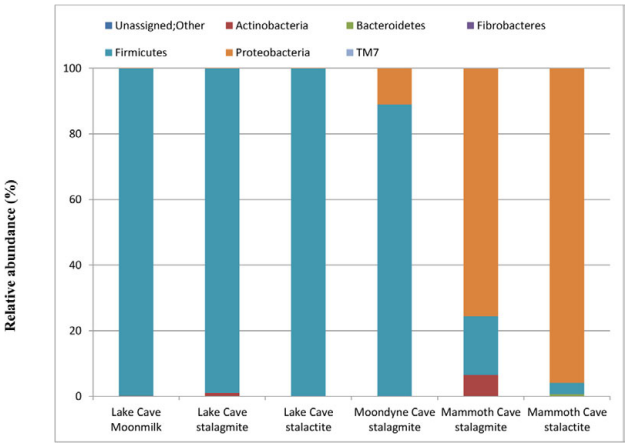

FIGURE 10 | Bacterial population composition at Phylum level in laboratory enriched conditions (based upon 16S rRNA gene sequencing presented as a fraction from total population).

Enrichment of Mineralizing Communities and Characterization of Biominerals

Microbial carbonate precipitation processes in Cave environments have been reported to be primarily driven by heterotrophic communities which alter the local conditions to promote $CaCO_3$ precipitation (Castanier et al., 2000; Banks et al., 2010; Rusznyak et al., 2012; Maciejewska et al., 2017). In order to gain insights into the actual biogenic process associated with mineral precipitation in caves, mimicking cave conditions in the laboratory will be imperative, including maintenance of similar temperature cycles, humidity, dark conditions, minimal nutrients, and subsurface situations. Establishing field-like conditions in the laboratory has always been challenging, so most of the previous studies investigating the role of biogenic carbonate formation have relied upon the use of acetate rich B4 media at ambient temperatures (Zamarreno et al., 2009; Banks et al., 2010; Shirakawa et al., 2011; Rodriguez-Navarro et al., 2012). Although rich nutrient conditions and ambient temperatures in the laboratory are not a true representation of actual cave processes, such experiments do shed light on the carbonate biomineralization potential of native microbial communities.

In order to further confirm the presence and association of speleothem surface microbes, their growth in B4 media was recorded. A significant increase in optical density after 4 days was recorded in all the biogenic sets (varying from 1.2 ± 0.31 – 2.6 ± 0.53) while little change was observed in the abiogenic set (with sterile speleothem sample input). The community structure and mineralization potential of the enriched cultures were then investigated. The relative abundance at Phylum level of the enriched communities under *in vitro* conditions can be seen in **Figure 10** and the relative abundance at genus level of the dominant microbial communities in all treatments is presented in Supplementary Table 2.

Variation in the composition of the enrichment microbial community were observed but Firmicutes were found to be the dominant phylum for Lake Cave and Moondyne Cave cultures while Proteobacteria were dominant in Mammoth Cave enrichments. Firmicutes and Proteobacteria has been previously found to be common genera involved in biomineralization (Rusznyak et al., 2012; Wu et al., 2015; Garcia et al., 2016; Andrei et al., 2017). Although Proteobacteria and Actinobacteria were dominant in the natural cave speleothems, under B4 media enrichments, Firmicutes were found to be the most prevalent along with Proteobacteria.

In the case of the Lake Cave enrichments, Firmicutes completely dominated the culture with a relative abundance of 99% while in the Moondyne Cave speleothem enrichments, it reached around 88% from an initial composition of around 1%. In the case of Mammoth Cave speleothems, dominance of Proteobacteria was recorded. The Firmicutes in case of Mammoth Cave were recorded at 17% in the stalagmite enrichments and around 3% in case of stalactite sample. At genus level, the Lake Cave moonmilk and stalactite enrichments comprised mainly of *Bacillus* while the stalagmite enrichment had a prevalence of *Planococcus* (Supplementary Table 2). In the case of the Moondyne speleothem sample, *Bacillus* and *Brevibacillus* genus dominated. The majority of communities in Mammoth Cave enrichment were found to be gram negative; belonging to *Caulobacter* and *Burkholderiales* genera in case of stalagmite sample and *Pseudomonas* in stalactite enrichments.

Firmicutes belonging to the Bacilli family have previously been reported to be the most dominant phylum in laboratory studies on bacteria isolated from cave environments (Cacchio et al., 2003; Banerjee and Joshi, 2014; Garcia et al., 2016). Cacchio et al. (2003) found that *Bacillus* sp. represented about 63% of all isolates from a limestone cave and a loamy soil. Recently Garcia et al. (2016) found that *Bacillus* sp. dominated the genera isolated from saline soils. Strains of *Pseudomonas* have also been isolated in a few studies from speleothems in caves (Chekroun et al., 2004; Rusznyak et al., 2012; Garcia et al., 2016). In a recent study of Andrei et al. (2017), both *Bacillus* and *Pseudomonas*

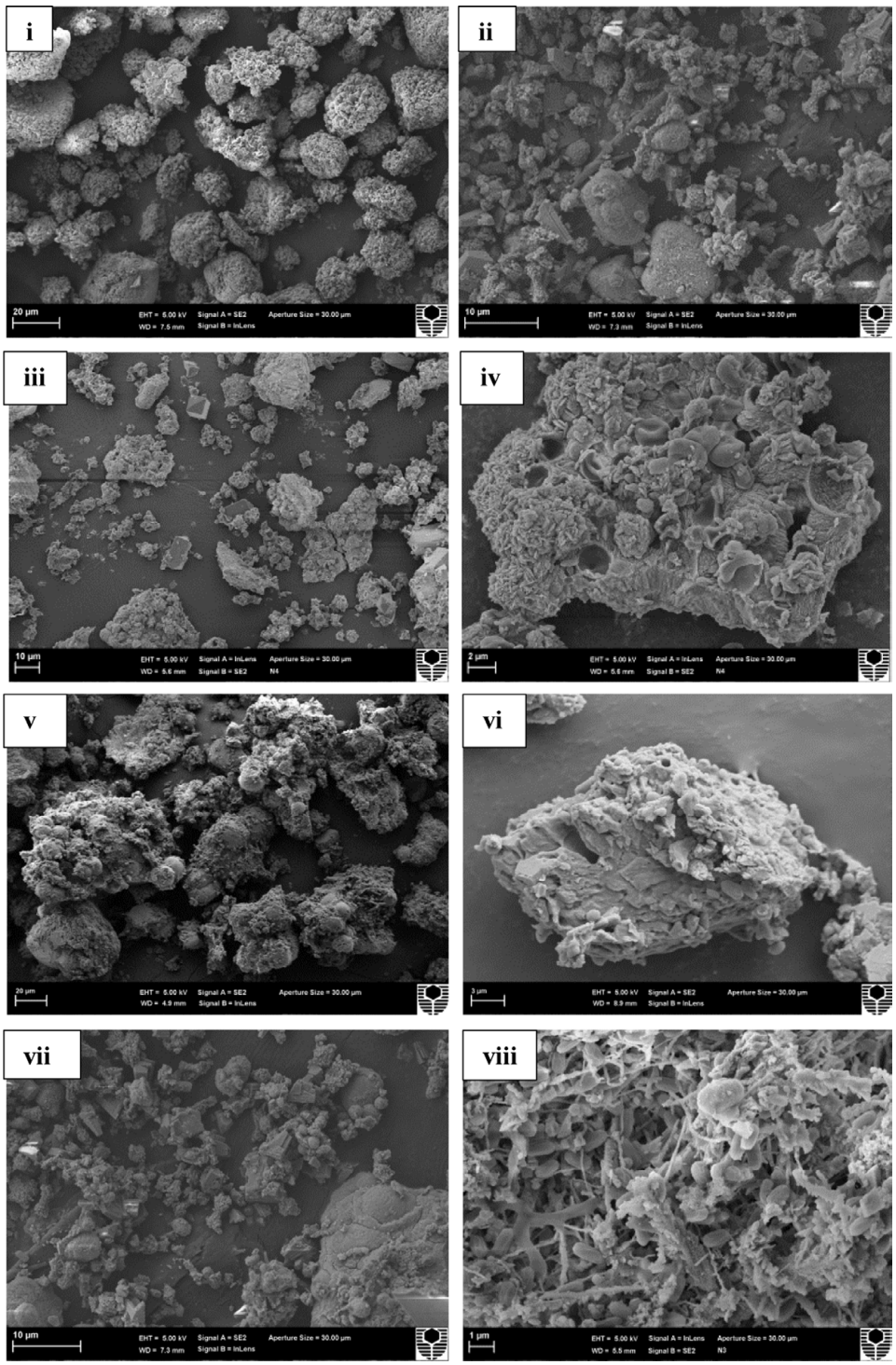

FIGURE 11 | Scanning electron micrograph of crystals precipitated in **(i,ii)** Lake Cave moonmilk enrichment set; **(iii,iv)** Lake Cave stalagmite enrichment set; **(v,vi)** Moondyne Cave stalagmite enrichment set **(vii,viii)** Mammoth Cave stalagmite enrichment set.

genera were found to be the predominant strains enriched from a limestone statue. It was also demonstrated that the predominance of *Pseudomonas* is linked to its common occurrence in soils. In this study, more *Pseudomonas* was enriched from the silica rich Mammoth Cave speleothems compared to calcitic speleothems suggesting a connection. The increased biomass (in biogenic sets) and observed diversity indicate the potential of acetate rich B4 media in promoting the growth of culturable bacteria

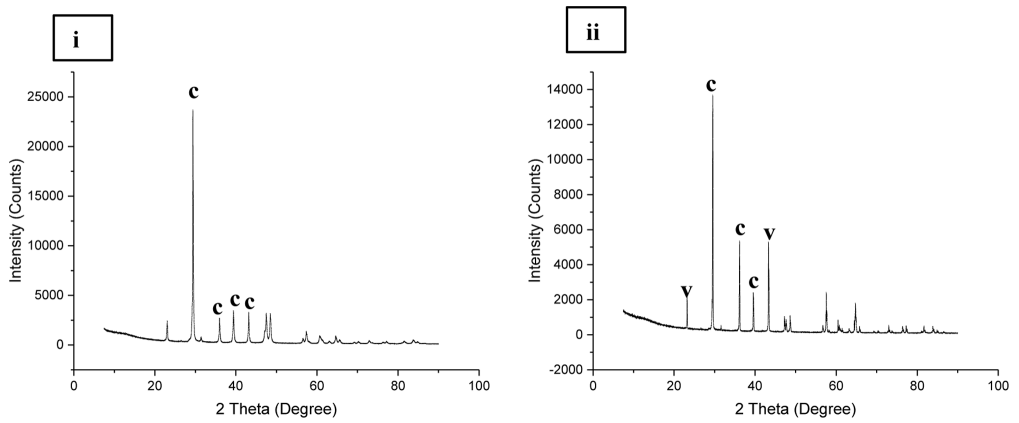

FIGURE 12 | X ray diffraction analysis of carbonate crystals precipitated in **(i)** Lake Cave moonmilk enrichment set **(ii)** Mammoth Cave stalagmite enrichment set (where c denotes calcite; v denotes vaterite).

from cave speleothems under laboratory conditions. However, it also highlights the shift in community structure seen in laboratory conditions which proves that nutrient availability and physical conditions play crucial role in selection of microbial metabolism and community structure. As laboratory enriched community structures are completely different from the natural conditions, preferring a few communities over the others; this study highlights the importance of future studies wherein natural conditions should be mimicked more closely. Variations in microbial community structures associated with different speleothems grown in different media have also been reported by other researchers (Rusznyak et al., 2012; Garcia et al., 2016; Maciejewska et al., 2017). Continuous monitoring of community shifts over regular intervals of time under those conditions will provide a better picture of the real field mechanisms.

Micrographic and mineralogical analysis of the crystals precipitated by microbes associated with the speleothems grown in B4 medium showed successful precipitation in all the biogenic speleothems. SEM analysis of the crystals confirmed the formation of crystals of varying sizes in all the biotic sets. **Figure 11** shows crystals formed by bacterial communities associated with different speleothems under laboratory conditions. In general, a mixture of smooth, rhombohedral, and spherical crystals with sizes varying from 20 to 100 μm was observed in the case of enrichments from Lake Cave (**Figures 11i–iv**), rhombohedral crystals in the case of enrichments from Moondyne Cave (**Figures 11v,vi**) and needle shaped crystals of sizes between 10 and 30 μm were recorded for enrichments from Mammoth Cave speleothems (**Figures 11vii,viii**). Some EPS formation was also noticed in a few sections. In all cases, the carbonate crystals were seen associated with bacterial cells indicating that they acted as nucleation sites, leading to their entrapment and formation of calcium carbonate. XRD analysis of the crystals identified various polymorphs of calcium carbonates in different sets (**Figure 12**). Calcite was seen as the predominant form in the Lake and Moondyne Cave enrichments (with Firmicutes) while vaterite was the major phase in the case of Proteobacteria dominated Mammoth Cave enrichments. No precipitates were seen in the control sets indicating that biotic process plays a crucial role in carbonate formation. The variations in carbonate polymorphs seen in the different communities could be a result of differing bacterial metabolic activities affecting dissolved inorganic carbon (DIC), and saturation index which could influence the type and properties of the calcium carbonate polymorphs (Rodriguez-Navarro et al., 2012; Dhami et al., 2013a; Okyay and Rodrigues, 2015). As microbial metabolic activity plays a role in determining the fate of the carbonate polymorph, this may explain the predominance of calcite formation with Firmicutes and vaterite formation with Proteobacteria as seen in the current study (Jimenez-Lopez et al., 2008; Jroundi et al., 2014; Zhu and Dittrich, 2016). A number of previous studies have reported the formation of biogenic carbonate crystals via bacterial strains isolated from cave environments (Cacchio et al., 2003; Rusznyak et al., 2012; Banerjee and Joshi, 2014). This work further supplements the hypothesis that biomineral production is a general phenomenon by different bacterial isolates and similar microbial activities might play an important role in the formation of speleothems in natural environments but still there is a lack of evidence of cause and effect. The associations between bacterial species, metabolic activities and their effects on mineral polymorphs need further studies. Advanced OMICS and radiolabelling techniques to identify active metabolic processes in speleothem formations from different climatic environments can be carried out in future studies. Our previous studies recorded the nanomechanical properties of different polymorphs of calcium carbonate crystals via ureolytic and carbonic anhydrase route wherein they varied in modulus from 36 ± 10 – 64 ± 2.7 GPa and hardness of 2.32 ± 0.15 – 3.92 ± 0.43 GPa; which are quite low compared to calcite rich cave speleothems of current study (Dhami et al., 2016). Further studies on nanomechanical properties of carbonate minerals synthesized by speleothem surface associated bacterial strains needs to be carried out in the future to investigate how these properties change at different time scales under cave simulated environments to provide deeper understanding of the bio-geo-chemical processes in

nature. Though the generation of calcium carbonate biominerals has been successfully achieved in laboratory conditions but in comparison to their natural counterparts, their mechanical performance is much lower. In order to widen the scope of MICP technology for engineering applications, comprehensive analysis and optimization of physical and chemical conditions to copy mechanical properties of natural biomineralized materials in shorter time spams is required. This challenge demands researchers from diverse areas as microbiology, molecular biology, geology, material/civil engineers and chemists to work together and bridge the gap for production of sustainable bio-cement with properties of naturally biomineralized formations.

CONCLUSION

In the current study, combined mineralogical, elemental, microbial, and nanomechanical characterization of different cave speleothems such as moonmilk, stalagmite, and stalactite has been conducted for the first time. Mineralogical and elemental analysis of cave speleothems varied from calcite, aragonite, dolomite, ankerite to silicates while micrographic analysis recorded differences in size, type, and shape of structures under different conditions. This analysis indicated the influence of geochemistry on mineralogical properties of different formations. Nanomechanical properties of these mineralized formations indicated that mineralogical signatures had profound effect on the mechanical properties. The moonmilk speleothem sample which was composed purely of calcite had higher strength properties compared to other speleothems indicating a connection between the two. On the other side, microbial diversity study of bacterial communities associated with the different cave speleothems specified that variations in assemblages were related to the mineralogy and geochemistry. Under *in vitro* conditions, microbial cultures associated with speleothem surfaces were enriched in nutrient rich conditions and all the biotic sets successfully precipitated calcium carbonate minerals. The generation of carbonate biominerals by cave speleothem associated bacterial communities in laboratory conditions support the hypothesis that similar processes may occur in nature. Even in lab conditions, noticeable variations in carbonate polymorphs were recorded highlighting the effect of microbial metabolism and species on carbonate mineralogy. Microbial diversity data under enriched conditions revealed significant variations in the assemblages from real field communities which highlighted the importance of physical and environmental conditions in selection of microbial communities under different conditions. Though the community structures and their metabolisms are selected by nutrient conditions and physico-chemical environments, they in return further affect the mineralogical and nanomechanical fate of the biominerals. Comparison of nanomechanical properties of naturally biomineralized formations with laboratory synthesized carbonate biominerals formed by MICP technology showed significantly higher performance of natural materials. In order to truly mimic the formation of such materials in laboratory conditions for engineering applications and synthesis of sustainable cements, further investigations combining geochemistry, mineralogy and next generation OMICS tools need to be carried out. Whether the performance of laboratory based biominerals formed harnessing different bacterial metabolic routes can be improved through optimization of physical and chemical conditions in shorter time spams; will help in determining the fate of MICP technology.

AUTHOR CONTRIBUTIONS

ND contributed by providing with concepts and ideas, fieldwork, experiments, and writing. AM contributed with concepts and ideas, fieldwork organization, data interpretation, and writing. EW contributed with microbiological data interpretation and writing.

FUNDING

The funding for this study was supported by University Western Australia, Australia.

ACKNOWLEDGMENTS

The authors thank the staff of the Augusta Margaret River Tourism Association (AMRTA) for their technical support in sample collection. Special acknowledgment is owed to Mr. Peter Bell (AMRTA Resource Officer) and Mr. Lindsay Hatcher (Natural Environment and Projects manager) for their assistance in the field and sharing their knowledge of the Margaret River Caves. They acknowledge the use of Curtin University's Microscopy and Microanalysis Facility, whose instrumentation has been partially funded by the University, State and Commonwealth Governments.

SUPPLEMENTARY MATERIAL

The Supplementary Material for this article can be found online at: https://www.frontiersin.org/articles/10.3389/fmicb.2018.00040/full#supplementary-material

REFERENCES

Adetutu, E., Thorpe, K., Shahsavari, E., Bourne, S., Cao, X., Fard, R., et al. (2012). Bacterial community survey of sediments at Naracoorte Caves, Australia. *Int. J. Speleol.* 41, 137–147. doi: 10.5038/1827-806X.41.2.2

Alonso-Zarza, A. M., and Wright, V. P. (2010). Carbonates in continental settings: facies, environments and processes. *Dev. Sedimentol.* 61, 225–267. doi: 10.1016/S0070-4571(09)06105-6

Andrei, A.-Ş., Păuşan, M. R., Tămaş, T., Har, N., Barbu-Tudoran, L., Leopold, N., et al. (2017). Diversity and biomineralization potential of the epilithic bacterial

communities inhabiting the oldest public stone monument of Cluj-Napoca (Transylvania, Romania). *Front. Microbiol.* 8:372. doi: 10.3389/fmicb.2017.00372

Bains, A., Dhami, N., Mukherjee, A., and Reddy, M. (2015). Influence of exopolymeric materials on bacterially induced mineralization of carbonates. *Appl. Biochem. Biotechnol.* 175, 3531–3541. doi: 10.1007/s12010-015-1524-3

Banerjee, S., and Joshi, S. R. (2014). Ultrastructural analysis of calcite crystal patterns formed by biofilm bacteria associated with cave speleothems. *J. Microsc. Ultrastruct.* 2, 217–223. doi: 10.1016/j.jmau.2014.06.001

Banks, E. D., Taylor, N. M., Gulley, J., Lubbers, B. R., Giarrizzo, J. G., Bullen, H. A., et al. (2010). Bacterial calcium carbonate precipitation in cave environments: a function of calcium homeostasis. *Geomicrobiol. J.* 27, 444–454. doi: 10.1080/01490450903485136

Barabesi, C., Galizzi, A., Mastromei, G., Rossi, M., Tamburini, E., and Perito, B. (2007). *Bacillus subtilis* gene cluster involved in calcium carbonate biomineralization. *J. Bacteriol.* 189, 228–235. doi: 10.1128/JB.01450-06

Barton, H. A., Giarrizzo, J. G., Suarez, P., Robertson, C. E., Broering, M. J., Banks, E. D., et al. (2014). Microbial diversity in a Venezuelan orthoquartzite cave is dominated by the *Chloroflexi* (Class *Ktedonobacterales*) and *Thaumarchaeota* Group I.1c. *Front. Microbiol.* 5:615. doi: 10.3389/fmicb.2014.00615

Barton, H. A., Taylor, N. M., Kreate, M., Springer, A. J., Oehrle, S. A., and Bertog, J. L. (2007). The impact of host rock geochemistry on bacterial community structure in oligotrophic cave environments. *Int. J. Speleol.* 36, 93–104. doi: 10.5038/1827-806X.36.2.5

Baskar, S., Baskar, R., Lee, N., Kaushik, A., and Theophilus, P. K. (2008a). Precipitation of iron in microbial mats of the spring waters of Borra Caves, Vishakapatnam, India: some geomicrobiological aspects. *Environ. Geol.* 56, 237–243. doi: 10.1007/s00254-007-1159-y

Baskar, S., Baskar, R., Lee, N., and Theophilus, P. K. (2008b). Speleothems from Mawsmai and Krem Phyllut caves, Meghalaya, India: some evidences on biogenic activities. *Environ. Geol.* 57, 1169–1186. doi: 10.1007/s00254-008-1413-y

Bastian, F., Alabouvette, C., and Saiz-Jimenez, C. (2009). Bacteria and free-living amoeba in the Lascaux Cave. *Res. Microbiol.* 160, 38–40. doi: 10.1016/j.resmic.2008.10.001

Borsato, A., Frisia, S., Jones, B., and Van Der Borg, K. (2000). Calcite moonmilk: crystal morphology and environment of formation in caves in the Italian alps. *J. Sediment. Res.* 70, 1171–1182. doi: 10.1306/032300701171

Broughton, P. L. (1983a). Environmental implications of competitive growth fabrics in stalactitic carbonate. *Int. J. Speleol.* 13, 31–41. doi: 10.5038/1827-806X.13.1.3

Broughton, P. L. (1983b). Lattice deformation and curvature in stalactitic carbonate. *Int. J. Speleol.* 13, 19–30. doi: 10.5038/1827-806X.13.1.2

Broughton, P. L. (1983c). Secondary origin of the radial fabric in stalactitic carbonate. *Int. J. Speleol.* 13, 43–66. doi: 10.5038/1827-806X.13.1.4

Buhmann, D., and Dreybrodt, W. (1984). The kinetics of calcite dissolution and precipitation in geologically relevant situations of karst areas Open system. *J. Chem. Geol.* 48, 189–211. doi: 10.1016/0009-2541(85)90046-4

Cacchio, P., Ercole, C., Cappuccio, G., and Lepidi, A. (2003). Calcium carbonate precipitation by bacterial strains isolated from a limestone cave and from a loamy soil. *Geomicrobiol. J.* 20, 85–98. doi: 10.1002/jobm.20130 0560

Cacchio, P., Ercole, C., Contento, R., Cappuccio, G., Preite Martinez, M., Del Gallo, M., et al. (2012). Involvement of bacteria in the origin of a newly described speleothem in the gypsum cave of grave grubbo (Crotone, Italy). *J. Cave Karst Stud.* 74, 7–18. doi: 10.4311/2010MB0136R

Calvaresi, M., Falini, G., Pasquini, L., Reggi, M., Fermani, S., Gazzadi, G. C., et al. (2013). Morphological and mechanical characterization of composite calcite/SWCNT-COOH single crystals. *Nanoscale* 5, 6944–6949. doi: 10.1039/c3nr01568h

Cañveras, C., and Sanchez-Moral, V. S. J. (2001). Microorganisms and microbially induced fabrics in cave walls. *Geomicrobiol. J.* 18, 223–240. doi: 10.1080/01490450152467769

Caporaso, J. G., Kuczynski, J., Stombaugh, J., Kyle, B., Bushman, F. D., Costello, E. K., et al. (2010). QIIME allows analysis of high-throughput community sequencing data. *Nat. Methods* 7, 335–336. doi: 10.1038/nmeth.f.303

Castanier, S., Métayer-Levrel, G., and Perthuisot, J.-P. (2000). "Bacterial roles in the precipitation of carbonate minerals," in *Microbial Sediments*, eds R. Riding and S. Awramik (Berlin: Springer), 32–39.

Chekroun, K. B., Rodríguez-Navarro, C., González-Muñoz, M. T., Arias, J. M., Cultrone, G., and Rodríguez-Gallego, M. (2004). Precipitation and growth morphology of calcium carbonate induced by *Myxococcus xanthus*: implications for recognition of bacterial carbonates. *J. Sediment. Res.* 74, 868–876. doi: 10.1306/050504740868

Chen, Y., Wu, L., Boden, R., Hillebrand, A., Kumaresan, D., Moussard, H., et al. (2009). Life without light: microbial diversity and evidence of sulfur- and ammonium-based chemolithotrophy in Movile Cave. *ISME J.* 3, 1093–1104. doi: 10.1038/ismej.2009.57

Constantinides, G., and Ulm, F. J. (2007). The nanogranular nature of C–S–H. *J. Mech. Phys. Solids* 55, 64–90. doi: 10.1016/j.jmps.2006.06.003

Cuezva, S., Fernandez-Cortes, A., Porca, E., Pasic, L., Jurado, V., Hernandez-Marine, M., et al. (2012). The biogeochemical role of Actinobacteria in Altamira Cave, Spain. *FEMS Microbiol. Ecol.* 81, 281–290. doi: 10.1111/j.1574-6941.2012.01391.x

Cunningham, K. I., Northup, D. E., Pollastro, R. M., Wright, W. G., and Larock, E. J. (1995). Bacteria, fungi and biokarst in Lechuguilla Cave, Carlsbad Caverns National Park, New Mexico. *Environ. Geol.* 25, 2–8. doi: 10.1007/BF01061824

De Muynck, W., De Belie, N., and Verstraete, W. (2010). Microbial carbonate precipitation in construction materials: a review. *Ecol. Eng.* 36, 118–136. doi: 10.1016/j.ecoleng.2009.02.006

Dejong, J., Burbank, M., Kavazanjian, E., Weaver, T., Montoya, B., Hamdan, N., et al. (2013). Biogeochemical processes and geotechnical applications: progress, opportunities and challenges. *Géotechnique* 63, 287–301. doi: 10.1680/geot.SIP13.P.017

DeJong, M. J., and Ulm, F. J. (2007). The nanogranular behavior of C-S-H at elevated temperatures (up to 700°C). *Cem. Concr. Res.* 37, 1–12. doi: 10.1016/j.cemconres.2006.09.006

Demény, A., Németh, P., Czuppon, G., Leél-Őssy, S., Szabó, M., Judik, K., et al. (2016). Formation of amorphous calcium carbonate in caves and its implications for speleothem research. *Sci. Rep.* 6:39602. doi: 10.1038/srep39602

Dhami, N. K., Alsubhi, W. R., Watkin, E., and Mukherjee, A. (2017a). Bacterial community dynamics and biocement formation during stimulation and augmentation: implications for soil consolidation. *Front. Microbiol.* 8:1267. doi: 10.3389/fmicb.2017.01267

Dhami, N. K., Mukherjee, A., and Reddy, M. S. (2013a). Biomineralization of calcium carbonate polymorphs by the bacterial strains isolated from calcareous sites. *J. Microbiol. Biotechnol.* 23, 707–714.

Dhami, N. K., Mukherjee, A., and Reddy, M. S. (2016). Micrographical, minerological and nano-mechanical characterisation of microbial carbonates from urease and carbonic anhydrase producing bacteria. *Ecol. Eng.* 94, 443–454. doi: 10.1016/j.ecoleng.2016.06.013

Dhami, N. K., Quirin, M. E. C., and Mukherjee, A. (2017b). Carbonate biomineralization and heavy metal remediation by calcifying fungi isolated from karstic caves. *Ecol. Eng.* 103, 106–117. doi: 10.1016/j.ecoleng.2017.03.007

Dhami, N. K., Reddy, M. S., and Mukherjee, A. (2012). "Biofilm and microbial applications in biomineralized concrete," in *Advanced Topics in Biomineralization*, ed. J. Seto (Rijeka: InTech), 137–164.

Dhami, N. K., Reddy, M. S., and Mukherjee, A. (2013b). Biomineralization of calcium carbonates and their engineered applications: a review. *Front. Microbiol.* 4:314. doi: 10.3389/fmicb.2013.00314

Dhami, N. K., Reddy, M. S., and Mukherjee, A. (2014). Application of calcifying bacteria for remediation of stones and cultural heritages. *Front. Microbiol.* 5:304. doi: 10.3389/fmicb.2014.00304

Douglas, S., and Beveridge, T. (1998). Mineral formation by bacteria in natural microbial communities. *FEMS Microbiol. Ecol.* 26, 79–88. doi: 10.1111/j.1574-6941.1998.tb00494.x

Eberhard, S., and Davies, S. (2011). Impacts of drying climate on aquatic cave fauna in Jewel cave and other caves in Southwest Western Australia. *J. Australas. Cave Karst Manag. Assoc.* 83, 6–13.

Eberhard, S. M. (2004). *Ecology and Hydrology of a Threatened Groundwater-dependent Ecosystem: The Jewel Cave Karst System in Western Australia*. Ph.D. thesis, Murdoch University, Perth, WA.

Edgar, R. C., Haas, B. J., Clemente, J. C., Quince, C., and Knight, R. (2011). UCHIME improves sensitivity and speed of chimera detection. *Bioinformatics* 27, 2194–2200. doi: 10.1093/bioinformatics/btr381

Folk, R. L., Chafetz, H. S., and Tiezzi, P. A. (1985). "Bizarre forms of depositional and diagenetic calcite in hot-spring travertines, central Italy," in *Carbonate Cements,* eds N. Schneidermann and P. M. Harris (Tulsa, OK: Society of Economic Paleontologists and Mineralogists), 349–369.

Fortin, D., Ferris, F., and Beveridge, T. (1997). Surface-mediated mineral development by bacteria. *Rev. Mineral. Geochem.* 35, 161–180.

Garcia, M. G., Marco Antonio, M. G., and Claudia Ximena, M. H. (2016). Characterization of bacterial diversity associated with calcareous deposits and drip-waters, and isolation of calcifying bacteria from two Colombian mines. *Microbiol. Res.* 182, 21–30. doi: 10.1016/j.micres.2015.09.006

Googlemaps (2016). *Margaret River Western Australia*. Available at: https://www.google.com.au/maps/@-26.6076557,127.8053516,5z

Grüneberg, E., Schöning, I., Kalko, E. K. V., and Weisser, W. W. (2010). Regional organic carbon stock variability: a comparison between depth increments and soil horizons. *Geoderma* 155, 426–433. doi: 10.1016/j.jenvman.2015.03.039

Hamilton, W. A. (2003). Microbially influenced corrosion as a model system for the study of metal microbe interactions: a unifying electron transfer hypothesis. *Biofouling* 19, 65–76. doi: 10.1080/0892701021000041078

Hammes, F., and Verstraete, W. (2002). Key roles of pH and calcium metabolism in microbial carbonate precipitation. *Rev. Environ. Sci. Biotechnol.* 1, 3–7. doi: 10.1111/j.1472-4669.2012.00342.x

Harmon, R. S., Atkinson, T. C., and Atkinson, J. L. (1983). The mineralogy of Castleguard Cave, Columbia Icefields, Alberta, Canada. *Arctic Alp. Res.* 15, 503–506. doi: 10.2307/1551236

Hill, C. A., and Forti, P. (1986). *Cave Minerals of the World*, 1st Edn. Huntsville, AL: National Speleological Society.

Hill, C. A., and Forti, P. (1997). *Cave Minerals of the World*. Huntsville, AL: National Speleological Society.

Hoffman, G. (1991). *VDLUFA-Methodenbuch: Die Untersuchung von Böden,* Band I. Darmstadt: Verband Deutscher Landwirtschaftlicher Untersuchungs.

Holmes, A. J., Tujula, N. A., Holley, M., Contos, A., James, J. M., Rogers, P., et al. (2001). Phylogenetic structure of unusual aquatic microbial formations in Nullarbor caves, Australia. *Environ. Microbiol.* 3, 256–264. doi: 10.1046/j.1462-2920.2001.00187.x

Jasinska, E. J. (1997). *Fauna of Aquatic Root Mats in Caves of Southwestern Australia: Origins and Ecology*. Crawley, WA: University of Western Australia.

Jimenez-Lopez, C., Jroundi, F., Pascolini, C., Rodriguez-Navarro, C., Piñar-Larrubia, G., Rodriguez-Gallego, M., et al. (2008). Consolidation of quarry calcarenite by calcium carbonate precipitation induced by bacteria activated among the microbiota inhabiting the stone. *Int. Biodeterior. Biodegradation* 62, 352–363. doi: 10.1016/j.ibiod.2008.03.002

Jones, B. (2001). Microbial activity in caves-A geological perspective. *Geomicrobiol. J.* 18, 345–357. doi: 10.1080/01490450152467831

Jones, B. (2010). The preferential association of dolomite with microbes in stalactites from Cayman Brac, British West Indies. *Sediment. Geol.* 226, 94–109. doi: 10.1016/j.sedgeo.2010.03.004

Jroundi, F., Gonzalez-Munoz, M. T., Garcia-Bueno, A., and Rodriguez-Navarro, C. (2014). Consolidation of archaeological gypsum plaster by bacterial biomineralization of calcium carbonate. *Acta Biomater.* 10, 3844–3854. doi: 10.1016/j.actbio.2014.03.007

Kendall, A. C., and Broughton, P. L. (1978). Origin of fabrics in speleothems composed of columnar calcite crystals. *J. Sediment. Res.* 48, 519–538.

Larouche, J. R., Bowden, W. B., Giordano, R., Flinn, M. B., and Crump, B. C. (2012). Microbial biogeography of arctic streams: exploring influences of lithology and habitat. *Front. Microbiol.* 3:309. doi: 10.3389/fmicb.2012.00309

Leél-Őssy, S., Szanyi, G., and Surányi, G. (2011). Minerals and speleothems of the József-hegy Cave (Budapest. Hungary). *Int. J. Speleol.* 40, 191–203. doi: 10.5038/1827-806X.40.2.11

Lowenstam, H. A. (1981). Minerals formed by organisms. *Science* 211, 1126–1131. doi: 10.1126/science.7008198

Macalady, J. L., Jones, D. S., and Lyon, E. H. (2007). Extremely acidic, pendulous cave wall biofilms from the Frasassi cave system, Italy. *Environ. Microbiol.* 9, 1402–1414. doi: 10.1111/j.1462-2920.2007.01256.x

Maciejewska, M., Adam, D., Naômé, A., Martinet, L., Tenconi, E., Całusińska, M., et al. (2017). Assessment of the potential role of *Streptomyces* in cave moonmilk formation. *Front. Microbiol.* 8:1181. doi: 10.3389/fmicb.2017.01181

Melim, A., Kristen, M., and Shinglman, P. L. (2001). Evidence for microbial involvement in pool finger precipitation, Hidden Cave, New Mexico. *Geomicrobiol. J.* 18, 311–329. doi: 10.1080/01490450152467813

Melim, L. A., Northup, D. E., Spilde, M. N., Jones, B., Boston, P. J., and Bixby, R. J. (2008). Reticulated filaments in cave pool speleothems: microbe or mineral? *J. Cave Karst Study* 70, 135–141.

Morse, J. W. (1983). The kinetics of calcium carbonate dissolution and precipitation. *Rev. Mineral. Geochem.* 11, 227–264.

Müller, W. E. G., Neufurth, M., Schlossmacher, U., Schröder, H. C., Pisignano, D., and Wang, X. (2014). The sponge silicatein-interacting protein silintaphin-2 blocks calcite formation of calcareous sponge spicules at the vaterite stage. *RSC Adv. J.* 4, 2577–2585. doi: 10.1039/C3RA45193C

Northup, D. E., Barns, S. M., Yu, L. E., Spilde, M. N., Schelble, R., Dano, K., et al. (2003). Diverse microbial communities inhabiting ferromanganese deposits in Lechuguilla and Spider Caves. *Environ. Microbiol.* 5, 1071–1086. doi: 10.1046/j.1462-2920.2003.00500.x

Northup, E., and Lavoie Diana, K. (2001). Geomicrobiology of caves: a review. *Geomicrobiol. J.* 18, 199–222. doi: 10.1080/01490451052467750

Okyay, T. O., and Rodrigues, D. F. (2015). Biotic and abiotic effects on CO_2 sequestration during microbially-induced calcium carbonate precipitation. *FEMS Microbiol. Ecol.* 91:fiv017. doi: 10.1093/femsec/fiv017

Onac, B. P., and Ghergari, L. (1993). Moonmilch mineralogy in some Romanian and Norwegian Caves. *Cave Sci.* 20, 107–111.

Pacton, M., Breitenbach, S. F. M., Lechleitner, F. A., Vaks, A., Rollion-Bard, C., Gutareva, O. S., et al. (2013). The role of microorganisms in the formation of a stalactite in Botovskaya Cave, Siberia – paleoenvironmental implications. *Biogeosciences* 10, 6115–6130. doi: 10.5194/bg-10-6115-2013

Phillips, A. J., Gerlach, R., Lauchnor, E., Mitchell, A. C., Cunningham, A. B., and Spangler, L. (2013). Engineered applications of ureolytic biomineralization: a review. *Biofouling* 29, 715–733. doi: 10.1080/08927014.2013.796550

Pogson, R. E., Osborne, A. L., and Colchester, M. (2014). Minerals of Jenolan Caves, New South Wales, Australia: geological and biological interactions. *Proc. Linn. Soc. N. S. W. J.* 136, 1–18.

Porter, H., Dhami, N. K., and Mukherjee, A. (2017). Synergistic chemical and microbial cementation for stabilization of aggregates. *Cem. Concr. Compos.* 83, 160–170. doi: 10.1016/j.cemconcomp.2017.07.015

Portillo, M. C., Gonzalez, J. M., and Saiz-Jimenez, C. (2008). Metabolically active microbial communities of yellow and grey colonizations on the walls of Altamira Cave, Spain. *J. Appl. Microbiol.* 104, 681–691. doi: 10.1111/j.1365-2672.2007.03594.x

Presser, V., Gerlach, K., Vohrer, A., Nickel, K. G., and Dreher, W. F. (2010). Determination of the elastic modulus of highly porous samples by nanoindentation: a case study on sea urchin spines. *J. Mater. Sci.* 45, 2408–2418. doi: 10.1007/s10853-010-4208-y

Quast, C., Pruesse, E., Yilmaz, P., Gerken, J., Schweer, T., Yarza, P., et al. (2013). The SILVA ribosomal RNA gene database project: improved data processing and web-based tools. *Nucleic Acids Res.* 41, D590–D596. doi: 10.1093/nar/gks1219

Ren, D., Meyers, M. A., Zhou, B., and Feng, Q. (2013). Comparative study of carp otolith hardness: lapillus and asteriscus. *Mater. Sci. Eng. C Mater. Biol. Appl.* 33, 1876–1881. doi: 10.1016/j.msec.2012.10.015

Rodriguez-Navarro, C., Jroundi, F., Schiro, M., Ruiz-Agudo, E., and Gonzalez-Munoz, M. T. (2012). Influence of substrate mineralogy on bacterial mineralization of calcium carbonate: implications for stone conservation. *Appl. Environ. Microbiol.* 78, 4017–4029. doi: 10.1128/AEM.07044-11

Ronholm, J., Schumann, D., Sapers, H., Izawa, M., Applin, D., Berg, B., et al. (2014). A mineralogical characterization of biogenic calcium carbonates precipitated by heterotrophic bacteria isolated from cryophilic polar regions. *Geobiology* 12, 542–556. doi: 10.1111/gbi.12102

Rooney, D. C., Hutchens, E., Clipson, N., Baldini, J., and Dermott, F. M. (2010). Microbial community diversity of moonmilk deposits at Ballynamintra Cave, Co. WaterfordI, Ireland. *Environ. Microbiol.* 60, 753–761. doi: 10.1007/s00248-010-9693-7

Rusznyak, A., Akob, D. M., Nietzsche, S., Eusterhues, K., Totsche, K. U., Neu, T. R., et al. (2012). Calcite biomineralization by bacterial isolates from the recently discovered pristine karstic Herrenberg cave. *Appl. Environ. Microbiol.* 78, 1157–1167. doi: 10.1128/AEM.06568-11

Sánchez-Román, M., Rivadeneyra, M. A., Vasconcelos, C., and Mckenzie, J. A. (2007). Biomineralization of carbonate and phosphate by moderately halophilic bacteria. *FEMS Microbiol. Ecol.* 61, 273–284. doi: 10.1111/j.1574-6941.2007.00336.x

Self, C. A., and Hill, C. A. (2003). How speleothems grow: an introduction to the ontogeny of cave minerals. *J. Cave Karst Stud.* 65, 130–151.

Shirakawa, M. A., Cincotto, M. A., Atencio, D., Gaylarde, C. C., and John, V. M. (2011). Effect of culture medium on biocalcification by *Pseudomonas putida*, *Lysinibacillus sphaericus* and *Bacillus subtilis*. *Braz. J. Microbiol.* 42, 499–507. doi: 10.1590/S1517-838220110002000014

Short, M. B., Baygents, J. C., Beck, J. W., Stone, D. A., Toomey, R. S. III, and Goldstein, R. E. (2005). Stalactite growth as a free-boundary problem: a geometric law and its platonic ideal. *Phys. Rev. Lett.* 94:018501. doi: 10.1103/PhysRevLett.94.018501

Skinner, H., and Jahren, A. (2004). "Biomineralization," in *Biochemistry*, ed. W. H. Schlesinger (Atlanta, GA: Elsevier), 117–184.

Tomczyk-Żak, K., and Zielenkiewicz, U. (2015). Microbial diversity in caves. *Geomicrobiol. J.* 33, 20–38. doi: 10.1080/01490451.2014.1003341

Wang, J., and Becker, U. (2009). Structure and carbonate orientation of vaterite ($CaCO_3$). *Am. Mineral.* 94, 380–386. doi: 10.2138/am.2009.2939

White, W. B. (1962). Introduction to the symposium on cave mineralogy. *Natl. Speleol. Soc. Bull.* 24, 55–56.

Wu, Y., Tan, L., Liu, W., Wang, B., Wang, J., Cai, Y., et al. (2015). Profiling bacterial diversity in a limestone cave of the western Loess Plateau of China. *Front. Microbiol.* 6:244. doi: 10.3389/fmicb.2015.00244

Zamarreno, D. V., Inkpen, R., and May, E. (2009). Carbonate crystals precipitated by freshwater bacteria and their use as a limestone consolidant. *Appl. Environ. Microbiol.* 75, 5981–5990. doi: 10.1128/AEM.02079-08

Zamiri, A., and De, S. (2011). Mechanical properties of hydroxyapatite single crystals from nanoindentation data. *J. Mech. Behav. Biomed. Mater.* 4, 146–152. doi: 10.1016/j.jmbbm.2010.11.001

Zepeda Mendoza, M. L., Lundberg, J., Ivarsson, M., Campos, P., Nylander, J. A., Sallstedt, T., et al. (2016). Metagenomic analysis from the interior of a speleothem in Tjuv-Ante's Cave, Northern Sweden. *PLOS ONE* 11:e0151577. doi: 10.1371/journal.pone.0151577

Zhang, J., Kobert, K., Flouri, T., and Stamatakis, A. (2014). PEAR: a fast and accurate Illumina paired-end reAd mergeR. *Bioinformatics* 30, 614–620. doi: 10.1093/bioinformatics/btt593

Zhu, T., and Dittrich, M. (2016). Carbonate precipitation through microbial activities in natural environment, and their potential in biotechnology: a review. *Front. Bioeng. Biotechnol.* 4:4. doi: 10.3389/fbioe.2016.00004

Zhu, W., Hughes, J. J., Bicanic, N., and Pearce, C. J. (2007). Nanoindentation mapping of mechanical properties of cement paste and natural rocks. *Mater. Charact.* 58, 1189–1198. doi: 10.1016/j.matchar.2007.05.018

Conflict of Interest Statement: The authors declare that the research was conducted in the absence of any commercial or financial relationships that could be construed as a potential conflict of interest.

frontiers in Microbiology

PERSPECTIVE
published: 13 February 2018
doi: 10.3389/fmicb.2018.00180

Bioenergetic Controls on Microbial Ecophysiology in Marine Sediments

James A. Bradley[1]*, *Jan P. Amend*[1,2] and *Douglas E. LaRowe*[1]

[1] Department of Earth Sciences, University of Southern California, Los Angeles, CA, United States, [2] Department of Biological Sciences, University of Southern California, Los Angeles, CA, United States

Marine sediments constitute one of the most energy-limited habitats on Earth, in which microorganisms persist over extraordinarily long timescales with very slow metabolisms. This habitat provides an ideal environment in which to study the energetic limits of life. However, the bioenergetic factors that can determine whether microorganisms will grow, lie dormant, or die, as well as the selective environmental pressures that determine energetic trade-offs between growth and maintenance activities, are not well understood. Numerical models will be pivotal in addressing these knowledge gaps. However, models rarely account for the variable physiological states of microorganisms and their demand for energy. Here, we review established modeling constructs for microbial growth rate, yield, maintenance, and physiological state, and then provide a new model that incorporates all of these factors. We discuss this new model in context with its future application to the marine subsurface. Understanding the factors that regulate cell death, physiological state changes, and the provenance of maintenance energy (i.e., endogenous versus exogenous metabolism), is crucial to the design of this model. Further, measurements of growth rate, growth yield, and basal metabolic activity will enable bioenergetic parameters to be better constrained. Last, biomass and biogeochemical rate measurements will enable model simulations to be validated. The insight provided from the development and application of new microbial modeling tools for marine sediments will undoubtedly advance the understanding of the minimum power required to support life, and the ecophysiological strategies that organisms utilize to cope under extreme energy limitation for extended periods of time.

Keywords: bioenergetics, numerical modeling, dormancy, maintenance energy, geobiology, life in extreme environments, low energy, endogenous and exogenous metabolism

OPEN ACCESS

Edited by:
Virginia P. Edgcomb, Woods Hole Oceanographic Institution, United States

Reviewed by:
Brent Craig Christner, University of Florida, United States
Thomas Maskow, Helmholtz-Zentrum für Umweltforschung (UFZ), Germany

***Correspondence:**
James A. Bradley
jbradley8365@gmail.com

Specialty section:
This article was submitted to Extreme Microbiology, a section of the journal Frontiers in Microbiology

Received: *26 October 2017*
Accepted: *26 January 2018*
Published: *13 February 2018*

Citation:
Bradley JA, Amend JP and LaRowe DE (2018) Bioenergetic Controls on Microbial Ecophysiology in Marine Sediments. Front. Microbiol. 9:180. doi: 10.3389/fmicb.2018.00180

INTRODUCTION

Marine sediments across the globe host a rich microbial biosphere, whose dynamics are important analogs to oligotrophic and extra-terrestrial environments, and whose activity bears a major control on organic carbon (OC) burial and thus global climate. Microbial cells in oligotrophic marine sediments catabolize 10^4–10^6 fold more slowly than model organisms in nutrient-rich media (Hoehler and Jørgensen, 2013), yet despite enduring prolonged starvation, they persist over geological timescales (D'Hondt et al., 2015). The vast majority of marine sediments constitute one of the most energy-limited habitats on Earth (Lever et al., 2015) and provide ideal test-cases to study the extreme limits of life over timescales that challenge fundamental notions of what it means to be alive. By studying life at its limit (i.e., low energy, low nutrients), much can be

learned about the fundamental ecophysiology of microorganisms. Since most microorganisms in marine sediments appear to be merely surviving rather than growing, factors such as metabolic state and maintenance energy utilization become increasingly important over the long timescales (i.e., thousands to millions of years) associated with this habitat.

Despite much effort to characterize and understand the ecophysiology associated with microorganisms and microbial communities from the deep subsurface biosphere, it is generally still unknown which factors govern whether microorganisms buried in sediments will grow and produce daughter cells, lie dormant for thousands to millions of years, or die at an extremely slow rate. A more comprehensive understanding of the factors that determine physiological state, as well as energy utilized for growth and maintenance, are crucial in addressing these fundamental questions facing deep biosphere research.

Here, we discuss bioenergetics, dormancy and maintenance energy in the subsurface, and consider how quantitative approaches (i.e., modeling) provide opportunities to complement ongoing research. We provide mathematical constructs for simulating microbial growth, yield, maintenance activities, and physiological state changes (i.e., active and dormant), and discuss them in the context of application to the marine subsurface biosphere. We hope to encourage a better integration of theoretical and experimental approaches to subsurface bioenergetics, which we believe is required to advance deep biosphere investigations beyond what can presently be captured by observations alone.

BIOENERGETICS AS A DRIVER OF MICROBIAL DYNAMICS IN MARINE SEDIMENTS

All organisms require energy to stay alive. That energy is ultimately harvested from the catalysis of redox reactions. Exergonic (energy-yielding) reactions are catalyzed within or nearby living cells at some rate to provide power. This power may ultimately be used to fuel endergonic (energy-requiring) reactions to maintain a cellular steady-state and sometimes (but not always) to grow. The amount of energy available from the catalysis of exergonic redox reactions can be determined by calculating the Gibbs energy of a potential reaction under a given set of geochemical conditions. Gibbs energy calculations demonstrate not only which reactions are thermodynamically favorable and thus constitute conceivable catabolic strategies for microorganisms, but also which environmental variables, including temperature, pressure, pH, salinity, and the concentrations of electron donors and terminal electron acceptors, influence the amount of energy available to microorganisms. In marine sediments, these factors are largely driven by the flux and burial of organic and mineral particles, and living organisms, to the ocean floor. Physical processes such as bioturbation, the diffusion of aqueous species including electron acceptors (e.g., O_2, SO_4^{2-}) and secondary redox products (e.g., Fe^{2+}, CH_4, H_2S), the sorption of OC to mineral surfaces, and mineral precipitation, also alter sediment properties. OC is the primary electron donor for microorganisms in marine sediments (Arndt et al., 2013) and O_2 and SO_4^{2-} are the primary electron acceptors for its oxidation (Thullner et al., 2009).

ENERGY FOR GROWTH AND MAINTENANCE

Growth yields and cellular maintenance requirements are subject to trade-offs based on selective pressures in different environments (Lele and Watve, 2014). Under low-energy conditions, such as in marine sediments, it is thought that microbial activity is limited, more or less, to maintaining cellular integrity through biomolecular repair and replacement (Westerhoff et al., 1983; Tijhuis et al., 1993; del Giorgio and Cole, 1998; Smith and Prairie, 2004; Carlson et al., 2007; Orcutt et al., 2013). Maintenance activities constitute the sum of activities that do not produce growth (e.g., regeneration of enzymes, maintaining membrane integrity, motility, etc.). Accordingly, maintenance activities potentially constitute a much greater fraction of total power utilized by microbial communities in marine sediments compared to other natural settings, or those grown in laboratories.

However, data from (or representative of) marine sediments are lacking, and an accurate determination of the *in situ* maintenance power utilization of microorganisms in any natural setting is challenging. Empirical approaches are plagued by methodological problems, experimental artifacts, and inconsistencies across studies (Hobson, 1965; Hempfling and Mainzer, 1975; Russell and Baldwin, 1979). Laboratory-determined values of maintenance powers are also likely a gross over-estimation of power requirement in natural settings due to the favorable (high-energy) conditions under which microorganisms are grown in the laboratory compared to the conditions that microorganisms experience in nature (LaRowe and Amend, 2015a). However, by integrating experimental datasets with numerical modeling, LaRowe and Amend (2015b) derived microbial power use by microorganisms from oligotrophic sediments in the South Pacific Gyre that were several orders of magnitude lower than laboratory-measured maintenance powers. Given the extreme energy-limitation of these sediments, the low rates of OC processing, and the net decline in biomass over the multi-million-year timescales over which cells are buried, it can be assumed that cells present in these sediments are not growing, and thus calculated power utilization represents mostly (if not exclusively) maintenance activities.

Maintenance energy for microorganisms in marine sediments might come from (i) endogenous catabolism, i.e., the utilization of biomass (Herbert, 1958), (ii) exogenous catabolism, i.e., the consumption of additional substrate (Pirt, 1965), or (iii) a combination of the two, which might vary depending on thermodynamic and environmental factors (Wang and Post, 2012).

ACTIVITY AKIN TO DORMANCY

The idealized conditions under which microorganisms are grown in the laboratory rarely occur in nature. The apparent ubiquity of microorganisms in natural environments that exhibit extraordinarily slow growth, intermittent growth, or even no growth, reflects a general lack of available energy (Morita, 1988). Microorganisms in marine sediments may be considered some of the slowest, most energy-limited living organisms on Earth, generally exhibiting levels of activity that are several orders of magnitude lower than anything measured via cultivation (Jørgensen and Boetius, 2007; D'Hondt et al., 2009, 2015; Røy et al., 2012; Hoehler and Jørgensen, 2013; Jørgensen and Marshall, 2016). The typical vegetative-like state of microorganisms in marine sediments is tantamount to dormancy (Jørgensen and Marshall, 2016), a transient and reversible state of low metabolic activity. Dormancy is thought to enable microorganisms to endure extended periods of unfavorable conditions such as energy-limitation, without the need to divide (Lever et al., 2015). Despite the omnipresence of dormant cells in marine sediments, the exact nature of dormancy and of its bioenergetic controls in relation to the marine sedimentary environment are not well understood. For instance, the rate at which energy is used by dormant cells, or the thermodynamic and environmental parameters that initiate or terminate dormancy, are not known. A quantitative approach toward microbial dormancy incorporating bioenergetics is thus required to truly understand the deep biosphere.

BIOENERGETICS AND MODELING

Microbial and geochemical models can help determine the fluxes of energy and material between ecosystem components, disentangle processes that are observed experimentally as a net outcome, and predict the sensitivity and response of ecosystems and geochemical environments to perturbations and changing conditions. Further, they are useful to bridge scales, interpolate between observations, and help identify important data and knowledge gaps. Models are also particularly helpful for deep biosphere investigations since the marine subsurface is notoriously difficult to study using traditional sampling strategies, because of its remoteness and relative inaccessibility, the exceedingly slow rates of energy processing, and the vast timescales over which measurements represent.

A review of the diagenetic models commonly used to simulate the degradation of OC, a process that drives biogeochemical reactions in marine sediments, is presented by Arndt et al. (2013). Thermodynamic models have also been used to quantify the power supply to and demand by microorganisms in marine sediments (e.g., LaRowe and Amend, 2015b), and Gibbs energy calculations have been used to infer what types of reactions microorganisms may be catalyzing in the subsurface (e.g., Teske et al., 2014; McKay et al., 2016; Sylvan et al., 2016). However, the majority of models assume that microbial biomass is in a steady state or has negligible influence beyond transient timescales (Thullner et al., 2005). Models need to be complex enough to describe the required properties and processes of the system, but structurally and mechanistically simple enough to be able to constrain and validate parameters and simulations from available data and literature. At present, a suitable microbial-biogeochemical model for the marine subsurface, capturing the ecophysiological factors discussed here, does not exist. In the following sections, we provide formulations for how such factors may be represented. The models presented here are based on differential equations that describe ecological processes in a mathematical sense. For a comprehensive guide to formulating ecological models, we direct the reader to Soetaert and Herman (2009).

Heterotrophic Growth and Organic Carbon Degradation

The following model (Equations 1 and 2), and some variations of these expressions including logistic growth, a rate limiting term, and mortality, form the basis of many ecosystem models (Soetaert and Herman, 2009; Sierra et al., 2015). Here, heterotrophic growth is dependent on the availability of OC as a substrate, and can be described by:

$$\frac{\delta B}{\delta t} = \left(V_{max} \cdot B \cdot \frac{OC}{K_{OC} + OC} \right) - (\alpha \cdot B) \tag{1}$$

where B denotes the concentration of microbial carbon, t is time, V_{max} corresponds to maximum microbial growth rate, OC denotes OC concentration (the non-living organic component), K_{OC} is the half-saturation constant for OC, a kinetic parameter that describes the dependency of microbial growth on OC concentration, and α represents the specific death rate.

The change in OC due to microbial processes can then be represented by:

$$\frac{\delta OC}{\delta t} = -\left(\frac{1}{Y} \cdot V_{max} \cdot B \cdot \frac{OC}{K_{OC} + OC} \right) + (\alpha \cdot B) \tag{2}$$

where Y represents an observed growth yield, which is the efficiency of converting carbon into microbial products (Sinsabaugh et al., 2013). The contribution of dead biomass to OC is represented by ($\alpha \cdot B$). Equations (1) and (2) constitute the "Basic" model (**Figure 1A**). This approach lumps maintenance and growth costs into a single parameter (Y), and assumes that all microorganisms are active. Thus, it is not sufficient to describe microbial processes in marine sediments.

Incorporating Maintenance and Growth Yields

Mechanistically distinguishing between maintenance energy and growth yield is important to accurately quantify bioenergetics in low-energy environments such as marine sediments where non-growing organisms expend a larger proportion of their total power utilization on maintenance.

Two well-known approaches to simulating maintenance energy are provided by Herbert (1958) and Pirt (1965). These approaches differ by the provenance of maintenance energy.

The first of these model types, commonly referred to as the Herbert approach, considers maintenance costs as endogenous

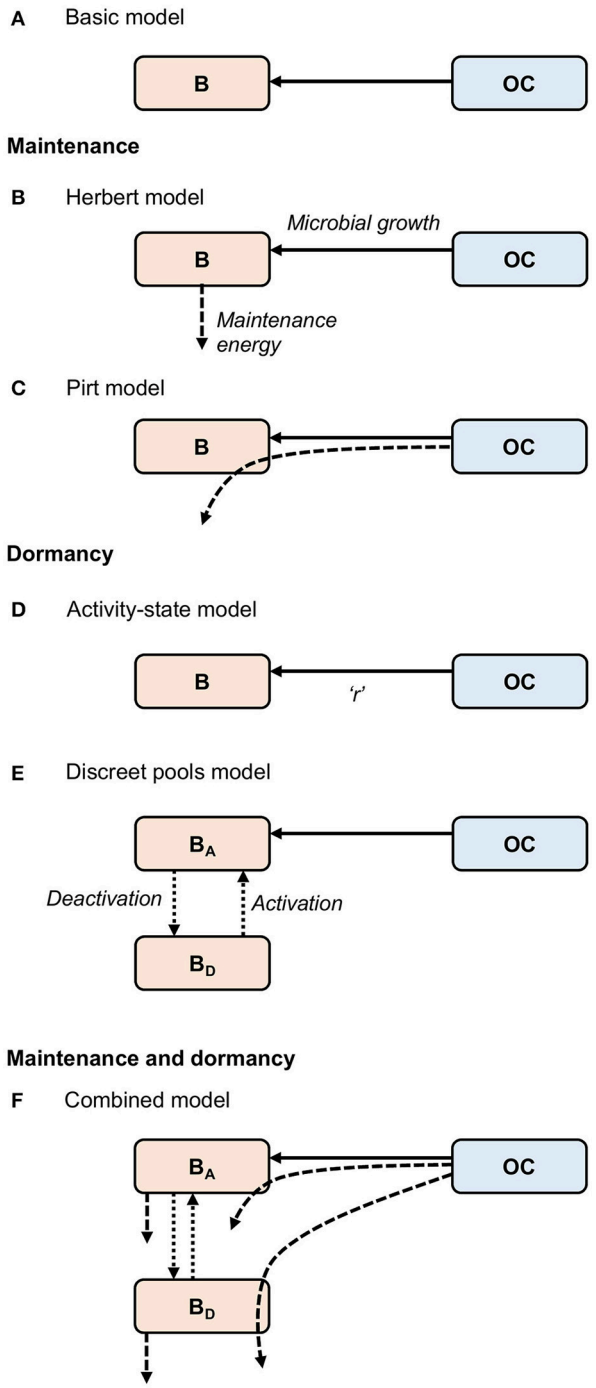

FIGURE 1 | Conceptual models for **(A)** "Basic" microbial growth, maintenance utilizing **(B)** Herbert, and **(C)** Pirt formulations, dormancy utilizing **(D)** "Activity-state" and **(E)** "Discreet pools" approaches, and **(F)** a "Combined model," developed here, combining formulations for maintenance and dormancy. Solid arrows represent biomass growth, dashed arrows represent maintenance energy, and dotted arrows represent transfers between active (B_A) and dormant (B_D) states. Microbial death [transfer from biomass (B) to organic carbon (OC)] is not shown. *"r"* in the "Activity-state" model **(D)** represents the proportion of actively growing microbial biomass (B), and varies from zero to one.

catabolism, i.e., the consumption of biomass (**Figures 1B**, **2A**) (Herbert, 1958; Knapp et al., 1983; Kim and Or, 2016). Thus, the specific maintenance rate is regarded as a negative growth rate:

$$\frac{\delta B}{\delta t} = \left(V_{max} \cdot B \cdot \frac{OC}{K_{OC} + OC}\right) - (\alpha \cdot B) - (a \cdot B) \qquad (3)$$

where a indicates maintenance requirement. Correspondingly, the change in OC is:

$$\frac{\delta OC}{\delta t} = -\left(\frac{1}{Y_G} \cdot V_{max} \cdot B \cdot \frac{OC}{K_{OC} + OC}\right) + (\alpha \cdot B) \qquad (4)$$

Here, Y_G represents the "true growth yield" (Pirt, 1965) reflected by the expenditure of energy solely to generate new biomass (Lipson, 2015). This formulation allows for maintenance activities to continue independently of substrate availability, and thus is potentially useful and appropriate for simulating microbial maintenance under substrate-starved conditions, such as in the vast majority of marine sediments. However, this expression does not allow for microorganisms to cover maintenance requirements from substrate, which may occur when substrate is plentiful (Dawes and Ribbons, 1964), and features a maximum specific growth rate (V_{max}) and a "true growth yield" (Y_G) that are less suitable from an empirical point of view as they cannot be observed or measured directly (Beeftink et al., 1990).

The second model type, commonly referred to as the Pirt approach (Pirt, 1965; Darrah, 1991) considers the additional consumption of substrate for maintenance (**Figures 1C**, **2B**), coupling "Basic" microbial growth (Equation 1) with the consumption of substrate according to:

$$\begin{aligned} \frac{\delta B}{\delta t} &= \left(V_{max} \cdot B \cdot \frac{OC}{K_{OC} + OC}\right) - (\alpha \cdot B) \\ \frac{\delta OC}{\delta t} &= -\left(\frac{1}{Y_G} \cdot V_{max} \cdot B \cdot \frac{OC}{K_{OC} + OC}\right) - (a \cdot B) + (\alpha \cdot B) \end{aligned} \qquad (5)$$

Here, however, the consumption of substrate is numerically possible even in its absence, due to the term that is included for maintenance ($a \cdot B$). Thus, this expression could be problematic for simulating marine sediments, because continual uptake of OC in low-energy, OC-poor sediments that characterize the deep biosphere may cause a mass imbalance.

In natural settings, the specific maintenance rate, as well the provenance of maintenance energy, can vary under different environmental conditions (Van Bodegom, 2007). A "Variable" model that allows for environmental factors to dictate the supply of maintenance energy from biomass and/or substrate, adapted from Wang and Post (2012), is:

$$\frac{\delta B}{\delta t} = \left(V_{max} \cdot B \cdot h\,(OC)\right) - \left(m_q \cdot B \cdot (1 - h\,(OC))\right) - (\alpha \cdot B) \qquad (6)$$

where m_q represents the specific maintenance rate, and $h(OC)$ is a function that varies from 0 to 1, and allows for microorganisms

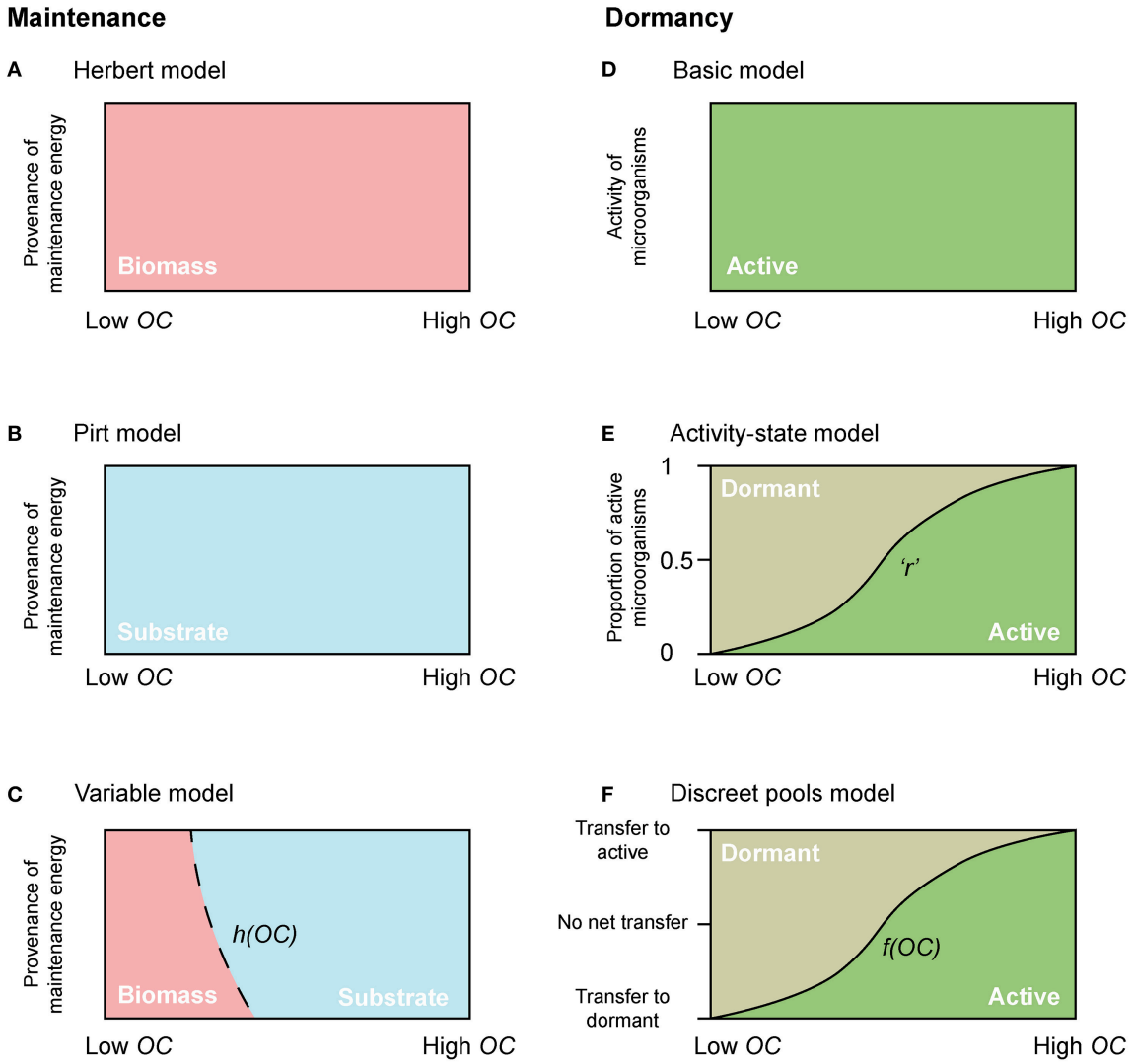

FIGURE 2 | Conceptual diagrams of maintenance energy provenance and dormancy. The dependency of maintenance energy provenance on organic carbon concentration with **(A)** Herbert, **(B)** Pirt, and **(C)** a "Variable" approach. Dependency of physiological state change of microorganisms with **(D)** the "Basic model," **(E)** the "Activity-state model," and **(F)** the "Discreet pools model". "*r*" in the "Activity-state model" represents the proportion of actively growing microbial biomass (*B*), and varies from 0 to 1. "*h(OC)*" in the "Variable model" and "*f(OC)*" in the "Discreet pools model" are functions that vary from 0 to 1.

to cover their maintenance requirements from OC when it is plentiful [$h(OC) \rightarrow 1$ when $OC \gg K_{OC}$], but from biomass when OC becomes scarce ($h(0) = 0$) (**Figure 2C**).

The change in OC is calculated according to:

$$\frac{\delta OC}{\delta t} = -\left(\frac{1}{Y_G} \cdot V_{max} \cdot B \cdot h\,(OC)\right) - \left(m_q \cdot B \cdot h\,(OC) \cdot \frac{1}{Y_G}\right) + (\alpha \cdot B) \quad (7)$$

This model follows the assumptions of (*i*) net negative growth at limiting concentrations of OC ($OC \rightarrow 0$), (*ii*) no OC consumption when OC is exhausted ($OC = 0$), and (*iii*) no biomass degradation (due to endogenous maintenance) and maximum microbial growth when OC is plentiful ($OC \gg K_{OC}$).

Incorporating Active and Dormant Microorganisms

With few exceptions, microbial models do not account for active and dormant biomass, and cells are considered either alive and active, or dead (**Figure 2D**). Of those models that incorporate multiple physiological states, there are two general approaches. First is to directly regard the active fraction of biomass (i.e., the ratio of active biomass to total living biomass) as a state variable (**Figures 1D**, **2E**) (e.g., Panikov, 1995; Blagodatsky and Richter, 1998; Ingwersen et al., 2008):

$$\frac{\delta B}{\delta t} = r\left(V_{max} \cdot B \cdot \frac{OC}{K_{OC} + OC} - \alpha \cdot B\right) \quad (8)$$

where r represents the proportion of actively growing biomass (B) ($0 \leq r \leq 1$), and its value may depend on multiple environmental and biological factors.

The corresponding change in OC is:

$$\frac{\delta OC}{\delta t} = -r\left(\frac{1}{Y} \cdot V_{max} \cdot B \cdot \frac{OC}{K_{OC} + OC}\right) + r\,(\alpha \cdot B) \quad (9)$$

Equations (8) and (9) constitute the "Activity-state" model.

Second is to explicitly separate the total live biomass into active (B_A) and dormant (B_D) pools (**Figures 1E**, **2F**, e.g., Bär et al., 2002; Stolpovsky et al., 2011):

$$\frac{\delta B_A}{\delta t} = V_{max} \cdot B_A \cdot \frac{OC}{K_{OC} + OC} - \alpha_A \cdot B_A - \xi + \epsilon \quad (10)$$

$$\frac{\delta B_D}{\delta t} = -\alpha_D \cdot B_D - \epsilon + \xi \quad (11)$$

$$\frac{\delta OC}{\delta t} = -\left(\frac{1}{Y_G} \cdot V_{max} \cdot B_A \cdot \frac{OC}{K_{OC} + OC}\right) + (\alpha_A \cdot B_A) + (\alpha_D \cdot B_D) \quad (12)$$

where α_A and α_D denote the specific death rate of active and dormant microorganisms respectively, ϵ denotes the transfer of biomass from dormant to active (B_D to B_A) (i.e., activation), and ξ denotes the transfer of biomass from active to dormant (B_A to B_D) (i.e., deactivation). Equations (10–12) constitute the "Discreet pools" model. The transitions between active and dormant microbial pools are typically dependent on environmental or thermodynamic factors. Under favorable conditions there is net activation, and vice-versa.

Integrating Dormancy and Maintenance

We have developed a new approach that allows for biomass and substrate to supply maintenance energy and that resolves the fraction of active and dormant microorganisms, combining the "Variable" model to represent maintenance (Equations 6 and 7) and the "Discreet pools" model to represent dormancy (Equations 10–12):

$$\frac{\delta B_A}{\delta t} = \left(V_{max} \cdot B_A \cdot h\,(OC)\right) - \left(m_{q,BA} \cdot B_A \cdot (1 - h\,(OC))\right) - (\alpha_A \cdot B_A) - \xi + \epsilon \quad (13)$$

$$\frac{\delta B_D}{\delta t} = -\left(m_{q,BD} \cdot B_D \cdot (1 - h\,(OC))\right) - (\alpha_D \cdot B_D) - \epsilon + \xi \quad (14)$$

$$\frac{\delta OC}{\delta t} = -\left(\frac{1}{Y_G} \cdot V_{max} \cdot B_A \cdot h\,(OC)\right) - \left(m_{q,BA} \cdot B_A \cdot h\,(OC) \cdot \frac{1}{Y_G}\right) - \left(m_{q,BD} \cdot B_D \cdot h\,(OC) \cdot \frac{1}{Y_G}\right) + (\alpha_A \cdot B_A) + (\alpha_D \cdot B_D) \quad (15)$$

where m_{qBA} and m_{qBD} denote specific maintenance requirements of active and dormant microorganisms respectively (**Figure 1F**). Dormant cells must carry out maintenance (Johnson et al., 2007), and like living cells, are able to utilize biomass and substrate to cover their maintenance demands. Equations (13–15) constitute the "Combined" model. We believe that this model incorporates sufficiently detailed microbial ecophysiology to form the basis of an ecosystem model for the deep biosphere without being overly complex.

Integration with Experimental Data

We are confident that the "Combined" numerical approach outlined here can be used as a foundation to effectively simulate microbial processes in marine sediments across a range of scales. Plausible values for parameters may be taken from existing datasets and modeling studies (e.g., Stolpovsky et al., 2011; Lomstein et al., 2012; Arndt et al., 2013). We also stress that this approach would be improved by future laboratory and field investigations considering the following measurements:

(i) Microbial growth rate (V_{max}).
(ii) True growth yield, Y_G.
(iii) Baseline rates of cellular metabolic activity, equivalent to the specific maintenance requirements of active and dormant microorganisms ($m_{q,BA}$ and $m_{q,BD}$).
(iv) The environmental conditions or biological factors under which maintenance energy is supplied by either substrate or biomass ($h(OC)$).
(v) The environmental conditions or biological factors under which microorganisms are active or dormant (ϵ and ξ).
(vi) The causes and rate of cell death for active and dormant microorganisms (α_A and α_D).

Model Developments and Data Integration

The "Combined" model provided in Equations (13–15) can be expanded in the following ways:

- Geochemistry: Primary and secondary redox reactions and equilibrium reactions involving important electron donors and acceptors are implemented in existing reaction-transport models, e.g., BRNS (Jourabchi et al., 2005; Thullner et al., 2009).
- Multiple functional groups: Microorganisms can be distinguished and classified based on functional traits (e.g., spore forming, motile) and metabolism (e.g., heterotroph, chemoautotroph).
- Additional biological dependencies: Microorganisms in a natural setting may be limited by the availability of electron donors, electron acceptors, and/or other environmental/geochemical factors. Biological responses to environmental conditions can be accounted for, e.g., via Michaelis-Menten kinetics (Michaelis and Menten, 1913).
- Thermodynamic factors: Explicit determination of thermodynamic factors, such as threshold energy requirements and cell growth yields on an electron-equivalent basis, and the energetic cost of biomass synthesis (Lever et al., 2015; LaRowe and Amend, 2016).
- Implementation in a 1D framework: In order to simulate diagenetic processes over the timescales of burial in a sediment column, transport processes such as advection, diffusion and bioturbation can be implemented in a 1D framework (Jourabchi et al., 2005; Arndt et al., 2013).

OUTLOOK

The insight provided from the development and application of a new microbial modeling tool for the deep marine subsurface will undoubtedly advance the current understanding of the minimum

energy requirements to support life in marine sediments, and the ecophysiological strategies that organisms utilize to survive low-energy conditions. Such insight might then explain the extraordinary persistence of microbial communities that endure unfavorable conditions over geological timescales.

AUTHOR CONTRIBUTIONS

All authors listed have made a substantial, direct and intellectual contribution to the work, and approved it for publication.

ACKNOWLEDGMENTS

This research was supported by a Center for Dark Energy Biosphere Investigations (C-DEBI, OCE-0939564) postdoctoral fellowship to JB. JA and DL acknowledge support from C-DEBI and NASA Astrobiology Institute–Life Underground (NAI-LU, NNA13AA92A). This is C-DEBI contribution 415 and NAI-LU contribution 127. Both organizations are based at the University of Southern California. We would like to thank the two reviewers who provided valuable comments on the manuscript.

REFERENCES

Arndt, S., Jørgensen, B. B., LaRowe, D. E., Middelburg, J. J., Pancost, R. D., and Regnier, P. (2013). Quantifying the degradation of organic matter in marine sediments: a review and synthesis. *Earth Sci. Rev.* 123, 53–86. doi: 10.1016/j.earscirev.2013.02.008

Bär, M., von Hardenberg, J., Meron, E., and Provenzale, A. (2002). Modelling the survival of bacteria in drylands: the advantage of being dormant. *Proc. R. Soc. London. Ser. B Biol. Sci.* 269, 937–942. doi: 10.1098/rspb.2002.1958

Beeftink, H. H., van der Heijden, R. T. J. M., and Heijnen, J. J. (1990). Maintenance requirements: energy supply from simultaneous endogenous respiration and substrate consumption. *FEMS Microbiol. Lett.* 73, 203–209. doi: 10.1111/j.1574-6968.1990.tb03942.x

Blagodatsky, S. A., and Richter, O. (1998). Microbial growth in soil and nitrogen turnover: a theoretical model considering the activity state of microorganisms. *Soil Biol. Biochem.* 30, 1743–1755. doi: 10.1016/S0038-0717(98)00028-5

Carlson, C., del Giorgio, P., and Herndl, G. (2007). Microbes and the dissipation of energy and respiration: from cells to ecosystems. *Oceanography* 20, 89–100. doi: 10.5670/oceanog.2007.52

D'Hondt, S., Inagaki, F., Zarikian, C. A., Abrams, L. J., Dubois, N., Engelhardt, T., et al. (2015). Presence of oxygen and aerobic communities from sea floor to basement in deep-sea sediments. *Nat. Geosci.* 8, 299–304. doi: 10.1038/ngeo2387

D'Hondt, S., Spivack, A. J., Pockalny, R., Ferdelman, T. G., Fischer, J. P., Kallmeyer, J., et al. (2009). Subseafloor sedimentary life in the South Pacific Gyre. *Proc. Natl. Acad. Sci. U.S.A.* 106, 11651–11656. doi: 10.1073/pnas.0811793106

Darrah, P. R. (1991). Models of the rhizosphere.1. microbial-population dynamics around a root releasing soluble and insoluble carbon. *Plant Soil* 133, 187–199. doi: 10.1007/BF00009191

Dawes, E. A., and Ribbons, D. W. (1964). Some aspects of the endogenous metabolism of bacteria. *Bacteriol. Rev.* 28, 126–149.

del Giorgio, P. A., and Cole, J. J. (1998). Bacterial growth efficiency in natural aquatic systems. *Annu. Rev. Ecol. Syst.* 29, 503–541. doi: 10.1146/annurev.ecolsys.29.1.503

Hempfling, W. P., and Mainzer, S. E. (1975). Effects of varying the carbon source limiting growth on yield and maintenance characteristics of *Escherichia coli* in continuous culture. *J. Bacteriol.* 123, 1076–1087.

Herbert, D. (1958). "Some principles of continuous culture," in *Recent Progress in Microbiology*, ed E. Tunevall (Stockholm: Almqvist & Wiksell), 381–396.

Hobson, P. N. (1965). Continuous culture of some anaerobic and facultativelyanaerobic Rumen bacteria. *J. Gen. Microbiol.* 38, 167–180. doi: 10.1099/00221287-38-2-167

Hoehler, T. M., and Jørgensen, B. B. (2013). Microbial life under extreme energy limitation. *Nat. Rev. Microbiol.* 11, 83–94. doi: 10.1038/nrmicro2939

Ingwersen, J., Poll, C., Streck, T., and Kandeler, E. (2008). Micro-scale modelling of carbon turnover driven by microbial succession at a biogeochemical interface. *Soil Biol. Biochem.* 40, 864–878. doi: 10.1016/j.soilbio.2007.10.018

Johnson, S. S., Hebsgaard, M. B., Christensen, T. R., Mastepanov, M., Nielsen, R., Munch, K., et al. (2007). Ancient bacteria show evidence of DNA repair. *Proc. Natl. Acad. Sci. U.S.A.* 104, 14401–14405. doi: 10.1073/pnas.0706787104

Jørgensen, B. B., and Boetius, A. (2007). Feast and famine - microbial life in the deep-sea bed. *Nat. Rev. Microbiol.* 5, 770–781. doi: 10.1038/nrmicro1745

Jørgensen, B. B., and Marshall, I. P. G. (2016). Slow microbial life in the seabed. *Ann. Rev. Mar. Sci.* 8, 311–332. doi: 10.1146/annurev-marine-010814-015535

Jourabchi, P., Van Cappellen, P., and Regnier, P. (2005). Quantitative interpretation of pH distributions in aquatic sediments: a reaction-transport modeling approach. *Am. J. Sci.* 305, 919–956. doi: 10.2475/ajs.305.9.919

Kim, M., and Or, D. (2016). Individual-based model of microbial life on hydrated rough soil surfaces. *PLoS ONE* 11:e0147394. doi: 10.1371/journal.pone.0147394

Knapp, E. B., Elliott, L. F., and Campbell, G. S. (1983). Carbon, nitrogen and microbial biomass interrelationships during the decomposition of wheat straw - a mechanistic simulation-model. *Soil Biol. Biochem.* 15, 455–461. doi: 10.1016/0038-0717(83)90011-1

LaRowe, D. E., and Amend, J. P. (2015a). Catabolic rates, population sizes and doubling/replacement times of microorganisms in natural settings. *Am. J. Sci.* 315, 167–203. doi: 10.2475/03.2015.01

LaRowe, D. E., and Amend, J. P. (2015b). Power limits for microbial life. *Front. Microbiol.* 6:718. doi: 10.3389/fmicb.2015.00718

LaRowe, D. E., and Amend, J. P. (2016). The energetics of anabolism in natural settings. *ISME J.* 10, 1–11. doi: 10.1038/ismej.2015.227

Lele, U., and Watve, M. (2014). Bacterial growth rate and growth yield: is there a relationship? *Proc. Indian Natn. Sci. Acad.* 80, 537–546. doi: 10.16943/ptinsa/2014/v80i3/55129

Lever, M. A., Rogers, K. L., Lloyd, K. G., Overmann, J., Schink, B., Thauer, R. K., et al. (2015). Life under extreme energy limitation: a synthesis of laboratory- and field-based investigations. *FEMS Microbiol. Rev.* 39, 688–728. doi: 10.1093/femsre/fuv020

Lipson, D. A. (2015). The complex relationship between microbial growth rate and yield and its implications for ecosystem processes. *Front. Microbiol.* 6:615. doi: 10.3389/fmicb.2015.00615

Lomstein, B. A., Langerhuus, A. T., D'Hondt, S., Jørgensen, B. B., and Spivack, A. J. (2012). Endospore abundance, microbial growth and necromass turnover in deep sub-seafloor sediment. *Nature* 484, 101–104. doi: 10.1038/nature10905

McKay, L., Klokman, V. W., Mendlovitz, H. P., LaRowe, D. E., Hoer, D. R., Albert, D., et al. (2016). Thermal and geochemical influences on microbial biogeography in the hydrothermal sediments of Guaymas Basin, Gulf of California. *Environ. Microbiol. Rep.* 8, 150–161. doi: 10.1111/1758-2229.12365

Michaelis, L., and Menten, M. (1913). The kinetics of invertase activity. *Biochem. Z* 49, 333–369.

Morita, R. Y. (1988). Bioavailability of energy and its relationship to growth and starvation survival in nature. *Can. J. Microbiol.* 34, 436–441. doi: 10.1139/m88-076

Orcutt, B. N., LaRowe, D. E., Biddle, J. F., Colwell, F. S., Glazer, B. T., Reese, B. K., et al. (2013). Microbial activity in the marine deep biosphere: Progress and prospects. *Front. Microbiol.* 4:189. doi: 10.3389/fmicb.2013.00189

Panikov, N. S. (1995). "Kinetics, microbial growth," in *Encyclopedia of Bioprocess Technology*, eds M. C. Flickinger and S. W. Drew (Moscow: John Wiley & Sons, Inc.).

Pirt, S. J. (1965). The maintenance energy of bacteria in growing cultures. *Proc. R. Soc. London. Ser. B. Biol. Sci.* 163, 224–231.

Røy, H., Kallmeyer, J., Adhikari, R. R., Pockalny, R., Jørgensen, B. B., and D'Hondt, S. (2012). Aerobic microbial respiration in 86-Million-Year-Old Deep-Sea Red Clay. *Science* 336, 922–925. doi: 10.1126/science.1219424

Russell, J. B., and Baldwin, R. L. (1979). Comparison of maintenance energy expenditures and growth yields among several rumen bacteria grown on continuous culture. *Appl. Environ. Microbiol.* 37, 537–543.

Sierra, C. A., Malghani, S., and Muller, M. (2015). Model structure and parameter identification of soil organic matter models. *Soil Biol. Biochem.* 90, 197–203. doi: 10.1016/j.soilbio.2015.08.012

Sinsabaugh, R. L., Manzoni, S., Moorhead, D. L., and Richter, A. (2013). Carbon use efficiency of microbial communities: stoichiometry, methodology and modelling. *Ecol. Lett.* 16, 930–939. doi: 10.1111/ele.12113

Smith, E. M., and Prairie, Y. T. (2004). Bacterial metabolism and growth efficiency in lakes: the importance of phosphorus availability. *Limnol. Oceanogr.* 49, 137–147. doi: 10.4319/lo.2004.49.1.0137

Soetaert, K., and Herman, P. (2009). *A Practical Guide to Ecological Modelling: Using R as a Simulation Platform*. London: Springer.

Stolpovsky, K., Martinez-Lavanchy, P., Heipieper, H. J., Van Cappellen, P., and Thullner, M. (2011). Incorporating dormancy in dynamic microbial community models. *Ecol. Model.* 222, 3092–3102. doi: 10.1016/j.ecolmodel.2011.07.006

Sylvan, J. B., Wankel, S. D., LaRowe, D. E., Charoenpong, C. N., Huber, J. A., Moyer, C. L., et al. (2016). Evidence for microbial mediation of subseafloor nitrogen redox processes at Loihi Seamount, Hawaii. *Geochim. Cosmochim. Acta*. 198, 131–150. doi: 10.1016/j.gca.2016.10.029

Teske, A., Callaghan, A. V., and LaRowe, D. E. (2014). Biosphere frontiers of subsurface life in the sedimented hydrothermal system of Guaymas Basin. *Front. Microbiol.* 5:362. doi: 10.3389/fmicb.2014.00362

Thullner, M., Dale, A. W., and Regnier, P. (2009). Global-scale quantification of mineralization pathways in marine sediments: a reaction-transport modeling approach. *Geochem. Geophys. Geosyst.* 10, 131–150. doi: 10.1029/2009GC002484

Thullner, M., Van Cappellen, P., and Regnier, P. (2005). Modeling the impact of microbial activity on redox dynamics in porous media. *Geochim. Cosmochim. Acta* 69, 5005–5019. doi: 10.1016/j.gca.2005.04.026

Tijhuis, L., Van Loosdrecht, M. C. M., and Heijnen, J. J. (1993). A thermodynamically based correlation for maintenance gibbs energy requirements in aerobic and anaerobic chemotrophic growth. *Biotechnol. Bioeng.* 42, 509–519. doi: 10.1002/bit.260420415

Van Bodegom, P. (2007). Microbial maintenance: a critical review on its quantification. *Microb. Ecol.* 53, 513–523. doi: 10.1007/s00248-006-9049-5

Wang, G., and Post, W. M. (2012). A theoretical reassessment of microbial maintenance and implications for microbial ecology modeling. *FEMS Microbiol. Ecol.* 81, 610–617. doi: 10.1111/j.1574-6941.2012.01389.x

Westerhoff, H. V., Hellingwerf, K. J., and Van Dam, K. (1983). Thermodynamic efficiency of microbial growth is low but optimal for maximal growth rate. *Proc. Natl. Acad. Sci. U.S.A.* 80, 305–309. doi: 10.1073/pnas.80.1.305

Conflict of Interest Statement: The authors declare that the research was conducted in the absence of any commercial or financial relationships that could be construed as a potential conflict of interest.

frontiers in Microbiology

ORIGINAL RESEARCH
published: 27 April 2018
doi: 10.3389/fmicb.2018.00858

Low-Light Anoxygenic Photosynthesis and Fe-S-Biogeochemistry in a Microbial Mat

Sebastian Haas[1,2], Dirk de Beer[1], Judith M. Klatt[1,3], Artur Fink[1], Rebecca McCauley Rench[4], Trinity L. Hamilton[5], Volker Meyer[1], Brian Kakuk[6] and Jennifer L. Macalady[4]*

[1] Max Planck Institute for Marine Microbiology, Bremen, Germany, [2] Department of Oceanography, Dalhousie University, Halifax, NS, Canada, [3] Department of Earth and Environmental Sciences, University of Michigan, Ann Arbor, MI, United States, [4] Geosciences Department, Pennsylvania State University, University Park, PA, United States, [5] Department of Plant and Microbial Biology, University of Minnesota, Minneapolis, MN, United States, [6] Bahamas Caves Research Foundation, Marsh Harbour, Bahamas

We report extremely low-light-adapted anoxygenic photosynthesis in a thick microbial mat in Magical Blue Hole, Abaco Island, The Bahamas. Sulfur cycling was reduced by iron oxides and organic carbon limitation. The mat grows below the halocline/oxycline at 30 m depth on the walls of the flooded sinkhole. *In situ* irradiance at the mat surface on a sunny December day was between 0.021 and 0.084 μmol photons m^{-2} s^{-1}, and UV light (<400 nm) was the most abundant part of the spectrum followed by green wavelengths (475–530 nm). We measured a light-dependent carbon uptake rate of 14.5 nmol C cm^{-2} d^{-1}. A 16S rRNA clone library of the green surface mat layer was dominated (74%) by a cluster (>97% sequence identity) of clones affiliated with *Prosthecochloris*, a genus within the green sulfur bacteria (GSB), which are obligate anoxygenic phototrophs. Typical photopigments of brown-colored GSB, bacteriochlorophyll *e* and (β-)isorenieratene, were abundant in mat samples and their absorption properties are well-adapted to harvest light in the available green and possibly even UV-A spectra. Sulfide from the water column (3–6 μmol L^{-1}) was the main source of sulfide to the mat as sulfate reduction rates in the mats were very low (undetectable-99.2 nmol cm^{-3} d^{-1}). The anoxic water column was oligotrophic and low in dissolved organic carbon (175–228 μmol L^{-1}). High concentrations of pyrite (FeS_2; 1–47 μmol cm^{-3}) together with low microbial process rates (sulfate reduction, CO_2 fixation) indicate that the mats function as net sulfide sinks mainly by abiotic processes. We suggest that abundant Fe(III) (4.3–22.2 μmol cm^{-3}) is the major source of oxidizing power in the mat, and that abiotic Fe-S-reactions play the main role in pyrite formation. Limitation of sulfate reduction by low organic carbon availability along with the presence of abundant sulfide-scavenging iron oxides considerably slowed down sulfur cycling in these mats.

Keywords: anoxygenic photosynthesis, green sulfur bacteria, low-light photosynthesis, sulfide scavenging, microbial mat, bacteriochlorophyll e, iron-sulfur-cycling, Proterozoic ocean

Abbreviations: AVS, acid volatile sulfide; BChl, bacteriochlorophyll; CRS, chromium reducible sulfur; DIC, dissolved inorganic carbon; DOMS, diver operated microsensor system; GSB, green sulfur bacteria; MBH, magical blue hole; ORP, oxidation-reduction potential; PMT, photomultiplier; RT, retention time.

OPEN ACCESS

Edited by:
Doug LaRowe, University of Southern California, United States

Reviewed by:
John Senko, University of Akron, United States
Mustafa Yucel, Middle East Technical University, Turkey

****Correspondence:***
Sebastian Haas
sebastian_haas@web.de;
s.haas@dal.ca

Specialty section:
This article was submitted to Microbiological Chemistry and Geomicrobiology, a section of the journal Frontiers in Microbiology

Received: *31 December 2017*
Accepted: *13 April 2018*
Published: *27 April 2018*

Citation:
Haas S, de Beer D, Klatt JM, Fink A, Rench RM, Hamilton TL, Meyer V, Kakuk B and Macalady JL (2018) Low-Light Anoxygenic Photosynthesis and Fe-S-Biogeochemistry in a Microbial Mat. Front. Microbiol. 9:858. doi: 10.3389/fmicb.2018.00858

INTRODUCTION

A significant part of the Earth's biosphere is exposed to regimes of extreme energy limitation, such as the terrestrial deep biosphere, the deep sea, and deep zones of most marine sediments. Energy limitation may have been even more significant on early Earth in the absence of oxygenic photosynthesis and the associated production of electron acceptors such as molecular oxygen and oxidized forms of nitrogen, iron, and sulfur. Although studies of low-energy communities are technically challenging and therefore relatively rare, they demonstrate how biotic and abiotic processes compete and interact, and may approximate conditions on early Earth and other planetary bodies.

The lower limits of biotic utilization of light are reached by anoxygenic photosynthesis, especially by members of the monophyletic clade of the GSB (*Chlorobiaceae*), which are obligate anaerobes and obligate anoxygenic phototrophs. They can proliferate at the interface of the sulfidic and photic zone in meromictic or eutrophic lakes (Montesinos et al., 1983; Mori et al., 2013; Crowe et al., 2014) or in microbial mats (Engel et al., 2004; Lau et al., 2009). The extremely low-light-adapted strain *Prosthecochloris phaeobacteroides* BS1 (formerly *Chlorobium phaeobacteroides* BS1; Manske et al., 2005; Imhoff and Thiel, 2010; Marschall et al., 2010) forms monospecific assemblages in the Black Sea chemocline and has been shown to fix inorganic carbon by the phototrophic oxidation of sulfide at light intensities as low as 0.015 μmol photons m^{-2} s^{-1}, which is five orders of magnitude lower than daylight (Manske et al., 2005). With estimated *in situ* carbon fixation rates as low as 200 to 1800 ng C m^{-2} d^{-1}, however, they have virtually no quantitative effect on the carbon and sulfur cycles in their habitat (Manske et al., 2005). Low-light-adapted GSB are referred to as brown-colored GSB, a non-monophyletic group of low-light specialists (Montesinos et al., 1983) that possess the BChl *a* and *e* as well as the carotenes isorenieratene and β-isorenieratene (Glaeser et al., 2002). BChl *e* and these carotenes are responsible for light-harvesting and energy transfer to BChl *a* in model GSB strains (Overmann et al., 1992; Hauska et al., 2001). GSB with this combination of pigments have an *in vivo* absorption maximum at 505 nm (Overmann et al., 1992). Since the physical light attenuation of water is lowest between 400 and 500 nm (Sogandares and Fry, 1997), they are able to thrive at great water depths.

Anoxygenic phototrophs can use a variety of electron donors, including nitrite (Griffin et al., 2007), ferrous iron (Widdel et al., 1993; in GSB: Heising et al., 1999), molecular hydrogen or reduced sulfur compounds (Pfennig, 1975; Overmann and Pfennig, 1989). Hydrogen sulfide is the electron donor most commonly used by GSB. It is converted according to the following stoichiometry:

$$2\,HS^- + CO_2 + 2\,H^+ \rightarrow \; 2\,S^0 + CH_2O + H_2O \qquad (1)$$

Hydrogen sulfide is produced biologically by sulfate reduction, a process most prominent in marine sediments, but also frequently observed in biofilms and microbial mats (Canfield and Des Marais, 1991; Kühl and Jørgensen, 1992; Visscher et al., 1992). Wieland et al. (2005) demonstrated how photosynthates in a microbial mat induced significantly increased sulfate reduction rates (SRRs) during the day. CO_2 produced by sulfate reduction in turn enhanced photosynthesis. The same study also showed how large amounts of Fe(III) can affect sulfur cycling by precipitating sulfide. In the present study, we describe how a similar effect can slow down sulfur cycling in a mat that is significantly more limited in light and organic carbon.

Green sulfur bacteria may produce sulfate from hydrogen sulfide or more oxidized sulfur compounds (Overmann and Pfennig, 1989), but can also produce elemental sulfur (S^0), which is deposited extracellularly (Pfennig, 1975). The production of sulfur compounds of intermediate oxidation states rather than sulfate is common also to non-phototrophic sulfide oxidation processes. In fact, the presence of incompletely oxidized sulfur in the form of CRS can be used as an indication for sulfide oxidation (e.g., Thode-Andersen and Jørgensen, 1989; Holmkvist et al., 2011; Lichtschlag et al., 2013), because sulfate reduction typically does not produce sulfur compounds of intermediate oxidation states. In the absence of light, biological sulfide oxidation typically requires either oxygen, nitrate or nitrite as electron acceptor.

Blue holes are sinkholes: vertical, water-filled karst features open to the surface (Mylroie et al., 1995). Inland blue holes of the Bahamas are anchialine caves (Iliffe, 2000), landlocked bodies of water with subterranean connections to the ocean containing meromictic water columns with an upper freshwater lens separated from a lower saltwater column by a stable halocline (Seymour et al., 2007; Gonzalez et al., 2011). Each blue hole displays distinct geochemical traits, making them unique natural laboratories that allow exploring the limits of photosynthesis and the interplay between biotic and abiotic sulfur cycling. Inland blue holes are therefore of particular interest for geomicrobiology, because the unique geochemical features of each blue hole (e.g., depth of halocline, concentration of sulfide, water flow rates, organic matter input) are associated with the formation of specific types of microbial communities (Gonzalez et al., 2011). Few studies have been conducted on the microbiology of inland blue holes to date (Bottrell et al., 1991; Schwabe and Herbert, 2004; Macalady et al., 2010; Gonzalez et al., 2011).

A thick, orange-colored microbial mat with a thin green top layer was discovered in the suboxic, sulfidic water below the halo-chemocline of MBH, The Bahamas (Gonzalez et al., 2011). The green color of surface cells and an abundance of GSB-affiliated 16S rRNA genes in clone libraries suggested the mats were phototrophic (Gonzalez et al., 2011). δ-*Proteobacteria* were also highly abundant in the clone libraries, suggesting that sulfate reduction might be an important process in the mats (Gonzalez et al., 2011). We aimed to test the hypothesis that the mats are phototrophic and dominated by GSB that are optimally adapted to the quality and low intensity of the ambient light. Secondly, we aimed to test whether the sulfide needed for the GSB activity is supplied by sulfate reduction in the mats. We used a highly sensitive light detection system to quantify ambient irradiance and determine the light quality. The ambient spectra were compared with the absorption spectra of photopigments from the mats. Activities were determined by light dependency

of carbon uptake and sulfate reduction rate measurements. To constrain the Fe-S-cycling in the mats, solid phase fractions of the iron and sulfur pools were quantified.

MATERIALS AND METHODS

Study Site and Mat

Magical Blue Hole (also known as Cherokee Road Extension Blue Hole, 26°22′31.96″N, 77°6′14.91″W) is an anchialine sinkhole on Abaco Island (The Bahamas). It is approximately 80 m deep and has a surface diameter of approximately 10 m. A stable halo- and chemocline is present at 25 m depth, separating oxic freshwater from anoxic, sulfidic seawater (Gonzalez et al., 2011). Below the surface, the diameter widens and the cave is roughly 40 m wide at 30 m depth. The narrow entry and the shading effect of the overhanging cave walls result in low light intensities below the halo-chemocline. The cave walls below the halo-chemocline are extensively covered by a thick microbial mat. It grows thickest (up to ∼6 cm) on a ledge in the otherwise vertical cave wall situated at approximately 30 m depth. The mat is stratified with a thin green layer of fluffy biological material on top (∼1 mm), a gelatinous orange middle layer (up to ∼3 cm) and a brown bottom-layer (up to ∼3 cm; **Figure 1**).

Sampling Techniques

Geochemical parameters of the water column were measured in vertical profiles. Water samples were collected in lockable plastic syringes by a diver and sterile-filtered (0.2 μm) immediately after sampling. Samples for dissolved inorganic and organic carbon analysis were stored at 4°C while samples for ammonium (NH_4^+) and nitrate (NO_3^-) quantification (n = 5 for 30 m and 40 m; n = 2 for remaining depths) were stored frozen. Total sulfide ($H_2S + HS^- + S^{2-}$) and sulfate (SO_4^{2-}; n = 3 for all depths, respectively) samples were preserved by mixing 1:1 (v/v) with 20% Zn-acetate solution.

Samples for incubation with ^{13}C-labeled substrates and subsamples for photosynthetic pigment analysis (n = 3) were taken by vacuuming the upper green part of the mat into lockable syringes. For clone library construction, a large piece of mat was cut out with a knife and immediately placed into a light-shielded and airtight plastic box by a diver for transport to the laboratory. Clone library samples were separated into the three natural layers based on location and color, preserved with RNAlater and stored at 4°C until analysis.

Microbial mat samples from around 30 m water depth were taken with push-cores, which were immediately closed by a diver with airtight plugs. Push-cores used to sample for pigment analysis (n = 3; core lengths: 1.2–5.7 cm) and ^{35}S incubation experiments (n = 10; lengths: 3.6–5.4 cm) were wrapped in black tape to shield the samples from light. Cores for solid phase analyses were immediately cut into 0.6 cm slices (AVS/ CRS/ sulfate; lengths: 3.6–5.4 cm) and 0.25 cm slices (dithionite reactive iron/ S^0; lengths: 3.5–4.5 cm) and fixed in 4 mL 5% Zn-acetate and 3 mL 20% Zn-acetate, respectively. Along with samples for pigment analysis, they were stored frozen. Samples for porosity (n = 4) and density (n = 1) measurements were also taken with push-cores.

Solid Phase Analyses

Mat porosity was determined as weight reduction after drying at 60°C in four mat cores (result: 0.92 ± 0.02). Density was determined as wet weight per mat volume. The density average of 0.6 cm/ 1 mL slices (n = 8) from one core sample (1.11 ± 0.12 g cm^{-3}) was used for conversions of mat weight into volume.

Acid volatile sulfide (AVS = FeS + Fe_3S_4 + H_2S: Cornwell and Morse, 1987) and CRS (CRS = S^0 + FeS_2: Cornwell and Morse, 1987) were extracted from six mat core samples in a two-step HCl and Cr(II) distillation according to Fossing and Jørgensen (1989). After distillation of the pellets, AVS and CRS trapped as ZnS were determined according to Cline (1969). Porewater sulfate content was quantified in the supernatant after a centrifugation step, which preceded these distillations. The detection limit was at 12.9 nmol S cm^{-3}. From five parallel cores, S^0 was extracted by methanol and measured as cyclo-S_8 by UPLC (Waters, United States) as described previously (Zopfi et al., 2004). Pyrite-S was defined as the difference between CRS and S^0.

A citrate-acetate-dithionite solution was used to extract iron from three mat samples. The procedure extracts most crystalline and amorphous Fe(III) as well as FeS (Kostka and Luther, 1994). Extraction was preceded by a centrifugation step after which the supernatant was discarded. Since Zn-acetate was used to preserve the samples, iron concentrations may be underestimated due to possible formation of non-extractable Fe-acetate. Dithionite extracts were analyzed with the ferrozine method according to Viollier et al. (2000).

Geochemical Water Analyses

Standard procedures were used to analyze chemical compounds in samples from the water column and in microbial mat extracts. Total sulfide was measured according to Cline (1969). Sulfate ion concentration was analyzed with ion chromatography (761 Compact Ion Chromatographer including 812 valve unit and 838 Advanced Sample Processor, Metrohm, Germany). Phosphate, nitrate and ammonium were quantified with a continuous flow analyzer (San^{++}, Skalar, Netherlands) using standard detection methods (Hansen and Koroleff, 2009). DIC was calculated as the difference between total carbon and non-purgeable organic carbon measured using a Total Carbon Analyzer (TOC-5000A, Shimadzu, Japan) after acidification and N_2-purging.

Photosynthetic Pigment Analysis

Frozen mat cores were horizontally sliced with a resolution of 3 mm. Pigments from both core slices and vacuumed surface layer samples were extracted with acetone as described previously (Al-Najjar et al., 2012). The filtered extract containing the pigments was then injected into a reversed-phase High-performance liquid chromatograph (HPLC; 2695 Separations Module, Waters, United States). The pigments were separated according to Wright (1991) and absorption spectra were measured using a 996 Photodiode Array Detector. Identification

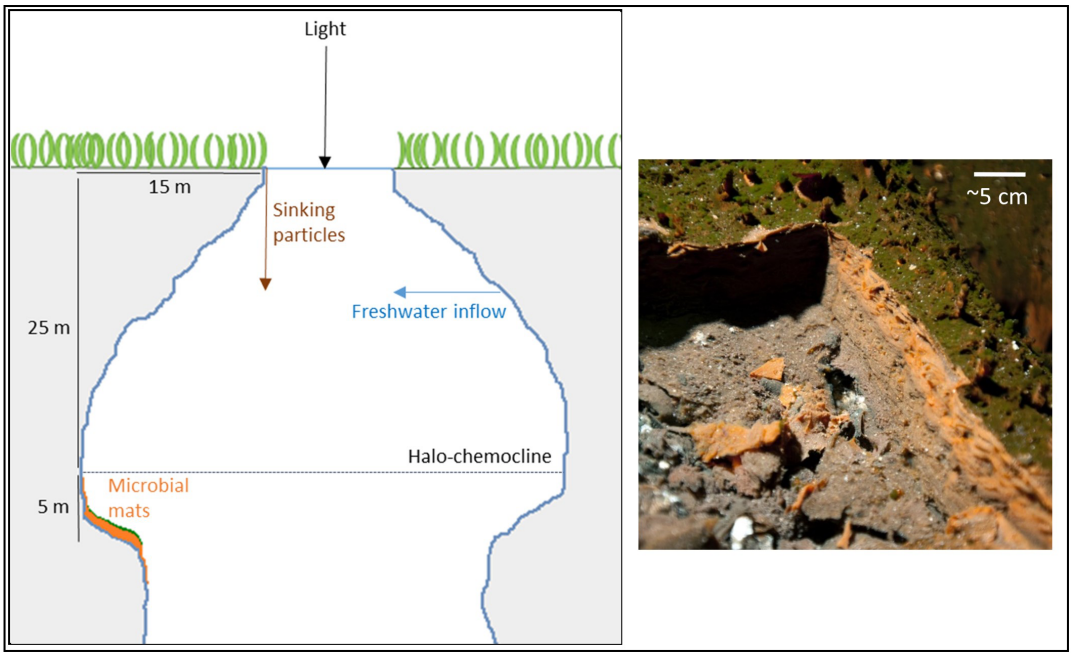

FIGURE 1 | Schematic drawing of Magical Blue Hole and a picture of the microbial mat of which a piece was cut out to reveal its three-layered structure.

of pigments was based on RT and absorption spectra. A β-carotene standard (beta-122; 0.813 mg L^{-1} in 100% acetone, Sigma-Aldrich, United States) and freeze-dried pure culture material of a low-light-adapted *Prosthecochloris phaeobacteroides* BS1strain isolated from the Black Sea chemocline by Overmann et al. (1992) (DSMZ Braunschweig) were analyzed in parallel as standards.

Isotope Incubations for Process Rate Determination

Rates of sulfate reduction, photoautotrophic carbon uptake and photoheterotrophic carbon uptake were assessed by incubations with isotopic labels. To assess SRRs inside the mat, the whole-core injection method based on radioactively labeled sulfate was carried out (Jørgensen, 1978). Under N_2-atmosphere, 4 µl per cm^3 sample of radioactively labeled $^{35}SO_4^{2-}$ in Na_2SO_4 carrier solution (~33 kBq cm^{-3}) were vertically injected into push-cores (20 mm diameter) containing up to 20 mL freshly sampled microbial mat. Incubation under anoxic conditions and approximate *in situ* temperature was stopped after four (n = 6) and six (n = 4) hours by horizontally slicing the cores into 6 mm pieces and immediately mixing them 1:1 (v/v) with 20% Zn-acetate to stop sulfate reduction and fix hydrogen sulfide as ZnS. After cold Cr(II) distillation (Kallmeyer et al., 2004; as modified by Røy et al., 2014), SRRs were determined (Jørgensen, 1978). A detection limit of 43.73 radioactive decays per minute (95% confidence interval) was calculated based on means and standard deviations of sample blanks prepared (Kallmeyer et al., 2004).

To determine phototrophic carbon uptake, parts of the green surface layer of the mat were incubated *in situ* in cave water amended with labeled ^{13}C-DIC ($NaH^{13}CO_3$) or ^{13}C-acetate ($^{13}CH_3{}^{12}CO_2Na$) at 30 m depth in the center of the cave (maximum irradiance: 0.27 µmol photons m^{-2} s^{-1}; **Figure 2A**) for different time periods. Under anoxic N_2-atmosphere and protected from high light exposure, samples were suspended in cave water (collected oxygen-free next to the mat) to a final volume of 500 ml. To ensure that the medium was completely anoxic, 18 µl of 1 M Na_2S were added to a final sulfide concentration of 84 µmol L^{-1} at pH 6.85 ± 0.35. Glass vials (6 mL) with plastic lids featuring integrated septa were filled with medium containing the inoculum and isotope label depending on the treatment. Vials were supplemented with 73.8 nmol of ^{13}C-labeled DIC or ^{13}C-labeled acetate, which resulted in ^{13}C-labeling percentages of 10.5% for DIC and 50% for acetate, calculated based on observed *in situ* DIC concentrations and by assuming negligible *in situ* amounts of acetate. Triplicate aliquots for determination of natural isotope abundance were preserved before label addition. The ^{13}C content of three incubation vials was immediately preserved after addition of label (t = 0). The remainder of the closed incubation vials were incubated in the center of the blue hole at 30 m depth. Dark controls were incubated in light-shielded vials. One set of vials (low-light incubated: n = 3; dark controls: n = 3) was recovered after approximately 2 days and a second set after 6 days. At the prevailing daylight length of 10.5 h, this corresponded to an incubation time in natural light of 24 h and 60 h, respectively. All incubations were terminated by filtration through pre-combusted (3 h, 450°C) GF/F-filters (0.7 µm pore size), which were then dried at 60°C and subsequently treated and analyzed as described in Halm et al. (2012). Rates of total DIC and acetate assimilation were calculated as the increase in $^{13}C/^{12}C$ over time, corrected for natural abundance and ^{13}C-labeling percentage.

Carbon uptake rates per single cell and per mat area were calculated assuming that all cells were phototrophic and covering the mat surface without gaps. Phototrophic cell numbers per incubation vial were estimated based on total carbon determined by isotope ratio mass spectrometry per incubation vial and using literature values of cell radius (0.6125 μm in Black Sea strain *P. phaeobacteroides* BS1 cells cultivated at 0.1 μmol photons m^{-2} s^{-1}; Manske et al., 2005) and carbon content (106 fg μm^{-3}; Nagata, 1986). They were corrected for carbon content determined in *in situ* cave water in the same way. To calculate quantum yields of photosynthesis - the amount of carbon fixed per incoming photons - we assumed a total absorptive cell surface of 0.716 cm^2 per incubation vial. This was based on the product of the mean phototrophic cell numbers per vial (1.16×10^8 cells $vial^{-1}$) and an assumed single-cell absorption cross section (= average light absorbing cell surface) of 0.62 μm^2 (Black Sea *P. phaeobacteroides*: Marschall et al., 2010).

Phylogenetic Analyses

Mat microbial DNA was extracted from mat samples using chloroform-phenol extraction and 16S rRNA genes were amplified by PCR using Bacteria-specific 27f and 1492r primers as described in Macalady et al. (2008). One library was constructed for each mat layer. Potential chimeras were excluded from further analysis. Full length and partial sequences for the green layer (n = 74), orange layer (n = 65) and brown layer (n = 67) were obtained from the respective libraries. Sequences were aligned with the Silva aligner available at http://www.arb-silva.de, imported into ARB (Ludwig et al., 2004) and manually refined. Operational taxonomic units (OTUs) were identified using a sequence identity threshold of 97% (0.03) using mothur (v.1.39.5) (Schloss et al., 2009). Taxonomy was assigned using BlastN (Altschul et al., 1997) and ARB (Ludwig et al., 2004). For phylogenetic analyses of sequences affiliated with *Chlorobi* and δ-*Proteobacteria*, the top BLAST matches and nearest relative to each OTU in the ARB database were included. Representative sequences were added to an existing 16S rRNA alignment in ARB, and manually refined. Maximum likelihood analyses were performed using RAxML (Stamatakis et al., 2008) with 1000 bootstrap replicates and the general time-reversible model with G+I rate variation as determined by JModelTest v.2.1.10 (Darriba et al., 2012). The resulting trees were viewed and edited using iTOL[1] (Letunic and Bork, 2016). The 16S rRNA gene sequences recovered in this study were submitted to the GenBank database and assigned the following accession numbers: MG601241–MG601445.

In Situ Measurements of Physico-Chemical Parameters

For measurements of physico-chemical parameters, a data-logging device was designed and constructed to measure (i) downwelling scalar irradiance and (ii) physico-chemical parameters as well as (iii) spectra of downwelling light available to the mat. Irradiance was measured with a modified DOMS (Weber et al., 2007). A scalar irradiance sensor (21.21 mm^2 sensing surface; US-SQS/LI, Walz, Germany) with a glass fiber was attached to a H5702-50 PMT (Hamamatsu Photonics, Japan). The control voltage and thereby the PMT sensitivity was scaled to ambient light conditions by a diver during measurements using a magnetic switch. The scalar irradiance sensor installed on the PMT measured irradiance over an angle of approximately 270°.

The DOMS logger, its NiMH rechargeable battery, the modified PMT, a cosine-corrected PAR sensor (QCP-2000; Biospherical Instruments, United States) and a multiparameter sonde (YSI 5200A, YSI, United States) equipped with sensors for pressure, ORP, pH, dissolved oxygen, temperature and salinity, were mounted on a vertical frame. This array could then be lowered into the blue hole with a rope for vertical profiling (descent rate: 4.3 m min^{-1}) or made neutrally buoyant and moored to the cave wall. By attaching both PAR- and PMT-sensors in one plane and upward orientation, parallel signals of the two sensors were obtained during the descent of the array through upper cave regions, where sufficient irradiance covered the sensitivity ranges of both light sensors. Using the PAR sensor's internal calibration, these overlapping data could be used to create a calibration curve for PMT measurements at greater depths.

The spectral quality of the light reaching the mat was determined by using a filter wheel containing optical longpass filters (FSR-GG-400 nm and -475 nm, FSR-OG-530 nm and -590 nm, FSR-RG-645 nm; Newport, United States) in front of the sensor. The sensor was shaded from below with a movable cup and the filter wheel was operated manually by a diver. Based on the amplitude of irradiance reduction measured by the sensor after each filter switch, an *in situ* wavelength spectrum was obtained. The filters reduced the light intensity above their respective threshold by 10% (manufacturer information), for which the spectrum was corrected. The PMT covered an irradiance spectrum of 200–700 nm with sensitivity dropping above and below this spectrum. Within this spectrum, sensitivity was approximately even, except for slightly increased sensitivity in the wavelength range 500–680 nm (manufacturer information) that may have led to a small overestimation (<2%) of the percentage of light from this wavelength range.

RESULTS

Water Column Geochemistry and Irradiance

Between 20 and 25 m depth, a distinct halo-chemocline was observed, below which the water was sulfidic and anoxic (**Figure 2**). Dissolved oxygen and temperature profiles displayed negative anomalies at about 10 m depth, probably due to lateral water inflow. Below the halo-chemocline, most chemical parameters and temperature remained approximately constant. Deviating from this trend, sulfide displayed two maxima, namely at 27.5 m, i.e., directly below the halo-chemocline and close to the depth of highest mat abundance, and at 45 m. There was no detectable sulfide above the halo-chemocline. Close to the depth of thickest mat growth, we observed a minimum in sulfide concentration (**Figure 2D**).

[1] http://itol.embl.de/

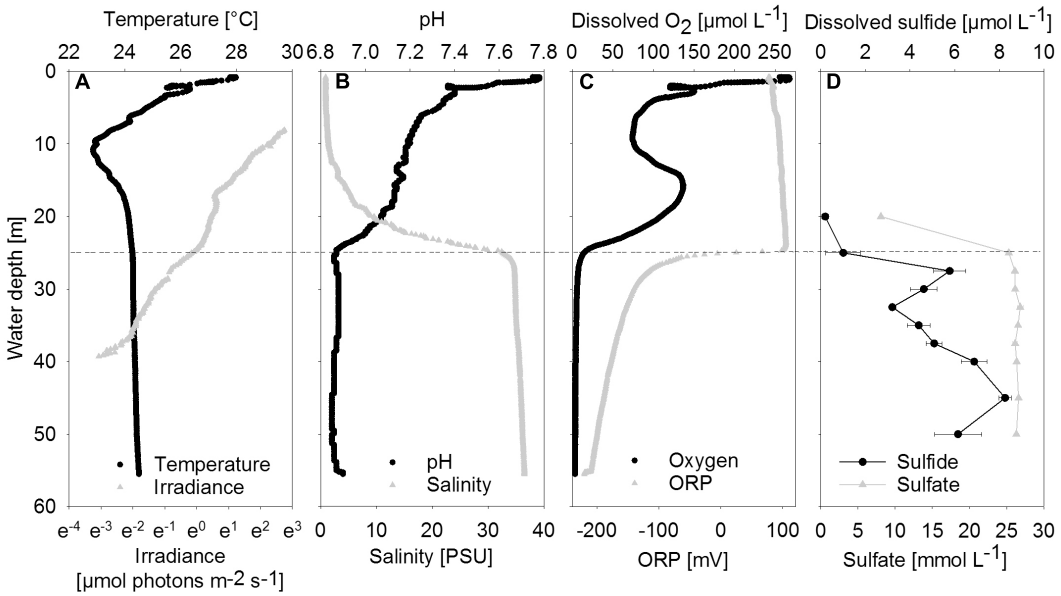

FIGURE 2 | Vertical profiles of chemical and physical parameters in the center of the water column. **(A)** Temperature and irradiance. Irradiance is plotted on a logarithmic scale. **(B)** PH and Salinity. **(C)** Dissolved oxygen and ORP, oxidation-reduction potential. **(D)** Dissolved sulfide and sulfate shown as mean concentrations (n = 3); error bars represent the standard deviation. The halo-chemocline is indicated by the dashed line at 25 m.

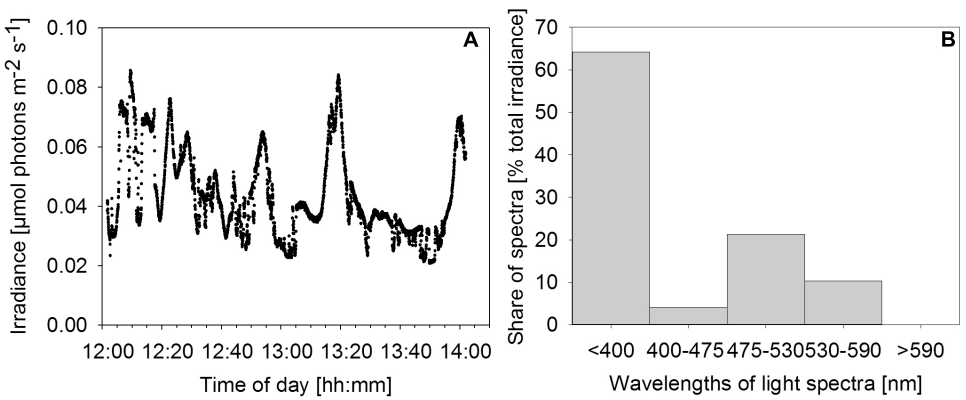

FIGURE 3 | Irradiance and relative wavelength abundance *in situ*. **(A)** Time series of *in situ* irradiance (270°) available to the mat over 2 h starting at noon on December 1st, 2013. Weather: sunny with occasional clouds. **(B)** Percentage share of wavelength ranges in total downwelling light reaching the mat as determined by application of a series of longpass filters.

Nutrient and dissolved organic carbon concentrations were low (data not shown). Phosphate concentrations ranged between 0.2 µmol L^{-1} in the deep water (40 m) and 0.5 µmol L^{-1} in the halo-chemocline (25 m). Dissolved inorganic nitrogen was present below the halo-chemocline in the form of ammonium (approximately 10 µmol L^{-1}) and above the halo-chemocline as nitrate (3 µmol L^{-1}). Dissolved non-purgeable organic carbon concentrations ranged from 171 µmol L^{-1} in the deep water (47 m) to 258 µmol L^{-1} in the oxic water column (9 m) with intermediate concentrations around 30 m.

Downwelling scalar irradiance declined with depth above 17 m and slightly more steeply with depth between 17 and 25 m (**Figure 2A**). Below the halo-chemocline, the light attenuation just below 25 m depth was stronger compared to the zone around 30 m depth. Irradiance at 30 m depth in the cave center was 0.27 µmol photons m^{-2} s^{-1}. At the same depth near the cave wall - the site of thickest mat growth - irradiance was notably lower (**Figure 3A**), in the range of 0.021 to 0.084 µmol photons m^{-2} s^{-1} during 2 h of measurement on a sunny day around noon. Occasional clouds caused sudden decreases in irradiance.

Measurements with a series of longpass filters revealed that the light attenuation varied substantially with wavelength. Intriguingly, 64% of the total irradiance available to the mat was light in the UV region of the spectrum (<400 nm). A second peak

of relative wavelength abundance (21%) was in the green part of the spectrum (475–530 nm). Red/near-IR light (>590 nm) did not reach the mat surface (**Figure 3B**).

Clone Libraries Dominated by Green Sulfur Bacteria and δ-*Proteobacteria*

We created separate 16S rRNA clone libraries from the green, the orange and the brown mat layers (**Figure 4**). The vast majority of the clones (74%) from the thin green upper layer were affiliated with GSB (*Chlorobi*). GSB were much less abundant in the middle, orange layer, which was dominated by δ-*Proteobacteria* related clones (37%). In the brown bottom layer, clones affiliated with *Aminicenantes* (OP8), δ-*Proteobacteria*, *Planctomycetes* and *Chloroflexi* were found most abundant, while GSB (1%) were virtually absent.

The GSB-affiliated 16S rRNA gene sequences shared >97% sequence identity and clustered together in the phylogenetic tree (Supplementary Figure S1). The MBH GSB cluster was situated in a wider cluster of *Prosthecochloris* reference sequences and the closest relative we identified was a clone from the chemocline of Sawmill Sink, a blue hole on the same island as MBH (Macalady et al., unpublished data). Unlike GSB, most δ-*Proteobacteria* clones did not cluster with each other, but were each affiliated with a variety of uncultured reference sequences from diverse habitats (Supplementary Figure S2). A majority of clones were widely clustered with *Desulfobacteraceae*, and a few more with *Syntrophobacteraceae*.

The Mat Contains the Photopigments Bacteriochlorophyll *e* and (β-)isorenieratene

High-performance liquid chromatography analysis was used to assess whether the mat contains photopigments with absorption properties congruent with the *in situ* light quality. To a depth of 57 mm below the mat surface, a carotene identified as either isorenieratene or β-isorenieratene was abundant. It was detected in both *P. phaeobacteroides* BS1 pure culture reference material and in the mat based on identical absorption spectra and RTs (**Figures 5B,D**). Based on difference in RT, it was clearly distinguished from β-carotene, which has the same absorption spectrum as β-isorenieratene and isorenieratene (Takaichi, 2000; Fuciman et al., 2010). Further distinction could not be made, because the reference culture contained both β-isorenieratene and isorenieratene.

Additionally, we found BChl *e* to be abundant in the upper 0.8 to 15 mm of the three core samples as well as in most samples from vacuum-collected green mat surface material. It was identified based on identical absorption spectra and RT of a pigment from *P. phaeobacteroides* BS1 biomass. The absorption spectrum matched published *ex vivo* spectra of BChl *e* (Gloe et al., 1975; Borrego et al., 1999), displaying a maximum at 468 nm, a smaller peak at 651 nm and a double peak at 315/343 nm (**Figures 5A,C**). In both *P. phaeobacteroides* BS1 and mat samples, we detected a variety of BChl *e* homologs (Borrego and Garcia-Gil, 1994) that all displayed the described absorption spectrum, but had different RTs ranging from 11.2 to 16.9 min. Besides BChl *e* we did not detect any type of BChl or chlorophyll.

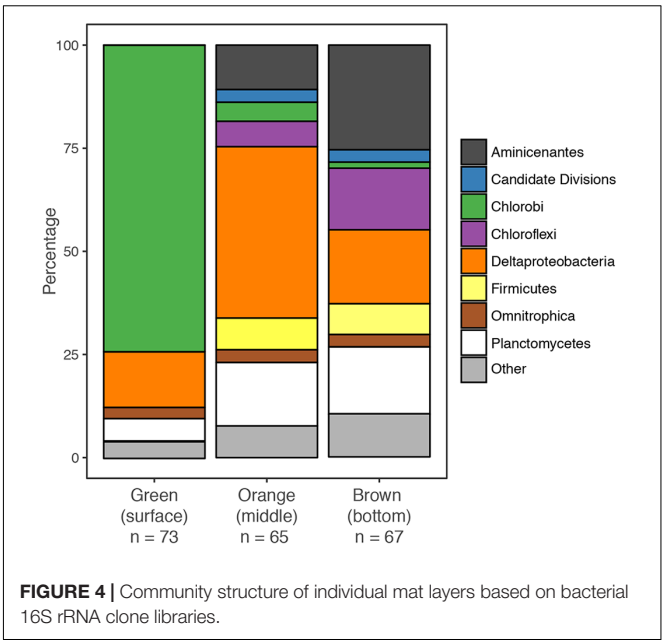

FIGURE 4 | Community structure of individual mat layers based on bacterial 16S rRNA clone libraries.

Low-Light Dependent Uptake of ^{13}C-Labeled DIC and Acetate

In situ incubation with ^{13}C-labeled DIC or acetate revealed light-dependent uptake of inorganic and organic carbon (at 0.27 μmol photons m^{-2} s^{-1}) by surface-layer mat bacteria. Light dependent uptake of DIC was sevenfold higher than uptake of acetate (**Figure 6**). Dark uptake rates of both acetate and DIC were considerably lower.

Single-cell net phototrophic uptake rates were determined from estimated cell numbers per incubation vial and experimentally determined carbon uptake rates (DIC: 7.1×10^{-9} nmol C $cell^{-1}$ h^{-1}; acetate: 1.2×10^{-10} nmol C $cell^{-1}$ h^{-1}). Assuming that the mat surface is homogeneously covered by active photoautotrophic cells, we used single-cell rates to estimate an *in situ* autotrophic carbon fixation rate of 14.5 nmol C cm^{-2} d^{-1}. If photosynthetic sulfide oxidation strictly proceeded according to Eq. 1, this corresponded to a phototrophic sulfide oxidation rate of 29.0 nmol S cm^{-2} d^{-1}. The photosynthetic quantum yield under experimental conditions was calculated from the photon flux of light between 475–530 nm (1.93×10^{-5} μmol photons m^{-2} s^{-1}) per total incubated cell surface area (7.16×10^{-5} m^2 per vial, see section "Isotope Incubations for Process Rate Determination") and the ^{13}C-uptake rate per incubation vial (0.83 nmol C $vial^{-1}$ h^{-1}) resulting in 0.056 moles of inorganic carbon fixed per mole photon reaching the incubated cells. This only takes into consideration the part of the light spectrum (475–530 nm) that can be absorbed by the photopigments found in the mats (**Figure 5** and see section "Discussion"). We assumed that all cells in the incubation vials were photoautotrophic GSB, that there was no shading and that all photons hitting a cell

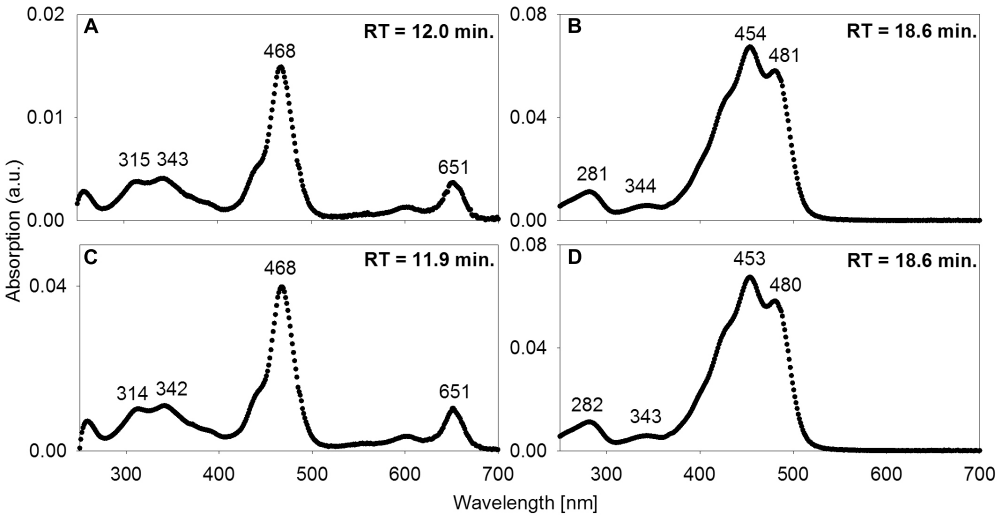

FIGURE 5 | Absorption spectra of acetone-extracted photosynthetic pigments. **(A,B)** from the mats; **(C,D)** and from freeze-dried culture material of low-light-adapted *Prosthecochloris phaeobacteroides* BS1 strain from the Black Sea. Wavelengths [nm] of absorption maxima are indicated as well as RT in the HPLC column.

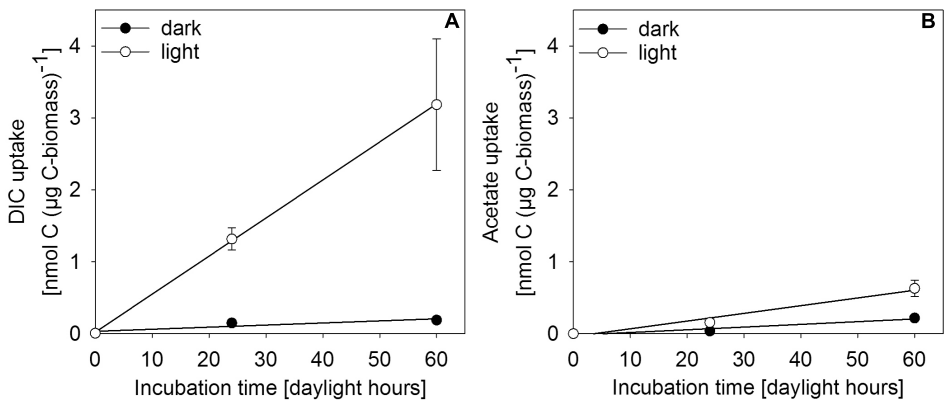

FIGURE 6 | Incorporation of **(A)** DIC and **(B)** acetate as uptake per carbon biomass of upper-layer mat material during incubation in *in situ* water at 30 m depth in the center of MBH. Dark controls were shielded from light during incubation. Error bars indicate standard deviation of the mean of parallel incubations (n = 3).

were absorbed. Depending on absorption efficiency and the share of non-photoautotrophic cells in our incubation vials, the photoautotrophic quantum yield was likely higher than our rough estimate of 0.056 mol C (mol photon)$^{-1}$.

Fe-S-Biogeochemistry

Sulfate reduction rates in 10 mat cores were typically very low, but highly variable between mat samples and highly heterogeneous within each core (**Figure 7F**). SRRs in the majority of subsamples fell below the detection limit. No consistent trend with depth within the mat was observed. The vertically integrated areal fluxes of sulfide caused by sulfate reduction determined in all ten samples were highly variable. Their average (30.4 nmol S cm^{-2} d^{-1}) was in the range of sulfide consumption by anoxygenic photosynthesis we found in the mats. Sulfate was available in large amounts throughout the mat (**Figure 7C**). More than the other analyzed Fe-S parameters, S^0 concentration showed a consistent vertical distribution within most mat core replicates. The highest S^0 concentrations (average ± standard deviation: 0.12 ± 0.06 µmol S cm^{-3}) were found in the top 0.25 cm decreasing to an average of 0.02 ± 0.01 µmol S cm^{-3} below 0.5 cm below the mat surface (**Figure 7E**). This indicated influx of S^0 produced by aerobic sulfide oxidation in the halo-chemocline or *in situ* production by anoxygenic phototrophs and removal by S^0 reduction or disproportionation below the photic layer.

Next to sulfate, dithionite reactive iron (≈ Fe(III) + FeS) and CRS (= FeS_2 + S^0) were by far the most abundant pools of iron and sulfur we found in the mats (**Figure 7**). High concentrations of CRS indicated that the mats were rich in pyrite given the relatively low concentrations of S^0. FeS and H_2S were almost absent, as indicated by low AVS values (**Figure 7A**). Since its FeS component was negligible, the abundant dithionite reactive iron

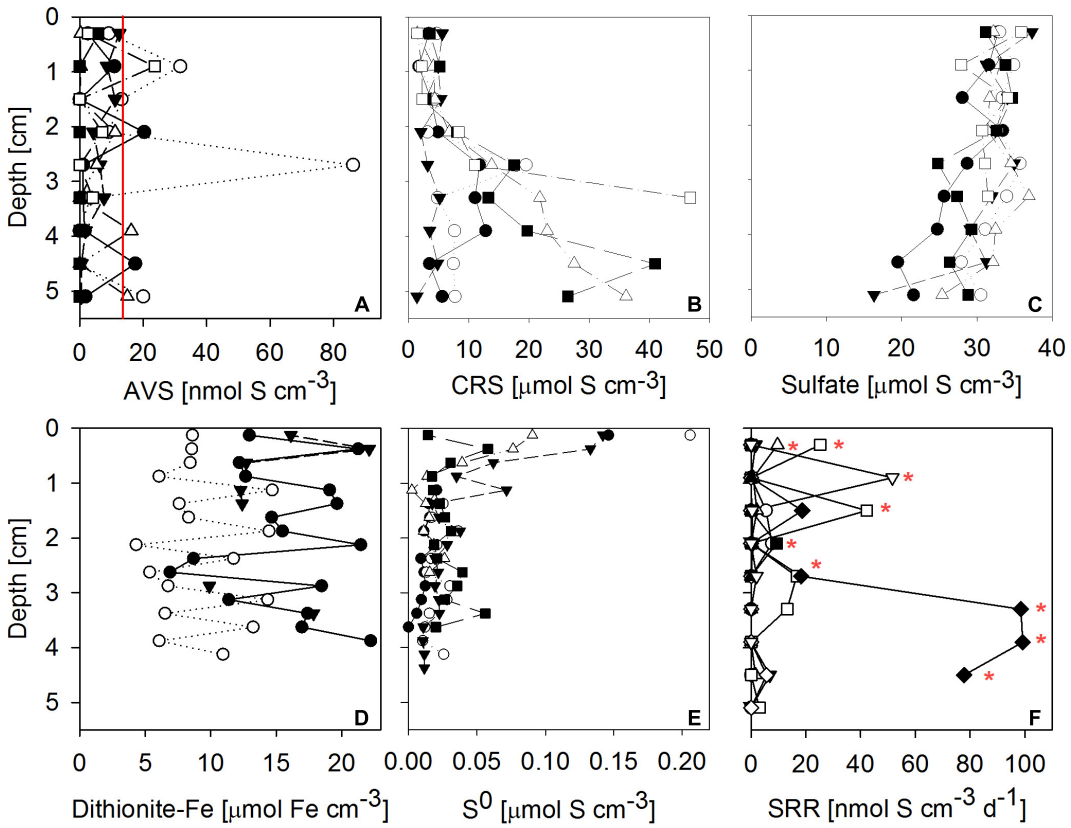

FIGURE 7 | Vertical profiles of Fe-S biogeochemical parameters through microbial mat cores. Different symbols identify replicate measurements from replicate mat cores. **(A)** Solid phase AVS (= FeS + Fe_3S_4 + H_2S; n = 6 replicate cores, the red line indicates detection limit); **(B)** solid phase CRS (= FeS_2 + S^0; n = 6); **(C)** porewater sulfate concentration (n = 6); **(D)** solid phase dithionite reactive iron (≈ Fe(III) + FeS; n = 3); **(E)** solid phase + porewater S^0 concentrations (n = 5); **(F)** sulfate reduction rates (SRR; n = 10, red stars indicate sulfate reduction rates above detection limit). AVS, CRS and sulfate concentrations were measured on the same cores, the remaining parameters were measured on independent cores.

largely consisted of oxidized iron [Fe(III)]. Fe(III) concentrations were in the same range as CRS concentrations. In some but not all samples, CRS showed a clear increase below 2 cm mat depth (**Figure 7B**). For dithionite reactive iron, no trend with depth could be identified.

DISCUSSION

Extremely Low-Light-Adapted Anoxygenic Photosynthesis

Our results show that bacteria in the mats of MBH perform anoxygenic photosynthesis under extremely low light conditions. Based on the mat color and on the abundance of 16S rRNA genes affiliated with GSB in clone libraries, it is likely that GSB are the dominating phylum in the upper layer (**Figure 4**). The single cluster of GSB we identified in MBH mats is closely related to the extremely low-light-adapted strain *P. phaeobacteroides* BS1 (Supplementary Figure S1) from the Black Sea chemocline (Marschall et al., 2010). Pigment analysis revealed the presence of (β-)isorenieratene in all layers and BChl *e* in the upper layers of the mat, which are the typical photopigments of brown-colored GSB including *P. phaeobacteroides* BS1 (Marschall et al., 2010). The 505 nm *in vivo* absorption maximum of the brown-colored and extremely low-light-adapted *Chlorobium* strain MN1 (Overmann et al., 1992) coincided with the part of the spectrum between 475 nm and 530 nm that is relatively abundant at the cave wall (**Figure 3B**). Incubation with ^{13}C-labeled compounds directly demonstrated light-dependent carbon uptake by mat microorganisms under close-to *in situ* irradiance (≤ 0.27 µmol photons m^{-2} s^{-1}). Photoautotrophic fixation of DIC was considerably more efficient than photoheterotrophic incorporation of acetate (**Figure 6**). Indeed, GSB can be mixotrophic regarding their utilized carbon sources (Feng et al., 2010; Tang and Blankenship, 2010). Given that all GSB sequences in our clone libraries formed a single cluster (Supplementary Figure S1), it is likely that heterotrophic and autotrophic phototrophy were performed by the same population.

Anoxygenic photosynthesis under similarly extreme low-light conditions as observed in MBH has previously been described by phylogenetically similar bacteria in the Black Sea chemocline. Photoautotrophic activity at light intensities as low as 0.055 µmol photons m^{-2} s^{-1} *in situ* (Marschall et al., 2010) and as low as

0.015 μmol photons m^{-2} s^{-1} in laboratory cultures (Manske et al., 2005) was reported. Maximum scalar irradiance, measured on a sunny December day shortly after noon at the cave wall next to the MBH mats, was 0.084 μmol photons m^{-2} s^{-1} (**Figure 3**). Since light is strongly attenuated with depth in microbial mats (Kühl et al., 1997), cells in deeper layers will experience even less light and might display extreme phototrophic quantum efficiencies. The photoautotrophic quantum yield observed during incubation of MBH mat cells of 0.056 mol C (mol photons)$^{-1}$ was low compared to previously reported values in GSB (Brune, 1989). However, we likely underestimated the real quantum yield in our assumption that all cells in our experimental vials were photoautotrophs which absorbed 100% of available photons of adequate wavelength. Also, sulfide and light *in situ* were much lower than under the experimental conditions these quantum yields were measured. We would expect to find a much higher quantum yield under more controlled experimental conditions.

Light Harvesting Niches

The irradiance maxima in the UV (<400 nm) and blue-green (475–530 nm) parts of the *in situ* light spectrum (**Figure 3B**) can be understood from the absorption coefficient of water, which has its minimum between 400 and 500 nm (Sogandares and Fry, 1997). The observed shift toward short wavelengths measured at 30 m depth is thus explained by physical attenuation in the overlying water column (Sogandares and Fry, 1997), making the MBH light spectrum resemble spectra from other oligotrophic water columns (Stomp et al., 2007). Oxygenic photosynthesis in the upper water column is the most plausible explanation for the observed minimum between 400 and 475 nm in our light spectra (**Figure 3B**) as it coincides with the short-wavelength absorption peak of Chlorophylls *a*/*b* (430/460 nm). This zone is probably located above 17 m depth, where relatively rapid light attenuation with depth was observed (**Figure 2A**) and dissolved organic carbon concentration was highest.

A typical strategy of anoxygenic phototrophs from mats at shallow water depths is to harvest near-IR light of wavelengths longer than the long-wavelength maxima of chlorophylls *a*/*b* (Overmann et al., 1991). In deeper water columns including MBH, long-wavelength light is attenuated, thus phototrophic mat bacteria must make use of the remaining blue-green light (around 500 nm) and under extreme light limitation might be forced to use the UV-A (320–400 nm) parts of the spectrum. The low-light-adapted *Chlorobium* strain MN1 with the same photosynthetic pigment setup we found in MBH mats [BChl *e* and (β)-isorenieratene] has an *in vivo* absorption maximum around 500 nm (Overmann et al., 1992), which is attributable to BChl *e* (Cox et al., 1998; Glaeser et al., 2002).

Bacteriochlorophyll *e* also has an *ex vivo* absorption maximum around 340 nm within the UV-A part of the light spectrum (**Figures 5A,C**). UV light is commonly thought to be damaging rather than utilizable for phototrophic organisms due to its high energy content (Post and Larkum, 1993; Moisan and Mitchell, 2001; Xue et al., 2005). However, several studies demonstrated that UV-A light can enhance oxygenic photosynthesis (Helbling et al., 2003; Gao et al., 2007; Xu and Gao, 2010). Since irradiance <400 nm constitutes the most abundant source of light energy in their environment, anoxygenic phototrophs in MBH mats may be able to harvest UV-A light for anoxygenic photosynthesis. This hypothesis remains to be tested in future work.

Fe-S-Biogeochemistry: The MBH Mat as Net Sulfide Sink

The Role of Phototrophic Sulfide Oxidation

Low sulfide (as indicated by AVS) and large amounts of pyrite-S (as indicated by high CRS and low S^0) suggest the role of the mats as sulfide sinks (**Figure 7**). Due to the extreme light limitation, it is questionable whether phototrophic sulfide oxidation can play a quantitatively significant role in MBH sulfur biogeochemistry. Our rough estimates of sulfide fluxes from phototrophic sulfide oxidation were in the range of the mean areal SRRs (both approximately 30 nmol S cm^{-2} d^{-1}), suggesting other, quantitatively more important, processes are causing the mats to be sulfide sinks.

The Role and Provenance of Fe-Oxides

Surprisingly large amounts of Fe-oxides were likely the main source of oxidation power in the mats. Fe(III) and CRS concentrations were in the range of values from coastal North Sea sediments (Thamdrup et al., 1994; Holmkvist et al., 2011) and sediments around Dvurechenskii mud volcano, where Lichtschlag et al. (2013) reported sulfide oxidation by Fe- or Mn-oxides. Fe-oxides can react with sulfide to form FeS and S^0 (Jørgensen and Nelson, 2004):

$$3\,H_2S + 2\,FeOOH \rightarrow S^0 + 2\,FeS + 4H_2O \qquad (2)$$

The reaction of S^0 with sulfide yields polysulfide (S_x^{2-}), which can enhance the rate of pyrite (FeS_2) formation (Luther, 1991):

$$FeS + S_x^{2-} \rightarrow FeS_2 + S_{(x-1)}^{2-} \qquad (3)$$

A variety of reaction types for pyrite formation by reaction of sulfide with Fe(III)-minerals, Fe^{2+} and FeS are possible (discussed in Holmkvist et al., 2011). Low concentrations of AVS compared to pyrite-S in the mat suggested that the FeS quickly reacts further to form pyrite (Eq. 3), which is quite stable under reduced conditions (Fossing and Jørgensen, 1990).

The origin of very abundant Fe(III) in the mats might be dust from the Sahara, particularly the Sahel zone (Shinn et al., 2000). This Fe-containing dust was deposited episodically during climatic fluctuations (Swart et al., 2010) on the land surface, on forming soils, and in air-filled caves, which later flooded to become anchialine caves. Millimeter- to centimeter-thick red dust layers, filling crevices and niches in flooded passages, have been observed by cave divers including B. Kakuk (personal communication). Bottrell et al. (1991) found large amounts of pyrite in the cave wall of another Bahamian blue hole. Iron reducing bacteria may have settled on such iron rich dust features in the cave wall of MBH and initialized formation of the mats. Initial input of Fe(III) from the bottom of the mats

in combination with continuous iron settling on the mats from the water column may explain the constant distribution of large amounts of Fe(III) throughout the mat.

Additionally, Fe(III) may be produced by iron oxidizing anoxygenic phototrophs (Widdel et al., 1993) on the mat surface. Photoferrotrophs may take up dissolved Fe^{2+} from the water column or as the product of reductive dissolution of iron from the limestone rock and also prevent the diffusive loss of Fe^{2+} produced during pyrite formation (Holmkvist et al., 2011), making the mats effective traps for dissolved and colloidal iron. This would create a niche for iron reducers, which would close the iron cycle. However, evidence for photoferrotrophy in MBH mats is lacking. *Chlorobium phaeoferrooxidans* is the first known photoferrotrophic GSB containing BChl *e*, which could theoretically enable it to harvest the part of the light spectrum available at the MBH cave wall (Llirós et al., 2015; Crowe et al., 2017). The MBH GSB cluster was neither affiliated with *C. phaeoferrooxidans* nor the other known or putative photoferrotrophic GSB *Chlorobium ferrooxidans* and *Chlorobium luteolum* (Supplementary Figure S1; Heising et al., 1999; Frigaard and Bryant, 2008).

Shortages of Organic Carbon and Sulfide

Despite the presence of photosynthesizing bacteria, MBH mats appear limited in chemical reductants, notably sulfide and organic carbon. Even if surplus organic carbon is produced in anoxygenic photosynthesis, it may be unavailable for organoheterotrophs, because it can be used by photoheterotrophs (**Figure 6B**). Low concentrations of nutrients and dissolved organic matter in the overlying water column were well below average lake water concentrations (Chen et al., 2015). Organic carbon shortage within the mats is suggested by low to undetectable SRRs despite high concentrations of sulfate (**Figure 7F**), which were much lower than in similar microbial mats and biofilms (Canfield and Des Marais, 1991; Kühl and Jørgensen, 1992; Visscher et al., 1992). A locally restricted anomaly of elevated SRRs in one sample may be explained by a pocket of high organic carbon, perhaps from sunken terrestrial material (**Figure 7F**).

Due to the low SRRs within the mats, the primary source of sulfide to the mats is from the water column. Vertical profiles of sulfide concentration (**Figure 2**) suggested small sources of sulfide from the bottom of the blue hole and in the halo-chemocline, where sulfate reduction has previously been observed in another Bahamian blue hole (Bottrell et al., 1991). Sulfate reduction in the halo-chemocline may be more active than in the mats due to better access to organic carbon from oxygenic phototrophy in the oxic water column, and potential anoxygenic phototrophy in the halo-chemocline (Macalady et al., 2010).

δ-*Proteobacterial* sulfate reducers and other heterotrophs seem to be abundant in the mats but their activity limited by organic carbon availability. Sulfate reduction may also experience competition for the scarce organic carbon by anoxygenic photoheterotrophy and iron reduction. While a majority of

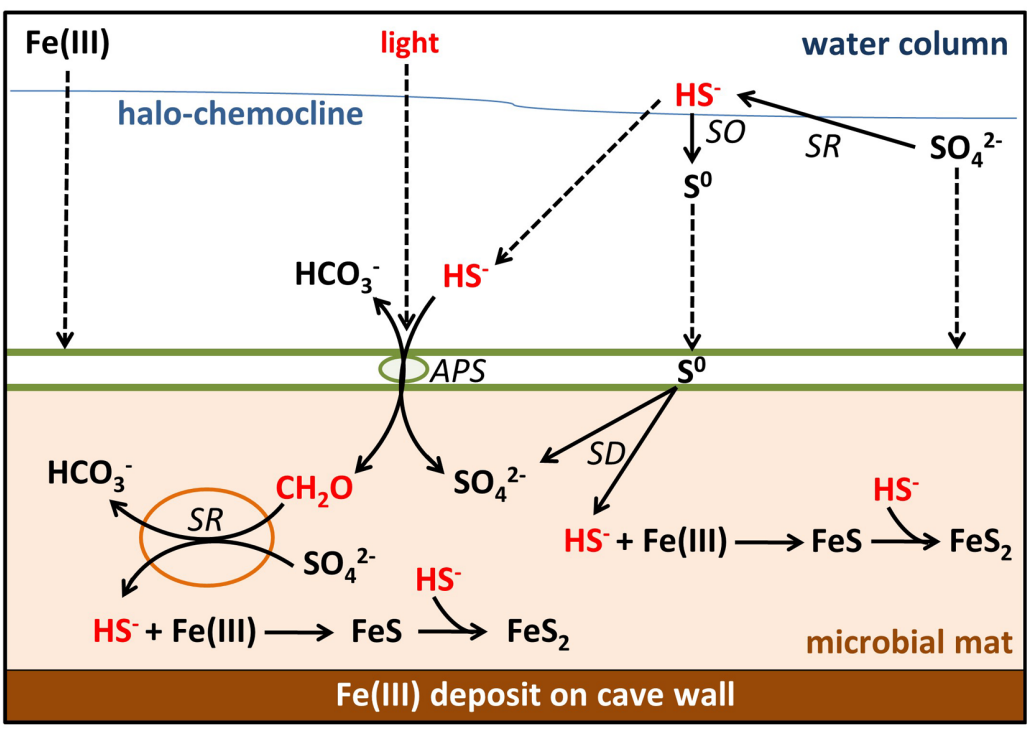

FIGURE 8 | Sulfur, carbon, and iron biogeochemical cycling in the MBH microbial mat. Biotic processes are labeled SD (S^0 disproportionation), SO (sulfide oxidation), SR (sulfate reduction), and APS (anoxygenic photosynthesis). Remaining processes are abiotic. Parameters limiting the sulfur cycle in the mat are marked with red color. Dashed arrows indicate input by sinking or diffusion from outside the mats. Green spheres = GSB; orange spheres = δ-Proteobacteria.

the δ-*Proteobacteria* in our clone libraries were affiliated with *Desulfobacteraceae* and *Syntrophobacteraceae* (Supplementary Figure S2), indicating that they are likely sulfate reducers (Kuever, 2014a,b), the affiliation of several other clones within the δ-*Proteobacteria* was unresolved and leaves room to speculate that they might reduce iron (Lovley et al., 2004) or disproportionate S^0 (Thamdrup et al., 1993). Generally, the community composition of the orange and brown portions of the MBH mats was defined by groups (δ-*Proteobacteria*, *Chloroflexi*, *Planctomycetes*, *Aminicenantes, and Omnitrophica*; **Figure 2**) that have previously been linked to heterotrophic and fermenting carbon degradation in similar environments (Inagaki et al., 2006; Gies et al., 2014). In MBH mats, the activity of these heterotrophic bacteria must be assumed to be limited by the scarce organic carbon. We therefore propose that the mats have grown slowly but largely undisturbed over long time scales - a hypothesis that warrants future research.

The Sulfur Cycle Was Slow in the Presence of Iron and Low Organic Carbon

Despite the presence of large amounts of sulfate, sulfur cycling within the mats was slowed down due to organic carbon shortage and the accumulations of Fe(III). Anoxygenic phototrophs were limited by light and probably also by sulfide, given slow production by sulfate reduction and competition by abiotic precipitation indicated by the pyrite accumulations. Therefore, mat-internal primary production was low and so was organic matter input from the oligotrophic water column. Low SRRs can thus be explained by organic carbon limitation.

In oxic shallow-water environments light energy can enable a phototrophic community to supply the deeper anoxic layers of a microbial mat with enough organic carbon to enable sulfate reduction to compete with FeS formation even in the presence of considerable amounts of iron (Wieland et al., 2005). If iron is present in anoxic environments under oligotrophic and light-limited conditions, sulfur cycling is slowed down considerably. In principle, this shortage in reductants would provide a niche for oxygenic photosynthesis, but the MBH light level is too low for the high energy water splitting reaction. High influx of organic carbon or sulfide would be needed to stimulate more active sulfur cycling in low-light mats.

Conclusions and Implications

The biogeochemistry of MBH is characterized by limitation of energy sources like light and organic carbon. This leads to slow rates of anoxygenic photosynthesis and heterotrophic processes like sulfate reduction (**Figure 8**). Low SRRs and AVS concentrations falsified our hypothesis of the mats functioning as a net sulfide source. Instead, high concentrations of pyrite-S indicated abiotic sulfide scavenging as the mechanism responsible for making the mats a net sulfide sink. The role of very abundant δ-*Proteobacteria* in clone libraries has yet to be finally resolved, but most of them appear to be sulfate reducers whose activity is low due to organic carbon limitation.

Most sulfide produced by any *in situ* sulfate reduction or diffusing into the mat from the water column will be scavenged by abundant iron oxides rather than oxidized by light-limited anoxygenic phototrophs. Thus, little organic carbon is produced *in situ*, preventing sulfate reduction or limiting it to very low rates. In the absence of significant external input of sulfide, light and organic carbon, the sulfur cycling in these mats is slowed down. Further investigations of these mechanisms may ultimately help to understand the creation of ferruginous conditions in the presence of sulfate which is relevant for Proterozoic ocean water columns. Ferruginous conditions prevailed in the Meso- (Planavsky et al., 2011) and Neoproterozoic ocean (Canfield et al., 2008) despite the presence of approximately 1 mM sulfate (Canfield and Farquhar, 2009), which requires limitation of sulfate reduction for example by organic carbon delivery (Johnston et al., 2010; Planavsky et al., 2011).

Despite extreme light limitation, anoxygenic photosynthesis by GSB could be detected. Barely explored traits in anoxygenic photosynthesis may be hypothesized based on our data and demand further investigation including the possibility of UV-A utilization by low-light-adapted GSB. Our data show that phylogenetically very similar organisms using the same photopigment setup are responsible for anoxygenic photosynthesis in two contrasting habitats with the lowest irradiance at which photosynthesis has been reported: as planktonic cells in the Black Sea chemocline (Overmann et al., 1992) and associated as a microbial mat on the cave wall of MBH. Their photopigments BChl *e* and (β-)isorenieratene in combination with 16S rRNA from known brown-colored GSB species are therefore promising biomarkers for low-light anoxygenic photosynthesis in a range of modern and ancient environments.

AUTHOR CONTRIBUTIONS

SH, JM, DdB, and AF contributed to the design of the study and the experiments. VM designed and built the custom-made light sensor. SH planned and SH, BK, and JM led the field work to which TH contributed. SH did the main laboratory work, supported by AF and JK. RMR contributed a subset of the data (clone libraries and carbon concentrations) from her work in collaboration with JM and their additional exploratory data helped to guide this study. SH, DdB, JM, AF, JK, and TH contributed to data evaluation and interpretation. SH was the main author of the manuscript. SH, DdB, JM, and JK developed the intellectual content of the manuscript, to which TH and AF contributed. All authors contributed to manuscript revision and approved the submitted version.

FUNDING

This study was funded by the Max-Planck Institute for Marine Microbiology, the National Science Foundation (EAR-0525503 to JM), the NASA Astrobiology Institute (PSARC, NNA04CC06A to JM), a Lewis and Clark Fund for Exploration and Field Research in Astrobiology Fellowship (to RM), a National Science Foundation Graduate Research Fellowship Travel Grant (to RM),

the Canadian Excellence Research Chair in Oceanography (SH), and the NASA Astrobiology Institute Postdoctoral Program (TH).

ACKNOWLEDGMENTS

We are indebted to Jörg Overmann and his group at DSMZ Braunschweig for providing freeze-dried *Chlorobium* culture material. We thank Marit van Erk for the S^0 analyses, Arjun Chennu, Tim Ferdelman, Mohammad al-Najjar, and Gaute Lavik for the expert advice on methodology, as well as Martina Alisch, Gabriele Klockgether, and all MPI Microsensor TAs for helping with sample analysis and microsensor preparation. Furthermore, we thank Tomas Wilkop and Manfred Schlösser for their support in preparing the field excursion, and the MPI Electronics and Mechanics workshops for their technical ingenuity. Sean Crowe provided valuable inspiration for Proterozoic Ocean implications. Three anonymous reviewers from an unsuccessful previous submission of the manuscript gave valuable suggestions for improvement. SH feels indebted to the Max-Planck society and the MarMic program for the excellent scientific training and funding.

SUPPLEMENTARY MATERIAL

The Supplementary Material for this article can be found online at: https://www.frontiersin.org/articles/10.3389/fmicb.2018.00858/full#supplementary-material

REFERENCES

Al-Najjar, M. A., de Beer, D., Kühl, M., and Polerecky, L. (2012). Light utilization efficiency in photosynthetic microbial mats. *Environ. Microbiol.* 14, 982–992. doi: 10.1111/j.1462-2920.2011.02676.x

Altschul, S. F., Madden, T. L., Schäffer, A. A., Zhang, J., Zhang, Z., Miller, W., et al. (1997). Gapped BLAST and PSI-BLAST: a new generation of protein database search programs. *Nucleic Acids Res.* 25, 3389–3402. doi: 10.1093/nar/25.17.3389

Borrego, C. M., Arellano, J. B., Abella, C. A., Gillbro, T., and Garcia-Gil, J. (1999). The molar extinction coefficient of bacteriochlorophyll e and the pigment stoichiometry in *Chlorobium phaeobacteroides*. *Photosynth. Res.* 60, 257–264. doi: 10.1023/A:1006230820007

Borrego, C. M., and Garcia-Gil, L. J. (1994). Separation of bacteriochlorophyll homologues from green photosynthetic sulfur bacteria by reversed-phase HPLC. *Photosynth. Res.* 41, 157–164. doi: 10.1007/BF02184156

Bottrell, S. H., Smart, P. L., Whitaker, F., and Raiswell, R. (1991). Geochemistry and isotope systematics of sulphur in the mixing zone of Bahamian blue holes. *Appl. Geochem.* 6, 97–103. doi: 10.1016/0883-2927(91)90066-X

Brune, D. C. (1989). Sulfur oxidation by phototrophic bacteria. *Biochim. Biophys. Acta* 975, 189–221. doi: 10.1016/S0005-2728(89)80251-8

Canfield, D. E., and Des Marais, D. J. (1991). Aerobic sulfate reduction in microbial mats. *Science* 251, 1471–1473. doi: 10.1126/science.11538266

Canfield, D. E., and Farquhar, J. (2009). Animal evolution, bioturbation, and the sulfate concentration of the oceans. *Proc. Natl. Acad. Sci. U.S.A.* 106, 8123–8127. doi: 10.1073/pnas.0902037106

Canfield, D. E., Poulton, S. W., Knoll, A. H., Narbonne, G. M., Ross, G., Goldberg, T., et al. (2008). Ferruginous conditions dominated later neoproterozoic deep-water chemistry. *Science* 321, 949–952. doi: 10.1126/science.1154499

Chen, M., Zeng, G., Zhang, J., Xu, P., Chen, A., and Lu, L. (2015). Global landscape of total organic carbon, nitrogen and phosphorus in lake water. *Sci. Rep.* 5:15043. doi: 10.1038/srep15043

Cline, J. D. (1969). Spectrophotometric determination of hydrogen sulfide in natural waters. *Limnol. Oceanogr.* 14, 454–458. doi: 10.4319/lo.1969.14.3.0454

Cornwell, J. C., and Morse, J. W. (1987). The characterization of iron sulfide minerals in anoxic marine sediments. *Mar. Chem.* 22, 193–206. doi: 10.1016/0304-4203(87)90008-9

Cox, R. P., Miller, M., Aschenbrücker, J., Ma, Y.-Z., and Gillbro, T. (1998). "The role of bacteriochlorophyll *e* and carotenoids in light harvesting in brown-colored green sulfur bacteria," in *Photosynthesis: Mechanisms and Effects*, ed. G. Garab (Amsterdam: Springer), 149–152.

Crowe, S. A., Hahn, A. S., Morgan-Lang, C., Thompson, K. J., Simister, R. L., Llirós, M., et al. (2017). Draft genome sequence of the pelagic photoferrotroph *Chlorobium phaeoferrooxidans*. *Genome Announc.* 5:e01584-16. doi: 10.1128/genomeA.01584-16

Crowe, S. A., Maresca, J. A., Jones, C., Sturm, A., Henny, C., Fowle, D. A., et al. (2014). Deep-water anoxygenic photosythesis in a ferruginous chemocline. *Geobiology* 12, 322–339. doi: 10.1111/gbi.12089

Darriba, D., Taboada, G. L., Doallo, R., and Posada, D. (2012). jModelTest 2: more models, new heuristics and parallel computing. *Nat. Methods* 9:772. doi: 10.1038/nmeth.2109

Engel, A. S., Porter, M. L., Stern, L. A., Quinlan, S., and Bennett, P. C. (2004). Bacterial diversity and ecosystem function of filamentous microbial mats from aphotic (cave) sulfidic springs dominated by chemolithoautotrophic "*Epsilonproteobacteria*". *FEMS Microbiol. Ecol.* 51, 31–53. doi: 10.1016/j.femsec.2004.07.004

Feng, X., Tang, K.-H., Blankenship, R. E., and Tang, Y. J. (2010). Metabolic flux analysis of the mixotrophic metabolisms in the green sulfur bacterium *Chlorobaculum tepidum*. *J. Biol. Chem.* 285, 39544–39550. doi: 10.1074/jbc.M110.162958

Fossing, H., and Jørgensen, B. B. (1989). Measurement of bacterial sulfate reduction in sediments: evaluation of a single-step chromium reduction method. *Biogeochemistry* 8, 205–222. doi: 10.1007/BF00002889

Fossing, H., and Jørgensen, B. B. (1990). Oxidation and reduction of radiolabeled inorganic sulfur compounds in an estuarine sediment, Kysing Fjord, Denmark. *Geochim. Cosmochim. Acta* 54, 2731–2742. doi: 10.1016/0016-7037(90)90008-9

Frigaard, N.-U., and Bryant, D. A. (2008). "Genomic insights into the sulfur metabolism of phototrophic green sulfur bacteria," in *Sulfur Metabolism in Phototrophic Organisms. Advances in Photosynthesis and Respiration*, eds R. Hell, C. Dahl, D. Knaff, and T. Leustek (Dordrecht: Springer), 337–355. doi: 10.1007/978-1-4020-6863-8_17

Fuciman, M., Chábera, P., Župèanová, A., Høíbek, P., Arellano, J. B., Vácha, F., et al. (2010). Excited state properties of aryl carotenoids. *Phys. Chem. Chem. Phys.* 12, 3112–3120. doi: 10.1039/B921384H

Gao, K., Wu, Y., Li, G., Wu, H., Villafane, V. E., and Helbling, E. W. (2007). Solar UV radiation drives CO_2 fixation in marine phytoplankton: a double-edged sword. *Plant Physiol.* 144, 54–59. doi: 10.1104/pp.107.098491

Gies, E. A., Konwar, K. M., Beatty, J. T., and Hallam, S. J. (2014). Illuminating microbial dark matter in meromictic Sakinaw Lake. *Appl. Environ. Microbiol.* 80, 6807–6818. doi: 10.1128/AEM.01774-14

Glaeser, J., Bañeras, L., Rütters, H., and Overmann, J. (2002). Novel bacteriochlorophyll e structures and species-specific variability of pigment composition in green sulfur bacteria. *Arch. Microbiol.* 177, 475–485. doi: 10.1007/s00203-002-0416-4

Gloe, A., Pfennig, N., Brockmann, H. Jr., and Trowitzsch, W. (1975). A new bacteriochlorophyll from brown-colored *Chlorobiaceae*. *Arch. Microbiol.* 102, 103–109. doi: 10.1007/BF00428353

Gonzalez, B. C., Iliffe, T. M., Macalady, J. L., Schaperdoth, I., and Kakuk, B. (2011). Microbial hotspots in anchialine blue holes: initial discoveries from the Bahamas. *Hydrobiologia* 677, 149–156. doi: 10.1007/s10750-011-0932-9

Griffin, B. M., Schott, J., and Schink, B. (2007). Nitrite, an electron donor for anoxygenic photosynthesis. *Science* 316:1870. doi: 10.1126/science.1139478

Halm, H., Lam, P., Ferdelman, T. G., Lavik, G., Dittmar, T., LaRoche, J., et al. (2012). Heterotrophic organisms dominate nitrogen fixation in the South Pacific Gyre. *ISME J.* 6, 1238–1249. doi: 10.1038/ismej.2011.182

Hansen, H. P., and Koroleff, F. (2009). "Determination of nutrients," in *Methods of Seawater Analysis*, eds K. Grasshoff, K. Kremling, and M. Ehrhardt (Weinheim: Verlag Chemie), 159–228.

Hauska, G., Schoedl, T., Remigy, H., and Tsiotis, G. (2001). The reaction center of green sulfur bacteria. *Biochim. Biophys. Acta* 1507, 260–277. doi: 10.1016/S0005-2728(01)00200-6

Heising, S., Richter, L., Ludwig, W., and Schink, B. (1999). *Chlorobium ferrooxidans* sp. nov., a phototrophic green sulfur bacterium that oxidizes ferrous iron in coculture with a "*Geospirillum*" sp. strain. *Arch. Microbiol.* 172, 116–124. doi: 10.1007/s002030050748

Helbling, E. W., Gao, K., Gonçalves, R. J., Wu, H., and Villafañe, V. E. (2003). Utilization of solar UV radiation by coastal phytoplankton assemblages off SE China when exposed to fast mixing. *Mar. Ecol. Prog. Ser.* 259, 59–66. doi: 10.3354/meps259059

Holmkvist, L., Ferdelman, T. G., and Jørgensen, B. B. (2011). A cryptic sulfur cycle driven by iron in the methane zone of marine sediment (Aarhus Bay, Denmark). *Geochim. Cosmochim. Acta* 75, 3581–3599. doi: 10.1016/j.gca.2011.03.033

Iliffe, T. M. (2000). "Anchialine cave ecology," in *Ecosystems of the World: Subterranean Ecosystems*, eds H. Wilkens, D. C. Culver, and W. F. Humphreys (Amsterdam: Elsevier), 59–76.

Imhoff, J. F., and Thiel, V. (2010). Phylogeny and taxonomy of *Chlorobiaceae*. *Photosynth. Res.* 104, 123–136. doi: 10.1007/s11120-009-9510-7

Inagaki, F., Nunoura, T., Nakagawa, S., Teske, A., Lever, M., Lauer, A., et al. (2006). Biogeographical distribution and diversity of microbes in methane hydrate-bearing deep marine sediments on the Pacific Ocean Margin. *Proc. Natl. Acad. Sci. U.S.A.* 103, 2815–2820. doi: 10.1073/pnas.0511033103

Jørgensen, B. B. (1978). A comparison of methods for the quantification of bacterial sulfate reduction in coastal marine sediments. *Geomicrobiol. J.* 1, 11–27. doi: 10.1080/01490457809377721

Jørgensen, B. B., and Nelson, D. C. (2004). Sulfide oxidation in marine sediments: geochemistry meets microbiology. *Geol. Soc. Am.* 379, 63–81. doi: 10.1130/0-8137-2379-5.63

Johnston, D. T., Poulton, S. W., Dehler, C., Porter, S., Husson, J., Canfield, D. E., et al. (2010). An emerging picture of Neoproterozoic ocean chemistry: insights from the Chuar Group, Grand Canyon, USA. *Earth Planet. Sci. Lett.* 290, 64–73. doi: 10.1016/j.epsl.2009.11.059

Kallmeyer, J., Ferdelman, T. G., Weber, A., Fossing, H., and Jørgensen, B. B. (2004). A cold chromium distillation procedure for radiolabeled sulfide applied to sulfate reduction measurements. *Limnol. Oceanogr. Methods* 2, 171–180. doi: 10.4319/lom.2004.2.171

Kostka, J. E., and Luther, G. W. (1994). Partitioning and speciation of solid phase iron in saltmarsh sediments. *Geochim. Cosmochim. Acta* 58, 1701–1710. doi: 10.1016/0016-7037(94)90531-2

Kuever, J. (2014a). "The family *Desulfobacteraceae*," in *The Prokaryotes: Deltaproteobacteria and Epsilonproteobacteria*, eds E. Rosenberg, E. F. DeLong, S. Lory, E. Stackebrandt, and F. Thompson (Berlin: Springer), 45–73.

Kuever, J. (2014b). "The family *Syntrophobacteraceae*," in *The Prokaryotes: Deltaproteobacteria and Epsilonproteobacteria*, eds E. Rosenberg, E. F. DeLong, S. Lory, E. Stackebrandt, and F. Thompson (Berlin: Springer), 289–299.

Kühl, M., and Jørgensen, B. B. (1992). Microsensor measurements of sulfate reduction and sulfide oxidation in compact microbial communities of aerobic biofilms. *Appl. Environ. Microbiol.* 58, 1164–1174.

Kühl, M., Lassen, C., and Revsbech, N. P. (1997). A simple light meter for measurements of PAR (400 to 700 nm) with fiber-optic microprobes: application for P vs E_0 (PAR) measurements in a microbial mat. *Aquat. Microb. Ecol.* 13, 197–207. doi: 10.3354/ame013197

Lau, M. C. Y., Aitchison, J. C., and Pointing, S. B. (2009). Bacterial community composition in thermophilic microbial mats from five hot springs in central Tibet. *Extremophiles* 13, 139–149. doi: 10.1007/s00792-008-0205-3

Letunic, I., and Bork, P. (2016). Interactive tree of life (iTOL) v3: an online tool for the display and annotation of phylogenetic and other trees. *Nucleic Acids Res.* 44, W242–W245. doi: 10.1093/nar/gkw290

Lichtschlag, A., Kamyshny, A., Ferdelman, T. G., and de Beer, D. (2013). Intermediate sulfur oxidation state compounds in the euxinic surface sediments of the Dvurechenskii mud volcano (Black Sea). *Geochim. Cosmochim. Acta* 105, 130–145. doi: 10.1016/j.gca.2012.11.025

Llirós, M., García–Armisen, T., Darchambeau, F., Morana, C., Triadó–Margarit, X., Inceoğlu, Ö., et al. (2015). Pelagic photoferrotrophy and iron cycling in a modern ferruginous basin. *Sci. Rep.* 5:13803. doi: 10.1038/srep13803

Lovley, D. R., Holmes, D. E., and Nevin, K. P. (2004). Dissimilatory Fe(III) and Mn(IV) reduction. *Adv. Microb. Physiol.* 49, 219–286. doi: 10.1016/S0065-2911(04)49005-5

Ludwig, W., Strunk, O., Westram, R., Richter, L., Meier, H., Buchner, A., et al. (2004). ARB: a software environment for sequence data. *Nucleic Acids Res.* 32, 1363–1371. doi: 10.1093/nar/gkh293

Luther, G. W. (1991). Pyrite synthesis via polysulfide compounds. *Geochim. Cosmochim. Acta* 55, 2839–2849. doi: 10.1016/0016-7037(91)90449-F

Macalady, J. L., Dattagupta, S., Schaperdoth, I., Jones, D. S., Druschel, G. K., and Eastman, D. (2008). Niche differentiation among sulfur-oxidizing bacterial populations in cave waters. *ISME J.* 2, 590–601. doi: 10.1038/ismej.2008.25

Macalady, J. L., Schaperdoth, I., Fulton, J. M., Freeman, K. H., and Hanson, T. E. (2010). Microbial biogeochemistry of a meromictic blue hole. *Geochim. Cosmochim. Acta* 74:A651.

Manske, A. K., Glaeser, J., Kuypers, M. M., and Overmann, J. (2005). Physiology and phylogeny of green sulfur bacteria forming a monospecific phototrophic assemblage at a depth of 100 meters in the Black Sea. *Appl. Environ. Microbiol.* 71, 8049–8060. doi: 10.1128/AEM.71.12.8049-8060.2

Marschall, E., Jogler, M., Henssge, U., and Overmann, J. (2010). Large-scale distribution and activity patterns of an extremely low-light-adapted population of green sulfur bacteria in the Black Sea. *Environ. Microbiol.* 12, 1348–1362. doi: 10.1111/j.1462-2920.2010.02178.x

Moisan, T. A., and Mitchell, B. G. (2001). UV absorption by mycosporine-like amino acids in *Phaeocystis antarctica* Karsten induced by photosynthetically available radiation. *Mar. Biol.* 138, 217–227. doi: 10.1007/s002270000424

Montesinos, E., Guerrero, R., Abella, C., and Esteve, I. (1983). Ecology and physiology of the competition for light between *Chlorobium limicola* and *Chlorobium phaeobacteroides* in natural habitats. *Appl. Environ. Microbiol.* 46, 1007–1016.

Mori, Y., Kataoka, T., Okamura, T., and Kondo, R. (2013). Dominance of green sulfur bacteria in the chemocline of the meromictic Lake Suigetsu, Japan, as revealed by dissimilatory sulfite reductase gene analysis. *Arch. Microbiol.* 195, 303–312. doi: 10.1007/s00203-013-0879-5

Mylroie, J. E., Carew, J. L., and Moore, A. I. (1995). Blue holes: definition and genesis. *Carb. Evap.* 10, 225–233. doi: 10.1007/BF03175407

Nagata, T. (1986). Carbon and nitrogen content of natural planktonic bacteria. *Appl. Environ. Microbiol.* 52, 28–32.

Overmann, J., Beatty, J. T., Hall, K. J., Pfennig, N., and Northcote, T. G. (1991). Characterization of a dense, purple sulfur bacterial layer in a meromictic salt lake. *Limnol. Oceanogr.* 36, 846–859. doi: 10.4319/lo.1991.36.5.0846

Overmann, J., Cypionka, H., and Pfennig, N. (1992). An extremely low-light-adapted phototrophic sulfur bacterium from the Black Sea. *Limnol. Oceanogr.* 37, 150–155. doi: 10.4319/lo.1992.37.1.0150

Overmann, J., and Pfennig, N. (1989). *Pelodictyon phaeoclathratiforme* sp. nov., a new brown-colored member of the Chlorobiaceae forming net-like colonies. *Arch. Microbiol.* 152, 401–406. doi: 10.1007/BF00425181

Pfennig, N. (1975). The phototrophic bacteria and their role in the sulfur cycle. *Plant Soil* 43, 1–16. doi: 10.1007/BF01928472

Planavsky, N. J., McGoldrick, P., Scott, C. T., Li, C., Reinhard, C. T., Kelly, A. E., et al. (2011). Widespread iron-rich conditions in the mid-Proterozoic ocean. *Nature* 477, 448–451. doi: 10.1038/nature10327

Post, A., and Larkum, A. W. (1993). UV-absorbing pigments, photosynthesis and UV exposure in Antarctica: comparison of terrestrial and marine algae. *Aquat. Bot.* 45, 231–243. doi: 10.1016/0304-3770(93)90023-P

Røy, H., Weber, H. S., Tarpgaard, I. H., Ferdelman, T. G., and Jørgensen, B. B. (2014). Determination of dissimilatory sulfate reduction rates in marine sediment via radioactive 35S tracer. *Limnol. Oceanogr. Methods* 12, 196–211. doi: 10.4319/lom.2014.12.196

Schloss, P. D., Westcott, S. L., Ryabin, T., Hall, J. R., Hartmann, M., Hollister, E. B., et al. (2009). Introducing mothur: open-source, platform-independent, community-supported software for describing and comparing microbial communities. *Appl. Environ. Microbiol.* 75, 7537–7541. doi: 10.1128/AEM.01541-09

Schwabe, S., and Herbert, R. A. (2004). Black holes of the Bahamas: what they are and why they are black. *Quat. Int.* 121, 3–11. doi: 10.1016/j.quaint.2004.01.019

Seymour, J. R., Humphreys, W. F., and Mitchell, J. G. (2007). Stratification of the microbial community inhabiting an anchialine sinkhole. *Aquat. Microb. Ecol.* 50, 11–24. doi: 10.3354/ame01153

Shinn, E. A., Smith, G. W., Prospero, J. M., Betzer, P., Hayes, M. L., Garrison, V., et al. (2000). African dust and the demise of Caribbean coral reefs. *Geophys. Res. Lett.* 27, 3029–3032. doi: 10.1029/2000GL011599

Sogandares, F. M., and Fry, E. S. (1997). Absorption spectrum (340–640 nm) of pure water. I. Photothermal measurements. *Appl. Optics* 36, 8699–8709. doi: 10.1364/AO.36.008699

Stamatakis, A., Hoover, P., and Rougemont, J. (2008). A rapid bootstrap algorithm for the RAxML web servers. *Syst. Biol.* 57, 758–771. doi: 10.1080/10635150802429642

Stomp, M., Huisman, J., Stal, L. J., and Matthijs, H. C. (2007). Colorful niches of phototrophic microorganisms shaped by vibrations of the water molecule. *ISME J.* 1, 271–282. doi: 10.1038/ismej.2007.59

Swart, P. K., Arienzo, M., Broad, K., Clement, A., and Kakuk, B. (2010). Blue Holes in Bahamas: repositories of climate, anthropogenic, and archaeological changes over the past 300 000 years. *J. Earth Sci.* 21:265. doi: 10.1007/s12583-010-0231-9

Takaichi, S. (2000). Characterization of carotenes in a combination of a C18 HPLC column with isocratic elution and absorption spectra with a photodiode-array detector. *Photosynth. Res.* 65, 93–99. doi: 10.1023/A:1006445503030

Tang, K.-H., and Blankenship, R. E. (2010). Both forward and reverse TCA cycles operate in green sulfur bacteria. *J. Biol. Chem.* 285, 35848–35854. doi: 10.1074/jbc.M110.157834

Thamdrup, B. O., Finster, K., Hansen, J. W., and Bak, F. (1993). Bacterial disproportionation of elemental sulfur coupled to chemical reduction of iron or manganese. *Appl. Environ. Microbiol.* 59, 101–108.

Thamdrup, B., Fossing, H., and Jørgensen, B. B. (1994). Manganese, iron and sulfur cycling in a coastal marine sediment, Aarhus Bay, Denmark. *Geochim. Cosmochim. Acta* 58, 5115–5129. doi: 10.1016/0016-7037(94)90298-4

Thode-Andersen, S., and Jørgensen, B. B. (1989). Sulfate reduction and the formation of 35S-labeled FeS, FeS2, and S0 in coastal marine sediments. *Limnol. Oceanogr.* 34, 793–806. doi: 10.4319/lo.1989.34.5.0793

Viollier, E., Inglett, P. W., Hunter, K., Roychoudhury, A. N., and van Cappellen, P. (2000). The ferrozine method revisited: Fe(II)/Fe(III) determination in natural waters. *Appl. Geochem.* 15, 785–790. doi: 10.1016/S0883-2927(99)00097-9

Visscher, P. T., Prins, R. A., and van Gemerden, H. (1992). Rates of sulfate reduction and thiosulfate consumption in a marine microbial mat. *FEMS Microbiol. Lett.* 86, 283–293. doi: 10.1016/0378-1097(92)90792-M

Weber, M., Faerber, P., Meyer, V., Lott, C., Eickert, G., Fabricius, K. E., et al. (2007). In situ applications of a new diver-operated motorized microsensor profiler. *Environ. Sci. Technol.* 41, 6210–6215. doi: 10.1021/es070200b

Widdel, F., Schnell, S., Heising, S., Ehrenreich, A., Assmus, B., and Schink, B. (1993). Ferrous iron oxidation by anoxygenic phototrophic bacteria. *Nature* 362, 834–836. doi: 10.1038/362834a0

Wieland, A., Zopfi, J., Benthien, M., and Kühl, M. (2005). Biogeochemistry of an iron-rich hypersaline microbial mat (Camargue, France). *Microb. Ecol.* 49, 34–49. doi: 10.1007/s00248-003-2033-4

Wright, S. W. (1991). Improved HPLC method for the analysis of chlorophylls and carotenoids from marine phytoplankton. *Mar. Ecol. Prog. Ser.* 77, 183–196. doi: 10.3354/meps077183

Xu, J., and Gao, K. (2010). Use of UV-a energy for photosynthesis in the red macroalga *Gracilaria lemaneiformis*. *Photochem. Photobiol.* 86, 580–585. doi: 10.1111/j.1751-1097.2010.00709.x

Xue, L., Zhang, Y., Zhang, T., An, L., and Wang, X. (2005). Effects of enhanced ultraviolet-B radiation on algae and cyanobacteria. *Crit. Rev. Microbiol.* 31, 79–89. doi: 10.1080/10408410590921727

Zopfi, J., Ferdelman, T. G., and Fossing, H. (2004). Distribution and fate of sulfur intermediates—sulfite, tetrathionate, thiosulfate, and elemental sulfur—in marine sediments. *Geol. Soc. Am.* 379, 97–116. doi: 10.1130/0-8137-2379-5.97

Conflict of Interest Statement: The authors declare that the research was conducted in the absence of any commercial or financial relationships that could be construed as a potential conflict of interest.

frontiers in Environmental Science

ORIGINAL RESEARCH
published: 01 May 2018
doi: 10.3389/fenvs.2018.00021

pH as a Primary Control in Environmental Microbiology: 1. Thermodynamic Perspective

Qusheng Jin[1]* *and Matthew F. Kirk*[2]

[1] Geobiology, Department of Earth Sciences, University of Oregon, Eugene, OR, United States, [2] Department of Geology, Kansas State University, Manhattan, KS, United States

pH influences the occurrence and distribution of microorganisms. Microbes typically live over a range of 3–4 pH units and are described as acidophiles, neutrophiles, and alkaliphiles, depending on the optimal pH for growth. Their growth rates vary with pH along bell- or triangle-shaped curves, which reflect pH limits of cell structural integrity and the interference of pH with cell metabolism. We propose that pH can also affect the thermodynamics and kinetics of microbial respiration, which then help shape the composition and function of microbial communities. Here we use geochemical reaction modeling to examine how environmental pH controls the energy yields of common redox reactions in anoxic environments, including syntrophic oxidation, iron reduction, sulfate reduction, and methanogenesis. The results reveal that environmental pH changes energy yields both directly and indirectly. The direct change applies to reactions that consume or produce protons whereas the indirect effect, which applies to all redox reactions, comes from the regulation of chemical speciation by pH. The results also show that energy yields respond strongly to pH variation, which may modulate microbial interactions and help give rise to the pH limits of microbial metabolisms. These results underscore the importance of pH as a control on microbial metabolisms and provide insight into potential impacts of pH variation on the composition and activity of microbial communities. In a companion paper, we continue to explore how the kinetics of microbial metabolisms responds to pH variations, and how these responses control the outcome of microbial interactions, including the activity and membership of microbial consortia.

Keywords: geochemical modeling, available energy, microbial kinetics, syntrophic oxidation, iron reduction, sulfate reduction, methanogenesis

OPEN ACCESS

Edited by:
Alain F. Plante, University of Pennsylvania, United States

Reviewed by:
Jeffrey M. Dick, Central South University, China
Rose M. Jones, Bigelow Laboratory for Ocean Sciences, United States
Jacob P. Beam, Bigelow Laboratory for Ocean Sciences, United States

***Correspondence:**
Qusheng Jin
qjin@uoregon.edu

Specialty section:
This article was submitted to Microbiological Chemistry and Geomicrobiology, a section of the journal Frontiers in Environmental Science

Received: *14 December 2017*
Accepted: *09 April 2018*
Published: *01 May 2018*

Citation:
Jin Q and Kirk MF (2018) pH as a Primary Control in Environmental Microbiology: 1. Thermodynamic Perspective. Front. Environ. Sci. 6:21. doi: 10.3389/fenvs.2018.00021

INTRODUCTION

Microorganisms are widespread in natural environments, from hot springs to deep aquifers, and to ocean floors (Chapelle et al., 1995; Ward et al., 1998; Edwards et al., 2012). They drive a series of biogeochemical processes, from redox reactions, to weathering, and to the global cycling of carbon and other elements (Bennett et al., 2001; Falkowski et al., 2008; Maguffin et al., 2015). In return, their metabolisms are controlled by a wide range of environmental variables, including pH, temperature, salinity, nutrient availability, and geographic locations (Lennon and Jones, 2011; Amend et al., 2013). Among these factors, pH emerges as a primary control (Chen et al., 2004; Kemmitt et al., 2006; Bethke et al., 2011; Zhalnina et al., 2015). pH correlates strongly

with microbial communities across a wide range of biogeochemical conditions (Thompson et al., 2017). In addition, variations in environmental pH also induce significant responses of metabolic activities of natural communities (Kotsyurbenko et al., 2004; Ye et al., 2012).

pH shapes microbial metabolisms in different ways. First, it affects the environmental conditions that are relevant to microbial growth and survival. pH describes the chemical activity of protons, a key player in redox reactions, mineral dissolution and precipitation, surface complexation, and other geochemical reactions (Stumm and Morgan, 1996; Bethke et al., 2011). These reactions determine the salinity and composition of aqueous solutions and control the bioavailability of nutrients and trace elements. In addition, pH also affects the activities of extracellular enzymes, and the reactivity of natural organic matter (Leprince and Quiquampoix, 1996; Paul et al., 2006). In this way, pH becomes an indicator of overall environmental settings that shape the composition and activity of microbial communities (Lauber et al., 2009).

Second, pH may interfere with microbial metabolisms. Most laboratory cultures live within a pH range of 3–4 units—that is 3–4 orders of magnitude difference in the chemical activity of protons (Rosso et al., 1995). The pH of maximum growth rate is called the optimal growth pH. Based on optimal growth pH, microbes can be separated into three groups: acidophiles grow best at pH < 5, neutrophiles grow optimally at pH between 5 and 9, and alkaliphiles grow fastest above pH 9 (Horikoshi, 1999; Baker-Austin and Dopson, 2007). Where environmental pH deviates from optimal pH levels, microbial growth rates decrease (Rosso et al., 1995). For a microbe with a pH range spanning 4 pH units, assuming that its optimal pH is near the middle point of the pH range, a deviation of one unit from this pH optimal can reduce its growth rate by about 50% (see Maestrojuan and Boone, 1991; O'Flaherty et al., 1998, and others). In natural environments, decreasing or increasing the environmental pH by one unit can also lower the metabolic activity of microbial communities by up to 50% (Kotsyurbenko et al., 2004; Fernández-Calviño and Bååth, 2010).

pH may also affect microbial metabolisms and hence microbial community structures by modulating the thermodynamics and kinetics of redox reactions. Microbial respiration catalyzes redox reactions in order to synthesize ATPs. Respiration rates thus depend on thermodynamic drives, the differences between the energy available from redox reactions and the energy conserved by respiration (Jin and Bethke, 2002, 2003). Many redox reactions produce or consume protons, and thus, their free energy yields vary with pH (Bethke et al., 2011). Where the available energies equal or fall below the conserved energies, respiration reactions become thermodynamic unfavorable (Jin and Bethke, 2005, 2007, 2009). In this way, environmental pH helps control the progress of microbial respiration and growth, which in turn shapes the community composition.

The goal of this study is to illustrate how environmental pH influences the thermodynamics of redox reactions, and how these influences may shape microbial metabolisms and interactions. We focus on syntrophic oxidation, iron reduction, sulfate reduction, and methanogenesis, common microbial redox reactions in anoxic environments (Lovley and Chapelle, 1995; Bethke et al., 2011). We evaluate their thermodynamic responses to environmental pH using geochemical reaction modeling. In a companion paper (Jin and Kirk, under review), we continue to explore how the pH-induced thermodynamic responses affect the kinetics of microbial metabolisms and the outcome of microbial interactions.

METHODS

Microbes catalyze different redox reactions and, accordingly, can be separated into fermenters and respirers (Jin and Roden, 2011). Fermenting microbes degrade natural organic matter to a series of products, including short-chain fatty acids (e.g., acetate, lactate, and propionate), and primary alcohols (e.g., methanol and ethanol) (Schink and Stams, 2013). Some respirers oxidize short-chain fatty acids and primary alcohols to acetate and CO_2, and transfer the released electrons to the reduction of protons to dihydrogen (H_2). Others oxidize the products of organic matter degradation, and transfer the released electrons to the reduction of O_2, ferric minerals, sulfate, bicarbonate, and other electron acceptors.

Table 1 lists the stoichiometric equations for microbial redox reactions commonly found in anoxic environments. Following standard practice in biochemistry and low-temperature geochemistry, we write these reactions using dominant chemical species at neutral pH. For example, at pH 7, short-chain fatty acids occur mainly as their conjugate bases, and most dissolved inorganic carbon (DIC) appears as bicarbonate (**Figure 1**). In contrast, sulfide occurs in nearly equal proportions as dihydrogen sulfide (H_2S) and monohydrogen sulfide (HS^-). We choose dihydrogen sulfide, instead of both dihydrogen sulfide and monohydrogen sulfide in writing the equations for sulfate reduction (reaction 14–20 in **Table 1**). Following previous practice (Bethke et al., 2011; Jin, 2012), we write reaction equations that transfer 8 electrons, or the consumption of one acetate or four dihydrogen molecules.

Energy available from a redox reaction, ΔG_A [J·(mol reaction)$^{-1}$, or J·mol^{-1}], is calculated as the negative of its Gibbs free energy change,

$$\Delta G_A = -\Delta G^o - RT\left[\ln\left(\prod_P a_P^{\nu_P}\right) - \ln\left(\prod_S a_S^{\nu_S}\right)\right], \quad (1)$$

where ΔG° is the standard Gibbs free energy change, a_P and a_S are the activities of products and reactants, respectively, ν_P and ν_S are the stoichiometric coefficients, R is the gas constant (J·mol^{-1}·K^{-1}), and T is the temperature in kelvin (K). Chemical activity is calculated as the product of activity coefficients (M^{-1}) and molal concentrations of chemical species. The activity coefficients are calculated according to an extended form of the Debye-Hückel equation (Helgeson, 1969). **Table 1** lists the available energy calculated under the biochemical standard conditions of pH 7, 25°C, 1 atm, and chemical activities of unity.

We compute available energies ΔG_A for a hypothetical solution in contact with goethite. The composition of the

TABLE 1 | Redox reactions, standard available energy $\Delta G_A^{o\prime}$, and the energy ΔG_A available in the assumed environment.

Redox reaction	$\Delta G_A^{o\prime}$ [(a)] (kJ·mol^{-1})	ΔG_A^{o} [(b)] (kJ·mol^{-1})
SYNTROPHIC OXIDATION		
1. Acetate + $4H_2O \leftrightarrows 4H_2(aq) + 2HCO_3^- + H^+$	−175.25	−13.89
2. 2Lactate + $4H_2O \leftrightarrows$ 2Acetate + $4H_2(aq) + 2HCO_3^- + 2H^+$	−52.65	68.81
3. $\frac{4}{3}$Propionate + $4H_2O \leftrightarrows \frac{4}{3}$Acetate + $4H_2(aq) + \frac{4}{3}HCO_3^- + \frac{4}{3}H^+$	−175.58	3.37
4. 2Butyrate + $4H_2O \leftrightarrows$ 4Acetate + $4H_2(aq) + 2H^+$	−170.90	23.31
5. $\frac{4}{3}$Methanol + $\frac{8}{3}H_2O \leftrightarrows 4H_2(aq) + \frac{4}{3}HCO_3^- + \frac{4}{3}H^+$	−102.24	35.51
6. 2Ethanol + $2H_2O \leftrightarrows$ 2Acetate + $4H_2(aq) + 2H^+$	−89.42	29.84
GOETHITE REDUCTION		
7. $4H_2(aq)$ + 8Goethite + $16H^+ \leftrightarrows 16H_2O + 8Fe^{2+}$	89.90	169.78
8. Acetate + 8Goethite + $15H^+ \leftrightarrows 2HCO_3^- + 12H_2O + 8Fe^{2+}$	−85.35	155.88
9. 2Lactate + 8Goethite + $14H^+ \leftrightarrows$ 2Acetate + $2HCO_3^- + 12H_2O + 8Fe^{2+}$	37.25	307.40
10. $\frac{4}{3}$Propionate + 8Goethite + $\frac{38}{3}H^+ \leftrightarrows \frac{4}{3}$Acetate + $\frac{4}{3}HCO_3^- + 12H_2O + 8Fe^{2+}$	−85.68	174.26
11. 2Butyrate + 8Goethite + $14H^+ \leftrightarrows$ 4Acetate + $12H_2O + 8Fe^{2+}$	−81.00	216.41
12. $\frac{4}{3}$Methanol + 8Goethite + $\frac{44}{3}H^+ \leftrightarrows \frac{4}{3}HCO_3^- + 8Fe^{2+} + \frac{40}{3}H_2O$	−12.34	209.54
13. 2Ethanol + 8Goethite + $14H^+ \leftrightarrows$ 2Acetate + $8Fe^{2+} + 14H_2O$	0.48	240.80
SULFATE REDUCTION		
14. $4H_2(aq) + SO_4^{2-} + 2H^+ \leftrightarrows H_2S + 4H_2O$	223.23	80.68
15. Acetate + $SO_4^{2-} + H^+ \leftrightarrows 2HCO_3^- + H_2S$	47.97	66.79
16. 2Lactate + $SO_4^{2-} \leftrightarrows$ 2Acetate + $2HCO_3^- + H_2S$	170.57	218.30
17. $\frac{4}{3}$Propionate + $SO_4^{2-} + \frac{2}{3}H^+ \leftrightarrows \frac{4}{3}$Acetate + $\frac{4}{3}HCO_3^- + H_2S$	47.64	85.16
18. 2Butyrate + $SO_4^{2-} \leftrightarrows$ 4Acetate + H_2S	52.33	127.31
19. $\frac{4}{3}$Methanol + $SO_4^{2-} + \frac{2}{3}H^+ \leftrightarrows H_2S + \frac{4}{3}H_2O + \frac{4}{3}HCO_3^-$	120.98	120.44
20. 2Ethanol + $SO_4^{2-} \leftrightarrows$ 2Acetate + $H_2S + 2H_2O$	133.80	151.70
METHANOGENESIS		
21. $4H_2(aq) + H^+ + HCO_3^- \leftrightarrows CH_4(aq) + 3H_2O$	190.33	49.56
22. Acetate + $H_2O \leftrightarrows HCO_3^- + CH_4(aq)$	15.07	35.67

[(a)] *$\Delta G_A^{o\prime}$ is calculated as the negative of the Gibbs free energy at 25°C, pH 7, 1 atm pressure, and chemical activities of unity.*
[(b)] *ΔG_A is calculated according to Equation (1) and the assumed environmental conditions for the hypothetical freshwater environment.*

solution is consistent with dilute groundwater. The solution has 1 atm pressure and a temperature of 25°C and contains 10 mM Na^+, 10 mM Cl^-, 2.0 mM Ca^{2+}, and 3 mM DIC. The solution also contains 1 mM sulfate, 10 μM acetate, lactate, propionate, butyrate, methanol, ethanol, and ferrous iron, 1 μM sulfide and methane, and 0.1 μM H_2.

Chemical compounds dissolved in water may react with water molecules, acquire or give up protons and hydroxide, and combine with other molecules and ions. As a result, they appear in different forms or chemical species—a process called chemical speciation. To calculate available energies, we simulate the speciation of dissolved chemical compounds and compute the activities of chemical species using the program React of the software package Geochemist's Workbench version 9.0 (Bethke, 2008). The simulation assumes that chemical speciation is at thermodynamic equilibrium, and describes these reactions on the basis of the updated LLNL Thermodynamic Database (Delany and Lundeen, 1990). The simulation also assumes that goethite and ferrihydrite dissolution are at equilibrium. We added into the thermodynamic database the entries for natural goethite and ferrihydrite (Lindsay, 1979; Bigham et al., 1996). The input script and the modeling output are available in the Supplementary Material.

To investigate the impact of pH, we take the available energies at pH 7 as references, and compute the changes in the available energies at pH ranging from 1 to 14. We consider changes in available energies, rather than absolute values, in order to highlight the relative responses of different microbial redox reactions to pH variations. This approach also simplifies the discussion of ferric mineral reduction. Different ferric minerals, such as ferrihydrite, goethite, hematite, and lepidocrocite, have different chemical potentials (Cornell and Schwertmann, 2003), but their potentials respond in the same fashion to pH, because the reduction of these ferric minerals consumes the same number of protons per electron. Here we take goethite as an example, but the results are applicable to ferrihydrite, hematite, and lepidocrocite.

We use the thermodynamic potential factor F_T to quantify the control of the available energy on the rate of microbial respiration,

$$F_T = 1 - \exp\left(-\frac{f}{\chi RT}\right), \tag{2}$$

where f is the thermodynamic drive (J·mol^{-1}), and χ is the average stoichiometric number (Jin and Bethke, 2007, 2009). The

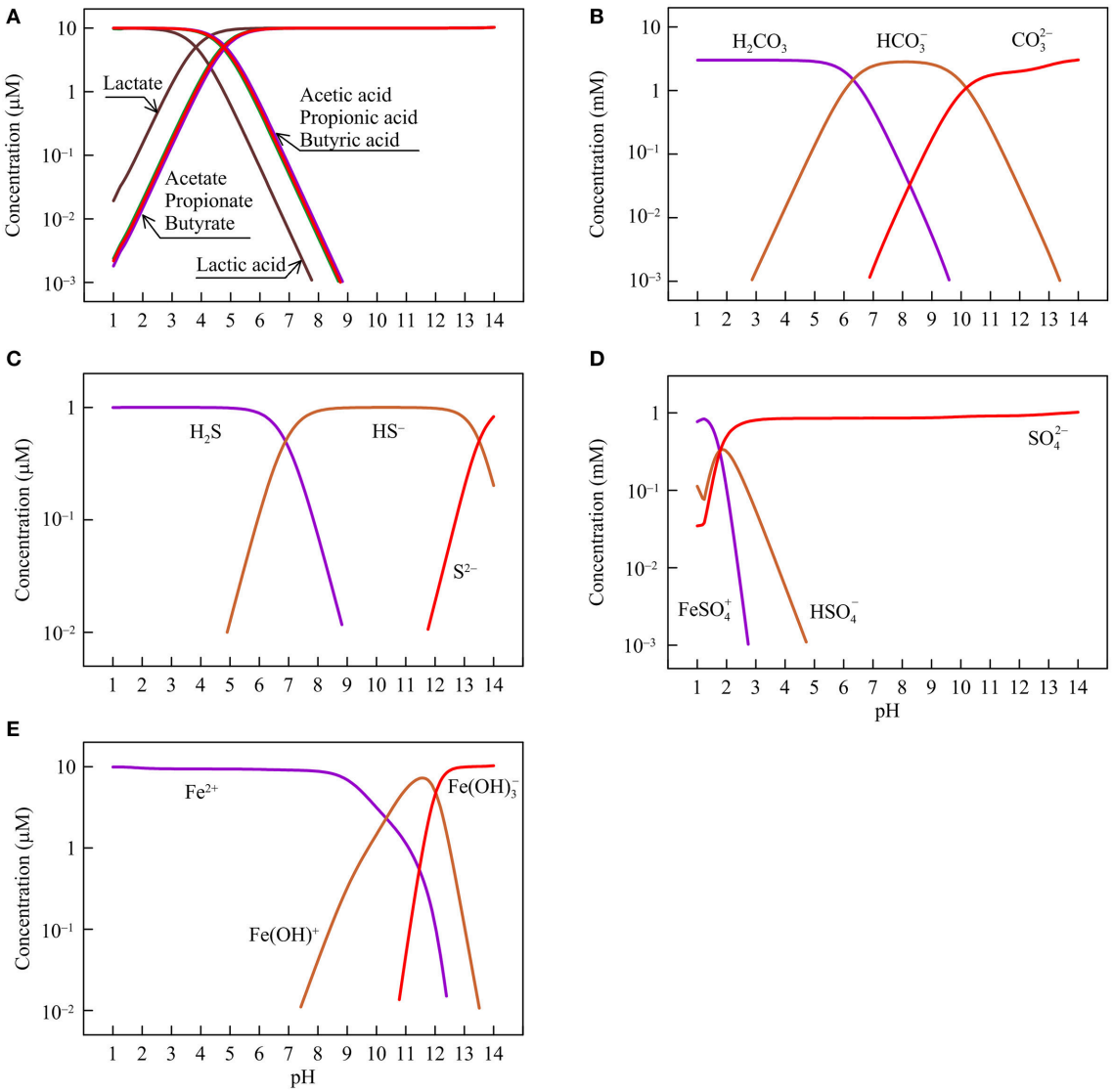

FIGURE 1 | Variations with pH in the concentrations of short-chain fatty acids and their conjugate bases **(A)**, dissolved inorganic carbon (carbonic acid H_2CO_3, bicarbonate HCO_3^-, and carbonate CO_3^{2-}) **(B)**, sulfide (dihydrogen sulfide H_2S, monohydrogen sulfide HS^-, and sulfide S^{2-}) **(C)**, sulfate (ferric iron-sulfate complex $FeSO_4^+$, hydrogen sulfate HSO_4^-, and sulfate SO_4^{2-}) **(D)**, and ferrous iron (ferrous iron Fe^{2+}, and ferrous iron-hydroxide complex $Fe(OH)^+$ and $Fe(OH)_3^-$) **(E)** in the hypothetical solution.

χ value is 8 per reaction for syntrophic oxidation of organic compounds and the reduction of goethite (reaction 1–13 in **Table 1**), 6 per reaction for the reduction of sulfate (reaction 14–20), and 2 per reaction for methanogenesis (reaction 21 and 22) (Jin and Bethke, 2005; Jin and Roden, 2011). The thermodynamic drive is

$$f = \Delta G_A - \Delta G_C, \tag{3}$$

the difference between the energy ΔG_A available in the environment and the energy ΔG_C conserved by respiration (Jin and Bethke, 2002, 2003). For microbial iron reduction, sulfate reduction, and methanogenesis, we calculate the conserved energy,

$$\Delta G_C = \nu_P \cdot \Delta G_P, \tag{4}$$

as the product of the ATP yield ν_P–the number of ATPs synthesized per reaction–and the phosphorylation energy ΔG_P–the energy required by ATP synthesis from ADP and phosphate in the cytoplasm. Based on Jin (2012), we take the ΔG_P value as 45 kJ·(mol ATP)$^{-1}$, and the ATP yields ν_P as 1, 0.75, and 0.5 ATPs per 8 electron transfer (or per acetate or 4 H_2) for iron reducers, sulfate reducers, and methanogens, respectively.

RESULTS

Respiring microbes harvest energy from a wide range of redox reactions. Here we focus on the electron donors generated from organic matter degradation, including dihydrogen (H_2), acetate, lactate, propionate, butyrate, methanol, and ethanol, and consider the common electron acceptors in anoxic environments, such as goethite, sulfate, bicarbonate, and protons (Lovley and Chapelle, 1995; Bethke et al., 2011).

Available Energy

Table 1 lists the energies available from different redox reactions in the assumed freshwater environment. Among the different redox reactions, goethite reduction provides the largest available energies, followed by sulfate reduction, methanogenesis, and syntrophic oxidation of organic compounds. This order in energy yield follows the well-known redox tower in microbiology (Bethke et al., 2011). Under acidic or alkaline conditions, however, the redox tower is not applicable anymore because pH affects the available energies of different redox reactions to different extents, as described in the subsections that follow.

Proton Reaction

Most redox reactions in **Table 1** consume or produce protons. Therefore, pH variations, or in other words, changes in the chemical activity of protons, affect the energy yields of the reactions. The slope L of the change in available energy depends on how many protons participate in the reaction,

$$L = RT \ln(10) \cdot \nu_H. \quad (5)$$

Here ν_H is the stoichiometric coefficient for protons in the reaction, which is positive where protons are produced.

Equation (5) predicts that energy available from syntrophic oxidation reactions increases linearly with pH because syntrophic reactions generate protons (**Figure 2**). For reactions that consume protons, their energies decrease linearly with increasing pH. These reactions include iron reduction, hydrogenotrophic methanogenesis, and sulfate reduction by oxidizing H_2, acetate, propionate, and methanol (**Figures 3**, **4A–C**, **5A**). No proton appears in acetoclastic methanogenesis or sulfate reduction by oxidizing lactate, butyrate, and ethanol. As such, pH variation does not directly influence their energy yields (**Figures 4D**, **5B**).

Chemical Speciation

We also compute available energies at different pHs using the results of geochemical reaction modeling. **Figures 2–5** compare the simulation results to those predicted by Equation (5). For most microbial redox reactions, the modeling results overlap with the equation predictions only over a limited range around neutral pH. The differences between the two predictions arise from the speciation of dissolved mass, which determines the activities of chemical species and hence the energy available from redox reactions.

Figure 1 shows, according to the simulation results, how the concentrations of different chemical species change with pH. Specifically, short-chain fatty acids occur in the solution as both acids and their conjugate bases (**Figure 1A**). The relative abundances of the two chemical species depend on acidity constants. Lactate has the smallest logarithmic acidity constant (pKa) of 3.9, and acetate, propionate, and butyrate have pKa values of 4.8–4.9 (Lide, 2003). Where pH is smaller than the pKa values, the acids are dominant. At pH > the pKa values, the conjugate bases take over.

DIC occurs mainly as carbonic acid, bicarbonate, and carbonate (**Figure 1B**). At pH between 6 and 10.5, bicarbonate dominates. Carbonic acid and carbonate are the main forms at pH below 6 and above 10.5, respectively. Dissolved sulfide also has three main species—dihydrogen sulfide, monohydrogen sulfide, and sulfide (S^{2-}), which appear as the dominant species at pH < 7, between 7 and 13.5, and above 13.5, respectively (**Figure 1C**). Sulfate occurs mainly as sulfate anion at pH > 2.5, and as ferric iron/sulfate-complex at lower pH (**Figure 1D**). We assume that the hypothetical solution is in contact with goethite and as such, ferric iron in the sulfate complex species comes from the dissolution of goethite.

Ferrous iron occurs as a free cation (Fe^{2+}) and two hydroxide-complexes (**Figure 1E**). The free cation dominates the solution at pH below 9. At pH around 11, ferrous monohydroxide $Fe(OH)^+$ is the main species whereas at pH above 13, ferrous trihydroxide $Fe(OH)_3^-$ becomes dominant.

Syntrophic Oxidation

Syntrophic oxidation reactions can be separated into two groups, depending on whether bicarbonate is produced (reaction 1–6 in **Table 1**). The group that produces bicarbonate includes the oxidations of acetate, lactate, propionate, and methanol. **Figures 2A–C** show according to the modeling results how the energies available from these reactions respond to pH variations. Below pH 6, available energies remain roughly constant. Above pH 7, the energies increase with pH with the highest rate of increase above pH 10.

This variation in available energy reflects changes in DIC speciation. Below pH 6, bicarbonate concentration declines with decreasing pH, which works to raise available energies (**Figure 1B**). At the same time, however, decreasing pH works to reduce available energies because the reactions generate protons. The thermodynamic effects of DIC speciation and proton generation cancel each other and, as a result, the available energies remain relatively constant. pH also affects the speciation of acetate, lactate, and propionate (**Figure 1A**), but the concentrations of these chemical species co-vary with pH, and their thermodynamic effects are either balanced by each other (such as in the oxidation of lactate and propionate) or by the speciation of DIC (acetate oxidation).

Between pH 7 and 10, bicarbonate concentration varies relatively little with pH (**Figure 1B**). As such, the thermodynamic effect of DIC speciation dissipates, and the thermodynamic effect of proton production causes energies to rise with increasing pH. Above pH 10, bicarbonate concentration falls with increasing pH, which further raises the available energies.

Reactions that do not generate bicarbonate include the oxidations of butyrate and ethanol. Their available energies depend on pH and the speciation of acetate—a product of the two reactions. Below pH 4, acetate concentration falls with

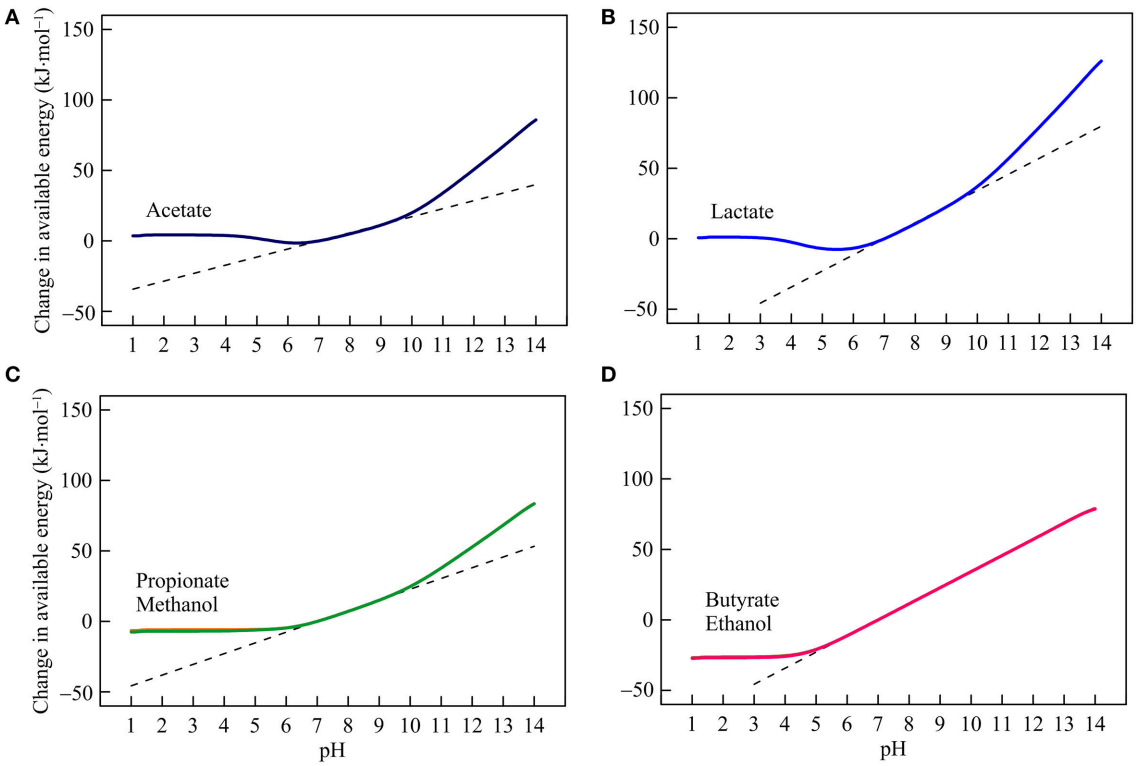

FIGURE 2 | Variations with pH in the energy available from syntrophic oxidation of acetate **(A)**, lactate **(B)**, propionate, methanol **(C)**, butyrate, and ethanol **(D)** in the hypothetical solution. Solid lines are results of geochemical modeling, and dashed lines are calculated according to Equation (5). The variations are calculated in reference to the available energies at pH 7.

decreasing pH (**Figure 1A**). While pH decreases work to lower the available energies, falling acetate concentration works to raise the available energies. The two effects balance each other, and hold the available energies constant. At pH above 5, the available energies depend primarily on pH, and increase linearly with increasing pH.

Iron Reduction

The available energies of iron reduction respond strongly to changes in pH (**Figure 3**). Between pH 1 and 9, the available energies fall almost linearly with rising pH. The slopes of the fall depend on the number of protons consumed in the reactions, and range from 72 to 91 kJ·mol^{-1} per pH unit (reaction 7–13 in **Table 1**). Speciation of short-chain fatty acids and DIC also responds to pH (**Figures 1A,B**). However, their thermodynamic effects are relatively insignificant compared to the energy variations induced directly by proton consumption.

Between pH 9 and 12, the available energies continue to decline with increasing pH but the slopes of the decline are smaller than those between pH 1 and 9. Here, the speciation of ferrous iron starts to take effect—ferrous iron concentration drops with increasing pH, due to the formation of ferrous iron/hydroxide-complexes (**Figure 1E**). The diminished concentration works to raise the available energies, which counteracts the thermodynamic effect of proton consumption. Ultimately, above pH 12, the speciation effect becomes dominant, leading to the rising available energies with increasing pH.

Sulfate Reduction

The response of sulfate reduction to pH varies between reactions. For hydrogenotrophic sulfate reduction (reaction 14 in **Table 1**), available energy declines at varying rates with increasing pH (**Figure 4A**). The energy change reflects proton consumption by the reaction but other factors also contribute. For example, at pH < 2, the sulfate ion is a secondary species of dissolved sulfate, and its concentration rises with increasing pH (**Figure 1D**), which partially counteracts the thermodynamic effect of proton consumption and slows down the decline in the available energy. At pH > 7, dihydrogen sulfide concentration starts to fall with increasing pH (**Figure 1C**), which also slows down the energy decline.

For sulfate reduction by the oxidation of acetate, propionate, and methanol (reaction 15, 17, and 19), energy variations separate into two phases (**Figures 4B,C**). Below pH 7, available energies largely fall with increasing pH, reflecting proton consumption and bicarbonate production by the reactions. Above pH 7, available energies rise with increasing pH, because the thermodynamic effect of proton consumption is counteracted by those of the speciation of DIC and sulfide. As pH increases, bicarbonate and dihydrogen sulfide concentrations diminish (**Figures 1B,C**).

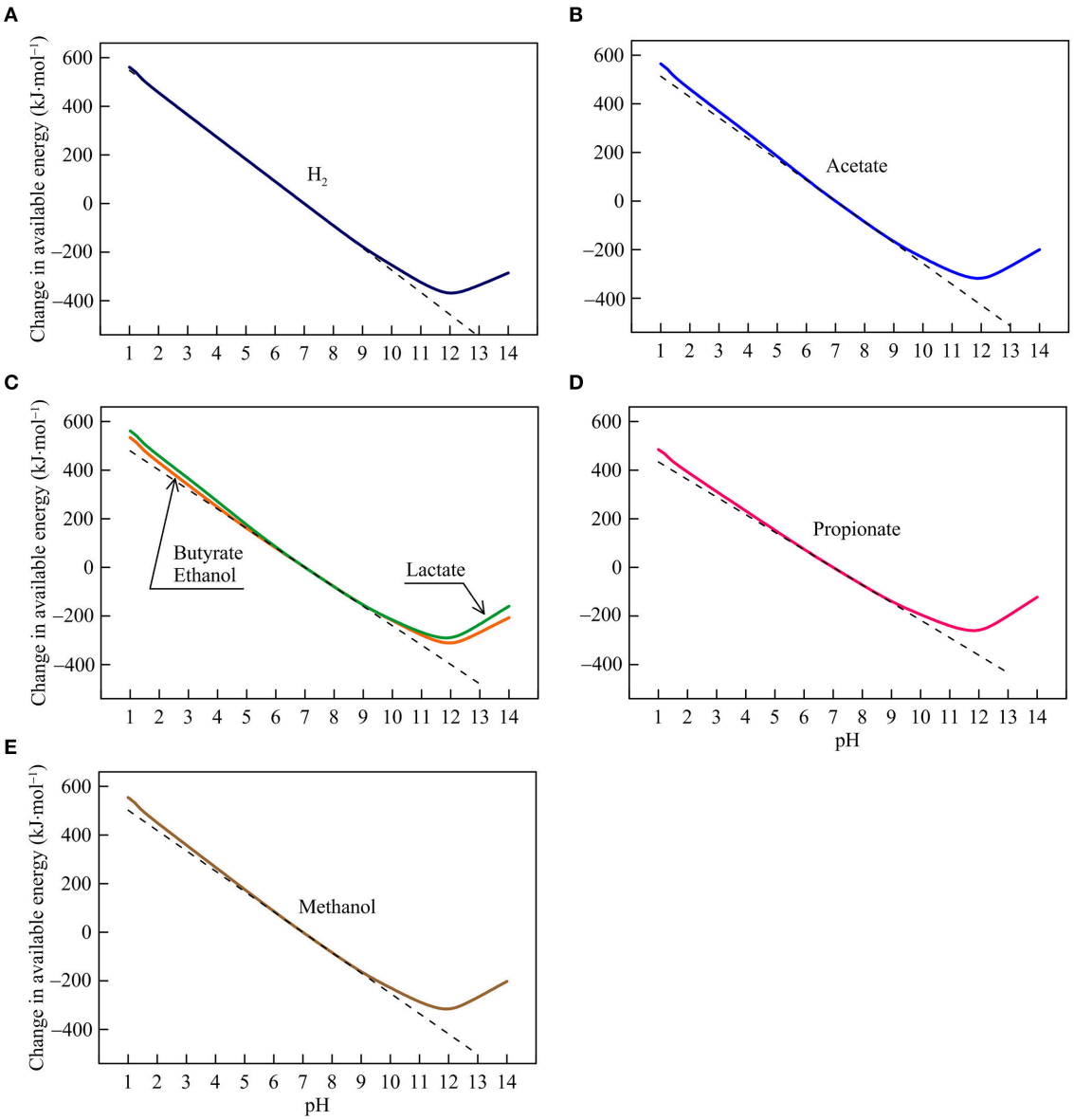

FIGURE 3 | Variations with pH in the energy available from the reduction of goethite coupled to the oxidation of H_2 **(A)**, acetate **(B)**, lactate, butyrate, ethanol **(C)**, propionate **(D)**, and methanol **(E)** in the hypothetical solution. Solid lines are results of geochemical modeling, and dashed lines are calculated according to Equation (5). The variations are calculated in reference to the available energies at pH 7.

For sulfate reductions by the oxidation of lactate, butyrate, and ethanol (reaction 16, 18, and 20), Equation (5) predicts that pH variations have no impact on the available energies, because no protons participate in the reactions. But the modeling results show that the available energies do respond considerably to pH changes (**Figure 4D**). These responses reflect variation with pH in the speciation of acetate, bicarbonate, sulfate, and sulfide (**Figure 1**). Between pH 1 and 7, an increase in pH raises the concentrations of acetate and bicarbonate, thereby lowering the available energies. In contrast, above pH 7, an increase in pH lowers the concentrations of bicarbonate and dihydrogen sulfide, which raises the available energies.

Methanogenesis

Hydrogenotrophic and acetoclastic methanogenesis respond differently to pH variation (**Figure 5**). Hydrogenotrophic pathway consumes proton and bicarbonate (reaction 21 in **Table 1**). Below pH 6, its available energy remains largely unchanged because the thermodynamic effects of proton consumption and DIC speciation counteract each other (see **Figure 1B**). Above pH 6, increases in pH cause available energy to decline because of proton consumption by the reaction. Above pH 9, the slope of the decrease becomes steeper because pH increases also lower the concentration of bicarbonate.

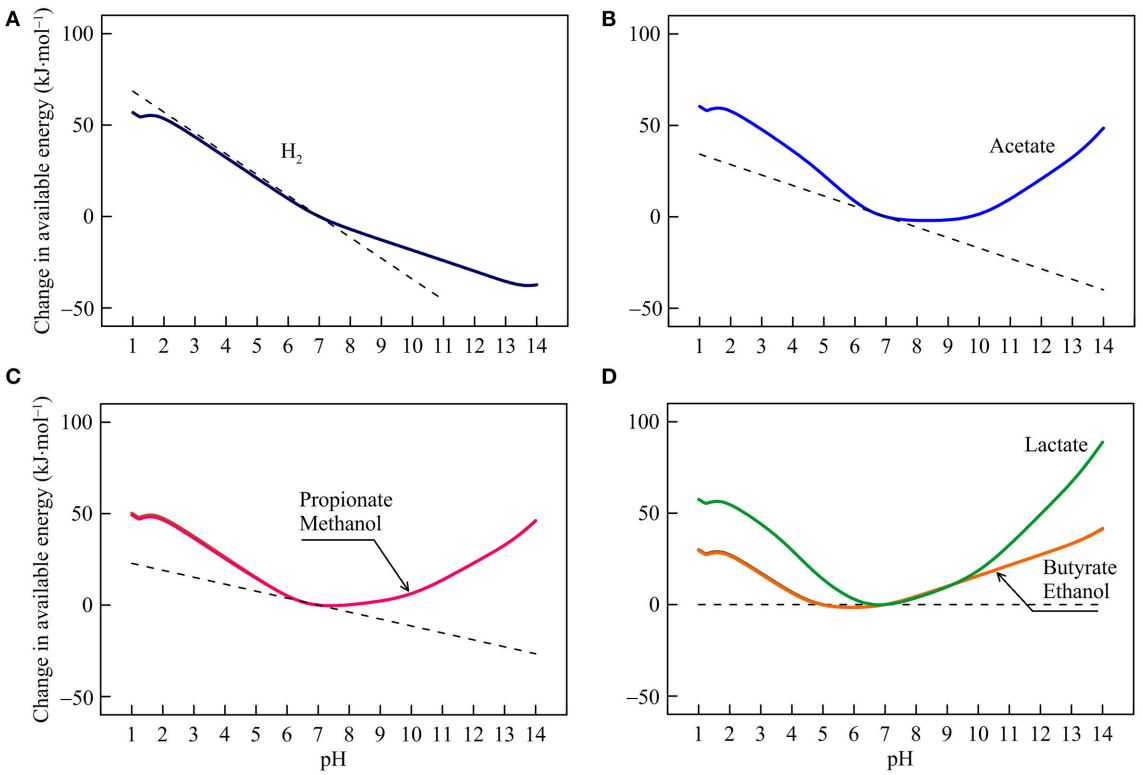

FIGURE 4 | Variations with pH in the energy available from the reduction of sulfate coupled to the oxidation of H_2 **(A)**, acetate **(B)**, propionate, methanol **(C)**, lactate, butyrate, and ethanol **(D)** in the hypothetical solution. Solid lines are results of geochemical modeling, and dashed lines are calculated according to Equation (5). The variations are calculated in reference to the available energies at pH 7.

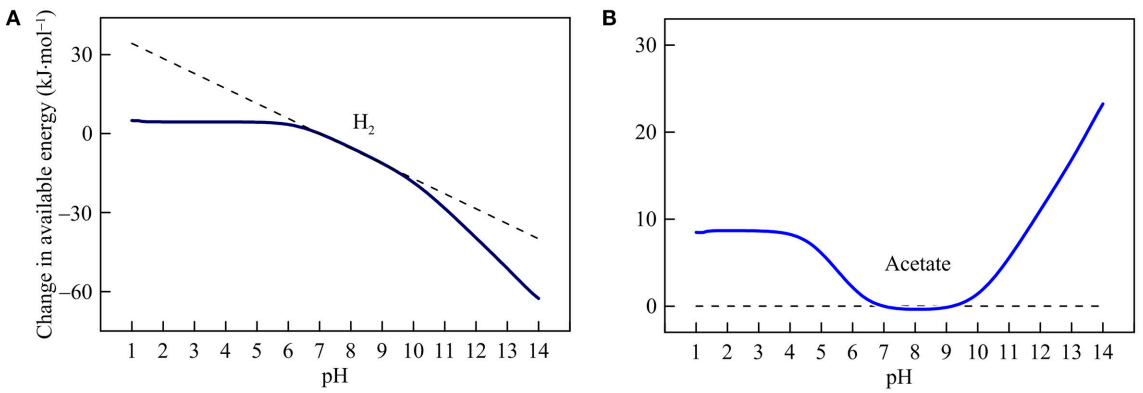

FIGURE 5 | Variations with pH in the energy available from hydrogenotrophic **(A)** and acetoclastic methanogenesis **(B)** in the hypothetical solution. Solid lines are results of geochemical modeling, and dashed lines are calculated according to Equation (5). The variations are calculated in reference to the available energies at pH 7.

For acetoclastic methanogenesis (reaction 22), Equation (5) predicts no response in the available energy with pH. However, the simulation results show that this prediction only applies between pH 7 and 9. Above pH 9, pH increases raise the available energy by lowering bicarbonate concentrations. Below pH 7, a decrease in pH also decreases bicarbonate concentration and hence raises available energy. Below pH 4, however, acetate concentration begins to decrease with decreasing pH, which counteracts the thermodynamic effect of decreasing bicarbonate concentration. Hence, the available energy varies little below pH 4.

Thermodynamic Drive

Microbes conserve a part of the energy available in the environment by making ATP, and spend the other part to drive respiration reactions. By changing the energy available in the environment, pH also changes the thermodynamic drive, which in turn changes the rate of respiration (Equations 2, 3).

For the purpose of this analysis, we focus on syntrophic oxidation of butyrate, and acetotrophic and hydrogenotrophic iron reduction, sulfate reduction, and methanogenesis, and compute how their thermodynamic drives respond to pH in the assumed environment. Butyrate is a key product of organic matter degradation, and acetate and H_2 are common electron donors in subsurface environments (Monokova, 1975; Molongoski and Klug, 1980; Lovley and Klug, 1982).

Environmental Conditions

Like energy availability, microbial energy conservation also depends on environmental conditions. For example, the amount of energy conserved by syntrophs depends on dihydrogen of the environment. Jin (2007) constructed a kinetic model for syntrophic butyrate oxidation. This model considers reverse electron transfer, a key step in the pathway of syntrophic oxidation (Schink, 1992), and describes the energy conserved by microbes, ΔG_C [J·(mol butyrate)$^{-1}$], as a function of molal concentration of dissolved dihydrogen m_{H_2},

$$\Delta G_C = -3.55 \times 10^4 - RT \cdot \ln\left(m_{H_2}\right). \quad (6)$$

According to this model, the conserved energy equals 15.8 kJ·mol^{-1} at 1 nM H_2 and decreases with increasing H_2 concentration. In the assumed environment, the conserved energy takes a value of 4.5 kJ·(mol butyrate)$^{-1}$. At H_2 concentration of more than 0.6 μM, the conserved energy decreases to 0.

pH also affects microbial energy conservation. Respiring microbes conserve energy by translocating protons across their cytoplasmic membrane to create proton motive force. Proton motive force includes electrical potential difference and the gradient in proton activity across the membrane. Changes in environmental pH directly affect the proton gradient as well as the electrical potential difference across the membrane (Sprott et al., 1985). In addition, microbes also respond to pH changes by changing the number of protons translocated across the membrane (Steigmiller et al., 2008).

Currently, no model is available to quantitatively predict how conserved energy changes with pH. Thus the impact of pH on conserved energies cannot be evaluated as rigorously as we have done for energy availability. For this reason, we follow the current practice, and calculate the conserved energy of syntrophic butyrate oxidizers according to Equation (6). For iron reducers, sulfate reducers, and methanogens, we calculate the conserved energies using Equation (4).

Thermodynamic Control

Figure 6 shows how thermodynamic drives respond to changes in pH. By fixing conserved energies, variations in thermodynamic drives follow the same patterns of the available energies. In the assumed environment, the thermodynamic drive of butyrate syntrophic oxidation is 14.3 kJ mol^{-1} at pH 7 and decreases with decreasing pH. Below pH 5.7, the drive becomes negative, and thus butyrate syntrophic oxidation becomes thermodynamically unfavorable. Hydrogenotrophic and acetotrophic iron reducers have a thermodynamic drive of 125 and 111 kJ·mol^{-1}, respectively, at pH 7. Their thermodynamic drives decrease with increasing pH and become negative above pH 7.9.

In the assumed environment, hydrogenotrophic and acetotrophic sulfate reducers have positive thermodynamic drives over the pH range of 1–14. Acetoclastic methanogen also has positive thermodynamic drives over the entire pH range but its thermodynamic drives fall to a minimum level around pH 8. On the other hand, hydrogenotrophic methanogens have a relatively large drive at low pH. Above pH 6, the thermodynamic drive begins to decrease and becomes negative above 10.9.

Figure 7 shows how the thermodynamic potential factors F_T vary with pH. The thermodynamic potential factor quantifies the significance of thermodynamic limitation on respiration rate (Equation 2). This factor approaches unity where available energy is much larger than conserved energy. In this case, thermodynamic control is considered insignificant; respiration rate is relatively large, and varies little with the thermodynamic drive. However, where available energy approaches conserved energy, the thermodynamic drive and hence the thermodynamic potential factor approach zero. Under this condition, respiration rate increases linearly with the thermodynamic drive, and the thermodynamic control is significant. Where the thermodynamic drive is negative, microbial respiration reaction is thermodynamically unfavorable. Here, respiration reaction ceases and the thermodynamic potential factor is set to 0.

In the assumed environment, the thermodynamic factors of different microbial respiration reactions respond differently to pH. For syntrophic butyrate oxidation, the thermodynamic factor is positive above pH 5.7 and increases nonlinearly with pH. At pH above 9.8, the thermodynamic factor increases to over 0.9.

The thermodynamic factors of hydrogenotrophic and acetotrophic iron reduction remain close to unity below pH 7.3. Above pH 7.3, increases in pH decrease sharply the thermodynamic factors for both reactions. At a pH of 7.9, the factors decrease to 0.

The thermodynamic factor of hydrogenotrophic sulfate reduction stays close to unity at pH $<$ 5.0. Above pH 5.0, increases in pH gradually decrease the thermodynamic factor to a value of 0.48 at pH 14. The thermodynamic factor of acetotrophic sulfate reduction remains relatively large over the entire pH range, with a minimum of 0.88 at pH 8.3.

The thermodynamic factor of hydrogenotrophic methanogenesis stay close to unity below pH 10.3. Above that level, the thermodynamic factor decreases sharply to 0 at pH 10.9. The thermodynamic factor of acetoclastic methanogenesis stays close to unity across the entire pH range because of its relatively large thermodynamic drive. Taking together the variations of the thermodynamic potential factors, we see that pH variations are capable of modifying the thermodynamic states of respiration reactions between favorable and unfavorable, and

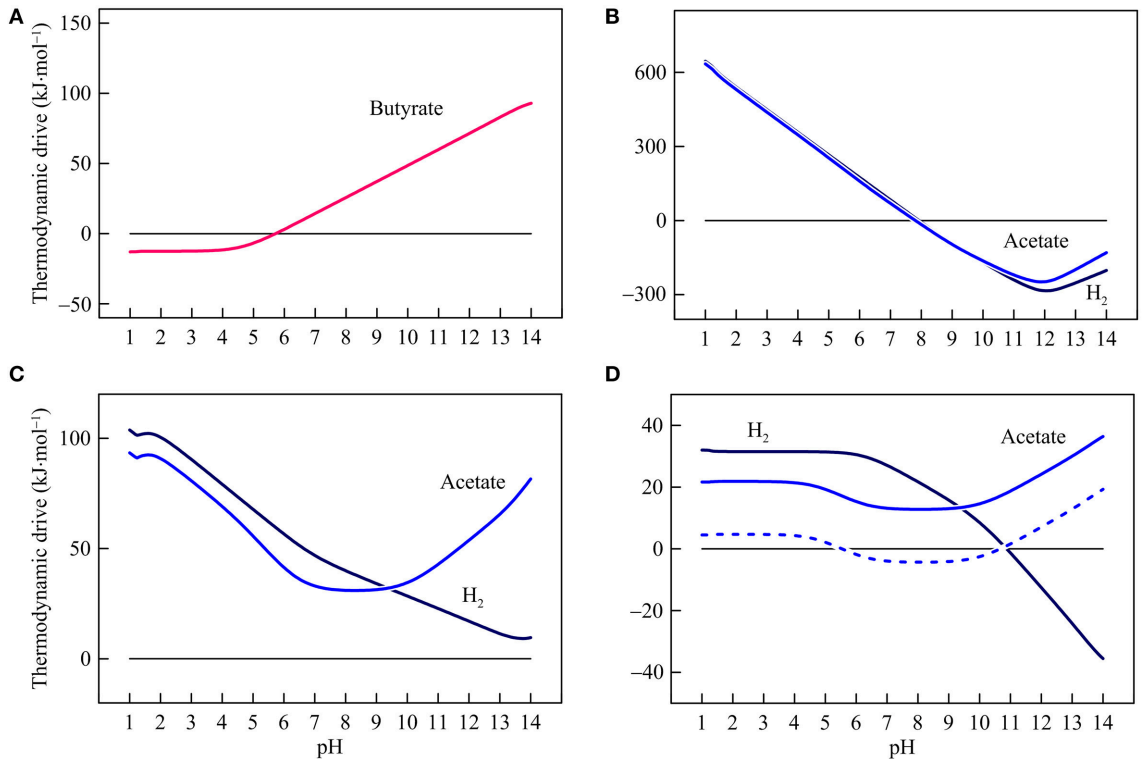

FIGURE 6 | Variations with pH in the thermodynamic drives of syntrophic butyrate oxidation **(A)**, hydrogenotrophic and acetotrophic goethite reduction **(B)**, sulfate reduction **(C)**, and methanogenesis **(D)**. Solid lines are results of the hypothetical solution, and dashed line is the result of acetoclastic methanogenesis by raising methane concentration in the hypothetical solution to 1 mM.

regulating the progress of the reactions, from relatively fast pace to complete rest.

DISCUSSION

We used geochemical reaction modeling and analyzed the thermodynamic and kinetic responses of microbial redox reactions to environmental pH. The results illustrate how pH can act as a key controlling parameter on microbial activities and interactions.

Thermodynamic Response

We first analyzed how the thermodynamics of microbial redox reactions respond to pH variations. Bethke et al. (2011) analyzed how the energies available from acetotrophic and hydrogenotrophic iron reduction, sulfate reduction, and methanogenesis respond to variation in pH between 4 and 10. We expand their analyses by varying pH from 1 to 14 and by including additional microbial redox reactions involved in the degradation of natural organic matter. These reactions include the oxidation of short-chain fatty acids and primary alcohols by proton reduction, iron reduction, and sulfate reduction. Our analyses confirm the previous conclusion that changes in environmental pH directly alter energy available from redox reactions that produce or consume protons, and the significances of the changes depend on the numbers of protons produced or consumed (Bethke et al., 2011).

Our simulation results also resonate with the previous studies that emphasize the indirect thermodynamic role of pH—pH affects chemical energies in the environment indirectly by affecting chemical speciation and thereby the concentrations of chemical species involved in microbial redox reactions (Windman et al., 2007; Dolfing et al., 2010; Shock et al., 2010; Hedrich et al., 2011; Johnson et al., 2012). We often write stoichiometric reaction equations and compute their Gibbs free energy changes using the main chemical species at pH 7 (**Table 1** and Equation 1). By doing so, we implicitly account for the speciation effect at pH 7.

But chemical speciation depends on pH, which impacts chemical reactions and their energies in two ways. First, chemical species participating in protonation and deprotonation have different concentrations at different pHs. As a result, the main chemical species of pH 7 may give way to alternative forms at other pHs. Second, the stoichiometries of proton consumption and production are not fixed, but vary with pH. At a given pH, proton consumption and production depend on the relative significances of acids and their conjugate bases. In response to pH variations, the concentrations of acids and their conjugate bases change (**Figure 1**) and thus so do the stoichiometries of proton reactions. Consequently, for reactions that include proton

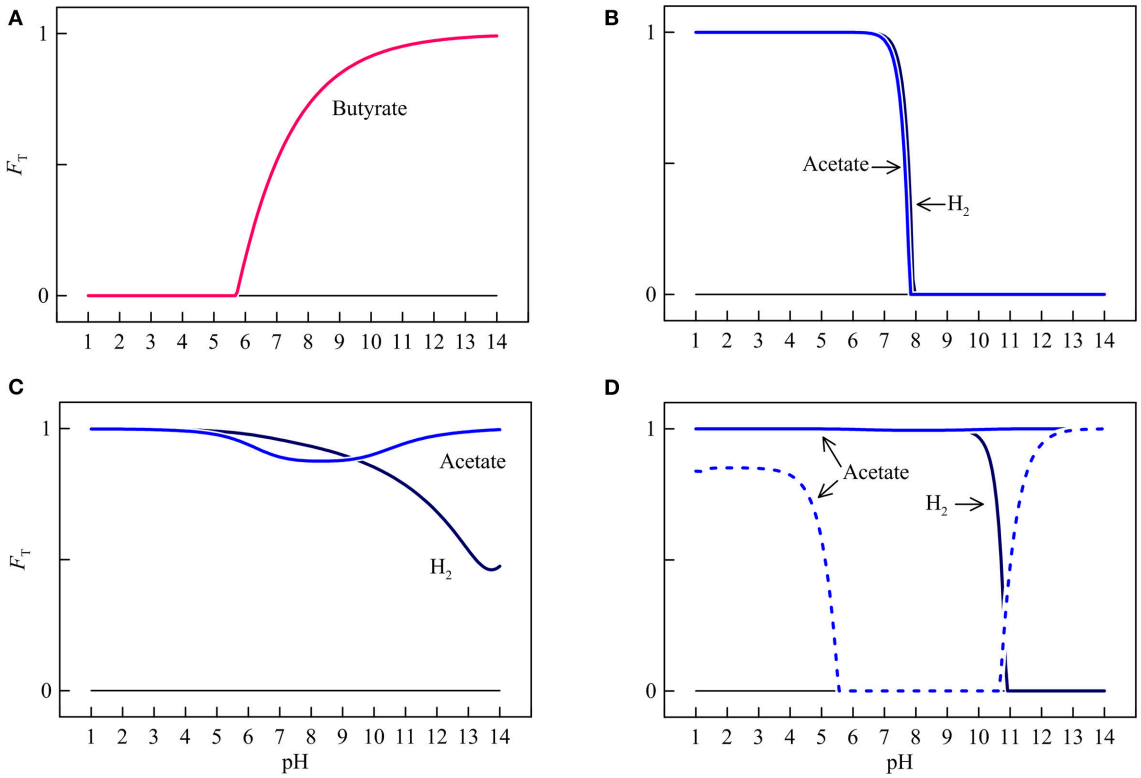

FIGURE 7 | Variations with pH in the thermodynamic factors F_T of syntrophic butyrate oxidation **(A)**, hydrogenotrophic and acetotrophic goethite reduction **(B)**, sulfate reduction **(C)**, and methanogenesis **(D)**. Solid lines are results of the hypothetical solution, and dashed line is the result of acetoclastic methanogenesis by raising methane concentration in the hypothetical solution to 1 mM.

consumption and production, the direct pH effect is not set but varies in magnitude with pH.

The indirect thermodynamic impact of pH is most notable for sulfate reduction by the oxidation of lactate, butyrate, and ethanol, and for acetoclastic methanogenesis (reaction 16, 18, 20, and 22 in **Table 1**). At pH 7, no proton would be produced or consumed by these reactions, and the available energies are not affected directly by pH. But according to the simulation results, their available energies vary significantly with the pH of the environment (**Figures 4D**, **5B**). We account for the variations using pH-dependent chemical speciation—these reactions involve bicarbonate, sulfide, and other chemical species, whose concentrations vary significantly with pH.

Figures 2–5 compare the direct and the total thermodynamic impacts of pH (the dashed and solid lines, respectively). The differences between the two lines highlight the indirect energy contribution by chemical speciation. Two patterns arise from these figures.

First, microbial thermodynamic responses are not uniform. The available energies of syntrophic oxidation reactions increase with increasing pH. For hydrogenotrophic sulfate reduction and methanogenesis, their available energies decrease with increasing pH. For other microbial redox reactions, in response to pH increases, available energies first decrease and then, after reaching minimum values, begin to increase.

These heterogeneous responses arise in part from the indirect speciation impact of pH. The speciation impact is not consistent throughout the entire pH range of 1–14. For example, for redox reactions that produce bicarbonate, energy available always increases as pH moves away from 7, regardless of whether pH is increasing or decreasing. As a second example, the speciation of ferrous iron only affects significantly the available energy of iron reduction at pH above 9. At lower pHs, the speciation impact is negligible.

Second, microbial iron reduction stands out from the other reactions in its strong response to pH. Energy available from the reduction of iron oxides and hydroxides depends significantly on pH. This sensitivity reflects consumption of relatively large numbers of protons, from 12.7 to 16 protons per reaction (8 electron transfer). As a result, a one-unit change in pH can lead to a change of 72–91 kJ·(mol reaction)$^{-1}$ in the available energy. In comparison, thermodynamic responses are relatively modest for other microbial redox reactions—a one-unit change in pH can lead to up to 20 kJ·(mol reaction)$^{-1}$ of change in the available energies of these reactions.

Kinetic Response

Microbial thermodynamic responses to pH lead to a cascade of metabolic effects, including impacts to the thermodynamic drives of respiration. We took butyrate syntrophic oxidation,

and acetotrophic and hydrogenotrophic iron reduction, sulfate reduction, and methanogenesis as examples, and analyzed how environmental pH controls the thermodynamic drives and hence the rates of these reactions in the assumed freshwater environment.

Like the energies available in the environment, the thermodynamic drives of different microbial respiration reactions respond differently to changes in pH. Specifically, a pH increase from 1 to 14 raises the thermodynamic drive of syntrophic butyrate oxidation from negative to positive and hence moves the reaction from thermodynamically unfavorable to favorable. On the other hand, increasing pH changes iron reduction and hydrogenotrophic methanogenesis from thermodynamically favorable to unfavorable. pH variation can also push hydrogenotrophic sulfate reduction close to thermodynamic equilibrium but this reaction always remains thermodynamically favorable in the assumed environment across the pH range considered.

It should be made clear that our thermodynamic drive calculations are specific for the assumed environment. In an environment of different geochemical conditions, thermodynamic drives may be different, and hence pH variations may modify respiration rates to different extents. For example, in the hypothetical solution, pH variation does not change much the thermodynamic potential factor of acetoclastic methanogenesis, and hence has little influence on the rate of the process (**Figure 7D**). However, if we raise methane concentration in the solution from 1 μM to 1 mM, we would decrease the thermodynamic drive by 17.1 $kJ \cdot mol^{-1}$ (**Figure 6D**). At pH between 5.7 and 10.6, the thermodynamic drive decreases below 0, and methanogenesis stops (**Figure 7D**). But the pattern in the responses of the thermodynamic drive should be similar, regardless of the concentration of methane or other chemical compounds. As shown in **Figure 6D**, the thermodynamic drive always increases as pH moves away from 7.

Microbial pH Response

The pH limits of microbial metabolisms are a classical physiological parameter. Previous studies have attributed these pH limits to different physiological mechanisms, including cellular structures and metabolisms. First, both acidophiles and alkaliphiles need to employ unique surface structures to develop acid or alkaline tolerance. For example, the cell walls of alkaliphiles have acidic polymers, which may protect cells from hydroxide ions (Horikoshi, 1999). Acidophiles, such as the members of *Ferroplasma*, mix caldarchaetidylglycerol tetraether lipids into their membranes to make a barrier to protons in the environment (Golyshina and Timmis, 2005).

Acidic or alkaline conditions also present a challenge to cell metabolism. For both acidophiles and alkaliphiles, cytoplasmic pH is often closer to neutral pH than the environments (Lowe et al., 1993). Maintaining a pH gradient across the membrane consumes energy (Booth, 1985). In addition, under acidic conditions, conjugate acids become significant in the environment, and diffuse through the cell membrane, which destabilizes the membrane and dissipates proton motive force (Russell, 1992). Very low or high pH levels also interfere with solute transport across the membrane and energy conservation by respiration (Matin, 1990; Krulwich et al., 1998).

Our thermodynamic analyses show that environmental pH affects the thermodynamics of microbial redox reactions, and determines whether microbial respiration reactions are thermodynamically favorable or not. Therefore, in addition to microbial physiology, the pH limits may arise, at least in part, from the response of reaction thermodynamics to pH.

For example, reaction thermodynamics sets the lower pH limit for syntrophic butyrate oxidizers. In the assumed environment, syntrophic butyrate oxidation becomes thermodynamically unfavorable and thus stops at pH below 5.7. In laboratory experiments, both butyrate and acetate have relatively large concentrations (Dwyer et al., 1988; Schmidt and Ahring, 1993). We repeat the calculation by taking their concentrations as 5 mM, and setting H_2 partial pressures at 10^{-4} atm (or dissolved H_2 at 77 nM), and find that butyrate oxidation would stop at pH < 6.3.

The predicted pH limits are consistent with previous laboratory observations. For example, *S. wolfei* is one of the first isolates that can grow syntrophically on butyrate, and it can grow at pH above 6.5 (Wu et al., 2007). Its close relatives, including *S. bryantii*, also have pH limit above 6.0 (Zhang et al., 2004, 2005).

As a second example, the thermodynamics of iron reduction sets the upper limit for microbes reducing ferric oxides and oxyhydroxides. In the assumed environment, at pH above 7.9, both hydrogenotrophic and acetotrophic reduction of goethite become thermodynamically unfavorable. In laboratory reactors, H_2, acetate, and ferrous iron often have concentrations orders magnitude above the concentrations in the assumed environment. If we take acetate concentration at 5 mM and ferrous iron at 1 mM, the reduction of goethite would remain thermodynamically favorable only at pH < 7.6.

The upper pH limit for iron reduction depends on ferric minerals (Postma and Jakobsen, 1996). For example, if we choose natural ferrihydrite as an electron acceptor, acetotrophic reduction of ferrihydrite becomes thermodynamically unfavorable at pH 8.3. This upper limit is consistent with the value determined using laboratory experiments. Straub et al. (1998) reported that by reducing ferrihydrite, two *Geobacter* strains grow optimally at pH around 7, and can grow at pH up to 7.5.

Implications for Environmental Microbiology

By promoting or inhibiting microbial redox reactions, environmental pH is capable of shaping the interactions between microbial groups. For example, previous studies of microbial syntrophy have emphasized the importance of H_2 levels of the environment—a key parameter that dictates the thermodynamics and occurrence of syntrophic degradation (Schink, 1997). The above results show that like H_2 levels, pH can change the thermodynamic status and rates of syntrohic oxidation of short-chain fatty acids and primary alcohols, and hence determine the occurrence and significance of these processes in the environment.

By promoting or inhibiting microbial respiration, environmental pH is also capable of shaping microbial community composition. Microbial iron reduction and sulfate reduction, for example, occur widely in subsurface environments and compete against each other for the common electron donors of H_2 and acetate. The current paradigm describing their interactions follows the tragedy of commons and assumes that iron reducers hold either a thermodynamic or kinetic advantage and as a result, always win the competition against sulfate reducers (Chapelle and Lovley, 1992; Bethke et al., 2008).

Our modeling results show that the competitive advantage of iron reducers is pH dependent. Specifically, the thermodynamic drive of microbial iron reduction responds significantly to pH. In the assumed environment, that response lowers iron reduction rates from maximum values to 0 over a narrow pH range of 1 unit. In comparison, sulfate reduction responds relatively modestly to pH and stays thermodynamically favorable over the entire pH range between 1 and 14. These results suggest iron reducers can win the competition against sulfate reducers under acidic conditions but might lose the competition under alkaline conditions. Thus, changes in pH have the potential to alter the proportions of iron reducers relative to sulfate reducers in an environment.

Results of laboratory experiments by Kirk et al. (2013) are consistent with this possibility. In their study, microbial consortia from a freshwater aquifer grew on acetate under two different pHs, 7.2 and 5.7, and the microbial community that developed in each reactor was sampled at the end of the study and analyzed by sequencing 16S rRNA gene amplicons. The relative abundance of sequences that grouped within *Geobacteraceae* and *Myxococcaceae* was twice as high in pH 5.7 reactors than pH 7.2 reactors. Members of *Geobacteraceae* and *Myxococcaceae*, such as *Geobacter* and *Anaeromyxobacter*, are capble of iron reduction (Lonergan et al., 1996; Treude et al., 2003). Conversely, sequences that grouped within taxa commonly associated with sulfate reduction, such as *Desulfobulbaceae*, *Desulfovibrionaceae*, *Desulfuromonadaceae*, and *Desulfobacteraceae*, were primarly only present in pH 7.2 reactors.

These differences in relative abundance are consistent with contributions of iron reduction and sulfate reduction to acetate oxidation evaluated using mass-balance calculations. According to their results, in pH 7.2 reactors, sulfate reduction overwhelmed iron reduction; sulfate reduction consumed 85% of acetate, and the rest is accounted for by iron reduction. At pH 5.7, iron reduction consumed at least 90% of acetate while sulfate reduction consumed a negligible amount (<1%). In agreement with these findings, furthermore, Kirk et al. (2016) found that broad-scale patterns in groundwater geochemistry in U.S. aquifers are also consistent with an increase in the significance of iron reduction relative to sulfate reduction as pH decreases.

Concluding Comments

We applied geochemical reaction modeling, and explored the thermodynamic responses of microbial redox reactions to environmental pH. Our modeling focused on the energy yields of redox reactions, and neglected other impacts brought upon cell metabolisms by pH. For example, low pH conditions promotes the diffusion of formic acid, acetic acid, and other short-chain fatty acids across the membrane, which dissipates proton motive force across the membrane and inhibits microbial growth (Russell, 1992). Low pH also helps dissolve ferric and ferrous minerals, which makes available ferric iron to iron reducers and ferrous iron to iron oxidizers, and promotes the biogeochemical cycling of iron (Coupland and Johnson, 2008; Emerson et al., 2010).

Our work represents a step forward toward a mechanistic view of the pH control on microbial metabolisms and community structures. Current studies rely on phenomenological models to describe the apparent microbial responses to pH. Here we focused on microbial respiration, and illustrated that environmental pH influences the thermodynamics of microbial redox reactions and that this influence can be strong enough to cause significant changes in respiration kinetics.

The simulation results illustrate that environmental pH can impact the energies of microbial redox reactions in two ways. Chemical energies are a direct function of pH—the chemical activity of protons—for reactions that consume and produce protons. In addition, pH also controls the speciation and concentrations of electron donors, acceptors, and reaction products, which in turn determine the energy yields of redox reactions. For microbial reduction of goethite and other ferric oxyhydroxides, the effect of proton consumption is dominant. For other reactions, the indirect speciation effect is of similar magnitude as the proton activity effect. These thermodynamic responses are strong enough that they can switch the thermodynamic states of microbial respiration between favorable and unfavorable and change microbial rates from 0 to their maximum values. Thermodynamic responses also help give rise to the lower or upper pH limits of microbial respiration reactions and pH-dependent changes in microbial community composition. By changing the thermodynamics of individual microbial redox reactions, pH variations are capable of shifting microbial community structures and modulating the interactions among microbes.

Taken together, our results provide a mechanistic understanding of how environmental pH regulates microbial respiration and affects the community composition of natural microbes. They expand our view on the evaluation of microbial processes using routine environmental parameters, such as pH and chemical energies. In addition to microbial respiration, microbial growth, and maintenance are also influenced by environmental pH (Russell and Dombrowski, 1980). Future efforts should explore the pH impact on growth and maintenance in order to achieve a holistic view of microbial response to environmental pH.

AUTHOR CONTRIBUTIONS

QJ and MK designed the research. QJ carried out the simulation, and wrote the first draft of the manuscript, and MK revised the manuscript.

ACKNOWLEDGMENTS

This research was funded by the National Science Foundation under Award EAR-1636815 and by National Aeronautics and Space Administration under Grant NNX16AJ59G.

SUPPLEMENTARY MATERIAL

The Supplementary Material for this article can be found online at: https://www.frontiersin.org/articles/10.3389/fenvs.2018.00021/full#supplementary-material

REFERENCES

Amend, A. S., Oliver, T. A., Amaral-Zettler, L. A., Boetius, A., Fuhrman, J. A., Horner-Devine, M. C., et al. (2013). Macroecological patterns of marine bacteria on a global scale. *J. Biogeogr.* 40, 800–811. doi: 10.1111/jbi.12034

Baker-Austin, C., and Dopson, M. (2007). Life in acid: pH homeostasis in acidophiles. *Trends Microbiol.* 15, 165–171. doi: 10.1016/j.tim.2007.02.005

Bennett, P. C., Rogers, J. R., Choi, W. J., and Hiebert, F. K. (2001). Silicates, silicate weathering, and microbial ecology. *Geomicrobiol. J.* 18, 3–19. doi: 10.1080/01490450151079734

Bethke, C. M. (2008). *Geochemical and Biogeochemical Reaction Modeling*, *2nd Edn*. Cambridge: Cambridge University Press.

Bethke, C. M., Ding, D., Jin, Q., and Sanford, R. A. (2008). Origin of microbiological zoning in groundwater flows. *Geology* 36, 739–742. doi: 10.1130/G24859A.1

Bethke, C. M., Sanford, R. A., Kirk, M. F., Jin, Q., and Flynn, T. M. (2011). The thermodynamic ladder in geomicrobiology. *Am. J. Sci.* 311, 183–210. doi: 10.2475/03.2011.01

Bigham, J. M., Schwertmann, U., Traina, S. J., Winland, R. L., and Wolf, M. (1996). Schwertmannite and the chemical modeling of iron in acid sulfate waters. *Geochim. Cosmochim. Acta* 60, 2111–2121. doi: 10.1016/0016-7037(96)00091-9

Booth, I. R. (1985). Regulation of cytoplasmic pH in bacteria. *Microbiol. Rev.* 49, 359–378.

Chapelle, F. H., and Lovley, D. R. (1992). Competitive exclusion of sulfate reduction by Fe(lll)-reducing bacteria: a mechanism for producing discrete zones of high-iron ground water. *Ground Water* 30, 29–36. doi: 10.1111/j.1745-6584.1992.tb00808.x

Chapelle, F. H., McMahon, P. B., Dubrovsky, N. M., Fujii, R. F., Oaksford, E. T., and Vroblesky, D. A. (1995). Deducing the distribution of terminal electron-accepting processes in hydrologically diverse groundwater systems. *Water Resour. Res.* 31, 359–371. doi: 10.1029/94WR02525

Chen, G., He, Z., and Wang, Y. (2004). Impact of pH on microbial biomass carbon and microbial biomass phosphorus in red soils. *Pedosphere* 14, 9–15.

Cornell, R. M., and Schwertmann, U. (2003). *The Iron Oxides: Structure, Properties, Reactions, Occurrences and Uses*, *2nd Edn*. Weinheim: Wiley-VCH.

Coupland, K., and Johnson, D. B. (2008). Evidence that the potential for dissimilatory ferric iron reduction is widespread among acidophilic heterotrophic bacteria. *FEMS Microbiol. Lett.* 279, 30–35. doi: 10.1111/j.1574-6968.2007.00998.x

Delany, J. M., and Lundeen, S. R. (1990). *The LLNL Thermodynamical Database*. Lawrence Livermore National Laboratory Report UCRL-21658, 150.

Dolfing, J., Xu, A., and Head, I. M. (2010). Anomalous energy yields in thermodynamic calculations: importance of accounting for pH-dependent organic acid speciation. *ISME J.* 4, 463. doi: 10.1038/ismej.2010.14

Dwyer, D. F., Weeg-Aerssens, E., Shelton, D. R., and Tiedje, J. M. (1988). Bioenergetic conditions of butyrate metabolism by a syntrophic, anaerobic bacterium in coculture with hydrogen-oxidizing methanogenic and sulfidogenic bacteria. *Appl. Environ. Microbiol.* 54, 1354–1359.

Edwards, K. J., Becker, K., and Colwell, F. (2012). The deep, dark energy biosphere: intraterrestrial life on Earth. *Annu. Rev. Earth Planet. Sci.* 40, 551–568. doi: 10.1146/annurev-earth-042711-105500

Emerson, D., Fleming, E. J., and McBeth, J. M. (2010). Iron-Oxidizing bacteria: an environmental and genomic perspective. *Annu. Rev. Microbiol.* 64, 561–583. doi: 10.1146/annurev.micro.112408.134208

Falkowski, P. G., Fenchel, T., and Delong, E. F. (2008). The Microbial engines that drive earth's biogeochemical cycles. *Science* 320, 1034–1039. doi: 10.1126/science.1153213

Fernández-Calviño, D., and Bååth, E. (2010). Growth response of the bacterial community to pH in soils differing in pH. *FEMS Microbiol. Ecol.* 73, 149–156. doi: 10.1111/j.1574-6941.2010.00873.x

Golyshina, O. V., and Timmis, K. N. (2005). Ferroplasma and relatives, recently discovered cell wall-lacking archaea making a living in extremely acid, heavy metal-rich environments. *Environ. Microbiol.* 7, 1277–1288. doi: 10.1111/j.1462-2920.2005.00861.x

Hedrich, S., Schlömann, M., and Johnson, D. B. (2011). The iron-oxidizing proteobacteria. *Microbiology* 157, 1551–1564. doi: 10.1099/mic.0.045344-0

Helgeson, H. C. (1969). Thermodynamics of hydrothermal systems at elevated temperatures and pressures. *Am. J. Sci.* 267, 729–804. doi: 10.2475/ajs.267.7.729

Horikoshi, K. (1999). Alkaliphiles: some applications of their products for biotechnology. *Microbiol. Mol. Biol. Rev.* 63, 735–750.

Jin, Q. (2007). Control of hydrogen partial pressures on the rates of syntrophic microbial metabolisms: a kinetic model for butyrate fermentation. *Geobiology* 5, 35–48. doi: 10.1111/j.1472-4669.2006.00090.x

Jin, Q. (2012). Energy conservation of anaerobic respiration. *Am. J. Sci.* 312, 573–628. doi: 10.2475/06.2012.01

Jin, Q., and Bethke, C. M. (2002). Kinetics of electron transfer through the respiratory chain. *Biophys. J.* 83, 1797–1808. doi: 10.1016/S0006-3495(02)73945-3

Jin, Q., and Bethke, C. M. (2003). A new rate law describing microbial respiration. *Appl. Environ. Microbiol.* 69, 2340–2348. doi: 10.1128/AEM.69.4.2340-2348.2003

Jin, Q., and Bethke, C. M. (2005). Predicting the rate of microbial respiration in geochemical environments. *Geochim. Cosmochim. Acta* 69, 1133–1143. doi: 10.1016/j.gca.2004.08.010

Jin, Q., and Bethke, C. M. (2007). The thermodynamics and kinetics of microbial metabolism. *Am. J. Sci.* 307, 643–677. doi: 10.2475/04.2007.01

Jin, Q., and Bethke, C. M. (2009). Cellular energy conservation and the rate of microbial sulfate reduction. *Geology* 36, 739–742. doi: 10.1130/G30185A.1

Jin, Q., and Roden, E. E. (2011). Microbial physiology-based model of ethanol metabolism in subsurface sediments. *J. Contam. Hydrol.* 125, 1–12. doi: 10.1016/j.jconhyd.2011.04.002

Johnson, D. B., Kanao, T., and Hedrich, S. (2012). Redox transformations of iron at extremely low pH: fundamental and applied aspects. *Front. Microbiol.* 3:96. doi: 10.3389/fmicb.2012.00096

Kemmitt, S. J., Wright, D., Goulding, K. W. T., and Jones, D. L. (2006). pH regulation of carbon and nitrogen dynamics in two agricultural soils. *Soil Biol. Biochem.* 38, 898–911. doi: 10.1016/j.soilbio.2005.08.006

Kirk, M. F., Jin, Q., and Haller, B. R. (2016). Broad-scale evidence that pH influences the balance between microbial iron and sulfate reduction. *Groundwater* 54, 406–413. doi: 10.1111/gwat.12364

Kirk, M. F., Santillan, E. F. U., Sanford, R. A., and Altman, S. J. (2013). CO2-induced shift in microbial activity affects carbon trapping and water quality in anoxic bioreactors. *Geochim. Cosmochim. Acta* 122, 198–208. doi: 10.1016/j.gca.2013.08.018

Kotsyurbenko, O. R., Chin, K.-J., Glagolev, M. V., Stubner, S., Simankova, M. V., Nozhevnikova, A. N., et al. (2004). Acetoclastic and hydrogenotrophic methane production and methanogenic populations in an acidic West-Siberian peat bog. *Environ. Microbiol.* 6, 1159–1173. doi: 10.1111/j.1462-2920.2004.00634.x

Krulwich, T. A., Ito, M., Hicks, D. B., Gilmour, R., and Guffanti, A. A. (1998). pH homeostasis and ATP synthesis: studies of two processes that necessitate inward proton translocation in extremely alkaliphilic Bacillus species. *Extremophiles* 2, 217–222. doi: 10.1007/s007920050063

Lauber, C. L., Hamady, M., Knight, R., and Fierer, N. (2009). Pyrosequencing-based assessment of soil pH as a predictor of soil bacterial community structure at the continental scale. *Appl. Environ. Microbiol.* 75, 5111–5120. doi: 10.1128/AEM.00335-09

Lennon, J. T., and Jones, S. E. (2011). Microbial seed banks: the ecological and evolutionary implications of dormancy. *Nat. Rev. Microbiol.* 9, 119–130. doi: 10.1038/nrmicro2504

Leprince, F., and Quiquampoix, H. (1996). Extracellular enzyme activity in soil: effect of pH and ionic strength on the interaction with montmorillonite of two acid phosphatases secreted by the ectomycorrhizal fungus *Hebeloma cylindrosporum* Activité enzymatique extracellulaire dans Ie sol: effet du pH et de la force ionique sur l'interaction avec la montmorillonite de deux phosphates acides sécrdteés par le champignon ectomycorhizien *Hebeloma cylindrosporum*. *Eur. J. Soil Sci.* 47, 511–522. doi: 10.1111/j.1365-2389.1996.tb01851.x

Lide, D. R. (2003). *Handbook of Chemistry and Physcis, 83rd Edn*. Boca Raton, FL: CRC Press.

Lindsay, W. L. (1979). *Chemical Equilibria in Soils*. New York, NY: John Wiley and Sons Ltd.

Lonergan, D. J., Jenter, H. L., Coates, J. D., Phillips, E. J., Schmidt, T. M., and Lovley, D. R. (1996). Phylogenetic analysis of dissimilatory Fe(III)-reducing bacteria. *J. Bacteriol.* 178, 2402–2408. doi: 10.1128/jb.178.8.2402-2408.1996

Lovley, D. R., and Chapelle, F. H. (1995). Deep subsurface microbial processes. *Rev. Geophys.* 33, 365–382. doi: 10.1029/95RG01305

Lovley, D. R., and Klug, M. J. (1982). Intermediary metabolism of organic matter in the sediments of a eutrophic lake. *Appl. Environ. Microbiol*. 43, 552–560.

Lowe, S. E., Jain, M. K., and Zeikus, J. G. (1993). Biology, ecology, and biotechnological applications of anaerobic bacteria adapted to environmental stresses in temperature, pH, salinity, or substrates. *Microbiol. Rev.* 57, 451–509.

Maestrojuan, G. M., and Boone, D. R. (1991). Characterization of *Methanosarcina barkeri* MST and 227, *Methanosarcina mazei* S-6T, and *Methanosarcina vacuolata* Z-761T. *Int. J. Syst. Evol. Microbiol.* 41, 267–274. doi: 10.1099/00207713-41-2-267

Maguffin, S. C., Kirk, M. F., Daigle, A. R., Hinkle, S. R., and Jin, Q. (2015). Substantial contribution of biomethylation to aquifer arsenic cycling. *Nat. Geosci.* 8, 290–293. doi: 10.1038/ngeo2383

Matin, A. (1990). Bioenergetics parameters and transport in obligate acidophiles. *Biochim. Biophys. Acta Bioenerg.* 1018, 267–270. doi: 10.1016/0005-2728(90)90264-5

Molongoski, J. J., and Klug, M. J. (1980). Anaerobic metabolism of particulate organic matter in the sediments of hypereutrophic lake. *Freshwater Biol.* 10, 507–518.

Monokova, S. V. (1975). Volatile fatty acids in bottom sediments of the Rybinsk reservoir. *Hydrobiol. J.* 11, 45–48.

O'Flaherty, V., Mahony, T., O'Kennedy, R., and Colleran, E. (1998). Effect of pH on growth kinetics and sulphide toxicity thresholds of a range of methanogenic, syntrophic and sulphate-reducing bacteria. *Process Biochem.* 33, 555–569. doi: 10.1016/S0032-9592(98)00018-1

Paul, A., Stösser, R., Zehl, A., Zwirnmann, E., Vogt, R. D., and Steinberg, C. E. W. (2006). Nature and abundance of organic radicals in natural organic matter: effect of pH and irradiation. *Environ. Sci. Technol.* 40, 5897–5903. doi: 10.1021/es060742d

Postma, D., and Jakobsen, R. (1996). Redox zonation: equilibrium constraints on the Fe(III)/SO4-reduction interface. *Geochim. Cosmochim. Acta* 60, 3169–3175. doi: 10.1016/0016-7037(96)00156-1

Rosso, L., Lobry, J. R., Bajard, S., and Flandrois, J. P. (1995). Convenient model to describe the combined effects of temperature and pH on microbial growth. *Appl. Environ. Microbiol.* 61, 610–616.

Russell, J. B. (1992). Another explanation for the toxicity of fermentation acids at low pH: anion accumulation versus uncoupling. *J. Appl. Bacteriol.* 73, 363–370. doi: 10.1111/j.1365-2672.1992.tb04990.x

Russell, J. B., and Dombrowski, D. B. (1980). Effect of pH on the efficiency of growth by pure cultures of rumen bacteria in continuous culture. *Appl. Environ. Microbiol.* 39, 604–610.

Schink, B. (1992). "Syntrophism among prokaryotes," in *The Prokaryotes,* eds A. Balows, H. Trüper, M. Dworkin, W. Harder, and K. Schleifer (New York, NY: Springer-Verlag), 276–299.

Schink, B. (1997). Energetics of syntrophic cooperation in methanogenic degradation. *Microbiol. Mol. Biol. Rev.* 61, 262–280.

Schink, B., and Stams, A. J. M. (2013). "Syntrophism among prokaryotes," in *The Prokaryotes: Prokaryotic Communities and Ecophysiology,* eds E. Rosenberg, E. F. DeLong, S. Lory, , E. Stackebrandt, and F. Thompson (Heidelberg; Berlin: Springer), 471–493.

Schmidt, J. E., and Ahring, B. K. (1993). Effects of hydrogen and formate on the degradation of propionate and butyrate in thermophilic granules from an upflow anaerobic sludge blanket reactor. *Appl. Environ. Microbiol.* 59, 2546–2551.

Shock, E. L., Holland, M., Meyer-Dombard, D. A., Amend, J. P., Osburn, G. R., and Fischer, T. P. (2010). Quantifying inorganic sources of geochemical energy in hydrothermal ecosystems, Yellowstone National Park, USA. *Geochim. Cosmochim. Acta* 74, 4005–4043. doi: 10.1016/j.gca.2009.08.036

Sprott, G. D., Bird, S. E., and McDonald, I. J. (1985). Proton motive force as a function of the pH at which *Methanobacterium bryantii* is grown. *Can. J. Microbiol.* 31, 1031–1034. doi: 10.1139/m85-194

Steigmiller, S., Turina, P., and Gräber, P. (2008). The thermodynamic H+/ATP ratios of the H+-ATPsynthases from chloroplasts and *Escherichia coli*. *Proc. Natl. Acad. Sci. U.S.A.* 105, 3745–3750. doi: 10.1073/pnas.0708356105

Straub, K. L., Hanzlik, M., and Buchholz-Cleven, B. E. E. (1998). The use of biologically produced ferrihydrite for the isolation of novel iron-reducing bacteria. *Syst. Appl. Microbiol.* 21, 442–449. doi: 10.1016/S0723-2020(98)80054-4

Stumm, W., and Morgan, J. J. (1996). *Aquatic Chemistry*. *Chemical Equilibria and Rates in Natural Waters*, *3rd Edn*. New York, NY: John Wiley and Sons, Inc.

Thompson, L. R., Sanders, J. G., McDonald, D., Amir, A., Ladau, J., Locey, K. J., et al. (2017). A communal catalogue reveals Earth's multiscale microbial diversity. *Nature* 551, 457. doi: 10.1038/nature24621

Treude, N., Rosencrantz, D., Liesack, W., and Schnell, S. (2003). Strain FAc12, a dissimilatory iron-reducing member of the Anaeromyxobacter subgroup of Myxococcales. *FEMS Microbiol. Ecol.* 44, 261–269. doi: 10.1016/S0168-6496(03)00048-5

Ward, D. M., Ferris, M. J., Nold, S. C., and Bateson, M. M. (1998). A natural view of microbial biodiversity within hot spring cyanobacterial mat communities. *Microbiol. Mol. Biol. Rev.* 62, 1353–1370.

Windman, T., Zolotova, N., Schwandner, F., and Shock, E. L. (2007). Formate as an energy source for microbial metabolism in chemosynthetic zones of hydrothermal ecosystems. *Astrobiology* 7, 873–890. doi: 10.1089/ast.2007.0127

Wu, C., Dong, X., and Liu, X. (2007). *Syntrophomonas wolfei* subsp. *methylbutyratica* subsp. nov., and assignment of *Syntrophomonas wolfei* subsp. saponavida to *Syntrophomonas saponavida* sp. nov. comb. nov. *Syst. Appl. Microbiol.* 30, 376–380. doi: 10.1016/j.syapm.2006.12.001

Ye, R., Jin, Q., Bohannan, B., Keller, J. K., McAllister, S. A., and Bridgham, S. D. (2012). pH controls over anaerobic carbon mineralization, the efficiency of methane production, and methanogenic pathways in peatlands across an ombrotrophic–minerotrophic gradient. *Soil Biol. Biochem.* 54, 36–47. doi: 10.1016/j.soilbio.2012.05.015

Zhalnina, K., Dias, R., de Quadros, P. D., Davis-Richardson, A., Camargo, F. A. O., Clark, I. M., et al. (2015). Soil pH determines microbial diversity and composition in the park grass experiment. *Microb. Ecol.* 69, 395–406. doi: 10.1007/s00248-014-0530-2

Zhang, C., Liu, X., and Dong, X. (2004). *Syntrophomonas curvata* sp. nov., an anaerobe that degrades fatty acids in co-culture with methanogens. *Int. J. Syst. Evol. Microbiol.* 54, 969–973. doi: 10.1099/ijs.0.02903-0

Zhang, C., Liu, X., and Dong, X. (2005). *Syntrophomonas erecta* sp. nov., a novel anaerobe that syntrophically degrades short-chain fatty acids. *Int. J. Syst. Evol. Microbiol.* 55, 799–803. doi: 10.1099/ijs.0.63372-0

Conflict of Interest Statement: The authors declare that the research was conducted in the absence of any commercial or financial relationships that could be construed as a potential conflict of interest.

frontiers in Environmental Science

ORIGINAL RESEARCH
published: 04 May 2018
doi: 10.3389/fenvs.2018.00015

Discerning Microbially Mediated Processes During Redox Transitions in Flooded Soils Using Carbon and Energy Balances

Kristin Boye[1,2]*, *Anke M. Herrmann*[3], *Michael V. Schaefer*[2,4], *Malak M. Tfaily*[5] and *Scott Fendorf*[2]

[1] Stanford Synchrotron Radiation Lightsource, SLAC National Accelerator Laboratory, Menlo Park, CA, United States, [2] Earth System Science, Stanford University, Stanford, CA, United States, [3] Department of Soil and Environment, Swedish University of Agricultural Sciences, Uppsala, Sweden, [4] Department of Environmental Sciences, University of California, Riverside, Riverside, CA, United States, [5] Environmental Molecular Sciences Laboratory, Pacific Northwest National Laboratory, Richland, WA, United States

Recurring dry-wet cycles of soils, such as in rice paddies and on floodplains, have a dramatic impact on biogeochemical processes. The rates and trajectories of microbial metabolic functions during transition periods from drained to flooded conditions affect the transformation rates and phase partitioning of carbon, nutrients, and contaminants. However, the regulating mechanisms responsible for diverging functional metabolisms during such transitions are poorly resolved. The chemistry of organic carbon within the microbially available pool likely holds key information regarding carbon cycling and redox transformation rates. In this study, we used mesocosms to examine the influence of different carbon sources (glucose, straw, manure, char) on microbial energetics, respiration rates, and carbon balances in rice paddy soils during the transition from drained to flooded conditions following inundation. We found that variability in carbon solubility (1.6–400 mg g^{-1}) and chemical composition of the amendments led to non-uniform stimulation of carbon dioxide production per unit carbon added (0.4–32.9 mmol CO_2 mol^{-1} added C). However, there was a clear linear correlation between energy release and net CO_2 production rate (R^2 = 0.85), between CO_2 and initial soluble C (R^2 = 0.91, excluding glucose treatment) and between heat output and Gibbs free energy of initial soluble C (R^2 = 0.78 and 0.69, with/without glucose respectively). Our results further indicated that the chemical composition of the soluble C from amendments initiated divergent anaerobic respiration behavior, impacting methane production and the partitioning of elements between soil solid phase and solution. This study shows the benefit of monitoring energy and element mass balances for elucidating the contribution of various microbial metabolic functions in complex systems. Further, our results highlight the importance of organic carbon composition within the water soluble pool as a key driver of microbially mediated redox transformations with major impacts on greenhouse gas emissions, contaminant fate, and nutrient cycling in paddy soils and similar ecosystems.

Keywords: soil carbon, microbial respiration, organic amendments, anaerobic metabolism, paddy soil, calorimetry, FT-ICR-MS

OPEN ACCESS

Edited by:
Jennifer Pett-Ridge, Lawrence Livermore National Laboratory (DOE), United States

Reviewed by:
Aaron Thompson, University of Georgia, United States
Nabeel Khan Niazi, University of Agriculture, Faisalabad, Pakistan

***Correspondence:**
Kristin Boye
kboye@slac.stanford.edu

Specialty section:
This article was submitted to Microbiological Chemistry and Geomicrobiology, a section of the journal Frontiers in Environmental Science

Received: *23 December 2017*
Accepted: *26 March 2018*
Published: *04 May 2018*

Citation:
Boye K, Herrmann AM, Schaefer MV, Tfaily MM and Fendorf S (2018) Discerning Microbially Mediated Processes During Redox Transitions in Flooded Soils Using Carbon and Energy Balances. Front. Environ. Sci. 6:15. doi: 10.3389/fenvs.2018.00015

INTRODUCTION

Microbial processes within rice paddy soils have profound impacts on crop production and the environment, ranging from changes in nutrient (e.g., N and P) and contaminant (e.g., As) availability to production and emission of greenhouse gases (GHG; e.g., CO_2, CH_4). Rice paddies consistently go through drainage and re-flooding between cropping cycles. Flooding of soils induce dramatic, temporary increases in microbial respiration rates (Fierer and Schimel, 2003; Corstanje and Reddy, 2004; Valett et al., 2005; Wilson et al., 2011), and the microbial response is influenced by the period of drainage and C input history (Bodelier et al., 2012; Göransson et al., 2013; Meisner et al., 2013; Shi and Marschner, 2014). However, the specific microbial metabolic response with flooding progression (as the soil becomes increasingly depleted in oxygen) and with different inputs remains unresolved. In general, anaerobic respiration conforms to thermodynamic predictions, owing to partial equilibrium, to proceed with progressively less favorable electron acceptors, i.e., $Mn(IV) > NO_3^- > Fe(III) > SO_4^{2-} > CO_2$ (Postma and Jakobsen, 1996; Arndt et al., 2013), but increasing evidence shows that the available electron donors (e.g., organic C compounds, H_2) and high variability in local conditions (e.g., pH, gas pressure, diffusion rates, concentrations of reactants and products) can off-set the metabolic transitions from this predicted trajectory (Jin and Bethke, 2005; LaRowe and Van Cappellen, 2011; Arndt et al., 2013; Hansel et al., 2015). The period immediately following flooding, when the system transitions from aerobic to anaerobic conditions, exhibits dramatic changes in reaction rates and metabolic activity, with a critical impact on C fate, rate of nutrient release, extent of denitrification, iron (and sulfate) reduction, contaminant release, and methanogenesis (Baldwin and Mitchell, 2000; Burns and Ryder, 2001; Newman and Pietro, 2001; Corstanje and Reddy, 2004; Wilson et al., 2011). Therefore, in order to predict C turnover rates in paddy soils and consequential processes impacting crop growth and environmental quality, it is necessary to determine the variability in microbial C oxidation, and its causes, in the response to flooding of paddy soils.

Soil organic matter serves as both C source and energy source for microorganisms, and the distribution between anabolic (biomass-yielding) and catabolic (energy-yielding) C use varies between different types of microorganisms and available substrates. Interestingly, independent of changes in enthalpy and metabolic pathway, the Gibbs energy (ΔG) dissipation per unit biomass produced exhibits little variability (von Stockar and Liu, 1999; Roden and Jin, 2011), i.e., the energy requirement for anabolism is relatively constant. Thus, the large variation in energy yield from different catabolic reactions results in a relatively proportional variation in growth, but with important differences in how the decrease in entropy from building biomass is handled (von Stockar and Liu, 1999). Aerobic metabolism achieves energy balance almost entirely through heat dissipation, i.e., the overall metabolic reaction is exothermic with the enthalpy change, ΔH, roughly equaling ΔG. Anaerobic metabolism, on the other hand, can range from being highly exothermic (methanogenesis from CO_2+H_2 has $\Delta H > \Delta G$) to being endothermic ($\Delta H < 0$) and entropy-driven (e.g., methanogenesis from acetate) (von Stockar and Liu, 1999; Liu et al., 2001). Thus, valuable information about differences in microbial metabolic activity can be gained through simultaneous measurements of microbial C utilization (e.g., respiration and/or biomass yield) and changes in enthalpy (by isothermal calorimetry) (Hansen et al., 2004; Herrmann et al., 2014; Barros et al., 2015; Bölscher et al., 2016; Arcand et al., 2017), particularly if the ΔG and/or ΔH of the substrate is known.

In well-aerated, moist soils, the calorespirometric ratio, R_q/R_{CO2} (heat dissipation per unit CO_2 produced), varies depending on soil management and land use history (e.g., fertilization, deforestation, reforestation, crop rotations) (Barros Pena et al., 2014; Herrmann and Bölscher, 2015; Barros et al., 2016; Bölscher et al., 2016) and this has been linked to differences in microbial community composition (Bölscher et al., 2016) and organic matter sources (Barros et al., 2016). Such evaluations are based on the thermodynamic relationship between heat and respiration in aerobic systems at steady-state (i.e., no growth), where R_q/R_{CO2} is dependent only on the oxidation state of the substrate (Hansen et al., 2004):

$$\frac{R_q}{R_{CO_2}} = -\left(1 - \frac{NOSC}{4}\right) \Delta H_{O_2} \text{ [kJ mol}^{-1} \text{ CO}_2\text{]} \qquad (1)$$

where R_q is the heat output rate (J g^{-1} soil day^{-1}), R_{CO2} is the CO_2 production rate (μmol g^{-1} soil day^{-1}), NOSC is the nominal oxidation state of C in the substrate (ranging from -4 to $+4$), and ΔH_{O2} is Thornton's constant or the oxycaloric equivalent (-455 ± 15 kJ mol^{-1} O_2) (Hansen et al., 2004). Deviations from the predicted value in fully aerated systems with a known substrate can then be attributed to growth (R_q/R_{CO2} smaller than predicted) or metabolic inefficiency due to environmental stressors (R_q/R_{CO2} larger than predicted) (Hansen et al., 2004). In systems with mixed or purely anaerobic metabolisms, the relationship between R_q and R_{CO2} is more complicated. Most commonly, anaerobic metabolism dissipates less heat than aerobic metabolism per unit biomass formed, due to the increase in entropy associated with fermentation and production of gaseous metabolites from dissolved substrates (von Stockar and Liu, 1999; Hansen et al., 2004). However, the relationship between heat and CO_2-production is less straightforward than the biomass yield; for example, CO_2 can be produced essentially without heat generation (e.g., through anaerobic respiration with sulfate or nitrate and an organic electron donor, or disproportionation of substrates) (Hansen et al., 2004; Ozuolmez et al., 2015). Contrastingly, CO_2 can be consumed with extreme heat dissipation (methanogenesis from CO_2 and H_2) (von Stockar and Liu, 1999), and heat can be generated without CO_2 being part of the metabolic reaction at all (e.g., fermentation of glucose to lactate). Therefore, the relationships between respiration rate, oxygen consumption, heat dissipation, and microbial growth in complex systems with mixed substrates and/or metabolisms need further evaluation in order to be useful for assessing microbial processes.

One of the fundamental prerequisites for thermodynamic evaluations of metabolic activities is to know the reactants and

products. For incubations with single (or few) organisms and simple substrates (e.g., glucose, acetate, propionate, ethanol, methanol) the metabolic reactions can largely be predicted and the enthalpy of combustion for substrates and products, as well as their NOSC, are generally known. Thus, the thermodynamic energy yield of such a system can be calculated and compared to measured heat and CO_2 generation to deduce which types of metabolic pathways are active and how efficiently energy, carbon, and nutrients are converted into biomass (Herrmann et al., 2014; Bölscher et al., 2016). Such predictions also hold true for mixed aerobic/anaerobic and growing systems (von Stockar and Liu, 1999; Hansen et al., 2004; Roden and Jin, 2011). However, soils are complex heterogeneous environments, where it is practically impossible to determine which substrate compounds are being metabolized through a certain metabolic pathway at any given point in time. Nevertheless, the Gibbs free energy of complex organic matter can be estimated based on its elemental stoichiometry (LaRowe and Van Cappellen, 2011). Recently, we used Fourier-transform ion cyclotron resonance mass spectrometry (FT-ICR-MS) to estimate a ΔG of water soluble organic C from sediment extracts, and we revealed that thermodynamic limitations for anaerobic respiration result in preferential removal of substrates with a favorable ΔG when coupled to sulfate reduction in typical anoxic conditions (Boye et al., 2017). Combining FT-ICR-MS determination of NOSC, and by extension the composite ΔG of soluble C, illuminates a potential solution to overcoming the challenges associated with quantifying metabolic pathways in systems with complex substrates. Such an approach greatly enhances the possibilities of constraining the thermodynamics of metabolic reactions in soil systems, as long as the rates of production or consumption of other participating compounds can be determined (e.g., O_2, anaerobic electron acceptors (Mn(IV), NO_3^-, Fe(III), SO_4^{2-} *etc.*), methane, H_2).

Therefore, the objectives of this study were to (1) evaluate the relationship between heat and carbon flow in non-steady-state soil systems with complex natural organic substrates and multiple types of active microbial metabolic strategies, and (2) test the hypothesis that the variability in microbial response to flooding is dependent on organic matter source and soil type and can be explained by thermodynamic theory and relatively easily obtained mass and energy balances. We thus determine key drivers of microbially mediated redox transformations, which have profound impacts on greenhouse gas emissions and other important element cycles in paddy soils and similar ecosystems. A better understanding of these mechanisms and their dependence on initial properties of soil and organic matter, will help simplify the predictions of carbon fate and other environmental impacts from flooding.

MATERIALS AND METHODS

Soil and Amendment Sampling and Characterization

In order to investigate the variability in microbial activity in response to flooding, we used three different types of rice paddy soils and three types of organic matter that are commonly present on rice paddies: dried rice straw (DS), charred rice straw (CS), and cattle manure (M). Straw amendments were collected from two separate Cambodian rice fields where harvested straw was deposited (DS) or piled and burned (CS). The "charred straw", thus, consisted of a mix of ashes (more aerated outer portions of the pile) and charred material (from the interior of the pile). Cattle manure was collected from grazing fields. Paddy soils were collected from the top 10 cm of rice fields in the Mekong delta of Vietnam (peaty paddy soil and acid sulfate soil) and Cambodia (mineral paddy soil). All soils and amendments were dried at room temperature for 1–2 weeks prior to analyses and experiments. Soils were gently ground to crush aggregates >2 mm and sieved (2 mm). Amendment material was ground to a fine powder in a ball mill. Soils and amendments were analyzed (in triplicate) for total C and N concentration (weight-% of dry material) by a Carlo Erba NA 1500 elemental analyzer. Total concentrations of other elements in soils were determined by X-ray fluorescence (XRF) spectroscopy (Spectro Xepos HE). Amendments were digested (in triplicate) in 70% nitric acid (trace metal grade) using a CEM MarsXpress™ microwave digester (CEM, Matthews, NC, USA). The digests were diluted 1:5 with ultrapure DI water and analyzed for total Fe and S concentrations with inductively coupled plasma optical emission spectroscopy (ICP-OES, iCAP6000, Thermo Scientific, Cambridge, UK). The pH of soil and amendments (except M, due to insufficient material) was determined in 1:5 (v/v) of material:DI-water slurries after shaking 5 min and settling for 2–8 h. Total enthalpy of combustion for all soils and amendments (except M, due to insufficient material), was determined by bomb calorimetry (6300 automatic isoperibol calorimeter, USA).

Incubation Experiment

For each soil, 50 aliquots of 4 g dry soil were weighed into 20 ml glass vials and separated into two sets, one for calorimetry measurements (in duplicate) and one for gas/solution analyses (with 4 sampling points, each in duplicate). Within each set of mesocosms, each soil was subjected to five treatments: DS, CS, M, glucose, and control [i.e., 5 treatments × 2 duplicates × 5 measurements (1 calorimetry + 4 gas/solution) = 50 vials]. Amendments were distributed so that 36 mg C were added to each vial (no amendment added to control vials). Thereafter, 15 ml TRIS buffer solution (10 mM, pH 7.03) was added, the vials were crimp-sealed, and thoroughly shaken to mix the amendments with the soil and ensure complete saturation of solids. The vials were then left to settle without further disturbance to allow anaerobiosis to gradually establish away from the headspace, similar to the progression in a flooded paddy field. For glucose amended vials, glucose was dissolved in the TRIS buffer solution and added with the solution to the vials; all other amendments were added as powdered solids prior to adding the solution. The first set of duplicates from each treatment and soil were placed in a TAM Air isothermal microcalorimeter (TA Instruments, Sollentuna, Sweden) at 25°C, along with reference vials filled with DI water to match the estimated heat capacity of the soil samples. After sample equilibration for 6.5 h, heat flow (corrected for baseline and instrument drift, <2 μW over the incubation period) was measured continuously for ca. 5 days, allowing the initially

fully aerated system (headspace and solution) to convert to anoxic conditions; a preliminary test (with another, but very similar, mineral paddy soil) using optical spot sensors (PreSens, Germany) showed that O_2 was depleted (<3 μmol/L) in the solution of all amended vials after 2–3 days of incubation (data not shown), although O_2 still remained in the headspace of some treatments. At the end-point, the solution from vials treated with glucose was filtered (0.2 μm) and analyzed for residual glucose, using an assay kit (Sigma-Aldrich, Stockholm, Sweden). The second set of mesocosms was kept in an incubator at 25°C and used to measure CO_2, CH_4, and O_2 on a Shimadzu GC-2014 at four time points: 0.5, 1.5, 2.5, and 5.5 days after flooding. The total CO_2/CH_4-production and O_2-consumption were calculated as the sum molar content of each gas in the headspace and solution using Henry's law (assuming equilibrium, atmospheric pressure, and negligible chemical reactions between gases and water). Solution samples were taken by a luer-lock needle/syringe assembly after gas sampling at the same time points (and same vials). Solutions were passed through a syringe filter (0.2 μm) and immediately analyzed for pH and acidified to 2% with nitric acid for analyses of dissolved concentrations of Fe and S by ICP-OES. Sampled mesocosms were removed from the experiment (i.e., each gas/solution measurement point was performed on unique replicate vials).

Water Soluble C Characterization

Water soluble organic C concentrations in soils and amendments (except glucose) was determined on water extracts (1:10 soil:DI-water, w/v) by the non-purgeable organic C (NPOC) method on a Shimadzu TOC-L analyzer with in-line acidification (phosphoric acid) and He-purging of samples to volatilize inorganic C. The chemical composition of water-soluble organic C was examined using a 12 Tesla Bruker SolariX Fourier transform ion cyclotron resonance mass spectrometer (FT-ICR-MS) within the Environmental Molecular Sciences Laboratory (EMSL), Richland, WA, USA. Extracts were diluted 1:2 (v/v) with LC-MS grade methanol less than 30 min before analysis to minimize potential esterification. Samples were injected directly into the mass spectrometer at a concentration of 20 ppm. A standard Bruker electrospray ionization (ESI) source was used to generate negatively charged molecular ions. Samples were introduced to the ESI source equipped with a fused silica tube (30 μm i.d.) through an Agilent 1200 series pump (Agilent Technologies) at a flow rate of 3.0 μL/min. Experimental settings followed previously established optimal parameterization: needle voltage +4.4 kV; Q1 set to 50 *m/z*; heated resistively coated glass capillary operated at 180 °C. All samples were run with instrument settings optimized by tuning on the IHSS Suwannee River fulvic acid standard. The instrument was externally calibrated weekly with a tuning solution from Agilent, which calibrates to a mass accuracy of <0.1 ppm and contains the following compounds: $C_2F_3O_2$, $C_6HF_9N_3O$, $C_{12}HF_{21}N_3O$, $C_{20}H_{18}F_{27}N_3O_8P_3$, and $C_{26}H_{18}F_{39}N_3O_8P_3$ with an *m/z* range of 112–1,333. Forty-four individual scans were averaged for each sample, and they were internally calibrated using an organic matter homologous series separated by 14 Da ($-CH_2$ groups). Mass measurement accuracy was typically within 1 ppm for singly charged ions across a broad *m/z* range (100–1,100). The mass resolution was ∼350,000 at *m/z* 321. All observed ions in the spectra were singly charged, as confirmed by the 1.0034 Da spacing found between isotopic forms of the same molecule (between $^{12}C_n$ and $^{12}C_{n-1}-^{13}C_1$). DataAnalysis software (BrukerDaltonik version 4.2) was used to convert raw spectra to a list of peak locations applying FTMS peak picker with the absolute intensity threshold set to the default value of 100. To further reduce cumulative errors, all sample peak lists within a dataset were aligned to each other prior to formula assignment to eliminate possible mass shifts that would impact formula assignment.

Chemical formulas were assigned using Formularity software (Tolić et al., 2017). The following criteria were used for formula assignments: signal to noise ratio, S/N >7, mass measurement error <1 ppm, and C, H, N, O, S, and P were the only elements considered. The presence of P cannot be confirmed through isotope analogs in the same way as the other elements. Therefore, P was only included in formulas where a single P atom was accompanied by at least four O atoms and two P atoms by at least seven O atoms. Additionally, we consistently picked the formula with the lowest error and the lowest number of heteroatoms, since molecules containing both P and S are relatively rare. All calculated formulas were screened according to a list of selection criteria previously applied to eliminate those unlikely to occur in natural organic matter (Koch and Dittmar, 2006; Kujawinski and Behn, 2006; Stubbins et al., 2010). The possibility for other potential formula assignments within our mass error ranges increases with increasing mass or mass to charge ratios. Thus, peaks with large mass to charge ratios (*m/z* values >500) often have multiple possible formulas. These peaks were assigned formulas through the detection of homologous series (CH_2, O, H_2). Specifically, whenever an observed *m/z* >500 could be assigned by adding the *m/z* of a group (CH_2, O, H_2) consistent with a homologous series to the *m/z* of an already putative assignment for a smaller compound, the formula for the large compound was assigned in this manner. If no chemical formula matched an *m/z* value within the allowed error, the peak was not included in the list of elemental formulas (i.e., the peak was unassigned).

Organic compound composition was assigned to major biochemical classes based on the molar H/C (y-axis) and O/C (x-axis) ratios (Kim et al., 2003; Šantl-Temkiv et al., 2013; Hodgkins et al., 2014; Tfaily et al., 2015). Our abundance calculations assumed equal concentrations for all compounds with an assigned molecular formula; in other words, the intensity of the peak was disregarded and a simple presence/absence approach was employed to assign relative abundance. This approach avoids biases incurred by different ionization efficiencies for different types of compounds and potential interferences between compounds or from complexation with metals. In general, the ionization efficiency is determined by the ability of different functional groups to stabilize the charge. In negative ion mode, ESI preferentially ionizes molecules that can carry a negative charge as a result of deprotonation. For example, acidic functional groups, such as carboxylic acids, are easily deprotonated and preferentially ionized relative to alcohols or nitrogen-containing compounds. This leads to

charge competition when both compound types are present in an extract. For example, compounds that contain carboxylic functional groups will be more readily ionized than compounds like lignin, tannins, and sugars, which are rich in hydroxyl functional groups. In general, compound classes ionize in the following order: lipids > lignin > hydrophilic tannins/sugars. In this study, all samples were run under similar condition, with similar starting concentrations. The effect of noise peaks was minimized by only assigning formulas to peaks with S/N >7.

Calculations and Statistical Analyses

All statistical analyses (ANOVA and linear regression analyses) were performed in R Studio® Version 1.1.383 (RStudio, Inc.).

We used the FT-ICR-MS data from the water extracts of soils and organic substrates to calculate the predicted heat output based on Equation 1 and the Gibbs free energy of the C oxidation reaction (ΔG°_{ox}) for respiration. For this purpose the stoichiometry of each assigned formula was used to calculate the nominal oxidation state of C (NOSC) for that compound (LaRowe and Van Cappellen, 2011):

$$NOSC = 4 - \frac{4c + h - 2o - 3n - 2s + 5p - z}{c} \quad (2)$$

where the letters represent the stoichiometric numbers for the elements with the corresponding capital symbol (C, H, O, N, S, P) and z is the charge of the molecule. The average NOSC for all identified compounds in the water extract was then used to calculate the Gibbs free energy of the initial water soluble C (LaRowe and Van Cappellen, 2011):

$$\Delta G^{\circ}_{ox} = 60.3 - 28.5 \cdot NOSC \text{ [kJ per mol C]} \quad (3)$$

We used this average multiplied by the total amount (mol-C) of water soluble C in each vial (soil+amendment) to calculate the maximum Gibbs free energy that would be released through complete oxidation of all water soluble C to CO_2 with O_2 as the electron acceptor (i.e., if all soluble C was oxidized through aerobic respiration) (**Table 1**). Using the measured net O_2-consumption, net dissolution of Fe, and net consumption of dissolved S, and the stoichiometrically proportional production of CO_2 per mol terminal electron acceptors (TEA) consumed (**Table 2**), we also calculated the total Gibbs free energy that was generated from respiration with O_2, ferrihydrite [$Fe(OH)_3$], and SO_4^{2-} as TEA, respectively (**Table 2**).

RESULTS

For all three soils, both heat output and respiration increased in the order control<CS<M<DS<Gluc over a ∼5 d period, although initially the microbial response to flooding in the different treatments deviated slightly from this order (**Figure 1**). The duplicate vials generated very similar heat signals (**Figures 1A–C**) and respiration data (**Figures 1D–F**), which validates the comparison of calorimetry and gas measurements conducted on separate vials. Statistical analyses (one-way ANOVA, all soils combined, $N = 6$) confirmed significant treatment differences in heat and CO_2 output ($P < 0.05$). Although the calorespirometric ratios ranged from 440 to 1,110 kJ per mol CO_2 (**Table 3**), there was a clear linear relationship between heat dissipation and CO_2 generation across all treatments and soils (**Figure 2**), with a slope of 0.86 and an intercept of −0.57 J at 0 μmol CO_2, suggesting an average R_q/R_{CO2} of ∼800 kJ $mol^{-1}CO_2$ for these systems ($R^2 = 0.77$, $P < 0.001$, linear regression not shown in **Figure 2**). However, the mineral paddy soil exhibited a different response pattern to the glucose treatment with substantial heat emissions compared to all other treatments (including glucose in the two other soils) (**Figure 3**), suggesting this system comprised an extreme case. Excluding this potential outlier, the linear fit improved ($R^2 = 0.85$, $P < 0.001$) and the slope changed to 0.65 with

TABLE 1 | Soil and amendment properties.

Soil	Country	Texture	pH	Total C (%)	Total N (%)	Total S (mg g^{-1})	Water-soluble C (mg g^{-1})	Average NOSC of soluble C	ΔG of soluble C (J g^{-1})
Peaty Paddy Soil	Vietnam	Silty clay loam	3.9	9.4 (0.3)	0.33 (0.02)	8.5	0.21 (0.00)	−0.50	1.0
Acid Sulfate Soil	Vietnam	Silt loam	3.5	13.0 (0.1)	0.57 (0.01)	9.8	0.40 (0.01)	−0.56	2.5
Mineral Paddy Soil	Cambodia	Silty clay	5.4	1.6 (0.0)	0.17 (0.00)	0.36	0.16 (0.06)	−0.53	1.3
Amendment	**Acronym**	**Enthalpy of combustion (MJ kg^{-1})**	**pH**	**Total C (%)**	**Total N (%)**	**Total S (mg g^{-1})**	**Water-soluble C (mg g^{-1})**	**Average NOSC of soluble C**	**ΔG of soluble C (J g^{-1})**
Glucose	Gluc	15.6†	n/a	40.0	0.00	0.00	400.0	0.00	1332
Dried rice straw	DS	14.7 (0.1)	6.3	37.3 (0.8)	0.89 (0.10)	0.19 (0.01)	24.9	−0.65	163
Charred rice straw	CS	6.8 (0.7)	9.1	14.6 (0.4)	0.62 (0.02)	0.42 (0.03)	1.6	−0.21	9
Cattle Manure	M	n/a	n/a	40.2 (0.6)	2.40 (0.14)	0.34 (0.01)	20.0	−0.71	134

Values in parentheses denote standard deviation from triplicate measurements where applicable, n/a denotes not analyzed. †Value taken from Herrmann et al. (2014), Supplementary Material.

TABLE 2 | Half-reactions for reduction of terminal electron acceptors (TEA) considered for the respiration calculations with Gibbs free energy (kJ per mol e^-) from Arndt et al. (2013) and stoichiometric relation to oxidized C, assuming complete oxidation to CO_2.

Reaction	ΔG°_{red} (kJ per mol e^-)	mol CO_2 produced per mol TEA consumed
$O_2 + 4H^+ + 4e^- \rightarrow 2H_2O$	−122.7	4/(4-NOSC of C substrate)
$Fe(OH)_3 + 3H^+ + e^- \rightarrow Fe^{2+} + 3H_2O$	−94.7	1/(4-NOSC of C substrate)
$SO_4^{2-} + 9H^+ + 8e^- \rightarrow HS^- + 4H_2O$	−24.0	8/(4-NOSC of C substrate)

an intercept close to 0, suggesting an average R_q/R_{CO2} of 650 kJ $mol^{-1}CO_2$, which is similar to previously reported values for saturated soils (Barros et al., 2016). Also shown in **Figure 2** is the calculated heat output from Equation (1) (open diamond symbols, thin solid regression line), assuming (i) all CO_2 was produced from O_2 consumption and (ii) that the average NOSC of initial soluble C (**Table 3**) is representative of the substrate used. However, O_2-consumption did not match the CO_2-production (**Table 3**), suggesting anaerobic metabolism accounted for 33–62% of the CO_2 production. Thus, we also calculated the heat that would be generated from no-growth aerobic respiration using the measured O_2 consumption data and the oxycaloric equivalent (Equation 1), and plotted this against the measured CO_2 production in **Figure 2** (x symbols, dashed regression line). The deviation between this and the measured data represents heat generating processes that do not consume oxygen, which we interpret as anaerobic metabolic processes. Indeed, we observed a net increase in dissolved Fe and detected methane in all vials (**Table 3**), although the methane production was limited in the peaty paddy soil. Methane production in the mineral paddy soil was more than an order of magnitude higher than in the other two soils. The DS treatment produced the most methane in each soil, followed by Gluc in the peaty paddy and acid sulfate soils and M in the mineral paddy soil. The Fe-dissolution followed the same order as the heat and CO_2 production (control<CS<M<DS<Gluc). Net S removal, an indicator of sulfate reduction, only occurred in the CS, M, and DS treatments in the mineral paddy soil (**Table 3**). In spite of the use of pH 7 TRIS buffer, pH was remarkably lower in the peaty paddy and the acid sulfate soils than in the mineral paddy soil (**Table 4**). In general, pH remained within ±0.5 units of the values measured on day 1 throughout the incubation, with the exception of the M and DS treatments in the mineral paddy soil, which increased by 0.7 and 0.8 pH units respectively from day 1 to day 5.

In order to better understand the causes of variability in metabolic response between the different soils and treatments, we examined the organic matter solubility (**Table 1**) and chemical composition in water extracts from soils and substrates with FT-ICR-MS (**Figure 4**, **Table 5**). All three soils had average NOSC values ∼-0.5 and the amendments ranged from 0 to −0.71 in the order Gluc>CS>DS>M, but due to the large variation in solubility of the amendment C (**Table 1**), the calculated total Gibbs free energy of the added soluble C varied immensely (**Table 1**). Linear regression analyses showed that the amount of added soluble C in complex organic matter (i.e., excluding glucose) was clearly correlated with respiration rate, with an $R^2 = 0.91$ ($P < 0.001$) (**Figure 5A**). Excluding glucose from this analysis is reasonable given it was added in solution and, hence, substrate solubility would not be a limiting factor in this system. Considering the strong correlation with soluble C and that CO_2-production comprised <40% of this pool (**Figure 5C**), we assumed that all CO_2 produced during the incubation originated from the initial soluble C pool, which was comprised of soluble organic matter from the soil plus the soluble portion of the amendment. Thus, we calculated the Gibbs free energy that would have been released by respiration, based on the fraction of total soluble C that had been converted to CO_2, using O_2- and S-consumption and Fe-dissolution to stoichiometrically partition CO_2 production between aerobic, Fe(III), and SO_4^{2-} respiration (which were the only respiration pathways we could approximately constrain in this study) according to values in **Table 2**. This generated a strong correlation between calculated ΔGs and the heat outputs ($R^2 = 0.69$, $P < 0.001$; **Figure 5B**, dashed line), in spite of evidence of other metabolic pathways, such as methanogenesis (**Table 3**) and fermentation, being active to some extent in all soils and treatments. The relationship between ΔGs and heat outputs improved when the glucose treatment was excluded ($R^2 = 0.78$, $P < 0.001$; **Figure 5B**, solid line). Post-experiment analyses of the glucose treated vials showed that no glucose remained in solution after 5 days of incubation, although only a small fraction of the added C (2–3% mol-C/mol-C basis, **Figure 5C**) had been converted to CO_2, indicating fermentation and/or other non-CO_2 generating metabolism must have been active in this treatment.

In contrast to soluble C, there was no correlation between CO_2 or heat production and the initial amount of total C or combustion enthalpy of the materials (data not shown).

DISCUSSION

Our results show that there is a correlation between heat generation and respiration even at non-steady state conditions in heterogeneous systems with complex substrates and a mix of metabolisms. As expected, in systems with mixed aerobic/anaerobic metabolism, the relationship (∼650 kJ per mol CO_2) deviated from the 460 kJ per mol CO_2 that was predicted by Equation (1) using the oxycaloric equivalent, the total CO_2 generation, and the average NOSC of soluble organic C (**Figure 2**). Given the complexity of the systems, we cannot rule out abiotic processes that may have contributed to offsetting either heat or CO_2 production rates, but they are likely to be minor relative to the microbial activity following C addition and re-wetting of soils; Herrmann et al. (2014) did

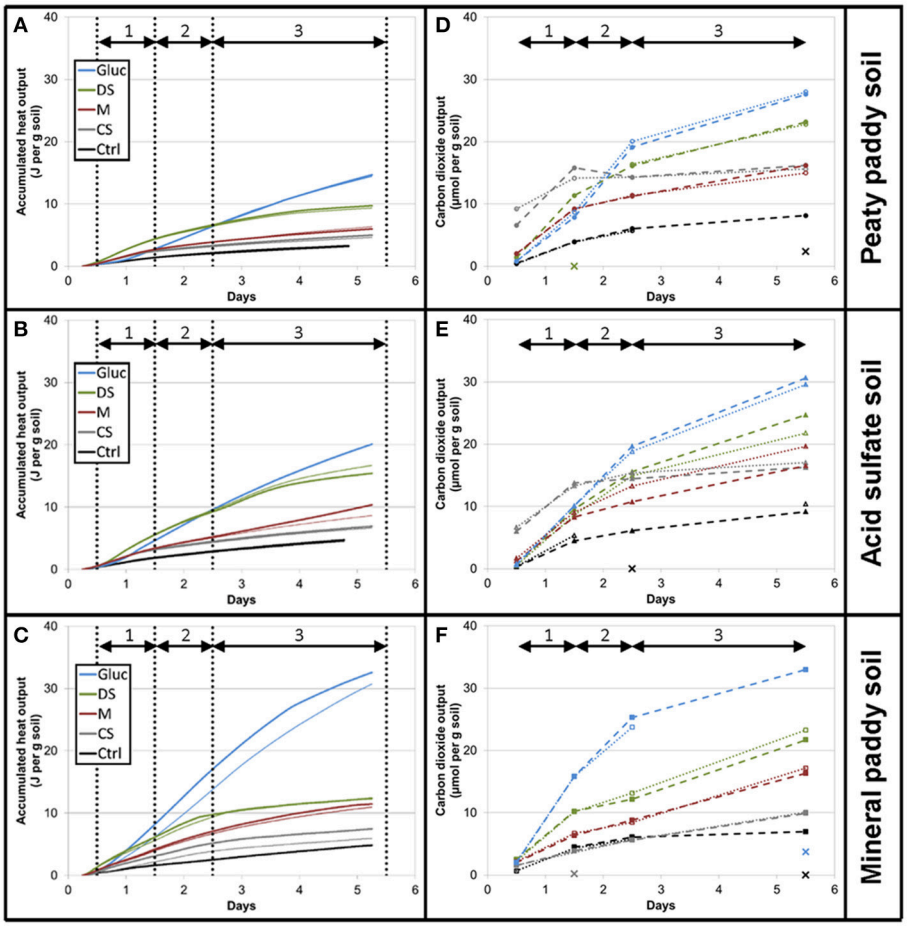

FIGURE 1 | Cumulative heat output **(A–C)** and respiration **(D–F)** for the first 5 days after flooding. Soils from top to bottom: peaty paddy soil **(A,D)**, acid sulfate soil **(B,E),** and mineral paddy soil **(C,F)**. Colors represent treatments: Control, black; CS, gray; M, red; DS, green; Gluc, blue. Duplicate vials are depicted by thick and thin lines. The dashed and dotted lines in the respiration figures **(D–F)** are only intended as guides for the eye as sampling was made on separate vials for each time point (i.e., there is no direct connection between the vials plotted within the same series other than that they belong to the same treatment). Data points marked with X denote gas samples where the GC measurements failed. Vertical dotted lines in the heat figures **(A–C)** indicate sampling times for the respiration measurements. Arrows denote intervals (1–3) used for calculating rates between sampling points.

not observe any abiotic heat dissipation in gamma-irradiated sterilized soils amended with glucose. Thus, the deviation from predicted values must be attributed to anaerobic metabolism, as the R_q values calculated from O_2-consumption were even lower than those predicted by Equation (1) (**Figure 2**). Given the generally lower enthalpy dissipation per unit biomass formed for fermentation and anaerobic respiration compared to aerobic respiration (von Stockar and Liu, 1999), this may seem surprising. However, it is important to distinguish between the relationship of heat to anabolic reactions, as examined in von Stockar and Liu (1999), and that of heat to catabolic reactions, as examined here and in other calorespirometry studies (Hansen et al., 2004). Therefore, to elucidate the influence of anaerobiosis on the calorespirometric ratios, we divided the incubation period into an initial, aerobic phase (sampling points 0.5–1.5 days) and a mixed aerobic/anaerobic phase (1.5–5.5 days) and calculated the deviation of measured R_q/R_{CO2} from those predicted by Equation (1) and the average NOSC in the initial soluble C pool (**Figure 6**). This revealed that the measured R_q/R_{CO2} in the initial phase in most cases was close to or lower than that predicted from Equation (1), which indicates growth (i.e., endothermic anabolism) and dominance of aerobic catabolism, although minor contributions from early anaerobiosis cannot be ruled out. After 1.5 days, the measured R_q/R_{CO2} values were always higher (and often much higher) than those predicted from Equation (1) (**Figure 6**). Thus, in this experiment, increasing contribution from anaerobic metabolism resulted in increasing R_q/R_{CO2} values, which is in contradiction to predictions based on heat dissipation relative to biomass yield (von Stockar and Liu, 1999) and expectations from thermodynamic calculations of CO_2-yielding fermentation and anaerobic respiration reactions (Hansen et al., 2004). However, an R_q/R_{CO2} higher than predicted by Equation (1), can be explained in several ways:

TABLE 3 | Net change in dissolved Fe and S concentrations, total methane production, total O_2-consumption, and calorespirometric ratios for the 5 days of incubation.

Soil	Treatment	ΔFe (μmol g^{-1}soil)	ΔS (μmol g^{-1}soil)	CH_4 (nmol g^{-1}soil)	$-\Delta O_2$ (μmol g^{-1}soil)	ΔCO_2 (μmol g^{-1}soil)	R_q/R_{CO2} (kJ $mol^{-1}CO_2$)
Peaty paddy soil	Control	1.4	1.1	0.7	5.8	7.7	443
	CS	2.0	0.4	6.5	4.7	8.0	607
	M	4.3	1.4	6.1	6.4	13.6	469
	DS	6.2	1.6	19.9	11.6	21.6	468
	Gluc	12.6	2.5	19.5	12.6	27.0	567
Acid sulfate soil	Control	6.5	0.7	12.0	5.8	9.4	536
	CS	6.2	2.8	23.1	6.9	10.3	669
	M	10.4	5.0	35.5	7.4	16.6	579
	DS	15.8	8.0	89.3	11.4	22.7	771
	Gluc	26.3	5.7	54.0	15.1	29.4	725
Mineral paddy soil	Control	0.6	0.5	0.2	3.0	6.3	770
	CS	0.9	−0.7	34.4	4.5	8.4	828
	M	5.9	−1.4	1080	12.1	14.7	795
	DS	17.4	−1.4	3300	14.1	20.1	623
	Gluc	44.0	0.3	149	13.9	30.9	1103

Reported values are differences between averages of duplicate measurements on day 5.5 and averages of duplicate measurements on day 0.5 of the incubation (different vials at days 0.5 and 5.5).

- *Incomplete metabolic oxidation of organic substrates to CO_2.* This is the case for fermentation, which is accomplished through disproportionation of a substrate into smaller molecules, with variable thermodynamic implications. For example, glucose fermented to lactate leads to a standard enthalpy change of −120 kJ per mol glucose (i.e., 20 kJ of dissipated heat per mol C fermented), with no simultaneous CO_2-production. Hence, R_q/R_{CO2} is infinitely large for this process. In contrast, fermentation of glucose to ethanol produces 2 mol CO_2 per mol glucose plus H_2 and ethanol, a process that at standard state releases 37.2 kJ heat per mol CO_2. This is an order of magnitude less than the 468 kJ per mol CO_2 released for glucose oxidation with O_2. However, the subsequent use of H_2 (and/or CO_2) in anoxic systems, for example by autotrophic methanogens, can be highly exothermic (von Stockar and Liu, 1999). Thus, although fermentation is a low-enthalpy metabolic process in terms of heat dissipation per unit biomass formed, the heat per unit CO_2 can still be higher than for aerobic respiration. The relationship between the two is dependent on the fermentation pathway and the subsequent fate of the metabolites. Incomplete oxidation of substrates is also common for anaerobic respiration (Coates et al., 1999; Detmers et al., 2001; Heidelberg et al., 2004), again potentially resulting in higher heat dissipation per unit CO_2 even if the heat dissipation per unit biomass yield is lower.
- *Autotrophic metabolism*. Microorganisms that use CO_2 for synthesizing biomass still need to dissipate heat from their catabolic processes, which can be highly exothermic (e.g., methanogenic autotrophy) (von Stockar and Liu, 1999). Thus, chemoautotrophic metabolism by itself would yield a negative calorespirometric ratio. However, in a mixed metabolic environment, where CO_2 is simultaneously produced by heterotrophs and consumed by autotrophs, the net effect will be seen as an increase in R_q/R_{CO2} relative to a system with only heterotrophic metabolic processes (as that considered in Equation 1).
- *Other "hidden" metabolic cycles & recycling of metabolites*. In addition to fermentation and autotrophy, chemolithoheterotrophic strategies (inorganic energy source, organic biomass source) also deviate from R_q/R_{CO2} values predicted by Equation (1), as they generate (some) heat without producing CO_2 or consuming O_2.
- *Utilization of more reduced compounds than the average available substrate.* This is technically not an exception from the rule represented in Equation (1), but a matter of knowing which substrate was used for the metabolic reaction, which is difficult in complex systems. Because R_q/R_{CO2} depends on the oxidation state of the substrate, deviations from the predicted value in a fully aerobic system can be interpreted as an indication that a more reduced (higher R_q/R_{CO2}) or more oxidized (lower R_q/R_{CO2}) substrate than predicted was used (Barros et al., 2016).

With the experimental approach used here, we cannot fully decipher which of these processes led to the high R_q/R_{CO2} values, but all could have contributed to some extent. In the glucose treatment, fermentation and/or respiration with incomplete oxidation must have occurred as the CO_2 production only accounted for 2–3% of the removed glucose (mol-C/mol-C basis). It is likely that fermentation was also active in the other treatments, although we cannot confirm this without post-experimental analyses of the soluble C fraction. The dissolution of Fe (all soils and treatments) and disappearance of S (some soils and treatments) from solution, strongly suggests that one or more

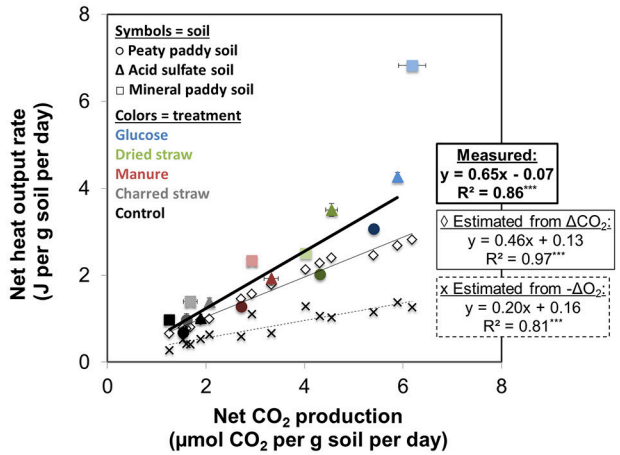

FIGURE 2 | Average respiration rate (μmol CO_2 per g soil per day) during 5 days of incubation, plotted against the average heat output rate (J per g soil per day) for the same period. Soils are represented by different symbols and shades (light □ = mineral paddy soil, medium Δ = acid sulfate soil, dark ○ = peaty paddy soil) and the colors correspond to treatments: Control, black; CS, gray; M, red; DS, green; Gluc, blue. Error bars denote standard error of the mean of the duplicates. Open diamonds show the predicted heat dissipation (Equation 1) if all CO_2 had been produced from aerobic respiration (assuming no-growth). Crosses show predicted heat output from aerobic respiration based on O_2-consumption and the oxycaloric equivalent (455 kJ mol^{-1} O_2) plotted against measured CO_2-production. Lines indicate regression fits (with equations and R^2-values given in the figure) for calculated aerobic respiration heat output (thin solid line and dashed line for CO_2-based and O_2-based calculations, respectively) and measured respiration and heat output (thick solid line), excluding the glucose treatment in the mineral paddy soil.

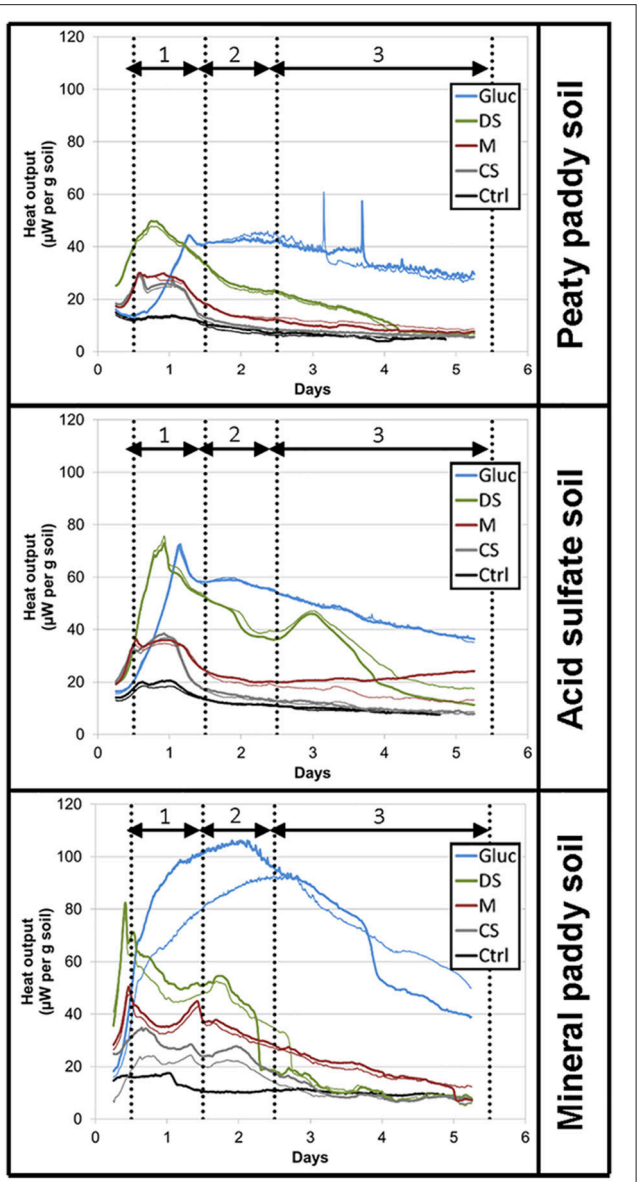

FIGURE 3 | Heat flow (μW per g soil) over the course of the 5-day incubation. Colors represent treatments: Control, black; CS, gray; M, red; DS, green; Gluc, blue. Duplicate vials are depicted by thick and thin lines. Vertical dotted lines indicate sampling times for the respiration measurements.

anaerobic respiration pathways were active and contributed to heat release without proportional CO_2 production (predicted by Equation 1), if the substrate was not completely oxidized. Both Fe and sulfate reduction are further subject to recycling of reaction intermediates and products (Weber et al., 2006; Canfield et al., 2010; Holler et al., 2011; Pester et al., 2012; Friedrich and Finster, 2014; Hansel et al., 2015; Berg et al., 2016), which constitute "hidden" or "cryptic" cycles when net measurements of total concentrations are used. Similarly, the detection of methane in all vials suggests that recycling of CO_2 to methane may have contributed to lowering the net CO_2 production, while emitting more heat than that expected from heterotrophic metabolism. However, we cannot partition between methane produced from acetate (or other organic compounds) and that produced from CO_2 with the simplified approach used here and, thus, cannot reliably estimate heat generation from methanogenesis.

In complex systems, such as those examined here, it is impossible to determine exactly what substrate(s) were used at what time. However, the correlation between CO_2 production and the initially available soluble C, as well as that between produced heat and the calculated ΔG released by aerobic and anaerobic (Fe(III), SO_4^{2-}) respiration of C from this pool (**Figure 5**), strongly suggests that the utilized substrates were in the soluble C pool. Even so, it is likely that the substrate used in the metabolic reactions (both aerobic and anaerobic) differed in NOSC from the average NOSC of the water-soluble C, as some compounds are more suitable for direct metabolism than others. Linear correlation analyses of produced CO_2 relative to the estimated amount of different types of compounds that were present in the initial soluble C pool, provided strongest fits for the carbohydrate- and aminosugar-like groups (**Table 5**). These groups contain compounds that are commonly used substrates and that on average have NOSC values similar to the overall average for the soluble C. However, protein-like and (although less strongly) lipid-like and unsaturated hydrocarbon types of compounds also correlated with CO_2, suggesting substrates with a considerably lower NOSC than the overall average were also metabolized. This explains, in part, the higher R_q/R_{CO2}

TABLE 4 | pH (average of duplicate vials ± standard deviation) in solution after 1.5 and 5.5 days of incubation, respectively.

Soil	Treatment	pH (0.5 days)	pH (5.5 days)
Peaty paddy soil	Control	4.1 ± 0.1	4.1†
	CS	5.2 ± 0.2	5.0 ± 0.0
	M	4.3 ± 0.1	4.8 ± 0.0
	DS	4.5†	4.8 ± 0.0
	Gluc	4.1†	4.0 ± 0.0
Acid sulfate soil	Control	3.5 ± 0.0	4.0 ± 0.0
	CS	4.8 ± 0.2	4.7 ± 0.0
	M	4.4 ± 0.3	4.7 ± 0.1
	DS	n/a	5.0 ± 0.4
	Gluc	4.3†	4.4 ± 0.0
Mineral paddy soil	Control	5.9 ± 0.3	6.2 ± 0.3
	CS	7.0 ± 0.0	6.9 ± 0.1
	M	6.3†	7.0 ± 0.0
	DS	6.1 ± 0.1	6.9 ± 0.1
	Gluc	5.5 ± 0.3	5.2 ± 0.1

n/a = not analyzed. †Only one measurement taken.

ratios observed than predicted in this experiment. Indeed, using Equation (1) we can calculate the NOSC that would be required to generate the measured R_q/R_{CO2} values with purely aerobic respiration, and arrive at values ranging from 0.1 to −3.3 (excluding the glucose treatment in the mineral paddy soil), with most values falling below −1. However, there were no molecules identified in any of the soil or amendment water extracts with a NOSC below −1.83 (minimum NOSC ranged from −1.7 to −1.83), which corresponds to a R_q/R_{CO2} ratio of 663 kJ per mol CO_2 i.e., almost identical to the 650 kJ per mol CO_2 we arrived at with the linear regression of measured values (**Figure 2**). Therefore, we can conclude that anaerobic metabolism must have contributed to off-setting the R_q/R_{CO2} from the prediction, as shown above, as it is unlikely that only the most reduced substrates were used. Except for the glucose treatment in the mineral paddy soil, the calorespirometric ratios obtained in our study are reasonable and within range of what can be expected even in purely aerobic systems with the identified soluble substrates. The extreme R_q/R_{CO2} value obtained for the glucose treatment in the mineral paddy soil would have required a substrate with a NOSC < -4 if only aerobic respiration was active. Thus, low CO_2-yielding anaerobic metabolism, such as fermentation and methanogenesis from CO_2, must have occurred in this treatment.

We conclude that much of the variability between soils and treatments in overall microbial response to flooding can be explained by organic substrate solubility and the oxidation state of water soluble C (a corollary to thermodynamic yield and viability of microbial C oxidation). However, at a more detailed level, we observed highly variable responses in the types of metabolic processes that were stimulated by the different amendments, particularly in the mineral paddy soil. This could potentially be attributed to the differences in pH (**Table 4**) or variabilities in the microbial community composition among the soils. Given the overall higher metabolic activity (respiration and heat production) in glucose-amended vials, which is consistent with its thermodynamic and kinetic favorability for metabolic reactions, it is intriguing that both the dried straw and manure treatments generated a higher methane-production than the glucose treatment (**Table 3**). It is possible that the lower pH in the glucose treatment (**Table 4**) contributed to this effect, as methanogens are most active at circumneutral pH (Oh et al., 2003; Liu et al., 2008). It is also possible that the first pulse of aerobic respiration depleted the smaller pool of soluble and favorable organic substrates available in the dried straw and manure treatments, while generating enough CO_2 to allow autotrophic methanogens to compete with heterotrophs (for H_2); the first respiration pulse occurred earlier in these two treatments than in the glucose treatment (**Figure 3**). More surprising, perhaps, is that we only observed indications of sulfate reduction in the charred straw, dried straw, and manure treatments of the mineral paddy soil, which had the lowest initial sulfur concentration (**Table 1**) and the highest pH (**Table 4**). Further, the estimated proportion of anaerobically generated CO_2 produced by sulfate reduction (0.27, 0.56, and 0.56 μmol CO_2 per g soil and day for CS, M, and DS, respectively) was larger than that of iron reduction (0.04, 0.25, and 0.40 μmol CO_2 per g soil and day) in all three treatments in this soil. It is likely that the gross rates of iron and sulfate reduction were higher than those measured by net changes in total dissolved Fe and S concentrations, as considerable recycling of Fe(II) and S redox intermediates is known to occur (Weber et al., 2006; Canfield et al., 2010; Holler et al., 2011; Pester et al., 2012; Friedrich and Finster, 2014; Hansel et al., 2015; Berg et al., 2016). Therefore, future work that includes more detailed measurements of Fe and S speciation [e.g., Fe(III) mineralogy, soluble Fe^{2+}, HS^-, and SO_4^{2-} concentrations], would elucidate whether the unexpected absence of sulfate reduction in the peaty paddy and acid sulfate soils is real or hidden due to the recycling of sulfur. Likewise, such measurements would help resolve the reasons for the high methanogen-activity and apparent dominance of sulfate reduction over Fe-reduction after amendment with organic substrates in the mineral paddy soil.

In summary, this experiment showed that the microbial activity in soils (heat release and respiration) is strongly correlated with the availability and oxidation state of soluble organic C, indicating that the substrates used for metabolic reactions are found in this pool. This enhances the possibilities to use thermodynamic calculations to predict and evaluate metabolic processes in environments with complex organic matter, as long as the stoichiometric composition of the soluble organic C pool can be determined (e.g., by FT-ICR-MS). Our results further indicated that the chemical composition of the soluble C added with the amendments initiated divergent anaerobic respiration behavior, impacting methane production and the partitioning of elements between soil solid phase and solution. This variability led to non-uniform stimulation of carbon dioxide production per unit carbon added and off-set the calorespirometric ratios (R_q/R_{CO2}) from predicted values for aerobic respiration; but there was still a strong linear

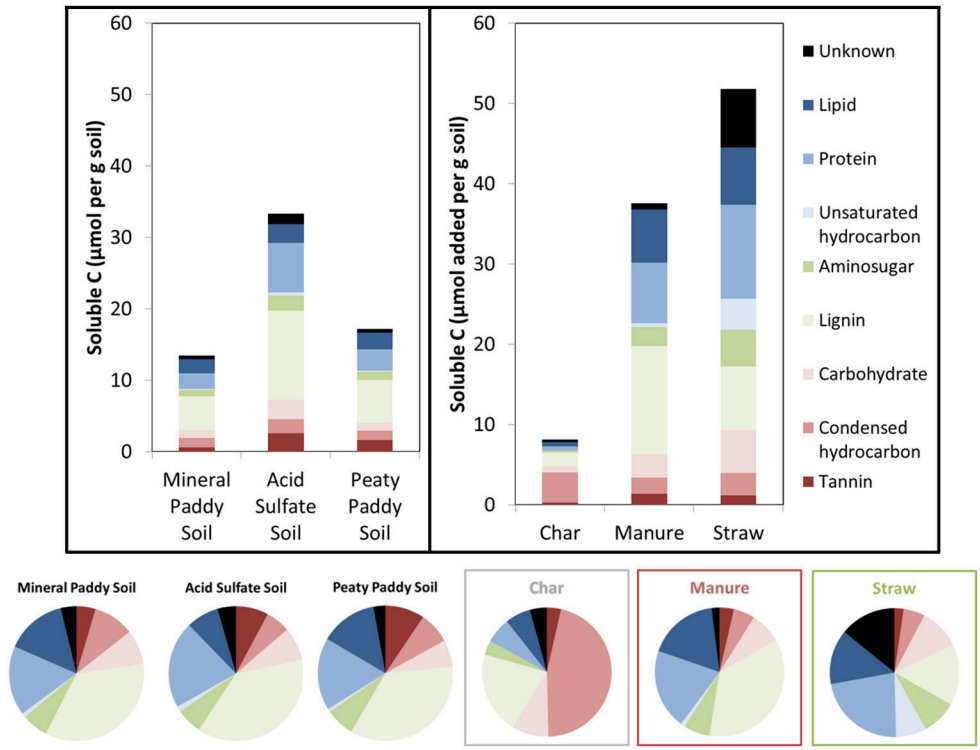

FIGURE 4 | Initial total water soluble C (µmol per g soil) in soils and added substrate materials (bars). Pie charts and bar colors show the relative distribution of compound classes determined from H/C and O/C ratios in molecule formulas identified by FT-ICR-MS.

TABLE 5 | Initially available substrates (µmol C g^{-1} soil) in solutions, estimated from relative distribution among different compound classes, based on H/C and O/C ratios (Kim et al., 2003; Šantl-Temkiv et al., 2013; Hodgkins et al., 2014; Tfaily et al., 2015) in molecular formulas identified with FT-ICR-MS, in water extracts and the total amount of water soluble C per g of soil.

Soil	Treatment	Tannin	Condensed hydrocarbon	Carbohydrate	Lignin	Amino-sugar	Unsaturated hydrocarbon	Protein	Lipid	Unknown
Peaty paddy soil	Control	1.6	1.3	1.1	6.0	1.2	0.1	3.0	2.3	0.5
	CS	1.9	5.1	1.9	7.7	1.5	0.1	3.5	2.9	0.8
	M	3.0	3.3	4.1	19.5	3.6	0.6	10.5	9.0	1.3
	DS	2.8	4.1	6.5	13.9	5.7	4.1	14.6	9.5	7.8
Acid sulfate soil	Control	2.6	2.0	2.7	12.6	2.1	0.4	7.0	2.6	1.5
	CS	2.9	5.7	3.4	14.2	2.4	0.4	7.5	3.1	1.8
	M	4.0	4.0	5.6	26.0	4.5	0.8	14.5	9.2	2.2
	DS	3.8	4.7	8.0	20.5	6.6	4.4	18.7	9.7	8.8
Mineral paddy soil	Control	0.6	1.3	1.1	4.7	0.9	0.1	2.2	2.0	0.5
	CS	0.9	5.1	1.9	6.4	1.1	0.1	2.8	2.5	0.9
	M	2.0	3.3	4.1	18.1	3.3	0.6	9.8	8.6	1.3
	DS	1.8	4.1	6.5	12.6	5.4	4.1	13.9	9.1	7.8
R^2 (CO_2)		0.33	ns	**0.96**	0.39	**0.98**	**0.80**	**0.93**	**0.82**	n/a
NOSC		0.09	0.41	−0.42	−0.44	−0.64	−0.62	−0.97	−1.37	n/a

Also noted are the R^2-values for significant linear regressions of the substrate amount with total net CO_2 production (µmol C g^{-1} soil) for the 5 day incubation period. R^2 values in bold have $P < 0.001$, otherwise $P < 0.05$, and ns denotes non-significant correlations. Note that the glucose treatment was excluded from these regression analyses.

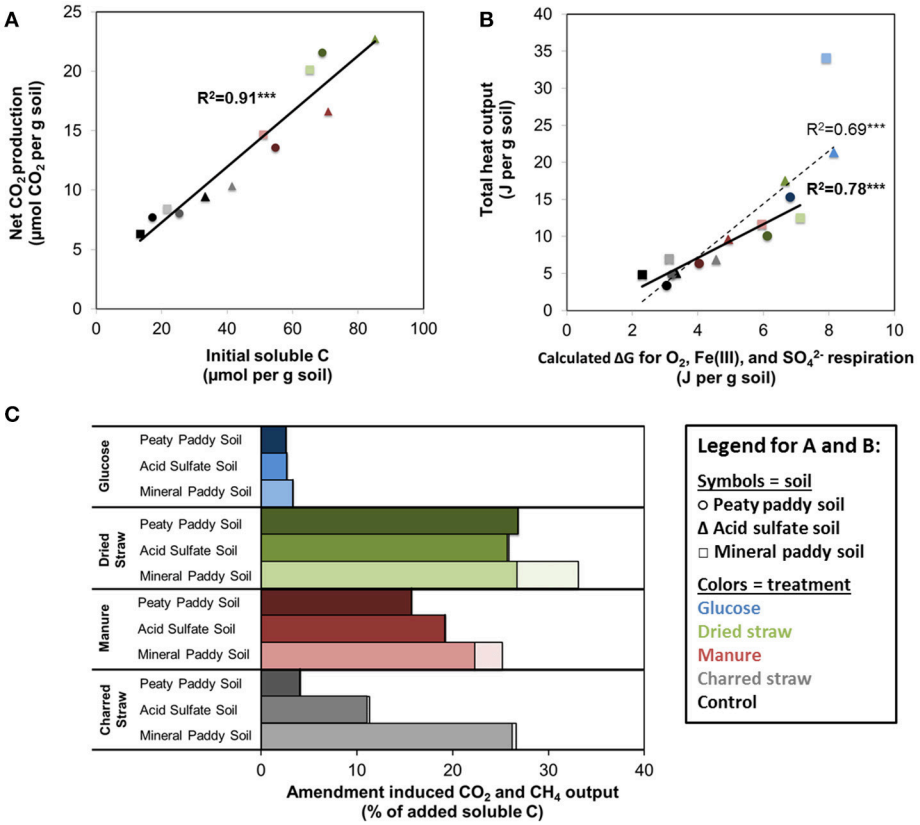

FIGURE 5 | Relationship between **(A)** initial amount of water soluble C and total respiration (µmol per g soil), excluding glucose treatment, and **(B)** total heat dissipation during the incubation (J per g soil) and the calculated Gibbs free energy of respired C, calculated from average NOSC of initial water soluble C and the fraction of this C that was respired with O_2, Fe(III), and SO_4^{2-} (assuming NOSC-unbiased utilization and complete oxidation to CO_2, using stoichiometric balances and values from **Table 1**). In both **(A,B)** soils are represented by different symbols and shades (light □ = mineral paddy soil, medium Δ = acid sulfate soil, dark ○ = peaty paddy soil) and the colors correspond to treatments: Control, black; CS, gray; M, red; DS, green; Gluc, blue. Linear regression fits and R^2-values are shown in solid and bold for fits excluding glucose and dashed, normal font **(B)** for fit including glucose. **(C)** shows total amendment induced output of CO_2 (solid) and CH_4 (light, shaded) as % of added water soluble C.

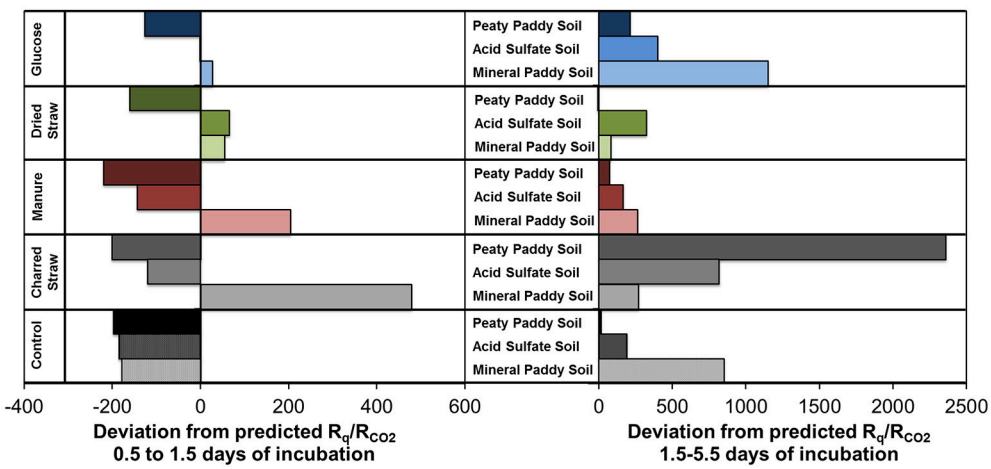

FIGURE 6 | Deviations of measured R_q/R_{CO2}, from those calculated by Equation (1) using NOSC of initial soluble C in soils and amendments, during the first day of incubation **(Left)** and the subsequent 4 days **(Right)**. Negative values indicate the measured R_q/R_{CO2} was lower than the predicted value.

correlation between energy release and respiration rate. We conclude that measurements which allow for energy and major elemental mass balances to be established can provide insights into the partitioning between main metabolic functions that govern C, nutrient, and contaminant fate in highly complex and transitory systems, such as paddy soils after flooding. Continued investigations to this end would be useful in order to further enlighten the mechanisms behind the observed variability. A deepened understanding of these mechanisms and their dependence on initial soil and organic matter properties will facilitate the development of simplified models for predicting the environmental outcomes of flooding.

AUTHOR CONTRIBUTIONS

This study was conceived and designed by KB in consultation with SF and AMH. Field sampling was conducted by MS with assistance from KB and AMH. Experimental work was conducted by KB with assistance from MS and AMH. MT performed the FT-ICR-MS analyses and assisted with the data processing and interpretation. KB processed the experimental data and wrote the manuscript with assistance from all co-authors.

FUNDING

This work was funded by the Swedish Foundation for International Cooperation in Research and Higher Education (STINT Initiative Grant IB2013-5275). KB was supported in part by the Marcus and Amalia Wallenberg Foundation, Sweden, and in part by the SLAC SFA research program (SLAC FWP 10094), which is funded by the U.S. Department of Energy (DOE) Subsurface Biogeochemical Research (SBR) program within the Office of Biological and Environmental Research. Work by SF on this project was supported by US Department of Energy, Office of Biological and Environmental Research, Terrestrial Ecosystem Program (Award Number DE-FG02-13ER65542) and Subsurface Biogeochemistry Program (Award Number DE-SC0016544). AMH was supported by the Swedish Research Council for Environment, Agricultural Sciences and Spatial Planning (Formas 2012-530). MS was funded through the U.S. National Science Foundation Graduate Research Fellowship Program (Grant Number DGE-114747). A portion of the research (FT-ICR-MS analysis) was performed using EMSL, a DOE Office of Science User Facility sponsored by the Office of Biological and Environmental Research under proposal ID 49333.

ACKNOWLEDGMENTS

We are very grateful to Professor Ngo Ngoc Hung and Do Thi Xuan at Can Tho University, Vietnam and Resource Development International, Cambodia for access to field sites and sampling assistance. Many thanks also to Shikha Avancha, Lilia Barragan, Guangchao Li, and Douglas Turner for laboratory assistance and analytical measurements.

REFERENCES

Arcand, M. M., Levy-Booth, D. J., and Helgason, B. L. (2017). Resource legacies of organic and conventional management differentiate soil microbial carbon use. *Front. Microbiol.* 8:2293. doi: 10.3389/fmicb.2017.02293

Arndt, S., Jørgensen, B. B., LaRowe, D. E., Middelburg, J., Pancost, R., and Regnier, P. (2013). Quantifying the degradation of organic matter in marine sediments: a review and synthesis. *Earth Sci. Rev.* 123, 53–86. doi: 10.1016/j.earscirev.2013.02.008

Baldwin, D. S., and Mitchell, A. M. (2000). The effects of drying and re-flooding on the sediment and soil nutrient dynamics of lowland river–floodplain systems: a synthesis. *Regul. Rivers* 16, 457–467. doi: 10.1002/1099-1646(200009/10)16:5<457::AID-RRR597>3.0.CO;2-B

Barros, N., Hansen, L. D., Piñeiro, V., Pérez-Cruzado, C., Villanueva, M., Proupín, J., et al. (2016). Factors influencing the calorespirometric ratios of soil microbial metabolism. *Soil Biol. Biochem.* 92(Suppl. C), 221–229. doi: 10.1016/j.soilbio.2015.10.007

Barros, N., Piñeiro, V., and Hansen, L. D. (2015). Calorespirometry: a novel tool to assess the effect of temperature on soil organic matter decomposition. *Thermochim. Acta* 618(Suppl. C), 15–17. doi: 10.1016/j.tca.2015.09.005

Barros Pena, N., Merino García, A., Martín Pastor, M., and Pérez Cruzado, C. (2014). Changes in soil organic matter in a forestry chronosequence monitored by thermal analysis and calorimetry. *SJSS* 4, 239–253. doi: 10.3232/SJSS.2014.V4.N3.03

Berg, J. S., Michellod, D., Pjevac, P., Martinez-Perez, C., Buckner, C. R. T., Hach, P. F., et al. (2016). Intensive cryptic microbial iron cycling in the low iron water column of the meromictic Lake Cadagno. *Environ. Microbiol.* 18, 5288–5302. doi: 10.1111/1462-2920.13587

Bodelier, P. L., Bär-Gilissen, M.-J., Meima-Franke, M., and Hordijk, K. (2012). Structural and functional response of methane-consuming microbial communities to different flooding regimes in riparian soils. *Ecol. Evol.* 2, 106–127. doi: 10.1002/ece3.34

Bölscher, T., Wadsö, L., Börjesson, G., and Herrmann, A. M. (2016). Differences in substrate use efficiency: impacts of microbial community composition, land use management, and substrate complexity. *Biol. Fertil. Soils* 52, 547–559. doi: 10.1007/s00374-016-1097-5

Boye, K., Noël, V., Tfaily, M. M., Bone, S. E., Williams, K. H., Bargar, J. R., et al. (2017). Thermodynamically controlled preservation of organic carbon in floodplains. *Nat. Geosci.* 10, 415–419. doi: 10.1038/ngeo2940

Burns, A., and Ryder, D. S. (2001). Response of bacterial extracellular enzymes to inundation of floodplain sediments. *Freshw. Biol.* 46, 1299–1307. doi: 10.1046/j.1365-2427.2001.00750.x

Canfield, D. E., Stewart, F. J., Thamdrup, B., De Brabandere, L., Dalsgaard, T., Delong, E. F., et al. (2010). A cryptic sulfur cycle in oxygen-minimum–zone waters off the Chilean Coast. *Science* 330, 1375–1378. doi: 10.1126/science.1196889.

Coates, J. D., Ellis, D. J., Gaw, C. V., and Lovley, D. R. (1999). Geothrix fermentans gen. nov., sp. nov., a novel Fe (III)-reducing bacterium from a hydrocarbon-contaminated aquifer. *Int. J. Syst. Evol. Microbiol.* 49, 1615–1622.

Corstanje, R., and Reddy, K. R. (2004). Response of biogeochemical indicators to a drawdown and subsequent reflood. *J. Environ. Qual.* 33, 2357–2366. doi: 10.2134/jeq2004.2357

Detmers, J., Brüchert, V., Habicht, K. S., and Kuever, J. (2001). Diversity of sulfur isotope fractionations by sulfate-reducing prokaryotes. *Appl. Environ. Microbiol.* 67, 888–894. doi: 10.1128/AEM.67.2.888-894.2001

Fierer, N., and Schimel, J. P. (2003). A proposed mechanism for the pulse in carbon dioxide production commonly observed following the rapid rewetting of a dry soil. *Soil Sci. Soc. Am. J.* 67, 798–805. doi: 10.2136/sssaj2003.0798

Friedrich, M. W., and Finster, K. W. (2014). How sulfur beats iron. *Science* 344, 974–975. doi: 10.1126/science.1255442

Göransson, H., Godbold, D. L., Jones, D. L., and Rousk, J. (2013). Bacterial growth and respiration responses upon rewetting dry forest soils: impact of drought-legacy. *Soil Biol. Biochem.* 57, 477–486. doi: 10.1016/j.soilbio.2012.08.031

Hansel, C. M., Lentini, C. J., Tang, Y., Johnston, D. T., Wankel, S. D., and Jardine, P. M. (2015). Dominance of sulfur-fueled iron oxide reduction in low-sulfate freshwater sediments. *ISME J.* 9, 2400–2412. doi: 10.1038/ismej.2015.50

Hansen, L. D., MacFarlane, C., McKinnon, N., Smith, B. N., and Criddle, R. S. (2004). Use of calorespirometric ratios, heat per CO2 and heat per O2, to quantify metabolic paths and energetics of growing cells. *Thermochim. Acta* 422, 55–61. doi: 10.1016/j.tca.2004.05.033

Heidelberg, J. F., Seshadri, R., Haveman, S. A., Hemme, C. L., Paulsen, I. T., Kolonay, J. F., et al. (2004). The genome sequence of the anaerobic, sulfate-reducing bacterium *Desulfovibrio vulgaris* Hildenborough. *Nat. Biotechnol.* 22:554. doi: 10.1038/nbt959

Herrmann, A. M., and Bölscher, T. (2015). Simultaneous screening of microbial energetics and CO2 respiration in soil samples from different ecosystems. *Soil Biol. Biochem.* 83(Suppl. C), 88–92. doi: 10.1016/j.soilbio.2015.01.020

Herrmann, A. M., Coucheney, E., and Nunan, N. (2014). Isothermal Microcalorimetry provides new insight into terrestrial carbon cycling. *Environ. Sci. Technol.* 48, 4344–4352. doi: 10.1021/es403941h

Hodgkins, S. B., Tfaily, M. M., McCalley, C. K., Logan, T. A., Crill, P. M., Saleska, S. R., et al. (2014). Changes in peat chemistry associated with permafrost thaw increase greenhouse gas production. *Proc. Natl. Acad. Sci. U.S.A.* 111, 5819–5824. doi: 10.1073/pnas.1314641111

Holler, T., Wegener, G., Niemann, H., Deusner, C., Ferdelman, T. G., Boetius, A., et al. (2011). Carbon and sulfur back flux during anaerobic microbial oxidation of methane and coupled sulfate reduction. *Proc. Natl. Acad. Sci. U.S.A.* 108, E1484–E1490. doi: 10.1073/pnas.1106032108

Jin, Q., and Bethke, C. M. (2005). Predicting the rate of microbial respiration in geochemical environments. *Geochim. Cosmochim. Acta* 69, 1133–1143. doi: 10.1016/j.gca.2004.08.010

Kim, S., Kramer, R. W., and Hatcher, P. G. (2003). Graphical method for analysis of ultrahigh-resolution broadband mass spectra of natural organic matter, the Van Krevelen Diagram. *Anal. Chem.* 75, 5336–5344. doi: 10.1021/ac034415p

Koch, B. P., and Dittmar, T. (2006). From mass to structure: an aromaticity index for high-resolution mass data of natural organic matter. *Rapid Commun. Mass Spectr.* 20, 926–932. doi: 10.1002/rcm.2386

Kujawinski, E. B., and Behn, M. D. (2006). Automated analysis of electrospray ionization fourier transform ion cyclotron resonance mass spectra of natural organic matter. *Anal. Chem.* 78, 4363–4373. doi: 10.1021/ac0600306

LaRowe, D. E., and Van Cappellen, P. (2011). Degradation of natural organic matter: a thermodynamic analysis. *Geochim. Cosmochim. Acta* 75, 2030–2042. doi: 10.1016/j.gca.2011.01.020

Liu, C. F, Yuan, X. Z., Zeng, G. M., Li, W. W., and Li, J. (2008). Prediction of methane yield at optimum pH for anaerobic digestion of organic fraction of municipal solid waste. *Bioresour. Technol.* 99, 882–888. doi: 10.1016/j.biortech.2007.01.013

Liu, J. S., Marison, I. W., and von Stockar, U. (2001). Microbial growth by a net heat up-take: a calorimetric and thermodynamic study on acetotrophic methanogenesis by Methanosarcina barkeri. *Biotechnol. Bioeng.* 75, 170–180. doi: 10.1002/bit.1176

Meisner, A., Bååth, E., and Rousk, J. (2013). Microbial growth responses upon rewetting soil dried for four days or one year. *Soil Biol. Biochem.* 66, 188–192. doi: 10.1016/j.soilbio.2013.07.014

Newman, S., and Pietro, K. (2001). Phosphorus storage and release in response to flooding: implications for Everglades stormwater treatment areas. *Ecol. Eng.* 18, 23–38. doi: 10.1016/S0925-8574(01)00063-5

Oh, S. E., Van Ginkel, S., and Logan, B. E. (2003). The relative effectiveness of pH control and heat treatment for enhancing biohydrogen gas production. *Environ. Sci. Technol.* 37, 5186–5190. doi: 10.1021/es034291y

Ozuolmez, D., Na, H., Lever, M., Kjeldsen, K., Jørgensen, B., and Plugge, C. (2015). Methanogenic archaea and sulfate reducing bacteria co-cultured on acetate: teamwork or coexistence? *Front. Microbiol.* 6:492. doi: 10.3389/fmicb.2015.00492

Pester, M., Knorr, K. H., Friedrich, M., Wagner, M., and Loy, A. (2012). Sulfate-reducing microorganisms in wetlands – fameless actors in carbon cycling and climate change. *Front. Microbiol.* 3:72. doi: 10.3389/fmicb.2012.00072

Postma, D., and Jakobsen, R. (1996). Redox zonation: equilibrium constraints on the Fe (III)/SO4-reduction interface. *Geochim. Cosmochim. Acta* 60, 3169–3175. doi: 10.1016/0016-7037(96)00156-1

Roden, E. E., and Jin, Q. (2011). Thermodynamics of microbial growth coupled to metabolism of glucose, ethanol, short-chain organic acids, and hydrogen. *Appl. Environ. Microbiol.* 77, 1907–1909. doi: 10.1128/AEM.02425-10

Shi, A., and Marschner, P. (2014). Drying and rewetting frequency influences cumulative respiration and its distribution over time in two soils with contrasting management. *Soil Biol. Biochem.* 72, 172–179. doi: 10.1016/j.soilbio.2014.02.001

Stubbins, A., Spencer, R. G. M., Chen, H., Hatcher, P. G., Mopper, K., Hernes, P. J., et al. (2010). Illuminated darkness: molecular signatures of Congo River dissolved organic matter and its photochemical alteration as revealed by ultrahigh precision mass spectrometry. *Limnol. Oceanogr.* 55, 1467–1477. doi: 10.4319/lo.2010.55.4.1467

Šantl-Temkiv, T., Finster, K., Dittmar, T., Hansen, B. M., Thyrhaug, R., Nielsen, N. W., et al. (2013). Hailstones: a window into the microbial and chemical inventory of a storm cloud. *PLoS ONE* 8:e53550. doi: 10.1371/journal.pone.0053550

Tfaily, M. M., Chu, R. K., Tolić, N., Roscioli, K. M., Anderton, C. R., Paša-Tolić, L., et al. (2015). Advanced solvent based methods for molecular characterization of soil organic matter by high-resolution mass spectrometry. *Anal. Chem.* 87, 5206–5215. doi: 10.1021/acs.analchem.5b00116

Tolić, N., Liu, Y., Liyu, A., Shen, Y., Tfaily, M. M., Kujawinski, E. B., et al. (2017). Formularity: software for automated formula assignment of natural and other organic matter from ultrahigh-resolution mass spectra. *Anal. Chem.* 89, 12659–12665. doi: 10.1021/acs.analchem.7b03318

Valett, H. M., Baker, M. A., Morrice, J. A., Crawford, C. S., Molles, M. C., Dahm, C. N., et al. (2005). Biogeochemical and metabolic responses to the flood pulse in a semiarid floodplain. *Ecology* 86, 220–234. doi: 10.1890/03-4091

von Stockar, U., and Liu, J.-S. (1999). Does microbial life always feed on negative entropy? Thermodynamic analysis of microbial growth. *Biochim. Biophys. Acta Bioener.* 1412, 191–211. doi: 10.1016/S0005-2728(99)00065-1

Weber, K. A., Achenbach, L. A., and Coates, J. D. (2006). Microorganisms pumping iron: anaerobic microbial iron oxidation and reduction. *Nat. Rev. Microbiol.* 4, 752–764. doi: 10.1038/nrmicro1490

Wilson, J. S., Baldwin, D. S., Rees, G. N., and Wilson, B. P. (2011). The effects of short-term inundation on carbon dynamics, microbial community structure and microbial activity in floodplain soil. *River Res. Appl.* 27, 213–225. doi: 10.1002/rra.1352

Conflict of Interest Statement: The authors declare that the research was conducted in the absence of any commercial or financial relationships that could be construed as a potential conflict of interest.

frontiers in Microbiology

REVIEW
published: 18 July 2018
doi: 10.3389/fmicb.2018.01605

Low Energy Subsurface Environments as Extraterrestrial Analogs

*Rose M. Jones, Jacqueline M. Goordial and Beth N. Orcutt**

Bigelow Laboratory for Ocean Sciences, East Boothbay, ME, United States

Earth's subsurface is often isolated from phototrophic energy sources and characterized by chemotrophic modes of life. These environments are often oligotrophic and limited in electron donors or electron acceptors, and include continental crust, subseafloor oceanic crust, and marine sediment as well as subglacial lakes and the subsurface of polar desert soils. These low energy subsurface environments are therefore uniquely positioned for examining minimum energetic requirements and adaptations for chemotrophic life. Current targets for astrobiology investigations of extant life are planetary bodies with largely inhospitable surfaces, such as Mars, Europa, and Enceladus. Subsurface environments on Earth thus serve as analogs to explore possibilities of subsurface life on extraterrestrial bodies. The purpose of this review is to provide an overview of subsurface environments as potential analogs, and the features of microbial communities existing in these low energy environments, with particular emphasis on how they inform the study of energetic limits required for life. The thermodynamic energetic calculations presented here suggest that free energy yields of reactions and energy density of some metabolic redox reactions on Mars, Europa, Enceladus, and Titan could be comparable to analog environments in Earth's low energy subsurface habitats.

Keywords: deep biosphere, subsurface, astrobiology, low energy, energy limitation

OPEN ACCESS

Edited by:
Doug LaRowe,
University of Southern California,
United States

Reviewed by:
Doug Bartlett,
University of California, San Diego,
United States
Christopher Kenneth Algar,
Marine Biological Laboratory,
United States

***Correspondence:**
Beth N. Orcutt
borcutt@bigelow.org

Specialty section:
This article was submitted to Extreme Microbiology, a section of the journal Frontiers in Microbiology

Received: *27 February 2018*
Accepted: *27 June 2018*
Published: *18 July 2018*

Citation:
Jones RM, Goordial JM and Orcutt BN (2018) Low Energy Subsurface Environments as Extraterrestrial Analogs. Front. Microbiol. 9:1605. doi: 10.3389/fmicb.2018.01605

INTRODUCTION

Astrobiology and Life Under Energy Limitation

Astrobiology includes the search for the presence of life outside the Earth (Domagal-Goldman et al., 2016). The immensity of this challenge requires a focused search, which involves setting constraints on where life may and may not be possible. Setting the boundaries of this habitable zone in a meaningful way (i.e., neither too broad nor too limiting) is not trivial and can be defined by a number of parameters (**Figure 1**), each with its own advantages and limitations that compete and complement each other (Cockell et al., 2016).

Analog sites on Earth are those that share past or present characteristics with other planetary bodies, providing natural systems for study of the limits of life, which are often quite different from lab conditions (Arndt et al., 2013). This concept is based on the idea that laws of physics and chemistry are universal, a principle that underlies a large proportion of astrobiology research (Léveillé, 2010; Preston and Dartnell, 2014). Therefore, sites on Earth can provide information on how physical and chemical conditions interact to form environments conducive to life

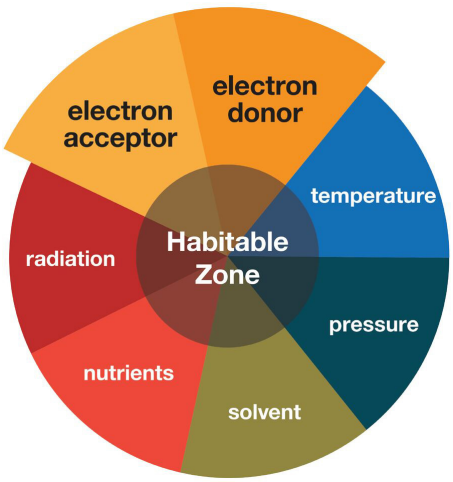

FIGURE 1 | Schematic illustrating the different parameters that contribute to habitability. This review primarily focuses on the electron donor and electron acceptor parameters on extraterrestrial targets and Earth's low energy subsurface environments.

elsewhere (Lederberg, 1960; Léveillé, 2010). "Extreme" environments [where conditions fall outside of the "standard" of 4–40°C, pH 5–8.5, and salinity above 37 g kg^{-1} water (Kristjánsson and Hreggvidsson, 1995; Bartlett and Bidle, 1999)] are common analog targets used as a way to identify and develop tools to search for identifying signs that life is or was ever present under a range of conditions (Preston and Dartnell, 2014). The current primary targets for astrobiology investigations within the solar system are Mars, Enceladus, Europa, and possibly Titan. These planetary bodies have surface conditions that are largely considered inhospitable to life, but where subsurface conditions are potentially habitable.

To better understand life under low energy conditions for extrapolation to extraterrestrial targets, studying environments on Earth that experience limited energetic disequilibria is useful. This "follow the energy" approach to evaluating whether life is possible relies on the idea that chemical disequilibria are important, providing differences in potential energy that can be used to drive reactions required by life (Kappler et al., 2005; Barge and White, 2017). The difference between equilibrium states of a given redox couple (i.e., an electron donor and an electron acceptor) defines this disequilibrium and how much energy could be released, with the equilibrium tipping point dependent on state variables like temperature and pressure. A gradient of redox pairs is generated; those of highest yield are generally removed preferentially and redox pairs of least energy yield persist. This corresponds to an approximate trend for decreasing microbial activity (Zhang et al., 2016), particularly in low disturbance environments such as sediments. Thus, defining the habitable zone (**Figure 1**) requires identifying electron donor/acceptor pairs that supply sufficient potential energy to satisfy the energetic limits of life under realistic state variables.

The energetic limit of life is the minimum energy (i.e., difference in redox potential) necessary for a cell. Electron transport in a cell works either by having each protein along the path at a slightly lower redox potential than the previous protein to facilitate movement of electrons from one to the next (Anraku, 1988) or by having an ion concentration gradient across the membrane to drive ATP production (Müller and Hess, 2017). Pathways and energetic requirements vary between genus and metabolism, with some microbes able to use multiple transport pathways (Kracke et al., 2015; Lever et al., 2015; Müller and Hess, 2017). Physical constraints such as resources required to perform and maintain particular metabolic reactions have an effect on which redox reactions are metabolically favorable (Amenabar et al., 2017).

The purpose of this review is to provide an overview of Earth's low energy subsurface sites as potential analog environments with particular emphasis on how they inform the study of the energetic limits required for life to exist, which has implications for refining the search for extraterrestrial life. These resource limits have applications in defining the energetic aspect of habitability, including minimum thresholds and identification of possible electron acceptor/donor reactions. This review compliments other recent reviews of astrobiology and analogs (Domagal-Goldman et al., 2016; Martins et al., 2017), habitability (Cockell et al., 2016), energetics and astrobiology (Barge and White, 2017), forward contamination (Fairén et al., 2017), deep marine environments (Fisher, 2005; Orcutt et al., 2013a), deep continental environments (Fredrickson and Balkwill, 2006; Colman et al., 2017), and energy within these (Amend and Teske, 2005; Edwards et al., 2012a; Hoehler and Jørgensen, 2013; Bach, 2016; Bradley et al., 2018). After reviewing basic features of Earth's subsurface environments and extraterrestrial targets, we review current understanding of energy limitation for life, and conclude with new assessments of possible chemotrophic energy availability in the subsurface analogs and extraterrestrial sites.

Defining the Low Energy Subsurface

The subsurface begins below the solid surface of the earth and includes a wide range of conditions across microscopic and macroscopic scales, substrate age and accumulation rates. The subsurface is classified into various continental and marine environments (**Figure 2**). These terms are rarely explicitly defined but usually refer to whether there is land or ocean above a location (Whitman et al., 1998; McMahon and Parnell, 2014), or to whether a location is situated in a continental or marine tectonic plate (Cogley, 1984). The continental definition generally includes continental shelves as continental, whereas the former will class them as marine. Note that the term "terrestrial" is often used in place of "continental" in the literature; however, we avoid use of the term terrestrial in this context, as this term encompasses the entire Earth system [i.e., "intraterrestrial" life (Edwards et al., 2012a) and "extraterrestrial" life].

Current definitions of the boundaries of the subsurface are somewhat imprecise, and yet highlight why the subsurface is relevant as a source of analog sites. Classifications of the shallowest boundary of the "deep subsurface" have included depth (Jørgensen and Boetius, 2007; Edwards et al., 2012a), pressure (Oger and Jebbar, 2010), water flow (Lovley and Chapelle, 1995), and operational considerations

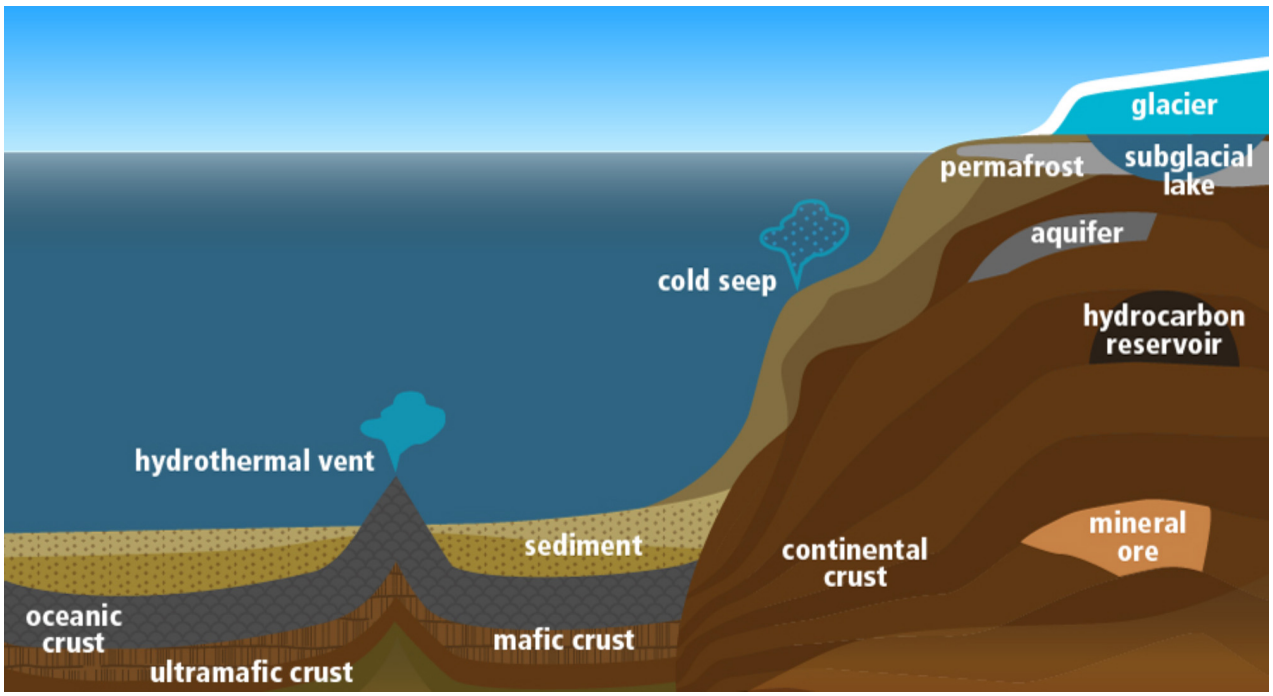

FIGURE 2 | Cross-section schematic of low energy subsurface environments on Earth.

(Orcutt et al., 2011). These thresholds generally follow the principle that surface processes influence shallow sites while deep subsurface sites are more isolated (i.e., do not interact with surface products and processes) and less prone to disturbance. However, this definition does not hold up when considering all environments within continental and marine environments, such as subglacial lakes and desert varnishes. Likewise, the downward extent to which life penetrates is poorly constrained. The upper temperature limit for life is generally taken as the ultimate constraint for the lower depth limit (Takai et al., 2008), and likely varies between environments due to the influence of other physical and chemical characteristics (Wilhelms et al., 2001; Head et al., 2003; LaRowe et al., 2017). The working definition used here (as in Edwards et al., 2012a; Wu et al., 2016; Colman et al., 2017) is of a low energy subsurface environment with all requirements for life are sourced from surrounding substrate. As such, the environments considered herein come from a variety of depths as we considered the threshold at which this definition becomes a true function of local conditions. For example, using our definition, sites with slow deposition rates and little disturbance such as oligotrophic sediment and Antarctic permafrost may have a subsurface that begins only a few cm below the actual surface. We also considered the overlaying surface immaterial. Therefore, ice covered sites are included within our definition.

Some characteristics are common to subsurface environments of Earth. Light is mostly absent (Van Dover et al., 1996; Reynolds and Lutz, 2001; White et al., 2002; Beatty et al., 2005), generally eliminating phototrophy as a lifestyle. Chemical-based lithotrophic reactions support a large fraction of life in Earth's subsurface environments, though transport of organic matter and oxidants of photosynthetic origin (i.e., oxygen) introduces influences from Earth's surface. In comparison to surface environments, deep subsurface sites on Earth are often limited by low concentrations of electron donors, electron acceptors, carbon and/or nutrients (D'Hondt et al., 2009, 2015; Hoehler and Jørgensen, 2013; Lever et al., 2015). Subsurface environments often have limited permeability and/or porosity, restricting transport and motility and experience higher pressures compared to the surface world, in addition to occasional extremes in pH and elevated temperature (Lysnes et al., 2004; Kelley et al., 2005; Prokofeva et al., 2005; Slobodkin and Slobodkina, 2014).

EARTH'S SUBSURFACE HABITAT TYPES

Marine

Beginning beneath the seafloor, there are three major habitat types: marine sediment, oceanic crust, and seep environments (**Figure 2**). Boundaries between these provide gradients and thresholds that provide additional opportunities for life.

Marine Sediment

The marine sediment subsurface begins below the bioturbation zone, where burrowing animals actively disturb the sediment. Bioturbation depth varies depending on the rate of sedimentation of particles and the organic content of the particles (Jørgensen and Boetius, 2007; Teal et al., 2008). Generally, sedimentation rate and organic content load is highest near continental margins where particles and nutrients are shed from land, and lowest

beneath the center of ocean gyres. Marine sediment composition varies from sands to fine-grained clays, and from biologically derived oozes to continentally derived particles and volcanic ashes. Porosity of marine sediment, and consequently the volume of liquid within it, decreases with depth due to compaction, and recent estimates suggest that roughly 5% of Earth's water is in the form of pore water within sediment (LaRowe et al., 2017). In locations with significant organic carbon burial, typically on continental shelves, methane production from terminal electron accepting processes can lead to the formation of large quantities of dissolved and free methane gas. Some of this gas escapes the seafloor, supporting "cold seep" environments where methane oxidation supports chemotrophic communities, with the majority of the gas stored as gas hydrates or clathrate ices (Whiticar, 1990; Clennell et al., 1999; Koh, 2002; Katayama et al., 2016).

There is vertical zonation of chemotrophic biogeochemical processes in marine sediment as more energy-rich terminal electron acceptors are preferentially used to oxidize organic carbon, generally in the order of dissolved oxygen, nitrate, metal oxides, sulfate, and carbon dioxide, followed by fermentation (Froelich et al., 1979; Orcutt et al., 2011; Arndt et al., 2013). Labile organic carbon is used first, with less favorable fractions persisting for hundreds to millions of years (Arndt et al., 2013). In areas with little organic carbon delivery, like beneath ocean gyres, the rate of organic carbon oxidation is so slow that relatively energy rich electron acceptors (i.e., oxygen, nitrate) penetrate throughout the entire sediment column (D'Hondt et al., 2009, 2015; Orcutt et al., 2013b). These low-resource sediments are not necessarily extremely limited across all metabolisms, however, as rates of activity for particular metabolic reactions are comparable to those of less oligotrophic sediments (Orcutt et al., 2013a). Growth and persistence rates in the order of <1–∼350 years are proposed in such oligotrophic sediments (Biddle et al., 2006; Braun et al., 2017; Volpi et al., 2017), reflecting metabolic limitations caused by scarcity of electron donors in addition to nutrients. In such conditions, it is necessary to consider dormancy and maintenance (Orcutt et al., 2013a; Lever et al., 2015; Reese et al., 2018). Yet the latest biomass estimates in sediment are $\sim 2.9 \times 10^{29}$ cells or ∼0.6% of earth's total biomass (Kallmeyer et al., 2012), indicating that it is possible for communities to persist in these environments.

Oceanic Crust

The oceanic crust begins beneath sediment cover or as exposed seafloor where ocean crust is newly formed or not blanketed by sediment. There are two main lithologies in the oceanic crust: an upper mafic layer of extrusive and intrusive basalts above intrusive gabbros, and a deeper ultramafic layer (Karson, 2002). Mafic rocks are generally low in silica (55–45 weight percent) and have a relatively high iron and magnesium oxide content. Ultramafic rocks have less silica (<45 weight percent) and more iron and magnesium. In contrast to sediments, the ocean crust is generally scarce in organic carbon and nitrogen-poor and includes increased trace elements depending on the host geology (Staudigel et al., 1998).

The oceanic crust encompasses not just the host rocks, but the fluids that circulate through them (Furnes and Staudigel, 1999; Edwards et al., 2005; Orcutt et al., 2011). Ocean water enters exposed areas of crust and moves through cracks and fissures in the crust, exiting as diffuse or focused flow due to pressure and temperature changes driving siphon effects (Fisher, 2005). Circulation depth is poorly constrained, extending >500 m below the crustal surface (Furnes and Staudigel, 1999). Fluid volume in the oceanic crust is estimated at ∼2% of the total ocean volume (Edwards et al., 2005) and circulates the entire ocean volume equivalent every $\sim 10^5$–10^6 years (Becker and Fisher, 2000). It is a complex habitat, with interactions between rocks (primarily iron-silicates such as basalt) and fluids that vary in temperature (cool to several hundreds of degrees Celsius), redox state (oxic to highly reducing), and pH (acidic to basic). Variation over time occurs with continual creation of freshly exposed rock surfaces due to volcanic eruptions or tectonic events and closing off of flow pathways due to alteration or deformation. Faster rates of subseafloor flow could therefore result in a more diverse, larger, and active community as more resources are delivered and inhibitors removed per unit of time compared to a system with a slower rate (Zhang et al., 2016). Where this altered fluid seeps into the sediment above, it introduces new sources of electron acceptors and donors (Engelen et al., 2008; Ziebis et al., 2012; Orcutt et al., 2013b; Labonté et al., 2017).

It was only recently appreciated that large portions of oceanic crust are oxic, due to seafloor hydrothermal circulation replenishing oxygen at depth and limited drawdown of oxygen in oligotrophic sediment above (Røy et al., 2012; Ziebis et al., 2012; Arndt et al., 2013; Orcutt et al., 2013b; D'Hondt et al., 2015; Braun et al., 2017). Chemolithotrophic electron donors and acceptors such as oxidized and reduced sulfur, iron, and manganese compounds are common in the crust (Bach and Edwards, 2003; Edwards et al., 2012a). The majority of these metal oxides are in solid form under near-neutral to alkaline subsurface conditions, but there are microbes that directly transfer electrons directly from the mineral for use in energy pathways (Lovley, 2008; Smith et al., 2014; Badalamenti et al., 2016). Hydrogen may be an important electron source, particularly in the lower layers (Amend and Shock, 2001; Bach, 2016), though the generation mechanism is as yet unclear (Chapelle et al., 2002; Brazelton et al., 2013; Dzaugis et al., 2016). Less is known about the ocean crustal subsurface in general, partially due to the operational challenges of sampling this environment. Crustal estimates of biomass and rates of activity are currently poorly constrained, though energetic calculation suggest this environment could support up to $\sim 1 \times 10^{12}$ g C yr^{-1} of new biomass (Bach and Edwards, 2003; Edwards et al., 2005), and recent empirical measurement of chemotrophic carbon fixation support this (Orcutt et al., 2015).

Seep Habitats

The marine environment has two types of seep habitats: cold seeps (described above) and hydrothermal seeps (commonly referred to as hydrothermal vents). Though not strictly deep subsurface environments, these environments provide natural "windows" into otherwise challenging to access environments and are therefore considered. Fluids in these environments

are subject to interactions with the local geology, resulting in an altered physiochemical character such as enrichment with dissolved minerals and metals (Staudigel et al., 1998). Marine hydrothermal vent systems represent concentrated regions of chemotrophic life in the otherwise oligotrophic deep-sea floor, as warm, mineral rich subseafloor fluids mix with cold, oxic, resource-deficient surface waters. This enrichment provides a potentially energy rich environment, particularly where reduced chemical species mix with oxic seawater in plume environments (Dick et al., 2013).

Continental

The continental subsurface begins beneath the top active layers of soil and ice or directly under exposed crust (**Figure 2**). There are three main habitat types in the continental subsurface: the crust, ores (here including hydrocarbon deposits) and aquifers. There are also "windows into the subsurface" environments such as hydrothermal springs and ophiolites.

Continental Crust

The continental crust has an estimated volume of approximately 2×10^8 km^2 or 40% of the Earth's solid volume, depending on the definition (Cogley, 1984). It is primarily granitic (high concentration of silica) and highly heterogeneous, becoming mafic at depth (Wedepohl, 1995; Rudnick and Gao, 2003). This contrasts with the broadly homogeneous marine crust which has a low silica content (Rudnick and Fountain, 1995). This heterogeneity provides a wide variety of habitats for chemolithotrophs, as there is more substrate variability in addition to temperature and pressure gradients. "Window" sections of the deepest subsurface are accessible as uplifted ophiolites (Neubeck et al., 2017; Rempfert et al., 2017). These environments provide information on deeper geology and interactions between these and microbial communities, though the degree to which these sites are reflective of the true deep subsurface varies according to local conditions.

Water in the terrestrial subsurface is primarily in channels and pore spaces. The solid to water ratio tends to increase with depth, causing a more constrained environment further down (Stober and Bucher, 2004; Parnell and McMahon, 2016). Water becomes more saline at depth, as long residence times of thousands of years results in the accumulation of dissolved minerals from contact with rock. Total groundwater volume in the terrestrial subsurface crust is estimated at 2.43×10^{19} L (Wirsen and Jannasch, 1978), with an estimated max volume of 98% in aquifers (Gleeson et al., 2016). These aquifers are areas of more permeable rock and sediment where groundwater has less restricted flow (Foster and Chilton, 2003). Aquifer conditions vary according to surrounding geology and sometimes anthropogenic effects, but are in general oligotrophic.

Similar to the marine crust, electron acceptors and donors include iron (Emerson et al., 2007; Heim et al., 2017), manganese (Peng et al., 2015; Sylvan et al., 2015), sulfur species and hydrogen (Osburn et al., 2014). Use of other metal species is reported but their significance is often unclear (Kashefi and Lovley, 2000; Oremland, 2003; Lee et al., 2015). Clays and sediments are occasionally present, which can have a higher organic carbon content than rock crust (Bagnoud et al., 2016). Elevated concentrations of hydrogen in particular are present in the deeper subsurface due to radiolysis, or as a product of serpentinization, a geochemical alteration process that produces methane, hydrogen, and abiotically produced hydrocarbons as a result of water-ultramafic rock interactions. Similar to the deep crustal marine subsurface, estimated rates of activity in the continental deep subsurface are poorly constrained, due in part to difficulties and costs involved in collecting quality samples from deep boreholes and mine systems (Miettinen et al., 2015; Momper et al., 2017).

Ores and Mineral Deposits

Concentrations of a particular mineral can alter local conditions and microbiology (Lehman et al., 2001), though they are rarely of significant volume in comparison to the total crustal volume (Williams and Cloete, 2008; Daly et al., 2016). Ores are mineral concentrations of economic interest, and here includes hydrocarbon (e.g., coal) and halite deposits in addition to metal-containing ores. These ores are sometimes the subject of commercial exploitation, which provides opportunities for site access though mining activity (Osburn et al., 2014; Miettinen et al., 2015; Daly et al., 2016). However, these environments are by definition altered by anthropogenic activity, changing local conditions, and local microbiology. Examples include generation of acid mine drainage (Druschel et al., 2004; Chen et al., 2016), souring of hydrocarbon deposits (Head et al., 2014), and alterations by explosive activity (Martins et al., 2017).

The range of electron acceptors and donors in these environments can be very different from typical crust. Hydrocarbon deposits such as oil and coal contain abundant organic carbon, though this is usually not labile and often includes toxic aromatic compounds (Larter et al., 2006; Head et al., 2014). Depending on host geology, sulfate in particular provides a reasonably energy rich electron acceptor (Sánchez-Andrea et al., 2011; Dopson and Johnson, 2012; Tsesmetzis et al., 2016). Other metals such as manganese (Spilde et al., 2005), arsenic (Escudero et al., 2013), uranium (Beller et al., 2013), and others (Johnson et al., 2017) are used in addition to iron as electron sources and sinks (Hedrich et al., 2011; Toner et al., 2016). Metal species in particular are usually present in low dissolved concentrations in the environment regardless of their concentration in solid mineral because of their respective solubility under environmental conditions. There are exceptions such as low pH environments associated with some ores and hydrothermal fluids, where a high concentration of H^+ shifts the thermodynamics of solid/liquid/gas state equilibrium, changing solubility so more metals stay in solution (Hedrich et al., 2011; Johnson et al., 2012). There is evidence that iron, sulfur, and methane oxidizing microbes use hydrogen as an electron donor in these environments (Lau et al., 2016; Carere et al., 2017; Hernsdorf et al., 2017).

Cold Subsurface Environments

Cold, hyperarid deserts are some of the closest analogs to current extraterrestrial targets for life, such as high elevation McMurdo Dry Valleys in Antarctica (Heldmann et al., 2013)

and the Atacama Desert in Chile (Navarro-González et al., 2003; Fairén et al., 2010). Temperatures in these environments rarely reach above freezing, resulting in a soil profile almost exclusively of permafrosts. These are oligotrophic systems, with potential electron acceptors such as nitrates, sulfates, and perchlorates as well as electron donors such as formate, acetate, and other small organic acids are present in these primarily mineral soils (Kounaves et al., 2010b; Parro et al., 2011; Jackson et al., 2016; Faucher et al., 2017).

Subglacial lakes such as those in Greenland, Iceland, and Antarctica (Siegert et al., 2016) are considered as 'subsurface' herein, as they fit the definition of an environment relatively isolated from surface processes. These are bodies of water of varying fluid dynamics, physiochemical properties, and residence times that may or may not have a rocky bottom, capped by kilometers of ice (Bell et al., 2002; Mikucki et al., 2016; Siegert et al., 2016). Microbial studies of these sub-glacial lakes show lithotrophic communities with unique microbial members and metabolisms with a range of electron donors and acceptors, with less biomass associates with the higher ice-water boundaries (Murray et al., 2012; Bulat, 2016; Mikucki et al., 2016).

EXTRATERRESTRIAL ASTROBIOLOGICAL TARGETS WITH SUBSURFACE ANALOGS ON EARTH

Mars, Europa, Enceladus, and Titan have received the most attention as the most likely to harbor signs of past or present extraterrestrial life. These sites possess characteristics or specific sites that share similar aspects of particular low energy subsurface sites, in terms of physical characteristics and possible energy sources.

Mars

Present day Mars is cold and hyper arid with low atmospheric pressure (∼7 mbar), high ionizing radiation, and highly oxidizing surface soil conditions (Fairén et al., 2010). Surface conditions on Mars are currently considered inhospitable because of this and due to the instability of liquid water on the surface. Water is present on Mars in the near subsurface in the form of ground ice and potentially as ground water residing in deeper crust (Clifford and Parker, 2001; Byrne et al., 2009; Clifford et al., 2010). Subsurface conditions such as pressure above the triple point of water, radiogenic heating and the presence of dissolved solutes could allow for liquid water with depth (Clifford et al., 2010). Evidence indicates that past Mars was relatively warmer than at present and liquid water was widespread (Fairén et al., 2010), resulting in possible previously habitable conditions. There are microorganisms on Earth that grow at subzero temperatures (Mykytczuk et al., 2013) and under present Martian atmosphere conditions (Mickol and Kral, 2017). Extant life could potentially remain in the more clement subsurface conditions due to protection provided from ionizing radiation and surface soil oxidizing conditions.

Basalts, clays and ultramafic minerals are found across Mars, and provide possible lithotrophic electron donors and acceptor sources. Iron and sulfur in particular are abundant (Squyres et al., 2004; Nixon et al., 2013), and there is evidence of perchlorates (Catling et al., 2010; Navarro-González et al., 2010), nitrogen (Stern et al., 2015), and other metal-containing minerals (Squyres et al., 2004). Oxygen is present in the atmosphere in extremely low concentrations of 0.1%, likely due to abiotic formation (Kounaves et al., 2010a). Evidence that Martian conditions have been locally extremely acidic (Horgan et al., 2017; Peretyazhko et al., 2017), means that metal and sulfur ions in particular could have been more bioavailable similar to low pH environments on Earth (Fernández-Remolar et al., 2008; Amils et al., 2014). Serpentine deposits have been identified associated with impact craters and surface terrains by the Mars Reconnaissance Orbiter in a number of sites on Mars (Ehlmann et al., 2010), including Nili Fossae, a site possibly linked with enriched methane concentrations (Mumma et al., 2009). Since methane is thought to have a short lifespan in the Martian atmosphere, a potential source for the variable detection of methane on Mars (Webster et al., 2015) could be present-day and/or past serpentinization processes in the subsurface (Oehler and Etiope, 2017) as relevant minerals are present (Hoefen et al., 2003; Ody et al., 2012). Some have theorized that the Martian subsurface could be supplied with an energy source from the oxidation of photochemically produced H_2 and CO diffusing into regolith, penetrating down to 100–1,000 meters (Weiss et al., 2000). Microorganisms in surface cold and hyper-arid soils are identified that utilize these substrates as a carbon and energy source in trace atmospheric amounts (Ji et al., 2017), and CO oxidation has been identified as a metabolism in the subsurface on Earth (Brazelton et al., 2012; Baker et al., 2016; Hoshino and Inagaki, 2017).

Analog environments to the cold and hyper-arid conditions on Mars include the subsurface of the hyperarid Atacama desert in Chile as well as polar deserts (Navarro-González et al., 2003; Fairén et al., 2010). While the dry surface mineral soils of the Atacama desert harbor little to no active microbial life (Navarro-González et al., 2003; Crits-Christoph et al., 2013), there is a "microbial oasis" at depth (∼2 m), where small films of liquid water is formed due to deliquescence caused by hygroscopic salts (Parro et al., 2011). In Antarctica, the McMurdo Dry Valleys are a polar desert analog similar to observations at the *Phoenix* landing site, where dry permafrost soil with negligible water content overlays ice-cemented ground (Heldmann et al., 2013). Life is likely constrained more by available liquid water than low energy in these oligotrophic environments (Goordial et al., 2016) as active microbial life in these cold, dry valleys can be observed at lower elevations where liquid water is more prevalent seasonally (Bakermans et al., 2014).

Considering the abundance of basalts and ultramafics on Mars, the subsurface provides analogs for Martian minerals, including basalts, clays, and serpentine (Stevens and Mckinley, 1995; Schulte et al., 2006) among others. Serpentinite hosted microbial ecosystems are found in subsurface environments in marine (e.g., Atlantis Massif) and in terrestrial settings (e.g., the Tablelands Ophiolite, The Ceders) (Kelley et al., 2005; Brazelton et al., 2006; Hernsdorf et al., 2017; Rempfert et al., 2017). Ophiolites on earth are identified as analogs for similar

lithologies on Mars as a source of hydrogen in particular, and depending on the host substrate, other energy sources such as iron or manganese may also be present (Schulte et al., 2006; Szponar et al., 2013; Dilek and Furnes, 2014). Deeply occurring clays (Bagnoud et al., 2016; Leupin et al., 2017) and particularly oligotrophic marine sediment (D'Hondt et al., 2009) may be useful analogs for Martian organic-poor clays.

Icy Moons With Liquid Oceans

There are currently two primary icy ocean world targets for possible extraterrestrial life: Saturn's moon Enceladus, and Europa, a moon of Jupiter. Enceladus probably has a rocky core covered at least partially by an approximately 10 km deep body of probably alkaline (pH 8.0–12: Postberg et al., 2009; Glein et al., 2015; Hsu et al., 2015) brine (Vance et al., 2016), with a cap of 30–40 km of ice (Iess et al., 2014). There is a geyser in the southern hemisphere (the so-called 'tiger stripes'), speculated to be sourced from hydrothermal activity (Glein et al., 2015; Hsu et al., 2015; Sekine et al., 2015) or clathrate decomposition (Kieffer et al., 2006). Information collected from the geyser indicate the presence of carbon, nitrogen and organic compounds (CH_4, NH_4), silicates (Postberg et al., 2009; Waite et al., 2009), sodium, potassium and carbonates (Postberg et al., 2009) and moderate salinity (Glein et al., 2015; Hsu et al., 2015). Temperature estimates for subsurface ocean range from $<$90°C in the assumed crustal subsurface to approximately 0°C near the ice-water interface. There are indications of possibly significant water-rock interactions between the liquid body and a hypothesized solid rock core (Glein et al., 2015; Hsu et al., 2015).

Europa is hypothesized to contain a rocky basaltic core (Vance et al., 2016) in contact with a liquid brine ocean ∼80–100 km deep (Kivelson et al., 2000; Lowell and DuBose, 2005), with a ∼15–25 km shell of ice (Kivelson et al., 2000) and lakes encased within (Schmidt et al., 2011). Conditions of pH, temperature, and composition of brines in Europa are less constrained than Enceladus. though the presence of H_2O_2, O_2, SO_2, CO_2, carbonates, and sulfates are inferred from spectral data of surface ice (McCord et al., 1998; Carlson et al., 1999; Hand et al., 2007), which are theorized to enter the subsurface in some instances (Teolis et al., 2017). Proposed possible metabolisms include methanogenesis and sulfate reduction pathways (McCollom, 1999), though evidence of compounds involved in these pathways have yet to be detected in the surface ice (Hand et al., 2007). If oxygen enters the subsurface, then this may also function as an electron acceptor, though the actual concentrations involved may be low and localized (Teolis et al., 2017). Hydrothermal activity and subsurface flow, are speculated based on features of the ice surface (Lowell and DuBose, 2005; Quick and Marsh, 2016).

Considering the ultramafic, saline, and alkaline conditions hypothesized to exist on these icy moon targets, marine ultramafic subsurface sites such as Lost City on the Atlantis Massif are useful to consider as they are broadly similar (Postberg et al., 2009; Preston and Dartnell, 2014; Glein et al., 2015; Vance et al., 2016; Lunine, 2017). The Lost City vent system consists of a succession of alkaline (pH 9–11) vents of ∼45–90°C fluids. The Europa site at the Mid-Cayman Ridge is another cool, ultramafic-hosted system with elevated methane (German et al., 2010). In these sites, seawater is entrained within the ultramafic system and undergoes fluid-rock reactions that remove carbonate, adds alkalinity, and enriches hydrogen, methane, and other small weight organics that are byproducts of serpentinization reactions. Serpentinization systems such as these have been speculated as a possible energy source on Enceladaus (Glein et al., 2015; Holm et al., 2015), with a possible H_2 generation value of approximately 3 mol H_2 kg^{-1} of water (Glein et al., 2015). This compares to 0.25–15 mmol H_2 kg^{-1} of water in the Lost City hydrothermal vent system (Kelley et al., 2001, 2005; Proskurowski et al., 2008). Methane and sulfates are a possible electron donor and acceptor (Kelley et al., 2001; Lang et al., 2010; Brazelton et al., 2013; Schrenk et al., 2013); however, a recent study suggests sulfate-reducers dominate this environment despite abundant methane (Lang et al., 2018). There is little sulfate yet detected on Enceladus, so sulfur couples may not be a significant source of energy on this target (Glein et al., 2015).

Basaltic oceanic crust environments also serve as useful analogs to icy ocean worlds, given the interaction of saline fluids with crust inferred on these targets. The best-studied subsurface environments on Earth where fluid moves through oceanic crust are on the flanks of mid-ocean ridges, namely the eastern flank of the Juan de Fuca Ridge and the western flank of the Mid-Atlantic Ridge at the "North Pond" site (Edwards et al., 2012b; Orcutt and Edwards, 2014). Recent studies at these sites have revealed dynamic microbial ecosystems thriving in this subsurface environment (Jungbluth et al., 2016; Meyer et al., 2016; Tully et al., 2018).

Considering the ice-water interface on these icy moons, proposed analogs for ice-water interfaces include sea ice-water channels (Martin and McMinn, 2017) and sub-glacial lakes such as Lake Vida, an Antarctic permanently ice-covered brine lake (Murray et al., 2012; Garcia-Lopez and Cid, 2017). Sub-glacial lake studies show chemotrophic communities with unique community members and evidence of more life at substrate-water interfaces than ice-water interface, indicating life is possible in these conditions (Murray et al., 2012; Bulat, 2016; Mikucki et al., 2016). Identified metabolisms include sulfate reduction, methanogenesis, nitrate as an electron acceptor (Skidmore et al., 2000; Michaud et al., 2017) and, at the crust-water interface, lithotrophic sources such as manganese and iron (Murray et al., 2012).

Considering the presence of brines in contact with crust on icy moons, salt ores and cold seep brine pools offer additional subsurface analogs for icy moons. Brine pools with distinct microbial communities are present in the marine subsurface, forming as buried salt deposits interact with upwelling subsurface ocean fluids (Joye et al., 2009, 2010; Antunes et al., 2011). Deep terrestrial halite ores harbor microbial communities, including inclusions within the deposits (Lowenstein et al., 2011; Jaakkola et al., 2016; Payler et al., 2017). Ionic strength of solution is generally more limiting than energy in these environments,

as there can be sulfur, methane, hydrogen and CO_2 present, depending on host lithology.

Titan

Titan is a cold, hydrocarbon-rich extraterrestrial body, so cold subsurface environments rich in hydrocarbons are possible analogs for this target. Titan has an atmosphere assumed to contain primarily N_2, CH_4 and H_2, surface temperatures of ∼90 K and a surface pressure of ∼1.46 bar (Jakosky et al., 2003; Niemann et al., 2005; Jennings et al., 2009). It has liquid reservoirs of N_2, CH_4, Ar, CO, C_2H_2–C_4H_{10}, and H_2 (Cordier et al., 2012, 2013) in addition to other complex C–H and C–N chains (Desai et al., 2017) on the surface, which possibly permeate the subsurface (Hayes et al., 2008; Mousis et al., 2014). The temperature of Titan's surface precludes all but the most psychrophilic lifestyles, though there are indications that life at these temperatures is within the realms of possibility (Price and Sowers, 2004; Panikov and Sizova, 2007; Amato and Christner, 2009). Evidence of cryovolcanism also indicates possible areas of warmer temperatures (Lopes et al., 2013). Conditions of Titan are likely to increase reactivity of silicon compounds, leading to some speculation on the possibility of silicon-based life in such conditions (Bains, 2004).

Subsurface hydrocarbon deposits are proposed as possible analogs for Titan (L'Haridon et al., 1995). Microbial life in these environments metabolize hydrocarbons under challenging conditions of temperature, pressure and oxygen limitation, in addition to limitations imposed by the properties of hydrocarbons as substrates. However, there is little information on minimum temperatures in hydrocarbon deposits on earth. Water is important in these hydrocarbon reservoirs, with a positive correlation between cell activity and water availability (Head et al., 2003; Larter et al., 2006); however temperatures on Titan likely limit the availability of this solvent to warmer areas linked to cryovolcanism (Kargel, 1994; Lopes et al., 2013). Methane has been proposed as a possible alternative solvent for Titan (Stofan et al., 2007), though its chemical properties are somewhat different from water. The conditions on Titan as currently understood allow for more extensive gas hydrate formation, including in the subsurface and on the surface (Osegovic and Max, 2005; Fortes et al., 2007). Methane hydrates and associated microbial communities form on Earth in deep sediment and permafrost (Osegovic and Max, 2005).

ENERGETICS AND THE SUBSURFACE

Growth, Activity, and Dormancy

The physiological state of microorganisms in the subsurface can be grouped into three categories based on metabolic activity: (1) *Growth*, where the energy/nutrient demands of the cell are met, and there is sufficient energy for cell division and biomolecule synthesis; (2) *basal maintenance* (alternatively termed vegetative) in which cell division is not occurring, but cells are carrying out essential housekeeping functions for cell viability such as repair and replacement of biomolecules, and maintenance of membrane integrity (Hoehler and Jørgensen, 2013); and (3) *dormancy* (endo-spores), a reversible state of low to zero metabolic activity that is generally thought to be an evolutionary strategy to overcome unfavorable conditions for growth (Jones and Lennon, 2010; Lennon and Jones, 2011; Bradley et al., 2018). The majority of microorganisms in most environmental systems spend their time in non-dividing and energy limited states (Bergkessel et al., 2016). Environmental and energetic cues causing microorganisms to switch between growth, activity and dormancy are unclear, though these physiological states have important implications for the evolution and ecology of low energy subsurface settings.

Many microorganisms on Earth are capable of temporarily resisting stresses such as temperature, desiccation and antibiotics by entering resting states or by forming spores (Jones and Lennon, 2010). These dormant microorganisms act as a seed bank, contributing to future microbial diversity when conditions become favorable again. Dormancy might be a relevant life strategy for considering life on planetary bodies with possible past habitable conditions or where environmental conditions fluctuate temporally. Due to the estimated life-span of viability for an endospore and measured endospore abundance with depth in subseafloor sediments, one strategy for extended longevity in the subsurface appears to be periodic germination of spores to carry out repair functions (Braun et al., 2017). Nonetheless, long term survival on geological timescales through low metabolic activity may be superior to dormancy since a minimum metabolic activity for maintenance is required to counteract damage to biomolecules accumulated over time caused by background radiation, hydrolysis, oxidation, etc. (Johnson et al., 2007).

Energy requirements of growth, maintenance activities and dormancy are difficult to directly measure, but is estimated to differ by orders of magnitude (10^6: 10^3: 1) (Price and Sowers, 2004). Investigations into limits of energy required for growth in cultured microbes vary from −20 to −9 kJ mol^{-1} of energy as a limiting threshold for actively growing populations (Schink, 1997; Hoehler, 2004; Schink and Stams, 2006). Values for *in situ* investigations are lower again, with values of 190 zeptoWatts (zW) per cell in ultra-oligotrophic sediments and theoretical values as low as 1 zW per cell (LaRowe and Amend, 2015a). For comparison, a J mol^{-1} is a unit of energy whereas W is a unit of power, which is energy use over time. Therefore, 190 zW is equivalent to 1.9×10^{-22} kJ mol^{-1} s^{-1}. More recent work suggests that −20 to −10 kJ mol^{-1} is the minimum energy required for ATP synthesis (Müller and Hess, 2017), suggesting that lower values are more representative of cells under vegetative states. However, modeling energy requirements of *in situ* populations of cells requires several assumptions about growth requirements such as cellular biomolecule content, cell size and microbial taxa (Lever et al., 2015; Bergkessel et al., 2016; Kempes et al., 2017). Likewise, the molecular mechanisms and physiological characteristics associated with non-growth activity in cultured microorganisms remains poorly understood, due partly to the challenges associated with controlling, reproducing, and measuring non-growing states (Bergkessel et al., 2016). It is unclear how mechanisms (such as those reviewed in Lever et al., 2015) and energy consumption in generally fast-growing,

mesophilic model microorganisms relate to those employed by extremophiles such as those of low energy subsurface environments.

Despite low energy and nutrients, multiple lines of evidence indicate active microbial life in the subsurface. These include rates of metabolic sulfate reduction and methane cycling inferred from geochemical profiles in environmental samples, and activity measurements in microcosm experiments through radioisotope and stable isotope labeling of compounds (Morono et al., 2011; Wegener et al., 2012; Orcutt et al., 2013a; Glombitza et al., 2016; Robador et al., 2016b; Trembath-Reichert et al., 2017). Detection of bulk transcriptional activity and translational activity has the advantage of ascribing taxonomy and function to active microbiota (Orsi et al., 2013, 2016; Hatzenpichler et al., 2016; Marlow et al., 2016). Calorimetry measurements detected microbial activity in oceanic crustal fluids, measuring cellular energy consumption ranging from 0.2 to 5.7 pW cell^{-1} (Robador et al., 2016a). Additionally, highly sensitive techniques such as nanometer-scale secondary ion mass spectrometry (nanoSIMS), and bioorthogonal non-canonical amino acid tagging (BONCAT), have detected activity down to the single cell level in slow growing microorganisms (Morono et al., 2011; Hatzenpichler et al., 2016; Trembath-Reichert et al., 2017), providing insight into individual cell-to-cell variation in metabolism in low energy settings. Such activity measurements have led to proposed cell turnover rates of months to 10s of 1000s of years (Phelps et al., 1994; Biddle et al., 2006; Hoehler and Jørgensen, 2013; Braun et al., 2017; Trembath-Reichert et al., 2017).

Energy Yield of Various Redox Reactions in the Low Energy Subsurface and on Extraterrestrial Environments

According to the "follow the energy" approach to identifying habitable zones (Hoehler, 2007), electron acceptors and donors must be present in large enough quantities, and the energy released needs to be sufficient for life to make use of it (Nixon et al., 2012). The energy of a reaction differs according to environmental conditions, particularly in "extreme" environments such as the subsurface and current potential extraterrestrial targets, where temperature, pressure, pH and concentration of available reactants and products deviate significantly from standard conditions of 25°C, 1 atm, 1 M substrate concentration (D'Hondt, 2002; Hoehler, 2004, 2007; LaRowe and Van Cappellen, 2011; Bradley et al., 2018). Additionally, Gibbs free energy yield calculations for various reactions give only the maximum theoretical available energy at a given set of conditions. Calculations of the energy yield of a reaction (i.e., kJ per mole of substrate) should be considered against the availability of the substrate to consider energy yield in a given volume of the environment (i.e., kJ per liter) (LaRowe and Van Cappellen, 2011; LaRowe and Amend, 2015b; Orcutt et al., 2015). This volumetric energy yield is particularly relevant in subsurface sites, where certain electron acceptors and donors can be in short supply.

To evaluate the feasibility of various redox reactions in low energy subsurface analog sites and extraterrestrial targets (**Table 1**), we calculated the Gibbs free energy yield of reactions under *in situ* conditions for a suite of reactions (**Table 2**),

TABLE 1 | Extraterrestrial and Earth low energy subsurface analog sites considered in energy calculations.

Site	Overview of site characteristics
Extraterrestrial	
Mars	Low estimate
	High estimate
Enceladus	Hypothesized crustal seafloor-liquid interface
Europa	Hypothesized crustal seafloor-liquid interface
Titan	Surface
Marine	
North Pond	Basaltic crust, cool, and oxic
Juan de Fuca	Basaltic crust, warm, and anoxic
Lost City	Ultramafic crust, warm hydrothermal vents
South Pacific Gyre	Extremely oligotrophic, oxic sediment
Gulf of Mexico	Cold anoxic brine seeps
Continental	
Sanford Underground Research Facility	Metamorphic crust
Mont Terri	Opalinus clay
Rio Tinto	Massive pyrite ore deposit
University Valley	Polar desert permafrost, low estimate
	Polar desert permafrost, high estimate
Atacama	Hyperarid desert, low temperature, high pH
	Hyperarid desert, high temperature, low pH
Lake Vida	Ice-enclosed hypersaline lake

*Environmental concentrations (listed in **Supplementary Table S1**) from references listed in **Supplementary Table S2**.*

TABLE 2 | Reactions considered in Gibbs free energy and energy density calculations.

Redox pair	Equation
H_2/O_2	$H_{2(aq)} + 0.5O_{2(aq)} \rightarrow H_2O_{(l)}$
H_2/NO_3^- (NO_2^-)	$H_{2(aq)} + NO_3^- \rightarrow NO_2^- + H_2O_{(l)}$
H_2/NO_3^- (NH_3)	$4H_{2(aq)} + NO_3^- + H^+ \rightarrow NH_{3(aq)} + 3H_2O_{(l)}$
H_2/SO_4^{2-}	$4H_{2(aq)} + SO_4^{2-} + 2H^+ \rightarrow H_2S_{(aq)} + 4H_2O_{(l)}$
H_2/CO_2	$4H_{2(aq)} + CO_{2\ (aq)} \rightarrow CH_{4(aq)} + 2H_2O_{(l)}$
H_2S/O_2	$H_2S_{(aq)} + 2O_{2(aq)} \rightarrow SO_4^{2-} + 2H^+$
H_2S/NO_3^-	$5H_2S_{(aq)} + 8NO_3^- \rightarrow 4N_{2(aq)} + 5SO_4^{2-} + 4H_2O_{(l)} + 2H^+$
Fe^{2+}/O_2	$2Fe^{2+} + 0.5O_{2(aq)} + 2H^+ \rightarrow 2Fe^{3+} + H_2O_{(l)}$
FeS_2/O_2	$FeS_{2(s)} + 3.5O_{2(aq)} + H_2O_{(l)} \rightarrow Fe^{2+} + 2SO_4^{2-} + 2H^+$
NH_3/O_2	$NH_{3(aq)} + 1.5O_{2(aq)} \rightarrow NO_2^- + H_2O_{(l)} + H^+$
NH_3/NO_2^-	$NH_{3(aq)} + NO_2^- + H^+ \rightarrow N_{2(aq)} + 2H_2O_{(l)}$
NH_3/SO_4^{2-}	$NH_{3(aq)} + SO_4^{2-} + H^+ \rightarrow NO_3^- + H_2S_{(aq)} + H_2O_{(l)}$
CH_4/O_2	$CH_{4(aq)} + 2O_{2(aq)} \rightarrow CO_{2(aq)} + 2H_2O_{(l)}$
CH_4/NO_3^-	$CH_{4(aq)} + 4NO_3^- \rightarrow 4NO_2^- + CO_{2(aq)} + H_2O_{(l)}$
CH_4/SO_4^{2-}	$CH_{4(aq)} + SO_4^{2-} + 2H^+ \rightarrow H_2S_{(aq)} + CO_{2(aq)} + 2H_2O_{(l)}$

*Note that redox pairs of Fe^{2+} with NO_3^- or SO_4^{2-} were also considered, but as the reactions were always endergonic (see **Supplementary Table S1**), they were excluded from further presentation.*

following approaches outlined in detail elsewhere (Amend and Shock, 2001; Osburn et al., 2014). We scaled the activity coefficients in the Gibbs free energy equations to account for ionic strength in the various environments, as well as temperature effects on standard conditions; pressure effects were not included as these have far less of an impact than temperature (Amend and Shock, 2001). Where available, we used measured or interpreted *in situ* concentrations of reactants and products available from the primary literature (**Supplementary Table S1**). Care was taken to select subsurface values wherever possible, particularly for sites such as Rio Tinto that have surface components. Where concentrations were unknown, we assumed an end-member limiting concentration of 1 nmol substrate per liter (**Supplementary Table S1**). Gibbs free energy yields were normalized to the number of electrons exchanged in the reaction, to calculate energy yields as kJ per mole of electrons for cross comparison of reactions. The energy density of the selected reactions in an environment were calculated by scaling the reactions to a mole of the limiting reactant, which was assumed to be the electron donor in all cases. While this assumption is not always true, such as in organic rich marine sediment where electron acceptors become limiting (Orcutt et al., 2011), its use allows more direct comparison within the presented dataset and other work (Osburn et al., 2014). Finally, we summed the free energy available from all calculated reactions together to compare sites to one another, although this presents an overestimate as there would be competing reactions for some substrates.

Despite the large variation in environmental conditions – such as temperature, ionic strength, and concentrations – our calculations show that there is remarkable consistency in the energy yields per electron transferred across all subsurface and extraterrestrial sites considered (**Table 1**), with most reactions varying by less than 100 kJ mol electron^{-1} (**Figure 3** and **Supplementary Table S1**). The most variable reaction energetic yield is the CH_4/O_2 redox pair, whereas the least variable is the H_2/CO_2 pair. Only the CH_4/SO_4 redox pair is expected to be endergonic under some conditions (though just barely exergonic and at or below the theoretical minimum energy limit in others); all other reactions are estimated to be exergonic under all conditions considered (note that calculations for Fe^{2+} paired with either NO_3^- or SO_4^{2-} was endergonic under all conditions and was excluded from further analysis). This indicates that a wide range of redox reactions could theoretically be supported on the extraterrestrial targets, and that the energy yields can be similar to what can be found in Earth's subsurface environments. However, given that the presence of some electron donors and acceptors in extraterrestrial targets are poorly constrained [e.g., unknown electron acceptors on Enceladus, despite confirmation of electron donors methane, ammonium, and possibly hydrogen (Postberg et al., 2009; Waite et al., 2009)], theoretical feasibility needs to be constrained by probability of both electron donors and acceptors being present.

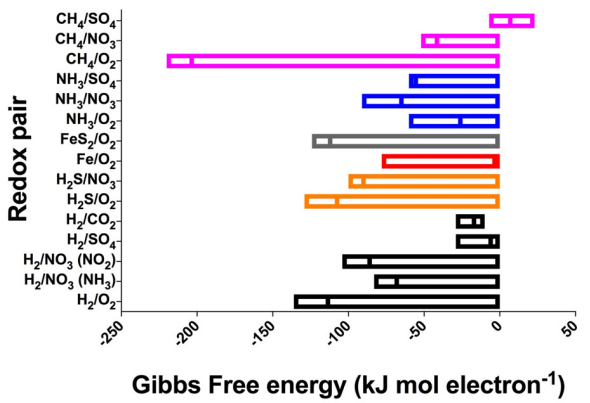

FIGURE 3 | Range and mean of Gibbs Free energy yields, normalized to kJ per mole electron transferred per reaction, across all sites for the redox pairs listed in **Table 1**. Negative values indicate exergonic reactions. See **Supplementary Table S1** for all values. Reactions grouped by electron donor and color (pink, CH_4; blue, NH_3; gray, FeS_2; red, Fe^{2+}; orange, H_2S; black, H_2).

Strikingly, extraterrestrial sites are predicted to have similar cumulative energy densities as Earth's subsurface habitats (with conservative assumptions about electron donor and acceptor concentrations), although the dominant energy-rich processes vary (**Figure 4** and **Supplementary Table S1**). For example, cumulative volumetric energy densities on Mars are estimated to range from 0.03 to 3 kJ L^{-1}, supported primarily by the electron donors NH_3, H_2S, or hydrogen reacting with sulfate, nitrate, or oxygen, depending on the scenario chosen for electron donor concentration, pH, and temperature. Under the scenario of low electron donor concentration, low pH, and low temperature, the predicted Martian energy density and dominant reactions are similar to those observed at the Earth analog site at the Juan de Fuca Ridge flank subsurface oceanic crust. Under the scenario of higher electron donor concentrations, pH, and temperature, the cumulative volumetric energy density and dominant reactions estimate is more similar to what is estimated from the Earth analog sites in the Rio Tinto. The base of the presumed Europan ocean has an estimated energy density of 400 kJ L^{-1} fueled primarily by iron oxidation, if dissolved oxygen is present (Teolis et al., 2017) and penetrates to the water-rock interface and if iron is released from water-rock reactions. This volumetric energy density and dominant reaction pattern is similar to that estimated for the Earth analog site at University Valley. By contrast, the ocean on Enceladus is estimated to have an energy density of 100 kJ L^{-1} fueled by ammonia oxidation with nitrate; none of our comparison Earth analog sites had similar energy density estimates from this reaction. The cumulative volumetric energy density estimates for Titan are the highest we estimate in this exercise, fueled by ammonia oxidation with sulfate or nitrate in a similar pattern as estimated for the Juan de Fuca analog system, but we highlight that this is the least well constrained system. Overall, although based on poorly constrained concentrations, these projections indicate that extraterrestrial sites could have sufficient overall energy to host chemolithotrophic communities.

The predicted relative contribution of each redox pair to each site is applicable information for the "follow the energy" approach to habitability (Hoehler, 2007), and can further be constrained by comparison studies of microbial metabolic processes in the Earth analog systems, to see if the predicted energy rich metabolisms

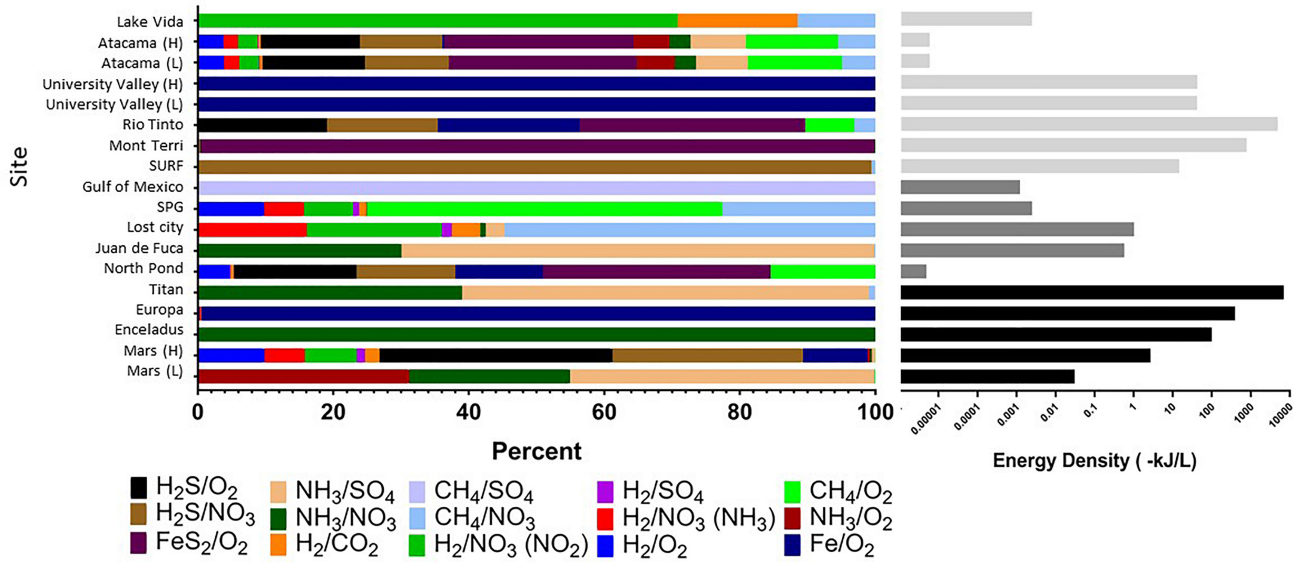

FIGURE 4 | Cumulative volumetric energy densities of redox reactions per site based on environmental concentrations of variables in each reaction (**Table 1**). **(Left)** Shows the percent contribution of various reactions as shown in the color legend. **(Right)** Shows combined absolute energy density (as kJ per liter) for all reactions, with gray scale reflecting habitat type. All calculations assumed that the electron donor was the limiting substrate. See **Supplementary Table S1** for all values and formulas.

are indeed those that occur. This approach of comparing energy density to microbial community function has recently been shown for some subsurface sites (Osburn et al., 2014; Reveillaud et al., 2016; Momper et al., 2017), demonstrating the power of this energy density approach to be a useful predictor of metabolic function. For example, North Pond energy is primarily from the FeS_2/O_2 couple (**Figure 4**), indicating that solid mineral substrates may be significant in this environment. Oxidation of hydrogen sulfide is also predicted to yield more energy than other electron donors (**Figure 4**), which agrees well with information on metabolic function in the community indicating that sulfur oxidizers are present in greater relative abundance as compared to hydrogen, ammonia and nitrite metabolisms (Jørgensen and Zhao, 2016; Meyer et al., 2016). Lost City estimates showmethane and hydrogen oxidation reactions as significant sources of energy (**Figure 4**), which agrees with work indicating methane oxidizers are common in this system but contrasts with other recent work pointing to sulfate metabolisms as being more important than hydrogen metabolisms in this environment (Lang et al., 2018). At this site, the Gibbs free energy of the H_2/CO_2 couple is relatively high but the energy density low (**Figures 3**, **4**), as dissolved CO_2 concentration is scarce because it rapidly precipitates as carbonates in the high pH environment. As shown previously, sulfide oxidizing metabolisms are energy rich in the continental subsurface at the Sanford Underground Research Facility, and sulfide oxidizers are dominant in the microbial community (Osburn et al., 2014; Momper et al., 2017). In the subsurface portion of Rio Tinto, observation of iron and sulfur metabolisms matches with estimates of energy density (García-Moyano et al., 2012; Sánchez-Andrea et al., 2012; Amils et al., 2014). The Atacama analog site has a very low predicted energy availability, although we note that factors like water availability may be more important than energy availability in structuring the microbial community at the hyperarid and polar desert environments (Goordial et al., 2016). It is notable that the range of pH and temperature scenarios at the Atacama and University Valley sites did not particularly affect the predicted dominant reactions or volumetric energy densities at the hyper-arid sites, unlike the Mars sites, which notably changed, highlighting that the ion concentrations are key for determining dominant reactions and energy densities. Overall, this "follow the energy" approach of matching predicting energy density to microbial community structure and function may inform the likely metabolisms that might be found on extraterrestrial targets.

As with all such calculations however, there are caveats to the estimates presented. Many of these values are estimates, due to missing information for many of the extraterrestrial targets (**Supplementary Table S1**). The calculations assume steady state concentrations, whereas in Earth analog environments, current concentrations do not reflect the energy available from biogeochemical reactions that may have already occurred. Likewise, these steady state calculations do not consider the fluxes of electron donors or acceptors, which will also have strong influence on energetics. The calculations assume a cumulative energy from many different reactions that would consume the same electron donors and acceptors and do not take into account competition for these substrates between the reactions, nor the possible variabilities in reaction kinetics, which is beyond the scope of this paper. The extraterrestrial calculations were generalized across the entire target and not modified for variations in possible habitat type. These calculations also do not take any other habitability factor (i.e., **Figure 1**) such

as water, carbon availability and toxicity into consideration, though these also affect microbial communities in subsurface analog sites (Goordial et al., 2016; Purkamo et al., 2017). These speculations assume that limits of energy of life in earth systems would be applicable elsewhere. This is a rather significant assumption, but a key part of extraterrestrial-analog investigation in general. Finally, it must be noted that habitability does not necessarily mean a set of conditions will be inhabited (Cockell et al., 2016). With these limitations in mind, these figures nevertheless serve to refine the question of habitability in combination with other factors (**Figure 1**) by giving a rough indication of which microbial metabolic redox reactions in various deep subsurface sites and potential extraterrestrial targets potentially provide sufficient energy for life.

In conclusion, the low energy subsurface is a collective term for environments that are relatively isolated from surface processes, though the exact habitable range is yet largely unconstrained. The largely prokaryotic life in these environments survive a range of "extreme" conditions such as temperature and availability of electron donors or acceptors. These factors have a direct effect on the available energy of a redox reaction, which in turn affects the viability of a particular metabolism in a given set of environmental conditions. These characteristics make the low energy subsurface a source of potential analogs in the search for life elsewhere, as this combination of conditions and resource scarcity are useful in the search for the boundaries of where life is possible across a broad spectrum of possible extreme environments. Therefore, studying the subsurface in the context of analogs contributes to constraining the energetic boundaries of "following the energy" as an approach to the search for life.

AUTHOR CONTRIBUTIONS

RJ and BO developed the idea and calculated values. RJ and JG reviewed the literature. RJ wrote the paper with input from all coauthors.

FUNDING

Support for this work came from the NSF-funded Center for Dark Energy Biosphere Investigations Science and Technology Center (C-DEBI, OCE-0939564), the NASA Astrobiology Institute Life Underground program (NNA13AA92A), and the Deep Carbon Observatory funded by the Alfred P. Sloan Foundation. This is C-DEBI contribution number 431.

ACKNOWLEDGMENTS

We thank Josh Wood of the Deep Carbon Observatory for generating the graphics in **Figures 1**, **2**.

SUPPLEMENTARY MATERIAL

The Supplementary Material for this article can be found online at: https://www.frontiersin.org/articles/10.3389/fmicb.2018.01605/full#supplementary-material

TABLE S1 | Environmental values and equations used to calculate Gibbs free energy and energy density calculations.

TABLE S2 | Source references for values in **Supplementary Table S1**.

REFERENCES

Amato, P., and Christner, B. C. (2009). Energy metabolism response to low-temperature and frozen conditions in *Psychrobacter cryohalolentis*. *Appl. Environ. Microbiol.* 75, 711–718. doi: 10.1128/AEM.02193-08

Amenabar, M. J., Shock, E. L., Roden, E. E., Peters, J. W., and Boyd, E. S. (2017). Microbial substrate preference dictated by energy demand rather than supply. *Nat. Geosci.* 10, 577–581. doi: 10.1038/ngeo2978

Amend, J. P., and Shock, E. L. (2001). Energetics of overall metabolic reactions of thermophilic and hyperthermophilic Archaea and Bacteria. *FEMS Microbiol. Rev.* 25, 175–243.

Amend, J. P., and Teske, A. (2005). Expanding frontiers in deep subsurface microbiology. *Palaeogeogr. Palaeoclimatol. Palaeoecol.* 219, 131–155. doi: 10.1016/j.palaeo.2004.10.018

Amils, R., Fernández-Remolar, D. C., and IPBSL Team (2014). Río Tinto: a geochemical and mineralogical terrestrial analogue of mars. *Life* 4, 511–534. doi: 10.3390/life4030511

Anraku, Y. (1988). Bacterial electron transport Chains. *Annu. Rev. Biochem.* 57, 101–132. doi: 10.1146/annurev.biochem.57.1.101

Antunes, A., Ngugi, D. K., and Stingl, U. (2011). Microbiology of the Red Sea (and other) deep-sea anoxic brine lakes. *Environ. Microbiol. Rep.* 3, 416–433. doi: 10.1111/j.1758-2229.2011.00264.x

Arndt, S., Barker Jørgensen, B., LaRowe, D. E., Middelburg, J. J., Pancost, R. D., and Regnier, P. (2013). Quantifying the degradation of organic matter in marine sediments: a review and synthesis. *Earth Sci. Rev.* 123, 53–86. doi: 10.1016/j.earscirev.2013.02.008

Bach, W. (2016). Some compositional and kinetic controls on the bioenergetic landscapes in oceanic basement. *Front. Microbiol.* 7:107. doi: 10.3389/fmicb.2016.00107

Bach, W., and Edwards, K. J. (2003). Iron and sulfide oxidation within the basaltic ocean crust: Implications for chemolithoautotrophic microbial biomass production. *Geochim. Cosmochim. Acta* 67, 3871–3887. doi: 10.1016/S0016-7037(03)00304-1

Badalamenti, J. P., Summers, Z. M., Chan, C. H., Gralnick, J. A., and Bond, D. R. (2016). Isolation and genomic characterization of "*Desulfuromonas soudanensis* WTL", a metal- and electrode-respiring bacterium from anoxic deep subsurface brine. *Front. Microbiol.* 7:913. doi: 10.3389/fmicb.2016.00913

Bagnoud, A., de Bruijn, I., Andersson, A. F., Diomidis, N., Leupin, O. X., Schwyn, B., et al. (2016). A minimalistic microbial food web in an excavated deep subsurface clay rock. *FEMS Microbiol. Ecol.* 92:fiv138. doi: 10.1093/femsec/fiv138

Bains, W. (2004). Many chemistries could be used to build living systems. *Astrobiology* 4, 137–167. doi: 10.1089/153110704323175124

Baker, B. J., Saw, J. H., Lind, A. E., Lazar, C. S., Hinrichs, K.-U., Teske, A. P., et al. (2016). Genomic inference of the metabolism of cosmopolitan subsurface Archaea, Hadesarchaea. *Nat. Microbiol.* 1:16002. doi: 10.1038/nmicrobiol.2016.2

Bakermans, C., Skidmore, M. L., Douglas, S., and McKay, C. P. (2014). Molecular characterization of bacteria from permafrost of the Taylor Valley, Antarctica. *FEMS Microbiol. Ecol.* 89, 331–346. doi: 10.1111/1574-6941.12310

Barge, L. M., and White, L. M. (2017). Experimentally testing hydrothermal vent origin of life on enceladus and other Icy/ocean worlds. *Astrobiology* 47, 820–833. doi: 10.1089/ast.2016.1633

Bartlett, D. H., and Bidle, K. A. (1999). *Enigmatic Microorganism and Life in Extreme Environments*. Dordrecht: Kluwer Academic, 502–509. doi: 10.1017/CBO9781107415324.004

Beatty, J. T., Overmann, J., Lince, M. T., Manske, A. K., Lang, A. S., Blankenship, R. E., et al. (2005). An obligately photosynthetic bacterial anaerobe from a deep-sea hydrothermal vent. *Proc. Natl. Acad. Sci. U.S.A.* 102, 9306–9310. doi: 10.1073/pnas.0503674102

Becker, K., and Fisher, A. T. (2000). Permeability of upper oceanic basement on the eastern flank of the Juan de Fuca Ridge determined with drill-string packer experiments. *J. Geophys. Res. Atmos.* 105, 897–912. doi: 10.1029/1999jb900250

Bell, R. E., Studinger, M., Tikku, A. A., Clarke, G. K. C., Gutner, M. M., and Meertens, C. (2002). Origin and fate of Lake Vostok water frozen to the base of the East Antarctic ice sheet. *Nature* 416, 307–310. doi: 10.1038/416307a

Beller, H. R., Zhou, P., Legler, T. C., Chakicherla, A., Kane, S., Letain, T. E., et al. (2013). Genome-enabled studies of anaerobic, nitrate-dependent oxidation in the chemolithoautotrophic bacterium *Thiobacillus denitrificans*. *Front. Microbiol.* 4:249. doi: 10.3389/fmicb.2013.00249

Bergkessel, M., Basta, D. W., and Newman, D. K. (2016). The physiology of growth arrest: uniting molecular and environmental microbiology. *Nat. Rev. Microbiol.* 14, 549–562. doi: 10.1038/nrmicro.2016.107

Biddle, J. F., Lipp, J. S., Lever, M. A., Lloyd, K. G., Sorensen, K. B., Anderson, R., et al. (2006). Heterotrophic Archaea dominate sedimentary subsurface ecosystems off Peru. *Proc. Natl. Acad. Sci. U.S.A.* 103, 3846–3851. doi: 10.1073/pnas.0600035103

Bradley, J. A., Amend, J. P., and LaRowe, D. E. (2018). Bioenergetic controls on microbial ecophysiology in marine sediments. *Front. Microbiol.* 9:180. doi: 10.3389/fmicb.2018.00180

Braun, S., Mhatre, S. S., Jaussi, M., Røy, H., Kjeldsen, K. U., Pearce, C., et al. (2017). Microbial turnover times in the deep seabed studied by amino acid racemization modelling. *Sci. Rep.* 7:5680. doi: 10.1038/s41598-017-05972-z

Brazelton, W. J., Morrill, P. L., Szponar, N., and Schrenk, M. O. (2013). Bacterial communities associated with subsurface geochemical processes in continental serpentinite springs. *Appl. Environ. Microbiol.* 79, 3906–3916. doi: 10.1128/AEM.00330-13

Brazelton, W. J., Nelson, B., and Schrenk, M. O. (2012). Metagenomic evidence for H_2 oxidation and H_2 production by serpentinite-hosted subsurface microbial communities. *Front. Microbiol.* 2:268. doi: 10.3389/fmicb.2011.00268

Brazelton, W. J., Schrenk, M. O., Kelley, D. S., and Baross, J. A. (2006). Methane- and sulfur-metabolizing microbial communities dominate the lost city hydrothermal field ecosystem. *Appl. Environ. Microbiol.* 72, 6257–6270. doi: 10.1128/AEM.00574-06

Bulat, S. A. (2016). Microbiology of the subglacial Lake Vostok: first results of borehole-frozen lake water analysis and prospects for searching for lake inhabitants. *Philos. Trans. R. Soc. A Math. Phys. Eng. Sci.* 374:20140292. doi: 10.1098/rsta.2014.0292

Byrne, S., Dundas, C. M., Kennedy, M. R., Mellon, M. T., McEwen, A. S., Cull, S. C., et al. (2009). Distribution of mid-latitude ground ice on Mars from new impact craters. *Science* 325, 1674–1676. doi: 10.1126/science.1175307

Carere, C. R., Hards, K., Houghton, K. M., Power, J. F., McDonald, B., Collet, C., et al. (2017). Mixotrophy drives niche expansion of verrucomicrobial methanotrophs. *ISME J.* 11, 2599–2610. doi: 10.1038/ismej.2017.112

Carlson, R. W., Johnson, R. E., and Anderson, M. S. (1999). Sulfuric acid on europa and the radiolytic sulfur cycle. *Science* 286, 97–99. doi: 10.1126/science.286.5437.97

Catling, D. C., Claire, M. W., Zahnle, K. J., Quinn, R. C., Clark, B. C., Hecht, M. H., et al. (2010). Atmospheric origins of perchlorate on Mars and in the Atacama. *J. Geophys. Res.* 115:E00E11. doi: 10.1029/2009JE003425

Chapelle, F. H., O'Neill, K., Bradley, P. M., Methé, B. A., Ciufo, S. A., Knobel, L. L., et al. (2002). A hydrogen-based subsurface microbial community dominated by methanogens. *Nature* 415, 312–315. doi: 10.1038/415312a

Chen, L.-X., Huang, L.-N., Méndez-García, C., Kuang, J.-L., Hua, Z.-S., Liu, J., et al. (2016). Microbial communities, processes and functions in acid mine drainage ecosystems. *Curr. Opin. Biotechnol.* 38, 150–158. doi: 10.1016/j.copbio.2016.01.013

Clennell, M. B., Hovland, M., Booth, J. S., Henry, P., and Winters, W. J. (1999). Formation of natural gas hydrates in marine sediments: 1. Conceptual model of gas hydrate growth conditioned by host sediment properties. *J. Geophys. Res. Solid Earth* 104, 22985–23003. doi: 10.1029/1999JB900175

Clifford, S. M., Lasue, J., Heggy, E., Boisson, J., McGovern, P., and Max, M. D. (2010). Depth of the martian cryosphere: revised estimates and implications for the existence and detection of subpermafrost groundwater. *J. Geophys. Res. Planets* 115. doi: 10.1029/2009JE003462

Clifford, S. M., and Parker, T. J. (2001). The evolution of the martian hydrosphere: implications for the fate of a primordial ocean and the current state of the northern plains. *Icarus* 154, 40–79. doi: 10.1006/icar.2001.6671

Cockell, C. S., Bush, T., Bryce, C., Direito, S., Fox-Powell, M. G., Harrison, J. P., et al. (2016). Habitability: a review. *Astrobiology* 16, 89–117. doi: 10.1089/ast.2015.1295

Cogley, J. G. (1984). Continental margins and the extent and number of the continents. *Rev. Geophys.* 22, 101–122. doi: 10.1029/RG022i002p00101

Colman, D. R., Poudel, S., Stamps, B. W., Boyd, E. S., and Spear, J. R. (2017). The deep, hot biosphere: twenty-five years of retrospection. *Proc. Natl. Acad. Sci. U.S.A.* 114, 6895–6903. doi: 10.1073/pnas.1701266114

Cordier, D., Mousis, O., Lunine, J. I., Lavvas, P., and Vuitton, V. (2013). Erratum: an estimate of the chemical composition of titan's lakes. *Astrophys. J. Lett.* 768, L23–L26. doi: 10.1088/2041-8205/768/1/L23

Cordier, D., Mousis, O., Lunine, J. I., Lebonnois, S., Rannou, P., Lavvas, P., et al. (2012). Titan's lakes chemical composition: Sources of uncertainties and variability. *Planet. Space Sci.* 61, 99–107. doi: 10.1016/j.pss.2011.05.009

Crits-Christoph, A., Robinson, C. K., Barnum, T. P., Fricke, W., Davila, A. F., Jedynak, B., et al. (2013). Colonization patterns of soil microbial communities in the Atacama Desert. *Microbiome* 1:28. doi: 10.1186/2049-2618-1-28

Daly, R. A., Borton, M. A., Wilkins, M. J., Hoyt, D. W., Kountz, D. J., Wolfe, R. A., et al. (2016). Microbial metabolisms in a 2.5-km-deep ecosystem created by hydraulic fracturing in shales. *Nat. Microbiol.* 1:16146. doi: 10.1038/nmicrobiol.2016.146

Desai, R. T., Coates, A. J., Wellbrock, A., Vuitton, V., Crary, F. J., González-Caniulef, D., et al. (2017). Carbon chain anions and the growth of complex organic molecules in Titan's ionosphere. *Astrophys. J.* 844:L18. doi: 10.3847/2041-8213/aa7851

D'Hondt, S. (2002). Metabolic activity of subsurface life in deep-sea sediments. *Science* 295, 2067–2070. doi: 10.1126/science.1064878

D'Hondt, S., Inagaki, F., Zarikian, C. A., Abrams, L. J., Dubois, N., Engelhardt, T., et al. (2015). Presence of oxygen and aerobic communities from sea floor to basement in deep-sea sediments. *Nat. Geosci.* 8, 299–304. doi: 10.1038/ngeo2387

D'Hondt, S., Spivack, A. J., Pockalny, R., Ferdelman, T. G., Fischer, J. P., Kallmeyer, J., et al. (2009). Subseafloor sedimentary life in the South Pacific Gyre. *Proc. Natl. Acad. Sci. U.S.A.* 106, 11651–11656. doi: 10.1073/pnas.0811793106

Dick, G. J., Anantharaman, K., Baker, B. J., Li, M., Reed, D. C., and Sheik, C. S. (2013). The microbiology of deep-sea hydrothermal vent plumes: Ecological and biogeographic linkages to seafloor and water column habitats. *Front. Microbiol.* 4:124. doi: 10.3389/fmicb.2013.00124

Dilek, Y., and Furnes, H. (2014). Ophiolites and their origins. *Elements* 10, 93–100. doi: 10.2113/gselements.10.2.93

Domagal-Goldman, S. D., Wright, K. E., Adamala, K., Arina de la Rubia, L., Bond, J., Dartnell, L. R., et al. (2016). The astrobiology primer v2.0. *Astrobiology* 16, 561–653. doi: 10.1089/ast.2015.1460

Dopson, M., and Johnson, D. B. (2012). Biodiversity, metabolism and applications of acidophilic sulfur-metabolizing microorganisms. *Environ. Microbiol.* 14, 2620–2631. doi: 10.1111/j.1462-2920.2012.02749.x

Druschel, G. K., Baker, B. J., Gihring, T. M., and Banfield, J. F. (2004). Acid mine drainage biogeochemistry at Iron Mountain, California. *Geochem. Trans.* 5, 13–32. doi: 10.1063/1.1769131

Dzaugis, M. E., Spivack, A. J., Dunlea, A. G., Murray, R. W., and D'Hondt, S. (2016). Radiolytic hydrogen production in the subseafloor basaltic aquifer. *Front. Microbiol.* 7:76. doi: 10.3389/fmicb.2016.00076

Edwards, K. J., Bach, W., and McCollom, T. M. (2005). Geomicrobiology in oceanography: microbe-mineral interactions at and below the seafloor. *Trends Microbiol.* 13, 449–456. doi: 10.1016/j.tim.2005.07.005

Edwards, K. J., Becker, K., and Colwell, F. (2012a). The deep, dark energy biosphere: intraterrestrial life on earth. *Annu. Rev. Earth Planet. Sci.* 40, 551–568. doi: 10.1146/annurev-earth-042711-105500

Edwards, K. J., Fisher, A. T., and Wheat, C. G. (2012b). the deep subsurface biosphere in igneous ocean crust: frontier habitats for microbiological exploration. *Front. Microbiol.* 3:8. doi: 10.3389/fmicb.2012.00008

Ehlmann, B. L., Mustard, J. F., and Murchie, S. L. (2010). Geologic setting of serpentine deposits on Mars. *Geophys. Res. Lett.* 37:L06201. doi: 10.1029/2010GL042596

Emerson, D., Rentz, J. A., Lilburn, T. G., Davis, R. E., Aldrich, H. C., Chan, C. S., et al. (2007). A novel lineage of proteobacteria involved in formation of marine Fe-oxidizing microbial mat communities. *PLoS One* 2:e667. doi: 10.1371/journal.pone.0000667

Engelen, B., Ziegelmüller, K., Wolf, L., Köpke, B., Gittel, A., Cypionka, H., et al. (2008). Fluids from the oceanic crust support microbial activities within the deep biosphere. *Geomicrobiol. J.* 25, 56–66. doi: 10.1080/01490450701829006

Escudero, L. V., Casamayor, E. O., Chong, G., Pedrós-Alió, C., and Demergasso, C. (2013). Distribution of microbial arsenic reduction, oxidation and extrusion genes along a wide range of environmental arsenic concentrations. *PLoS One* 8:e78890. doi: 10.1371/journal.pone.0078890

Fairén, A. G., Davila, A. F., Lim, D. S. S., Bramall, N., Bonaccorsi, R., Zavaleta, J., et al. (2010). Astrobiology through the ages of mars: the study of terrestrial analogues to understand the habitability of mars. *Astrobiology* 10, 821–843. doi: 10.1089/ast.2009.0440

Fairén, A. G., Parro, V., Schulze-Makuch, D., and Whyte, L. (2017). Searching for life on mars before it is too late. *Astrobiology* 17, 962–970. doi: 10.1089/ast.2017.1703

Faucher, B., Lacelle, D., Davila, A. F., Pollard, W., Fisher, D., and McKay, C. P. (2017). Physicochemical and biological controls on carbon and nitrogen in permafrost from an ultraxerous environment, McMurdo Dry Valleys of Antarctica. *J. Geophys. Res. Biogeosci.* 122, 2593–2604. doi: 10.1002/2017JG004006

Fernández-Remolar, D. C., Prieto-Ballesteros, O., Rodríguez, N., Gómez, F., Amils, R., Gómez-Elvira, J., et al. (2008). Underground Habitats in the Río Tinto Basin: a model for subsurface life habitats on mars. *Astrobiology* 8, 1023–1047. doi: 10.1089/ast.2006.0104

Fisher, A. T. (2005). Marine hydrogeology: recent accomplishments and future opportunities. *Hydrogeol. J.* 13, 69–97. doi: 10.1007/s10040-004-0400-y

Fortes, A. D., Grindrod, P. M., Trickett, S. K., and Vočadlo, L. (2007). Ammonium sulfate on Titan: possible origin and role in cryovolcanism. *Icarus* 188, 139–153. doi: 10.1016/j.icarus.2006.11.002

Foster, S. S. D., and Chilton, P. J. (2003). Groundwater: the processes and global significance of aquifer degradation. *Philos. Trans. R. Soc. B Biol. Sci.* 358, 1957–1972. doi: 10.1098/rstb.2003.1380

Fredrickson, J. K., and Balkwill, D. L. (2006). Geomicrobial processes and biodiversity in the deep terrestrial subsurface. *Geomicrobiol. J.* 23, 345–356. doi: 10.1080/01490450600875571

Froelich, P. N., Klinkhammer, G. P., Bender, M. L., Luedtke, N. A., Heath, G. R., Cullen, D., et al. (1979). Early oxidation of organic matter in pelagic sediments of the eastern equatorial Atlantic: suboxic diagenesis. *Geochim. Cosmochim. Acta* 43, 1075–1090. doi: 10.1016/0016-7037(79)90095-4

Furnes, H., and Staudigel, H. (1999). Biological mediation in ocean crust alteration: how deep is the deep biosphere? *Earth Planet. Sci. Lett.* 166, 97–103. doi: 10.1016/S0012-821X(99)00005-9

Garcia-Lopez, E., and Cid, C. (2017). Glaciers and ice sheets as analog environments of potentially habitable Icy worlds. *Front. Microbiol.* 8:1407. doi: 10.3389/fmicb.2017.01407

García-Moyano, A., González-Toril, E., Aguilera, Á., and Amils, R. (2012). Comparative microbial ecology study of the sediments and the water column of the Río Tinto, an extreme acidic environment. *FEMS Microbiol. Ecol.* 81, 303–314. doi: 10.1111/j.1574-6941.2012.01346.x

German, C. R., Bowen, A., Coleman, M. L., Honig, D. L., Huber, J. A., Jakuba, M. V., et al. (2010). Diverse styles of submarine venting on the ultraslow spreading Mid-Cayman Rise. *Proc. Natl. Acad. Sci. U.S.A.* 107, 14020–14025. doi: 10.1073/pnas.1009205107

Gleeson, T., Befus, K. M., Jasechko, S., Luijendijk, E., and Cardenas, M. B. (2016). The global volume and distribution of modern groundwater. *Nat. Geosci.* 9, 161–164. doi: 10.1038/ngeo2590

Glein, C. R., Baross, J. A., and Waite, J. H. (2015). The pH of Enceladus' ocean. *Geochim. Cosmochim. Acta* 162, 202–219. doi: 10.1016/j.gca.2015.04.017

Glombitza, C., Adhikari, R. R., Riedinger, N., Gilhooly, W. P., Hinrichs, K.-U., and Inagaki, F. (2016). Microbial sulfate reduction potential in coal-bearing sediments down to ∼2.5 km below the seafloor off Shimokita Peninsula, Japan. *Front. Microbiol.* 7:1576. doi: 10.3389/fmicb.2016.01576

Goordial, J., Davila, A. F., Lacelle, D., Pollard, W., Marinova, M. M., Greer, C. W., et al. (2016). Nearing the cold-arid limits of microbial life in permafrost of an upper dry valley, Antarctica. *ISME J.* 10, 1613–1624. doi: 10.1038/ismej.2015.239

Hand, K. P., Carlson, R. W., and Chyba, C. F. (2007). Energy, chemical disequilibrium, and geological constraints on Europa. *Astrobiology* 7, 1006–1022. doi: 10.1089/ast.2007.0156

Hatzenpichler, R., Connon, S. A., Goudeau, D., Malmstrom, R. R., Woyke, T., and Orphan, V. J. (2016). Visualizing in situ translational activity for identifying and sorting slow-growing archaeal-bacterial consortia. *Proc. Natl. Acad. Sci. U.S.A.* 113, E4069–E4078. doi: 10.1073/pnas.1603757113

Hayes, A., Aharonson, O., Callahan, P., Elachi, C., Gim, Y., Kirk, R. L., et al. (2008). Hydrocarbon lakes on Titan: distribution and interaction with a porous regolith. *Geophys. Res. Lett.* 35:L09204. doi: 10.1029/2008gl033409

Head, I. M., Gray, N. D., and Larter, S. R. (2014). Life in the slow lane; biogeochemistry of biodegraded petroleum containing reservoirs and implications for energy recovery and carbon management. *Front. Microbiol.* 5:566. doi: 10.3389/fmicb.2014.00566

Head, I. M., Jones, D. M., and Larter, S. R. (2003). Biological activity in the deep subsurface and the origin of heavy oil. *Nature* 426, 344–352. doi: 10.1038/nature02134

Hedrich, S., Schlomann, M., and Johnson, D. B. (2011). The iron-oxidizing proteobacteria. *Microbiology* 157, 1551–1564. doi: 10.1099/mic.0.045344-0

Heim, C., Quéric, N. V., Ionescu, D., Schäfer, N., and Reitner, J. (2017). Frutexites-like structures formed by iron oxidizing biofilms in the continental subsurface (Äspö Hard Rock Laboratory, Sweden). *PLoS One* 12:e0177542. doi: 10.1371/journal.pone.0177542

Heldmann, J. L., Pollard, W., McKay, C. P., Marinova, M. M., Davila, A. F., Williams, K. E., et al. (2013). The high elevation Dry Valleys in Antarctica as analog sites for subsurface ice on Mars. *Planet. Space Sci.* 85, 53–58. doi: 10.1016/j.pss.2013.05.019

Hernsdorf, A. W., Amano, Y., Miyakawa, K., Ise, K., Suzuki, Y., Anantharaman, K., et al. (2017). Potential for microbial H2 and metal transformations associated with novel bacteria and archaea in deep terrestrial subsurface sediments. *ISME J.* 11, 1915–1929. doi: 10.1038/ismej.2017.39

Hoefen, T. M., Clark, R. N., Bandfield, J. L., Smith, M. D., Pearl, J. C., and Christensen, P. R. (2003). Discovery of olivine in the Nili Fssae region of Mars. *Science* 302, 627–630. doi: 10.1126/science.1089647

Hoehler, T. M. (2004). Biological energy requirements as quantitative boundary conditions for life in the subsurface. *Geobiology* 2, 205–215. doi: 10.1111/j.1472-4677.2004.00033.x

Hoehler, T. M. (2007). An Energy Balance Concept for Habitability. *Astrobiology* 7, 824–838. doi: 10.1089/ast.2006.0095

Hoehler, T. M., and Jørgensen, B. B. (2013). Microbial life under extreme energy limitation. *Nat. Rev. Microbiol.* 11, 83–94. doi: 10.1038/nrmicro2939

Holm, N. G., Oze, C., Mousis, O., Waite, J. H., and Guilbert-Lepoutre, A. (2015). Serpentinization and the Formation of H_2 and CH_4 on Celestial Bodies (Planets, Moons, Comets). *Astrobiology* 15, 587–600. doi: 10.1089/ast.2014.1188

Horgan, B. H. N., Smith, R. J., Cloutis, E. A., Mann, P., and Christensen, P. R. (2017). Acid weathering of basalt and basaltic glass: I. Near-infrared spectra, thermal-infrared spectra, and implications for Mars. *J. Geophys. Res. Planets* 122, 1–31. doi: 10.1002/2016JE005111

Hoshino, T., and Inagaki, F. (2017). Distribution of anaerobic carbon monoxide dehydrogenase genes in deep subseafloor sediments. *Lett. Appl. Microbiol.* 64, 355–363. doi: 10.1111/lam.12727

Hsu, H.-W., Postberg, F., Sekine, Y., Shibuya, T., Kempf, S., Horanyi, M., et al. (2015). Ongoing hydrothermal activities within Enceladus. *Nature* 519, 207–210. doi: 10.1038/nature14262

Iess, L., Stevenson, D. J., Parisi, M., Hemingway, D., Jacobson, R. A., Lunine, J. I., et al. (2014). The gravity field and interior structure of Enceladus. *Science* 344, 78–80. doi: 10.1126/science.1250551

Jaakkola, S. T., Ravantti, J. J., Oksanen, H. M., and Bamford, D. H. (2016). Buried alive: microbes from ancient halite. *Trends Microbiol.* 24, 148–160. doi: 10.1016/j.tim.2015.12.002

Jackson, A., Davila, A. F., Böhlke, J. K., Sturchio, N. C., Sevanthi, R., Estrada, N., et al. (2016). Deposition, accumulation, and alteration of Cl -, NO 3 -, ClO 4 - and ClO 3 - salts in a hyper-arid polar environment: Mass balance and isotopic constraints. *Geochim. Cosmochim. Acta* 182, 197–215. doi: 10.1016/j.gca.2016.03.012

Jakosky, B. M., Nealson, K. H., Bakermans, C., Ley, R. E., and Mellon, M. T. (2003). Subfreezing activity of microorganisms and the potential habitability of mars', polar regions. *Astrobiology* 3, 343–350. doi: 10.1089/153110703769016433

Jennings, D. E., Flasar, F. M., Kunde, V. G., Samuelson, R. E., Pearl, J. C., Nixon, C. A., et al. (2009). Titan's surface brightness temperatures. *Astrophys. J.* 691, L103–L105. doi: 10.1088/0004-637X/691/2/L103

Ji, F., Zhou, H., Yang, Q., Gao, H., Wang, H., and Lilley, M. D. (2017). Geochemistry of hydrothermal vent fluids and its implications for subsurface processes at the active Longqi hydrothermal field, Southwest Indian Ridge. *Deep Sea Res. Part 1 Oceanogr. Res. Pap.* 122, 41–47. doi: 10.1016/j.dsr.2017.02.001

Johnson, D. B., Hedrich, S., and Pakostova, E. (2017). Indirect redox transformations of iron, copper, and chromium catalyzed by extremely acidophilic bacteria. *Front. Microbiol.* 8:211. doi: 10.3389/fmicb.2017.00211

Johnson, D. B., Kanao, T., and Hedrich, S. (2012). Redox transformations of iron at extremely low pH: fundamental and applied aspects. *Front. Microbiol.* 3:96. doi: 10.3389/fmicb.2012.00096

Johnson, S. S., Hebsgaard, M. B., Christensen, T. R., Mastepanov, M., Nielsen, R., Munch, K., et al. (2007). Ancient bacteria show evidence of DNA repair. *Proc. Natl. Acad. Sci. U.S.A.* 104, 14401–14405. doi: 10.1073/pnas.0706787104

Jones, S. E., and Lennon, J. T. (2010). Dormancy contributes to the maintenance of microbial diversity. *Proc. Natl. Acad. Sci. U.S.A.* 107, 5881–5886. doi: 10.1073/pnas.0912765107

Jørgensen, B. B., and Boetius, A. (2007). Feast and famine — microbial life in the deep-sea bed. *Nat. Rev. Microbiol.* 5, 770–781. doi: 10.1038/nrmicro1745

Jørgensen, S. L., and Zhao, R. (2016). Microbial inventory of deeply buried oceanic crust from a young ridge flank. *Front. Microbiol.* 7:820. doi: 10.3389/fmicb.2016.00820

Joye, S. B., Bowles, M. W., Samarkin, V. A., Hunter, K. S., and Niemann, H. (2010). Biogeochemical signatures and microbial activity of different cold-seep habitats along the Gulf of Mexico deep slope. *Deep. Res. Pt. II Top. Stud. Oceanogr.* 57, 1990–2001. doi: 10.1016/j.dsr2.2010.06.001

Joye, S. B., Samarkin, V. A., Orcutt, B. N., MacDonald, I. R., Hinrichs, K.-U., Elvert, M., et al. (2009). Metabolic variability in seafloor brines revealed by carbon and sulphur dynamics. *Nat. Geosci.* 2, 349–354. doi: 10.1038/ngeo475

Jungbluth, S. P., Bowers, R. M., Lin, H. T., Cowen, J. P., and Rappé, M. S. (2016). Novel microbial assemblages inhabiting crustal fluids within mid-ocean ridge flank subsurface basalt. *ISME J.* 10, 2033–2047. doi: 10.1038/ismej.2015.248

Kallmeyer, J., Pockalny, R., Adhikari, R. R., Smith, D. C., and D'Hondt, S. (2012). Global distribution of microbial abundance and biomass in subseafloor sediment. *Proc. Natl. Acad. Sci. U.S.A.* 109, 16213–16216. doi: 10.1073/pnas.1203849109

Kappler, A., Emerson, D., Edwards, K. J., Amend, J. P., Gralnick, J. A., Grathwohl, P., et al. (2005). Microbial activity in biogeochemical gradients - New aspects of research. *Geobiology* 3, 229–233. doi: 10.1111/j.1472-4669.2005.00053.x

Kargel, J. S. (1994). Cryovolcanism on the icy satellites. *Earth Moon Planets* 67, 101–113. doi: 10.1007/BF00613296

Karson, J. A. (2002). Geologic structure of the uppermost oceanic crust created at fast- to intermediate-rate spreading centers. *Annu. Rev. Earth Planet. Sci.* 30, 347–384. doi: 10.1146/annurev.earth.30.091201.141132

Kashefi, K., and Lovley, D. R. (2000). Reduction of Fe (III), Mn (IV), and Toxic Metals at 100°C by *Pyrobaculum islandicum* Reduction of Fe (III), Mn (IV), and Toxic Metals at 100°C by *Pyrobaculum islandicum*. *Society* 66, 1050–1056. doi: 10.1128/AEM.66.3.1050-1056.2000

Katayama, T., Yoshioka, H., Takahashi, H. A., Amo, M., Fujii, T., and Sakata, S. (2016). Changes in microbial communities associated with gas hydrates in subseafloor sediments from the Nankai Trough. *FEMS Microbiol. Ecol.* 92:fiw093. doi: 10.1093/femsec/fiw093

Kelley, D. S., Karson, J. A., Blackman, D. K., Früh-Green, G. L., Butterfield, D. A., Lilley, M. D., et al. (2001). An off-axis hydrothermal vent field near the Mid-Atlantic Ridge at 30°N. *Nature* 412, 145–149. doi: 10.1038/35084000

Kelley, D. S., Karson, J. A., Früh-Green, G. L., Yoerger, D. R., Shank, T. M., Butterfield, D. A., et al. (2005). A serpentinite-hosted ecosystem: the Lost City hydrothermal field. *Science* 307, 1428–1434. doi: 10.1126/science.1102556

Kempes, C. P., van Bodegom, P. M., Wolpert, D., Libby, E., Amend, J. P., and Hoehler, T. M. (2017). Drivers of bacterial maintenance and minimal energy requirements. *Front. Microbiol.* 8:31. doi: 10.3389/fmicb.2017.00031

Kieffer, S. W., Lu, X., Bethke, C. M., Spencer, J. R., Marshak, S., and Navrotsky, A. (2006). A clathrate reservoir hypothesis for enceladus south polar plume. *Science* 314, 1764–1766. doi: 10.1126/science.1133519

Kivelson, M. G., Khurana, K. K., Russell, C. T., Volwerk, M., Walker, R. J., and Zimmer, C. (2000). Galileo magnetometer measurements: a stronger case for a subsurface ocean at Europa. *Science* 289, 1340–1343. doi: 10.1126/science.289.5483.1340

Koh, C. A. (2002). Towards a fundamental understanding of natural gas hydrates. *Chem. Soc. Rev.* 31, 157–167. doi: 10.1039/b008672j

Kounaves, S. P., Hecht, M. H., Kapit, J., Gospodinova, K., DeFlores, L., Quinn, R. C., et al. (2010a). Wet chemistry experiments on the 2007 phoenix mars scout lander mission: data analysis and results. *J. Geophys. Res.* 115:E00E10. doi: 10.1029/2009JE003424

Kounaves, S. P., Stroble, S. T., Anderson, R. M., Moore, Q., Catling, D. C., Douglas, S., et al. (2010b). Discovery of natural perchlorate in the Antarctic dry valleys and its global implications. *Environ. Sci. Technol.* 44, 2360–2364. doi: 10.1021/es9033606

Kracke, F., Vassilev, I., and Kromer, J. O. (2015). Microbial electron transport and energy conservation - The foundation for optimizing bioelectrochemical systems. *Front. Microbiol.* 6:575. doi: 10.3389/fmicb.2015.00575

Kristjánsson, J. K., and Hreggvidsson, G. O. (1995). Ecology and habitats of extremophiles. *World J. Microbiol. Biotechnol.* 11, 17–25. doi: 10.1007/BF00339134

Labonté, J. M., Lever, M. A., Edwards, K. J., and Orcutt, B. N. (2017). Influence of igneous basement on deep sediment microbial diversity on the eastern Juan de Fuca Ridge flank. *Front. Microbiol.* 8:1434. doi: 10.3389/fmicb.2017.01434

Lang, S. Q., Butterfield, D. A., Schulte, M., Kelley, D. S., and Lilley, M. D. (2010). Elevated concentrations of formate, acetate and dissolved organic carbon found at the Lost City hydrothermal field. *Geochim. Cosmochim. Acta* 74, 941–952. doi: 10.1016/j.gca.2009.10.045

Lang, S. Q., Früh-Green, G. L., Bernasconi, S. M., Brazelton, W. J., Schrenk, M. O., and McGonigle, J. M. (2018). Deeply-sourced formate fuels sulfate reducers but not methanogens at Lost City hydrothermal field. *Sci. Rep.* 8:755. doi: 10.1038/s41598-017-19002-5

LaRowe, D. E., and Amend, J. P. (2015a). Catabolic rates, population sizes and doubling/replacement times of microorganisms in natural settings. *Am. J. Sci.* 315, 167–203. doi: 10.2475/03.2015.01

LaRowe, D. E., and Amend, J. P. (2015b). Power limits for microbial life. *Front. Microbiol.* 6:718. doi: 10.3389/fmicb.2015.00718

LaRowe, D. E., Burwicz, E., Arndt, S., Dale, A. W., and Amend, J. P. (2017). Temperature and volume of global marine sediments. *Geology* 45, 275–278. doi: 10.1130/G38601.1

LaRowe, D. E., and Van Cappellen, P. (2011). Degradation of natural organic matter: a thermodynamic analysis. *Geochim. Cosmochim. Acta* 75, 2030–2042. doi: 10.1016/j.gca.2011.01.020

Larter, S. R., Huang, H., Adams, J., Bennett, B., Jokanola, O., Oldenburg, T., et al. (2006). The controls on the composition of biodegraded oils in the deep subsurface: part II - Geological controls on subsurface biodegradation fluxes and constraints on reservoir-fluid property prediction. *Am. Assoc. Pet. Geol. Bull.* 90, 921–938. doi: 10.1306/01270605130

Lau, M. C. Y., Kieft, T. L., Kuloyo, O., Linage-Alvarez, B., van Heerden, E., Lindsay, M. R., et al. (2016). An oligotrophic deep-subsurface community dependent on syntrophy is dominated by sulfur-driven autotrophic denitrifiers.

Proc. Natl. Acad. Sci. U.S.A. 113, E7927–E7936. doi: 10.1073/pnas.1612244113

Lederberg, J. (1960). Exobiology: approaches to life beyond the Earth. *Science* 132, 393–400.

Lee, J.-H., Fredrickson, J. K., Plymale, A. E., Dohnalkova, A. C., Resch, C. T., McKinley, J. P., et al. (2015). An autotrophic H_2 -oxidizing, nitrate-respiring, Tc(VII)-reducing A Cidovorax sp. isolated from a subsurface oxic-anoxic transition zone. *Environ. Microbiol. Rep.* 7, 395–403. doi: 10.1111/1758-2229.12263

Lehman, R. M., Roberto, F. F., Earley, D., Bruhn, D. F., Brink, S. E., O'Connell, S. P., et al. (2001). Attached and unattached bacterial communities in a 120-Meter Corehole in an Acidic, Crystalline Rock Aquifer. *Appl. Environ. Microbiol.* 67, 2095–2106. doi: 10.1128/AEM.67.5.2095-2106.2001

Lennon, J. T., and Jones, S. E. (2011). Microbial seed banks: the ecological and evolutionary implications of dormancy. *Nat. Rev. Microbiol.* 9, 119–130. doi: 10.1038/nrmicro2504

Leupin, O. X., Bernier-Latmani, R., Bagnoud, A., Moors, H., Leys, N., Wouters, K., et al. (2017). Fifteen years of microbiological investigation in Opalinus Clay at the Mont Terri rock laboratory (Switzerland). *Swiss J. Geosci.* 110, 343–354. doi: 10.1007/s00015-016-0255-y

Léveillé, R. (2010). A half-century of terrestrial analog studies: from craters on the Moon to searching for life on Mars. *Planet. Space Sci.* 58, 631–638. doi: 10.1016/j.pss.2009.04.001

Lever, M. A., Rogers, K. L., Lloyd, K. G., Overmann, J., Schink, B., Thauer, R. K., et al. (2015). Life under extreme energy limitation: a synthesis of laboratory- and field-based investigations. *FEMS Microbiol. Rev.* 39, 688–728. doi: 10.1093/femsre/fuv020

L'Haridon, S., Reysenbacht, A.-L., Glénat, P., Prieur, D., and Jeanthon, C. (1995). Hot subterranean biosphere in a continental oil reservoir. *Nature* 377, 223–224. doi: 10.1038/377223a0

Lopes, R. M. C., Kirk, R. L., Mitchell, K. L., Legall, A., Barnes, J. W., Hayes, A., et al. (2013). Cryovolcanism on Titan: new results from Cassini RADAR and VIMS. *J. Geophys. Res. E Planets* 118, 416–435. doi: 10.1002/jgre.20062

Lovley, D. R. (2008). Extracellular electron transfer: Wires, capacitors, iron lungs, and more. *Geobiology* 6, 225–231. doi: 10.1111/j.1472-4669.2008.00148.x

Lovley, D. R., and Chapelle, F. H. (1995). Deep subsurface microbial processes. *Rev. Geophys.* 33, 365–381. doi: 10.1029/95RG01305

Lowell, R. P., and DuBose, M. (2005). Hydrothermal systems on Europa. *Geophys. Res. Lett.* 32:L05202. doi: 10.1029/2005gl022375

Lowenstein, T. K., Schubert, B. A., and Timofeeff, M. N. (2011). Microbial communities in fluid inclusions and long-term survival in halite. *GSA Today* 21, 4–9. doi: 10.1130/GSATG81A.1

Lunine, J. I. (2017). Ocean worlds exploration. *Acta Astronaut.* 131, 123–130. doi: 10.1016/j.actaastro.2016.11.017

Lysnes, K., Thorseth, I. H., Steinsbu, B. O., Øvreås, L., Torsvik, T., and Pedersen, R. B. (2004). Microbial community diversity in seafloor basalt from the Arctic spreading ridges. *FEMS Microbiol. Ecol.* 50, 213–230. doi: 10.1016/j.femsec.2004.06.014

Marlow, J. J., Skennerton, C. T., Li, Z., Chourey, K., Hettich, R. L., Pan, C., et al. (2016). Proteomic stable isotope probing reveals biosynthesis dynamics of slow growing methane based microbial communities. *Front. Microbiol.* 7:563. doi: 10.3389/fmicb.2016.00563

Martin, A., and McMinn, A. (2017). Sea ice, extremophiles and life on extra-terrestrial ocean worlds. *Int. J. Astrobiol.* 17, 1–16. doi: 10.1017/s1473550416000483

Martins, Z., Cottin, H., Kotler, J. M., Carrasco, N., Cockell, C. S., Dela Torre, et al. (2017). Earth as a tool for astrobiology—a European perspective. *Space Sci. Rev.* 209, 43–81. doi: 10.1007/s11214-017-0369-1

McCollom, T. M. (1999). Methanogenesis as a potential source of chemical energy for primary biomass production by autotrophic organisms in hydrothermal systems on Europa. *J. Geophys. Res. Planets* 104, 30729–30742. doi: 10.1029/1999JE001126

McCord, T. B., Hansen, G. B., Fanale, F. P., Carlson, R. W., Matson, D. L., Johnson, T. V., et al. (1998). Salts on Europa's surface detected by Galileo's near infrared mapping spectrometer. *Science* 280, 1242–1245. doi: 10.1126/science.280.5367.1242

McMahon, S., and Parnell, J. (2014). Weighing the deep continental biosphere. *FEMS Microbiol. Ecol.* 87, 113–120. doi: 10.1111/1574-6941.12196

Meyer, J. L., Jaekel, U., Tully, B. J., Glazer, B. T., Wheat, C. G., Lin, H.-T., et al. (2016). A distinct and active bacterial community in cold oxygenated fluids circulating beneath the western flank of the Mid-Atlantic ridge. *Sci. Rep.* 6:22541. doi: 10.1038/srep22541

Michaud, A. B., Dore, J. E., Achberger, A. M., Christner, B. C., Mitchell, A. C., Skidmore, M. L., et al. (2017). Microbial oxidation as a methane sink beneath the West Antarctic Ice Sheet. *Nat. Geosci.* 10, 582–586. doi: 10.1038/ngeo2992

Mickol, R. L., and Kral, T. A. (2017). Low pressure tolerance by methanogens in an aqueous environment: implications for subsurface life on Mars. *Orig. Life Evol. Biosph.* 47, 511–532. doi: 10.1007/s11084-016-9519-9

Miettinen, H., Kietäväinen, R., Sohlberg, E., Numminen, M., Ahonen, L., and Itävaara, M. (2015). Microbiome composition and geochemical characteristics of deep subsurface high-pressure environment, Pyhasalmi mine Finland. *Front. Microbiol.* 6:1203. doi: 10.3389/fmicb.2015.01203

Mikucki, J. A., Lee, P. A., Ghosh, D., Purcell, A. M., Mitchell, A. C., Mankoff, K. D., et al. (2016). Subglacial Lake Whillans microbial biogeochemistry: a synthesis of current knowledge. *Philos. Trans. A Math. Phys. Eng. Sci.* 374:20140290. doi: 10.1098/rsta.2014.0290

Momper, L. M., Kiel Reese, B., Zinke, L. A., Wanger, G., Osburn, M. R., Moser, D. P., et al. (2017). Major phylum-level differences between porefluid and host rock bacterial communities in the terrestrial deep subsurface. *Environ. Microbiol. Rep.* 9, 501–511. doi: 10.1111/1758-2229.12563

Morono, Y., Terada, T., Nishizawa, M., Ito, M., Hillion, F., Takahata, N., et al. (2011). Carbon and nitrogen assimilation in deep subseafloor microbial cells. *Proc. Natl. Acad. Sci. U.S.A.* 108, 18295–18300. doi: 10.1073/pnas.1107763108

Mousis, O., Choukroun, M., Lunine, J. I., and Sotin, C. (2014). Equilibrium composition between liquid and clathrate reservoirs on Titan. *Icarus* 239, 39–45. doi: 10.1016/j.icarus.2014.05.032

Müller, V., and Hess, V. (2017). The minimum biological energy quantum. *Front. Microbiol.* 8:2019. doi: 10.3389/fmicb.2017.02019

Mumma, M. J., Villanueva, G. L., Novak, R. E., Hewagama, T., Bonev, B. P., DiSanti, M. A., et al. (2009). Strong release of methane on Mars in northern summer 2003. *Science* 323, 1041–1045. doi: 10.1126/science.1165243

Murray, A. E., Kenig, F., Fritsen, C. H., McKay, C. P., Cawley, K. M., Edwards, R., et al. (2012). Microbial life at -13 C in the brine of an ice-sealed Antarctic lake. *Proc. Natl. Acad. Sci. U.S.A.* 109, 20626–20631. doi: 10.1073/pnas.1208607109

Mykytczuk, N. C. S., Foote, S. J., Omelon, C. R., Southam, G., Greer, C. W., and Whyte, L. G. (2013). Bacterial growth at − 15°C; molecular insights from the permafrost bacterium *Planococcus halocryophilus* Or1. *ISME J.* 7, 1211–1226. doi: 10.1038/ismej.2013.8

Navarro-González, R., Rainey, F. A., Molina, P., Bagaley, D. R., Hollen, B. J., De La Rosa, J., et al. (2003). Mars-like soils in the Atacama desert, chile, and the dry limit of microbial life. *Science* 302, 1018–1021. doi: 10.1126/science.1089143

Navarro-González, R., Vargas, E., De La Rosa, J., Raga, A. C., and McKay, C. P. (2010). Reanalysis of the Viking results suggests perchlorate and organics at midlatitudes on Mars. *J. Geophys. Res. E Planets* 115:E12010. doi: 10.1029/2010JE003599

Neubeck, A., Sun, L., Müller, B., Ivarsson, M., Hosgörmez, H., Özcan, D., et al. (2017). Microbial community structure in a serpentine-hosted abiotic gas seepage at the Chimaera Ophiolite, Turkey. *Appl. Environ. Microbiol.* 83:e03430-16. doi: 10.1128/AEM.03430-16

Niemann, H. B., Atreya, S. K., Bauer, S. H., Carignan, G. R., Demick, J. E., Frost, R. L., et al. (2005). The abundances of constituents of Titan's atmosphere from the GCMS instrument on the Huygens probe. *Nature* 438, 779–784. doi: 10.1038/nature04122

Nixon, S. L., Cockell, C. S., and Tranter, M. (2012). Limitations to a microbial iron cycle on Mars. *Planet. Space Sci.* 72, 116–128. doi: 10.1016/j.pss.2012.04.003

Nixon, S. L., Cousins, C. R., and Cockell, C. S. (2013). Plausible microbial metabolisms on Mars. *Astron. Geophys.* 54, 13–11. doi: 10.1093/astrogeo/ats034

Ody, A., Poulet, F., Langevin, Y., Bibring, J. P., Bellucci, G., Altieri, F., et al. (2012). Global maps of anhydrous minerals at the surface of Mars from OMEGA/MEx. *J. Geophys. Res. E Planets* 117: E00J14. doi: 10.1029/2012JE004117

Oehler, D. Z., and Etiope, G. (2017). Methane seepage on Mars: where to look and why. *Astrobiology* 17, 1233–1264. doi: 10.1089/ast.2017.1657

Oger, P. M., and Jebbar, M. (2010). The many ways of coping with pressure. *Res. Microbiol.* 161, 799–809. doi: 10.1016/j.resmic.2010.09.017

Orcutt, B. N., and Edwards, K. J. (2014). Life in the ocean crust: lessons from subseafloor laboratories. *Dev. Mar. Geol.* 7, 175–196. doi: 10.1016/B978-0-444-62617-2.00007-4

Orcutt, B. N., Larowe, D. E., Biddle, J. F., Colwell, F. S., Glazer, B. T., Reese, B. K., et al. (2013a). Microbial activity in the marine deep biosphere: progress and prospects. *Front. Microbiol.* 4:189. doi: 10.3389/fmicb.2013.00189

Orcutt, B. N., Wheat, C. G., Rouxel, O. J., Hulme, S. M., Edwards, K. J., and Bach, W. (2013b). Oxygen consumption rates in subseafloor basaltic crust derived from a reaction transport model. *Nat. Commun.* 4:2539. doi: 10.1038/ncomms3539

Orcutt, B. N., Sylvan, J. B., Knab, N. J., and Edwards, K. J. (2011). Microbial ecology of the dark ocean above, at, and below the seafloor. *Microbiol. Mol. Biol. Rev.* 75, 361–422. doi: 10.1128/MMBR.00039-10

Orcutt, B. N., Sylvan, J. B., Rogers, D. R., Delaney, J., Lee, R. W., and Girguis, P. R. (2015). Carbon fixation by basalt-hosted microbial communities. *Front. Microbiol.* 6:904. doi: 10.3389/fmicb.2015.00904

Oremland, R. S. (2003). The ecology of Arsenic. *Science* 300, 939–944. doi: 10.1126/science.1081903

Orsi, W. D., Barker Jørgensen, B., and Biddle, J. F. (2016). Transcriptional analysis of sulfate reducing and chemolithoautotrophic sulfur oxidizing bacteria in the deep subseafloor. *Environ. Microbiol. Rep.* 8, 452–460. doi: 10.1111/1758-2229.12387

Orsi, W. D., Edgcomb, V. P., Christman, G. D., and Biddle, J. F. (2013). Gene expression in the deep biosphere. *Nature* 499, 205–208. doi: 10.1038/nature12230

Osburn, M. R., LaRowe, D. E., Momper, L. M., and Amend, J. P. (2014). Chemolithotrophy in the continental deep subsurface: Sanford Underground Research Facility (SURF), USA. *Front. Microbiol.* 5:610. doi: 10.3389/fmicb.2014.00610

Osegovic, J. P., and Max, M. D. (2005). Compound clathrate hydrate on Titan's surface. *J. Geophys. Res. E Planets* 110:E08004. doi: 10.1029/2005JE002435

Panikov, N. S., and Sizova, M. V. (2007). Growth kinetics of microorganisms isolated from Alaskan soil and permafrost in solid media frozen down to −35 degrees C. *FEMS Microbiol. Ecol.* 59, 500–512. doi: 10.1111/j.1574-6941.2006.00210.x

Parnell, J., and McMahon, S. (2016). Physical and chemical controls on habitats for life in the deep subsurface beneath continents and ice. *Philos. Trans. R. Soc. A Math. Phys. Eng. Sci.* 374:20140293. doi: 10.1098/rsta.2014.0293

Parro, V., de Diego-Castilla, G., Moreno-Paz, M., Blanco, Y., Cruz-Gil, P., Rodríguez-Manfredi, J. A., et al. (2011). A microbial oasis in the hypersaline Atacama subsurface discovered by a life detector chip: implications for the search for life on mars. *Astrobiology* 11, 969–996. doi: 10.1089/ast.2011.0654

Payler, S. J., Biddle, J. F., Coates, A. J., Cousins, C. R., Cross, R. E., Cullen, D. C., et al. (2017). Planetary science and exploration in the deep subsurface: results from the MINAR Program, Boulby Mine, UK. *Int. J. Astrobiol.* 16, 114–129. doi: 10.1017/S1473550416000045

Peng, X., Ta, K., Chen, S., Zhang, L., and Xu, H. (2015). Coexistence of Fe(II)- and Mn(II)-oxidizing bacteria govern the formation of deep sea umber deposits. *Geochim. Cosmochim. Acta* 169, 200–216. doi: 10.1016/j.gca.2015.09.011

Peretyazhko, T. S., Niles, P. B., Sutter, B., Morris, R. V., Agresti, D. G., Le, L., et al. (2017). Smectite formation in the presence of sulfuric acid: implications for acidic smectite formation on early Mars. *Geochim. Cosmochim. Acta* 220, 248–260.

Phelps, T. J., Murphy, E. M., Pfiffner, S. M., and White, D. C. (1994). Comparison between geochemical and biological estimates of subsurface microbial activities. *Microb. Ecol.* 28, 335–349. doi: 10.1007/BF00662027

Postberg, F., Kempf, S., Schmidt, J., Brilliantov, N., Beinsen, A., Abel, B., et al. (2009). Sodium salts in E-ring ice grains from an ocean below the surface of Enceladus. *Nature* 459, 1098–1101. doi: 10.1038/nature08046

Preston, L. J., and Dartnell, L. R. (2014). Planetary habitability: lessons learned from terrestrial analogues. *Int. J. Astrobiol.* 13, 81–98. doi: 10.1017/S1473550413000396

Price, P. B., and Sowers, T. (2004). Temperature dependence of metabolic rates for microbial growth, maintenance, and survival. *Proc. Natl. Acad. Sci. U.S.A.* 101, 4631–4636. doi: 10.1073/pnas.0400522101

Prokofeva, M. I., Kublanov, I. V., Nercessian, O., Tourova, T. P., Kolganova, T. V., Lebedinsky, A. V., et al. (2005). Cultivated anaerobic acidophilic/acidotolerant thermophiles from terrestrial and deep-sea hydrothermal habitats. *Extremophiles* 9, 437–448. doi: 10.1007/s00792-005-0461-4

Proskurowski, G., Lilley, M. D., Seewald, J. S., Früh-Green, G. L., Olson, E. J., Lupton, J. E., et al. (2008). Abiogenic hydrocarbon production at lost city hydrothermal field. *Science* 319, 604–607. doi: 10.1126/science.1151194

Purkamo, L., Bomberg, M., Nyyssönen, M., Ahonen, L., Kukkonen, I., and Itävaara, M. (2017). Response of deep subsurface microbial community to different carbon sources and electron acceptors during 2 months incubation in microcosms. *Front. Microbiol.* 8:232. doi: 10.3389/fmicb.2017.00232

Quick, L. C., and Marsh, B. D. (2016). Heat transfer of ascending cryomagma on Europa. *J. Volcanol. Geotherm. Res.* 319, 66–77. doi: 10.1016/j.jvolgeores.2016.03.018

Reese, B. K., Zinke, L. A., Sobol, M. S., LaRowe, D. E., Orcutt, B. N., Zhang, X., et al. (2018). Nitrogen cycling of active bacteria within oligotrophic sediment of the mid-atlantic ridge flank. *Geomicrobiol. J.* 35, 468–483. doi: 10.1080/01490451.2017.1392649

Rempfert, K. R., Miller, H. M., Bompard, N., Nothaft, D., Matter, J. M., Kelemen, P., et al. (2017). Geological and geochemical controls on subsurface microbial life in the Samail Ophiolite, Oman. *Front. Microbiol.* 8:56. doi: 10.3389/fmicb.2017.00056

Reveillaud, J., Reddington, E., McDermott, J., Algar, C., Meyer, J. L., Sylva, S., et al. (2016). Subseafloor microbial communities in hydrogen-rich vent fluids from hydrothermal systems along the Mid-Cayman Rise. *Environ. Microbiol.* 18, 1970–1987. doi: 10.1111/1462-2920.13173

Reynolds, G. T., and Lutz, R. A. (2001). Sources of Light in the Deep Ocean. *Rev. Geophys.* 39, 123–136. doi: 10.1029/1999RG000071

Robador, A., LaRowe, D. E., Jungbluth, S. P., Lin, H. T., Rappé, M. S., Nealson, K. H., et al. (2016a). Nanocalorimetric characterization of microbial activity in deep subsurface oceanic crustal fluids. *Front. Microbiol.* 7:454. doi: 10.3389/fmicb.2016.00454

Robador, A., Müller, A. L., Sawicka, J. E., Berry, D., Hubert, C. R. J., Loy, A., et al. (2016b). Activity and community structures of sulfate-reducing microorganisms in polar, temperate and tropical marine sediments. *ISME J.* 10, 796–809. doi: 10.1038/ismej.2015.157

Røy, H., Kallmeyer, J., Adhikari, R. R., Pockalny, R., Jørgensen, B. B., and D'Hondt, S. (2012). Aerobic microbial respiration in 86-million-year-old deep-sea red clay. *Science* 336, 922–925. doi: 10.1126/science.1219424

Rudnick, R. L., and Fountain, D. M. (1995). Nature and composition of the continental crust: a lower crustal perspective. *Rev. Geophys.* 33, 267–309. doi: 10.1029/95RG01302

Rudnick, R. L., and Gao, S. (2003). 3.01 – Composition of the continental crust. *Treatise Geochem.* 3, 1–64. doi: 10.1016/b0-08-043751-6/03016-4

Sánchez-Andrea, I., Knittel, K., Amann, R. I., Amils, R., and Sanz, J. L. (2012). Quantification of Tinto river sediment microbial communities: importance of sulfate-reducing bacteria and their role in attenuating acid mine drainage. *Appl. Environ. Microbiol.* 78, 4638–4645. doi: 10.1128/AEM.00848-12

Sánchez-Andrea, I., Rodríguez, N., Amils, R., and Sanz, J. L. (2011). Microbial diversity in anaerobic sediments at Río Tinto, a naturally acidic environment with a high heavy metal content. *Appl. Environ. Microbiol.* 77, 6085–6093. doi: 10.1128/AEM.00654-11

Schink, B. (1997). Energetics of syntrophic cooperation in methanogenic degradation. *Microbiol. Mol. Biol. Rev.* 61, 262–280.

Schink, B., and Stams, A. (2006). Syntrophism among prokaryotes. *Prokaryotes* 2, 309–335.

Schmidt, B. E., Blankenship, D. D., Patterson, G. W., and Schenk, P. M. (2011). Active formation of "chaos terrain" over shallow subsurface water on Europa. *Nature* 479, 502–505. doi: 10.1038/nature10608

Schrenk, M. O., Brazelton, W. J., and Lang, S. Q. (2013). Serpentinization, carbon, and deep life. *Rev. Mineral. Geochem.* 75, 575–606. doi: 10.2138/rmg.2013.75.18

Schulte, M., Blake, D., Hoehler, T. M., and McCollom, T. M. (2006). Serpentinization and It's Implication for Life on Early Earth and Mars. *Astrobiology* 6, 364–376.

Sekine, Y., Shibuya, T., Postberg, F., Hsu, H. W., Suzuki, K., Masaki, Y., et al. (2015). High-temperature water-rock interactions and hydrothermal environments in

the chondrite-like core of Enceladus. *Nat. Commun.* 6:8604. doi: 10.1038/ncomms9604

Siegert, M. J., Ross, N., and Le Brocq, A. M. (2016). Recent advances in understanding Antarctic subglacial lakes and hydrology. *Philos. Trans. R. Soc. A Math. Phys. Eng. Sci.* 374:20140306. doi: 10.1098/rsta.2014.0306

Skidmore, M. L., Foght, J. M., and Sharp, M. J. (2000). Microbial life beneath a high Arctic glacier. *Appl. Environ. Microbiol.* 66, 3214–3220. doi: 10.1128/AEM.66.8.3214-3220.2000

Slobodkin, A. I., and Slobodkina, G. B. (2014). Thermophilic prokaryotes from deep subterranean habitats. *Microbiology* 83, 169–183. doi: 10.1134/S0026261714030151

Smith, J. A., Tremblay, P. L., Shrestha, P. M., Snoeyenbos-West, O. L., Franks, A. E., Nevin, K. P., et al. (2014). Going wireless: Fe(III) oxide reduction without pili by Geobacter sulfurreducens strain JS-1. *Appl. Environ. Microbiol.* 80, 4331–4340. doi: 10.1128/AEM.01122-14

Spilde, M. N., Northup, D. E., Boston, P. J., Schelble, R. T., Dano, K. E., Crossey, L. J., et al. (2005). Geomicrobiology of cave ferromanganese deposits: a field and laboratory investigation. *Geomicrobiol. J.* 22, 99–116. doi: 10.1080/01490450590945889

Squyres, S. W., Grotzinger, J. P., Arvidson, R. E., Bell, J. F., Calvin, W., Christensen, P. R., et al. (2004). *In situ* evidence for an ancient aqueous environment at Meridiani Planum, Mars. *Science* 306, 1709–1714. doi: 10.1126/science.1104559

Staudigel, H., Yayanos, A., Chastain, R., Davies, G., Verdurmen, E. A., Schiffman, P., et al. (1998). Biologically mediated dissolution of volcanic glass in seawater. *Earth Planet. Sci. Lett.* 164, 233–244. doi: 10.1016/S0012-821X(98)00207-6

Stern, J. C., Sutter, B., Freissinet, C., Navarro-González, R., McKay, C. P., Archer, P. D., et al. (2015). Evidence for indigenous nitrogen in sedimentary and aeolian deposits from the Curiosity rover investigations at Gale crater, Mars. *Proc. Natl. Acad. Sci. U.S.A.* 112, 4245–4250. doi: 10.1073/pnas.1420932112

Stevens, T., and Mckinley, J. P. (1995). Lithoautotrophic microbial ecosystems in deep basalt aquifers. *Science* 270, 450–454. doi: 10.1038/s41467-017-01288-8

Stober, I., and Bucher, K. (2004). Fluid sinks within the earth's crust. *Geofluids* 4, 143–151. doi: 10.1111/j.1468-8115.2004.00078.x

Stofan, E. R., Elachi, C., Lunine, J. I., Lorenz, R. D., Stiles, B., Mitchell, K. L., et al. (2007). The lakes of Titan. *Nature* 445, 61–64. doi: 10.1038/nature05438

Sylvan, J. B., Hoffman, C. L., Momper, L. M., Toner, B. M., Amend, J. P., and Edwards, K. J. (2015). *Bacillus rigiliprofundi* sp. nov., an endospore-forming Mn-oxidizing, moderately halophilic bacterium isolated from deep subseafloor basaltic crust. *Int. J. Syst. Evol. Microbiol.* 65, 1992–1998. doi: 10.1099/ijs.0.000211

Szponar, N., Brazelton, W. J., Schrenk, M. O., Bower, D. M., Steele, A., and Morrill, P. L. (2013). Geochemistry of a continental site of serpentinization, the Tablelands Ophiolite, Gros Morne National Park: A Mars analogue. *Icarus* 224, 286–296. doi: 10.1016/j.icarus.2012.07.004

Takai, K., Nakamura, K., Toki, T., Tsunogai, U., Miyazaki, M., Miyazaki, J., et al. (2008). Cell proliferation at 122 C and isotopically heavy CH4 production by a hyperthermophilic methanogen under high-pressure cultivation. *Proc. Natl. Acad. Sci. U.S.A.* 105, 10949–10954. doi: 10.1073/pnas.0712334105

Teal, L. R., Bulling, M. T., Parker, E. R., and Solan, M. (2008). Global patterns of bioturbation intensity and mixed depth of marine soft sediments. *Aquat. Biol.* 2, 207–218. doi: 10.3354/ab00052

Teolis, B. D., Plainaki, C., Cassidy, T. A., and Raut, U. (2017). Water Ice Radiolytic O_2, H_2, and H_2O_2 yields for any projectile species, energy, or temperature: a model for icy astrophysical bodies. *J. Geophys. Res. Planets* 122, 1996–2012. doi: 10.1002/2017JE005285

Toner, B. M., Rouxel, O. J., Santelli, C. M., Bach, W., and Edwards, K. J. (2016). Iron transformation pathways and redox micro-environments in seafloor sulfide-mineral deposits: Spatially resolved Fe XAS and δ57/54Fe observations. *Front. Microbiol.* 7:648. doi: 10.3389/fmicb.2016.00648

Trembath-Reichert, E., Morono, Y., Ijiri, A., Hoshino, T., Dawson, K. S., Inagaki, F., et al. (2017). Methyl-compound use and slow growth characterize microbial life in 2-km-deep subseafloor coal and shale beds. *Proc. Natl. Acad. Sci. U.S.A.* 114, E9206–E9215. doi: 10.1073/pnas.1707525114

Tsesmetzis, N., Alsop, E. B., Vigneron, A., Marcelis, F., Head, I. M., and Lomans, B. P. (2016). Microbial community analysis of three hydrocarbon reservoir cores provides valuable insights for the assessment of reservoir souring potential. *Int. Biodeterior. Biodegrad.* 126, 177–188.

Tully, B. J., Wheat, C. G., Glazer, B. T., and Huber, J. A. (2018). A dynamic microbial community with high functional redundancy inhabits the cold, oxic subseafloor aquifer. *ISME J.* 12, 1–16. doi: 10.1038/ismej.2017.187

Van Dover, C. L., Reynolds, G. T., Chave, A. D., and Tyson, J. A. (1996). Light at deep-sea hydrothermal vents. *Geophys. Res. Lett.* 23, 2049–2052. doi: 10.1029/96GL02151

Vance, S. D., Hand, K. P., and Pappalardo, R. T. (2016). Geophysical controls of chemical disequilibria in Europa. *Geophys. Res. Lett.* 43, 4871–4879. doi: 10.1002/2016GL068547

Volpi, M., Lomstein, B. A., Sichert, A., Røy, H., Jørgensen, B. B., and Kjeldsen, K. U. (2017). Identity, abundance, and reactivation kinetics of thermophilic fermentative endospores in cold marine sediment and seawater. *Front. Microbiol.* 8:131. doi: 10.3389/fmicb.2017.00131

Waite, J. H., Lewis, W. S., Magee, B. A., Lunine, J. I., McKinnon, W. B., Glein, C. R., et al. (2009). Liquid water on Enceladus from observations of ammonia and40Ar in the plume. *Nature* 460, 487–490. doi: 10.1038/nature08153

Webster, C. R., Mahaffy, P. R., Atreya, S. K., Flesch, G. J., Mischna, M. A., Meslin, P.-Y., et al. (2015). Mars methane detection and variability at Gale crater. *Science* 347, 415–417. doi: 10.1126/science.1261713

Wedepohl, K. H. (1995). The composition of the continental crust. *Geochim. Cosmochim. Acta* 59, 1217–1232. doi: 10.1016/0016-7037(95)00038-2

Wegener, G., Bausch, M., Holler, T., Thang, N. M., Prieto Mollar, X., Kellermann, M. Y., et al. (2012). Assessing sub-seafloor microbial activity by combined stable isotope probing with deuterated water and 13C-bicarbonate. *Environ. Microbiol.* 14, 1517–1527. doi: 10.1111/j.1462-2920.2012.02739.x

Weiss, B. P., Yung, Y. L., and Nealson, K. H. (2000). Atmospheric energy for subsurface life on Mars? *Proc. Natl. Acad. Sci. U.S.A.* 97, 1395–1399. doi: 10.1073/pnas.030538097

White, S. N., Chave, A. D., and Reynolds, G. T. (2002). Investigations of ambient light emission at deep-sea hydrothermal vents. *J. Geophys. Res. Solid Earth* 107, EPM 1-1–EPM 1-13. doi: 10.1029/2000JB000015

Whiticar, M. J. (1990). A geochemial perspective of natural gas and atmospheric methane. *Org. Geochem.* 16, 531–547. doi: 10.1016/0146-6380(90)90068-B

Whitman, W. B., Coleman, D. C., and Wiebe, W. J. (1998). Prokaryotes: the unseen majority. *Proc. Natl. Acad. Sci. U.S.A.* 95, 6578–6583. doi: 10.1073/pnas.95.12.6578

Wilhelms, A., Larter, S. R., Head, I. M., Farrimond, P., Di-Primio, R., and Zwach, C. (2001). Biodegradation of oil in uplifted basins prevented by deep-burial sterilization. *Nature* 411, 1034–1037. doi: 10.1038/35082535

Williams, P. J., and Cloete, T. E. (2008). Microbial community study of the iron ore concentrate of the Sishen Iron Ore Mine, South Africa. *World J. Microbiol. Biotechnol.* 24, 2531–2538. doi: 10.1007/s11274-008-9777-4

Wirsen, C. O., and Jannasch, H. W. (1978). Physiological and morphological observations on *Thiovulum* sp. *J. Bacteriol.* 136, 765–774.

Wu, X., Holmfeldt, K., Hubalek, V., Lundin, D., Åström, M., Bertilsson, S., et al. (2016). Microbial metagenomes from three aquifers in the Fennoscandian shield terrestrial deep biosphere reveal metabolic partitioning among populations. *ISME J.* 10, 1192–1203. doi: 10.1038/ismej.2015.185

Zhang, X., Feng, X., and Wang, F. (2016). Diversity and metabolic potentials of subsurface crustal microorganisms from the western flank of the mid-atlantic ridge. *Front. Microbiol.* 7:363. doi: 10.3389/fmicb.2016.00363

Ziebis, W., McManus, J., Ferdelman, T. G., Schmidt-Schierhorn, F., Bach, W., Muratli, J., et al. (2012). Interstitial fluid chemistry of sediments underlying the North Atlantic gyre and the influence of subsurface fluid flow. *Earth Planet. Sci. Lett.* 32, 79–91. doi: 10.1016/j.epsl.2012.01.018

Conflict of Interest Statement: The authors declare that the research was conducted in the absence of any commercial or financial relationships that could be construed as a potential conflict of interest.

frontiers in Microbiology

CORRECTION
published: 27 August 2019
doi: 10.3389/fmicb.2019.01959

Corrigendum: Low Energy Subsurface Environments as Extraterrestrial Analogs

*Rose M. Jones, Jacqueline M. Goordial and Beth N. Orcutt**

Bigelow Laboratory for Ocean Sciences, East Boothbay, ME, United States

Keywords: deep biosphere, subsurface, astrobiology, low energy, energy limitation

A Corrigendum on

Low Energy Subsurface Environments as Extraterrestrial Analogs
by Jones, R. M., Goordial, J. M., and Orcutt, B. N. (2018). Front. Microbiol. 9:1605. doi: 10.3389/fmicb.2018.01605

In the original article, there was a mistake in the calculations in **Supplementary Table S1** as published, which affected **Figure 4** and the resulting text describing **Figure 4**.

In brief, there were errors in the equations for calculating the volumetric energy densities for some of the reactions, due to a copy/paste error, which affected the estimates of cumulative energy density and ratio of reactions presented in **Figure 4**. We have corrected these errors in the revised **Supplementary Table S1** file as well as in **Figure 4**, shown below. We thank the reader who brought this to our attention.

Supplementary Table S1: The file has been corrected in the original article.

Due to the error mentioned above, a correction has been made to section ***Energetics and the Subsurface***, subsection ***Energy Yield of Various Redox Reactions in the Low Energy Subsurface and on Extraterrestrial Environments***, paragraphs four and five:

"Strikingly, extraterrestrial sites are predicted to have similar cumulative energy densities as Earth's subsurface habitats (with conservative assumptions about electron donor and acceptor concentrations), although the dominant energy-rich processes vary (**Figure 4**, Supplementary Table S1). For example, cumulative volumetric energy densities on Mars are estimated to range from 0.03 to 3 kJ L^{-1}, supported primarily by the electron donors NH_3, H_2S, or hydrogen reacting with sulfate, nitrate, or oxygen, depending on the scenario chosen for electron donor concentration, pH, and temperature. Under the scenario of low electron donor concentration, low pH, and low temperature, the predicted Martian energy density and dominant reactions are similar to those observed at the Earth analog site at the Juan de Fuca Ridge flank subsurface oceanic crust. Under the scenario of higher electron donor concentrations, pH, and temperature, the cumulative volumetric energy density and dominant reactions estimate is more similar to what is estimated from the Earth analog sites in the Rio Tinto. The base of the presumed Europan ocean has an estimated energy density of 400 kJ L^{-1} fueled primarily by iron oxidation, if dissolved oxygen is present (Teolis et al., 2017) and penetrates to the water-rock interface and if iron is released from water-rock reactions. This volumetric energy density and dominant reaction pattern is similar to that estimated for the Earth analog site at University Valley. By contrast, the ocean on Enceladus is estimated to have an energy density of 100 kJ L^{-1} fueled by ammonia oxidation with nitrate; none of our comparison Earth analog sites had similar energy density estimates from this reaction. The cumulative volumetric energy density estimates for Titan are the highest

OPEN ACCESS

Approved by:
Frontiers Editorial Office, Frontiers Media SA, Switzerland

****Correspondence:***
Beth N. Orcutt
borcutt@bigelow.org

Specialty section:
This article was submitted to Extreme Microbiology, a section of the journal Frontiers in Microbiology

Received: *07 August 2019*
Accepted: *08 August 2019*
Published: *27 August 2019*

Citation:
Jones RM, Goordial JM and Orcutt BN (2019) Corrigendum: Low Energy Subsurface Environments as Extraterrestrial Analogs. Front. Microbiol. 10:1959. doi: 10.3389/fmicb.2019.01959

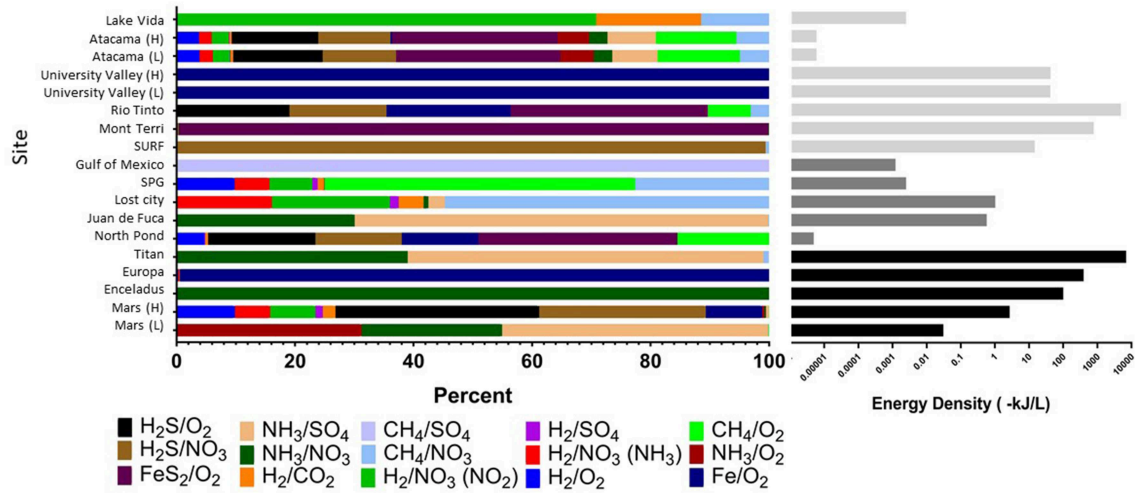

FIGURE 4 | Cumulative volumetric energy densities of redox reactions per site based on environmental concentrations of variables in each reaction (Table 1). **(Left)** Shows the percent contribution of various reactions as shown in the color legend. **(Right)** Shows combined absolute energy density (as kJ per liter) for all reactions, with gray scale reflecting habitat type. All calculations assumed that the electron donor was the limiting substrate. See Supplementary Table S1 for all values and formulas.

we estimate in this exercise, fueled by ammonia oxidation with sulfate or nitrate in a similar pattern as estimated for the Juan de Fuca analog system, but we highlight that this is the least well constrained system. Overall, although based on poorly constrained concentrations, these projections indicate that extraterrestrial sites could have sufficient overall energy to host chemolithotrophic communities."

"The predicted relative contribution of each redox pair to each site is applicable information for the "follow the energy" approach to habitability (Hoehler, 2007), and can further be constrained by comparison studies of microbial metabolic processes in the Earth analog systems, to see if the predicted energy rich metabolisms are indeed those that occur. This approach of comparing energy density to microbial community function has recently been shown for some subsurface sites (Osburn et al., 2014; Reveillaud et al., 2016; Momper et al., 2017), demonstrating the power of this energy density approach to be a useful predictor of metabolic function. For example, North Pond energy is primarily from the FeS_2/O_2 couple (**Figure 4**), indicating that solid mineral substrates may be significant in this environment. Oxidation of hydrogen sulfide is also predicted to yield more energy than other electron donors (**Figure 4**), which agrees well with information on metabolic function in the community indicating that sulfur oxidizers are present in greater relative abundance as compared to hydrogen, ammonia and nitrite metabolisms (Jørgensen and Zhao, 2016; Meyer et al., 2016). Lost City estimates show methane and hydrogen oxidation reactions as significant sources of energy (**Figure 4**), which agrees with work indicating methane oxidizers are common in this system but contrasts with other recent work pointing to sulfate metabolisms as being more important than hydrogen metabolisms in this environment (Lang et al., 2018). At this site, the Gibbs free energy of the H_2/CO_2 couple is relatively high but the energy density low (Figures 3, **4**), as dissolved CO_2 concentration is scarce because it rapidly precipitates as carbonates in the high pH environment. As shown previously, sulfide oxidizing metabolisms are energy rich in the continental subsurface at the Sanford Underground Research Facility, and sulfide oxidizers are dominant in the microbial community (Osburn et al., 2014; Momper et al., 2017). In the subsurface portion of Rio Tinto, observation of iron and sulfur metabolisms matches with estimates of energy density (García-Moyano et al., 2012; Sánchez-Andrea et al., 2012; Amils et al., 2014). The Atacama analog site has a very low predicted energy availability, although we note that factors like water availability may be more important than energy availability in structuring the microbial community at the hyperarid and polar desert environments (Goordial et al., 2016). It is notable that the range of pH and temperature scenarios at the Atacama and University Valley sites did not particularly affect the predicted dominant reactions or volumetric energy densities at the hyper-arid sites, unlike the Mars sites, which notably changed, highlighting that the ion concentrations are key for determining dominant reactions and energy densities. Overall, this "follow the energy" approach of matching predicting energy density to microbial community structure and function may inform the likely metabolisms that might be found on extraterrestrial targets."

In addition, in the original article, the following references were incorrectly written.

The reference for "Amend et al., 2015" should be "Sylvan, J. B., Hoffman, C. L., Momper, L. M., Toner, B. M., Amend, J. P., and Edwards, K. J. (2015). *Bacillus rigiliprofundi* sp. nov., an endospore-forming Mn-oxidizing, moderately halophilic bacterium isolated from deep seubseafloor basaltic crust. *Int. J. Syst. Evol. Microbiol.* 65, 1992–1998. doi: 10.1099/ijs.0.000211." The citation in the text has been updated accordingly.

The reference for "Amils et al., 2014" should be "Amils, R., Fernández-Remolar, D. C., and IPBSL Team (2014). Río Tinto: a geochemical and mineralogical terrestrial analogue of mars. *Life* 4, 511–534. doi: 10.3390/life4030511."

The reference for "Bate et al., 2004" should be "Gleeson, T., Befus, K. M., Jasechko, S., Luijendijk, E., and Cardenas, M. B. (2016). The global volume and distribution of modern groundwater. *Nat. Geosci.* 9, 161–164. doi: 10.1038/ngeo2590." The citation in the text has been updated accordingly.

The reference for "Lowell, 2005" should be "Lowell, R. P., and DuBose M. (2005). Hydrothermal systems on Europa. *Geophys. Res. Lett.* 32:L05202. doi: 10.1029/2005gl022375."

The reference for "McCord, 1998" should be "McCord, T. B., Hansen, G. B., Fanale, F. P., Carlson, R.W., Matson, D. L., Johnson, T. V., et al. (1998). Salts on Europa's surface detected by Galileo's near infrared mapping spectrometer. *Science* 280, 1242–1245. doi: 10.1126/science.280.5367.1242."

The reference for "Schink et al., 2006" should be "Schink, B., and Stams, A. (2006). Syntrophism among prokaryotes. *Prokaryotes* 2, 309–335."

The reference for "Squyres, 2004" should be "Squyres, S. W., Grotzinger, J. P., Arvidson, R. E., Bell, J. F., Calvin, W., Christensen, P. R., et al. (2004). *In situ* evidence for an ancient aqueous environment at Meridiani Planum, Mars. *Science* 306, 1709–1714. doi: 10.1126/science.1104559."

The authors apologize for these errors and state that they do not change the scientific conclusions of the article in any way. The original article has been updated.

REFERENCES

Amils, R., Fernández-Remolar, D. C., and IPBSL Team (2014). Río Tinto: a geochemical and mineralogical terrestrial analogue of mars. *Life* 4, 511–534. doi: 10.3390/life4030511

García-Moyano, A., González-Toril, E., Aguilera,Á., and Amils, R. (2012). Comparative microbial ecology study of the sediments and the water column of the Río Tinto, an extreme acidic environment. *FEMS Microbiol. Ecol.* 81, 303–314. doi: 10.1111/j.1574-6941.2012.01346.x

Goordial, J., Davila, A. F., Lacelle, D., Pollard, W., Marinova, M. M., Greer, C. W., et al. (2016). Nearing the cold-arid limits of microbial life in permafrost of an upper dry valley, Antarctica. *ISME J.* 10, 1613–1624. doi: 10.1038/ismej.2015.239

Hoehler, T. M. (2007). An Energy Balance Concept for Habitability. *Astrobiology* 7, 824–838. doi: 10.1089/ast.2006.0095

Jørgensen, S. L., and Zhao, R. (2016). Microbial inventory of deeply buried oceanic crust from a young ridge flank. *Front. Microbiol.* 7:820. doi: 10.3389/fmicb.2016.00820

Lang, S. Q., Früh-Green, G. L., Bernasconi, S. M., Brazelton, W. J., Schrenk, M. O., and McGonigle, J. M. (2018). Deeply-sourced formate fuels sulfate reducers but not methanogens at Lost City hydrothermal field. *Sci. Rep.* 8:755. doi: 10.1038/s41598-017-19002-5

Meyer, J. L., Jaekel, U., Tully, B. J., Glazer, B. T., Wheat, C. G., Lin, H.-T., et al. (2016). A distinct and active bacterial community in cold oxygenated fluids circulating beneath the western flank of the Mid-Atlantic ridge. *Sci. Rep.* 6:22541. doi: 10.1038/srep22541

Momper, L. M., Kiel Reese, B., Zinke, L. A., Wanger, G., Osburn, M. R., Moser, D. P., et al. (2017). Major phylum-level differences between porefluid and host rock bacterial communities in the terrestrial deep subsurface. *Environ. Microbiol. Rep.* 9, 501–511. doi: 10.1111/1758-2229.12563

Osburn, M. R., LaRowe, D. E., Momper, L. M., and Amend, J. P. (2014). Chemolithotrophy in the continental deep subsurface: Sanford Underground Research Facility (SURF), USA. *Front. Microbiol.* 5:610. doi: 10.3389/fmicb.2014.00610

Reveillaud, J., Reddington, E., McDermott, J., Algar, C., Meyer, J. L., Sylva, S., et al. (2016). Subseafloor microbial communities in hydrogen-rich vent fluids from hydrothermal systems along the Mid-Cayman Rise. *Environ. Microbiol.* 18, 1970–1987. doi: 10.1111/1462-2920.13173

Sánchez-Andrea, I., Knittel, K., Amann, R. I., Amils, R., and Sanz, J. L. (2012). Quantification of Tinto river sediment microbial communities: importance of sulfate-reducing bacteria and their role in attenuating acid mine drainage. *Appl. Environ. Microbiol.* 78, 4638–4645. doi: 10.1128/AEM.00848-12

Teolis, B. D., Plainaki, C., Cassidy, T. A., and Raut, U. (2017). Water Ice Radiolytic O_2, H_2, and H_2O_2 yields for any projectile species, energy, or temperature: a model for icy astrophysical bodies. *J. Geophys. Res. Planets* 122, 1996–2012. doi: 10.1002/2017JE005285

frontiers in Environmental Science

ORIGINAL RESEARCH
published: 25 September 2018
doi: 10.3389/fenvs.2018.00101

pH as a Primary Control in Environmental Microbiology: 2. Kinetic Perspective

Qusheng Jin[1]* *and Matthew F. Kirk*[2]

[1] Department of Earth Sciences, University of Oregon, Eugene, OR, United States, [2] Department of Geology, Kansas State University, Manhattan, KS, United States

In a companion paper, we examined the thermodynamic responses of microbial redox reactions to pH changes. Here we explore how these thermodynamic responses may affect the composition and function of microbial communities. We simulate butyrate syntrophic oxidation, sulfate reduction, and methanogenesis by microbial consortia at pH ranging from 7 to 5. The simulation accounts for the thermodynamics of microbial metabolisms and the interactions among microbes. The results show that thermodynamic responses to variation in pH can be strong enough to speed up or slow down microbial metabolisms. These kinetic changes then shape the outcome of microbial interactions, including the membership and activity of microbial consortia. Moreover, the kinetic changes modulate carbon fluxes and the efficiency of methane production. The simulation results support the hypothesis that environmental pH can shape the composition and metabolic function of microbial communities by changing the energy yields of redox reactions. They also add to the current theories of microbial ecology. Specifically, due to pH-induced thermodynamic responses, the principle of competitive exclusion fails for microbial processes with significant thermodynamic limitations, which allows the co-occurrence of competing respiration reactions in natural environments. Taken together, these results confirm that pH is a primary control in environmental microbiology. They also highlight the feasibility and potential of biogeochemical kinetic modeling in uncovering and illuminating mechanistic relationships between environmental parameters and microbial communities.

Keywords: bioenergetics, butyrate oxidation, sulfate reduction, methanogenesis, microbial kinetics

OPEN ACCESS

Edited by:
Alain F. Plante,
University of Pennsylvania,
United States

Reviewed by:
John W. Moreau,
The University of Melbourne, Australia
Juan M. Gonzalez,
Consejo Superior de Investigaciones Científicas (CSIC), Spain

***Correspondence:**
Qusheng Jin
qjin@uoregon.edu

Specialty section:
This article was submitted to Microbiological Chemistry and Geomicrobiology, a section of the journal Frontiers in Environmental Science

Received: *21 March 2018*
Accepted: *23 August 2018*
Published: *25 September 2018*

Citation:
Jin Q and Kirk MF (2018) pH as a Primary Control in Environmental Microbiology: 2. Kinetic Perspective. Front. Environ. Sci. 6:101. doi: 10.3389/fenvs.2018.00101

INTRODUCTION

Environmental pH is one of the most informative parameters for studying microbes in natural environments. pH represents the chemical activities of protons—a reactant that participates in biological energy conservation, interacts with cellular surface components and structures, and involves in metabolism-related chemical reactions, including redox reactions, mineral dissolution and precipitation, and reactions of natural organic matter (Kinniburgh et al., 1999; Konings et al., 2002; Paul et al., 2006). Reflecting these relationships, pH correlates with community composition across a wide range of biogeochemical conditions (Thompson et al., 2017), and pH variation induces significant changes in the metabolic functions of microbial communities (Kotsyurbenko et al., 2004; Ye et al., 2012).

In a companion paper (Jin and Kirk, 2018), we hypothesize that the correlation between pH and microbial communities may also reflect the thermodynamic and kinetic responses of microbial metabolisms to pH variation. This hypothesis is based on the dependence of chemotrophic microbes on chemical energy in the environment (Thauer et al., 1977; Jin, 2012). Chemotrophs liberate chemical energy in the environment by catalyzing redox reactions and save a part of the liberated energy by making adenosine triphosphate (ATP) molecules. They then spend the ATPs to maintain biomass and make new cells. Any factors that influence the energy available in the environment, therefore, have the potential to affect the metabolisms of individual microbial groups and the composition and metabolic activity of microbial communities.

To test this hypothesis, we examined the effect of pH variation on the energy yields of microbial redox reactions (Jin and Kirk, 2018). We focused on redox reactions involved in organic matter degradation, including syntrophic oxidation, iron reduction, sulfate reduction, and methanogenesis, and computed their energy yields at pH ranging from 1 to 14. The results show that energy yields vary significantly in response to both direct and indirect impacts of pH variation. The direct impact is due to the changes in proton chemical activities and applies to the reactions that consume or produce protons; the indirect impact comes from the control of pH on chemical speciation–pH variation affects the distribution of solute mass among possible chemical species and thus the activities of chemical species involved in microbial reactions.

These results demonstrate that pH variations can alter the energy yields of microbial redox reactions. However, thermodynamics alone is limited in its ability to predict the metabolic rates and population sizes of microbes or to account for the correlation between pH and microbial communities (Bethke et al., 2011; Amenabar et al., 2017). These limitations arise in part from the complexity of microbial metabolisms in natural settings. In addition to thermodynamics, microbial metabolisms are subject to control by a wide range of biogeochemical factors, including substrate availability, geochemical reactions, and microbial interactions (Panikov, 1995; Jin et al., 2013). But most thermodynamic calculations are reaction specific, and do not explicitly consider concurrent geochemical reactions or microbial metabolisms.

Here we apply kinetic modeling to explore how pH may influence the composition and metabolic activity of simple microbial consortia. According to microbial kinetic theory, the rates of microbial metabolisms depend on the thermodynamic drives of microbial respiration, the differences between the energy available in the environment and the energy conserved by ATP synthesis (Jin and Bethke, 2003, 2007). A change in pH could raise or lower the thermodynamic drives and speed up or slow down individual microbial metabolisms, which in turn shape microbial interactions and the membership of microbial consortia.

We simulate microbial metabolisms using biogeochemical reaction modeling (Bethke, 2008; Jin et al., 2013). In addition to changing the energy yields of redox reactions, pH also directly affects the kinetic parameters of microbes. In our simulation, we assume that pH only impacts the energy yields. This assumption is of course an oversimplification but it allows us to concentrate on the outcome of pH-induced changes of energy yields. We can include the changes of microbial kinetic parameters, but the results would bear the combined effects of microbial kinetic and thermodynamic responses. Thus, they would not be straightforward in illustrating the significance of the thermodynamic effect—the focus of the current study.

We focus on syntrophic butyrate oxidation, sulfate reduction, and methanogenesis. Butyrate is a common intermediate in the degradation of natural organic matter whereas sulfate reduction and methanogenesis are common microbial processes in anoxic environments (Monokova, 1975; Molongoski and Klug, 1980; Lovley and Klug, 1982). Our simulation considers microbial interactions, including competition and syntrophy, and computes rates of respiration and growth by accounting for the chemical energy in the environment. We seek to demonstrate how pH can influence the outcome of microbial interactions—the membership and activity of microbial consortia—by changing the energy yields of redox reactions.

METHODS

We simulate the progress of microbial metabolisms using the rates of microbial respiration, biosynthesis, and maintenance. Microbial respiration couples redox reactions to the synthesis of ATP. The redox reactions can be represented as

$$\sum_{\mathrm{D}} \nu_{\mathrm{D}} \mathrm{D} + \sum_{\mathrm{A}} \nu_{\mathrm{A}} \mathrm{A} \rightleftarrows \sum_{\mathrm{D}^+} \nu_{\mathrm{D}^+} \mathrm{D}^+ + \sum_{\mathrm{A}^-} \nu_{\mathrm{A}^-} \mathrm{A}^-, \qquad (1)$$

where D and D^+ are electron donors and their oxidized forms, respectively, A and A^- are electron acceptors and their reduced forms, respectively, and ν_D and others are stoichiometric coefficients. The energies ΔG_A available from the reactions are the negative of the Gibbs free energy changes [J·(mol reaction)$^{-1}$, or J·mol^{-1}], and are calculated according to

$$\Delta G_A = -\Delta G^o - RT \ln \left(\frac{\prod_{\mathrm{D}^+} \mathrm{a}_{\mathrm{D}^+}^{\nu_{\mathrm{D}^+}} \cdot \prod_{\mathrm{A}^-} \mathrm{a}_{\mathrm{A}^-}^{\nu_{\mathrm{A}^-}}}{\prod_{\mathrm{D}} \mathrm{a}_{\mathrm{D}}^{\nu_{\mathrm{D}}} \cdot \prod_{\mathrm{A}} \mathrm{a}_{\mathrm{A}}^{\nu_{\mathrm{A}}}} \right), \qquad (2)$$

where ΔG° is the standard Gibbs free energy change, a is the chemical activity, R is the gas constant (J·mol^{-1}·K^{-1}), and T is the temperature in kelvin (K). Chemical activity is calculated as the product of activity coefficients (M^{-1}) and molal concentrations of chemical species. Activity coefficients are calculated according to an extended form of the Debye-Hückel equation (Helgeson, 1969).

Respiration rate r (mol·kg^{-1}·s^{-1}, mol per kg water per s) can be calculated according to the thermodynamically consistent rate law (Jin and Bethke, 2005, 2007):

$$r = k \cdot [X] \cdot \prod_i F_i, \qquad (3)$$

where k is the rate constant [mol·(g dry weight)$^{-1}$·s^{-1}, or mol·g^{-1}·s^{-1}], [X] is the biomass concentration [g dry weight·(kg

water)$^{-1}$, or g·kg^{-1}], and F_i represents different controlling factors, including the kinetic factors of electron donor (F_D) and acceptor (F_A), and the thermodynamic potential factor (F_T). The kinetic factors are calculated according to

$$F_D = \frac{m_D}{K_D + m_D} \tag{4}$$

and

$$F_A = \frac{m_A}{K_A + m_A}, \tag{5}$$

where m_D and m_A are the molal concentrations of electron donor and acceptor, respectively, and K_D and K_A are the half-saturation constants (M) for electron donor and acceptor, respectively. The thermodynamic potential factor is calculated according to

$$F_T = 1 - \exp\left(-\frac{f}{\chi \cdot RT}\right), \tag{6}$$

where f is the thermodynamic drive (J·mol^{-1}), and χ is the average stoichiometric number. The thermodynamic drive,

$$f = \Delta G_A - \Delta G_C, \tag{7}$$

is the difference between the energy ΔG_A (J·mol^{-1}) available in the environment and the energy ΔG_C (J·mol^{-1}) conserved by respiration.

According to Jin (2007), the energy ΔG_C (J·mol^{-1}) conserved by syntrophic butyrate oxidizers is a function of hydrogen partial pressure P_{H_2} (atm),

$$\Delta G_C = \begin{cases} 3.5 \times 10^4, & P_{H_2} < 10^{-9}\text{atm} \\ -1.78 \times 10^4 - 2.5 \times 10^3 \cdot \ln\left(P_{H_2}\right), & 10^{-9}\text{atm} < P_{H_2} < 10^{-3}\text{atm} \\ 0, & P_{H_2} > 10^{-3}\text{atm} \end{cases}. \tag{8}$$

According to this model, the conserved energy reaches its largest value at H_2 partial pressure less than 10^{-9} atm, and declines with increasing H_2 partial pressure. At the partial pressure of 10^{-3} atm or more, the conserved energy declines to 0.

For sulfate reducers and methanogens, the conserved energy ΔG_C is calculated as

$$\Delta G_C = \nu_P \cdot \Delta G_P, \tag{9}$$

the product of the ATP yield ν_P of respiration and the phosphorylation energy ΔG_P (Jin and Bethke, 2002, 2003). The phosphorylation energy is the energy required to synthesize ATP from ADP and phosphate in the cytoplasm, and its value is taken as 45 kJ·(mol ATP)$^{-1}$ (Jin, 2012).

Microbes utilize the conserved energy ΔG_C to synthesize biomass. The rate at which the biomass concentration [X] changes with time, or the net growth rate, is

$$\frac{d[X]}{dt} = Y \cdot r - D \cdot [X], \tag{10}$$

where Y is the biomass yield, the grams of biomass dry weight synthesized per mol reaction (g·mol^{-1}), and D is the specific rate of maintenance and death (s^{-1}) (van Bodegom, 2007). The product of the growth yield and respiration rate, $Y \cdot r$, gives the biosynthesis rate. Equation (10) neglects that many microbes can persist through adverse environmental conditions via dormancy and other survival mechanisms. Instead, it assumes that microbial population sizes depend solely on biosynthesis rate relative to the rate of maintenance.

We simulate the metabolisms of neutrophilic syntrophic butyrate oxidizers, sulfate reducers, and methanogens using the React program of the software package Geochemist's Workbench version 9.0 (Bethke, 2008). The simulation assumes that aqueous chemical speciation is at thermodynamic equilibrium, and describes these reactions on the basis of the updated LLNL Thermodynamic Database (Delany and Lundeen, 1990). Evaluating microbial rate laws (Equations 3 and 10) requires a series of microbial parameters; their values are listed in **Table 1**.

We carry out the simulation by varying pH from 7 to 5. Most neutrophilic microbes live over 4 pH units (Rosso et al., 1995). Taking pH 7 as the optimal growth pH, a decrease of 2 pH units would decrease microbial growth rates to 0. Hence we simulate the metabolisms at pH ranging from 7 to 5. We assume that microbial parameters, such as rate constant k and half-saturation constants K_D and K_A, remain constant at different pHs. This assumption is necessary for testing the hypothesis that microbial thermodynamic responses to pH are strong enough to modulate the kinetics of microbial metabolisms and the outcome of microbial interactions. The input scripts are available in **Supplementary Material**.

RESULTS

In the companion paper (Jin and Kirk, 2018), we analyzed the thermodynamic responses of individual redox reactions to pH changes. Microbes rarely, if ever, live in isolation in nature. Instead, they often join each other in communities to carry out a network of biogeochemical reactions and perform a wide range of ecological functions (Nielsen et al., 2011; Xavier, 2011). By working together, microbes build different working relationships, such as competition and syntrophy. Here we apply biogeochemical reaction modeling to predict how the thermodynamic responses to pH may influence the outcome of microbial competition and syntrophy.

Competition

A classic example of microbial competition is the competition for acetate between sulfate reducers and methanogens (Lovley and Philips, 1987). Sulfate reducers oxidize acetate to inorganic carbon by reducing sulfate to sulfide,

$$\text{Acetate} + SO_4^{2-} + H^+ \rightleftarrows 2HCO_3^- + H_2S. \tag{11}$$

Methanogens convert acetate to CO_2 and methane,

$$\text{Acetate} + H_2O \rightleftarrows HCO_3^- + CH_4. \tag{12}$$

In the companion paper (Jin and Kirk, 2018), we show that a pH decrease from 7 to 5 raises the energy yields of both

TABLE 1 | Kinetic parameters (rate constant k, and half-saturation constant K_D and K_A), growth parameters (growth yield Y and specific maintenance rate D), and thermodynamic parameters (ATP yield ν_P and average stoichiometric number χ) of microbial metabolism.

Microbe	Reaction[a]	Kinetic parameter[b]			Growth parameter		Thermodynamic parameter[c]	
		k (mol·g^{-1}·s^{-1})	K_D (molal)	K_A (molal)[c]	Y[d] (g·mol^{-1})	D[e] (s^{-1})	ν_P	χ
Strain IB	Butyrate oxidation (Equation 13)	2.0×10^{-6}	6.5×10^{-5}		–[f]	10^{-7}	–[g]	2
D. postgatei	Sulfate reduction (Equation 11)	1.0×10^{-6}	2.3×10^{-4}	1.5×10^{-4}	5.0	10^{-7}	1.0	6
M. barkeri	Acetoclastic methanogenesis (Equation 12)	1.0×10^{-6}	3.0×10^{-3}		2.1	10^{-7}	0.5	2
M. mazei	Acetoclastic methanogenesis (Equation 12)	2.0×10^{-6}	2.0×10^{-3}		3.1	10^{-7}	0.74	2
M. formicium	Hydrogenotrophic methanogenesis (Equation 14)	2.0×10^{-6}	1.0×10^{-7}		2.5	10^{-7}	0.5	2

[a]*Numbers in parentheses are equation numbers in text.* [b]*Jin and Roden (2011) and Jin and Kirk (2016).* [c]*Only consider the kinetic factor of sulfate.* [d]*Jin (2012).* [e]*Jin and Roden (2011).* [f]*The yield is computed according to* $Y = Y_G \cdot \Delta G_C$*, where* Y_G *is the biomass yield per unit energy conserved, and the value is 0.1 g·kJ*$^{-1}$ *(Jin, 2007).* [g]*See text.*

reactions and thus has the potential to speed up the metabolisms of both microbial groups. Nevertheless, according to the principle of competitive exclusion, sulfate reducers win the competition against methanogens because sulfate reducers can hold acetate concentrations either below the thresholds required by running methanogenesis (Lovley et al., 1982) or below the levels required for sustaining methanogen populations (Bethke et al., 2008).

Closed Environment

We first simulate the competition between a sulfate reducer and a methanogen in a closed environment. Schönheit et al. (1982) monitored acetate oxidation in laboratory batch reactors by a representative sulfate reducer—*Desulfobacter postgatei*—and by a model methanogen—*Methanosarcina barkeri*. In their experiments, the two microbes grew together at 30°C in growth media with pH 6.9, 10 mmolal acetate, and 20 mmolal sulfate. We simulated the experiments by taking the initial biomass concentrations at 1.5 g·(kg H_2O)$^{-1}$ for *D. postgatei* and 2.0 g·(kg H_2O)$^{-1}$ for *M. barkeri*. These initial biomass concentrations are estimated by fitting the simulation results to the concentrations of acetate, methane, and sulfide during the first hour of the experiments (**Figure 1**). Also, to best fit the experimental observations, we set a lag time of 10 min before the two microbes start to consume acetate.

Figure 1 shows how chemical concentrations change with time according to the experimental observations and the simulation results. Acetate concentration decreases with time while sulfide and methane concentrations increase. After 1.5 h, methane concentration reaches a constant value. An hour later, sulfide also stabilizes. The simulation results predict that neither microbe grows much—during the experiments, their biomass concentrations increase by less than 2% of the initial concentrations (results not shown). But the rates of sulfate reduction and methanogenesis vary significantly over time (**Figure 2**). Both rates are about 1.5×10^{-6} molal·s^{-1} at the beginning of the experiments and decrease almost linearly with time. The rates of methanogenesis and sulfate reduction fall near 0 around hour 1.7 and 3, respectively. In other words, methanogenesis stops earlier than sulfate reduction. The modeling results also show that *D. postgatei* and *M. barkeri* differ from each other in the contribution to acetate consumption. Overall, 59% of the acetate is consumed by *D. postgatei* while *M. barkeri* uses the remaining 41%.

The simulation results demonstrate that the energy availability limits the progress of both sulfate reduction and methanogenesis (**Figure 3**). At the beginning of the experiments, the energy available to *D. postgatei* is 75 kJ·mol^{-1}, much larger than that to *M. barkeri*, 40 kJ·mol^{-1}. As the experiments progress, the acetate consumption and the accumulation of sulfide, bicarbonate, and methane decrease the available energy (**Figures 1**, **3A,B**). About 1.5 h into the experiments, energy available to *M. barkeri* decreases to 25 kJmol^{-1} and the thermodynamic drive disappears. As such, the thermodynamic potential factor decreases to zero and methanogenesis ceases (Equation 3). At this time, energy available to *D. postgatei* is 55 kJmol^{-1}, still larger than the energy it conserves, allowing sulfate reduction to continue. After 2 h into the experiment, however, energy available to *D. postgatei* approaches 45 kJmol^{-1}, the energy conserved by the organism, and the reaction slows. This result supports the hypothesis that sulfate reducers can win the competition by lowering acetate below the threshold level required for running methanogenesis (Lovley et al., 1982).

Figures 1, **2** also show the simulation results at pH 6 and 5. According to these results, sulfide production is faster at lower pH. For example, at the beginning of the experiments, sulfide is produced at 1.08×10^{-6}, 1.22×10^{-6}, and 1.35×10^{-6} molal·s^{-1} at pH 7, 6, and 5, respectively. Accordingly, sulfide reaches its maximum concentration after 2.5, 2, and 1.7 h, respectively. In comparison, the pH changes have little impact on methane production. Methane is produced $1.38 \pm 0.05 \times 10^{-6}$ molal·s^{-1} in each simulation.

Figure 3A shows that the energy yield of *D. postgatei* responds significantly to pH changes. The pH decreases from 7 to 6 and from 6 to 5 raise the energy yield by about 7.1 kJ·mol^{-1} and 13.6 kJ·mol^{-1}, respectively. As a result, the thermodynamic potential factor increases, speeding up sulfate reduction (**Figures 2A**, **3C**).

Figure 3B shows that the energy yield of methanogenesis also responds to the pH changes. The pH decreases from 7 to 6 and from 6 to 5 raise the energy yield by about 1.4 kJ·mol^{-1} and 3.6 kJ·mol^{-1}, respectively. These increases raise the thermodynamic potential factor (**Figure 3D**). However, the rate does not respond notably to the pH changes because, in

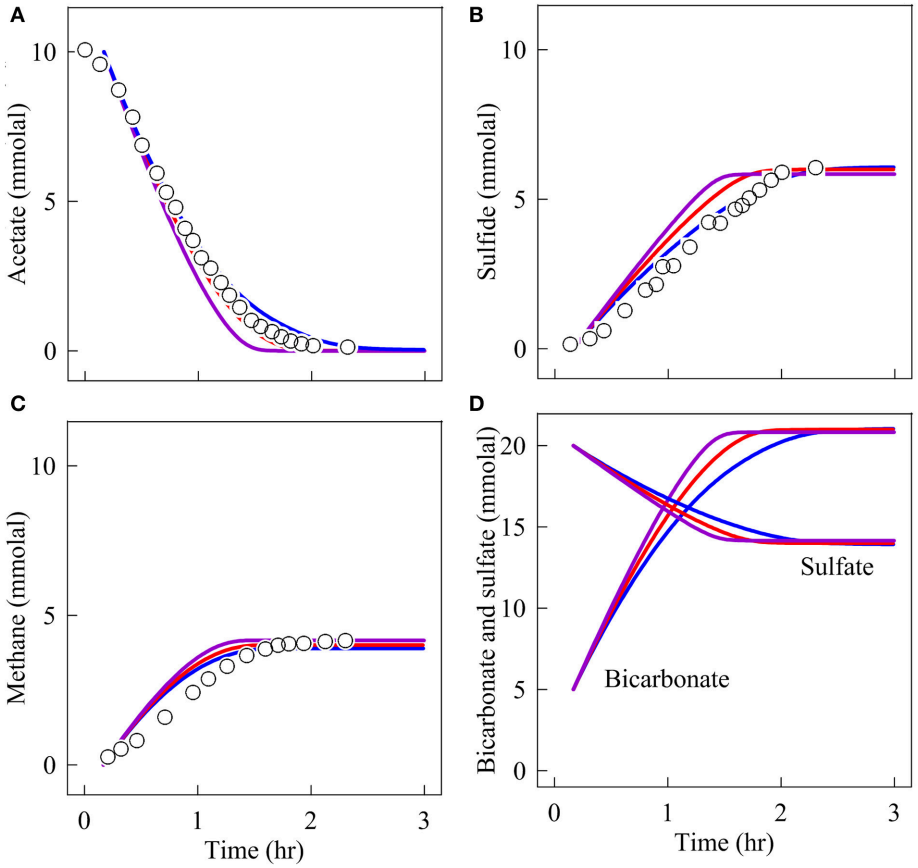

FIGURE 1 | Variation with time in the concentrations of acetate **(A)**, sulfide **(B)**, methane **(C)**, bicarbonate, and sulfate **(D)** in a batch reactor inoculated with *Desulfobacter postgatei* and *Methanosarcina barkeri*. Data points are the experimental results of Schönheit et al. (1982, their figure 3) at pH 7; the lines are the simulation results at pH 7 (blue), 6 (red), and 5 (purple) using microbial rate laws (Equations 3 and 10) and the parameters in **Table 1**.

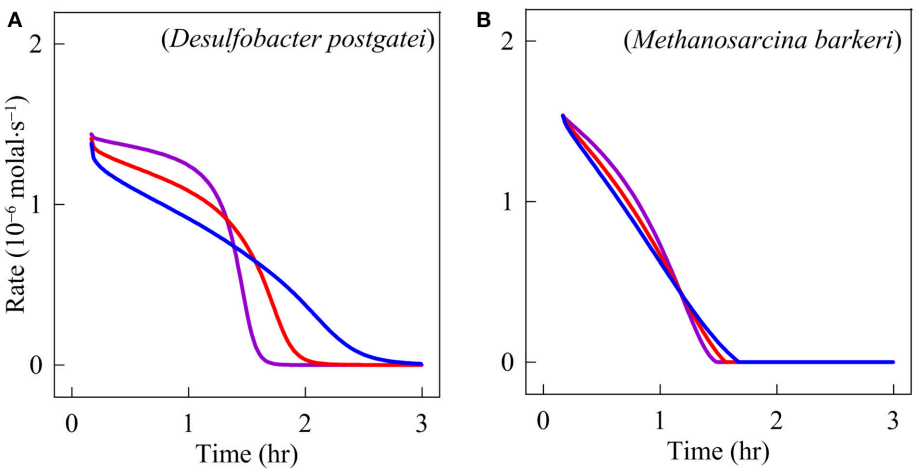

FIGURE 2 | Variation with time in respiration rates of *Desulfobacter postgatei* **(A)** and *Methanosarcina barkeri* **(B)**. The lines are the simulation results at pH 7 (blue), 6 (red), and 5 (purple).

addition to the thermodynamic control, methanogenesis rate is also limited by the concentration of acetate (Equation 3, **Figures 2B**, **3F**). Compared to *D. postgatei*, *M. barkeri* is more sensitive to the decrease in acetate concentrations because it has a relatively large half-saturation constant (**Table 1**). At pH 6 and 5, acetate concentration decreases faster than at pH 7, decreasing

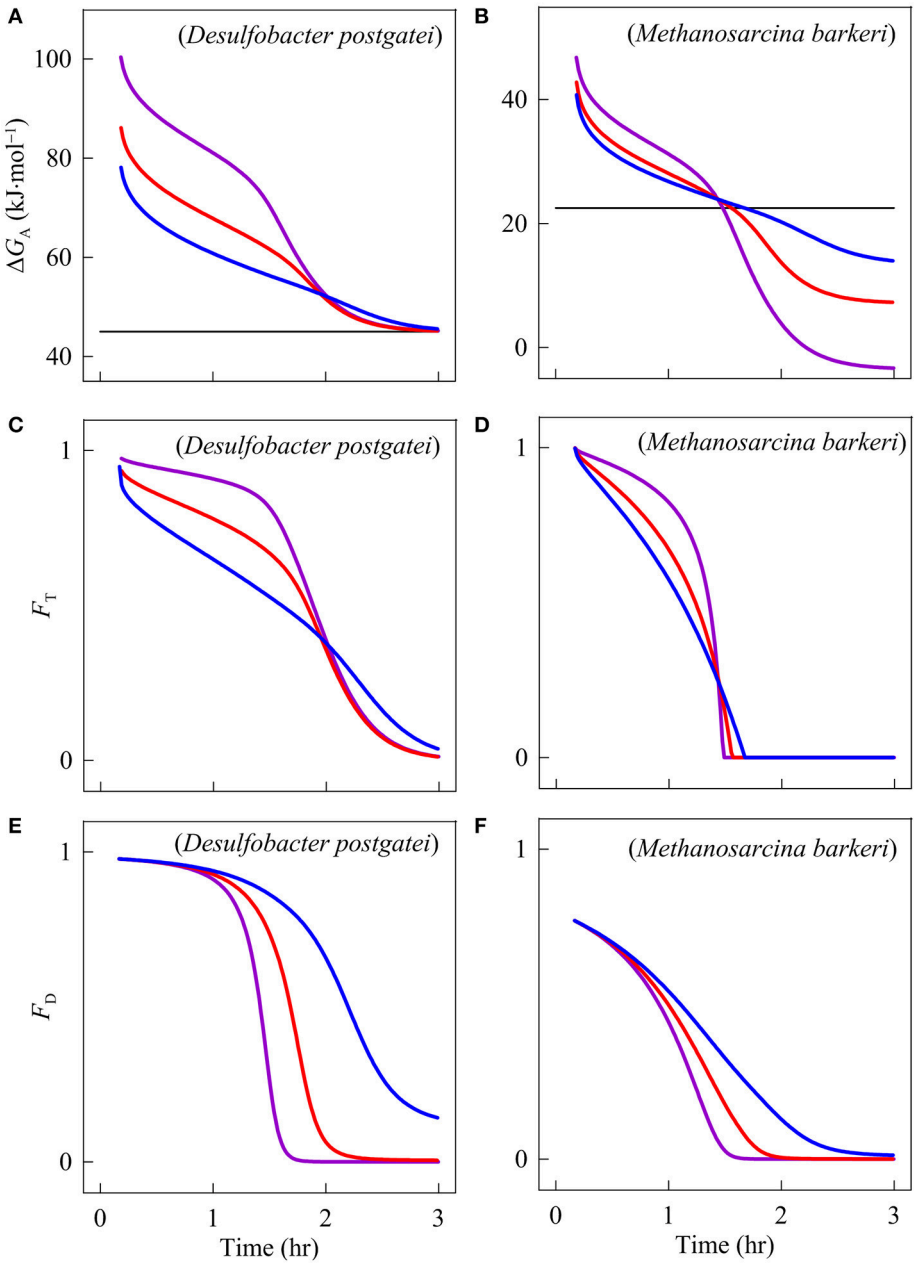

FIGURE 3 | Variation with time in the available energy ΔG_A **(A,B)**, the thermodynamic potential factor F_T **(C,D)**, and the kinetic factor F_D of *Desulfobacter postgatei* and *Methanosarcina barkeri* **(E,F)**. The lines are the simulation results at pH 7 (blue), 6 (red), and 5 (purple).

further the kinetic factor F_D of acetate (**Figures 1A**, **3F**). This change offsets the gain in energy provided by the decreasing pH and thus, the simulation predicts that the methanogenesis rate remains roughly unchanged at the different pHs.

Semi-open Environment

We then simulate the competition between *D. postgatei* and *M. barkeri* in a hypothetical semi-open system. We assume that fluid containing 5 mM acetate, 5 mM sulfate, and 1 mM bicarbonate has a temperature of 25°C and flows continuously through the system with a residence time of 3.7 day (or a turnover rate of 0.27 per day). We carry out the simulation at different pHs, from 5 to 7, for 10 years, well pass the time (0.5 year) when the system reaches steady state.

Figure 4 shows the simulation results. At pH 7, *D. postgatei* dominates the system but fails to drive out *M. barkeri*. At steady state, the hypothetical system contains 4.56 mM sulfide, 0.46 sulfide, 0.25 mM methane, and 0.21 mM acetate. *D. postgatei* grows to a concentration of 0.54 $g \cdot kg^{-1}$, and consumes 94.8% of the acetate flowing into the system. In contrast, *M. barkeri* has a

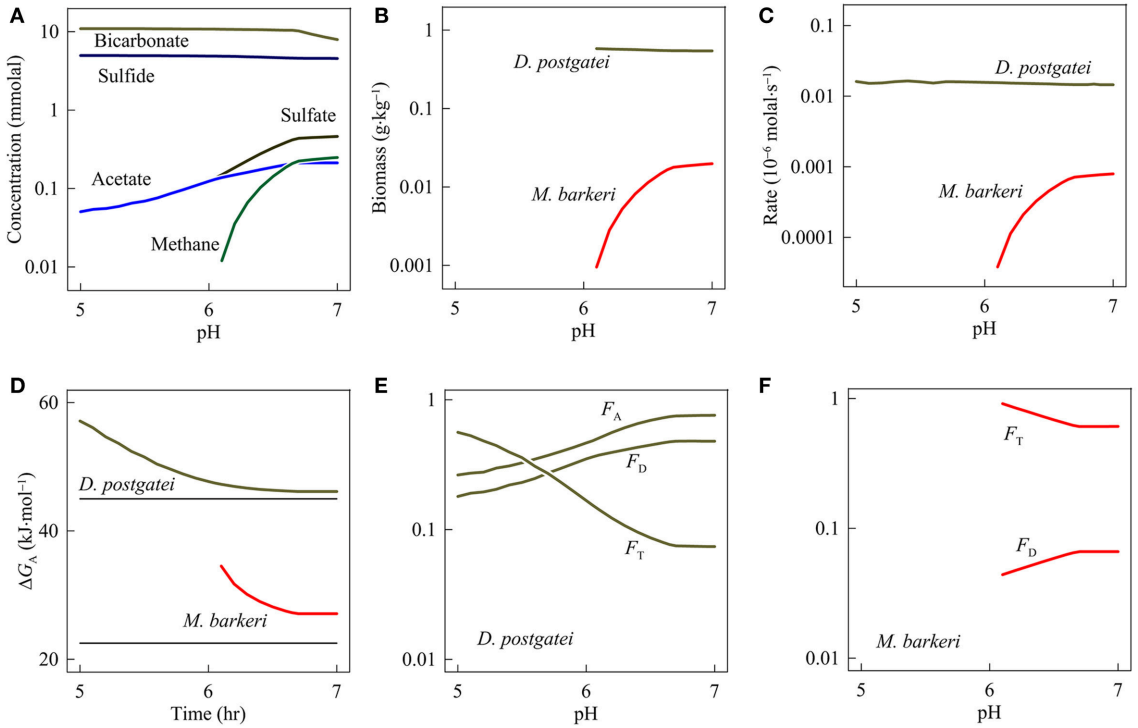

FIGURE 4 | Variation with pH in the concentrations of bicarbonate, sulfide, sulfate, acetate, and methane **(A)**, and the biomass concentrations **(B)**, the respiration rates **(C)**, the available energies ΔG_A **(D)**, the thermodynamic potential factors F_T, and the kinetic factors F_D and F_A of *Desulfobacter postgatei* **(E)** and *Methanosarcina barkeri* **(F)**.

concentration of 0.02 g·kg^{-1} and consumes the remaining 5.2% of the acetate.

As pH decreases from 7 to 6.1, *M. barkeri* persists but decreases in abundance relative to *D. postgatei*. Sulfate, acetate, and methane concentrations fall to 0.15, 0.14, and 0.01 mM, respectively, at pH 6.1 while sulfide concentration rises to 4.87 mM. Coupled with these changes, *D. postgatei* biomass rises slightly to 0.58 g·kg^{-1} as pH decreases to 6.1 while *M. barkeri* biomass decreases to 0.95 mg·kg^{-1}. At this point, methanogenesis only accounts for about 0.2% of the acetate consumption.

Only at pH equal to or less than 6, can *D. postgatei* drive *M. barkeri* out of the system. At pH 5, sulfate and acetate concentrations both decrease to 0.05 mM. The concentrations of sulfide and *D. postgatei* biomass rise to 4.97 mM and 0.59 g·kg^{-1}, respectively.

Above pH 6, the failure of *D. postgatei* to exclude *M. barkeri* is due to the significant thermodynamic limitation on sulfate reduction (**Figure 4D**). This control reflects the combined effects of neutral to near-neutral pH, acetate consumption, and bicarbonate and sulfide accumulation. As a consequence, the thermodynamic potential factor remains relatively small, lowering the rates of sulfate reduction and biosynthesis (Equations 3 and 10). To maintain biosynthesis rates above the rate of maintenance and cell death and thereby to avoid a decline in the biomass concentration, *D. postgatei* must balance the small thermodynamic potential factor by maintaining a modest kinetic factor of acetate. Specifically, it must maintain acetate concentrations above 0.13 mM, obtaining a kinetic factor above 0.4 (**Figure 4F**). In turn, these acetate concentrations are large enough for *M. barkeri* to achieve biosynthesis rates above the rate of maintenance and cell death (**Table 1**) and to survive in the system.

On the other hand, between pH 5 and 6, the energy available to *D. postgatei* rises well above the conserved energy (**Figure 4D**), raising the thermodynamic potential factor above 0.2. Under this condition, *D. postgatei* can lower acetate concentrations below the levels required for the survival of *M. barkeri*. These results are consistent with the hypothesis that sulfate reducers can drive methanogens out of the system by holding acetate concentrations below the levels needed for sustaining methanogen populations (Bethke et al., 2008). The results also support our hypothesis that pH can control the membership and metabolic activity of microbial consortia, and influence the outcome of microbial competition.

Syntrophy

A classic example of syntrophy is the interspecies hydrogen transfer, which takes place between H_2-producing and H_2-consuming microbes (Schink and Stams, 2013). Previous studies have emphasized H_2 levels as a determining factor of H_2-based syntrophic interactions. For example, butyrate-oxidizing microbes, such as *Syntrophomonas wolfei*, can oxidize butyrate to acetate by reducing protons to H_2. For butyrate oxidation

to remain thermodynamically favorable, butyrate oxidizers can partner with microbes that consume H_2 and thereby maintain H_2 levels low. In the companion paper (Jin and Kirk, 2018), we show that pH can play a similar role as H_2– pH affects the thermodynamics of both butyrate oxidation and hydrogentrophic redox reactions. Therefore, we expect that pH can also affect the kinetics of individual redox reactions in the syntrophic interaction and the dynamics of syntrophic consortia.

Laboratory Experiments

Wu et al. (1994) studied butyrate degradation using a consortium of three microbes, butyrate-oxidizing strain IB, *Methanobacterium formicium*, and *Methanosarcina mazei*. In their experiments, strain IB oxidizes butyrate and produces acetate and H_2,

$$\text{Butyrate} + 2H_2O \rightleftarrows 2\text{Acetate} + 2H_2 + H^+ \quad (13)$$

M. formicium catalyzes hydrogenotrophic methanogenesis,

$$4H_2 + H^+ + HCO_3^- \rightleftarrows CH_4 + 3H_2O \quad (14)$$

M. mazei drives acetoclastic methanogenesis (reaction 12). The three microbes grew at 37°C in batch reactors of 108 mL headspace and 50 mL growth medium. The medium had a pH of 7 and contained 4.3 mM butyrate, 4.1 mM isobutyate, 6.3 mM acetate, and 48.0 mM bicarbonate.

Jin (2007) developed a kinetic model for the three microbes. This model computes microbial reaction rates according to (Equations 3 and 10), and simulates butyrate degradation by accounting for the response of syntrophic energy conservation to H_2 partial pressure (Equation 8). Here we update the microbial parameters of the model to reflect recent developments of biogeochemical reaction modeling (see **Table 1**), and repeat the simulation.

According to the experimental observations and the simulation results at pH 7 (**Figure 5**), butyrate and isobutyrate concentrations decrease with time and are nearly depleted after day 25. Acetate concentration remains relatively stable during the first 10 days of the experiments and then accumulates to 10 mM after day 20. H_2 partial pressure peaks during the first couple of days and then decreases to 10^{-4} atm and remains at this level till day 20. Afterwards, H_2 partial pressure decreases to about 4.0×10^{-5} atm at day 27. The simulation also predicts the accumulations of dissolved inorganic carbon (DIC) and methane. At day 27, DIC reaches 57 mM and methane has a partial pressure of 0.17 atm.

Figure 6 shows the variations with time in the biomass concentrations and respiration rates of strain IB, *M. mazei*, and *M. formicium* according to the simulation results. The biomass concentrations of the three microbes vary similarly over time. They first increase to maximum values over about 20 days and then start to decrease slowly. Around day 20, the consortium is dominated by *M. mazeri*, whose maximum biomass concentration is 38.1 $mg{\cdot}kg^{-1}$. The biomass concentrations of strain IB and *M. formicium* are only 5.2 and 9.5 $mg{\cdot}kg^{-1}$, respectively. The rates of butyrate oxidation and hydrogenotrophic methanogenesis also vary similarly. The rates increase during the first 19 days, and then drop to 0. In comparison, the rate of *M. mazei* peaks twice during the experiments. The first peak appears around day 12 and the second comes on day 19, the same time when strain IB and *M. formicium* reach their maximum rates of butyrate oxidation and hydrogenotrophic methanogenesis, respectively.

Similar patterns of rates and biomass concentrations of strain IB and *M. formicium* confirm that the metabolisms of the two microbes depend on each other and thus interact syntrophically. On the other hand, the rate variation of *M. mazei* suggests that its metabolism is not closely coupled to butyrate oxidation, likely because acetate was provided at the beginning of the experiments.

pH Impact

To explore how pH may potentially affect butyrate degradation by the microbial consortium, we re-ran the updated model with medium at pH 6 and at pH 5. The results suggest that lowering pH can influence microbial metabolisms and interactions in at least three ways.

First, a decrease in pH affects butyrate degradation rates and hence the carbon fluxes from butyrate to CO_2 and methane. The simulation results indicate that, relative to pH 7, butyrate consumption slows by 4 and 15 days, respectively, at pH 6 and 5 (**Figure 5A**). Accordingly, lowering pH also delays variations in the biomass concentration and the respiration rate of strain IB (**Figures 6A,D**). For example, at pH 7, the biomass concentration reaches its maximum value at day 20. At pH 6 and 5, the maximum values appear on day 26 and 39, respectively. This delay in the metabolism explains the absence of an initial H_2 peak at pH 6 and 5 (**Figure 5E**).

The delay in butyrate degradation can be accounted for by the thermodynamic response of syntrophic butyrate oxidation. For strain IB, both the available energy and conserved energy depend on the partial pressures of H_2. At pH 7, the available energy first decreases briefly because of the H_2 peak and then increases to more than 10 $kJ{\cdot}mol^{-1}$ after day 5 (**Figure 7A**). Conserved energy also drops at the beginning of the experiments and then recovers, exceeding 5 $kJ{\cdot}mol^{-1}$ after day 5 (**Figure 7B**). As a result, the thermodynamic drive declines initially and then rises to about 7 $kJ{\cdot}mol^{-1}$ after day 5 (**Figure 7C**). The drive remains at this level until day 15 and then starts to decrease because of acetate accumulation. After day 20, the drive decreases to nearly 0.

Available energy also depends on pH. Specifically, available energy decreases with decreasing pH (Jin and Kirk, 2018). Thus, the thermodynamic drive is smaller at pH 6 than pH 7. At pH 5, during the first 10 days, the available energy is relatively large because of the small H_2 partial pressure. But the small partial pressure also allows strain IB to save more energy. As a result, the thermodynamic drive remains smaller than the value at pH 6. Smaller thermodynamic drives at pH 6 and 5 slow down the metabolism of strain IB (**Figure 7F**).

The delay in butyrate oxidation affects the metabolisms of *M. formicium* and *M. mazei*. *M. formicium* depends on strain IB for the supply of H_2. As a result, the delayed butyrate oxidation also delays the metabolism of *M. formicium*. The acetate for *M. mazei* comes from two sources, the acetate provided at the beginning of the experiments and the acetate produced by strain IB. The two different sources give rise to the two

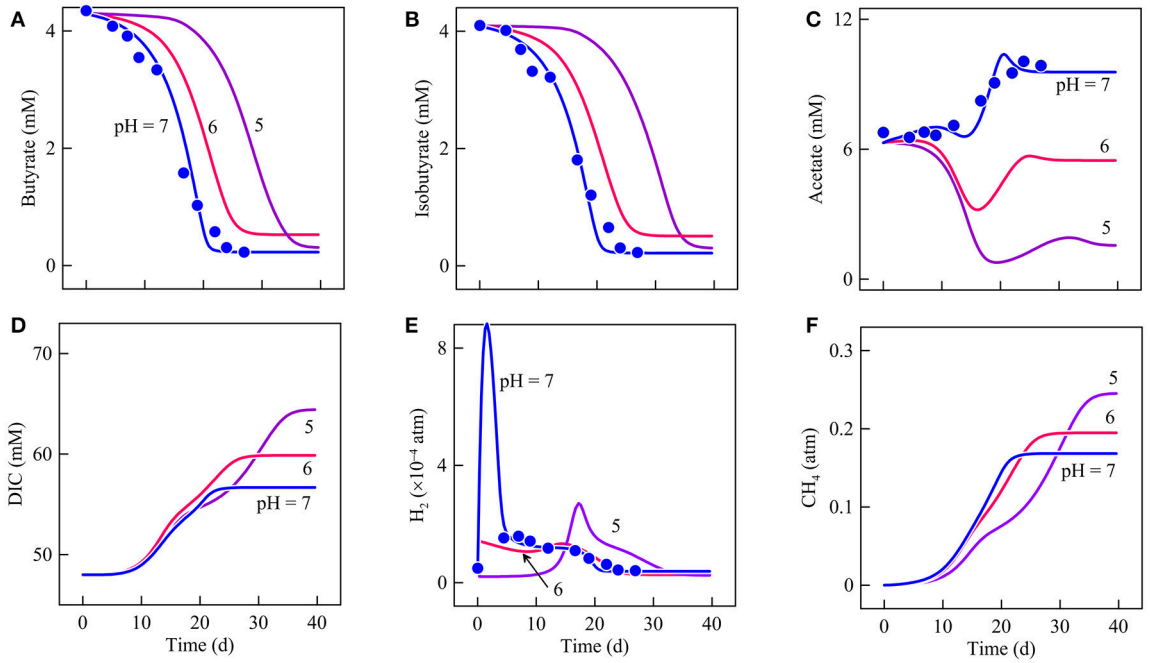

FIGURE 5 | Variation with time in the concentrations of butyrate **(A)**, isobutyrate **(B)**, acetate **(C)**, dissolved inorganic carbon (DIC, **D**), and the partial pressures of H_2 **(E)** and methane **(F)** in batch reactors of differ pHs. Data points are the results of Wu et al. (1994); lines are the results of biogeochemical reaction modeling, accounting for the impact of pH on the energy available from microbial reactions.

peak rates (**Figure 6E**). The first peak is made possible by the consumption of the initial acetate supply and the second is due to the acetate produced by butyrate oxidation. Delayed butyrate oxidation, therefore, delays the arrival of the second peak.

Second, a decrease in pH may also modulate the interactions between hydrogenotrophic and acetoclastic methanogenesis. In the reactors, methanogenesis by *M. mazei* is inhibited by the accumulation of methane. Methane accumulation decreases the thermodynamic drives and hence rates of both *M. formicium* and *M. mazei* (**Figures 7D,E,G,H**). But *M. mazei* is affected more because the energy available from acetoclastic methanogenesis (reaction 12) tends to be smaller than that of hydrogenotrophic methanogenesis (reaction 14), and because *M. mazei* conserves more energy than *M. formicium* per methane (Equations 6 and 7, **Table 1**). These thermodynamic differences allow *M. formicium* to make a proportionally larger contribution to methane production than *M. mazei.*

This effect can be evaluated in terms of the contribution of *M. mazei* to methane production. In the reactors, 4.3 mM butyrate, 4.1 mM isobutyrate and 6.3 mM acetate are provided. If the metabolisms of *M. mazei* and *M. formicium* are independent of each other and are not inhibited by methane accumulation, *M. formicium* would produce 4.2 mol methane, and *M. mazei* would produce 23.1 mol per liter of medium. In other words, *M. mazei* would account for 84.6% of methane production. According to the simulation results, at pH 7, *M. mazei* accounts for 76.1% of methane production. Thus, methane accumulation decreases the contribution of *M. mazei* by 8.5%.

At lower pH, this effect is lessened because methane production by *M. formicium* is delayed. The delay gives *M. mazei* an opportunity to consume more acetate and to make a bigger contribution to methane production (**Figures 5C,F, 6B,E**). At pH 6 and 5, *M. mazei* accounts for 80.9 and 83.9% of methane production, respectively. Corresponding to the increasing methane production, the biomass concentration of *M. mazeri* also increases (**Figures 6B,C**). At pH 6, *M. mazeri* reaches a maximum biomass concentration of 45.8 $mg{\cdot}kg^{-1}$ at day 28. At pH 5, the maximum biomass concentration of 57.4 $mg{\cdot}kg^{-1}$ is achieved on day 58.

Lastly, the pH decreases may regulate the efficiency of methane production. Microbial communities degrade organic carbon to CO_2 and methane. The efficiency of methane production is quantified as the ratio of methane production to the sum of CO_2 and methane productions (Ye et al., 2012),

$$\eta = \frac{C_{CH_4}}{C_{CO_2} + C_{CH_4}}, \tag{15}$$

where C_{CO_2} and C_{CH_4} are the total CO_2 and methane produced in the reactors. In the experiments, methane is produced by both acetoclastic and hydrogenotrophic methanogenesis but CO_2 is produced only by acetoclastic methanogenesis. The hydrogenotrophic pathway instead consumes CO_2. As such, the efficiency of methane generation increases with the increasing contribution of hydrogenotrophic methanogenesis. According to the simulation results, the proportion of acetoclastic to hydrogenotrophic methanogenesis changes with pH. Therefore,

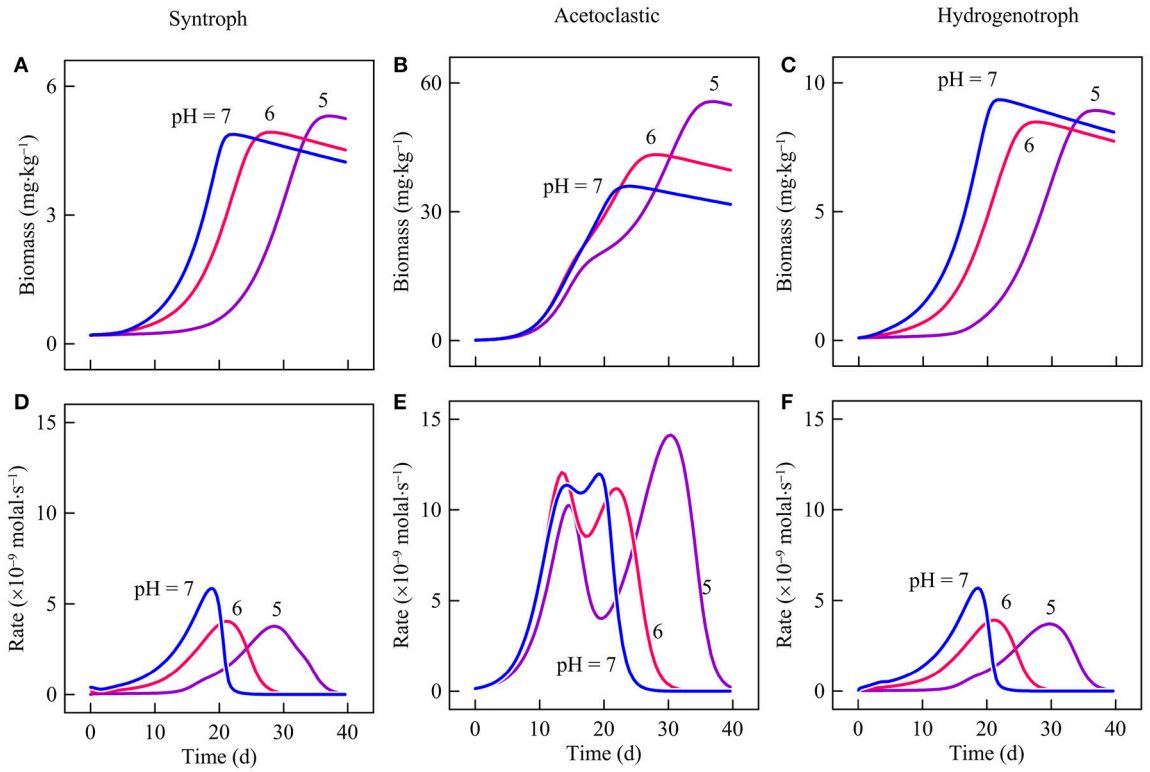

FIGURE 6 | Variation with time in the biomass concentrations and respiration rates of strain IB **(A,D)**, *Methanosarcina mazei* **(B,E)**, and *Methanobacterium formicium* **(C,F)** in batch reactors of differ pHs. Lines are the results of biogeochemical reaction modeling, accounting for the impact of pH on the energy available from microbial reactions.

the methane production efficiency η also varies with pH. Specifically, a decrease in pH lowers the efficiency of methane production. According to the simulation results, at pH 7, the efficiency of methane production is 65.7%. At pH 6 and 5, the efficiency decreases to 61.8 and 59.6%, respectively.

DISCUSSION

We explored the relationship between pH and microbial communities using biogeochemical kinetic modeling. We simulated how pH variation speeds up or slows down microbial respiration and growth and in turn influences microbial interactions, including the competition between sulfate reducers and methanogens and the syntrophy among butyrate oxidizers and methanogens.

Kinetic Response

In the companion paper (Jin and Kirk, 2018), we show that the variations in environmental pH change significantly the energy yields of syntrophic oxidation, sulfate reduction, and methanogenesis. In this paper, we simulate the kinetics of these processes using the thermodynamically consistent Monod equation (Equation 6)—this equation accounts for the energy yields of microbial redox reactions as well as the energy conserved by respiration. The simulation results show that a decrease in pH speeds up the metabolism of acetotrophic sulfate reducers. Specifically, decreases of one pH unit speed up the progress by 12%. The decrease in pH also slows down the metabolism of butyrate syntrophic oxidizers. A decrease of one pH unit decreases the rate by >10%. These results are consistent with the predictions from the thermodynamics of the redox reactions (reactions 11 and 13), and support that the thermodynamic responses of redox reactions can be strong enough to affect the kinetics of microbial metabolisms.

The pH decreases also raise the energy yields of acetoclastic and hydrogenotrophic methanogenesis (reactions 12 and 14) and hence have the potential of raising the metabolic activities of methanogens (Jin and Kirk, 2018). But our kinetic simulations fail to support these predictions. The inconsistencies between the thermodynamic and kinetic predictions highlight the complexity of microbial kinetics and the importance of microbial interactions.

For example, the rate of acetoclastic methanogenesis depends on the kinetic factor of acetate concentration as well as the thermodynamic factor of the energy yield. The modeling results show that in the batch reactor experiments of Schönheit et al. (1982), the pH decreases do raise the energy yields of acetoclastic methanogenesis, but this increasing effect is counteracted by the decreasing acetate concentrations. As a result, the rate doesn't respond much to the pH changes (**Figures 1–3**).

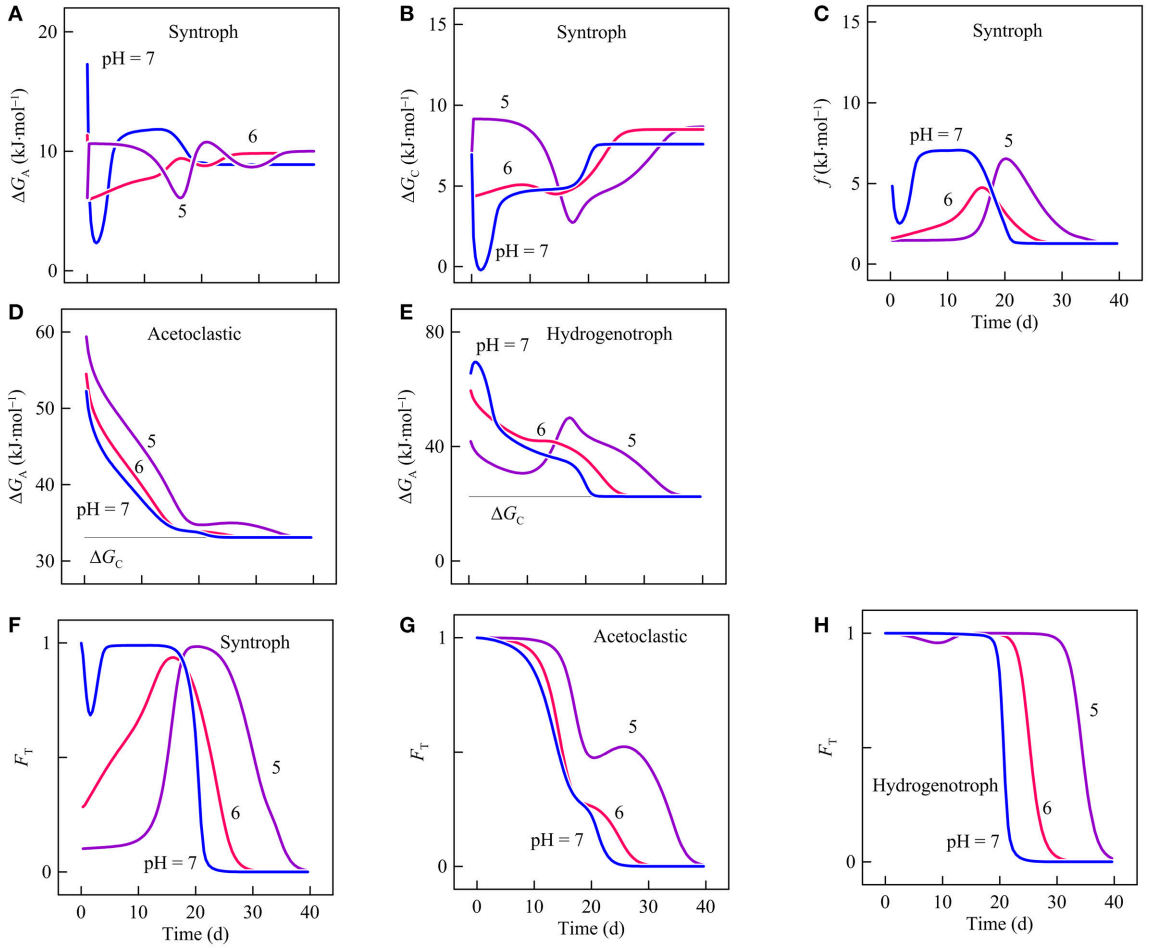

FIGURE 7 | Variation with time in the energy available **(A)**, the conserved energy **(B)**, and the thermodynamic drive **(C)** of strain IB, the energy available to *Methanosarcina mazei* **(D)** and to *Methanobacterium formicium* **(E)**, and the thermodynamic factor of syntrophic butyrate oxidation **(F)**, acetoclastic methanogenesis **(G)**, and hydrogenotrophic methanogenesis **(H)** in batch reactors of differ pHs. Lines are the results of biogeochemical reaction modeling, accounting for the impact of pH on the energy available from microbial reactions.

In the experiments of Wu et al. (1994), the pH decreases do not raise the energy yield of hydrogenotrophic methanogenesis. In the experiments, H_2-consuming *M. formicium* relies on H_2-producing strain IB for the supply of H_2. The energy yield of hydrogenotrophic methanogenesis depends not only on pH but also on the concentrations of H_2. At lower pH, H_2 production from butyrate oxidation slows down and H_2 concentration decreases, thereby lowering the energy yield at the beginning of the experiments and slowing down hydrogenotrophic methanogenesis.

The discrepancies between the thermodynamic predictions and kinetic modeling reiterate the difference between thermodynamic and kinetic modeling: the predictions made from reaction thermodynamics should be treated as the potential responses of microbial metabolisms. Whether the predictions are relevant or not requires biogeochemical modeling that considers not only the kinetics of microbial metabolisms of interest, but also the impact from concurrent biogeochemical processes.

Competitive Exclusion vs. Co-occurrence

In addition to the observation-based modeling, we also simulated the competition between *D. postgatei* and *M. barkeri* in a hypothetical semi-open environment (**Figure 4**). The results show that, despite its kinetic and thermodynamic advantages, *D. postgatei* is not always capable of excluding *M. barkeri* from the system, and that environmental pH can play a role in the outcome of microbial competition. The simulation demonstrates that pH can determine whether competitors coexist or are excluded from the environment. These results might help resolve the disagreement between the principle of competitive exclusion and metabolic diversities in natural environments.

According to the principle of competitive exclusion (Hardin, 1960), where different microbes reduce various electron acceptors by competing for a limiting electron donor, they cannot coexist, and only the one with competitive advantage can survive. In natural sediments and aquifers, common electron acceptors include O_2, nitrate, ferric minerals, sulfate, and CO_2,

and the apparent pattern in electron acceptor usage appears to conform to this principle (Kuivila et al., 1989; Chapelle et al., 1995; Bethke et al., 2011). Among these electron acceptors, O_2 is the most thermodynamically favorable one, followed by nitrate, ferric mineral, sulfate, and CO_2, respectively. Accordingly, O_2 is typically the first electron acceptor to be depleted from the environment, whereas CO_2 is the last.

But different anaerobic respiration reactions can take place simultaneously. The co-occurrence of iron reduction, sulfate reduction, and methanogenesis have been discovered in various settings, from biofilms to surface sediments and aquifers (Raskin et al., 1996; Metje and Frenzel, 2007; Flynn et al., 2013). Different mechanisms have been proposed to account for these co-occurrences, including spatial heterogeneity, dynamic biogeochemical conditions, and complex microbial interactions (Roy and Chattopadhyay, 2007; Bethke et al., 2011).

In our modeling example (**Figure 4**), *D. postgatei* can consume acetate and grow faster than *M. barkeri* (**Table 1**). But under the assumed flow and chemical conditions, the competitive exclusion principle only applies at pH $\leq$ 6.0. At pH above 6.0, the two microbes co-exist, due to the relatively significant thermodynamic limitation on the rates of sulfate reduction and biosynthesis. To balance the thermodynamic limitation, *D. postgatei* must maintain acetate at relatively large concentrations in order to achieve a relatively large kinetic factor F_D of acetate. These acetate concentrations exceed thresholds required for sustaining *M. barkeri* population.

Between pH 5 and 6, the relatively low pH raises the energy yield of sulfate reduction, which loosens the thermodynamic control and raises the rates of sulfate reduction and biosynthesis. Such favorable thermodynamic response allows *D. postgatei* to exclude *M. barkeri* by lowering acetate concentrations.

These results suggest that the competitive exclusion principle may not always be applicable, especially where microbes of competitive advantage are subject to significant thermodynamic limitations. They also illustrate a decisive role of pH in the outcome of microbial competition, and support our hypothesis that environmental pH is capable of shaping microbial community composition by affecting the thermodynamics and kinetics of individual microbial metabolisms.

Microbial Kinetic Model

This study focuses on how microbial thermodynamic responses to pH may affect the kinetics of individual microbial metabolism and the outcome of microbial interactions. In addition, pH also directly affects the catalytic capacity of microbes, therefore the kinetic parameters of microbial respiration and growth (Equation 3). This impact arises from the dependence of enzyme activities on cytoplasmic pH. Cytoplasmic pH modifies enzyme conformations and is critical for the formation and maintenance of the catalytically-competent active sites within enzymes (Leprince and Quiquampoix, 1996; Nielsen and McCammon, 2003). In addition, many enzymes are regulated allosterically by effector molecules. The presence of effector molecules and their interactions with enzymes depend on cytoplasmic pH (Makhlynets et al., 2015). Although cytoplasmic pH is tightly regulated by microbes, it does vary in accordance with the changes in environmental pH, albeit to lesser extents (Booth, 1985; Kobayashi et al., 2000; Padan et al., 2005).

Current models consider the direct pH impact on the forward rates by including a pH factor (Ng and Schaffner, 1997; Tienungoon et al., 2000). Enzyme activities respond to pH variations by following bell- or triangular-shaped curve. For example, the pH impact can be described using a triangular function,

$$F_{\mathrm{pH}} = \begin{cases} \frac{\mathrm{pH_{opt}} - \mathrm{pH}}{\mathrm{pH_{opt}} - \mathrm{pH_{min}}}, & \mathrm{pH_{min}} \leq \mathrm{pH} \leq \mathrm{pH_{opt}}; \\ \frac{\mathrm{pH_{max}} - \mathrm{pH}}{\mathrm{pH_{max}} - \mathrm{pH_{opt}}}, & \mathrm{pH_{opt}} < \mathrm{pH} \leq \mathrm{pH_{max}}. \end{cases} \quad (16)$$

Here pH_{opt}, pH_{min}, and pH_{max} are the optimal, minimum, and maximum pHs for growth. We propose to determine the values of pH_{opt}, pH_{min}, and pH_{max} based on the pH response of rate-limiting enzymes of microbial respiration. For example, methyl-coenzyme reductase is likely a rate-limiting step of methanogenesis (Bonacker et al., 1992). Based on previous laboratory observations of methyl-coenzyme M reductase of *Methanosarcina thermophila* (Jablonski and Ferry, 1991), we set pH_{opt} at 6.9, pH_{min} at 4.9, and pH_{max} at 8.9.

By combining the pH factor and the thermodynamic factor, we consider not only the direct impact of pH on respiration enzymes, but also the indirect impact by changing the thermodynamics of microbial respiration. These dual effects may explain a common pattern in the response of microbial metabolism to pH—the metabolic response is asymmetric about optimal pH. Specifically, between the minimum and optimal pHs, the slope of the increase in microbial rates differs from the slope of decrease between optimal and maximum pHs. The asymmetric responses have been widely reported for laboratory cultures, including syntrophs (Zhang et al., 2005; Hatamoto et al., 2007), iron reducers (Xu et al., 2005; Sun et al., 2014), sulfate reducers (Baena et al., 1998; O'Flaherty et al., 1998), and methanogens (Zehnder and Wuhrmann, 1977; Huser et al., 1982).

Taking acetoclastic methanogenesis as an example, according to the pH factor (Equation 16), a deviation from optimal pH always leads to the inhibition of microbial metabolism. Likewise, moving pH toward optimal pHs would promote microbial metabolism. However, for neutrophilic methanogens whose optimal pH is 7, increases in pH above the optimal pH raise their thermodynamic drives and hence rates, counteracting decreases by the direct pH effect on the forward rates of methanogenesis.

Combining the pH factor and the thermodynamic factor, the modified Monod equation predicts that rates of acetoclastic methanogenesis respond to pH asymmetrically. As shown in **Figure 8**, the slope predicted for the rate increase between pH_{min} and pH_{opt} is almost twice as large as the slope predicted for the decrease between pH_{opt} and pH_{max}. This prediction agrees with previous laboratory observations, such as those of *Methanosarcina mazei* (Maestrojuan and Boone, 1991).

In simulating microbial metabolisms, we purposely set the pH factor to one (Equation 16). In other words, we assumed that pH only impacts the thermodynamics of microbial redox reactions. This assumption allows us to focus on microbial thermodynamic responses. Despite this simplification, the simulation may still be relevant to natural environments, especially those that host

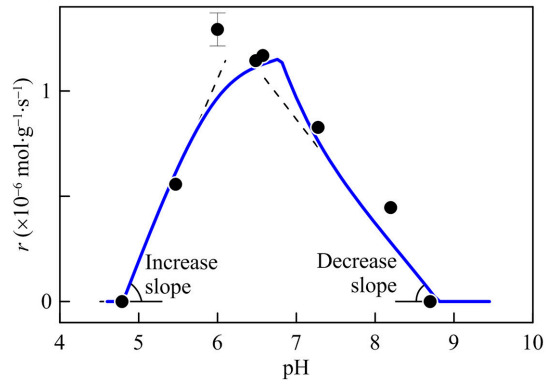

FIGURE 8 | Variation with time in the rate of acetoclastic methanogenesis. Solid line is the prediction by the pH factor and the thermodynamic factor, assuming that acetate is abundant and the kinetic factor F_D takes a value of one; data points are computed from the experimental results of *Methanosarcina mazei*, using a growth yield of 2 g·(mol acetate)$^{-1}$ (Maestrojuan and Boone, 1991). The slopes of increase and decrease are 0.86 and 0.49 mol·g^{-1}·s^{-1} per pH unit, respectively.

diverse microbial communities. For example, environments with neutral pH may host a seed bank of microbes whose optimal pHs are at pH 6 or 5. Thus, lowering pH to 6 lowers the respiration rate for microbes with optimal pH of 7, but would raise the rate for those with optimal pH of 6 (or their pH factors become one). As a result, microbes with an optimal pH of 6 would take over and drive out those whose optimal pHs are not 6, providing that other microbial properties, such as growth yields and maintenance rates, do not change.

Consistent with this interpretation, results of Petrie et al. (2003) and Kirk et al. (2013) suggest that the contribution of *Anaeromyxobacter* species to iron reduction increased as pH decreased in their field and bioreactor studies, respectively. As shown in the companion paper, iron reduction becomes more thermodynamically favorable as pH decreases. Thus, the shift in iron reducer identity was not likely a response to a thermodynamic limitation but possibly a reflection of differences in pH optima. These observations suggest that our results are best applied to environments that host diverse communities of microorganisms with different optimal pHs. We further propose that thermodynamics may provide insight into the kinetic response of microbial metabolisms to pH variations, whereas pH optima may dictate the identity of species that catalyze the reactions at a given pH.

Concluding Comments

We applied biogeochemical kinetic modeling to simulate the responses of syntrophic butyrate oxidation, sulfate reduction, and methanogenesis to pH changes. Our modeling is biased by two assumptions. We assume that pH does not affect the amount of energy conserved by microbes. We also assume that microbial kinetic parameters, including rate constants, half-saturation constants, and maintenance rates, do not change with pH. These assumptions overlook the complexity of microbial metabolisms and may have underestimated the extent to which pH impacts cell metabolisms. But these assumptions allow us to focus on microbial thermodynamic responses and to test whether the pH-induced thermodynamic responses alone are strong enough for significant changes in the composition and activity of microbial communities.

The simulation results show that, by accounting for the thermodynamics and kinetics of microbial reactions and the interactions among microbes, biogeochemical kinetic modeling can be applied to gauge and tune the predictions made from thermodynamics. For example, a pH decrease from 7 to 6 or to 5 raises the energy yield of acetotrophic sulfate reduction, but lowers the energy yield of syntrophic butyrate oxidation. Based on the thermodynamic responses, we predict that acetotrophic sulfate reduction would speed up, but syntrophic butyrate oxidation would slow down by the pH decrease. The kinetic modeling results confirm the predictions—a one-unit decrease in pH can raise the rate of acetotrophic sulfate reduction and lower the rate of syntrophic butyrate oxidation by >10%.

Our results also show that thermodynamic predictions are not always relevant. A pH decrease from 7 to 6 or to 5 raises the energy yield of acetoclastic and hydrogenotrophic methanogenesis, and hence can speed up the two reactions. But the kinetic modeling results suggest that, in closed environments, such as in laboratory batch reactors, the thermodynamic influence of pH on acetoclastic methanogenesis can be canceled by the impact of decreasing acetate concentrations. Also, where hydrogenotrophic methanogens live syntrophically with H_2-producing butyrate oxidizers, both the energy yield and rate of methanogenesis may depend primarily on the H_2 production by butyrate oxidizers, instead of environmental pH.

The simulation of the semi-open system supports the hypothesis that by changing the energy yields of microbial redox reactions, environmental pH is capable of changing the composition of microbial communities. According to the simulation results, environmental pH dictates the outcome of the competition between *D. postgatei* and *M. barkeri*. Between pH 6 and 7, despite the competitive advantage of *D. postgatei* over *M. barkeri*, the two microbes live together in the system. Between pH 5 and 6, only *D. postgatei* stays, and *M. barkeri* disappears. The different outcomes come from the influence of pH on the energy yield of sulfate reduction. Between pH 6 and 7, *D. postgatei* is subject to a significant thermodynamic limitation, and must balance that limitation by keeping acetate concentrations relatively large—large enough for sustaining the cells of *M. barkeri*. Decreasing pH to or below 6 alleviates the thermodynamic limitation and enables *D. postgatei* to expel *M. barkeri* by lowering acetate concentrations below the minimum levels required for sustaining *M. barkeri*.

By raising or lowering the energy yields of microbial redox reactions, environmental pH is also capable of shaping the ecological functions of microbial communities. The modeling results of butyrate syntrophic degradation show that pH variation is capable of changing microbially-driven carbon fluxes in three ways. First, environmental pH affects the magnitudes of carbon fluxes. Lowering pH from 7 to 5 decrease the rates of butyrate oxidation and hence the fluxes of C from butyrate to CO_2 and

methane. This decrease is mainly due to the decreases in the energy available from the syntrophic oxidation of butyrate.

Second, environmental pH regulates the contributions of hydrogenotrophic and acetoclastic methanogenesis to methane production. Compared to the hydrogenotrophic pathway, acetoclastic methanogenesis is more sensitive to the accumulation of methane in the environment because of its limited available energy. The simulation results show that lowering pH from 7 to 5 decreases the thermodynamic drive of the hydrogenotrophic pathway and subsequently its production of methane. In turn, this effect alleviates the methane inhibition of the acetoclastic pathway, allowing it to produce more methane.

Last, variation in pH changes the efficiency of methane production. By working together, syntrophic butyrate oxidation, and hydrogenotrophic and acetoclastic methanogenesis convert butyrate to CO_2 and methane. Environmental pH can influence the efficiency of methane production by changing the relative significances of the two methanogenesis pathways. Specifically, decreases in pH decrease the efficiency of methane production from butyrate, a result that is consistent with previous observations in wetlands (Ye et al., 2012). Taken together, these results provide a mechanistic view of how environmental pH modulate the fluxes and composition of C in the environment. Although we focused on butyrate degradation, we expect that pH also influence the C fluxes from other organic compounds and hence the biogeochemical cycling of C—a topic to be further investigated.

In addition, the modeling results add to the current theories of environmental microbiology. For example, current theories attribute microbial competitive advantages to two different mechanisms—by lowering substrate levels below the thresholds required for driving the catabolisms of competitors (Lovley et al., 1982) or below the thresholds for sustaining the populations of competitors (Bethke et al., 2008). Our simulation results suggest that the two mechanisms are applicable to two different environmental settings—the first is applicable to batch reactors and other closed environments, whereas the second applies to flow-through reactors or other semi-open environments.

The modeling results also suggest that the principle of competitive exclusion may not always be applicable. This principle predicts that where electron donors are limiting, microbial respiration reactions segregated into spatially-distinct zones. According to the simulation results, this principle may not be applicable to respiration reactions of significant thermodynamic limitations, where the energy yields of redox reactions are close to the energy conserved by respiration. Under this condition, respiration reactions of competitive advantage may take place simultaneously with reactions of competitive disadvantage. Only where the thermodynamic control becomes relatively insignificant, can the respiration reactions of competitive advantage exclude competing reactions from the environment by lowering electron donor concentrations. Thus, by modifying the energy yields of microbial redox reactions, environmental pH can determine whether the competitive exclusion principle is applicable, or whether different microbial redox reactions take place simultaneously or segregated into different zones.

AUTHOR CONTRIBUTIONS

All authors listed have made a substantial, direct and intellectual contribution to the work, and approved it for publication.

FUNDING

This research was funded by the National Science Foundation under Award EAR-1636815 and by National Aeronautics and Space Administration under Grant NNX16AJ59G.

SUPPLEMENTARY MATERIAL

The Supplementary Material for this article can be found online at: https://www.frontiersin.org/articles/10.3389/fenvs.2018.00101/full#supplementary-material

REFERENCES

Amenabar, M. J., Shock, E. L., Roden, E. E., Peters, J. W., and Boyd, E. S. (2017). Microbial substrate preference dictated by energy demand rather than supply: *Nat. Geosci*. 10, 577–581. doi: 10.1038/ngeo2978

Baena, S., Fardeau, M. L., Labat, M., Ollivier, B., Garcia, J. L., and Patel, B. K. C. (1998). *Desulfovibrio aminophilus* sp. nov., a novel amino acid degrading and sulfate reducing bacterium from an anaerobic dairy wastewater lagoon. *Syst. Appl. Microbiol*. 21, 498–504. doi: 10.1016/S0723-2020(98)80061-1

Bethke, C. M. (2008). *Geochemical and Biogeochemical Reaction Modeling.* Cambridge:Cambridge University Press.

Bethke, C. M., Ding, D., Jin, Q., and Sanford, R. A. (2008). Origin of microbiological zoning in groundwater flows. *Geology* 36, 739–742. doi: 10.1130/G24859A.1

Bethke, C. M., Sanford, R. A., Kirk, M. F., Jin, Q., and Flynn, T. M. (2011). The thermodynamic ladder in geomicrobiology. *Am. J. Sci*. 311, 183–210. doi: 10.2475/03.2011.01

Bonacker, L. G., Baudner, S., and Thauer, R. K. (1992). Differential expression of the two methyl-coenzyme M reductases in *Methanobacterium thermoautotrophicum* as determined immunochemically via isoenzyme-specific antisera. *Eur. J. Biochem.* 206, 87–92. doi: 10.1111/j.1432-1033.1992.tb16904.x

Booth, I. R. (1985). Regulation of cytoplasmic pH in bacteria. *Microbiol. Rev*. 49, 359–378.

Chapelle, F. H., McMahon, P. B., Dubrovsky, N. M., Fujii, R. F., Oaksford, E. T., and Vroblesky, D. A. (1995). Deducing the distribution of terminal electron-accepting processes in hydrologically diverse groundwater systems. *Water Resour. Res*. 31, 359–371. doi: 10.1029/94WR02525

Delany, J. M., and Lundeen, S. R. (1990). *The LLNL Thermodynamical Database.* Lawrence Livermore National Laboratory Report UCRL-21658.

Flynn, T. M., Sanford, R. A., Ryu, H., Bethke, C. M., Levine, A. D., Ashbolt, N. J., et al. (2013). Functional microbial diversity explains groundwater chemistry in a pristine aquifer. *BMC Microbiol.* 13:146. doi: 10.1186/1471-2180--146

Hardin, G. (1960). The competitive exclusion principle. *Science* 131, 1292–1297. doi: 10.1126/science.131.3409.1292

Hatamoto, M., Imachi, H., Fukayo, S., Ohashi, A., and Harada, H. (2007). *Syntrophomonas palmitatica* sp. nov., an anaerobic, syntrophic, long-chain

fatty-acid-oxidizing bacterium isolated from methanogenic sludge. *Int. J. Syst. Evolu. Microbiol.* 57, 2137–2142. doi: 10.1099/ijs.0.64981-0

Helgeson, H. C. (1969). Thermodynamics of hydrothermal systems at elevated temperatures and pressures. *Am. J. Sci.* 267, 729–804. doi: 10.2475/ajs.267.7.729

Huser, B. A., Wuhrmann, K., and Zehnder, A. J. B. (1982). *Methanothrix soehngenii* gen. nov. sp. nov., a new acetotrophic non-hydrogen-oxidizing methane bacterium. *Arch. Microbiol.* 132, 1–9.

Jablonski, P. E., and Ferry, J. G. (1991). Purification and properties of methyl coenzyme M methylreductase from acetate-grown *Methanosarcina thermophila*. *J. Bacteriol.* 173, 2481–2487. doi: 10.1128/jb.173.8.2481-2487.1991

Jin, Q. (2007). Control of hydrogen partial pressures on the rates of syntrophic microbial metabolisms: a kinetic model for butyrate fermentation. *Geobiology* 5, 35–48. doi: 10.1111/j.1472-4669.2006.00090.x

Jin, Q. (2012). Energy conservation of anaerobic respiration. *Am. J. Sci.* 312, 573–628. doi: 10.2475/06.2012.01

Jin, Q., and Bethke, C. M. (2002). Kinetics of electron transfer through the respiratory chain. *Biophys. J.* 83, 1797–1808. doi: 10.1016/S0006-3495(02)73945-3

Jin, Q., and Bethke, C. M. (2003). A new rate law describing microbial respiration. *Appl. Environ. Microbiol.* 69, 2340–2348. doi: 10.1128/AEM.69.4.2340-2348.2003

Jin, Q., and Bethke, C. M. (2005). Predicting the rate of microbial respiration in geochemical environments. *Geochim. Cosmochim. Acta* 69, 1133–1143. doi: 10.1016/j.gca.2004.08.010

Jin, Q., and Bethke, C. M. (2007). The thermodynamics and kinetics of microbial metabolism. *Am. J. Sci.* 307, 643–677. doi: 10.2475/04.2007.01

Jin, Q., and Kirk, M. F. (2016). Thermodynamic and kinetic response of microbial reactions to high CO2. *Front. Microbiol.* 7:1696. doi: 10.3389/fmicb.2016.01696

Jin, Q., and Kirk, M. F. (2018). pH as a primary control in environmental microbiology: 1. Thermodynamic perspective. *Front. Environ. Sci.* 6:21. doi: 10.3389/fenvs.2018.00021

Jin, Q., and Roden, E. E. (2011). Microbial physiology-based model of ethanol metabolism in subsurface sediments. *J. Contam. Hydrol.* 125, 1–12. doi: 10.1016/j.jconhyd.2011.04.002

Jin, Q., Roden, E. E., and Giska, J. R. (2013). Geomicrobial kinetics: extrapolating laboratory studies to natural environments. *Geomicrobiol. J.* 30, 173–185. doi: 10.1080/01490451.2011.653084

Kinniburgh, D. G., van Riemsdijk, W. H., Koopal, L. K., Borkovec, M., Benedetti, M. F., and Avena, M. J. (1999). Ion binding to natural organic matter: competition, heterogeneity, stoichiometry and thermodynamic consistency. *Colloids Surf. A Physicochem. Eng. Aspects* 151, 147–166. doi: 10.1016/S0927-7757(98)00637-2

Kirk, M. F., Santillan, E. F. U., Sanford, R. A., and Altman, S. J. (2013). CO2-induced shift in microbial activity affects carbon trapping and water quality in anoxic bioreactors. *Geochim. Cosmochim. Acta* 122, 198–208. doi: 10.1016/j.gca.2013.08.018

Kobayashi, H., Saito, H., and Kakegawa, T. (2000). Bacterial strategies to inhabit acidic environments. *J. Gen. Appl. Microbiol.* 46, 235–243. doi: 10.2323/jgam.46.235

Konings, W. N., Albers, S.-V., Koning, S., and Driessen, A. J. M. (2002). The cell membrane plays a crucial role in survival of bacteria and archaea in extreme environments. *Antonie van Leeuwenhoek* 81, 61–72. doi: 10.1023/A:1020573408652

Kotsyurbenko, O. R., Chin, K.-J., Glagolev, M. V., Stubner, S., Simankova, M. V., Nozhevnikova, A. N., et al. (2004). Acetoclastic and hydrogenotrophic methane production and methanogenic populations in an acidic West-Siberian peat bog. *Environ. Microbiol.* 6, 1159–1173. doi: 10.1111/j.1462-2920.2004.00634.x

Kuivila, K. M., Murray, J. W., Devol, A. H., and Novelli, P. C. (1989). Methane production, sulfate reduction and competition for substrates in the sediments of Lake Washington. *Geochim. Cosmochim. Acta* 53, 409–416. doi: 10.1016/0016-7037(89)90392-X

Leprince, F., and Quiquampoix, H. (1996). Extracellular enzyme activity in soil: effect of pH and ionic strength on the interaction with montmorillonite of two acid phosphatases secreted by the ectomycorrhizal fungus *Hebeloma cylindrosporum*. *Eur. J. Soil Sc.* 47, 511–522. doi: 10.1111/j.1365-2389.1996.tb01851.x

Lovley, D. R., Dwyer, D. F., and Klug, M. J. (1982). Kinetic analysis of competition between sulfate reducers and methanogens for hydrogen in sediments. *Appl. Environ. Microbiol.* 43, 1373–1379.

Lovley, D. R., and Klug, M.J. (1982). Intermediary metabolism of organic matter in the sediments of a eutrophic lake. *Appl. Environ. Microbiol.* 43, 552–560.

Lovley, D. R., and Philips, E. J. (1987). Competitive mechanisms of sulfate reduction and methane production in the zone of ferric iron reduction in sediments. *Appl. Environ. Microbiol.* 53, 2636–2641.

Maestrojuan, G. M., and Boone, D. R. (1991). Characterization of Methanosarcina barkeri MST and 227, *Methanosarcina mazei* S-6T, and *Methanosarcina vacuolata* Z-761T. *Int. J. Syst. Evolu. Microbiol.* 41, 267–274. doi: 10.1099/00207713-41-2-267

Makhlynets, O. V., Raymond, E. A., and Korendovych, I. V. (2015). Design of allosterically regulated protein catalysts. *Biochemistry* 54, 1444–1456. doi: 10.1021/bi5015248

Metje, M., and Frenzel, P. (2007). Methanogenesis and methanogenic pathways in a peat from subarctic permafrost. *Environ. Microbiol.* 9, 954–964. doi: 10.1111/j.1462-2920.2006.01217.x

Molongoski, J. J., and Klug, M. J. (1980). Anaerobic metabolism of particulate organic matter in the sediments of hypereutrophic lake. *Freshw. Biol.* 10, 507–518. doi: 10.1111/j.1365-2427.1980.tb01225.x

Monokova, S.V. (1975). Volatile fatty acids in bottom sediments of the Rybinsk reservoir. *Hydrobiol. J.* 11, 45–48.

Ng, T. M., and Schaffner, D. W. (1997). Mathematical models for the effects of pH, temperature, and sodium chloride on the growth of *Bacillus stearothermophilus* in salty carrots. *Appl. Environ. Microbiol.* 63, 1237–1243.

Nielsen, J. E., and McCammon, J. A. (2003). Calculating pKa values in enzyme active sites. *Protein Sci.* 12, 1894–1901. doi: 10.1110/ps.03114903

Nielsen, U. N., Ayres, E., Wall, D. H., and Bardgett, R. D. (2011). Soil biodiversity and carbon cycling: a review and synthesis of studies examining diversity–function relationships. *Eur. J. Soil Sci.* 62, 105–116. doi: 10.1111/j.1365-2389.2010.01314.x

O'Flaherty, V., Mahony, T., O'Kennedy, R., and Colleran, E. (1998). Effect of pH on growth kinetics and sulphide toxicity thresholds of a range of methanogenic, syntrophic and sulphate-reducing bacteria. *Process Biochem.* 33, 555–569. doi: 10.1016/S0032-9592(98)00018-1

Padan, E., Bibi, E., Ito, M., and Krulwich, T. A. (2005). Alkaline pH homeostasis in bacteria: new insights. *Biochim. Biophys. Acta Biomembranes* 1717, 67–88. doi: 10.1016/j.bbamem.2005.09.010

Panikov, N. S. (1995). *Microbial Growth Kinetics.* London: Chapman and Hall.

Paul, A., Stösser, R., Zehl, A., Zwirnmann, E., Vogt, R. D., and Steinberg, C. E. W. (2006). Nature and abundance of organic radicals in natural organic matter: effect of pH and irradiation. *Environ. Sci. Technol.* 40, 5897–5903. doi: 10.1021/es060742d

Petrie, L., North, N. N., Dollhopf, S. L., Balkwill, D. L., and Kostka, J. E. (2003). Enumeration and characterization of iron(III)-reducing microbial communities from acidic subsurface sediments contaminated with uranium(VI). *Appl. Environ. Microbiol.* 69, 7467–7479. doi: 10.1128/AEM.69.12.7467-7479.2003

Raskin, L., Rittmann, B. E., and Stahl, D. A. (1996). Competition and coexistence of sulfate-reducing and methanogenic populations in anaerobic biofilms: *Appl. Environ. Microbiol.* 62, 3847–57.

Rosso, L., Lobry, J. R., Bajard, S., and Flandrois, J. P. (1995). Convenient model to describe the combined effects of temperature and pH on microbial growth. *Appl. Environ. Microbiol.* 61, 610–616.

Roy, S., and Chattopadhyay, J. (2007). Towards a resolution of 'the paradox of the plankton': a brief overview of the proposed mechanisms. *Ecol. Complex* 4, 26–33. doi: 10.1016/j.ecocom.2007.02.016

Schink, B., and Stams, A. J. M. (2013). "Syntrophism among prokaryotes," in *The Prokaryotes: Prokaryotic Communities and Ecophysiology*, eds E. Rosenberg, E. F. DeLong, S. Lory, E. Stackebrandt, and F. Thompson (Berlin; Heidelberg: Springer), 471–493.

Schönheit, P., Kristjansson, J. K., and Thauer, R. K. (1982). Kinetic mechanism for the ability of sulfate reducers to out-compete methanogens for acetate. *Arch. Microbiol.* 132, 285–288.

Sun, D., Wang, A., Cheng, S., Yates, M., and Logan, B. E. (2014). *Geobacter anodireducens* sp. nov., an exoelectrogenic microbe in bioelectrochemical systems. *Int. J. Syst. Evolu. Microbiol.* 64, 3485–3491. doi: 10.1099/ijs.0.061598-0

Thauer, R. K., Jungermann, K., and Decker, K. (1977). Energy conservation in chemotrophic anaerobic bacteria. *Bacteriolog. Rev*. 41, 100–180.

Thompson, L. R., Sanders, J. G., McDonald, D., Amir, A., Ladau, J., Locey, K. J., et al. (2017). A communal catalogue reveals Earth's multiscale microbial diversity. *Nature* 551, 457–463. doi: 10.1038/nature24621

Tienungoon, S., Ratkowsky, D. A., McMeekin, T. A., and Ross, T. (2000). Growth limits of *Listeria monocytogenesas* a function of temperature, pH, NaCl, and lactic acid. *Appl. Environ. Microbiol*. 66, 4979–4987. doi: 10.1128/AEM.66.11.4979-4987.2000

van Bodegom, P. (2007). Microbial maintenance: a critical review on its quantification. *Microbiol Ecol*. 53, 513–523. doi: 10.1007/s00248-006-9049-5

Wu, W.-M., Jain, M. K., and Zeikus, J. G. (1994). Anaerobic degradation of normal- and branched-chain fatty acids with four or more carbons to methane by a syntrophic methanogenic triculture. *Appl. Environ. Microbiol*. 60, 2220–2226.

Xavier, J. B. (2011). Social interaction in synthetic and natural microbial communities. *Mol. Syst. Biol*. 7:483. doi: 10.1038/msb.2011.16

Xu, M., Guo, J., Cen, Y., Zhong, X., Cao, W., and Sun, G. (2005). *Shewanella decolorationis* sp. nov., a dye-decolorizing bacterium isolated from activated sludge of a waste-water treatment plant. *Int. J. Syst. Evolu. Microbiol*. 55, 363–368. doi: 10.1099/ijs.0.63157-0

Ye, R., Jin, Q., Bohannan, B., Keller, J. K., McAllister, S. A., and Bridgham, S. D. (2012). pH controls over anaerobic carbon mineralization, the efficiency of methane production, and methanogenic pathways in peatlands across an ombrotrophic–minerotrophic gradient. *Soil Biol. Biochem*. 54, 36–47. doi: 10.1016/j.soilbio.2012.05.015

Zehnder, A. J. B., and Wuhrmann, K. (1977). Physiology of a *Methanobacterium* strain AZ. *Arch. Microbiol*. 111, 199–205. doi: 10.1007/BF00549357

Zhang, C., Liu, X., and Dong, X. (2005). *Syntrophomonas erecta* sp. nov., a novel anaerobe that syntrophically degrades short-chain fatty acids. *Int. J. Syst. Evol. Microbiol*. 55, 799–803. doi: 10.1099/ijs.0.63372-0

Conflict of Interest Statement: The authors declare that the research was conducted in the absence of any commercial or financial relationships that could be construed as a potential conflict of interest.

frontiers in Earth Science

ORIGINAL RESEARCH
published: 26 September 2018
doi: 10.3389/feart.2018.00143

A Bioenergetic Framework for Assessing Soil Organic Matter Persistence

Elizabeth K. Williams and Alain F. Plante*

Department of Earth and Environmental Science, University of Pennsylvania, Philadelphia, PA, United States

The emerging view of soil organic matter (SOM) persistence asserts that SOM exists as a continuum of organic material, continuously processed by the decomposer community from large biopolymers to small monomers and with increasing oxidation and solubility, protected from decomposition through mineral aggregation and adsorption. Microbial community and ecosystem dynamics regulate the exchange of both nutrients and carbon between the soil and the atmosphere through the mineralization of SOM. Because these ecosystem dynamics are driven by net energy flows, analysis of SOM bioenergetics can provide complementary constraints to SOM models as well as insight into the fundamental conundrum of why thermodynamically unstable organic matter persists in soil. Microbial substrate preference has been shown to depend on the energy status of the potential substrates in terms of energy required and energy returned. Here we propose a framework for assessing the persistence of SOM utilizing thermally determined activation energy (E_a) and energy density (ED), tested on a suite of soils that have undergone alteration in field or laboratory experiments designed to isolate persistent SOM. Comparison of these energetic parameters in this framework will determine whether a chemical or physical change during SOM decomposition resulted in a change in its environmental persistence. An expanded framework of bioenergetics changes during SOM formation, decomposition, and stabilization is proposed as persistent SOM is characterized by decreased ED and E_a, relative to the bulk SOM.

Keywords: soil organic matter, bioenergetics, thermal analysis, carbon cycling, activation energy

OPEN ACCESS

Edited by:
Philippe C. Baveye, AgroParisTech Institut des Sciences et Industries du Vivant et de L'environnement, France

Reviewed by:
Carsten W. Mueller, Technische Universität München, Germany
Federico Maggi, University of Sydney, Australia

****Correspondence:***
Elizabeth K. Williams
weliz@sas.upenn.edu

Specialty section:
This article was submitted to Soil Processes, a section of the journal Frontiers in Earth Science

Received: *22 June 2018*
Accepted: *10 September 2018*
Published: *26 September 2018*

Citation:
Williams EK and Plante AF (2018) A Bioenergetic Framework for Assessing Soil Organic Matter Persistence. Front. Earth Sci. 6:143. doi: 10.3389/feart.2018.00143

INTRODUCTION

Soil organic matter (SOM) contains more actively cycling carbon than the atmosphere and global terrestrial biomass combined (Jobbágy and Jackson, 2000; Stockmann et al., 2013), and for this reason, even small changes in the size of this carbon pool can have large impacts on the release and storage of atmospheric CO_2 and other greenhouse gases (CH_4, etc.; Davidson and Janssens, 2006; Bond-Lamberty and Thomson, 2010). Microbial community and ecosystem dynamics regulate the exchange of both nutrients and carbon between the soil and the atmosphere through the mineralization of SOM (Falkowski et al., 2008). These microbial community dynamics are driven by net energy flows, in which soil heterotrophs oxidize organic matter, acquiring energy that was fixed during photosynthesis, and channeling this energy into storage in the form of tissues (i.e., microbial biomass) or other organic materials, or expending this energy in metabolic processes (i.e., respiration; Odum et al., 1962; Currie, 2003). Despite its importance, the mechanisms controlling SOM stability and persistence are still debated (Schmidt et al., 2011). However, the growing

consensus is that environmental and biological controls (i.e., microbial community composition, organo-mineral associations, temperature, and moisture) exert a stronger control over SOM stability than molecular structure alone (Schmidt et al., 2011; Lehmann and Kleber, 2015).

Microbial substrate preference has been shown to depend on the energy status of the potential substrates in terms of energy required to metabolize the substrate and energy returned from metabolism of the substrate. In a study of thermophilic microbes, Amenabar et al. (2017) showed that the microbial energy demand (or required energy input from the microbial community) dictated the substrate choice rather than the potential energy supply of the substrates, with microbes preferring easier to decompose substrates over more energy rich substrates. Studying pyrogenic carbon, Harvey et al. (2016) demonstrated that the microbial community exhibited a greater preference for organic matter that returned the most energy for the smallest energy investment, which they expressed as the return-on-energy-investment (ROI) ratio. The energy status of SOM should therefore also be an important factor in its persistence. Barré et al. (2016) demonstrated that for a variety of climates and soil types, persistent SOM showed specific thermally determined energetic signatures, namely, that persistent SOM became less energy dense (yielding less energy during ramped combustion) with increasing duration of minimal C inputs via bare fallow treatment, suggesting that soil microorganisms preferentially mineralize high-energy SOM. In a similar study employing thermal decomposition of SOM, Williams et al. (2018) demonstrated distinct bioenergetic signatures between particulate (faster cycling) SOM vs mineral-associated (slower cycling) SOM. The particulate SOM fractions were characterized by larger energy densities and activation energies, whereas the mineral-associated SOM fractions were characterized by smaller energy densities and activation energies.

Here we propose a framework for assessing the persistence of SOM using thermally determined activation energy and energy density (ED). ED is a measure of the total net bond energy released during ramped combustion and can be used as a proxy for the molecular composition of SOM, such that more condensed or polymerized compounds would have higher ED. ED also represents the amount of available or potential chemical energy the microbial community might thus gain through the complete decomposition of the SOM for growth and respiration. Activation energy (E_a) is a measure of the input energy required to combust SOM and can be used as a proxy for the molecular composition of SOM and as a proxy for the energetic barrier to decomposition, and thus SOM persistence. We will test this framework using several soils that have undergone alteration in field or laboratory experiments designed to isolate persistent SOM: bare fallow and chemical fallow field trials, land-use/land-cover changes, long-term laboratory incubations, and acid hydrolysis. Many fractionation methods intended to isolate persistent SOM are still hampered by methodological problems (Bruun et al., 2008). In several persistent-SOM isolation method comparison studies (Jenkinson, 1971; Balesdent, 1996; Balabane and Plante, 2004; Plante et al., 2005; Krull et al., 2006; Paul et al., 2006; Bruun et al., 2008), the authors found variable or no relationships between the isolated soil fractions and environmental persistence. Likewise, uncertainty in estimates of the size of labile and persistent SOM pools are a major source of error in modeling soil organic C turnover (Falloon and Smith, 2000) and response to climatic and environmental changes.

Because the energy status of SOM is a fundamental factor in its environmental persistence, we expect that comparison of changes in these two energetic parameters (ED and E_a) as discussed in the following bioenergetics framework will allow us to determine if a chemical or physical change during SOM decomposition has resulted in a change in its environmental persistence or biodegradability. We hypothesize that the ED will be lower in persistent SOM compared to the bulk soil as energy dense particulate organic matter (mostly comprised of plant residues) decompose into smaller particles and biomolecules. For E_a, we propose two competing hypotheses that offer the opportunity to test opposing theories of persistent SOM formation. If persistent SOM formation follows the humification theory, E_a is hypothesized to increase as persistent SOM would have been formed by the polymeric condensation of decomposition products into large and stable biopolymers (i.e., humus). If persistent SOM follows the progressive decomposition or selective preservation theories, E_a is hypothesized to decrease as the persistent SOM is comprised of smaller biomolecules.

MATERIALS AND METHODS

The Bioenergetic Framework

The stability and persistence of SOM is dependent upon the balance of the energetic barriers to decomposition (i.e., physical and chemical protection, availability of electron acceptors, or enzyme production) and the energy available or released to the microbial community upon decomposition for metabolic functions. Comparison of these energies (available energy and energy barrier) leads to four possible scenarios (**Figure 1**) varying in E_a and ED that have previously been postulated by Rovira et al. (2008) for litter decomposition and are now discussed in relation to SOM. Scenario 1, symbolized by the top-left quadrant (A), represents a substrate with a high energy availability for a low energetic investment. Microbial populations could easily grow on quadrant A substrates and thus SOM turnover would be fastest. Scenario 2, symbolized by the bottom-right quadrant (D), represents the opposite relationship in which the substrate has low energy availability but requires a high energy investment. Microbial populations growing on such a substrate will have low metabolic and growth rates and thus SOM would exhibit the slowest turnover and be considered persistent. Scenarios 3 and 4, represented by quadrants B and C, fall between the extremes of scenarios 1 and 2 (quadrants A and D) and in some cases may be equal in quality and biodegradability in terms of energy input and return. However, because of the greater available energy of quadrant B substrates, it is postulated that substrates in quadrant C are generally less biodegradable and more persistent than substrates in quadrant B.

In soils, the interpretation of E_a is complicated by the mineral matrix, which can bind with SOM, forming additional

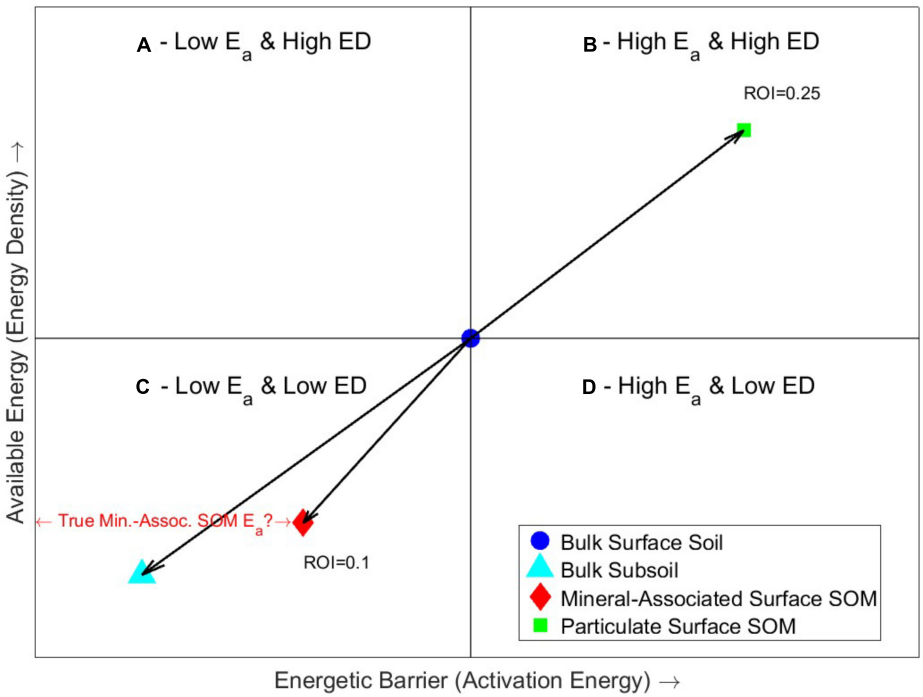

FIGURE 1 | The four possible scenarios of the bioenergetics framework, depicted in quadrants **A–D** (varying in E_a and ED) for SOM decomposition and the formation of persistent SOM. Quadrant **A** represents a substrate with high energy availability for a low energetic input on which microbial populations could easily grow; SOM turnover is hypothesized to be greatest in this quadrant. Quadrant **D** represents low energy availability for a high energy input and microbial populations growing on such a substrate will have low metabolic and growth rates; SOM turnover is hypothesized to be slowest in this quadrant. Quadrants **B** and **C** represent substrates with either a high/high or low/low energy input/return. We hypothesize that persistent SOM will be characterized by decreasing ED and either decreasing or increasing E_a. Also shown are the results of (Williams et al., 2018) of average changes in bulk soil (n = 16) with depth and fractionation into particulate (faster cycling) and mineral-associated (slower cycling) carbon pools. The centroid represents the starting energy status of the SOM and arrows represent observed trajectories of relatively stable and labile SOM with depth and density fractionation. It is hypothesized that the E_a of the mineral-associated SOM fraction is higher than the organic matter alone because of the presence of and interaction with the soil matrix.

barriers to decomposition reflected in both the thermal and natural decomposition of SOM (Leifeld and von Lützow, 2014). Counterintuitively, Williams et al. (2018) found that organic matter chemically protected by strong mineral bonds required less E_a than particulate organic matter (**Figure 1**). A similar difference was observed in respiration experiments of mineral and organic soils, in which E_a was lower in mineral soils (Leifeld and von Lützow, 2014). Williams et al. (2018) suggested that while the E_a of the bound-SOM was lower, it is still reflective of the additional barriers to decomposition provided by the mineral matrix, (as evidenced in experimental mixtures of kerogen and common soil minerals; Dembicki, 1994) as well as compositional differences between the particulate and mineral-associated SOM. Williams et al. (2018) also observed that with depth (and increased residence time) in the soil column, there was also a decrease in ED and E_a. Based on these energetic differences observed between mineral-associated and particulate organic matter, we hypothesize that there is a difference in environmental stability and persistence between quadrants B and C, such that organic matter trending toward quadrant C has a greater potential for environmental persistence likely because of increasing mineral association and the preferential loss of energy dense particulate organic matter.

Experimental Soil Sample Sets

Samples for this study were collected from archived soil samples from several previously published field-based and laboratory-based experiments designed to isolate or characterize persistent SOM through the loss or removal of labile SOM (**Table 1**). Additional details about these soils, experimental conditions, and additional analyses can be found in the following referenced works.

Field Experiments

We used soils from four long-term bare fallow (LTBF) field experiments from northwestern Europe, one chemical fallow field experiment from New Zealand, and five land-use conversion experiments located across a mean annual temperature gradient (**Table 1**). The LTBF soils used were from bare fallows located at Château de Versailles in Versailles, France, Rothamsted Research in Harpenden, United Kingdom, the Swedish University of Agricultural Sciences at Ultuna in Uppsala, Sweden, and at the Askov Experimental Station, Denmark (Barré et al., 2016). Surface soils (up to 25 cm depth) were collected from two field replicate plots at each location and from triplicate plots in Askov (see **Table 1** for soil depths). Bare fallow treatments span 27 years at Askov to 79 years at Versailles (**Table 1**),

TABLE 1 | Location, treatment, depth, soil carbon contents (pre and post), and percent carbon change for the field and laboratory based experiments.

Experiment		Location	Treatment	Soil depth (cm)	Initial soil C content (mg/g)	Final soil C content (mg/g)	ΔC (%)
Field-based	Fallow[1,2]	Versailles, FR	79 years	0–25	17.5	6.2	−64.6
		Rothamsted, United Kingdom	49 years	0–23	30.3	9.7	−67.9
		Ultuna, SW	53 years	0–20	15.0	9.2	−38.7
		Askov, DK	27 years	0–20	16.5	11.9	−27.9
		Canterbury, NZ	13 years	0–7.5	31.1	20.8	−33.1
			13 years	7.5–15	23.8	19.4	−18.5
			13 years	15–25	18.0	14.8	−17.8
	Land-use change[3]	Waggoner's Ranch, TX	Grassland to cropland	0–20	11.2	10.2	−8.9
		Mandan, ND	Grassland to cropland	0–20	32.4	28.0	−13.6
		Akron, CO	Grassland to cropland	0–20	11.6	6.9	−40.5
		Nova Vida Ranch, BR	Forest to pasture	0–20	10.6	14.1	+ 33.0
		Alajuela, CR	Forest to pasture	0–20	200.2	141.6	−29.3
Laboratory	Incubation[3]	TX, ND, CO	Grassland	0–20	18.4	14.7	−20.1
	(588 days, 35°C)	BR, CR	Forest	0–20	105.4	94.7	−10.2
		TX, ND, CO	Cropland	0–20	15.0	12.6	−16.0
		BR, CR	Pasture	0–20	77.9	72.3	−7.2
	Acid hydrolysis[4]	Breton, AB	Forest	0–5	67.2	48.5	−27.8
	(6 M HCl, 16 h,	Breton, AB	Conventional till	0–5	12.9	9.2	−28.7
	95°C)	Breton, AB	Conventional till	0–5	17.9	12.7	−29.1
		Scott, SK	Conventional till	0–5	40.8	41.1	+ 0.7
		Scott, SK	Grassland	0–5	59.6	26.3	−55.9

Superscript numbers refer to the following referenced works, in which these data have been previously reported and other site or experimental information including detailed soil descriptions can be obtained: [1]Barré et al. (2016), [2]Gregorich et al. (2015), [3]Haddix et al. (2011), and [4]Plante et al. (2006).

and samples were collected in the following years: (Versailles) 1929, 1934, 1939, 1950, 1960, 1968, 1980, 1991, 2002, 2008; (Rothamsted) 1959, 1963, 1971, 1987, 2000, 2008; (Ultuna) 1956, 1967, 1974, 1985, 1995, 2009; (Askov) 1956, 1962, 1968, 1976, 1983. During the duration of the bare fallows, soil organic C concentrations exhibited a relative decrease of 29–65% (Barré et al., 2016).

Chemical bare fallow soils were collected from three field replicate plots from Lincoln, New Zealand. Soils were sampled at three depths (0–7.5, 7.5–15, and 15–25 cm). These soils span 13 years (beginning in 2000) of chemical fallow conditions (Gregorich et al., 2015), resulting in a relative decrease of 33% in soil organic C concentrations in the surface soil and 18% in the two subsoils.

Soils from land-use conversion experiments were collected from five sites along a mean annual temperature gradient (2–25.6°C; Haddix et al., 2011). The temperate sites had paired native grassland and cultivated land uses (Mandan, ND, United States; Akron, CO, United States; and Waggoner Ranch, TX, United States) and the tropical sites had paired native forest and pasture land uses (Alajuela, Costa Rica, and Nova Vida Ranch, Brazil). Transitions from native grassland or forest to cultivated cropland or pasture occurred between 1957 and 1984. Surface soil samples (0–20 cm) were collected from each land-use, resulting in 10 land-use conversion samples (five native + five altered). The land-use conversion resulted in relative decreases in soil organic C concentration (9–40%) due to decades of intensive agriculture. Only the Brazil site experienced a 33% increase in soil C, where an increase in the proportions of carbohydrates and peptides was noted that was not observed in the other locations (Haddix et al., 2011).

Laboratory Experiments

The 10 previously described land-use conversion soils, comprised of three grassland, three cropland, two forests, and two pasture soils, were subjected to a long-term laboratory incubation experiment. Samples were incubated for 588 days at 35°C and optimal, constant moisture conditions to maximize the microbial mineralization of labile SOM. Based on the total respired carbon (Haddix et al., 2011), the long-term incubations resulted in a relative decrease of 7-20% in soil organic C concentrations.

Five surface soil samples (0–5 cm) were collected from two long-term agricultural field experiments in Alberta, Canada and Saskatchewan, Canada (Plante et al., 2006). The two sites had paired either grassland or forest and cultivated (conventional till) land uses. Soils were hydrolyzed with 25 mL of 6 M HCl at 95°C for 16 h, resulting in relative decreases in soil organic C concentration decreases of 28–56%, although one site experienced a 0.7% increase in soil C.

Activation Energy and Energy Density Determinations

Thermal analyses were performed by ramped combustion using a Netzsch STA 449PC Jupiter simultaneous thermal

analyzer equipped with an automatic sample carrier (ASC) and a type-S platinum/ rhodium (Pt/PtRh) sample carrier (Netzsch–Gerätebau GmbH, Selb, Germany). Thermal analysis has been demonstrated to be highly reproducible on a variety of soil types (Plante et al., 2009), and thus thermal analyses analytical replicate aliquots were not performed. Samples were weighed to contain approximately 1 mg C and were heated from ambient temperature (25°C) to 105°C at 10°C min^{-1} under an oxidizing atmosphere of 40 mL min^{-1} of CO_2-free synthetic air (20% O_2 and N_2 balance). Samples were held at 105°C for 15 min to allow for drying/moisture equilibration, then heated at 10°C min^{-1} to 800°C. Evolved CO_2 was analyzed using a coupled LICOR LI-820 infrared gas analyzer. Differential scanning calorimetry (DSC) heat flux (the exothermic or endothermic energy flux from the sample, referenced to an empty Pt/Rh crucible), thermogravimetric (TG) mass loss, and evolved CO_2 gas (CO_2-EGA) signals were recorded every second. DSC and CO_2 baselines were corrected *a posteriori* using the base R package and the smooth.spline() function using a spline and linear baseline, respectively (refer to Plante et al., 2011for additional information on baseline corrections). DSC integration was also performed using the base R package and the sintergral() function.

Total exothermic energy content (in mJ) was determined by integrating the DSC heat flux (in mW) over the exothermic region 190–600°C, which represents the temperature range in which SOM is oxidized (Rovira et al., 2008). TG mass loss was determined for the same range. This mass loss is attributable largely to SOM combustion, with minor contributions from dehydration of minerals such as kaolinite. ED (in J mg^{-1} OM) was thus determined by dividing energy content by TG mass loss (Rovira et al., 2008; Plante et al., 2011).

Activation energy (E_a, in kJ mol^{-1} CO_2) was determined following the methods of Burnham and Braun (1999) and Williams et al. (2014), assuming first-order reaction kinetics during ramped combustion. The fraction of sample C remaining (x) for each time step was calculated from the evolved CO_2 data. Each data point over the decomposition temperature range (105–800°C) is then assumed to represent an instantaneous measurement of the rate constant of combustion (k) at each temperature, and E_a is determined from a modified Arrhenius plot of $\ln|\ln(x)|$ vs 1/T, in which the slope of the regression is equal to $-E_a/R$ where $\ln|\ln(x)|$ is the natural log of the absolute value of the natural log of x and R is the universal gas constant. Thermally derived values of E_a are expected to be greater than what occurs naturally in soils or during laboratory soil incubations (Leifeld and von Lützow, 2014) because of the complete decomposition of each soil instead of a relatively biochemically labile portion and because of the lack of microbial and fungal enzymes to catalyze the decomposition reactions.

Additionally, the ROI ratio (Harvey et al., 2016) which has been demonstrated to be directly related to the biodegradability of specific types of organic matter and thus environmental persistence was calculated for each soil by dividing ED by E_a.

Statistical Analyses

Differences in ED, E_a, and ROI between pre- and post-treatment soils were analyzed using an independent one-way ANOVA. Statistical analyses were performed for each of the following paired pre- and post-treatment groupings: all soils (n = 38), soils separated by field (n = 23) or lab (n = 15) setting, and soils grouped by individual experiments [bare fallow; n = 2 (×4 experiments), chemical fallow; n = 3 (×3 soil depths), land-use; n = 5, incubation; n = 10, and hydrolysis; n = 5]. All analyses were performed using MATLAB and differences in E_a, ED, and ROI were considered statistically significant when $p \leq 0.05$.

RESULTS

The E_a and ED varied widely among the initial soils. E_a ranged from 57 to 69 kJ/mol CO_2 and ED ranged from 7 to 15 J/mg OM, reflecting the range of soil types, climates, land uses, vegetation types, and organic matter inputs. The ROI ratios varied between the initial and final soils, spanning 0.15–0.24 in the untreated soils to 0.07–0.33 in the final soils, implying changes in SOM biodegradability over the course of the experiments (**Table 2**). The changes in ROI were not strongly correlated to changes in carbon (R^2 = 0.20, p = 0.04; least squares linear regression). When analyzed collectively, only the E_a was statistically different (decreased) between pre- and post-treatment soils (ED p = 0.20; E_a p = 0.005; ROI p = 0.48).

Field-Based Experiments

In the field-based studies (i.e., bare/chemical fallow and land-use change), post-treatment soils displayed a decrease in E_a and ED (**Figure 2**) relative to the initial soils during the course of the experiments (ED $p < 0.001$; E_a p = 0.003), trending toward quadrant C. In the LTBF experiments, the evolution of and variation in ED and E_a with labile SOM loss over time is visible (**Figures 2A–D**). For the 79 year fallow at Versailles, only the decrease in ED over the course of the experiment was statistically significant (ED p = 0.001; E_a p = 0.08). For the other bare fallows, only the decrease in E_a was statistically significant: Askov (ED p = 0.16; E_a p = 0.03), Rothamsted (ED p = 0.28; E_a $p < 0.000$), Ultuna (ED p = 0.23; E_a p = 0.003).

In the one field study considering soil depth (**Figure 2E**), there was a statistically significant decrease in the E_a with depth and no change in ED (initial ED p = 0.14; initial E_a p = 0.03; final ED p = 0.12; final E_a p = 0.03). At all depths, the 13 year chemical fallow soils demonstrated statistically significant decreases in E_a (0–7.5 cm p = 0.03; 7.5–15 cm p = 0.001; 15–25 cm p = 0.001) over time. However, only the two subsoil samples exhibited significant decreases in ED over the course of the fallow treatment (0–7.5 cm p = 0.25; 7.5–15 cm p = 0.004; 15–25 cm p = 0.04). Neither the changes in ED nor E_a were statistically significant with the changes in land-use (**Figure 2F**) from forest/grassland to pasture/cropland (ED p = 0.44; E_a p = 0.22).

Although ROIs for the field samples (collectively) decreased after treatment (p = 0.04), the decrease in E_a and ED of the field soils was not always reflected by a decrease in ROI. Only the Rothamsted (p = 0.01), Versailles (p = 0.04), and Ultuna

TABLE 2 | The changes in the ROI ratio with labile SOM loss or removal from the field and laboratory based experiments.

Experiment		Treatment	Soil depth (cm)	Initial ROI	Final ROI	ΔROI (%)
Field-based	Fallow	79 years	0–25	0.16	0.07	−56.3
		49 years	0–23	0.17	0.11	−35.3
		53 years	0–20	0.19	0.17	−10.5
		27 years	0–20	0.16	0.13	−18.8
		13 years	0–7.5	0.23	0.23	0.0
		13 years	7.5–15	0.22	0.22	0.0
		13 years	15–25	0.24	0.22	−8.3
	Land-use change	Grassland to cropland	0–20	0.17	0.13	−23.5
		Grassland to cropland	0–20	0.21	0.19	−9.5
		Grassland to cropland	0–20	0.19	0.12	−36.8
		Forest to pasture	0–20	0.15	0.16	+6.7
		Forest to pasture	0–20	0.22	0.22	0.0
Laboratory	Incubation	Grassland	0–20	0.20	0.19	−5.0
		Forest	0–20	0.20	0.25	+25.0
		Cropland	0–20	0.16	0.18	+12.5
		Pasture	0–20	0.20	0.22	+10.0
	Acid hydrolysis	Forest	0–5	0.24	0.25	+4.2
		Conventional till	0–5	0.23	0.33	+43.5
		Conventional till	0–5	0.25	0.26	+4.0
		Conventional till	0–5	0.22	0.23	+4.5
		Grassland	0–5	0.20	0.23	+15.0

(p = 0.01) bare fallows displayed decreased ROI (and decreased hypothesized biodegradability), while the remaining bare fallow (Askov, p = 0.26), chemical fallow soils (0–7.5 cm p = 0.67; 7.5–15 cm p = 0.17; 15–25 cm p = 0.28), and the land-use soils (p = 0.20) displayed no change in ROI possibly due to proportional changes in ED and E_a.

Laboratory-Based Experiments

In the laboratory-based experiments (i.e., incubation and acid hydrolysis), post-treatment soils displayed no statistically significant changes in E_a and ED (**Figures 2G,H**) relative to the initial soils (ED p = 0.14; E_a p = 0.58), when analyzed collectively. The long-term laboratory incubation (35°C, 588 days) resulted in highly variable alterations in ED and E_a (**Figure 3A**), seemingly dependent upon land-use (ED p = 0.53; E_a p = 0.52). Grassland soils displayed decreased ED and E_a (toward quadrant C) following incubation similar to the signature of mineral associated SOM (Williams et al., 2018) and the fallow soils, whereas forest and pasture soils displayed a decrease in E_a and increase in ED (toward quadrant A) similar to the decomposition of forest litter (Rovira et al., 2008), and croplands displayed increased ED and E_a (toward quadrant B) similar to the response of the hydrolyzed soils (**Figure 2H**) and the energetic signature of the particulate organic matter (Williams et al., 2018) in **Figure 1**. However, none of the changes in ED and E_a due to long-term incubation were statistically significant when separated by land-use (grassland ED p = 0.22; grassland E_a p = 0.49; forest ED p = 0.84; forest E_a p = 0.42; cropland ED p = 0.63; cropland E_a p = 0.55; pasture ED p = 0.87; pasture E_a p = 0.68). Labile SOM removal by acid hydrolysis (**Figure 3B**) resulted in statistically significant increases in E_a and ED relative to the untreated soil, trending toward quadrant B (ED p = 0.02; E_a p = 0.01). The net changes in E_a and ED for all experiments are shown in **Figure 3**.

Return-on-energy-investments for the laboratory-based samples (collectively) did not change after treatment (p = 0.14). The ROI also did not change when the lab soils were separated by experiment (incubation; p = 0.29, hydrolysis; p = 0.12), possibly due to proportional changes in ED and E_a. Similar to the lack of pre- and post-treatment differences in ED and E_a with land-use, ROI also did not change (grassland p = 0.64; forest p = 0.21; cropland p = 0.53; pasture p = 0.36) with incubation.

DISCUSSION

The emerging view of SOM persistence asserts that SOM exists as a continuum of organic material, continuously processed by the decomposer community from large biopolymers to small monomers and with increasing oxidation and solubility, protected from decomposition through mineral aggregation and adsorption (Lehmann and Kleber, 2015) and that the persistence of SOM is thus a property of the ecosystem as a whole (Schmidt et al., 2011). Because these ecosystem dynamics are driven by net energy flows, analysis of SOM bioenergetics can provide complementary constraints to SOM models as well as insight into the fundamental conundrum of why thermodynamically unstable organic matter persists in soil.

Long-term bare fallow experiments present the best case for studying the bioenergetic status of persistent SOM (Ruhlmann, 1999). Soils are kept free of vegetation and additional organic inputs for extended periods of time (up to 79 years in the

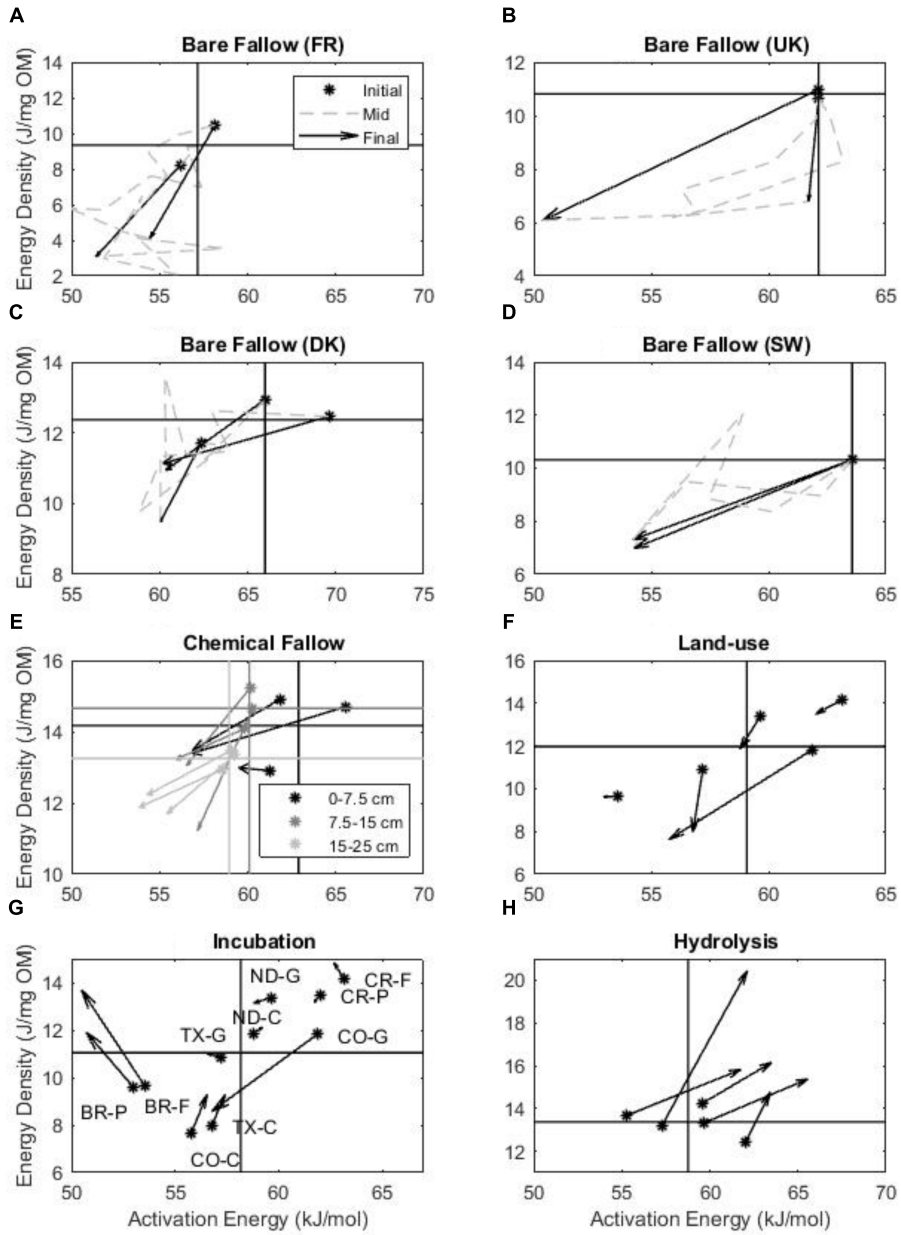

FIGURE 2 | The changes in E_a and ED with labile SOM loss or removal from the field and laboratory-based experiments presented in the bioenergetics framework. Changes are indicated by the circles (initial soils) and arrowheads (final soils). For each experiment, the axes cross at the average initial soil E_a and ED to demonstrate the trajectory into one of the four bioenergetics scenarios relative to the initial soil. **(A–D)** The change in ED and E_a over the course of the long-term bare fallow experiments (**A** Versailles, FR; **B** Rothamsted, United Kingdom; **C** Askov, DK; **D** Ultuna, SW). **(E)** The change in ED and E_a after 13 years of chemical fallow for surface soils and soils at depth. **(F)** The changes in ED and E_a after land-use change from grassland or forest to cultivated cropland or pasture. **(G)** The change in ED and E_a after laboratory incubation for 588 days at 35°C. Letters indicate the origin and land-use of each soil (G – grassland, P – pasture, C – cropland, F – forest) listed in **Table 1**. **(H)** Changes in the ED and E_a of SOM after acid hydrolysis. Please note the different axes scales.

experiments studied here), allowing initially present organic matter to decompose under field conditions and soils to become more enriched in persistent or stable SOM as the more labile SOM decomposes naturally (Barré et al., 2016). Although consisting of different durations and climatic conditions, all fallow experiments (**Figures 2A–E**) follow the first and third hypotheses of persistent SOM, trending into quadrant C of the bioenergetics framework characterized by decreased ED and decreased E_a. This trajectory is comparable to the observed changes in ED and E_a for bulk soils with depth and fractionation into particulate and mineral-associated SOM (**Figure 1**). These reductions in ED over time were previously observed (Barré et al., 2016). This trend in the 79 year bare fallow is supported by the observed reduction in energy dense

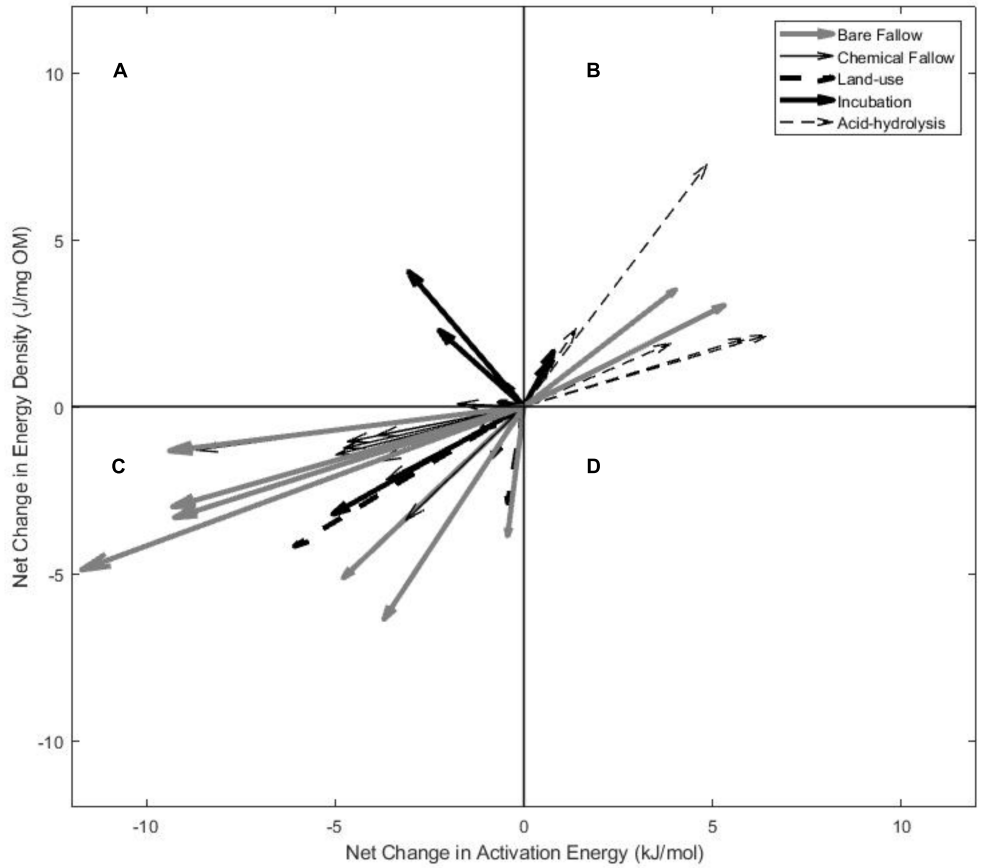

FIGURE 3 | Comparison of the net changes in E_a and ED with the removal or loss of labile SOM from the field and laboratory-based experiments. Changes (arrowheads) shown are relative to the initial pre-treatment soils, represented by the origin point (0,0). **A–D** represent the four scenarios (quadrants) of the bioenergetics framework, as described in **Figure 1**.

particulate organic matter (Balabane and Plante, 2004) over the course of the experiment, suggesting that organo-mineral complexes (similar to the mineral-associated SOM in Williams et al., 2018) dominate in the latter stages of the fallow and comprise the more persistent SOM. Mineral-associated soil fractions with the longest turnover are assumed to have larger proportions of easily metabolizable organic molecules with low thermodynamic stability (lowest abundance of aromatic groups, highest O-alkyl C/aromatic C ratio, highest proportion of thermally labile materials, and highest ratio of substituted fatty acids to lignin phenols), whereas the younger soil fractions are assumed to have higher proportions of stable organic matter considered more difficult to metabolize, as evidenced by Kleber et al. (2011). This decreased thermodynamic stability is evidenced in the decreased ED or E_a over time, simultaneously the decreased biodegradability is evidenced in the decreasing ROI ratios (**Table 2**).

Organic matter in subsoils is characterized by longer turnover times compared to surface material (Rumpel and Kögel-Knabner, 2011) and also presents a useful opportunity to investigate SOM biogenetic changes at depth as microbial activity may be reduced by suboptimal environmental conditions, nutrient or energy scarcity, and organic matter may be less accessible because of its association with mineral surfaces (Schmidt et al., 2011). At depth in the chemical fallow experiments (**Figure 2B**), soils also follow the third hypothesized trajectory of persistent SOM (**Figure 1**), with deeper soils trending into quadrant C with decreased E_a (as indicated in migrating origin points of the initial soils with depth). However, the ROI ratios (**Table 2**) do not suggest changes in SOM biodegradability with depth because of the lack of significant change in ED.

Changes in land-use are often disruptive to soil structure, alter natural C inputs, and often result in degradation of biogeochemically labile SOM (Guo and Gifford, 2002). However, when statistically analyzed collectively, changes in land-use in the soils were insufficient in addressing changes in the energy status of SOM, likely due to the continued input of labile organic matter inputs as well as the lack of field/site replicates, and thus there was no true isolation of persistent SOM with the land-use conversions.

Incubations offer a second-best option for studying the bioenergetic status of persistent SOM, as SOM is allowed to decompose in optimal conditions and positive correlations between ED and microbial respiration have been observed in

several studies (Plante et al., 2011; Peltre et al., 2013; Stone and Plante, 2015). Although conducted at an elevated temperature, compared to the native MATs, and for almost 2 years to speed the microbial degradation of labile SOM, these incubation experiments were also insufficient to observe differences in SOM E_a and ED. The variable responses in E_a and ED are likely a result of the different land-uses, soil types, climates, and vegetation and the interpretations are limited again by the lack of field/site replicates. Incubations are also limited by the fact that truly persistent SOM is not accessed by the microbes, but rather isolate a large intermediate pool of SOM (Haddix et al., 2011).

In direct contrast to the fallow experiments, the acid-hydrolyzed soils trend toward quadrant B (**Figure 3B**) following none of the hypothesized trajectories of persistent SOM but rather following the observed trajectories of labile SOM as presented in **Figure 1**. The use of acid hydrolysis (and other wet chemical oxidation methods such as with hydrogen peroxide) rests on the premise that organic molecules resistant to chemical hydrolysis are also resistant to soil enzymatic attack and are therefore also more biologically stable and persistent in the environment (Krull et al., 2006; Greenfield et al., 2013). While radiocarbon analysis of acid hydrolysis residues has been demonstrated to be older than the bulk soils (Trumbore et al., 1989; Paul et al., 2006), acid hydrolysis is known to preferentially hydrolyze nucleic acids, proteins, and carbohydrates with *O*-alkyl functional, while leaving alkyl and aromatic compounds (Kiem et al., 2000; Bruun et al., 2008) and has been shown to not equate with resistance (Greenfield et al., 2013). Additionally, in the study of young (40-days-old) and old (40-years-old) carbon mixtures, Bruun et al. (2008) found that acid hydrolysis consistently removed more old carbon, suggesting that the remaining material contained a large portion of faster cycling carbon. Similar to the results of Williams et al. (2018) in which unsaturated/aromatic soil (low H:C) carbon pools, trended toward scenario B, these results are also suggestive of the loss of non-aromatic organic material during acid hydrolysis or artifacts from the conversion of carbohydrates into molecules compositionally indistinguishable from non-hydrolyzable SOM (Greenfield et al., 2013).

The fact that none of the experimental soils trended into quadrant D (**Figures 2**, **3**), or the most energetically unfavorable pool of organic substrates characterized by low ED and high E_a (Hypotheses 1 and 2), supports emerging concepts and models of SOM formation and stabilization away from classic humification theories. Decreased ED is expected with SOM decomposition as larger plant biopolymers are processed into smaller molecules; however, increased E_a is postulated to be the result of mineral association, condensation or polymerization reactions, or the loss of less molecularly complex OM. Mineral association is not expected to significantly affect the E_a of SOM in organic soils, but is expected to increase the E_a of SOM in mineral soils due to additional organic matter-mineral adsorption and complexation bonds which must be broken for SOM decomposition, mineralization or combustion (as conceptualized in **Figure 1**). However, it is expected that this increased E_a may be relatively small as evidenced in a study of the effects of various mineral matrices (quartz, calcite, dolomite, kaolinite, and bentonite) on kerogen decomposition kinetics in which measured E_a was increased compared to kerogen alone, but only at low organic carbon concentrations (Dembicki, 1994) and by the observation that mineral-associated SOM displays lower E_a than particulate SOM (Williams et al., 2018). However, the presence of carbonates would increase the measured E_a as carbonates decompose into CO_2 at relatively high temperatures (∼600–800°C) and would be indiscriminately incorporated into the E_a calculation. Condensation reactions, such as those occurring during the classic soil humification models, suggest the synthesis of large and stable biopolymers and molecules (humus) from decomposition products. However, the lack of evidence for the physical existence of humic substances *in situ* independent of the alkaline extraction procedure (Schmidt et al., 2011; Lehmann and Kleber, 2015) has led to the acceptance of other models of SOM formation that can be observed in the soil. Additionally, condensation or polymerization reactions occurring during SOM processing would result in an increase in ED as well as an increase in E_a and would likely not appear in quadrant D, but instead in quadrant B. Similarly, the loss of less molecularly complex OM would increase E_a but would also increase ED, as what is postulated to have happened during the acid hydrolysis experiments. Hypothesized substrates in quadrant D were expected to have the slowest turnover and thus be the most environmentally persistent. However, it does not seem plausible within the accepted theories of SOM formation and stabilization for SOM to exist in this hypothetical state, rather the most persistent SOM likely exists in the lower ED extremes of quadrant C (**Figure 4**) as suggested by the fallow and density fractionation experiments.

Soil organic matter substrates characterized by high ED and low E_a (quadrant A) are expected to turnover relatively rapidly within the bioenergetics framework and thus would not become a dominant feature of the soils where persistent SOM dominates over labile SOM such as the post-treatment samples in this study. Only the coupled native forest/pasture incubation soils trended into quadrant A (**Figures 2**, **3**). A trajectory into quadrant A, however, was observed by Rovira et al. (2008) during litter decomposition (**Figure 4**). Litter decay products were characterized by increased ED and decreased DSC-T50 (the temperature at which half of the total exothermic energy has been released) relative to fresh litter. For all of the soils included in this study as well as the soils, soil density fractions, and litter of Williams et al. (2018), DSC-T50 is positively correlated with E_a ($n = 254$; $R^2 = 0.6$, $p < 0.0001$). Thus, E_a is expected to decrease with decreasing DSC-T50 ($E_a = 0.25 \times \text{DSC-T50} - 27.55$) and this relationship also reinforces the usage of DSC-T50 as a measure of SOM decomposability as utilized by Rovira et al. (2008), Plante et al. (2011), Peltre et al. (2013), and Leifeld and von Lützow (2014). The native forest/pasture soils were characterized by the highest carbon contents (**Table 1**) and it is possible that greater litter inputs into these soils compared to the grassland/cultivated soils caused them to respond to the incubation in the same way as litter, with increasing ED.

In an expanded conceptual bioenergetics framework (**Figure 4**), we combine the results of this study, the litter decomposition study of Rovira et al. (2008), and the soil

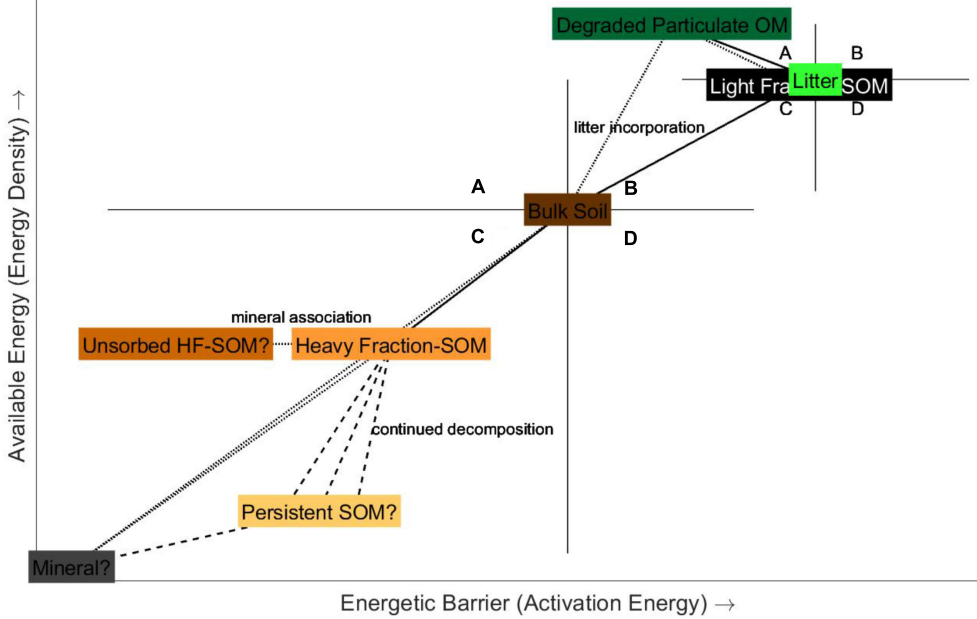

FIGURE 4 | Expanded conceptual bioenergetics framework for SOM persistence, based on the observed SOM ED and E_a with depth and fractionation into particulate (LF) and mineral-associated (HF) carbon pools and of litter relative to the bulk surface soil (Williams et al., 2018) and on the observed ED and E_a (modified from DSC-T50) of litter decomposition (Rovira et al., 2008), relative to litter. **A–D** represent the four scenarios (quadrants) of the bioenergetics framework, as described in **Figure 1**. Changes are linked by solid lines. Dashed lines represent hypothesized trajectories in ED-E_a space based on the results of this study. Dotted lines represent composition (i.e., the HF-SOM or mineral-associated SOM is comprised of the mineral matrix and the SOM adsorbed to or otherwise interacting with those mineral surfaces). The mineral matrix exists at a hypothetical zero ED and zero E_a.

density fractionation study of Williams et al. (2018) and summarize proposed bioenergetic changes during SOM formation, decomposition, and stabilization. Litter decomposes into relatively more energy-dense and biodegradable decay products (Rovira et al., 2008), plotting in quadrant A relative to the fresh litter. We expect that pyrogenic organic matter derived from litter would have a higher degree of molecular condensation and thus higher E_a (Harvey et al., 2012). The ED of pyrogenic organic matter would depend on the fire/charring intensity, as Harvey et al. (2016) demonstrated that chars produced at higher temperatures were characterized by lower net energies. However, some litter included in the study by Williams et al. (2018) contained visible pyrogenic organic matter and were from an energetics viewpoint indistinguishable from non-pyrogenic containing litter, thus pyrogenic organic matter is not explicitly depicted in **Figure 4**. When bulk soil is separated into particulate organic matter (represented by the LF from density fractionation) and mineral-associated organic matter (represented by the HF from density fractionation) pools, particulate SOM is more energy dense and requires greater energy input than bulk SOM or mineral-associated SOM. Particulate SOM is also likely composed to some extent of litter decay products or litter; hence, they are similar in ED and E_a in the framework. Mineral-associated SOM is comprised of the mineral matrix and the adsorbed or chemically complexed SOM, the former increasing the required energy input of the latter due to the additional bonds of SOM sorption onto mineral surfaces. As the bulk soil decomposes, there is a net loss of the more labile particulate SOM, bringing the energetic signature of the bulk soil closer to that of the mineral-associated SOM. The mineral matrix exists at the hypothesized point of zero ED and zero E_a, as it offers no SOM for microbial decomposition and thus would yield no CO_2. With continued decomposition, the energetic benefit to cost ratio continues to decrease, resulting in relatively thermodynamically unstable SOM being the most persistent.

CONCLUSION

By analyzing the energetics of a suite of soils from field and laboratory experiments designed to isolate persistent SOM within the proposed bioenergetics framework, this study has demonstrated that the signature of persistent SOM is that of decreasing available energy supply (ED) and of decreasing required energy input (E_a). This finding contradicts soil formation theories that propose that persistent SOM is formed by the polymeric condensation of decomposition products into large and stable biopolymers (humus), and instead supports theories that persistent SOM is comprised of smaller and smaller particulate SOM fragments and biomolecules, preserved due to interaction with soil minerals. SOM stabilization mechanisms, such as physical and chemical protection, can be viewed as energetic barriers to decomposition such that the stabilized SOM requires additional energies from the microbial community to

access. In this framework, we propose that this stabilized SOM is also less biodegradable than labile SOM because of its decreased energy contents. The conclusions of this framework should not be applied to carbonate soils as thermal decomposition of carbonate mineral may result in extraneous CO_2 incorporated into the calculation of E_a. The variable or increased ED and E_a exhibited by the laboratory experimental soils suggests that these methods do not always effectively isolate environmentally persistent SOM, but in some cases may target physically or chemically protected SOM.

AUTHOR CONTRIBUTIONS

EW conceived the conceptual framework, performed the thermal analyses, analyzed the data, and wrote the manuscript with input and contributions from AP.

FUNDING

Funding to support this project was provided by the University of Pennsylvania Vice Provost for Research – Postdoctoral Fellowship for Academic Diversity and the National Science Foundation (EAR 1541588).

ACKNOWLEDGMENTS

We thank Pierre Barré and Folk van Oort for supplying samples from the Long-Term Bare Fallow network, Mike Beare and Denis Curtin from Landcare New Zealand for supplying samples from the chemical fallow experiments, and Michelle Haddix and Rich Conant for supplying samples from the land-use conversion/MAT transect.

REFERENCES

Amenabar, M. J., Shock, E. L., Roden, E. E., Peters, J. W., and Boyd, E. S. (2017). Microbial substrate preference dictated by energy demand rather than supply. *Nat. Geosci.* 10, 577–581. doi: 10.1038/Ngeo2978

Balabane, M., and Plante, A. F. (2004). Aggregation and carbon storage in silty soil using physical fractionation techniques. *Eur. J. Soil Sci.* 55, 415–427. doi: 10.1111/j.1351-0754.2004.0608.x

Balesdent, J. (1996). The significance of organic separates to carbon dynamics and its modelling in some cultivated soils. *Eur. J. Soil Sci.* 47, 485–493. doi: 10.1111/j.1365-2389.1996.tb01848.x

Barré, P., Plante, A. F., Cecillon, L., Lutfalla, S., Baudin, F., Bernard, S., et al. (2016). The energetic and chemical signatures of persistent soil organic matter. *Biogeochemistry* 130, 1–12. doi: 10.1007/s10533-016-0246-0

Bond-Lamberty, B., and Thomson, A. (2010). Temperature-associated increases in the global soil respiration record. *Nature* 464, 579–582. doi: 10.1038/nature08930

Bruun, S., Thomsen, I. K., Christensen, B. T., and Jensen, L. S. (2008). In search of stable soil organic carbon fractions: a comparison of methods applied to soils labelled with C-14 for 40 days or 40 years. *Eur. J. Soil Sci.* 59, 247–256. doi: 10.1111/j.1365-2389.2007.00985.x

Burnham, A. K., and Braun, R. L. (1999). Global kinetic analysis of complex materials. *Energy Fuels* 13, 1–22. doi: 10.1021/ef9800765

Currie, W. S. (2003). Relationships between carbon turnover and bioavailable energy fluxes in two temperate forest soils. *Glob. Change Biol.* 9, 919–929. doi: 10.1046/j.1365-2486.2003.00637.x

Davidson, E. A., and Janssens, I. A. (2006). Temperature sensitivity of soil carbon decomposition and feedbacks to climate change. *Nature* 440, 165–173. doi: 10.1038/nature04514

Dembicki, H. (1994). The effects of the mineral matrix on the determination of kinetic-parameters using modified rock-eval pyrolysis - reply. *Organ. Geochem.* 21, 982–984.

Falkowski, P. G., Fenchel, T., and Delong, E. F. (2008). The microbial engines that drive Earth's biogeochemical cycles. *Science* 320, 1034–1039. doi: 10.1126/science.1153213

Falloon, P. D., and Smith, P. (2000). Modelling refractory soil organic matter. *Biol. Fertil. Soils* 30, 388–398.

Greenfield, L. G., Gregorich, E. G., van Kessel, C., Baldock, J. A., Beare, M. H., Billings, S. A., et al. (2013). Acid hydrolysis to define a biologically-resistant pool is compromised by carbon loss and transformation. *Soil Biol. Biochem.* 64, 122–126. doi: 10.1016/j.soilbio.2013.04.009

Gregorich, E. G., Gillespie, A. W., Beare, M. H., Curtin, D., Sanei, H., and Yanni, S. F. (2015). Evaluating biodegradability of soil organic matter by its thermal stability and chemical composition. *Soil Biol. Biochem.* 91, 182–191. doi: 10.1016/j.soilbio.2015.08.032

Guo, L. B., and Gifford, R. M. (2002). Soil carbon stocks and land use change: a meta analysis. *Glob. Change Biol.* 8, 345–360. doi: 10.1046/j.1354-1013.2002.00486.x

Haddix, M. L., Plante, A. F., Conant, R. T., Six, J., Steinweg, J. M., Magrini-Bair, K., et al. (2011). The role of soil characteristics on temperature sensitivity of soil organic matter. *Soil Sci. Soc. Am. J.* 75, 56–68. doi: 10.2136/sssaj2010.0118

Harvey, O. R., Kuo, L. J., Zimmerman, A. R., Louchouarn, P., Amonette, J. E., and Herbert, B. E. (2012). An index-based approach to assessing recalcitrance and soil carbon sequestration potential of engineered black carbons (Biochars). *Environ. Sci. Technol.* 46, 1415–1421. doi: 10.1021/es2040398

Harvey, O. R., Myers-Pigg, A. N., Kuo, L. J., Singh, B. P., Kuehn, K. A., and Louchouarn, P. (2016). Discrimination in degradability of soil pyrogenic organic matter follows a return-on-energy-investment principle. *Environ. Sci. Technol.* 50, 8578–8585. doi: 10.1021/acs.est.6b01010

Jenkinson, D. S. (1971). Studies on decomposition of C14 labelled organic matter in soil. *Soil Sci.* 111, 64–70. doi: 10.1097/00010694-197101000-00008

Jobbágy, E. G., and Jackson, R. B. (2000). The vertical distribution of soil organic carbon and its relation to climate and vegetation. *Ecol. Appl.* 10, 423–436.

Kiem, R., Knicker, H., Korschens, M., and Kogel-Knabner, I. (2000). Refractory organic carbon in C-depleted arable soils, as studied by C-13 NMR spectroscopy and carbohydrate analysis. *Organ. Geochem.* 31, 655–668. doi: 10.1016/S0146-6380(00)00047-4

Kleber, M., Nico, P. S., Plante, A. F., Filley, T., Kramer, M., Swanston, C., et al. (2011). Old and stable soil organic matter is not necessarily chemically recalcitrant: implications for modeling concepts and temperature sensitivity. *Glob. Change Biol.* 17, 1097–1107. doi: 10.1111/j.1365-2486.2010.02278.x

Krull, E. S., Swanston, C. W., Skjemstad, J. O., and McGowan, J. A. (2006). Importance of charcoal in determining the age and chemistry of organic carbon in surface soils. *J. Geophys. Res. Biogeosci.* 111:G04001.

Lehmann, J., and Kleber, M. (2015). The contentious nature of soil organic matter. *Nature* 528, 60–68. doi: 10.1038/nature16069

Leifeld, J., and von Lützow, M. (2014). Chemical and microbial activation energies of soil organic matter decomposition. *Biol. Fertil. Soils* 50, 147–153. doi: 10.1007/s00374-013-0822-6

Odum, E. P., Connell, C. E., and Davenport, L. B. (1962). Population energy-flow of 3 primary consumer components of old-field ecosystems. *Ecology* 43, 88–96. doi: 10.2307/1932043

Paul, E. A., Morris, S. J., Conant, R. T., and Plante, A. F. (2006). Does the acid hydrolysis-incubation method measure meaningful soil organic carbon pools? *Soil Sci. Soc. Am. J.* 70, 1023–1035. doi: 10.2136/sssaj2005.0103

Peltre, C., Fernandez, J. M., Craine, J. M., and Plante, A. F. (2013). Relationships between biological and thermal indices of soil organic matter stability differ with soil organic carbon level. *Soil Sci. Soc. Am. J.* 77, 2020–2028. doi: 10.2136/sssaj2013.02.0081

Plante, A. F., Conant, R. T., Paul, E. A., Paustian, K., and Six, J. (2006). Acid hydrolysis of easily dispersed and microaggregate-derived silt- and clay-sized fractions to isolate resistant soil organic matter. *Eur. J. Soil Sci.* 57, 456–467. doi: 10.1111/j.1365-2389.2006.00792.x

Plante, A. F., Fernandez, J. M., Haddix, M. L., Steinweg, J. M., and Conant, R. T. (2011). Biological, chemical and thermal indices of soil organic matter stability in four grassland soils. *Soil Biol. Biochem.* 43, 1051–1058. doi: 10.1016/j.soilbio.2011.01.024

Plante, A. F., Fernandez, J. M., and Leifeld, J. (2009). Application of thermal analysis techniques in soil science. *Geoderma* 153, 1–10. doi: 10.1016/j.geoderma.2009.08.016

Plante, A. F., Pernes, M., and Chenu, C. (2005). Changes in clay-associated organic matter quality in a C depletion sequence as measured by differential thermal analyses. *Geoderma* 129, 186–199. doi: 10.1016/j.geoderma.2004.12.043

Rovira, P., Kurz-Besson, C., Couteaux, M. M., and Vallejo, V. R. (2008). Changes in litter properties during decomposition: a study by differential thermogravimetry and scanning calorimetry. *Soil Biol. Biochem.* 40, 172–185. doi: 10.1016/j.soilbio.2007.07.021

Ruhlmann, J. (1999). A new approach to estimating the pool of stable organic matter in soil using data from long-term field experiments. *Plant Soil* 213, 149–160. doi: 10.1023/A:1004552016182

Rumpel, C., and Kögel-Knabner, I. (2011). Deep soil organic matter—a key but poorly understood component of terrestrial C cycle. *Plant Soil* 338, 143–158. doi: 10.1007/s11104-010-0391-5

Schmidt, M. W., Torn, M. S., Abiven, S., Dittmar, T., Guggenberger, G., Janssens, I. A., et al. (2011). Persistence of soil organic matter as an ecosystem property. *Nature* 478, 49–56. doi: 10.1038/nature10386

Stockmann, U., Adams, M. A., Crawford, J. W., Field, D. J., Henakaarchchi, N., Jenkins, M., et al. (2013). The knowns, known unknowns and unknowns of sequestration of soil organic carbon. *Agric. Ecosyst. Environ.* 164, 80–99.

Stone, M. M., and Plante, A. F. (2015). Relating the biological stability of soil organic matter to energy availability in deep tropical soil profiles. *Soil Biol. Biochem.* 89, 162–171. doi: 10.1016/j.soilbio.2015.07.008

Trumbore, S. E., Vogel, J. S., and Southon, J. R. (1989). Ams C-14 measurements of fractionated soil organic-matter - an approach to deciphering the soil carbon-cycle. *Radiocarbon* 31, 644–654.

Williams, E. K., Fogel, M. L., Berhe, A. A., and Plante, A. F. (2018). Distinct bioenergetic signatures in particulate versus mineral-associated soil organic matter. *Geoderma* 330, 107–116. doi: 10.1016/j.geoderma.2018.05.024

Williams, E. K., Rosenheim, B. E., McNichol, A. P., and Masiello, C. A. (2014). Charring and non-additive chemical reactions during ramped pyrolysis: applications to the characterization of sedimentary and soil organic material. *Organ. Geochem.* 77, 106–114. doi: 10.1016/j.orggeochem.2014.10.006

Conflict of Interest Statement: The authors declare that the research was conducted in the absence of any commercial or financial relationships that could be construed as a potential conflict of interest.

frontiers in Environmental Science

ORIGINAL RESEARCH
published: 01 October 2018
doi: 10.3389/fenvs.2018.00100

Using Maximum Entropy Production to Describe Microbial Biogeochemistry Over Time and Space in a Meromictic Pond

Joseph J. Vallino[1]* *and Julie A. Huber*[2]

[1] *Marine Biological Laboratory, Ecosystems Center, Woods Hole, MA, United States,* [2] *Woods Hole Oceanographic Institution, Marine Chemistry and Geochemistry, Woods Hole, MA, United States*

Determining how microbial communities organize and function at the ecosystem level is essential to understanding and predicting how they will respond to environmental change. Mathematical models can be used to describe these communities, but properly representing all the biological interactions in extremely diverse natural microbial ecosystems in a mathematical model is challenging. We examine a complementary approach based on the maximum entropy production (MEP) principle, which proposes that systems with many degrees of freedom will likely organize to maximize the rate of free energy dissipation. In this study, we develop an MEP model to describe biogeochemistry observed in Siders Pond, a phosphate limited meromictic system located in Falmouth, MA that exhibits steep chemical gradients due to density-driven stratification that supports anaerobic photosynthesis as well as microbial communities that catalyze redox cycles involving O, N, S, Fe, and Mn. The MEP model uses a metabolic network to represent microbial redox reactions, where biomass allocation and reaction rates are determined by solving an optimization problem that maximizes entropy production over time, and a 1D vertical profile constrained by an advection-dispersion-reaction model. We introduce a new approach for modeling phototrophy and explicitly represent oxygenic photoautotrophs, photoheterotrophs and anoxygenic photoautotrophs. The metabolic network also includes reactions for aerobic organoheterotrophic bacteria, sulfate reducing bacteria, sulfide oxidizing bacteria and aerobic and anaerobic grazers. Model results were compared to observations of biogeochemical constituents collected over a 24 h period at 8 depths at a single 15 m deep station in Siders Pond. Maximizing entropy production over long (3 day) intervals produced results more similar to field observations than short (0.25 day) interval optimizations, which support the importance of temporal strategies for maximizing entropy production over time. Furthermore, we found that entropy production must be maximized locally instead of globally where energy potentials are degraded quickly by abiotic processes, such as light absorption by water. This combination of field observations and modeling results indicate that natural microbial systems can be modeled by using the maximum entropy production principle applied over time and space using many fewer parameters than conventional models.

Keywords: maximum entropy production, microbial biogeochemistry, metabolic networks, phototrophy, community function, meromictic

OPEN ACCESS

Edited by:
Anke Marianne Herrmann, Swedish University of Agricultural Sciences, Sweden

Reviewed by:
Mustafa Yucel, Middle East Technical University, Turkey
John Senko, University of Akron, United States

***Correspondence:**
Joseph J. Vallino
jvallino@mbl.edu

Specialty section:
This article was submitted to Microbiological Chemistry and Geomicrobiology, a section of the journal Frontiers in Environmental Science

Received: *07 February 2018*
Accepted: *23 August 2018*
Published: *01 October 2018*

Citation:
Vallino JJ and Huber JA (2018) Using Maximum Entropy Production to Describe Microbial Biogeochemistry Over Time and Space in a Meromictic Pond. Front. Environ. Sci. 6:100. doi: 10.3389/fenvs.2018.00100

INTRODUCTION

Mass and energy flow associated with the growth and predation of bacteria, archaea and eukaryotes in microbial food webs, coupled with abiotic reactions and transport processes, define biogeochemical cycles that occur in ecosystems ranging in size from less than a liter (Marino et al., 2016) to the entire planet. Because organisms are ultimately responsible for most observed biogeochemical transformations, it is customary and natural to focus on the bioenergetics of growth and predation of organisms that constitute food webs in order to understand and predict biogeochemical transformations. This organismal focus has a long history and has advanced our understanding and prediction of ecosystem dynamics and the mass and energy flow through them (Riley, 1946; Fasham et al., 1990; Le Quere et al., 2005; Friedrichs et al., 2007; Schartau et al., 2017). While focusing on the growth, predator-prey and cooperative interactions of organisms will continue to contribute to our understanding of ecosystem bioenergetics, there are some challenges that limit this approach for microbial systems that form the basis of biogeochemical cycles. Microbial communities are diverse, complex and abundant, consisting, for example, of approximately 10^9 microorganisms per liter of seawater, with estimates that Earth hosts close to 1 trillion microbial species (Sogin et al., 2006; Locey and Lennon, 2016). With the advent of metagenomics, next generation sequencing and bioinformatics, the challenging task of deciphering and annotating the metabolic capabilities and activities of bacteria and other microorganisms has begun, but determining how information in genomes contributes to competition and cooperation is still in its infancy (Hallam and McCutcheon, 2015; Pasternak et al., 2015; Worden et al., 2015). Even more challenging is understanding and predicting community composition dynamics and succession as environmental conditions change, both from exogenous and endogenous drivers (Konopka et al., 2015). While considerable progress is being made in developing predictive models of biogeochemistry based on organisms and the genes they carry (Reed et al., 2014; Coles et al., 2017), the ability for this approach to encompass the complex biogeochemistry of the ecosystem will likely take many decades to compile and decipher. We believe the reductionist approach is essential, but there is also a complementary approach to understanding microbial biogeochemistry that is less studied and uses a more thermodynamic, or whole systems, approach.

Understanding how ecosystems function at the systems level has a long tradition in theoretical ecology (Chapman et al., 2016; Vallino and Algar, 2016), with the underlying premise that ecosystems organize so as to maximize an objective function, such as maximizing power proposed by Lotka (1922) nearly 100 years ago. The advantage of the systems approach is that optimization can be used to determine how an ecosystem will organize and function without the knowledge of which organisms are present and how their population changes over time. Understanding and modeling of ecosystems can focus on function rather than on organisms, and there is growing support that stable function arises from dynamic communities (Fernandez et al., 1999; Fernandez-Gonzalez et al., 2016; Louca and Doebeli, 2016; Needham and Fuhrman, 2016; Coles et al., 2017). Here, we build upon the assumption that microbial systems organize to use all available energy sources. To use the correct thermodynamic term, living organisms use Gibbs free energy, since energy is conserved, but Gibbs free energy (aka usable energy) is not. The destruction of Gibbs free energy or energy potentials results in entropy production, so the net action of life produces entropy, because contrary to conventional wisdom, living organisms are not low entropy structures (Morrison, 1964; Blumenfeld, 1981). This allows us to employ the maximum entropy production (MEP) principle, which proposes that systems with sufficient degrees of freedom will likely organize to maximize the dissipation of Gibbs free energy (Dewar, 2003; Lorenz, 2003; Martyushev and Seleznev, 2006). In an ecological context, if food (which includes organisms themselves) is available but not being consumed, then organisms will eventually adapt, invade or evolve to utilize it if biologically possible. This simple concept forms the basis of this manuscript. The MEP principle has been applied to both abiotic and biotic processes (Kleidon and Lorenz, 2005; Kleidon et al., 2010; Dewar et al., 2014b), and we have used MEP to model periodically forced methanotrophic microbial communities (Vallino et al., 2014) and investigate metabolic switching in nitrate reducing environments (Algar and Vallino, 2014). While MEP is consistent with Darwinian evolution, and likely guides its trajectory (Goldenfeld and Woese, 2011; Skene, 2015, 2017; Judson, 2017), it has yet to gain general acceptance in theoretical or experimental ecological communities largely because of an insufficient number of case studies and uncertainty in how to apply it.

In this study we develop an MEP-based model to predict microbial biogeochemistry in a meromictic pond located in Falmouth, MA (Siders Pond) that includes metabolic processes for phytoplankton, green sulfur bacteria, aerobic organoheterotrophic bacteria, sulfate reducing bacteria, sulfide oxidizing bacteria, photoheterotrophs and aerobic and anaerobic predators (**Figure 1**). However, the model's objective function is to dissipate energy potentials, not grow organisms. While previous MEP models have been developed for chemolithoautotrophs, chemolithoheterotrophs, and chemoorganoheterotrophs, this study expands the metabolic reaction repertoire to include photoautotrophs and photoheterotrophs. The approach is also extended to include an explicit spatial dimension, and we compare model output to observations in Siders Pond collected over a 24 h sampling period from eight depths. MEP solutions using two different optimization timescales (0.25 day vs. 3.0 days) are contrasted and compared to observations, and we discuss the problem of local vs. global MEP optimization for energy potentials that are quickly dissipated abiotically, such as light. Our results suggest that microbial systems in nature can be described by the maximum entropy production conjecture applied over time and space.

RATIONALE

Our interest in investigating the applicability of MEP theory for describing microbial communities has, in addition to the basic science question, an applied objective. Standard models used to describe microbial biogeochemistry contain a large number of

poorly constrained parameters, such as maximum growth rates, substrate affinity constants, growth efficiencies, prey preferences, substrate inhibition constant, and others. Consequently, data are required to determine parameter values, but since there is almost always more parameters than constraining observations, it is not difficult to obtain good agreement between model output and observations. Consequently, a good model fit does not equate to an understanding of the underlying mechanisms in a system. As a consequence, such models usually do poorly when extrapolated to different systems (Vallino, 2000; Ward et al., 2010). Parameters must be recalibrated for new conditions, but this defeats the purpose of developing a model, as we are often interested in using a model to predict how a system will respond to new conditions that have yet to occur. If the MEP principle fundamentally describes microbial communities, then models based on MEP should exhibit better extrapolation performance, since MEP would still be an appropriate objective function even under new conditions.

A challenging and unresolved aspect of MEP principle involves the temporal and spatial scales over which it applies (Dewar et al., 2014a). MEP theory has been developed for nonequilibrium steady-state systems where time is removed from the derivation, but natural microbial communities are dynamic and often far from steady state. For non-steady-state systems, we have proposed the following distinctions (Vallino, 2010). Abiotic processes, such as fire or a rock rolling down a hill, maximize instantaneous entropy production. That is, they follow a steepest descent trajectory down a potential energy surface in progress toward equilibrium, but this pathway can lead to metastable states that prevent further progress and entropy production. For instance, the flame gets extinguished or the rock gets stuck in a ditch partway down the hill. Biological systems, however, have evolved temporal strategies, such as circadian rhythms, that allow the system to take an alternate pathway that is not as steep, but it avoids metastable traps and enables further progress down the free energy surface. While instantaneous entropy production is lower in biological systems, when averaged over time, the integrated entropy production is greater than abiotic processes. Since MEP theory proposes that system configurations that produce more entropy are more likely to prevail (Lorenz, 2003), the higher average entropy production by biological systems allow them to persist over abiotic processes, at least in some situations. Similarly, when considering a spatial domain, entropy production can either be maximized locally at each point in the domain, or entropy production at each point can be adjusted so that entropy production is maximized globally over the entire domain. A simple numerical study indicated that when a system organizes over space, entropy produced by global optimization can exceed that from local optimization, but this requires spatial coordination by the community, while abiotic systems are likely to only maximize entropy production locally (Vallino, 2011). This paper will explore how changes in time and space scales over which entropy is maximized alters model predictions of microbial biogeochemistry. To provide some grounding in reality, model predictions are compared to biogeochemical observations. The purpose of this manuscript is to demonstrate one particular implementation of how MEP can be used to describe microbial biogeochemistry in natural systems that goes beyond a simple conceptual model, but ours is certainly not the only approach.

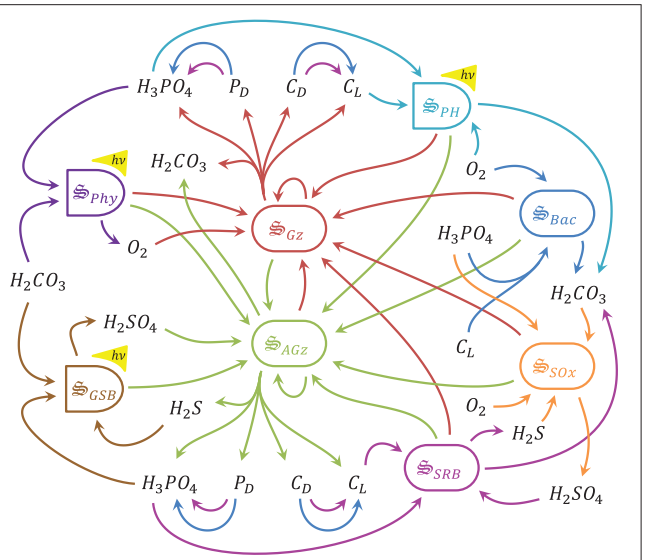

FIGURE 1 | Schematic of catalysts and associated reactions used in the MEP model for Siders Pond. Functional groups include: $\mathbb{S}_{Phy}$, phytoplankton, purple, 2 rxns; $\mathbb{S}_{GSB}$, green sulfur bacteria, brown, 2 rxns; $\mathbb{S}_{Gz}$, aerobic grazers, red, 8 rxns; $\mathbb{S}_{AGz}$, anaerobic grazers, green, 8 rxns; $\mathbb{S}_{Bac}$, aerobic organoheterotrophic bacteria, blue, 3 rxns; $\mathbb{S}_{SRB}$, sulfate reducing bacteria, magenta, 3 rxns; $\mathbb{S}_{PH}$, photoheterotrophs, cyan, 1 rxn; $\mathbb{S}_{SOx}$, sulfide oxidizing bacteria, orange, 1 rxn. Other abbreviations: $h\nu$, photon capture; C_L, labile organic carbon; C_D, refractory organic carbon; P_D, refractory organic phosphorous. See **Table 2** for qualitative representation of functional reactions and section 2.7 of the **Supplementary Material** for stoichiometrically balanced reactions.

METHODS

This section describes Siders Pond sample collection procedures and sample analyses followed by the development of the MEP model and associated 1D transport model for Siders Pond.

Siders Pond

Site Description

Siders Pond is a small coastal meromictic kettle hole (volume: 10^6 m^3; area: 13.4 ha; maximum depth: 15 m) that receives approximately 1×10^6 m^3 of fresh and 0.15×10^6 m^3 of saltwater each year (Caraco, 1986). The latter input occurs via a small creek that connects the pond to Vineyard Sound approximately 550 m to the south. Tritium-helium water dating confirmed vertical mixing across two observed chemoclines, but permanent stratification is maintained because the saltwater inputs enter the pond at depth, mix upward and become entrained with freshwater before exiting the pond (Caraco, 1986). Caraco (1986) also characterized N and P loading to the pond (50 g N m^2 y^{-1} and 1.3 g P m^{-2} y^{-1}, respectively), and an N+P enrichment study (Caraco et al., 1987) showed phytoplankton to be P limited, especially in the low salinity surface waters. Previous studies show

Siders Pond is eutrophic averaging 16 mg m^{-3} chlorophyll a (Chl a) in surface waters (but can exceed 100 mg m^{-3} at times) and an annual primary productivity of 315 g C m^{-2} (Caraco, 1986; Caraco and Puccoon, 1986). In anoxic bottom waters, bacterial Chl c, d and e associated with photosynthetic green sulfur bacteria averages 20 mg m^{-3} (purple sulfur bacteria were not found in high concentration), but BChl cde was also observed to reach high concentrations at times (> 75 mg m^{-3}). Even though green sulfur bacteria could attain high concentrations, their productivity was only 6% of the oxygenic photoautotroph (cyanobacteria + algae) production (Caraco, 1986). Siders Pond was chosen for this study because extensive redox cycling occurs over a 15 m deep water column, which greatly facilitates sampling due to the large water volumes that can be readily collected without perturbing the system.

Sampling and Measurements

Samples were collected from Siders Pond, Falmouth, MA over a 24 h period starting at 6:45 on Jun 25th and ending at 7:37 on Jun 26th, 2015 from a single station located within the deepest basin of the pond (41.548212°N, 70.622412°W). A total of 7 casts were conducted over the 24 hr period, and each cast sampled 8 depths to generate a 2D sampling grid designed for comparison to model outputs (**Figure 2**). A Hydrolab DS5 water quality sonde (OTT Hydromet, GmbH) was connected to a Hydrolab Surveyor 4 handheld display and used to record depth, temperature, salinity, pH, dissolved oxygen (DO), photosynthetic active radiation (PAR), and *in situ* Chl a fluorescence. All sensors were calibrated per manufacturer's instructions one day prior to sampling. One end of a 20 m long section of vinyl tubing with a 1 cm inside diameter was attached to the water quality sonde, while the other end passed through a Geopump 2 (Geotech, CO) peristaltic pump and then connected to 25 mm polypropylene, acid washed, in-line Swinnex filter holder (Millipore, MA), which housed a GF/F glass fiber filter (Whatman, GE Healthcare) that had been ashed at 450°C for 1 hr. At all depths, the vinyl tubing was first flushed for at least 2 min, sample collection vials were washed twice with filtrate and GF/F filters where changed as needed to maintain high flow. This design allowed water samples to be collected at the desired depths and processed on location then preserved on ice or dry ice for later analysis as described below.

Unless otherwise noted, all samples were filtered as described above and stored in 20 mL acid-washed, high-density polyethylene scintillation vials (Fisher Scientific). Samples were preserved for later analysis as follows. Inorganic phosphate: 15 mL samples were amended with 20 μL of 5 N HCl and placed on dry ice. Dissolved inorganic carbon (DIC) and sulfate: samples were collected in 12 mL exetainers (Labco, UK) by overfilling bottles from the bottom up, and then capped without bubbles and placed on ice. Hydrogen sulfide: while filling exetainers, 25 μL of sample was pipette transferred to 6 mL of 2% zinc acetate in a 20 mL scintillation vial and place on ice. Dissolved organic carbon (DOC): 25 mL of sample was collected in previously ashed 30 mL glass vials to which 40 μL of 5 N HCl was added then stored on ice. Particulate organic carbon (POC): approximately 300 mL of sample was passed through new, ashed, 25 mm GF/F filter then stored in a plastic Petri dish on dry ice.

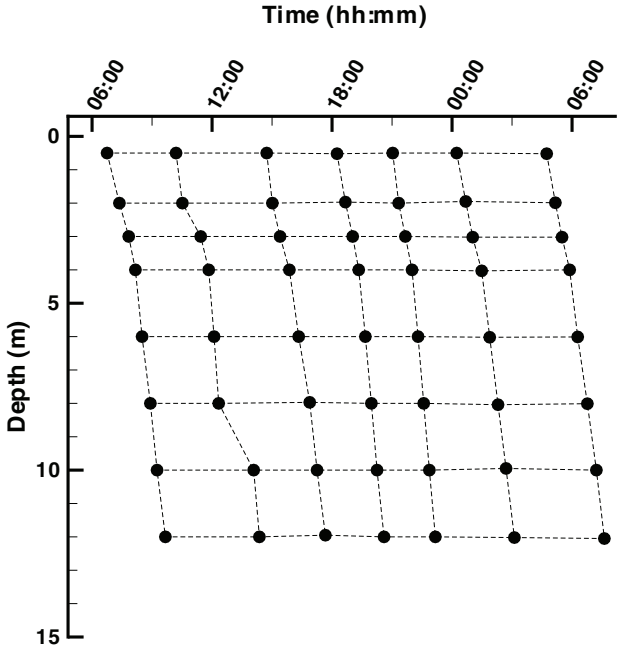

FIGURE 2 | Layout of the Siders Pond 2D (t, z) sample grid. Samples were collected over a 24 h diel cycle starting at ~ 6:00 on 25 Jun 2015 and ending at ~6:00 on 26 Jun 2015. Samples were collected at 0.5, 2, 3, 4, 6, 8, 10, and 12 m.

Samples were analyzed at the Ecosystems laboratory, MBL as follows. Phosphate: samples were stored at −20°C then later analyzed following the spectrophotometric method of Murphy and Riley (1962) on a UV-1800 spectrophotometer (Shimadzu, Kyoto, Japan). DIC: samples were immediately run on return to MBL on an Apollo AS-C3 DIC analyzer (Apollo SciTech, DE). Sulfate: samples were sparged with N_2 to strip H_2S on return to MBL and stored at 4°C then analyzed using ion chromatography on a Dionex DX-120 analyzer (Dionex, Sunnyvale, CA). Hydrogen sulfide: samples were briefly stored at 4°C for 5 days then analyzed using the spectrophotometric method of Gilboa-Garber (1971). DOC: samples were stored at 4°C then run on a Shimadzu TOC-L high temperature total organic carbon analyzer at 720°C. POC: samples were stored at −20°C then analyzed on a Thermo Scientific FLASH 2000 CHN analyzer using aspartic acid standards. To facilitate model comparison to observations, Chl a was estimated from modeled output of phototroph biomass concentrations using 12. $\left(\left[\mathbb{S}_{Phy}\right] + \left[\mathbb{S}_{GSB}\right] + \left[\mathbb{S}_{PH}\right]\right) / \theta_{C:Chla}$, where $\theta_{C:Chla}$ is the C:Chl a ratio, which was set to 50 μg C (μg Chl a)$^{-1}$ (Sathyendranath et al., 2009).

Model Development

The equations used to model biogeochemistry in Siders Pond are provided in detail in the **Supplementary Material**, so the descriptions in this section focus primarily on model concepts

that form the basis of the modeling approach and extensions to previous studies. The model consists of three main components: (1) a set of biologically catalyzed reactions that constitute the distributed metabolic network of the microbial community, including predators such as protist and viruses; (2) a 1D transport model; (3) an optimization component in which control variables that govern reaction stoichiometry, kinetics and thermodynamics are determined so as to maximize internal entropy production over a specified interval of time and space. We describe briefly below the three model components, but we focus first on the representation of the metabolic network, as this forms the foundation of the approach, and includes the concentrations of 11 chemical constituents and 8 functional groups (**Figure 1**, **Table 1**).

Catalysts and Metabolic Reaction Network

Our approach views a complex microbial community as a collection of catalysts (denoted with the special symbol $\mathbb{S}_j$ with the subscript j meaning any of the 8 functional groups in **Figure 1**) that each have a subset of $n_{r,\,j}$ functional reactions they catalyze. The catalyst has an elemental composition given by $CH_{\alpha_{\mathbb{S}}} O_{\beta_{\mathbb{S}}} N_{\gamma_{\mathbb{S}}} P_{\delta_{\mathbb{S}}}$. For this study all catalysts are assigned the same composition as yeast with associated thermodynamic properties (Battley et al., 1997), but this is not an overly constraining approximation (Vallino et al., 2014) and can be easily relaxed if needed. The catalysts and reactions included in the metabolic network represent the capabilities of the entire microbial community, but the reactions are distributed across $n_{\mathbb{S}}$ catalysts (8 for the case of Siders Pond, **Figure 1**), just as functions are distributed across phyla in natural communities (Vallino, 2003). The reactions are highly simplified and condensed, and consist of two essential components: an anabolic reaction that synthesizes catalyst from environmental resources, and a catabolic reaction that provides free energy to drive the anabolic reaction forward. A highly simplified list of metabolic reactions for the Siders Pond model is given in **Table 2**. To convey the basic ideas, we consider below the phyla responsible for sulfate reduction for chemotrophy and phytoplankton for phototrophy.

chemotrophyh

The catalyst $\mathbb{S}_{SRB}$ represents the capabilities of sulfate reducing bacteria (SRB) that oxidize labile organic matter, C_L, using sulfate as the electron acceptor. The anabolic and catabolic reactions are given by,

$$\begin{aligned} C_L \;+\; & \gamma_{\mathbb{S}}\mathrm{NH_3} + \delta_{\mathbb{S}}\mathrm{H_3PO_4} + a^A_{1,\,SRB}\mathrm{H_2SO_4} \rightarrow \mathbb{S}_{SRB} \\ & + a^A_{1,\,SRB}\mathrm{H_2S}(aq) + b^A_{1,SRB}\mathrm{H_2O} \end{aligned} \tag{1}$$

$$C_L \;+\; \frac{1}{2}\mathrm{H_2SO_4} \rightarrow \mathrm{H_2CO_3} + \frac{1}{2}\mathrm{H_2S}\left(aq\right), \tag{2}$$

respectively, where the stoichiometric coefficients, $a^A_{1,\,SRB}$ and $b^A_{1,SRB}$, are determined from elemental balances around O and H. Both reactions above must be catalyzed by $\mathbb{S}_{SRB}$, so the reaction rates are proportional to the concentration of the catalyst, $c_{\mathbb{S}_{SRB}}$, present (note, we also use bracket nomenclature, $[\mathbb{S}_{SRB}]$, for concentration below). These two reactions can be combined by introducing a reaction efficiency variable, ε_{SRB}, to produce an overall reaction representing growth and respiration of sulfate reducing bacteria, $r_{1,SRB}$, given by,

$$\begin{aligned} C_L \;+\; & \varepsilon_{SRB}\left(\gamma_{\mathbb{S}}\mathrm{NH_3} + \delta_{\mathbb{S}}\mathrm{H_3PO_4}\right) \\ & + \left(\frac{1}{2} + \varepsilon_{SRB}\left(a^A_{1,\,SRB} + \frac{1}{2}\right)\right)\mathrm{H_2SO_4} \rightarrow \varepsilon_{SRB}\mathbb{S}_{SRB} \\ & + (1-\varepsilon_{SRB})\,\mathrm{H_2CO_3} + \left(\frac{1}{2} + \varepsilon_{SRB}\left(a^A_{1,\,SRB} + \frac{1}{2}\right)\right)\mathrm{H_2S}\left(aq\right) \\ & + \varepsilon_{SRB} b^A_{1,SRB}\mathrm{H_2O}. \end{aligned} \tag{3}$$

The reaction efficiency variable, ε_{SRB}, is ***one of two classes of optimal control variables*** and a central design feature of the MEP model. As ε_{SRB} approaches 1, Equation (3) represents 100% conversion of labile carbon plus N and P resources to catalyst, while as ε_{SRB} approaches 0, the reaction changes to 100% anaerobic combustion of labile carbon. From an entropy production perspective, only the catabolic reaction dissipates significant free energy, so ε_{SRB} should be set to zero to maximize entropy production; however, the catabolic reaction cannot proceed without catalyst. There exists, then, an optimum value of ε_{SRB} that produces just enough $\mathbb{S}_{SRB}$ catalyst to dissipate the chemical potential between C_L and H_2SO_4, but ε_{SRB} must change as a function of C_L and H_2SO_4 supply rates as well as N and P availability. Conceptually, the MEP problem is to determine how ε_{SRB} should change over time and space to maximize free energy dissipation; however, there are a few other important details.

Gibbs free energies of reaction, $\Delta_r G_{i,j}$, are calculated using Alberty's (2003) approach, which accounts for substrate activities, pH and temperature. For chemotrophic reactions, an adaptive Monod equation parameterized by ε_j accounts for the tradeoffs between substrate affinity, maximum specific growth rate and growth efficiency and can approximate oligotrophic to copiotrophic growth kinetics by varying ε_j between 0 and 1 (Algar and Vallino, 2014; Vallino et al., 2014). In addition to this kinetic constraint, F_K, reaction rates, $r_{i,j}$, are also constrained by reaction thermodynamics, F_T, as described by La Rowe et al. (2012). Consequently, the rates of chemotrophic reactions take the following general form,

$$r_{i,j} = \nu^* \varepsilon_j^2 \Omega_{i,j} \left[\mathbb{S}_j\right] F_K(\mathbf{c}, \varepsilon_j; \kappa^*) F_T(\triangle_r G_{i,j}), \tag{4}$$

where $\mathbf{c}$ are substrate concentrations, ν^* and κ^* are universal constants and $\Omega_{i,j}$ is the second ***optimal control variable class***. Since each catalyst, $\mathbb{S}_j$, can catalyze $n_{r,j}$ sub-reactions (**Table 2**), $\Omega_{i,j}$ determines the fraction of catalyst j, $\mathbb{S}_j$, that is allocated to reaction $r_{i,j}$. For instance, the sulfate reducing bacteria have two others reactions in addition to $r_{1,SRB}$, Equation (3) (**Table 2**). Reactions $r_{2,SRB}$ and $r_{3,SRB}$ allow SRB to decompose recalcitrant organic carbon, C_D, and phosphorous, P_D, into labile organic carbon, C_L, and inorganic phosphate, respectively, and $\Omega_{i,SRB}$ determines the fraction of protein allocated to each of the three reactions. Consequently, each $\Omega_{i,j}$ is bound between 0 and 1, and $\Omega_{i,j}$ must sum to unity over all i for each catalyst; that is,

TABLE 1 | Names of state variables and associated symbols.

Variable	Sym.	Variable	Sym.
Salt	c_{Sal}	Phytoplankton	$c_{\mathfrak{S}_{Phy}}$
Dissolved oxygen	c_{O_2}	Green sulfur bacteria	$c_{\mathfrak{S}_{GSB}}$
Dissolved inorganic carbon	$c_{H_2CO_3}$	Aerobic predators	$c_{\mathfrak{S}_{Gz}}$
Inorganic phosphate	$c_{H_3PO_4}$	Anaerobic predators	$c_{\mathfrak{S}_{AGz}}$
Sulfate	$c_{H_2SO_4}$	Aerobic organoheterotrophic bacteria	$c_{\mathfrak{S}_{Bac}}$
Hydrogen sulfide	c_{H_2S}	Sulfate reducing bacteria	$c_{\mathfrak{S}_{SRB}}$
Phytoplankton carbohydrates	$c_{C_{Phy}}$	Photoheterotrophs	$c_{\mathfrak{S}_{PH}}$
Green sulfur bacteria carbohydrates	$c_{C_{GSB}}$	Sulfide oxidizing bacteria	$c_{\mathfrak{S}_{SOx}}$
Labile organic carbon	c_{C_L}		
Refractory organic carbon	c_{C_D}		
Refractory organic phosphate	c_{P_D}		

All state variables represent concentrations in mmol m^{-3}, except for salt, which is in PSU. Concentrations of NH_3 (c_{NH_3}) and detrital N (c_{N_D}) are included in chemical reactions for stoichiometric and thermodynamic calculations, but were held constant at 5 and 10 mmol m^{-3}, respectively, in all simulations.

TABLE 2 | Reactions associated with the 8 biological catalysts, $\mathfrak{S}_j$, used to model microbial biogeochemistry in Siders Pond, where $r_{i,j}$ represents sub-reaction i of biological catalyst $\mathfrak{S}_j$.

Rxn.	Abbreviated Stoichiometry	Cat.
$r_{1,Phy}$	$H_2CO_3 + h\nu \rightarrow C_{Phy} + O_2$	$\mathfrak{S}_{Phy}$
$r_{2,Phy}$	$C_{Phy} + NH_3 + H_3PO_4 + O_2 \rightarrow \mathfrak{S}_{Phy} + H_2CO_3$	$\mathfrak{S}_{Phy}$
$r_{1,GSB}$	$H_2CO_3 + H_2S + h\nu \rightarrow C_{GSB} + H_2SO_4$	$\mathfrak{S}_{GSB}$
$r_{2,GSB}$	$C_{GSB} + NH_3 + H_3PO_4 + H_2SO_4 \rightarrow \mathfrak{S}_{GSB} + H_2CO_3 + H_2S$	$\mathfrak{S}_{GSB}$
$r_{1-8,Gz}$	$\mathfrak{S}_i + C_i + O_2 \rightarrow \mathfrak{S}_{Gz} + H_2CO_3 + C_D + NH_3 + N_D + H_3PO_4 + P_D + C_L$	$\mathfrak{S}_{Gz}$
$r_{1-8,AGz}$	$\mathfrak{S}_i + C_i + H_2SO_4 \rightarrow \mathfrak{S}_{AGz} + H_2CO_3 + C_D + NH_3 + N_D + H_3PO_4 + P_D + H_2S + C_L$	$\mathfrak{S}_{AGz}$
$r_{1,Bac}$	$C_L + NH_3 + H_3PO_4 + O_2 \rightarrow \mathfrak{S}_{Bac} + H_2CO_3$	$\mathfrak{S}_{Bac}$
$r_{2,Bac}$	$C_D \rightarrow C_L$	$\mathfrak{S}_{Bac}$
$r_{3,Bac}$	$P_D \rightarrow H_3PO_4$	$\mathfrak{S}_{Bac}$
$r_{1,SRB}$	$C_L + NH_3 + H_3PO_4 + H_2SO_4 \rightarrow \mathfrak{S}_{SRB} + H_2CO_3 + H_2S$	$\mathfrak{S}_{SRB}$
$r_{2,SRB}$	$C_D \rightarrow C_L$	$\mathfrak{S}_{SRB}$
$r_{3,SRB}$	$P_D \rightarrow H_3PO_4$	$\mathfrak{S}_{SRB}$
$r_{1,PH}$	$C_L + NH_3 + H_3PO_4 + h\nu \rightarrow \mathfrak{S}_{PH} + H_2CO_3$	$\mathfrak{S}_{PH}$
$r_{1,SOx}$	$H_2CO_3 + H_2S + O_2 + NH_3 + H_3PO_4 \rightarrow \mathfrak{S}_{SOx} + H_2SO_4$	$\mathfrak{S}_{SOx}$

There are a total of 28 reactions, where $\mathfrak{S}_{Gz}$ and $\mathfrak{S}_{AGz}$ each catalyzed 8 sub-reactions. Reactions are shown to emphasize function only. Complete reaction stoichiometries, including influence of optimal control variables, are given in section 2.7 of the ***Supplementary Material****. See caption of* ***Figure 1*** *for nomenclature.*

$\sum_{i=1}^{n_{r,j}} \Omega_{i,j} = 1$. An example of how F_K, $\Delta_r G_{i,j}$, and F_T vary over time and space to influence reaction rates of sulfate reducing bacteria is given in **Supplementary Material 4.1**, **Figure S3**.

phototrophy

In this version of the MEP model we introduce catalysts associated with phototrophic growth, specifically phytoplankton (Phy), $\mathfrak{S}_{Phy}$, anaerobic green sulfur bacteria (GSB), $\mathfrak{S}_{GSB}$, and photoheterotrophs (PH), $\mathfrak{S}_{PH}$. Both Phy and GSB are modeled similarly using two sub-reactions (**Table 2**). One sub-reaction couples photon capture that drives CO_2 fixation into carbohydrates, C_{Phy} and C_{GSB}, and a second sub-reaction converts carbohydrates into biomass in a manner analogous to growth of chemotrophs described above. We focus on phytoplankton here because development for GSB is similar, and can be found in the **Supplementary Material**.

The carbon fixation reaction for phytoplankton is given by,

$$\varepsilon_{Phy}\mathrm{H_2CO_3} + n_{1,Phy}h\nu \rightarrow \varepsilon_{Phy}\left(\mathrm{C}_{Phy} + \mathrm{O_2}(aq)\right) \tag{5}$$

where $h\nu$ are captured photons of frequency ν, h is Plank's constant and $n_{1,Phy}$ is the moles of photons needed to fix 1 mole of CO_2 at 100% efficiency (i.e., $\varepsilon_{Phy} = 1$). The Gibbs free energy for a mole of photons is given by

$$\Delta_r G_\gamma = -\eta_I h\nu N_A, \tag{6}$$

where N_A is Avogadro's number and η_I is the thermodynamic efficiency for converting electromagnetic radiation into work

(Candau, 2003). If $\Delta_r G_{C_{Phy}}$ is the Gibbs free energy for fixing a mole of H_2CO_3 into C_{Phy} plus O_2, then moles of photons needed to fix 1 mole of CO_2 is given by,

$$n_{1,Phy} = -\frac{\Delta_r G_{C_{Phy}}}{\Delta_r G_\gamma}, \tag{7}$$

and the Gibbs free energy of reaction for CO_2 fixation defined by Equation (5) is given by,

$$\Delta_r G_{1,Phy} = -\left(1 - \varepsilon_{Phy}\right) \Delta_r G_{C_{Phy}}. \tag{8}$$

In this formulation, ε_{Phy} governs the efficiency for the conversation of electromagnetic potential into chemical potential. If 100% of photosynthetic active radiation is converted to chemical potential, no entropy is produced, and the free energy of reaction for Equation (5) is zero, so the reaction will not proceed due to thermodynamic constraints. However, as ε_{Phy} is decreased, some photons are dissipated as heat, which drives the reaction forward, and all photons are dissipated as heat when $\varepsilon_{Phy} = 0$, but no catalyst is synthesized.

The reaction rate for CO_2 fixation depends on the rate of photon capture, which is given by,

$$\Delta I_{Phy} = k_p \Omega_{1,Phy}[\mathbb{S}_{Phy}] I(t,z) \tag{9}$$

where k_p is the coefficient for light absorption by particles, $\Omega_{1,Phy}[\mathbb{S}_{Phy}]$ is the fraction of phytoplankton catalytic machinery allocated to capturing photons (i.e., chlorophyll and electron transfer proteins), and $I(t,z)$ is light intensity (mmol photons m^{-2} d^{-1}) at time t and depth z. Consequently, the reaction rate for CO_2 fixation is given by,

$$r_{1,Phy} = \frac{\Delta I_{Phy}}{n_{1,Phy}} F_K\left(\mathbf{c},\ \varepsilon_j;\ \kappa^*\right) F_T\left(\Delta_r G_{1,Phy}\right), \tag{10}$$

where F_K and F_T are the kinetic and thermodynamic drivers, respectively. This reaction has similarities to those typically used to describe phytoplankton growth (Macedo and Duarte, 2006), but our derivation focuses not on the local light intensity level, but rather on how much light is actually intercept by the phytoplankton, as governed by $k_p \Omega_{1,Phy}[\mathbb{S}_{Phy}] I$, and how much of that free energy is actually used to drive carbon fixation, as governed by ε_{Phy}. As evident in Equation (10), the maximum rate is directly tied to the rate of photon interception, ΔI_{Phy}, not by an arbitrary maximum specific growth parameter. The second reaction used by Phy and GSB (**Table 2**) is simply the conversion of reduced organic carbon, C_{Phy} and C_{GSB}, into more catalyst or CO_2 depending of the value of ε_{Phy}.

The reaction for photoheterotrophs (PH) differs slightly from that above. In this case only one reaction is used ($r_{1,PH}$, **Table 2**), where photon capture is linked to the conversion of labile carbon into PH catalyst. As above, photons captured can also be dissipated as heat for $\varepsilon_{PH} < 1$, or the free energy can be used to drive biosynthesis ($\varepsilon_{PH} > 0$), where photon free energy replaces chemical free energy used in chemotroph reactions.

Transport Model

Siders Pond is horizontally well mixed, so an advection-dispersion-reaction (ADR) model that includes particle sinking was used to approximate vertical transport of the 19 state variables (**Figure 1**). The origin of the vertical coordinate, z, is defined at the pond's surface, and the axis points in the positive direction downward toward the benthos and reaches a maximum depth of 15 m. Siders Pond 3D bathymetry surface was rendered from a contour plot in Caraco (1986), and an equation for cross-section area as a function of depth was derived therefrom (**Figure S1**). Equations for vertical volumetric flow rate, lateral groundwater inputs and seawater intrusion at the bottom boundary were derived from Caraco (1986), who used both tritium-helium-3 dating combined with mass balance calculations to estimate freshwater inputs and seawater intrusion. An equation for the dispersion coefficient was derived by fitting simulated salinity profiles to observations collected during this study.

The primary external drivers in the model are temperature, pH and photosynthetic active radiation. Surface irradiance was based on a model of solar zenith angle (Brock, 1981), which assumes a cloudless sky. To predict PAR light intensity as function of time and depth, a standard light adsorption model was used that includes coefficients for light absorption by water, k_w, and particulate material, k_p.

Neumann boundary conditions were used for state variables at the pond's surface and gas transport for O_2, CO_2, and H_2S across the air-water interface was accounted for using a stagnant-film model. Robin boundary conditions were used for the bottom boundary based on the flux of material entering the boundary associated with the intrusion of seawater diluted with groundwater. In addition, aerobic and anaerobic decomposition of sinking organic matter from the water column contributed to a sink for O_2 and H_2SO_4, and a source for H_3PO_4, H_2CO_3, and H_2S to the overlying water.

Entropy Production and Optimization

Entropy-production

Entropy production occurs when an energy potential is destroyed and dissipated as heat to the environment, but not when the potential is converted to another potential. For example, a flame converting chemical potential into heat or light being absorbed by water both result in maximum entropy production; these are irreversible processes and the Gibbs free energy is destroyed. On the other hand, entropy is not produced if electromagnetic potential is converted reversibly into chemical potential, but thermodynamic theory requires that reversible reactions must proceed infinitely slowly. In the model, as the reaction efficiency for phytoplankton, ε_{Phy}, approaches 1, electromagnetic potential is converted to chemical potential without entropy production, but the thermodynamic force, F_T, drivers the reaction rate to 0, and as ε_{Phy} approaches zero, all electromagnetic potential is dissipated as heat, but no catalyst is produced, as evident in Eq. (5). Consequently, living organisms operate between these two extremes. For organisms to grow at a non-zero rate, an energy potential must be partially dissipated and some entropy must be produced.

Instantaneous entropy production per unit volume, $\dot{\sigma}_{i,j}$, for chemotrophic reactions is readily calculated as the product of reaction rate times Gibbs free energy of reaction (Vallino, 2010) divided by temperature, T, as given by,

$$\dot{\sigma}_{i,j} = -\frac{1}{T} \triangle_r G_{i,j} r_{i,j}. \tag{11}$$

Average entropy production, $\langle \dot{\sigma}_{i,j} \rangle$, is calculated by integrating $\dot{\sigma}_{i,j}$ over an interval of time, Δt, as given by,

$$\langle \dot{\sigma}_{i,j} \rangle = \frac{1}{\triangle t} \int_t^{t+\triangle t} \dot{\sigma}_{i,j} d\tau. \tag{12}$$

The value of $\triangle t$ is unknown, but it is the fundamental parameter of interest in this study, because it represents the time scale over which biology has evolved to operate.

Entropy production associated with the dissipation of electromagnetic radiation is readily calculated from the Gibbs free energy for photons, Equation (6), and photon capture rate, Equation (9). The photon free energy can be dissipated as heat along two pathways: (1) interception by water or (2) particles, such as bacteria and grazers, as well as by the non-photosynthetic components of phytoplankton. Photons intercepted by the photosynthetic machinery of phototrophs can be either dissipated as heat, if $\varepsilon_j = 0$, or all energy potential can be transferred to chemical potential, if $\varepsilon_j = 1$, but typically it is a combination of both, so that $0 < \varepsilon_j < 1$. Consequently, total entropy production, $\dot{\sigma}_\Sigma$, is the sum of three processes: entropy production by light absorption by water, $\dot{\sigma}_W$, entropy production by light absorption by particles, $\dot{\sigma}_P$, and entropy production by chemical reactions, $\dot{\sigma}_R$, including photoreactions. All entropy production terms are accounted for in the MEP optimization problem, including that from light absorption by water and particles.

MEP-optimization

The stoichiometry, thermodynamics and kinetics of the 28 reactions that comprise the metabolic network (**Table 2**, **Figure 1**) vary as a function of the eight ε_j optimal control variables, and the partitioning of biological structure, $\mathbb{S}_j$, to sub-reactions $r_{i,j}$ that depends on the values of the $\Omega_{i,j}$ control variables, of which there are 20. A solution to the MEP model, and associated microbial biogeochemistry, is determined by adjusting ε_j and $\Omega_{i,j}$ over $\triangle t$ time and 1D space to maximize entropy production, the details of which are provided in **Supplementary Material** section 3.2, but also see Vallino et al. (2014). As $\triangle t$ approaches 0 in Equation (12), the average entropy production, $\langle \dot{\sigma}_{i,j} \rangle$, approaches the instantaneous value, $\dot{\sigma}_{i,j}$, and describes abiotic processes based on our hypothesis. Increasing $\triangle t$ permits other solutions that are not constrained to the steepest descent trajectory. By changing values of ε_j and $\Omega_{i,j}$ over time and space, pathways that avoid the ditch halfway down the hill are allowed, or strategies that anticipate the sun rising in the morning can be exploited. The critical aspect of the optimization is choosing the appropriate time interval over which to maximize entropy production and whether local or global optimization should be used (Vallino, 2011); consequently, these two aspects are the focus of this manuscript and form the bases of the Results section.

Physical parameters and model skill assessment

If the MEP model developed here were cast as a conventional biogeochemistry model, there would be 89 biological parameters associated with growth kinetics. Instead, there are 28 optimal control (OC) variables (8 ε_j and 20 $\Omega_{i,j}$), but only one biological parameter, because the OC variables are determined by maximizing entropy production described above. The sole biological parameter, Δt, specifies the time scale over which entropy is maximized, Equation (12), and its impact on solution dynamics is the focus of this manuscript. There are 11 uncertain physical parameters, 9 associated with particulate matter sinking velocities and two associated with light absorption by water and particles. Since fitting model output to observations is not an indication of good model forecasting fidelity, we only crudely adjusted the 11 physical parameters so that model outputs were within an order of magnitude of observations. These adjustments were made with fix values of the 28 OC variables that were set arbitrarily. The objective was to get the physics to reasonably approximate that occurring in Sider Pond.

To determine model performance, 2D linear interpolation was used to extract values of model state variables at times and depths corresponding to those taken for observations. Root mean squared errors were then calculated between interpolated model outputs and observations to quantify model skill (Fitzpatrick, 2009). The computational approach used for solving the 1D advection-dispersion-reaction equation is described in **Supplementary Material** section 2.9 and the approach used for solving the optimal control problem is described in **Supplementary Material** section 3.2.

RESULTS

All solutions presented here are from local entropy maximization at 10 depths (0, 1, 2, 3, 4, 6, 8, 10, 12, and 15 m). We investigated two optimization time intervals, $\triangle t$, for entropy maximization, a short interval of 0.25 days and a long interval of 3 days. Simulations were started on May 19th, but only the last 6 days of simulations from Jun 21st to Jun 27th are shown here and compared to observations collected on Jun 25th and 26th (**Figure 2**). Our results focus on how these two solutions compare to observations in the **Simulations Compared to Observations** section as well as how the short and long interval optimization windows differ from each other in the **Comparison Between SIO and LIO Simulations** section.

Simulations Compared to Observations

Solutions obtained from the short (0.25 day) and long (3 day) interval optimizations are compared to biogeochemical observations from Siders Pond that were collected to form a 2D sample grid on Jun 25th and 26th, 2015 (**Figure 2**). Simulated profiles for photosynthetic active radiation (PAR), Chl a and dissolved oxygen (DO) are compared to observations in Siders Pond in **Figure 3**. The short interval optimization (SIO) shows PAR extending to nearly the bottom of the pond (**Figure 3A**),

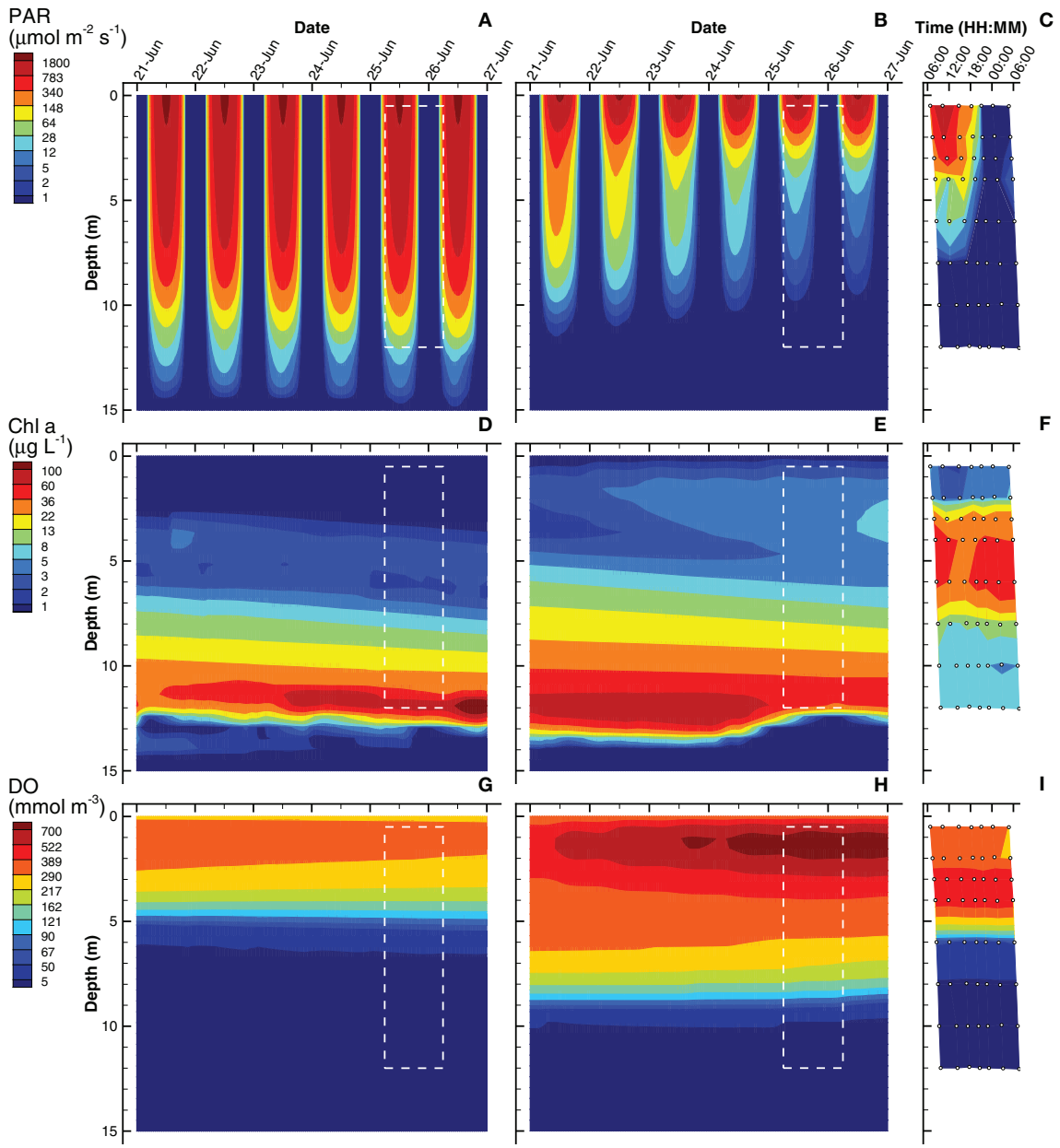

FIGURE 3 | Contour plots of photosynthetic active radiation (PAR) **(A–C)**, chlorophyll (Chl) a concentration **(D–F)** and dissolved oxygen (DO) **(G–I)** for six day simulations using short interval optimization (SIO) (left column), long interval optimization (LIO) (center column) and for observations collected from Siders Pond over a 24 h period on Jun 25 to Jun 26 2015 (right column). Rectangle (dashed white lines) in simulation plots corresponds to time and depths where observations are comparable (i.e., Jun 25/26, 0.5 to 12 m). Actual observations are shown as white circles with black perimeters (see also **Figure 2**).

while PAR from the long interval optimization (LIO) (**Figure 3B**) more closely matches observations (**Figure 3C**). The prediction for Chl a in both simulations do not match observations very well (**Figures 3D–F**), but this is partially due to how Chl a was estimated, since Chl a is not specifically modeled. The Chl a *in vivo* observations show a peak Chl a around 5 m, while both simulations have peaks around 12 m, but those peaks are due to accumulation of sinking phytoplankton rather than productivity at that depth. The LIO simulation does show a secondary Chl a peak developing around 3 m, but it is weaker than observations ($\sim$ 6 vs. 40 µg L^{-1}). Based on DO, the SIO shows anaerobic conditions begin at 6 m, while the LIO shows that occurring at 10 m. The observed transition to anoxia splits between the two simulations at 8 m. Observations also show a subsurface DO maximum at 3.5 m, while both simulations show max DO closer to 1.3 m. Furthermore, the SIO shows a decreasing DO max with time, while the LIO shows an increase over time, and the maximum reaches 800 mmol m^{-3} vs. 480 for observations.

In general, the SIO simulations show less phototrophic activity while LIO shows greater activity than what the observations indicate. The LIO solutions show better fits to observations for PAR and Chl a based on RMSE, while the SIO shows a better fit to DO (**Table 3**).

Simulations of substrate concentrations for autotrophs, namely inorganic phosphate and dissolved inorganic carbon (DIC), show qualitative agreement to observations for both SIO and LIO solutions (**Figure 4**), but some discrepancies are apparent. The phosphate chemoclines occur around 10, 11, and 8 m for the SIO, LIO, and observations, respectively (**Figures 4A–C**). Above the phosphate chemocline, the SIO simulation shows slightly elevated levels of H_3PO_4 (∼0.3 mmol m^{-3}) in the surface and 5 m layers, compare to observations (**Figure 4C**), which are near the level of detection (0.03 mmol m^{-3}) except for a few spikes. Below the phosphate chemocline, observations show slightly higher accumulations of phosphate, approaching 22 mmol m^{-3}, while the SIO and LIO simulations show max concentrations closer to 16 and 19 mmol m^{-3}, respectively. For DIC, both SIO and LIO simulations show much lower DIC concentrations below 10 m (3,000 and 5,400 mmol m^{-3}, respectively) than observed in Siders Pond (16,500 mmol m^{-3}), which would indicate much higher anaerobic remineralization in the pond than occurs in the simulations. The SIO and LIO also show greater draw down of DIC in the surface water above 2 and 4 m respectively, and the LIO simulation shows minimum DIC approaching just 2 mmol m^{-3} at 1 m, while minimum observed value is above 660 mmol m^{-3}. The SIO simulation fits phosphate observations slight better than the LIO simulation, but LIO does better at fitting the DIC observations (**Table 3**).

Simulations of hydrogen sulfide show a chemocline at approximately 9 and 10 m for the SIO and LIO solutions, respectively, which are slightly deeper than the H_2S chemocline observed in Siders Pond at about 8 m (**Figures 5A–C**). However, H_2S reaches concentrations as high as 7,000 mmol m^{-3} in Siders Pond, while maximum concentrations only reach 900 and 2,100 mmol m^{-3} in the SIO and LIO simulations, respectively. Simulations also show a peak H_2S concentration at 12 m, and a decrease in concentration below 12 m, which also indicates lower anaerobic respiration in the simulations. Simulated sulfate concentrations in the upper portion of the water column (0 to 4 m) are similar to those observed (**Figures 5D,E**), but the simulations show an abrupt sulfate chemocline starting at about 8 m, while observations show a more gradual increase in sulfate with depth. Furthermore, sulfate reaches much higher concentrations in the simulations at depth than do observations, showing maximums of 15,500 mmol m^{-3} in both simulations, while observation maximum is only 9,000 mmol m^{-3}. The lower simulated concentrations of H_2S and the higher simulated sulfate concentrations indicate that sulfate reduction in the model is lower than that actually occurring in Siders Pond, but the LIO simulations fit observations better for both H_2S and H_2SO_4 than do the SIO simulations (**Table 3**).

The last of the observations are dissolved organic carbon (DOC) and particulate organic carbon (POC) concentrations (**Figure 6**). For simulations, DOC is a derived quantity based on the sum of state variables $[C_L]$ and $[C_D]$, while POC is derived from the sum of internal carbohydrate stores, $\left[C_{Phy}\right]$ and $[C_{GSB}]$, plus the concentrations of all biological structures, $\left[\mathbb{S}_j\right]$. In the water column above 12 m, the SIO simulation shows very low concentrations of DOC (∼ 1 mmol m^{-3}), but then increases rapidly to a maximum of 1,900 mmol m^{-3} (**Figure 6A**). The LIO simulation shows a similarly high DOC concentration at 14 m, but above 12 m, the DOC concentration ranges from 2 to 140 mmol m^{-3}, which is closer to those observed in Siders Pond, which range from 200 to 300 mmol m^{-3} above 10 m, and increase to a maximum of about 1,000 mmol m^{-3} at 12 m. Similar to DOC, POC in the SIO simulation shows low values ($<$ 30 mmol m^{-3}) above 6 m, but POC peaks to 1,000 mmol m^{-3} at 12 m (**Figure 6D**). The POC concentrations from the LIO simulation are closer to observations, but the mid-water POC maximum in the LIO simulation is approximately 500 mmol m^{-3}, while the observations peak at 280 mmol m^{-3} around 4 m. Like the SIO simulation, the LIO simulation also shows high POC concentrations below 10 m, which was not observed in Siders Pond. It is possible that DOC and POC may reach higher concentrations in the funnel-like basin of Siders Pond below 12 m, but samples were not collected there. While the LIO simulations show better fit to DOC observations, the SIO simulations fit the POC observations better (**Table 3**). Overall, the LIO simulations fit six observations better, while the SIO simulations of fit three observations better, which indicates the LIO simulations are overall closer to observations (**Table 3**). On a qualitative measure, the LIO simulation produces a phytoplankton bloom near the surface of the pond (**Figure 3**), which is consistent with multiple years of student collected observations from Sider Pond. In that regard, the LIO solution appears better at predicting this important feature of Siders Pond.

Comparison Between SIO and LIO Simulations

Since the MEP optimization model generates a large number of outputs, this section highlights some of those outputs to contrast the simulations based on the short (0.25 d) interval optimization (SIO) to that from the long (3 d) interval optimization (LIO). Consider entropy production, which is the variable that is being sequentially maximized over a 0.25 d interval (SIO) or a 3 d interval (LIO) at 10 different depths (**Figure 7**). Total entropy production, $\dot{\sigma}_\Sigma$, for the SIO and LIO simulations differ significantly, in that $\dot{\sigma}_\Sigma$ in the SIO solution is spread out over a 12 m water column (**Figure 7A**) vs. the LIO solution (**Figure 7E**), where most of the entropy production occurs in the top 3 m of the pond. Furthermore, peak entropy production in the LIO simulation is 7.5 times great than the SIO solution (9.8 vs. 1.3 GJ m^{-1} K^{-1} d^{-1}), and the total integrated entropy produced over the water column and over the 6 day simulation, σ_T, was 21.3 GJ K^{-1} and 36.5 GJ K^{-1} for the SIO and LIO simulations, respectively. For comparison, if the pond was sterile, σ_T would equal 12.4 GJ K^{-1} from light absorption in the water column. The 71% higher total integrated entropy, σ_T, produced by the LIO simulation illustrates that extending the optimization time scale

TABLE 3 | Root mean squared errors between model predictions and observations for the short (SIO, $t = 0.25$ d) and long (LIO, $t = 3.0$ d) interval optimizations.

Δt (d)	PAR (μE m^{-2} s^{-1})	Chl a (μg L^{-1})	DO (μM)	H_3PO_4 (μM)	DIC (μM)	H_2S (μM)	H_2SO_4 (μM)	DOC (μM)	POC (μM)
0.25	484.	32.9	***137.***	***4.69***	6050.	2500.	3650.	388.	***167.***
3.00	***189.***	***24.4***	212.	4.88	***5610.***	***2280.***	***3390.***	***361.***	198.

Better (i.e., lower) scores are highlighted in bold italic font face.

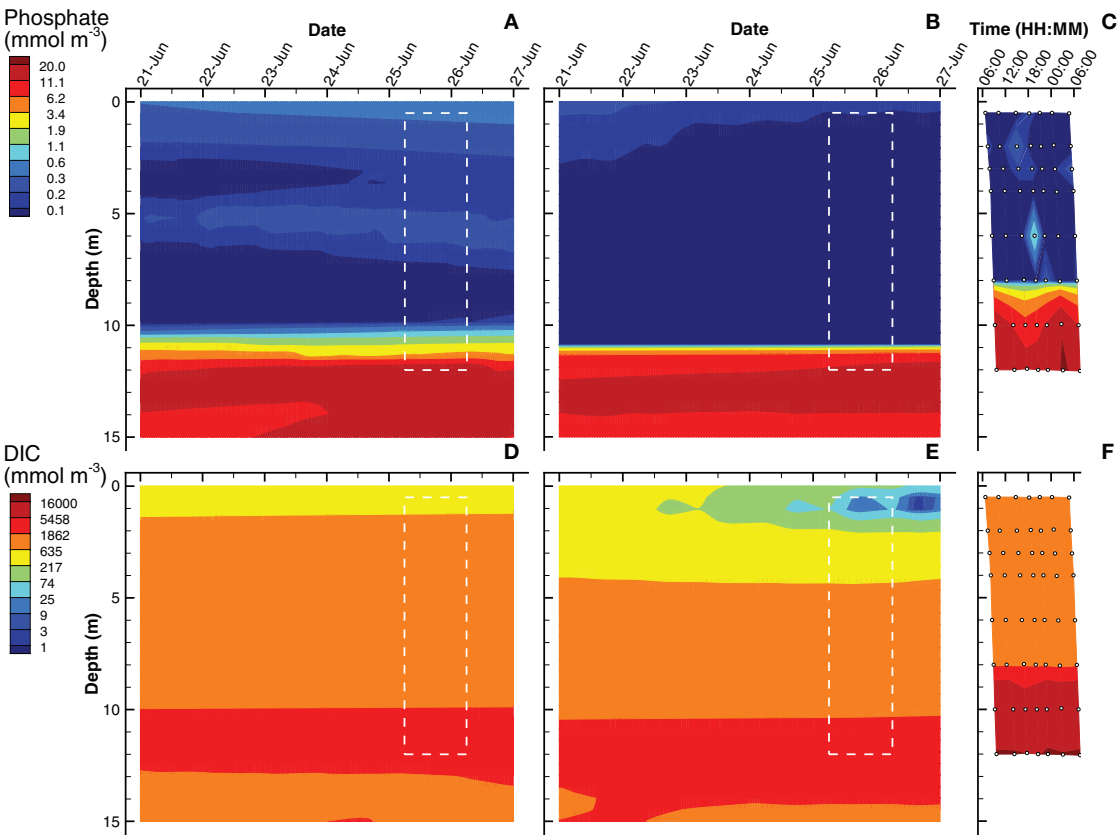

FIGURE 4 | Contour plots of inorganic phosphate **(A–C)** and dissolved inorganic carbon (DIC) **(D–F)** concentrations for SIO and LIO simulations (left and center columns, respectively) and Siders Pond observations (right column). See caption to **Figure 3** for other details.

results in greater entropy production, which is consistent with a previous study (Vallino et al., 2014).

The different contributors to total entropy production, namely by reaction, $\dot{\sigma}_R$, water, $\dot{\sigma}_W$, and particles, $\dot{\sigma}_P$, also differ significantly between the two simulations. For instance, total integrated entropy production associated with reactions was actually greater in the SIO than the LIO simulation (**Figure 7B** vs. **Figure 7F**), as well as exhibited a greater maximum $\dot{\sigma}_R$ (0.28 vs. 0.26 GJ m^{-1} K^{-1} d^{-1} for SIO versus LIO); however, entropy production by reaction during the day is rather small (< 25% in the upper 5 m) compared to light dissipation by water or particles, but the two simulations differ here as well. The SIO simulation dissipates most of the incoming radiation by water absorption in the upper 5 m of the water column (**Figure 7C** vs. **Figure 7G**), while the LIO simulation dissipates most of the electromagnetic potential via absorption by particles (**Figure 7D** vs. **Figure 7H**). As evident in the POC (**Figure 6**) and Chl a (**Figure 3**) concentrations, the LIO simulation produces more biomass in the upper portion of the water column, and biomass is effective at absorbing and dissipating light.

An analysis of phytoplankton (Phy) growth by the SIO and LIO simulations (**Figure 8**) illustrates not only how the two simulations differ, but also some of the mechanics of the MEP-based optimization approach. Phytoplankton density attains a maximum of 20 mmol m^{-3} in the LIO simulation by June 27th, but Phy are effectively absent in the SIO simulation, attaining a maximum of only 0.1 mmol m^{-3} (**Figures 8A,F**). While it is possible that the low phytoplankton density in the SIO simulation could be due to extensive predation, this is not the case because the rates of CO_2 fixation ($r_{1,Phy}$, **Table 2**) and conversion of fixed C to biomass ($r_{2,Phy}$, **Table 2**) are two orders of magnitude

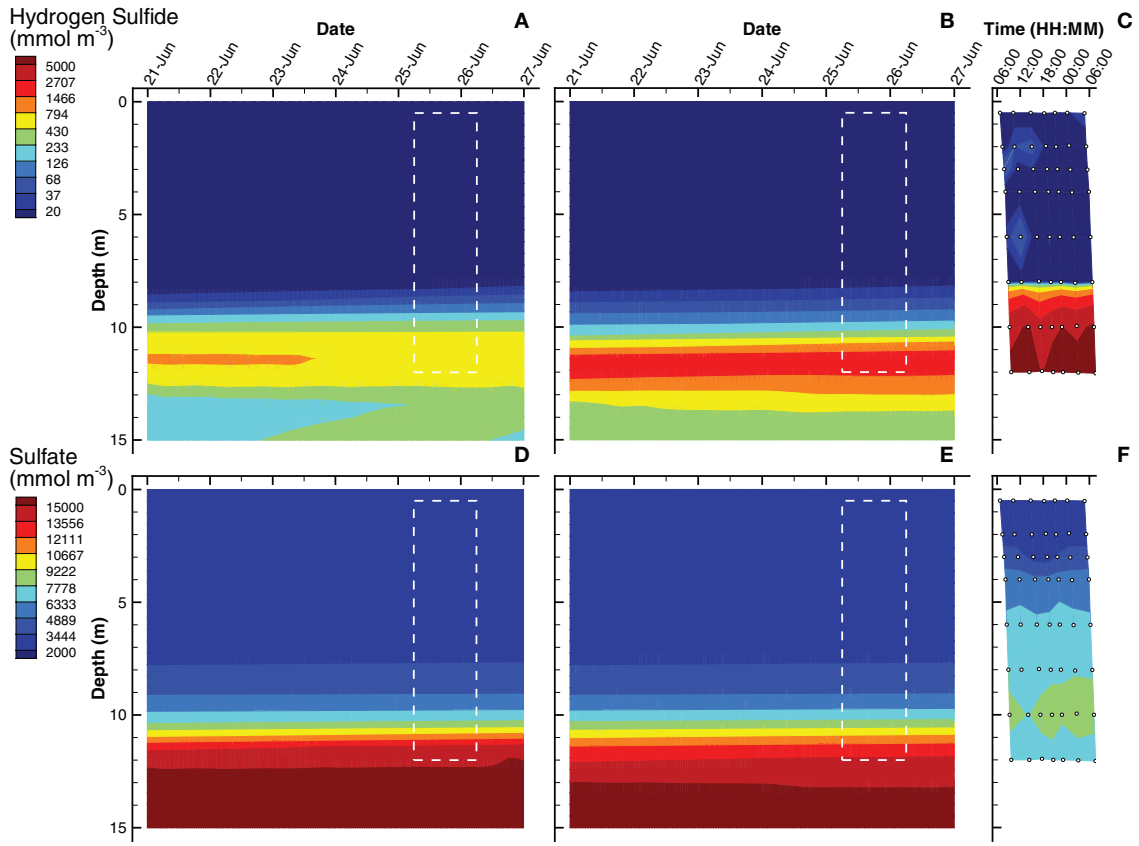

FIGURE 5 | Contour plots of hydrogen sulfide **(A–C)** and sulfate **(D–F)** concentrations for SIO and LIO simulations (left and center columns, respectively) and Siders Pond observations (right column). See caption to **Figure 3** for other details.

lower in the SIO versus LIO simulation (**Figures 8B,C** vs. **Figures 8G,H**). The differences in phytoplankton density and reaction rates between the SIO and LIO simulations are due to how the optimal control variables change over time and space (**Figures 8D,E,I,J**). Consider how reaction efficiency, ε_{Phy}, varies over time and space in the two simulations (**Figures 8D,I**). The SIO simulation shows rapid switching between very high efficiencies (>0.98) and very low efficiencies (<0.02) over time. While not on all days, reaction efficiency drops to very low levels around noon (**Figure 8D**), which results in high entropy production, but at the sacrifice of fixing CO_2, which is consistent with maximizing energy dissipation on a short term time scale. On the contrary, the LIO solution (**Figure 8I**) shows more gradual changes in ε_{Phy}, operating between 0.3 and 0.4 for most of the simulation. There is rapid changing of the biomass allocation variable, $\Omega_{1,Phy}$, in the LIO solution (**Figure 8J**), but this makes sense, because the control variable partitions phytoplankton biomass to the light requiring carbon fixation reaction, $r_{1,Phy}$, during peak daylight (**Figure 8G**), then switches to the biosynthesis reaction, $r_{2,Phy}$, at night (**Figure 8H**). Based on **Figure 7C**, the SIO solution instead uses water for the short term dissipation of electromagnetic potential in the pond's surface, but in deeper water the SIO solution does produce biomass.

Instead of producing phytoplankton, the SIO solution produces more green sulfur bacteria (GSB), which reach a maximum concentration of 735 mmol m^{-3}, compare to only 23 mmol m^{-3} in the LIO solution (**Figures 9A,D**). Furthermore, GSB increase during the SIO simulation, while they decrease in the LIO, which is evident in the greater biosynthesis reaction, $r_{2,GSB}$, in SIO vs. LIO solutions (**Figures 9B,E**) as well as in $r_{1,GSB}$ (not shown). However, the value of the reaction efficiency control variable, ε_{GSB}, does switch to low values around noon on several days in the SIO simulation, which implies again the solution favors entropy production over growth (**Figures 9C,F**). This SIO simulation also favors much higher reaction rates of photoheterotrophs (PH), $r_{1,PH}$, compared to the LIO solution, but interestingly, this does not lead to greater concentrations of PH biomass, $\mathbb{S}_{PH}$ (**Figure 10**). The reason is because high rates for PH growth, $r_{1,PH}$, are coupled with extremely low values of growth efficiency, ε_{PH} (**Figures 10B,C**). Based on the adaptive Monod equation that changes substrate affinity as a function of ε_{PH}^4, uptake of labile organic carbon, C_L, by PH can occur at extremely low concentrations when ε_{PH} is close to zero, but small ε_{PH} values means very little biomass is produced as a results. This is an interesting result, as light energy is being used to scavenge organic carbon at low concentrations, which contributes to the low labile organic carbon observed

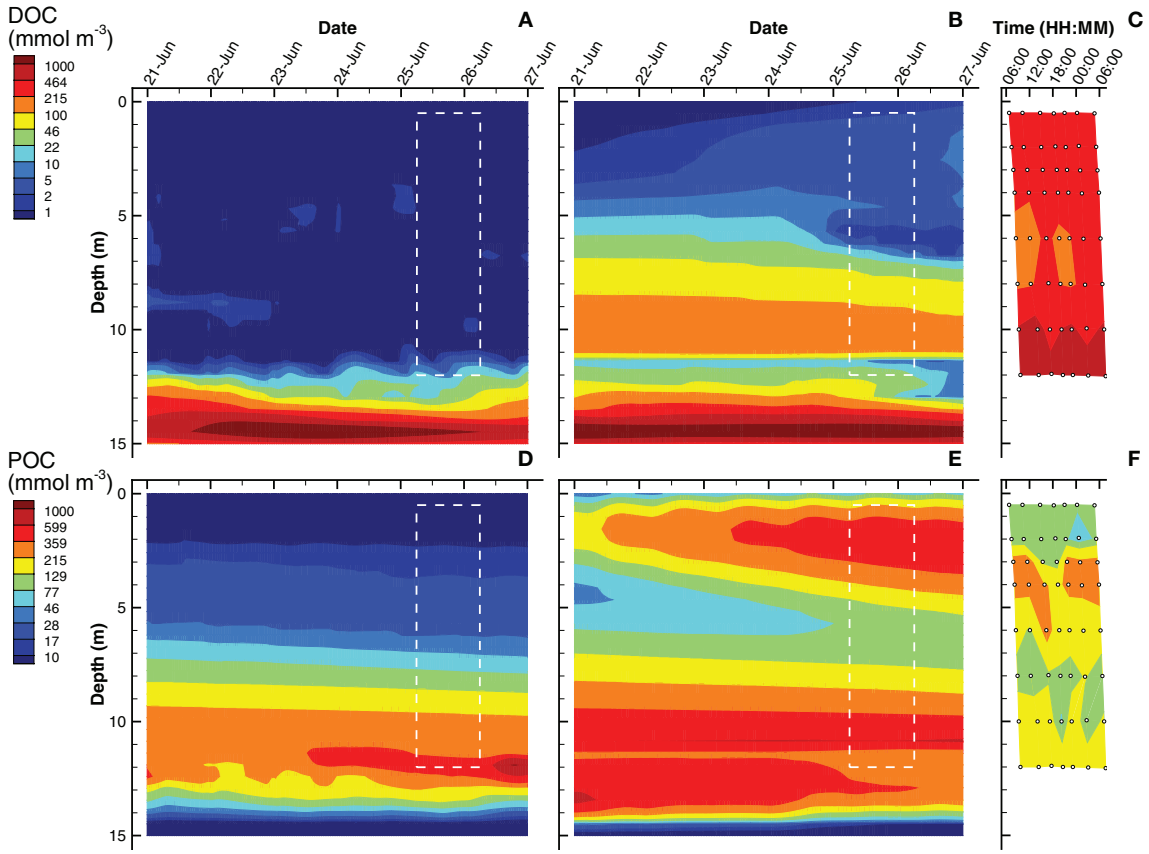

FIGURE 6 | Contour plots of dissolved organic carbon (DOC) **(A–C)** and particulate organic carbon (POC) **(D–F)** concentrations for SIO and LIO simulations (left and center columns, respectively) and Siders Pond observations (right column). See caption to **Figure 3** for other details.

in the SIO simulation (**Figure 6A**). Furthermore, the high entropy production from reaction, $\dot{\sigma}_R$ (**Figure 7B**), is almost entirely due to PH. One of the reasons both green sulfur bacteria and photoheterotrophs are more active in the SIO versus LIO simulations is that light is not being intercepted by phytoplankton like it is in the LIO simulation (**Figure 8A** vs. **Figure 8F**).

Bacterial densities are similar in the two simulations (**Figures S4a,d**), but there is significantly higher growth rate by bacteria in the LIO simulation between 4 and 10 m (**Figures S4b,e**). Both simulations allocate almost all of $\mathbb{S}_{Bac}$ to detrital carbon decomposition, $r_{2,Bac}$, below 13 m (**Figures S5c,f**), but the SIO simulation also allocates biomass to detrital carbon decomposition sporadically throughout the water column to produce C_L (**Figure S4c**). The anaerobic, sulfate reducing bacteria function similarly as bacteria, but operate in the anaerobic portion of the water column (**Figures S6, S7**). Like bacteria (Bac), the sulfate reducing bacteria (SRB) allocate biomass to detrital carbon decomposition, $r_{2,SRB}$, below 13 m in both SIO and LIO simulations (**Figures S7c,f**) and sporadically throughout the water column in the SIO simulation (**Figure S7c**). Overall, bacteria and SRB function in a complementary mode across the aerobic and anaerobic portions of the water column. Similar to phytoplankton, the control variables for both $\mathbb{S}_{Bac}$ and $\mathbb{S}_{SRB}$ show more rapid (bang-bang) control in the SIO compared to the LIO simulation (**Figures S5, S7**). The third bacterial group, sulfide oxidizing bacteria, $\mathbb{S}_{SOx}$, are largely unimportant in either of the 6 day simulations.

Another significant difference between the SIO and LIO simulations is a greater importance of predation, $\mathbb{S}_{Gz}$, in the SIO solution (**Figure 11**). Because predation is abstracted in the MEP model, it represents all predation mechanisms, including protists, predatory bacteria, viruses, and cannibalism. In addition to dissipating chemical potential stored as biomass, predation serves a more important task of recycling nutrients from biomass that are allocated to metabolic functions that are not needed under prevailing conditions. The SIO and LIO simulations show that the concentration of $\mathbb{S}_{Gz}$ is more than 4 times higher in SIO than LIO solutions, and $\mathbb{S}_{Gz}$ increases over time under the SIO objective. The primary prey items in the SIO solution are $\mathbb{S}_{Gz}$ (i.e., cannibalism), $\mathbb{S}_{Bac}$ and $\mathbb{S}_{PH}$ (**Figures 11B–D**), while only $\mathbb{S}_{Bac}$ predation is of significance in the LIO solution (**Figure 11G**). Closer inspection of **Figures 11B,C** reveals that predation occurs predominately at night, which is a result of temporal changes in the partitioning control variables, $\Omega_{i,Gz}$,

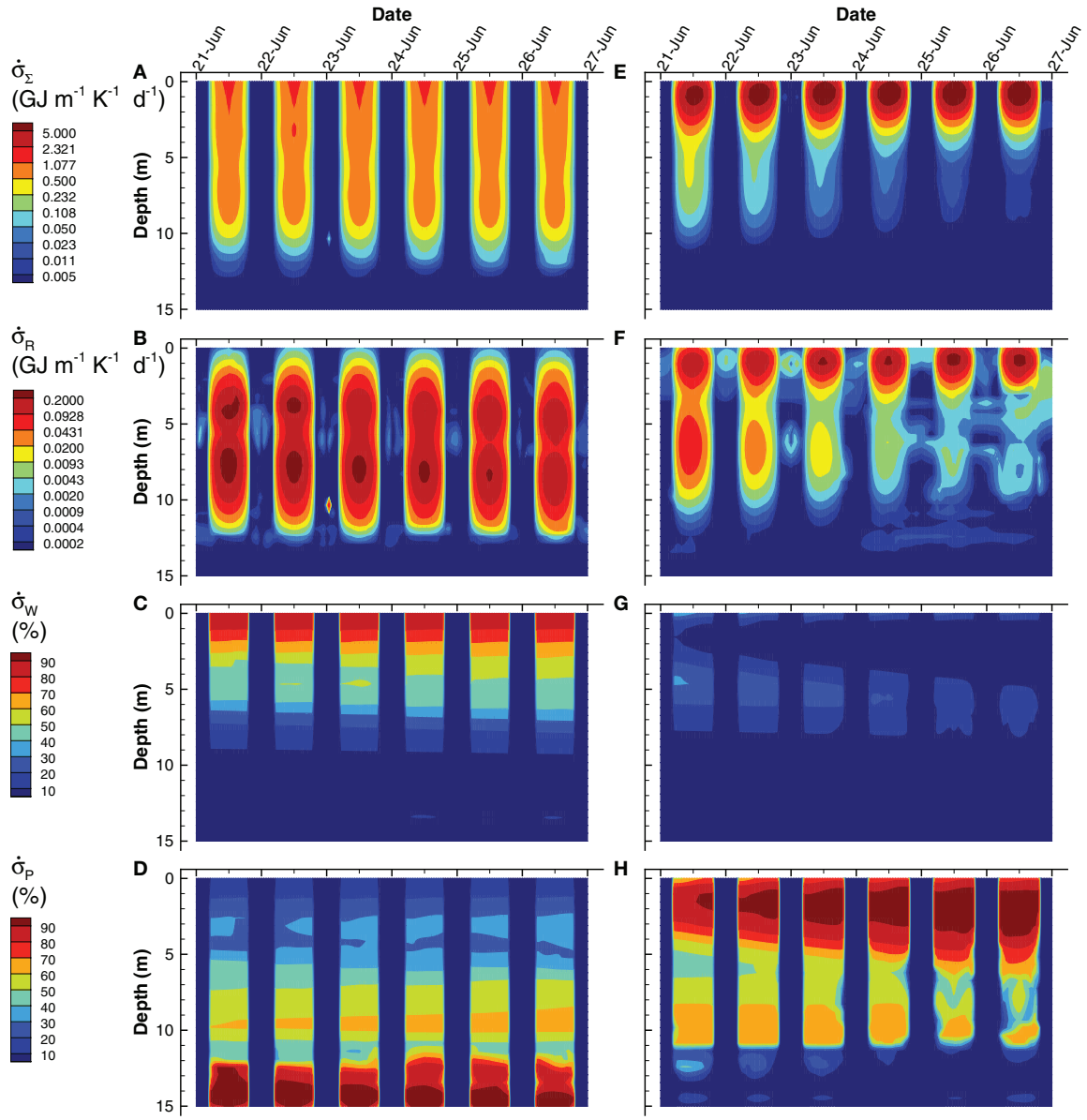

FIGURE 7 | Contour plots of simulated total entropy production, $\dot{\sigma}_\Sigma$ (Eq. (S178)) **(A,E)**, entropy production from reactions, $\dot{\sigma}_R$ [Equation (S178)] **(B,F)**, and entropy production from light absorption by water, $\dot{\sigma}_W(t,z)$ [Equation (S176)] **(C,G)** and particles, $\dot{\sigma}_P$ [Equation (S177)] **(D,H)** for the SIO (left column) and LIO (right column) simulations. Entropy production from light dissipation by water and particles are shown as a percentage of total entropy production.

rather than prey concentration (not shown). High concentration of $\mathbb{S}_{Gz}$ is found below 10 m, but growth of grazers actually occurs between 4 and 7 m, which indicates the high $\mathbb{S}_{Gz}$ concentration below 10 m is due to sinking and accumulation. Accumulation of biomass in the deep, anaerobic, portion of the water column becomes food for anaerobic predators, $\mathbb{S}_{AGz}$, which are important in both SIO and LIO simulations, but are slightly more active in the LIO simulation (**Figure S8**).

An interesting result that derives from the focus on dissipating energy potentials rather than on growing organisms is the importance of chemotrophs on dissipating electromagnetic potential. For instance, aerobic organoheterotrophic bacteria, $\mathbb{S}_{Bac}$, are well understood as dissipaters of chemical potential, as they typically respire significant amounts of organic carbon (i.e., $\varepsilon_{Bac} < 0.5$). In both the SIO and LIO simulations, however, far more free energy is dissipated by passive light absorption than it is by respiration (**Figure 12**), although the difference is more striking in the SIO simulation (**Figure 12A** vs. **Figure 12B**). Some prokaryotes in nature harness this abundant light energy via expression of proteorhodopsin (Béjà et al., 2000), which is perhaps more widespread than currently appreciated (Dubinsky et al., 2017).

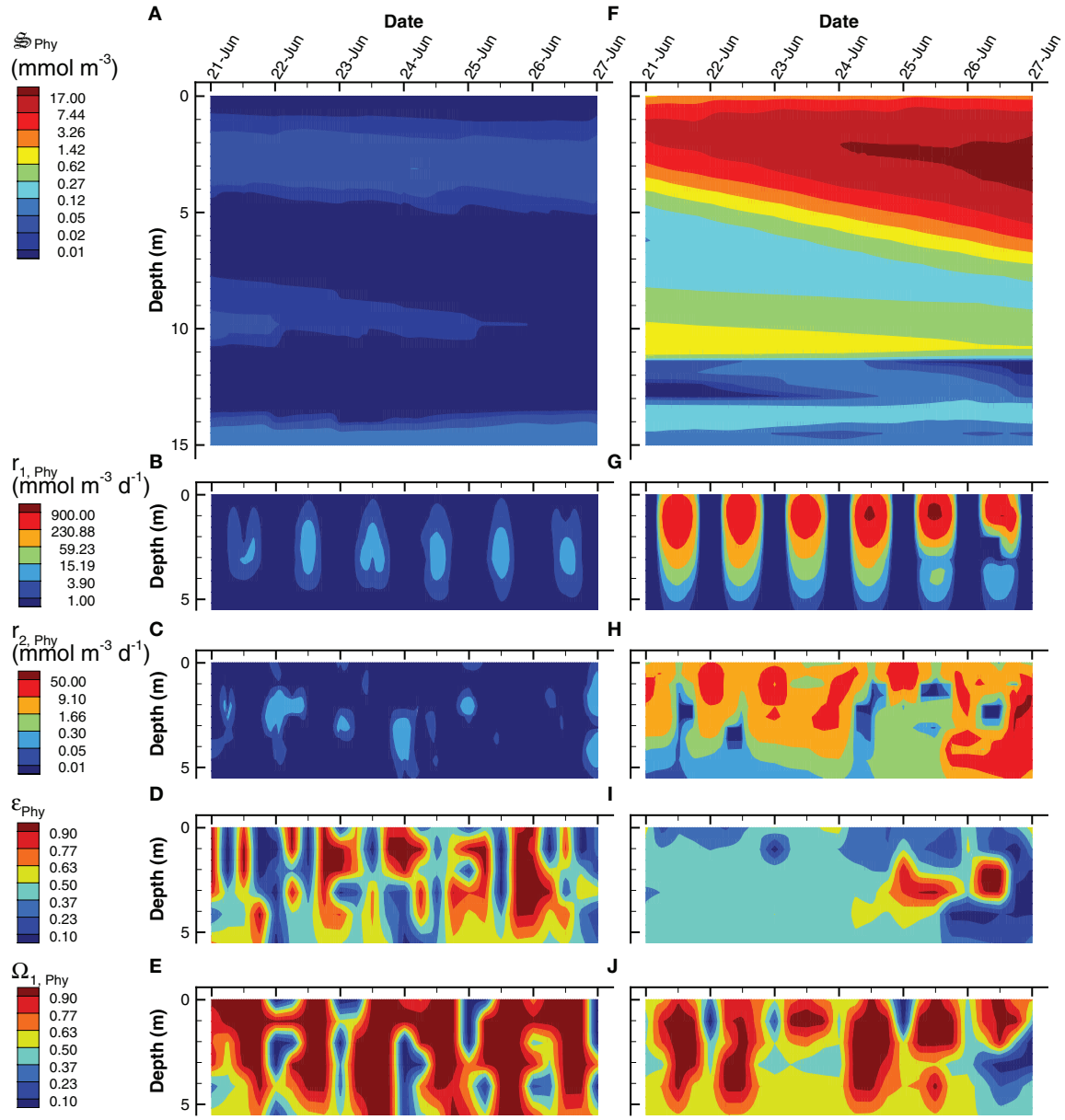

FIGURE 8 | Contour plots of phytoplankton concentration, [$\mathbb{S}_{Phy}$] **(A,F)**, rates for the two associated reactions, $r_{1,Phy}$ **(B,G)** and, $r_{2,Phy}$ **(C,H)** and two optimal control variables, ε_{Phy} **(D,I)**, and $\Omega_{1,Phy}$ **(E,J)** for the SIO **(A–E)** and LIO **(F–J)** simulations. Note, reaction rates and control variables are only plotted for the top 5 m of the water column where the processes are significant.

DISCUSSION

The two primary objectives of this study were to demonstrate that (1) a model based on free energy dissipation can reasonably describe microbial community organization and function with relatively few parameters and (2) that microbial systems operate collectively over characteristic timescales that are likely longer than what common wisdom would suggest. The secondary objectives were to demonstrate how the model can be used in systems with spatial dimensions and to extend the approach to include phototrophs. While improvements could be made with explicit data assimilation (Edwards et al., 2015), the MEP model did a reasonable job at simulating biogeochemistry in Siders Pond with few adjustable parameters, and the better fit of the long interval optimization (LIO) simulation to 6 out of 9 observations indicates that the microbial community has evolved to function over time scales that are longer than 0.25 days (**Table 3**). The MEP optimization approach removed approximately 89 parameters that would have had to be tuned if a conventional model had been used (Ward et al., 2010). Perhaps the most

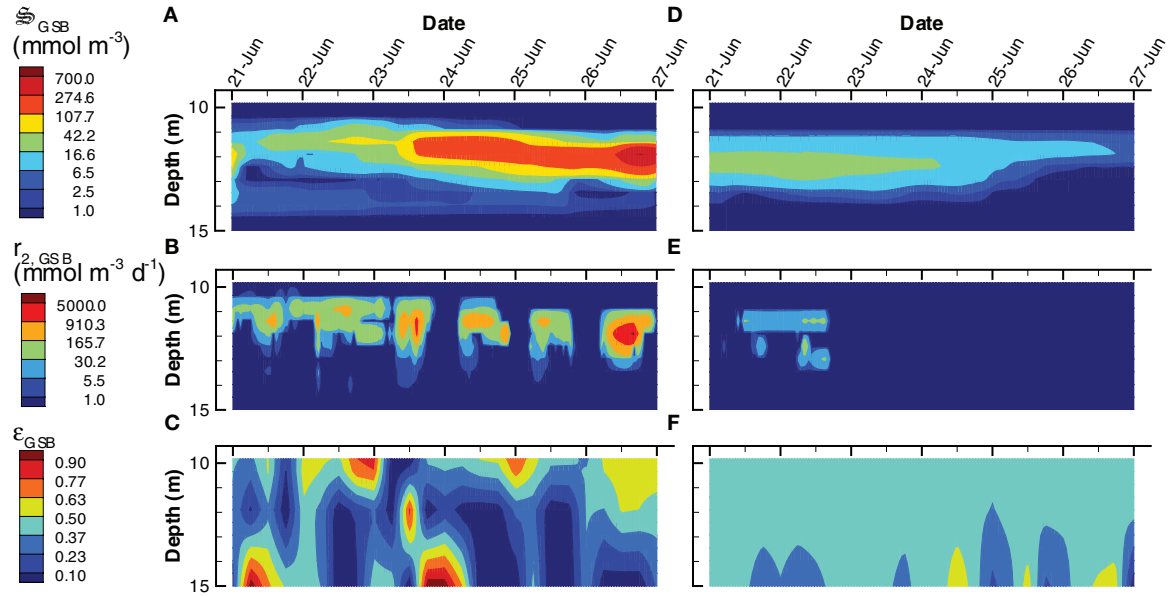

FIGURE 9 | Contour plots of green sulfur bacteria concentration, [$\mathbb{S}_{GSB}$] **(A,D)**, rate of the biosynthesis reaction, $r_{2,GSB}$ **(B,E)** and the growth efficiency optimal control variable, ε_{GSB} **(C,F)** for the SIO **(A–C)** and LIO **(D–F)** simulations. Note, variables are only plotted for 10 m to 15 m where the GSB are active.

useful aspect is that MEP provides a different perspective to view biology (Skene, 2017). For the Siders Pond model, the perspective focused our attention on how microbial functional activity changes with the length of the entropy integration interval, Δt.

Temporal strategies, such as circadian clocks (Wolf and Arkin, 2003), anticipatory control (Mitchell et al., 2009; Katz and Springer, 2016), energy and resource storage (Schulz et al., 1999; Grover, 2011), and dormancy (Lewis, 2010) are hallmarks of biology, yet they are often not given much consideration when theory and models are developed for understanding biogeochemistry, even though temporal strategies have also been observed in microbial communities (Ottesen et al., 2014). Here our model results indicate that different organizational timescales can dramatically impact biogeochemistry and how microbial communities function. For instance, the SIO simulation does not invest resources in phytoplankton growth, because over the short 0.25 day optimization, water dissipates more electromagnetic potential than a small increase in phytoplankton biomass over the short interval. Instead, the SIO solution allocates resources to growth of green sulfur bacteria (GSB) and photoheterotrophs (PH) deeper in the water column to dissipate light not adsorbed by water in the surface. The SIO solution also places more resources on decomposing refractory carbon, but also on respiring the liberated labile carbon. Grazing rates, especially under aerobic conditions, are higher in the SIO simulations as well. These types of resource allocations in the SIO solution appear more consistent with R* or resource-ratio theory (Tilman, 1982) and r-selection (Pianka, 1970; Fierer et al., 2007); that is, emphasis on fast growth. On the contrary, the LIO solution appears more similar to K-selection where resources are invested for longer term outcomes. These differences are also evident in the control variables. In the SIO simulations, the control variables show rapid bang-bang control fluctuations as resources vary (**Figure 8D**), while the LIO solution produces more gradual changes in control variables (**Figure 8I**). A microbial community that implements temporal strategies should outcompete a community that lacks temporal strategies, because long-term strategies result in greater acquisition and utilization of food resources under non steady-state conditions than short-term strategies (Cole et al., 2015), which is evident by the 71% greater entropy production over the 6 day simulations using LIO versus SIO (36.5 GJ K^{-1} vs. 21.3 GJ K^{-1}).

One of the main questions that arise in applying MEP is what is the appropriate timescale over which biology organizes? That is, in the current implementation of the model, what is an appropriate value for Δt used in the optimal control problem? In this study two values were explored, 0.25 days for the SIO and 3 days for the LIO. These choices were based on the observation time scale, where 0.25 day is "short" compared to 1 day, and 3 days is "long" in comparison to 1 day. Our results indicate that the SIO solution did not match observations or expectations as well as the LIO solution (**Table 3**). Comparing MEP model output to observations for differing values of Δt is one means to explore this fundamental property of ecosystems. But is a 3 d optimization window sufficient? It seems the appropriate MEP time scales do not depend on just the characteristic time scales of organisms, because our study on periodically forced methanotroph communities showed that the communities were well adapted to 20 day cyclic inputs of energy, even though the characteristic turnover time of bacteria is closer to hours (Vallino et al., 2014; Fernandez-Gonzalez et al., 2016). We know that terrestrial systems function on long timescales, at least on the order of the four seasons, but their time scales are likely much

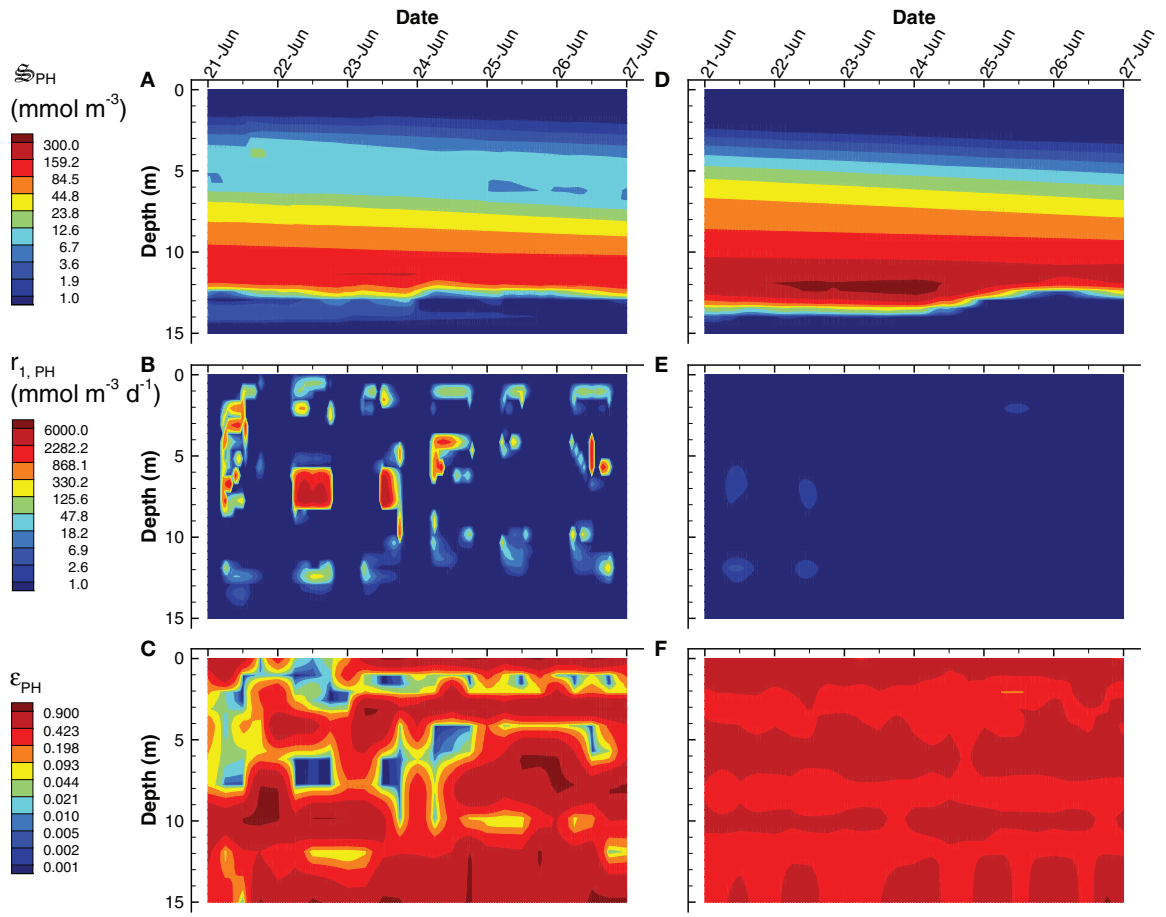

FIGURE 10 | Contour plots of photoheterotroph concentration, [$\mathfrak{S}_{PH}$] **(A,D)**, rate of the carbon fixation reaction, $r_{1,PH}$ **(B,E)** and the growth efficiency optimal control variable, ε_{PH} **(C,F)** for the SIO **(A–C)** and LIO **(D–F)** simulations. Note, contours for ε_{PH} were selected to emphasize ε_{PH} values near zero.

longer given that individual trees can live hundreds of years, and forest succession takes longer than that (Odum, 1969; Finegan, 1984). At this time, we do not have an answer to the question regarding an appropriate optimization time scale for microbial communities, but it is likely related to the time scales over which biological predictions, acquired by evolution, can be reliably made, such as the sun will return tomorrow, or winter is coming. Predicting the future has obvious evolutionary advantages, but it also results in greater dissipation of free energy and entropy production, as evident by the higher entropy produced by the LIO solution. We believe that determining the temporal scales over which microbial communities operate will be important for developing predictive biogeochemistry models, but space scales are also import.

Strategies that coordinate function over space also lead to greater free energy dissipation (Vallino, 2011). Some examples of such coordination include quorum sensing (Goo et al., 2012; Hmelo, 2017) and associated quorum policing (Whiteley et al., 2017), long-range metabolic signaling (Liu et al., 2015), stigmergy (Gloag et al., 2013), horizontal gene transfer (Treangen and Rocha, 2011), cables and nanowires (Reguera et al., 2005; Schauer et al., 2014), cross-feeding (Estrela et al., 2012; Rakoff-Nahoum et al., 2016), chemotaxis (Stocker and Seymour, 2012), vertical migration (Inoue and Iseri, 2012) and other types infochemical exchange (Moran, 2015). Our original intent was to compare local versus global MEP optimization, but global optimization in the Siders Pond model did not produce biologically relevant results due to the speed at which electromagnetic potential is dissipated abiotically. Because water and sediments rapidly absorb light, any water column of sufficient depth will dissipate all incoming radiation as entropy regardless of the presence of organisms, so an infinite number of solutions exist that all produce the same global entropy production. However, maximizing local entropy production at discrete depths, as was conducted in this study, does select for a unique solution, which our results show is biologically relevant. Our previous study with purely chemical reactions showed that global entropy production results in greater chemical potential destruction (Vallino, 2011). This study indicates that if abiotic processes can destroy an energy potential faster than biotic ones, then local MEP optimization will be the preferred solution. Global maximization of entropy production is more likely to be found in

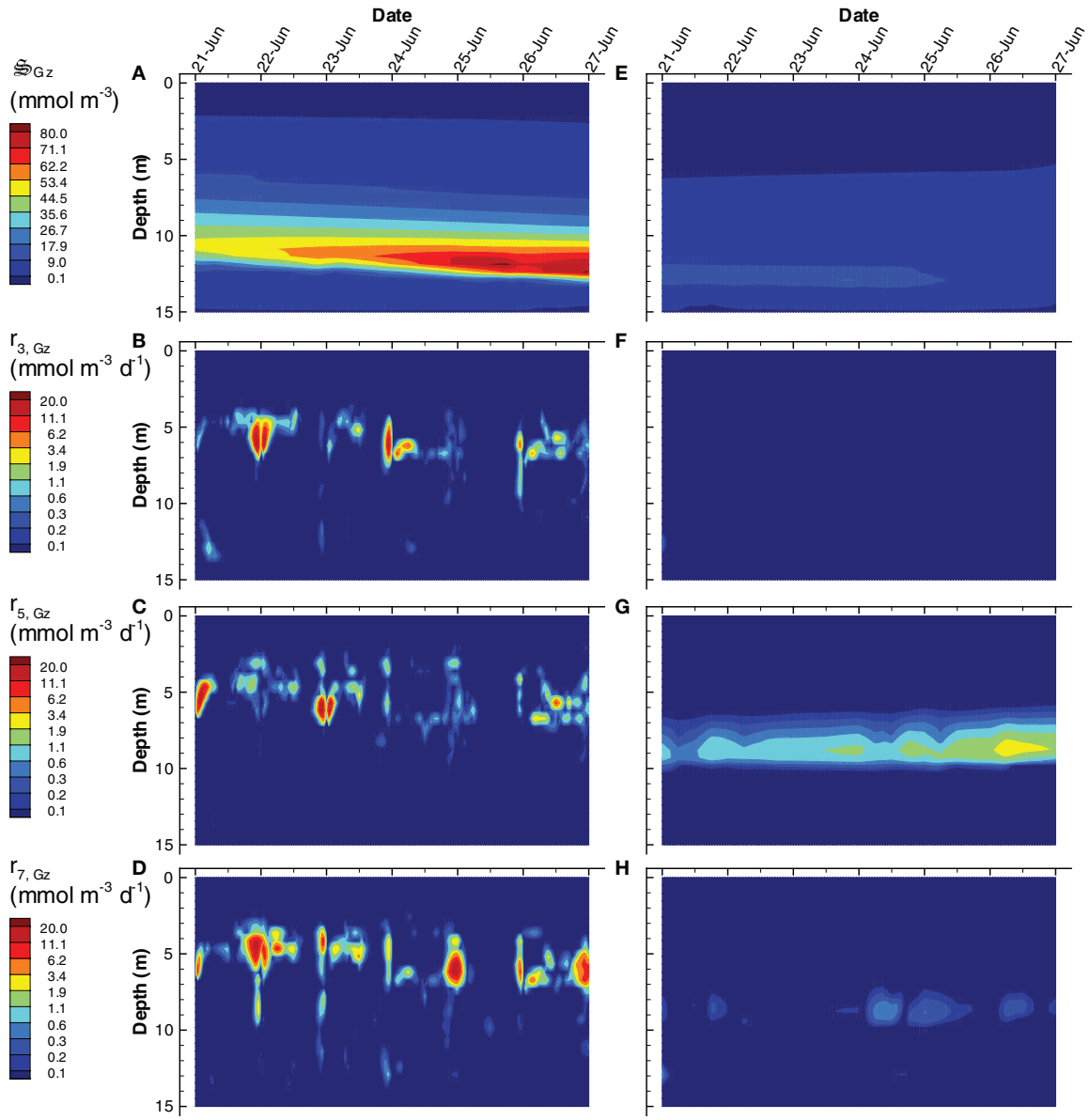

FIGURE 11 | Contour plots of grazer concentration, [$\mathbb{S}_{Gz}$] **(A,E)** and rates of predation on, grazers, $r_{3,Gz}$ **(B,F)**, bacteria, $r_{5,Gz}$ **(C,G)**, and photoheterotrophs, $r_{7,Gz}$ **(D,H)** for the SIO **(A–D)** and LIO **(D–H)** simulations.

systems where energy potentials are stable with respect to abiotic decay, such as chemical potentials. However, it seems possible that both local and global optimization could be operating simultaneously in systems given that both light and chemical potentials often exist, so further studies are needed.

Other areas that could improve the MEP modeling approach are as follows. Our metabolic network (**Figure 1**) was largely based on prior knowledge about Siders Pond biogeochemistry, but condensing genome-scale models may also be a means to construct more realistic whole community metabolic networks from genomic surveys (Hanson et al., 2014; Hanemaaijer et al., 2015), and exometabolomics could be used to identify metabolite nodes in the distributed metabolic network that are widely exchanged between functional groups (Klitgord and Segre, 2010; Baran et al., 2015; Fiore et al., 2015; Ponomarova and Patil, 2015). Also, our current approach relies on non-linear optimal control to locate MEP solutions, but this is a computationally intensive problem, and falls under the class of problems known as control of partial differential equations (Coron, 2007). Building on expertise from that field could reduce computation requirements, especially for problems involving two or three spatial dimensions, but it might be possible to avoid the formal optimization problem altogether. One possibility would be to use Darwinian inspired trait-based modeling approaches (Follows et al., 2007; Coles et al.,

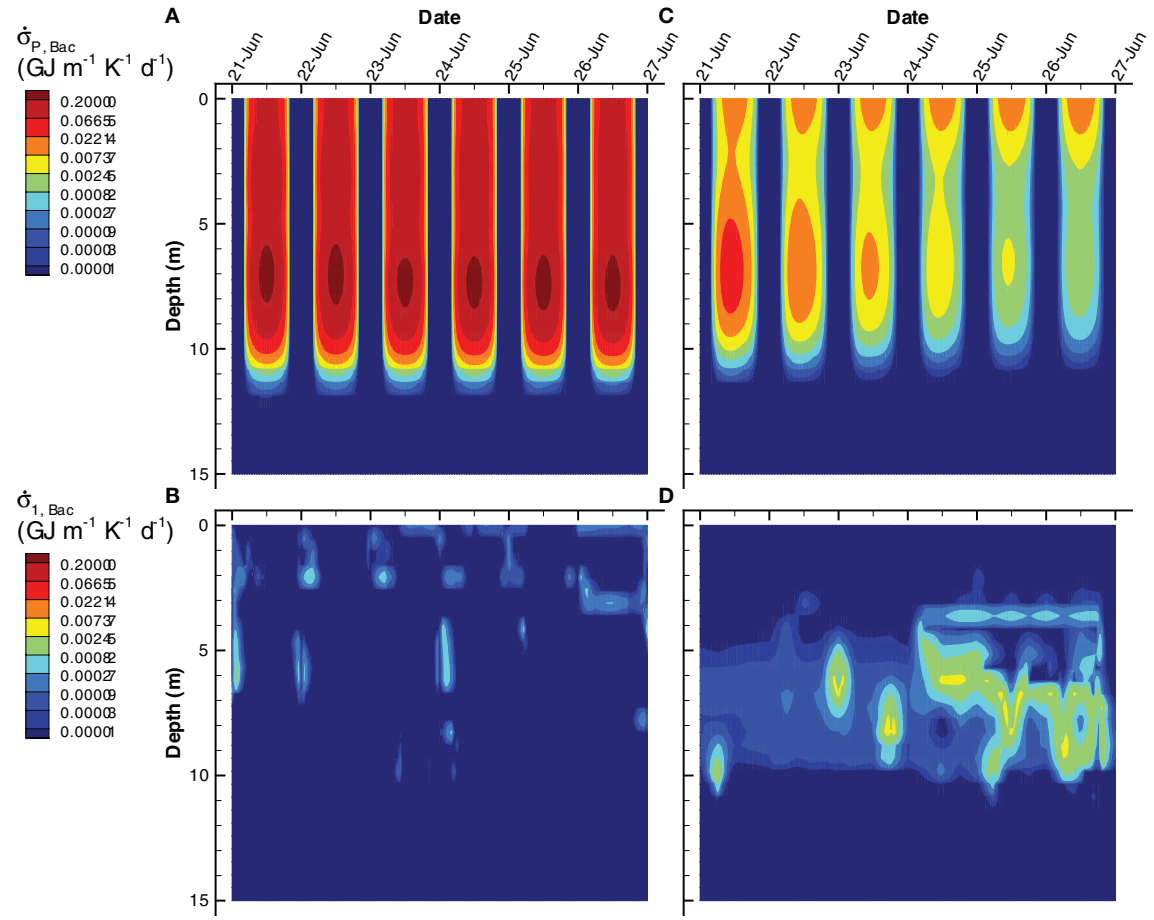

FIGURE 12 | Contour plots of entropy production by bacteria associated with light absorption by bacterial biomass, $\dot{\sigma}_{P,Bac}$ **(A,C)** and growth of bacteria, $r_{1,Bac}$, on organic carbon, $\dot{\sigma}_{1,Bac}$, Equation (S94) **(B,D)** for the SIO **(A,B)** and LIO **(C,D)** simulations.

2017), which is how biology actually solves the MEP problem. On the other hand, MEP could be useful for developing trait models that improve entropy production over time and space, such as traits that include resource storage, time delays (i.e., dormancy), migration across fronts and boundaries to acquire resources, clocks and oscillators, distribution and packaging of metabolic function, predation, remineralization, and other regulatory motifs (Wolf and Arkin, 2003). By placing emphasis on the mechanisms of how energy potentials are destroyed over time and space, rather than on the peculiarities of how organisms grow and survive, can lead to new insights that can improve our understanding of biogeochemistry and model predictions thereof.

CONCLUSIONS

Our results demonstrate that models based on MEP can reasonably simulate how microbial communities organize and function in Siders Pond over time and space while using a minimum of adjustable parameters. The improved qualitative and quantitative agreement between model predictions and observations using long (3 day, LIO) versus short (0.25 day, SIO) interval optimization supports the hypothesis that biological systems maximize entropy production over long time scales. The modeling presented here extends the MEP approach to include an explicit spatial dimension, and new metabolic reactions were introduced to model phototrophs and entropy production associated with the destruction of electromagnetic potential. By considering the dissipation of both chemical and electromagnetic potentials, the MEP model shows that heterotrophs, such as bacteria, dissipate far more free energy in the photic zone by passive light absorption than by chemical respiration. Short interval optimization results in higher grazing rates and turnover of organic carbon, as well as rapid (bang-bang) changes in the reaction control variables, while long interval optimization supports higher phytoplankton growth and standing stocks near the surface of the pond. We also found that maximization of local entropy production, as opposed to global entropy production, must be used for energy potentials that are quickly dissipated by abiotic processes, such as light absorption by water and particles. Taken together, results validate our general conjecture

that biological systems evolve and organize to maximize entropy production over the greatest possible spatial and temporal scales, while abiotic processes maximize instantaneous and local entropy production.

AUTHOR CONTRIBUTIONS

Both JV and JH contributed equally to project concepts and design, and both conducted the 24 h sampling of Siders Pond. Preliminary results from metatranscriptomics and metagenomics from JH were used to improve development of the metabolic network. JV developed the model and wrote first draft of the manuscript with editing and inputs during the process from JH. Both authors contributed to manuscript revision, read and approved the submitted version.

FUNDING

Primary funding for this project was from NSF GG grant EAR-1451356 to JV and JH, with additional support from Gordon and Betty Moore Foundation grant GBMF 3297. JV also received support from NSF Grants OCE-1637630 and OCE-1558710 and Simons Foundation grant 549941. The NSF Center for Dark Energy Biosphere Investigations (C-DEBI; OCE-0939564) also supported the participation of JH. This is C-DEBI contribution number 441.

ACKNOWLEDGMENTS

We thank Petra Byl for assistance in field work preparation and sampling of Siders Pond, as well as insightful conversations about the project. We also thank Jane Tucker for dissolved inorganic carbon analyses, Suzanne Thomas for hydrogen sulfide analyses, Sam Kelsey for dissolved organic carbon analyses, Kate Morkeski for sulfate, phosphate and particulate organic carbon analyses, and Rich McHorney, Leslie Murphy, Emily Reddington, and Gretta Serres for assistance with Siders Pond sampling logistics. We also thank the Semester in Environmental Science Program at MBL for use of their Hydrolab and Jon Boat used for sampling, and a special thank you to Tom Gregg who allowed us to access Siders Pond through his property as well as for providing logistical support.

SUPPLEMENTARY MATERIAL

The Supplementary Material for this article can be found online at: https://www.frontiersin.org/articles/10.3389/fenvs.2018.00100/full#supplementary-material

REFERENCES

Alberty, R. A. (2003). *Thermodynamics of Biochemical Reactions*. Hoboken, NJ: Wiley and Sons.

Algar, C. K., and Vallino, J. J. (2014). Predicting microbial nitrate reduction pathways in coastal sediments. *Aquat. Microb. Ecol.* 71, 223–238. doi: 10.3354/ame01678

Baran, R., Brodie, E. L., Mayberry-Lewis, J., Hummel, E., Da Rocha, U. N., Chakraborty, R., et al. (2015). Exometabolite niche partitioning among sympatric soil bacteria. *Nat. Commun.* 6:8289. doi: 10.1038/ncomms9289

Battley, E. H., Putnam, R. L., and Boerio-Goates, J. (1997). Heat capacity measurements from 10 to 300 K and derived thermodynamic functions of lyophilized cells of *Saccharomyces cerevisiae* including the absolute entropy and the entropy of formation at 298.15 K. *Thermochim. Acta* 298, 37–46. doi: 10.1016/S0040-6031(97)00108-1

Béjà, O., Aravind, L., Koonin, E. V., Suzuki, M. T., Hadd, A., Nguyen, L. P., et al. (2000). Bacterial rhodopsin: evidence for a new type of phototrophy in the sea. *Science* 289, 1902–1906. doi: 10.1126/science.289.5486.1902

Blumenfeld, L. A. (1981). *Problems of Biological Physics*. Berlin: Springer-Verlag.

Brock, T. D. (1981). Calculating solar radiation for ecological studies. *Ecol. Model.* 14, 1–19. doi: 10.1016/0304-3800(81)90011-9

Candau, Y. (2003). On the exergy of radiation. *Solar Energy* 75, 241–247. doi: 10.1016/j.solener.2003.07.012

Caraco, N. (1986). *Phosphorus, Iron, and Carbon Cycling in a Salt Stratified Coastal Pond*. Ph.D. thesis, Boston University.

Caraco, N., and Puccoon, A. H. (1986). The measurement of bacterial chlorophyll and algalchlorophyll a in natural waters. *Limnol. Oceanogr.* 31, 889–893. doi: 10.4319/lo.1986.31.4.0889

Caraco, N., Tamse, A., Boutros, O., and Valiela, I. (1987). Nutrient limitation of phytoplankton growth in brackish coastal ponds. *Can. J. Fish. Aquat. Sci.* 44, 473–476. doi: 10.1139/f87-056

Chapman, E. J., Childers, D. L., and Vallino, J. J. (2016). How the Second Law of Thermodynamics has informed ecosystem ecology through its history. *BioScience* 66, 27–39. doi: 10.1093/biosci/biv166

Cole, J. A., Kohler, L., Hedhli, J., and Luthey-Schulten, Z. (2015). Spatially-resolved metabolic cooperativity within dense bacterial colonies. *BMC Syst. Biol.* 9:15. doi: 10.1186/s12918-015-0155-1

Coles, V. J., Stukel, M. R., Brooks, M. T., Burd, A., Crump, B. C., Moran, M. A., et al. (2017). Ocean biogeochemistry modeled with emergent trait-based genomics. *Science* 358, 1149–1154. doi: 10.1126/science.aan5712

Coron, J.-M. (2007). *Control and Nonlinearity*. Providence, RI: American Mathematical Society.

Dewar, R. (2003). Information theory explanation of the fluctuation theorem, maximum entropy production and self-organized criticality in non-equilibrium stationary states. *J. Phys. A Math. Gen.* 36, 631–641. doi: 10.1088/0305-4470/36/3/303

Dewar, R., Lineweaver, C., Niven, R., and Regenauer-Lieb, K. (2014a). "Beyond the Second Law: an overview," in *Beyond the* Second *Law*, eds R. C. Dewar, C. H. Lineweaver, R. K. Niven and K. Regenauer-Lieb (Berlin; Heidelberg: Springer), 3–27.

Dewar, R. C., Lineweaver, C. H., Niven, R. K., and Regenauer-Lieb, K., (eds) (2014b). *Beyond the Second Law: Entropy Production and Non-Equilibrium Systems*. Berlin: Springer-Verlag.

Dubinsky, V., Haber, M., Burgsdorf, I., Saurav, K., Lehahn, Y., Malik, A., et al. (2017). Metagenomic analysis reveals unusually high incidence of proteorhodopsin genes in the ultraoligotrophic Eastern Mediterranean Sea. *Environ. Microbiol.* 19, 1077–1090. doi: 10.1111/1462-2920.13624

Edwards, C. A., Moore, A. M., Hoteit, I., and Cornuelle, B. D. (2015). Regional ocean data assimilation. *Ann. Rev. Mar. Sci.* 7, 21–42. doi: 10.1146/annurev-marine-010814-015821

Estrela, S., Trisos, C. H., and Brown, S. P. (2012). From metabolism to ecology: cross-feeding interactions shape the balance between polymicrobial conflict and mutualism. *Am. Nat.* 180, 566–576. doi: 10.1086/667887

Fasham, M. J. R., Ducklow, H. W., and McKelvie, S. M. (1990). A nitrogen-based model of plankton dynamics in the ocean mixed layer. *J. Mar. Res.* 48, 591–639. doi: 10.1357/002224090784984678

Fernandez, A., Huang, S., Seston, S., Xing, J., Hickey, R., Criddle, C., et al. (1999). How stable is stable? Function versus community composition. *Appl. Environ. Microbiol.* 65, 3697–3704.

Fernandez-Gonzalez, N., Huber, J. A., and Vallino, J. J. (2016). Microbial communities are well adapted to disturbances in energy input. *mSystems* 1:e00117–16. doi: 10.1128/mSystems.00117-16

Fierer, N., Bradford, M. A., and Jackson, R. B. (2007). Toward an ecological classification of soil bacteria. *Ecology* 88, 1354–1364. doi: 10.1890/05-1839

Finegan, B. (1984). Forest succession. *Nature* 312, 109–114. doi: 10.1038/312109a0

Fiore, C. L., Longnecker, K., Kido Soule, M. C., and Kujawinski, E. B. (2015). Release of ecologically relevant metabolites by the cyanobacterium *Synechococcus elongatus* CCMP 1631. *Environ. Microbiol.* 17, 3949–3963. doi: 10.1111/1462-2920.12899

Fitzpatrick, J. J. (2009). Assessing skill of estuarine and coastal eutrophication models for water quality managers. *J. Mar. Syst.* 76, 195–211. doi: 10.1016/j.jmarsys.2008.05.018

Follows, M. J., Dutkiewicz, S., Grant, S., and Chisholm, S. W. (2007). Emergent biogeography of microbial communities in a model ocean. *Science* 315, 1843–1846. doi: 10.1126/science.1138544

Friedrichs, M. A. M., Dusenberry, J. A., Anderson, L. A., Armstrong, R. A., Chai, F., Christian, J. R., et al. (2007). Assessment of skill and portability in regional marine biogeochemical models: role of multiple planktonic groups. *J. Geophys. Res.* 112:C08001. doi: 10.1029/2006JC003852

Gilboa-Garber, N. (1971). Direct spectrophotometric determination of inorganic sulfide in biological materials and in other complex mixtures. *Anal. Biochem.* 43, 129–133. doi: 10.1016/0003-2697(71)90116-3

Gloag, E. S., Javed, M. A., Wang, H., Gee, M. L., Wade, S. A., Turnbull, L., et al. (2013). Stigmergy: a key driver of self-organization in bacterial biofilms. *Commun. Integr. Biol.* 6:e27331. doi: 10.4161/cib.27331

Goldenfeld, N., and Woese, C. (2011). Life is physics: evolution as a collective phenomenon far from equilibrium. *Annu. Rev. Cond. Matt. Phys.* 2, 375–399. doi: 10.1146/annurev-conmatphys-062910-140509

Goo, E., Majerczyk, C. D., An, J. H., Chandler, J. R., Seo, Y. S., Ham, H., et al. (2012). Bacterial quorum sensing, cooperativity, and anticipation of stationary-phase stress. *Proc. Natl. Acad. Sci. U.S.A.* 109, 19775–19780. doi: 10.1073/pnas.1218092109

Grover, J. P. (2011). Resource storage and competition with spatial and temporal variation in resource availability. *Am. Nat.* 178, E124–E148. doi: 10.1086/662163

Hallam, S. J., and McCutcheon, J. P. (2015). Microbes don't play solitaire: how cooperation trumps isolation in the microbial world. *Environ. Microbiol. Rep.* 7, 26–28. doi: 10.1111/1758-2229.12248

Hanemaaijer, M., Röling, W. F., Olivier, B. G., Khandelwal, R. A., Teusink, B., and Bruggeman, F. J. (2015). Systems modeling approaches for microbial community studies: from metagenomics to inference of the community structure. *Front. Microbiol.* 6:213. doi: 10.3389/fmicb.2015.00213

Hanson, N. W., Konwar, K. M., Hawley, A. K., Altman, T., Karp, P. D., and Hallam, S. J. (2014). Metabolic pathways for the whole community. *BMC Genomics* 15:619. doi: 10.1186/1471-2164-15-619

Hmelo, L. R. (2017). Quorum sensing in marine microbial environments. *Ann. Rev. Mar. Sci.* 9, 257–281. doi: 10.1146/annurev-marine-010816-060656

Inoue, T., and Iseri, Y. (2012). Diel vertical migration and nutrient transport of the dinoflagellate *Peridinium bipes F.* occultatum in a thermally stratified reservoir. *Water Sci. Technol.* 66, 1212–1219. doi: 10.2166/wst.2012.302

Judson, O. P. (2017). The energy expansions of evolution. *Nat. Ecol. Evol.* 1:0138. doi: 10.1038/s41559-017-0138

Katz, Y., and Springer, M. (2016). Probabilistic adaptation in changing microbial environments. *Peer J.* 4:e2716. doi: 10.7717/peerj.2716

Kleidon, A., and Lorenz, R. D. (2005). *Non-equilibrium Thermodynamics and the Production of Entropy*. Berlin: Springer-Verlag.

Kleidon, A., Malhi, Y., and Cox, P. M. (2010). Maximum entropy production in environmental and ecological systems. *Philos. Trans. R. Soc. B Biol. Sci.* 365, 1297–1302. doi: 10.1098/rstb.2010.0018

Klitgord, N., and Segrè, D. (2010). Environments that induce synthetic microbial ecosystems. *PLoS Comput. Biol.* 6:e1001002. 1–17. doi: 10.1371/journal.pcbi.1001002

Konopka, A., Lindemann, S., and Fredrickson, J. (2015). Dynamics in microbial communities: unraveling mechanisms to identify principles. *ISME J.* 9, 1488–1495. doi: 10.1038/ismej.2014.251

La Rowe, D. E., Dale, A. W., Amend, J. P., and Van Cappellen, P. (2012). Thermodynamic limitations on microbially catalyzed reaction rates. *Geochim. Cosmochim. Acta* 90, 96–109. doi: 10.1016/j.gca.2012.05.011

Le Quere, C., Harrison, S. P., Colin Prentice, I., Buitenhuis, E. T., Aumont, O., Bopp, L., et al. (2005). Ecosystem dynamics based on plankton functional types for global ocean biogeochemistry models. *Glob. Chang. Biol.* 11, 2016–2040. doi: 10.1111/j.1365-2486.2005.1004.x

Lewis, K. (2010). Persister cells. *Annu. Rev. Microbiol.* 64, 357–372. doi: 10.1146/annurev.micro.112408.134306

Liu, J., Prindle, A., Humphries, J., Gabalda-Sagarra, M., Asally, M., and Lee, D. Y., et al. (2015). Metabolic co-dependence gives rise to collective oscillations within biofilms. *Nature* 523, 550–554. doi: 10.1038/nature14660

Locey, K. J., and Lennon, J. T. (2016). Scaling laws predict global microbial diversity. *Philos. Trans. R. Soc. B Biol. Sci.* 113, 5970–5975. doi: 10.1073/pnas.1521291113

Lorenz, R. (2003). Full steam ahead-probably. *Science* 299, 837–838. doi: 10.1126/science.1081280

Lotka, A. J. (1922). Contribution to the energetics of evolution. *Philos. Trans. R. Soc. B Biol. Sci.* 8, 147–151. doi: 10.1073/pnas.8.6.147

Louca, S., and Doebeli, M. (2016). Transient dynamics of competitive exclusion in microbial communities. *Environ. Microbiol.* 18, 1863–1874. doi: 10.1111/1462-2920.13058

Macedo, M. F., and Duarte, P. (2006). Phytoplankton production modelling in three marine ecosystems–static versus dynamic approach. *Ecol. Modell.* 190, 299–316. doi: 10.1016/j.ecolmodel.2005.05.012

Marino, N. A. C., Srivastava, D. S., and Farjalla, V. F. (2016). Predator kairomones change food web structure and function, regardless of cues from consumed prey. *Oikos* 125, 1017–1026. doi: 10.1111/oik.02664

Martyushev, L. M., and Seleznev, V. D. (2006). Maximum entropy production principle in physics, chemistry and biology. *Phys. Rep.* 426, 1–45. doi: 10.1016/j.physrep.2005.12.001

Mitchell, A., Romano, G. H., Groisman, B., Yona, A., Dekel, E., Kupiec, M., et al. (2009). Adaptive prediction of environmental changes by microorganisms. *Nature* 460, 220–224. doi: 10.1038/nature08112

Moran, M. A. (2015). The global ocean microbiome. *Science* 350:aac8455. doi: 10.1126/science.aac8455

Morrison, P. (1964). A thermodynamic characterization of self-reproduction. *Rev. Mod. Phys.* 36, 517–524. doi: 10.1103/RevModPhys.36.517

Murphy, J., and Riley, J. P. (1962). A modified single solution method for the determination of phosphate in natural waters. *Anal. Chim. Acta* 27, 31–36. doi: 10.1016/S0003-2670(00)88444-5

Needham, D. M., and Fuhrman, J. A. (2016). Pronounced daily succession of phytoplankton, archaea and bacteria following a spring bloom. *Nat. Microbiol.* 1:16005. doi: 10.1038/nmicrobiol.2016.5

Odum, E. P. (1969). The strategy of ecosystem development. *Science* 164, 262–270.

Ottesen, E. A., Young, C. R., Gifford, S. M., Eppley, J. M., Marin, R., Schuster, S. C., et al. (2014). Multispecies diel transcriptional oscillations in open ocean heterotrophic bacterial assemblages. *Science* 345, 207–212. doi: 10.1126/science.1252476

Pasternak, Z., Ben Sasson, T., Cohen, Y., Segev, E., and Jurkevitch, E. (2015). A new comparative-genomics approach for defining phenotype-specific indicators reveals specific genetic markers in predatory bacteria. *PLOS ONE* 10:e0142933. doi: 10.1371/journal.pone.0142933

Pianka, E. R. (1970). R-Selection and K-Selection. *Am. Nat.* 104, 592–597. doi: 10.1086/282697

Ponomarova, O., and Patil, K. R. (2015). Metabolic interactions in microbial communities: untangling the Gordian knot. *Curr. Opin. Microbiol.* 27, 37–44. doi: 10.1016/j.mib.2015.06.014

Rakoff-Nahoum, S., Foster, K. R., and Comstock, L. E. (2016). The evolution of cooperation within the gut microbiota. *Nature* 533, 255–259. doi: 10.1038/nature17626

Reed, D. C., Algar, C. K., Huber, J. A., and Dick, G. J. (2014). Gene-centric approach to integrating environmental genomics and biogeochemical models. *Proc. Natl. Acad. Sci. U.S.A.* 111, 1879–1884. doi: 10.1073/pnas.1313713111

Reguera, G., McCarthy, K. D., Mehta, T., Nicoll, J. S., Tuominen, M. T., and Lovley, D. R. (2005). Extracellular electron transfer via microbial nanowires. *Nature* 435, 1098–1101. doi: 10.1038/nature03661

Riley, G. A. (1946). Factors controlling phytoplankton population on Georges Bank. *J. Mar. Res.* 6, 54–73.

Sathyendranath, S., Stuart, V., Nair, A., Oka, K., Nakane, T., Bouman, H., et al. (2009). Carbon-to-chlorophyll ratio and growth rate of phytoplankton in the sea. *Mar. Ecol. Prog. Ser.* 383, 73–84. doi: 10.3354/meps07998

Schartau, M., Wallhead, P., Hemmings, J., Löptien, U., Kriest, I., Krishna, S., et al. (2017). Reviews and syntheses: parameter identification in marine planktonic ecosystem modelling. *Biogeosciences* 14, 1647–1701. doi: 10.5194/bg-14-1647-2017

Schauer, R., Risgaard-Petersen, N., Kjeldsen, K. U., Tataru Bjerg, J. J., B., Jørgensen, B., Schramm, A., et al. (2014). Succession of cable bacteria and electric currents in marine sediment. *ISME J.* 8, 1314—1322. doi: 10.1038/ismej.2013.239

Schulz, H. N., Brinkhoff, T., Ferdelman, T. G., Mariné, M. H., Teske, A., and Jørgensen, B. B. (1999). Dense populations of a giant sulfur bacterium in Namibian shelf sediments. *Science* 284, 493–495. doi: 10.1126/science.284.5413.493

Skene, K. (2015). Life's a gas: a thermodynamic theory of biological evolution. *Entropy* 17, 5522–5548. doi: 10.3390/e17085522

Skene, K. R. (2017). Thermodynamics, ecology and evolutionary biology: a bridge over troubled water or common ground? *Acta Oecologica* 85, 116–125. doi: 10.1016/j.actao.2017.10.010

Sogin, M. L., Morrison, H. G., Huber, J. A., Welch, D. M., Huse, S. M., Neal, P. R., et al. (2006). Microbial diversity in the deep sea and the underexplored "rare biosphere". *Proc. Natl. Acad. Sci. U.S.A.* 103, 12115—12120. doi: 10.1073/pnas.0605127103

Stocker, R., and Seymour, J. R. (2012). Ecology and physics of bacterial chemotaxis in the ocean. *Microbiol. Mol. Biol. Rev.* 76, 792–812. doi: 10.1128/MMBR.00029-12

Tilman, D. (1982). *Resource Competition and Community Structure.* Princeton, NJ: Princetown University Press.

Treangen, T. J., and Rocha, E. P. C. (2011). Horizontal transfer, not duplication, drives the expansion of protein families in prokaryotes. *PLoS Genet.* 7:e1001284. doi: 10.1371/journal.pgen.1001284

Vallino, J. J. (2000). Improving marine ecosystem models: use of data assimilation and mesocosm experiments. *J. Mar. Res.* 58, 117–164. doi: 10.1357/002224000321511223

Vallino, J. J. (2003). Modeling microbial consortiums as distributed metabolic networks. *Biol. Bull.* 204, 174–179. doi: 10.2307/1543554

Vallino, J. J. (2010). Ecosystem biogeochemistry considered as a distributed metabolic network ordered by maximum entropy production. *Philos. Trans. R. Soc. B Biol. Sci.* 365, 1417–1427. doi: 10.1098/rstb.2009.0272

Vallino, J. J. (2011). Differences and implications in biogeochemistry from maximizing entropy production locally versus globally. *Earth Syst. Dynam.* 2, 69–85. doi: 10.5194/esd-2-69-2011

Vallino, J. J., and Algar, C. K. (2016). The thermodynamics of marine biogeochemical cycles: lotka revisited. *Ann. Rev. Mar. Sci.* 8, 333–3s56. doi: 10.1146/annurev-marine-010814-015843

Vallino, J. J., Algar, C. K., González, N. F., and Huber, J. A. (2014). "Use of receding horizon optimal control to solve MaxEP-based biogeochemistry problems," in *Beyond the* Second *Law-Entropy Production and Non-Equilibrium Systems*, eds R. C. Dewar, C. H. Lineweaver, R. K. Niven, and K. Regenauer-Lieb (Berlin; Heidelberg: Springer), 337–359.

Ward, B. A., Friedrichs, M. A. M., Anderson, T. R., and Oschlies, A. (2010). Parameter optimisation techniques and the problem of underdetermination in marine biogeochemical models. *J. Mar. Syst.* 81, 34–43. doi: 10.1016/j.jmarsys.2009.12.005

Whiteley, M., Diggle, S. P., and Greenberg, E. P. (2017). Progress in and promise of bacterial quorum sensing research. *Nature* 551:313. doi: 10.1038/nature24624

Wolf, D. M., and Arkin, A. P. (2003). Motifs, modules and games in bacteria. *Curr. Opin. Microbiol.* 6, 125–134. doi: 10.1016/S1369-5274(03)00033-X

Worden, A. Z., Follows, M. J., Giovannoni, S. J., Wilken, S., Zimmerman, A. E., and Keeling, P. J. (2015). Rethinking the marine carbon cycle: factoring in the multifarious lifestyles of microbes. *Science* 347:1257594. doi: 10.1126/science.1257594

Conflict of Interest Statement: The authors declare that the research was conducted in the absence of any commercial or financial relationships that could be construed as a potential conflict of interest.

Advantages of publishing in Frontiers

OPEN ACCESS
Articles are free to read for greatest visibility and readership

FAST PUBLICATION
Around 90 days from submission to decision

HIGH QUALITY PEER-REVIEW
Rigorous, collaborative, and constructive peer-review

TRANSPARENT PEER-REVIEW
Editors and reviewers acknowledged by name on published articles

Frontiers
Avenue du Tribunal-Fédéral 34
1005 Lausanne | Switzerland

Visit us: www.frontiersin.org
Contact us: info@frontiersin.org | +41 21 510 17 00

REPRODUCIBILITY OF RESEARCH
Support open data and methods to enhance research reproducibility

DIGITAL PUBLISHING
Articles designed for optimal readership across devices

FOLLOW US
@frontiersin

IMPACT METRICS
Advanced article metrics track visibility across digital media

EXTENSIVE PROMOTION
Marketing and promotion of impactful research

LOOP RESEARCH NETWORK
Our network increases your article's readership